

Topics in Current Chemistry Collections

Juan Carlos Colmenares
Gregory Chatel *Editors*

Sonochemistry

From Basic Principles to Innovative
Applications

 Springer

Topics in Current Chemistry Collections

Journal Editors

Massimo Olivucci, Siena, Italy and Bowling Green, USA
Wai-Yeung Wong, Hong Kong

Series Editors

Hagan Bayley, Oxford, UK
Kendall N. Houk, Los Angeles, USA
Greg Hughes, Codexis Inc, USA
Christopher A. Hunter, Cambridge, UK
Seong-Ju Hwang, Seoul, South Korea
Kazuaki Ishihara, Nagoya, Japan
Barbara Kirchner, Bonn, Germany
Michael J. Krische, Austin, Texas
Delmar Larsen, Davis, USA
Jean-Marie Lehn, Strasbourg, France
Rafael Luque, Córdoba, Spain
Jay S. Siegel, Tianjin, China
Joachim Thiem, Hamburg, Germany
Margherita Venturi, Bologna, Italy
Chi-Huey Wong, Taipei, Taiwan
Henry N.C. Wong, Hong Kong
Vivian Wing-Wah Yam, Hong Kong
Chunhua Yan, Beijing, China
Shu-Li You, Shanghai, China

Aims and Scope

The series *Topics in Current Chemistry Collections* presents critical reviews from the journal *Topics in Current Chemistry* organized in topical volumes. The scope of coverage is all areas of chemical science including the interfaces with related disciplines such as biology, medicine and materials science.

The goal of each thematic volume is to give the non-specialist reader, whether in academia or industry, a comprehensive insight into an area where new research is emerging which is of interest to a larger scientific audience.

Each review within the volume critically surveys one aspect of that topic and places it within the context of the volume as a whole. The most significant developments of the last 5 to 10 years are presented using selected examples to illustrate the principles discussed. The coverage is not intended to be an exhaustive summary of the field or include large quantities of data, but should rather be conceptual, concentrating on the methodological thinking that will allow the non-specialist reader to understand the information presented.

Contributions also offer an outlook on potential future developments in the field.

More information about this series at <http://www.springer.com/series/14181>

Juan Carlos Colmenares • Gregory Chatel
Editors

Sonochemistry

From Basic Principles
to Innovative Applications

With contributions from

Muthupandian Ashokkumar • Sundaram Ganesh Babu
Alessandro Barge • Sukhvir Kaur Bhangu • Gregory Chatel
Juan C. Colmenares • Giancarlo Cravotto • Micheline Draye
David Fernandez Rivas • Parag R. Gogate • Jordan J. Hinman
Nathalie Kardos • Simon Kuhn • Ewelina Kuna • Paweł Lisowski
Katia Martina • Bernaurdshaw Neppolian • Pankaj N. Patil
Kenneth S. Suslick • Silvia Tagliapietra • Ewa Zielewicz

 Springer

Editors

Juan Carlos Colmenares
Institute of Physical Chemistry
Polish Academy of Sciences
Warsaw, Poland

Gregory Chatel
Laboratoire de Chimie Moléculaire et
Environnement (LCME)
Université Savoie Mont Blanc
Le Bourget-du-Lac Cedex
France

Originally published in *Top Curr Chem (Z)* Volume 374 (2016),
© Springer International Publishing Switzerland 2017

ISSN 2367-4067 ISSN 2367-4075 (electronic)
Topics in Current Chemistry Collections
ISBN 978-3-319-54270-6 ISBN 978-3-319-54271-3 (eBook)
DOI 10.1007/978-3-319-54271-3

Library of Congress Control Number: 2017933486

© Springer International Publishing AG 2017

This work is subject to copyright. All rights are reserved by the Publisher, whether the whole or part of the material is concerned, specifically the rights of translation, reprinting, reuse of illustrations, recitation, broadcasting, reproduction on microfilms or in any other physical way, and transmission or information storage and retrieval, electronic adaptation, computer software, or by similar or dissimilar methodology now known or hereafter developed.

The use of general descriptive names, registered names, trademarks, service marks, etc. in this publication does not imply, even in the absence of a specific statement, that such names are exempt from the relevant protective laws and regulations and therefore free for general use.

The publisher, the authors and the editors are safe to assume that the advice and information in this book are believed to be true and accurate at the date of publication. Neither the publisher nor the authors or the editors give a warranty, express or implied, with respect to the material contained herein or for any errors or omissions that may have been made. The publisher remains neutral with regard to jurisdictional claims in published maps and institutional affiliations.

Printed on acid-free paper

This Springer imprint is published by Springer Nature
The registered company is Springer International Publishing AG
The registered company address is: Gewerbestrasse 11, 6330 Cham, Switzerland

Contents

Sonochemistry: from Basic Principles to Innovative Applications	vii
Gregory Chatel, Juan Carlos Colmenares	
Theory of Sonochemistry	1
Sukhvir Kaur Bhangu, Muthupandian Ashokkumar	
Advances in Green Organic Sonochemistry	29
Micheline Draye, Nathalie Kardos	
Nanostructured Materials Synthesis Using Ultrasound	59
Jordan J. Hinman, Kenneth S. Suslick	
Synthesis of Photoactive Materials by Sonication: Application in Photocatalysis and Solar Cells	95
Juan C. Colmenares, Ewelina Kuna, Paweł Lisowski	
The Role of Ultrasound on Advanced Oxidation Processes	117
Sundaram Ganesh Babu, Muthupandian Ashokkumar, Bernardshaw Neppolian	
Effects of ultrasonic disintegration of excess sewage sludge	149
Ewa Zielewicz	
Combined Microwaves/Ultrasound, a Hybrid Technology	175
Katia Martina, Silvia Tagliapietra, Alessandro Barge, Giancarlo Cravotto	
Ultrasound in Combination with Ionic Liquids: Studied Applications and Perspectives	203
Gregory Chatel	
Synergy of Microfluidics and Ultrasound: Process Intensification Challenges and Opportunities	225
David Fernandez Rivas, Simon Kuhn	
Sonochemical Reactors	255
Parag R. Gogate, Pankaj N. Patil	

Sonochemistry: from Basic Principles to Innovative Applications

Gregory Chatel¹ · Juan Carlos Colmenares²

© Springer International Publishing Switzerland 2016

The term “sonochemistry” is used to describe the chemical and physical processes occurring in solution through energy provided by ultrasound (in the range from 20 kHz to 2 MHz). The effects of ultrasound are the consequence of the cavitation phenomenon, namely the formation, growth, and collapse of gaseous microbubbles in liquid phase. The intense local effects (mechanical, thermal, and chemical) due to the sudden collapse of these micrometric bubbles lie at the origin of all applications of sonochemistry. Use of ultrasound in chemical processes increased between 1980 and 2000, and the corresponding literature has increased enormously in volume from 2000 onwards, reporting many applications in several areas including but not limited to sonocatalysis, organic chemistry, materials preparation, polymer chemistry, biomass conversion, extraction, electrochemistry, enzymatic catalysis, and environmental remediation.

The potential of sonochemistry is often directly connected to the choice of the sonochemical parameters and experimental conditions. The first contribution to this topical collection, provided by Prof. Ashokkumar’s research group, provides theoretical considerations regarding the use of ultrasound in the laboratory, to better

This article is part of the Topical Collection “Sonochemistry: From basic principles to innovative applications” edited by Juan Carlos Colmenares Q. and Gregory Chatel.

✉ Gregory Chatel
gregory.chatel@univ-smb.fr;
<http://gregorychatel-chemistry.com/>

✉ Juan Carlos Colmenares
jcarloscolmenares@ichf.edu.pl;
<http://photo-catalysis.org>

¹ Laboratoire de Chimie Moléculaire et Environnement (LCME), UFR Sciences et Montagne (Scem), Université Savoie Mont Blanc, 73376 Le Bourget Du Lac Cedex, France

² Institute of Physical Chemistry of the Polish Academy of Sciences (PAS), Kasprzaka 44/52, 01-224 Warsaw, Poland

understand the mechanisms involved and determine which parameters can affect the observed results. Specifically, a detailed discussion on single-bubble sonochemistry is provided in this contribution.

Further contributions highlight how sonochemistry represents a key area for research and innovation in chemistry. Indeed, the conditions obtained in a medium submitted to ultrasound can account for a large number of physicochemical effects, such as enhanced kinetics of chemical reactions, changes in reaction mechanisms, emulsification effects, erosion, crystallization, and precipitation, among others. Sonochemistry is multidisciplinary, and recent advances highlighting this are reported in this topical collection, in particular applications such as organic chemistry (Prof. Draye's group), synthesis of nanostructured materials (Prof. Suslick), synthesis of photoactive materials (Prof. Colmenares' group), advanced oxidation processes (Prof. Neppolian's group), and treatment of sewage sludge (Prof. Zielewicz). Results in these areas show that the improvements achieved require use of recently developed sonochemical processes.

The combination of sonochemistry with other innovative technologies is also highlighted, using microwave irradiation (Prof. Cravotto's group), ionic liquids as solvent or catalyst (Dr. Chatel), and coupling with microfluidics (Prof. Rivas' group). In all these cases, synergistic effects are observed, representing a new source of innovation for further research.

The final contribution, provided by Prof. Gogate's group, covers laboratory equipment and the opportunity to scale up the technology for maximum process intensification benefits. We conclude by stating that scientific rigor is essential in the sonochemistry area to understand the associated mechanisms and benefit from the full potential offered by ultrasound.

The editors kindly acknowledge the *Topics in Current Chemistry* editorial office (Springer) for inviting us to compile this comprehensive topical collection on sonochemistry. We would also like to extend our most sincere gratitude to international experts for their time and consideration regarding this project, as well as for their general contributions to sonochemistry science; It was pleasing and instructive to work with them on this topical collection. Last but not least, we sincerely thank our publishing editor, Elizabeth Hawkins, and assistant editor, Na Xu, who patiently and kindly took us through the development of this topical collection over the past few months to achieve this impressive final result, which would not have been possible without such support.

We sincerely hope that this topical collection will be useful both to (bio)chemistry, chemical engineering, and materials science students, as well as to graduates interested in green chemical technologies, and wish you an enjoyable and satisfactory read.



Dr. Gregory Chatel received his Ph.D. degree in 2012 from the Université de Grenoble (France) under the supervision of Prof. M. Draye and Prof. B. Andrioletti, studying the fundamentals of and developing a sonochemical method involving ionic liquids for epoxidation of various alkenes. In 2013, he joined Prof. R. D. Rogers' group at the Center for Green Manufacturing at The University of Alabama (USA) as a postdoctoral research fellow. His research has focused on applications of ionic liquids in green chemistry, separation, and biomass processing. At the end of 2013, Dr. Chatel joined the Institut de Chimie des Milieux et Matériaux de Poitiers (IC2MP) of the Université de Poitiers (France) as an assistant professor to develop a biomass valorization program based on nonconventional media/techniques, in particular via sonochemistry. In 2014, he became the first president of the French national Young Chemists' Network (RJ-SCF) of the French Chemical Society. In 2016, he joined the Laboratoire de Chimie Moléculaire et Environnement (LCME) of the Université Savoie Mont Blanc (France) to develop his work in organic sonochemistry through new original processes and applications.





Prof. Dr. Juan Carlos Colmenares Q. graduated from Warsaw University of Technology (Chem. Eng. 1995) and obtained his M.Sc. (1997) in catalysis for organic technology and Ph.D. (2004) in chemical and material sciences from the same university, and his scientific degree of habilitation (D.Sc. 2015) from the Institute of Physical Chemistry of the Polish Academy of Sciences in Poland. His interests range from materials science, nanotechnology, and heterogeneous catalysis to biomass/CO₂ valorization, solar chemicals, sonication, photocatalysis, and water/air purification. After obtaining his Ph.D., he worked at the University of Córdoba, Spain (2005–2006) in Prof. Marinas' group as a postdoctoral fellow and at the University of Southern California, Los Angeles (USA) (2006–2009) in Prof. G. A. Olah's (Nobel Prize in Chemistry) group as a postdoctoral research associate. He is a Marie Skłodowska-Curie fellow. He serves as an expert evaluator for many important scientific journals/institutions and chemical companies (Colombia, USA, Poland, Spain), and as a member of the editorial advisory board of the *Sustainable Chemical Processes* journal (Chemistry Central-Springer). He has coauthored more than 60 works published in international scientific journals and books, and filed three patent applications. Presently, he is working as an associate professor at the Institute of Physical Chemistry of the Polish Academy of Sciences in Poland.



Theory of Sonochemistry

Sukhvir Kaur Bhangu¹ · Muthupandian Ashokkumar¹

Received: 28 May 2016 / Accepted: 12 July 2016 / Published online: 1 August 2016
© Springer International Publishing Switzerland 2016

Abstract Sonochemistry refers to ultrasound-initiated chemical processes in liquids. The interaction between bubbles and sound energy in liquids results in acoustic cavitation. This review presents the fundamental aspects of acoustic cavitation and theoretical aspects behind sonochemistry such as dynamics of bubble oscillation, the rectified diffusion process that is responsible for the growth of cavitation bubbles, near adiabatic collapse of cavitation bubbles resulting in extreme reaction conditions and several chemical species generated within collapsing bubbles that are responsible for various redox reactions. Specifically, a detailed discussion on single bubble sonochemistry is provided.

Keywords Sonochemistry · Acoustic cavitation · Single bubble dynamics · Sonoluminescence

1 Introduction

Ultrasound refers to sound waves beyond the frequency that can be detected by the human ear. Sound waves with a frequency greater than 20 kHz fall into this category. Ultrasound is divided into three main regions: low frequency (20–100 kHz), intermediate frequency (100 kHz–1 MHz) and high frequency (1–10 MHz) [1]; however, intermediate range is also sometimes referred to as high frequency. Ultrasound interacts with gas bubbles in liquids to generate chemical reactions and strong physical forces that can be used for various

This article is part of the Topical Collection “Sonochemistry: From basic principles to innovative applications”; edited by Juan Carlos Colmenares Q., Gregory Chatel.

✉ Muthupandian Ashokkumar
masho@unimelb.edu.au

¹ School of Chemistry, University of Melbourne, Victoria 3010, Australia

processing applications and for promoting chemical reactions. The driving force for the generation of chemical and physical forces is acoustic cavitation, which generates extreme temperatures and pressures. The consequences of these extreme conditions generated include radical generation, light emission-sonoluminescence (SL), shock waves, microjets, microstreaming, shear forces and turbulence [1]. As a result of these strong physical and chemical effects, various applications of acoustic cavitation have been developed for commercial use including wastewater treatment [2] and the formation of protein microbubbles which can be used for flavour encapsulation and drug delivery [3].

2 History

The phenomenon of cavitation was first reported by Thornycroft and Barnaby [4] in 1895. In 1917 Rayleigh published the first mathematical model describing cavitation in an incompressible liquid [5]. In the 1930s Brohult [6] and other groups discovered that sonication can be used for the degradation of bio- and synthetic polymers. In 1935 Frenzel and Schulze [7] reported for the first time that light emission occurred in water when exposed to intense ultrasound. In 1944 Weiss [8] observed that the sonication of water leads to the generation of hydrogen and hydroxyl radicals, and in 1956 Parke and Taylor [9] provided the first experimental evidence for the formation of OH radicals in aqueous solutions. The first observations on chemical reactions in organic solutions were made in the early 1950s. It was found that methanol solutions containing diphenylpicrylhydrazyl were decolourised, indicating the formation of free radicals [10]. Also, the first computer calculations modelling a cavitation bubble were published by Neppiras and Noltingk [11] in 1950. Makino et al. [12] used spin trapping agents and electron spin resonance measurements to verify the formation of H and OH radicals during the sonication of water. It was reported in 1987 by Henglein [13] that over 80 % of primary radicals originally generated in the hotspot recombine to produce water molecules. Since the 1930s, acoustic cavitation has gained popularity as it can be used for the enhancement of chemical reactions, emulsification of oils, degradation of chemical and biological pollutants, etc.

A number of books, review articles and book chapters have been published on acoustic cavitation and its applications are available in the literature. The fundamentals of an acoustic bubble have been discussed in detail by Leighton [14] in his book *The Acoustic Bubble*. Mason and Lorimer [15–17] have published various review articles and books dealing with different aspects of ultrasound such as theory of sonochemistry, applications of ultrasound in food technology, uses of ultrasound in chemical synthesis and physical aspects of sonochemistry. A review by Leong et al. focuses on the fundamentals of ultrasound-induced physical processes such as transient and stable cavitation, rectified diffusion, coalescence and sonoluminescence [18]. The current review provides an overview of various fundamental processes of acoustic cavitation with a particular emphasis on single bubble sonochemistry.

3 Acoustic Cavitation

3.1 Bubble Formation

Acoustic cavitation is the phenomenon of formation, growth and violent collapse induced by the pressure fluctuations generated by sound waves in a liquid medium. If the intensity of ultrasound is enough to overcome the tensile strength of the medium, there occurs a point where intermolecular forces are not able to hold the molecular structure together. This point leads to the formation of a cavity in the medium. A large amount of energy is required to create a void or cavity. Equation 1 can be used to calculate the critical pressure (P_B) required to create a cavity of radius R_c .

$$P_B \sim P_h + \frac{0.77\sigma}{R_c} \quad (1)$$

σ is the surface tension of the liquid and P_h is the hydrostatic pressure (could be approximated to atmospheric pressure under normal experimental conditions). The equation is valid when $2\sigma/R_c \ll P_h$ [19]. However, free gas bubbles and gas molecules trapped in solid impurities are inherently present in liquids, which can act as nuclei for cavitation. Hence, the actual pressure required for cavitation to occur is far lower. Hence, in practical terms, acoustic cavitation refers to the growth of pre-existing gas nuclei followed by the collapse of “grown” bubbles.

There are different mechanisms associated with the formation of bubbles [14]. Firstly, gas molecules trapped in crevices of the container walls, motes or on hydrophobic dust particles [20] can act as bubble source. Harvey’s crevice model depicts how an air bubble can be nucleated from crevices. A gas pocket, trapped in a crevice, responds to alternating compression and the rarefaction cycles of the applied ultrasound. The gas pocket expands considerably during the negative pressure cycle. When the gas pocket grows sufficiently it gets detached from the crevice and leads to the formation of a gas free bubble in the liquid [21]. Dissolved gas in the liquid then fills the residual gas cavity under the applied sound field and the cycle is repeated. The second mechanism is based on the skin model where inherently present bubble nuclei are stabilized against dissolution when their surface is completely covered with organic materials or surfactants [22]. It has also been suggested that such bubbles can be stabilized by hydrophobic impurities present in a liquid. These bubbles tend to grow in an acoustic field by coalescence or rectified diffusion [23, 24]. Recently Yasui et al. introduced a dynamic equilibrium model for the stabilization of bubbles covered with hydrophobic materials [25]; the chemical potential gradient that exists near the edge of hydrophobic materials generates a dynamic equilibrium state [25]. Another mechanism for the nucleation is fragmentation of the active cavitation bubbles [26]. The shape instability of a bubble which is mostly induced by asymmetric collapse leads to the fragmentation of the bubble into several daughter bubbles which then act as new nuclei for cavitation [27–30].

Before discussing the growth of an acoustic cavitation bubble, we discuss the fundamental equations used to study the motion of bubbles in an acoustic field in the following section.

3.2 Dynamics of Bubble Oscillation

This section focuses on the oscillation dynamics of a gas bubble in an acoustic field. Further details on this can be found in the book *The Acoustic Bubble* by Leighton [14]. The Rayleigh–Plesset equation is used to examine the dynamics of a bubble oscillating at finite amplitudes [5, 14, 31]. The equation describes the motion of a spherical bubble in response to a time-varying pressure field in an incompressible liquid. When time $t < 0$, a bubble of radius R_0 is at rest in an incompressible viscous liquid and hydrostatic pressure is p_0 which is constant. However, at $t > 0$ pressure p_t varies with time and is superimposed on p_0 , so that the pressure of liquid at certain point from the bubble, $p_\infty = p_0 + p_t$ which results in a change of bubble radius to some new value R_t . During this process, the liquid shell around the bubble acquires kinetic energy of

$$\frac{1}{2} \rho \int_R^\infty \dot{r}^2 4\pi r^2 dr \quad (2)$$

where shell at radius r has thickness dr , mass = $4\pi r^2 \rho dr$ (ρ = density of liquid) and \dot{r} is the speed.

Using the liquid incompressibility condition, $\dot{r}/\dot{R} = R^2/r^2$ (where R is the radius of the bubble when contracted, \dot{R} is the wall velocity) Eq. 2 can be integrated to give $2\pi\rho R^3 \dot{R}^2$. Equating this to the difference between the work done at a certain point from the bubble by p_∞ and the work done by the pressure p_L in the liquid outside the bubble wall gives

$$\int_{R_0}^R (p_L - p_\infty) 4\pi R^2 dR = 2\pi R^3 \dot{R}^2. \quad (3)$$

Equation (5) is obtained after differentiating Eq. (3) with respect to R , noting that

$$\frac{\partial (\dot{R})^2}{\partial R} = \frac{1}{R} \frac{\partial (\dot{R}^2)}{\partial t} = 2\ddot{R} \quad (4)$$

$$\frac{p_L - p_\infty}{\rho} = \frac{3\dot{R}^2}{2} + R\ddot{R} \quad (5)$$

where \dot{R} is the velocity of the cavity, \ddot{R} is the acceleration of the cavity.

The liquid pressure p_L for a pulsating bubble containing gas and vapour is given as

$$p_L = \left(p_0 + \frac{2\sigma}{R_0} - p_v \right) \left(\frac{R_0}{R} \right)^{3\gamma} + p_v - \frac{2\sigma}{R} \quad (6)$$

where p_v is the vapour pressure of the liquid, σ is the surface tension, p_0 is the ambient pressure, γ is the ratio of specific heat of gas at constant pressure to that of constant volume.

Substituting p_L from Eq. 6 and $p_\infty = p_0 + p_t$ into Eq. 4 gives

$$R\ddot{R} + \frac{3\dot{R}^2}{2} = \frac{1}{\rho} \left\{ \left(p_0 + \frac{2\sigma}{R_0} - p_v \right) \left(\frac{R_0}{R} \right)^{3\gamma} + p_v - \frac{2\sigma}{R} - p_0 - p_t \right\}. \quad (7)$$

The effect of viscosity on the above equation was considered by Poritsky [32], who found that viscosity effects arise through boundary conditions and not through the Navier–Stokes equation and obtained Eq. 8.

$$\ddot{R}R + \frac{3\dot{R}^2}{2} = \frac{1}{\sigma} \left\{ \left(p_0 + \frac{2\sigma}{R_0} - p_v \right) \left(\frac{R_0}{R} \right)^{3\gamma} + p_v - \frac{2\sigma}{R} - \frac{4\dot{R}}{R} - p_0 - p_t \right\} \quad (8)$$

where η is the viscosity of the liquid.

Equations 5, 7 and 8 are commonly known as Rayleigh–Plesset equations and they indicate that the motion of a bubble under the acoustic field is non-linear.

A spherical bubble is subjected to the time-varying pressure of amplitude p_A and circular frequency ω . Therefore,

$$p_t = -p_A \sin(t). \quad (9)$$

Substituting Eq. 9 into Eq. 8 gives

$$\ddot{R}R + \frac{3\dot{R}^2}{2} = \frac{1}{\sigma} \left\{ \left(p_0 + \frac{2\sigma}{R_0} - p_v \right) \left(\frac{R_0}{R} \right)^{3\gamma} + p_v - \frac{2\sigma}{R} - \frac{4\dot{R}}{R} - p_0 + p_A \sin(t) \right\}. \quad (10)$$

Equation 10 is the fundamental equation used to describe the bubble motion at different frequencies. Over the past few decades the equation has been extended significantly to account for damping effects, solution compressibility, condensation, non-linear evaporation etc. [33, 34].

3.3 Bubble Growth

Bubbles inherently present in liquids tend to grow to a critical size (which is influenced by several parameters such as acoustic pressure, ultrasonic power and frequency, viscosity of medium, etc.) in an ultrasonic field. The ultrasound-driven growth is due to rectified diffusion which is defined as the slow growth of a pulsating gas bubble due to an average flow of mass (dissolved gases and solvent vapour) into the bubble as a function of time. Crum [24] explained this “rectification of mass” in terms of two effects, viz. “area effect” and “shell effect”, schematically shown in Fig. 1.

A gas bubble trapped in a liquid tends to expand when the surrounding liquid experiences negative pressure of the sound wave. At this stage, the low internal pressure of the bubble results in the evaporation of solvent molecules and diffusion

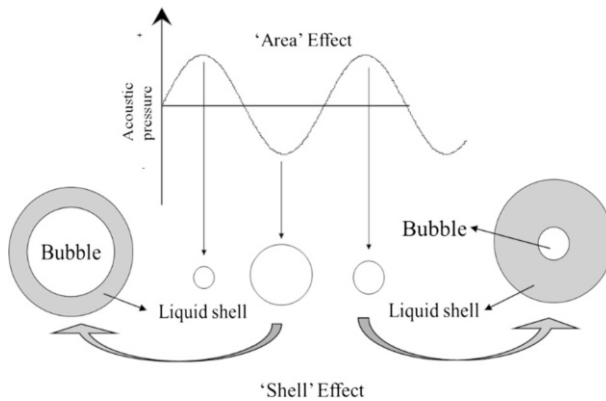


Fig. 1 Schematic description of the growth of a bubble in an acoustic field by “area” and “shell” effects (adapted from [35])

of dissolved gases into the bubble from the surrounding liquid. Therefore, the rarefaction cycle leads to “intake” of gas and vapour molecules. The bubble is compressed when the surrounding liquid experiences the positive pressure (compression cycle) of the sound wave. At this stage, the internal pressure of the bubble is high, which leads to the expulsion of the gas/vapour molecules from the bubble into the surrounding liquid. Thus, the compression cycle leads to the “loss” of bubble mass. Since the bubble collapse is relatively fast and less surface area is available for mass transport, the amount of material that diffuses out of the bubble during the compression cycle is always less than that which diffuses into the bubble during the expansion cycle, thereby leading to the net growth of the bubble. This is known as the area effect.

A change in the surface area of the bubble alone, however, is not sufficient to explain rectified diffusion. The concentration of dissolved gases and thickness of the liquid shell around the bubble change during the expansion and rarefaction cycle. During the compression half cycle, the bubble contracts and the shell thickness increases, thereby leading to a decrease in the concentration of gases within the shell. This generates a concentration difference between the gas at the interface and bulk. The rate of diffusion of gas in a liquid is proportional to the gradient of the concentration of the dissolved gas. However, the gas concentration gradient lowers as the shell thickness increases, which lowers the mass transfer of the gas coming out of the bubble. When the bubble is in its expanded state, the liquid shell becomes thinner (relative to the size of the bubble) with a relatively higher gas concentration. Since the gas concentration inside the bubble is lower, material diffuses into the bubble from the surrounding liquid shell. Two factors, i.e. gas concentration at the bubble wall and the shell thickness, work together when the bubble is in the expanded state and work against each other when the bubble is in the compressed state, thus resulting in a net bubble growth over time.

Crum [24] noted that both effects have to be considered to theoretically model the rectified diffusion process. The kinetics of the bubble growth and collapse is also

a crucial factor and expected to control the rectified diffusion. Therefore, a mathematical solution for the growth of a gas bubble by rectified diffusion requires equations of bubble motion, diffusion equations and heat conduction equations for both the liquid and bubble [24]. Consideration of these factors makes it complicated. Hsieh and Plesset [36] and Eller and Flynn [37] have taken into account the motion of the bubble wall and a diffusion equation for the concentration of gas dissolved in the liquid alone. The diffusion of gas in the liquid obeys Fick's law of mass transfer.

Eller and Flynn [37] showed that the rate of change of number of moles n of the gas in the bubble with the time is given as

$$\frac{dn}{dt} = 4\pi DR_0 C_0 \left[\left\langle \frac{R}{R_0} \right\rangle + \left(\frac{\langle (R/R_0) \rangle}{\pi Dt} \right)^{\frac{1}{2}} \right] H \tag{11}$$

where H is given by

$$H = \frac{C_i}{C_0} - \left\langle \left(\frac{R}{R_0} \right)^4 \left(\frac{p_{g,m}}{p_\infty} \right) \right\rangle \left\langle \left(\frac{R}{R_0} \right)^4 \right\rangle. \tag{12}$$

C_i is the concentration of dissolved gas in the liquid far from the bubble, $p_{g,m}$ is the instantaneous pressure of the gas in the bubble, C_0 is the saturation concentration of the gas in the liquid, D is the diffusivity of the gas, and $\left\langle \left(\frac{R}{R_0} \right)^4 \left(\frac{p_{g,m}}{p_\infty} \right) \right\rangle$, $\left\langle \left(\frac{R}{R_0} \right)^4 \right\rangle$ and $\left\langle \frac{R}{R_0} \right\rangle$ are the time averages.

Crum later extended Eq. 12 to obtain the rate of change of equilibrium bubble radius as a function of time, which is given as

$$\frac{dR_0}{dt} = \frac{Dd}{R_0} \left[\left\langle \frac{R}{R_0} \right\rangle + R_0 \left(\frac{\langle (R/R_0) \rangle}{\pi Dt} \right)^{1/2} \right] \left(1 + \frac{4\sigma}{3P_\infty R_0} \right)^{-1} \left(\frac{C_i}{C_0} - \left\langle \left(\frac{R}{R_0} \right)^4 \left(\frac{p_{g,m}}{p_\infty} \right) \right\rangle / \left\langle \left(\frac{R}{R_0} \right)^4 \right\rangle \right) \tag{13}$$

where, $d = kTC_0/P_\infty$ (K is the universal gas constant, T is the temperature).

The threshold acoustic pressure growth of a gas bubble is obtained by setting $dR_0/dt = 0$, and results in the equation

$$P_A^2 = \frac{(\rho R_0^2 \omega_0^2)^2 \left[(1 - \omega^2/\omega_0^2)^2 + b^2(\omega^2/\omega_0^2) \right] (1 + 2\sigma/R_0 P_\infty - C_i/C_0)}{(3 + 4K)(C_i/C_0) - \left\{ \left[\frac{3(\eta-1)(3\eta^4)}{4} \right] + (4-3)K \right\} (1 + 2\sigma/R_0 P_\infty)}. \tag{14}$$

Figure 2 represents the rectified diffusion threshold as a function of radius above and below the resonance values calculated using Eq. 14.

Later Fyrrillas and Szeri [38] developed a new mathematical analysis for describing the mass transportation during rectified diffusion. They extended the analysis to incorporate the effect of interfacial resistance to mass transfer caused by surfactants. Crum's experimental data was used to estimate the rectified diffusion growth of the cavitation bubbles. Lee et al. [39] and Leong et al. [18] studied rectified diffusion growth in the presence of various surfactants. They reported that

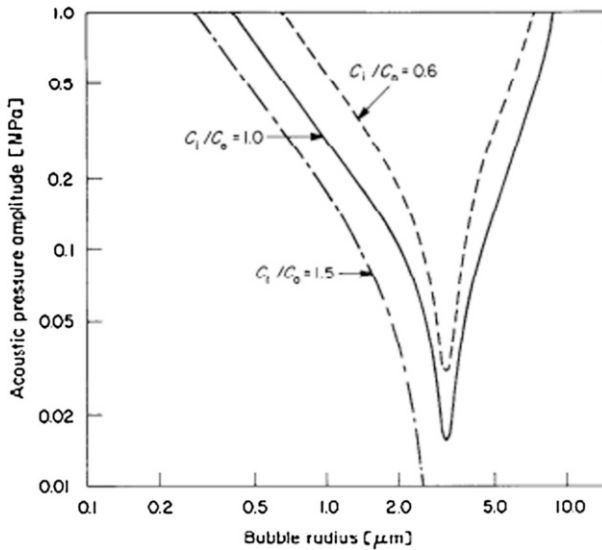


Fig. 2 Rectified diffusion threshold as a function of gas bubble radius at different dissolved gas concentration ratios. The curves can be calculated by Eq. 14, the acoustic frequency used was 1 MHz and the surface tension was 68 dyn/cm; the liquid is assumed to be water [reprinted with permission from Elsevier [24], copyright (1984)]

acoustic streaming, caused as a result of surfactant adsorption, plays a major role in rectified diffusion growth of bubbles in addition to surface activity and the nature of the head group of surfactants [18].

3.4 Bubble Collapse

Rectified diffusion leads to the growth of the bubble to a critical (resonance) size, at which the natural bubble oscillation frequency matches that of the driving ultrasound frequency. A simple relationship between the frequency of ultrasound and the resonance radius of a bubble is given by Eq. 15, which is called Minnaert's equation.

$$F \times R \approx 3 \quad (15)$$

F = frequency in hertz, R = radius of the bubble in metres

Yasui [26] suggests that resonance size is not a single value but consists of a range. While Eq. 15 theoretically predicts the relationship between ultrasound frequency and resonance size of the bubble, experimental data to support this equation was only recently reported. A pulsed ultrasound technique can be used to determine the resonance size range of sonoluminescence (SL) bubbles and sonochemically (SCL) active bubbles [40–43]. Brochie et al. [44] have shown for sonochemically active bubbles that with increasing frequency the mean bubble size becomes smaller, and the distribution becomes narrower (Fig. 3). SL and SCL

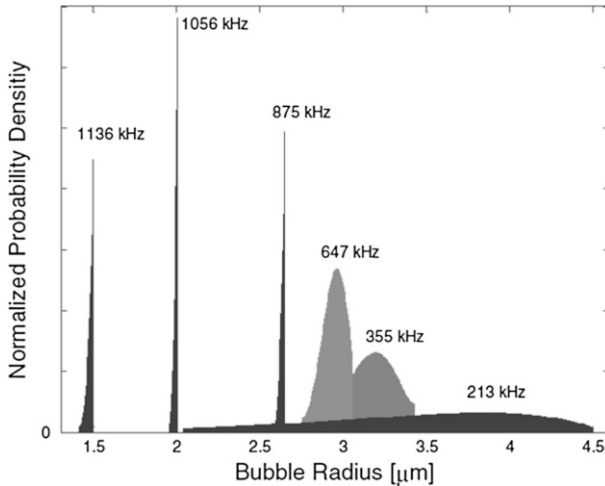


Fig. 3 Bubble size distributions for 213, 355, 647, 875, 1056 and 1136 kHz. For 875, 1056 and 1136 kHz data have been scaled down by a factor of 4. The acoustic power of all frequencies is 1.5 ± 0.4 W [reprinted with permission from American Physical Society [24]; copyright (2009)]

are discussed later in this review. Other experimental techniques used to measure the bubble size are laser light diffraction [45], active cavitation detection [46] and phase-Doppler [47].

Once a critical size is reached, the bubble grows to a maximum in a single acoustic cycle and implodes (collapses). The bubble implosion, from a thermodynamic consideration, is important because a large change in bubble volume occurs. Since the bubble collapse happens in a very short time domain (approx. $1 \mu\text{s}$), the “work done” (PdV) leads to a “near” adiabatic heating of the contents of the bubble, which results in the generation of very high temperatures (>5000 K) and pressures (>1000 atm) within the bubble.

Rayleigh initially developed the fundamental equation dealing with the collapse of gas cavity in 1917 for an isothermal process, which can be easily extended for an adiabatic process. The model was proposed for a bubble of initial radius of R_m and when $\dot{R} = 0$, the cavity would collapse, rebound and oscillate between maximum radius R_{max} and minimum radius R_{min} . $R = R_m$ and $\dot{R} = 0$ at the beginning of the collapse. The pressure of gas inside the bubble is $p_{g,m}$ and temperature is T_m . Assuming that there is no heat flow across the bubble wall, the gas pressure is given by Eq. 16, which follows adiabatic law.

$$p_g = p_{g,m} \left(\frac{R_m}{R} \right)^{3\gamma} \tag{16}$$

As a result of the presence of gases inside the bubble, the decrease in the potential energy will be equal to the sum of kinetic energy of the liquid and amount of work done in compressing the liquid when radius changes from R_m to R . The energy balance is given as

$$-\int_{R_m}^R p_\infty 4\pi R^2 dR = 2\pi R^3 \dot{R}^2 \rho - \int_{R_m}^R p_L 4\pi R^2 dR. \quad (17)$$

The work done can be expressed as

$$-\int_{R_m}^R p_L dV = \frac{1}{\gamma - 1} \frac{4\pi R_m^3}{3} p_{g,m} \left\{ \left(\frac{R_m}{R} \right)^{3\gamma-1} - 1 \right\}. \quad (18)$$

Therefore, Eq. 17 becomes

$$\int_{R_m}^R p_\infty 4\pi R^2 dR = 2\pi R^3 \dot{R}^2 \rho - \frac{1}{\gamma - 1} \frac{4\pi R_m^3}{3} p_{g,m} \left\{ \left(\frac{R_m}{R} \right)^{3\gamma-1} - 1 \right\}. \quad (19)$$

If in Eq. 19, vapour pressure and surface tension are negligible and external pressure is constant, the energy equation described by Noltingk and Neppiras for the collapse becomes

$$\frac{3\rho \dot{R}}{2} = p_\infty \left\{ \left(\frac{R_m}{R} \right)^3 - 1 \right\} - p_{g,m} \frac{1}{1 - \gamma} \left\{ \left(\frac{R_m}{R} \right)^3 - \left(\frac{R_m}{R} \right)^{3\gamma} \right\}. \quad (20)$$

This equation can be solved for calculating R_{\max} and R_{\min} when the velocity \dot{R} of the bubble wall is zero.

$$p_\infty (\gamma - 1) \left\{ \left(\frac{R_m}{R} \right)^3 - 1 \right\} = p_{g,m} \left\{ \left(\frac{R_m}{R} \right)^{3\gamma} - \left(\frac{R_m}{R} \right)^3 \right\} \quad (21)$$

where $R = R_{\max}$ or R_{\min} .

When $R = R_{\max}$ and if $R = R_{\min} \ll R_m$ then Eq. 21 reduces to

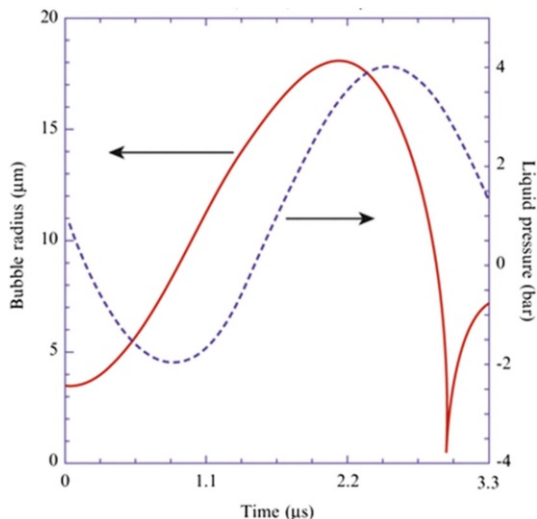
$$p_{g,m} \left(\frac{R_m}{R_{\min}} \right)^{3(\gamma-1)} = p_\infty (\gamma - 1). \quad (22)$$

As PV^γ and $TV^{(\gamma-1)}$ are constant during the reversible adiabatic compression, the maximum pressure P_{\max} and maximum temperature attained during collapse T_{\max} can be obtained from Eq. 22 and are given as

$$P_{\max} = p_{g,m} \left(\frac{R_m}{R_{\min}} \right)^{3\gamma} \approx p_{g,m} \left(\frac{p_\infty (\gamma - 1)}{p_{g,m}} \right)^{\frac{\gamma}{\gamma-1}} \quad (23)$$

$$T_{\max} = \left(\frac{R_m}{R_{\min}} \right)^{3\gamma-1} \approx T_m \left(\frac{p_\infty (\gamma - 1)}{p_{g,m}} \right). \quad (24)$$

Fig. 4 Result of the numerical simulation of the bubble radius as a function of time for one acoustic cycle (3.3 μs) when the frequency and pressure amplitude of an ultrasonic wave are 300 kHz and 3 bar, respectively. The ambient radius of an isolated spherical air bubble is 3.5 μm . The *dotted line* is the acoustic pressure (plus the ambient pressure) as a function of time [reprinted with permission from AIP Publishing LLC [48]; copyright (2007)]



Equation 24 for calculating the T_{\max} tends to overestimate the collapse temperature because it does not take into account the heat leaking from the bubble into the surrounding fluid or the thermal conductivity of the gases or the energy consumed in the decomposition of the vapour/gas within the bubble. Figures 4 and 5 show the results of the numerical simulation of the pulsation of an isolated spherical air bubble in water irradiated with 300 kHz and 3 bar as calculated by Yasui et al. [48] using the bubble dynamics equations. The temperature at the end of the bubble collapse (Rayleigh collapse) increased up to 5100 K (Fig. 5a) whereas pressure reaches 6×10^9 Pa (Fig. 5b).

The results obtained by Merouani et al. are similar (Fig. 6) [49]. The temperature and pressure calculated inside a bubble increase suddenly at the end of the bubble collapse up to 4600 K and 1400 atm (approx. 140 MPa), respectively.

A number of techniques have been developed for the experimental determination of T_{\max} . Mišík et al. [50], using kinetic isotope effect of the sonolysis of $\text{H}_2\text{O}/\text{D}_2\text{O}$ mixtures, found that the cavitation temperatures determined were dependent on the specific spin trap used and are in the range of 1000–4600 K. Mean temperatures in different regions of a “hot spot” were postulated by Suslick et al. [51], using comparative rate thermometry in alkane solutions. They proposed a gas phase zone within the collapsing cavity with an estimated temperature and pressure of 5200 ± 650 K and 500 atm, respectively, and a thin liquid layer immediately surrounding the collapsing cavity with an estimated temperature of 1900 K [51].

Henglein studied the sonolysis of methane using a methyl radical recombination (MRR) method to estimate the bubble core temperature [52]. Sonication of methane leads to the following reactions in the liquid medium:



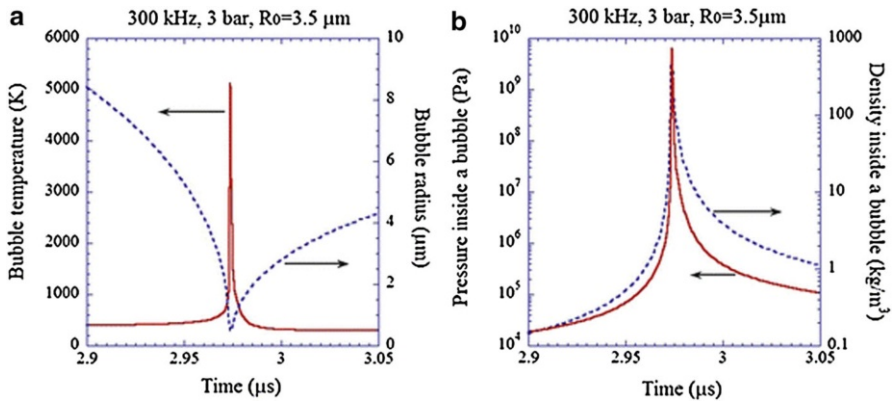


Fig. 5 Results of the numerical simulation. **a** The bubble radius (*dotted line*) and the temperature inside a bubble (*solid line*). **b** The pressure (*solid line*) and the density (*dotted line*) inside a bubble with logarithmic vertical axes. Reprinted with permission from AIP Publishing LLC [48]; copyright (2007)

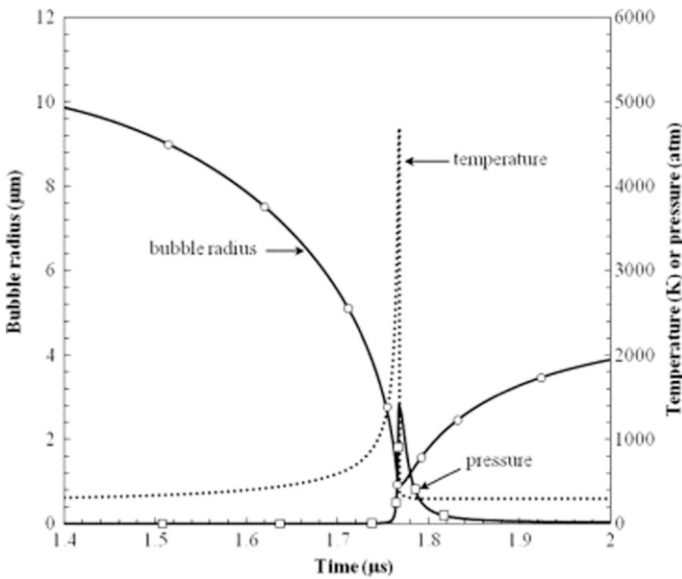
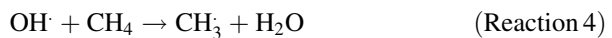


Fig. 6 Bubble radius and temperature and pressure inside a bubble as a function of time during the collapse phase of the bubble. The *horizontal axis* is only for 0.6 μs . A maximum bubble temperature and pressure of about 4600 K and 1400 atm (approx. 140 MPa), respectively, are achieved at the end of the collapse. Reprinted with permission from Elsevier [49]; copyright (2014)



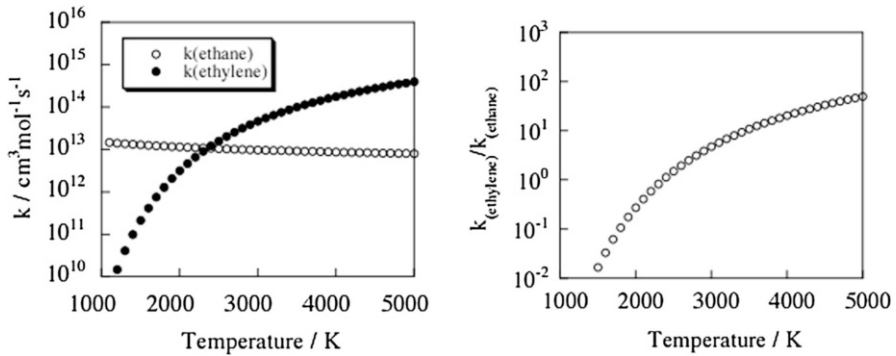
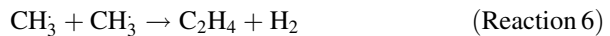


Fig. 7 Rate constants for the formation of ethane and ethylene as a function of temperature (*left*) and temperature dependence of the ratio $k_{\text{ethylene}}/k_{\text{ethane}}$ (*right*) [reprinted with permission from Elsevier [52]; copyright (1990)]



The temperature dependence of the rate constants involved during the formation of ethane and ethylene (Reactions 5, 6) is shown in Fig. 7. The rate constant for the formation of ethylene increases with an increase in temperature, whereas that for the formation of ethane has negligible dependence on the temperature. Figure 7 also shows the dependence of the ratio $k_{\text{ethylene}}/k_{\text{ethane}}$ ($=\text{yield}_{\text{ethylene}}/\text{yield}_{\text{ethane}}$) as a function of temperature which can be used to estimate the bubble temperature. Temperatures in the range of 1930–2720 K have been estimated using this method.

Tauber et al. estimated the temperature in the range of 2300 and 3600 K using the MRR method by studying the sonolysis of *t*-butanol [53]. Grieser and coworkers [54, 55] noted that cavitation bubble temperature is affected by the surface activity of alcohols used to generate methyl radicals.

4 Physical and Chemical Effects Generated by Acoustic Cavitation

The sudden violent collapse of a cavitation bubble gives rise to a number of physical and chemical effects in the liquid such as microstreaming, agitation, turbulence, microjetting, shock waves, generation of radicals, sonoluminescence etc. [19]. Shock waves are produced when the bubble collapses symmetrically [19]. However, when the bubble collapses unsymmetrically (mostly at a boundary), it leads to the formation of a jet in the liquid (Fig. 8) [56] due to the uneven acoustic field around the bubble.

The microjets have velocities of the order of 100 m/s. The effect of shock waves and microstreaming together with the transition from high to low flow velocities away from the bubble surface generates extensive amounts of shear stress [57]. The generation of very high temperatures on bubble collapse leads to local heating. The

Fig. 8 Microjet formation when a bubble collapses near a solid surface; adapted from [57]

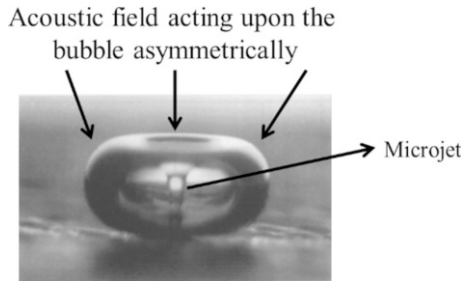
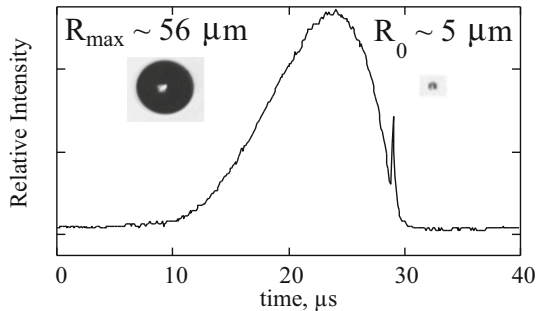


Fig. 9 Relative scattered light intensity, proportional to the size of the bubble, as a function of time. Bubble growth is a relatively slow process compared to the collapse. The *spike* observed near the end of the collapse phase is the SL emission, adapted from [1]



heat generated can raise the temperature of the core of the bubbles to thousands of degrees for a short period (micro- to nanoseconds). Such extreme thermal conditions lead to light emission from the bubbles, referred to as sonoluminescence [58]. It was first observed in 1933 by Marinesco and Trillant [59]. Frenzel and Schultes [7] and Griffing and Sette [60] were the first to detect sonoluminescence using photomultipliers with accurate temporal resolution. Sonoluminescence can be divided into two categories [61]. A large number of cavitation bubbles generates multibubble sonoluminescence (MBSL). Single bubble sonoluminescence (SBSL) refers to emission observed from a stably oscillating single bubble in a liquid. The change in radius of a single bubble within one acoustic cycle is shown in Fig. 9 [1, 61–63]. The relative scattered intensity is proportional to radius of the bubble. A stroboscopic technique was used to record the images of an oscillating bubble as shown in Fig. 9. SL emission could also be observed at the end of bubble collapse.

The intensity of SL depends on the nature of the liquid medium [64, 65], amount of dissolved gases [66, 67], hydrostatic pressure [68], acoustic pressure amplitude [9, 60] and acoustic frequency [60, 69]. Different theoretical models have been proposed for SL. One model is based on inward-moving shock waves during bubble collapse: it is believed that light is emitted from the bubble centre where plasma is created by the shock-wave convergences [70–72]. Another is quasiadiabatic compression model, where a bubble is heated by the quasiadiabatic compression [73, 74]. Both SBSL and MBSL originate from quasiadiabatic compression [62, 75]. However, Yasui proposed that sonoluminescence is originated by the heat generated from the whole bubble rather than a local point [62, 74] and constructed a

theoretical model for SL. Yasui suggested that SL is due to both electron–ion radiative recombination and electron–atom bremsstrahlung [75]. The mechanism behind the SL observed from noble gas bubbles is usually radiative recombination of electrons and ions and electron–atom bremsstrahlung [62].

The intensity of light emission from cavitation bubbles can be increased significantly by adding a small amount of luminol in aqueous alkaline solutions. This emission is referred to as sonochemiluminescence (SCL) [76–79], which arises because of the reaction between OH radicals and luminol. Thus, SCL indicates a chemically active region in a reactor. Ashokkumar et al. [78, 79] showed that two groups of cavitation bubbles exist: one group reaches higher temperatures for SL to occur and the second group causes chemical reactions (Fig. 10). It can be seen in the figure that SL occurs only in a small region closer to the liquid–water interface. It was speculated that these bubbles experience relatively larger acoustic force due to the reflected waves at the air–liquid interface. Note that chemical activity could also be observed throughout the reactor from cavitation bubbles that reach a relatively lower temperature enough to cause chemical reactions (OH radical generation).

The speculation that SL bubbles reach relatively higher temperatures is supported by the experimental data published later. A comparison between the size distributions of SL-emitting and sonochemistry-producing cavitation bubbles was studied by Brotchie et al. [44]. They showed that SL-emitting bubbles are larger than sonochemically active bubbles (Fig. 11) [44].

Another consequence of the extreme conditions of ultrasound is that it leads to a variety of chemical reactions (formation of highly reaction radical species). When an argon-saturated liquid is sonicated, formation of H[•] and OH[•] radicals (Reaction 2) takes place as the majority of the bubble contents is water vapour. H radicals are reducing in nature, whereas OH[•] radicals are oxidising in nature.

A number of techniques have been used to confirm the formation and quantification of radical species. ESR spin traps and chemical dosimeters have been used for the quantification of the radical produced during sonication [50, 80, 81]. Another method is the reaction between terephthalic acid and OH[•]

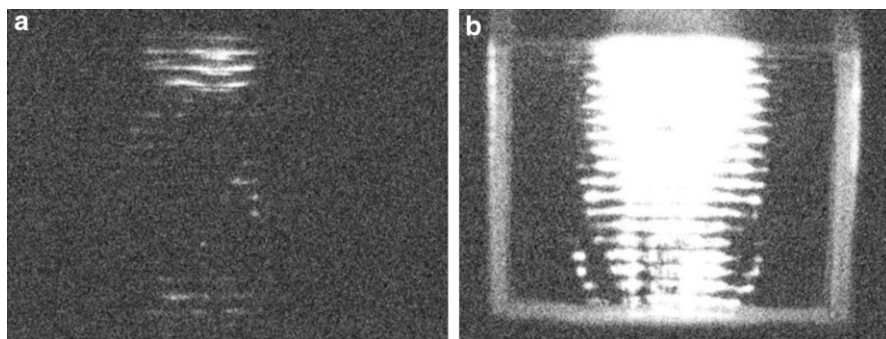


Fig. 10 Sonoluminescence from **a** water and **b** an aqueous solution containing luminol; frequency = 170 kHz; power = 12 W [reprinted with permission from John Wiley and Sons [78]; copyright (2010)]

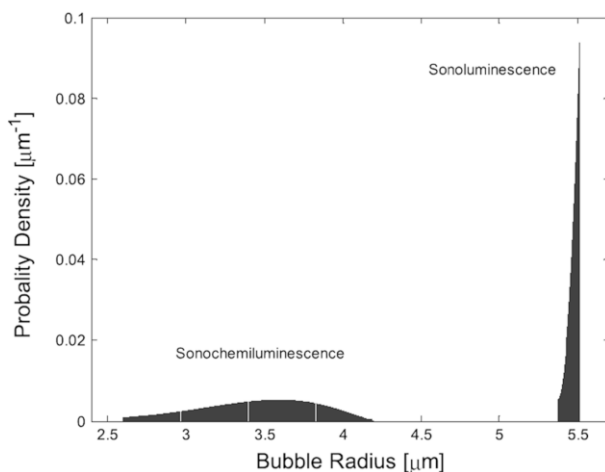
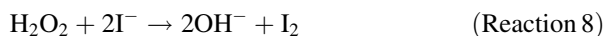


Fig. 11 Bubble radius distribution of SL and SC bubbles. Frequency = 575 kHz [reprinted with permission from American Physical Society [44]; copyright (2009)]

radicals which leads to the formation of fluorescent hydroxyterephthalic acid [81, 82]. The intensity of fluorescence can be utilized to quantify the amount of OH^\cdot radicals generated during cavitation. The Weissler method is a simple approach to quantify OH^\cdot radicals, which is based on the oxidation of iodide ions [1, 83]. In this method, OH^\cdot radicals react to produce hydrogen peroxide (Reaction 7) which can oxidize iodide ions to molecular iodine (Reaction 8). When excess iodide ions are present, molecular iodine is converted into the triiodide complex (Reaction 9). Triiodide has an absorption maximum at 353 nm which can be used to quantify the amount of iodine, and hence the amount of OH^\cdot radicals generated.



5 Single Bubble Sonochemistry

In air-saturated water, a variety of radicals and molecular products such as H_2O_2 , HO_2^\cdot , O^\cdot , O_3 , HNO_2 , HNO_3 , H_2 and OH^\cdot radicals (Reactions 2, 7, 10–15) are generated (Fig. 12c).



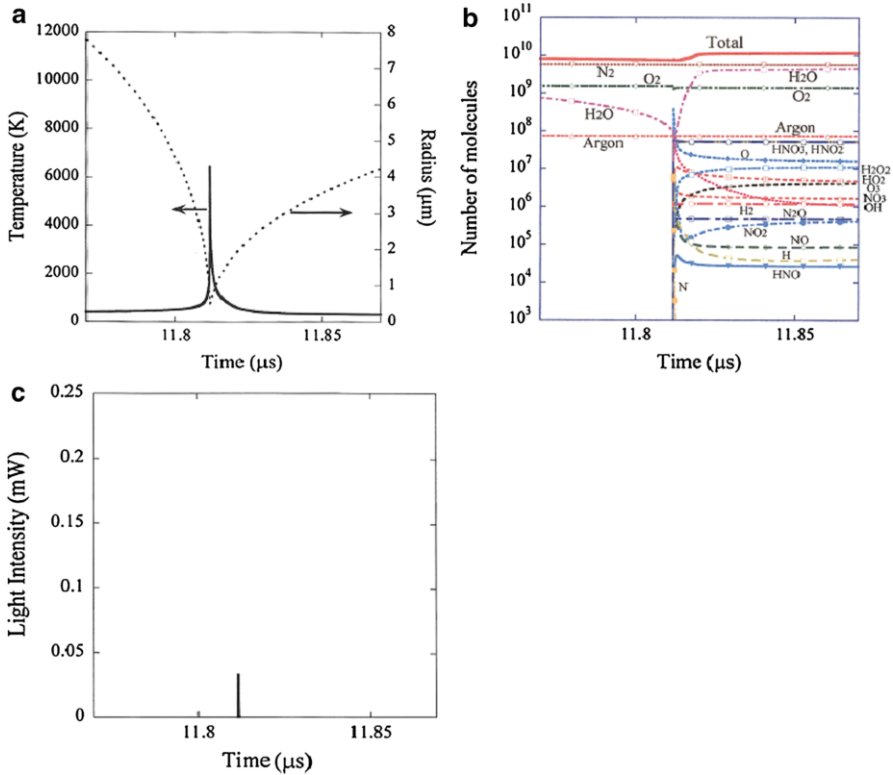


Fig. 12 Calculated results for an initial air bubble at around the end of the bubble collapse only for 0.1 ms. **a** The bubble radius and the temperature inside a bubble. **b** The number of molecules inside a bubble. **c** The intensity of the light emitted from a bubble [reprinted with permission from AIP Publishing LLC [89]; copyright (2005)]



The quantification of primary radicals and molecular products in multibubble systems has been extensively studied [26, 44, 55, 84–88]. Such information for a single bubble system has also been theoretically studied [48, 49, 89]. Only in the past decade, experimental details on the amount of radicals and molecular products generated for single bubble systems became available [62, 76, 90].

Yasui et al. [89] numerically calculated the chemical reaction yield for a single cavitation bubble. In Fig. 12a, the changes in bubble radius and temperature inside a bubble are shown. It is seen that the temperature inside a bubble increases at the end of bubble collapse up to 6500 K, which is much lower than that measured in argon-saturated bubbles because the molar specific heat of nitrogen and oxygen is larger

than that of argon. Figure 12b shows the number of different molecules produced inside a bubble. The bubble content mostly consists of nitrogen, oxygen and water vapour, and the main chemical products obtained in this case are HNO_3 , HNO_2 , O and H_2O_2 . Figure 12c shows the intensity of the light emitted from a bubble. SL is only emitted at the end of the bubble collapse and has a pulse width of about 60 ps. The number of photons emitted is 1.53×10^4 , which is 20 % less than in the case of argon-saturated bubbles as the SL intensity is affected by the amount and nature of the dissolved gases. Yasui observed that these results were consistent with the experimental observation by Matula and Crum [91].

Didenko and Suslick determined the amount of different chemical products experimentally. Table 1 shows the average amounts of chemical products per acoustic cycle. It can be seen from the data shown in Table 2 that the main chemical products are hydrogen molecule, oxygen atom, hydrogen peroxide, hydrogen atom, and nitrous acid. According to Didenko and Suslick [90], the number of OH radicals that diffuse into the liquid after one acoustic cycle is 8.2×10^5 , which is consistent with the calculated result of 6.6×10^5 . The generation of NO_2 and further reaction of NO_2 with H_2O leads to the formation of nitric acid [92]. It is for this reason that sonication of air-saturated water leads to a decrease in solution pH [1]. The number of NO_2^- ions produced in one acoustic cycle was experimentally determined by Didenko and Suslick [90] as 9.9×10^6 (Table 1). A similar number was reported by Koda et al. [93], which was found to be larger than the value numerically calculated by Yasui et al. [89].

In Table 2, the average amount of chemical products diffusing into a liquid per acoustic cycle for the case of *an air bubble* is shown. A single bubble trapped at the pressure antinode of a standing ultrasonic wave initially consists mainly of air, and its main content gradually changes to argon. Yasui et al. [89] showed that the average amount of HNO_2 (4.0×10^7) dissolving in the liquid per oscillation from an initial air bubble is an order of magnitude larger than that from an SBSL bubble in steady state (an argon bubble) and it is even larger than the experimentally reported value of 9.9×10^6 . This suggests that the experimentally reported production rate of NO_2^- ions may be the time-averaged value during the course of the gradual change of the bubble content from air to argon. The amount of OH

Table 1 Amounts of chemical products obtained in a single cavitation bubble at 52 kHz, acoustic pressure 1.5 atm

Conditions	22 °C	3 °C
R_{\max} (μm)	28.9	30.5
Number of OH· radicals per cycle	6.6×10^5	8.2×10^5
Number of photons per cycle	8.1×10^3	7.5×10^4
Number of NO_2^- ions per cycle	3.7×10^6	9.9×10^6
Potential energy at R_{\max} (eV)	6.4×10^{10}	7.5×10^{10}
Energy to form OH radicals (eV per cycle)	3.4×10^6	4.3×10^6
Energy to form NO_2^- ions (eV per cycle)	1.6×10^6	4.2×10^6

Reprinted with permission from Nature Publishing Group [90]. Copyright (2002)

Table 2 Average amount of chemical products that dissolve into the liquid from the interior of an initial air bubble in one acoustic cycle

Chemical species	Number of molecules per acoustic cycle
HNO ₂	4.0 × 10 ⁷
HNO ₃	3.7 × 10 ⁷
O	1.6 × 10 ⁷
H ₂ O ₂	5.1 × 10 ⁶
O ₃	2.7 × 10 ⁶
HO ₂	2.3 × 10 ⁶
NO ₃	1.1 × 10 ⁶
H ₂	1.0 × 10 ⁶
OH	9.9 × 10 ⁵
NO ₂	3.9 × 10 ⁵
N ₂ O	3.0 × 10 ⁵
NO	1.3 × 10 ⁵
H	1.1 × 10 ⁵
HNO	2.8 × 10 ⁴
N	2.7 × 10 ³
N ₂ O ₅	6.8 × 10 ²

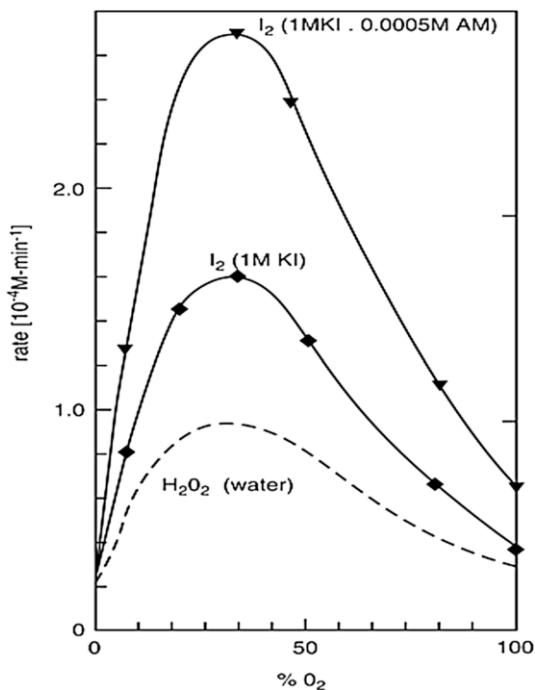
Reprinted with permission from AIP Publishing LLC [89]; Copyright (2005)

radicals dissolving into liquid from an initial air bubble (9.9×10^5) is not so different from that from an SBSL bubble in a steady state (6.6×10^5) and is consistent with the experimentally reported value of 8.2×10^5 .

The main oxidants dissolved in the liquid are oxygen and hydrogen peroxide besides the OH radicals. In a multibubble system, where a standing wave is established, many bubbles behave as single spherical SBSL bubbles [87, 89, 94–97]. The reason behind this is Bjerknes force. The radiation force, which acts on the bubbles, leads to the gathering of bubbles at the regions where the acoustic amplitude is comparable to the cavitation threshold. It has been concluded that even in a multibubble system oxidants produced are not only OH radicals but also oxygen atoms and hydrogen peroxide irrespective of the effect of neighbouring bubbles on the bubble dynamics, shielding of acoustic field, etc. [89, 98]. According to Yasui et al. [89], O atoms may have been created by the dissociation of oxygen molecules and water vapour molecules inside the collapsing bubble as given in Reactions 16–19 (M is an inert third body).



Fig. 13 Experimental results of the rate of production of H_2O_2 in pure water and I_2 in 1 M KI solution or 1 M KI + 0.0005 M ammonium molybdate solution under different mixtures of argon and oxygen dissolved in the solution [reprinted with permission from American Chemical Society [102]; copyright (1985)]



Different methods to estimate the amount of oxygen atoms have been reported in the literature [99–101]. In 1985, Hart and Henglein [102] suggested that O atoms created inside a bubble may oxidize I^- ions in an aqueous KI solution containing a mixture of argon and O_2 . In their experimental results (Fig. 13), the amount of I_2 produced in aqueous KI solution was considerably larger than that of H_2O_2 generated in pure water (in the absence of O_2). On the basis of this observation, they concluded that there should be some oxidant such as O in addition to OH radicals and H_2O_2 . Hart and Henglein [102] as well as Yasui [89] suggested that considerable amounts of O atoms can be produced in an air-filled collapsing bubble. Therefore sonochemistry can serve as an important tool to study the chemical reactions of oxygen atoms in liquids [103].

6 Effect of Ultrasound Frequency on Sonochemistry

The extent of sonochemical reactions (e.g. yield of primary and secondary radicals) and sonoluminescence intensity produced by acoustic cavitation depend on the frequency, power, etc. Various methods have been used to estimate the cavitation yield such as the amount chemical products obtained, T_{max} , SL intensity etc. as a function of acoustic frequency. Yasui et al. [48] estimated the average temperature and rate of production of the main oxidant OH at different frequencies (20, 100, 300 and 1 MHz) as a function acoustic amplitude (Fig. 14). At lower frequencies (20 and 100 kHz), maximum temperature was reached at relatively lower acoustic

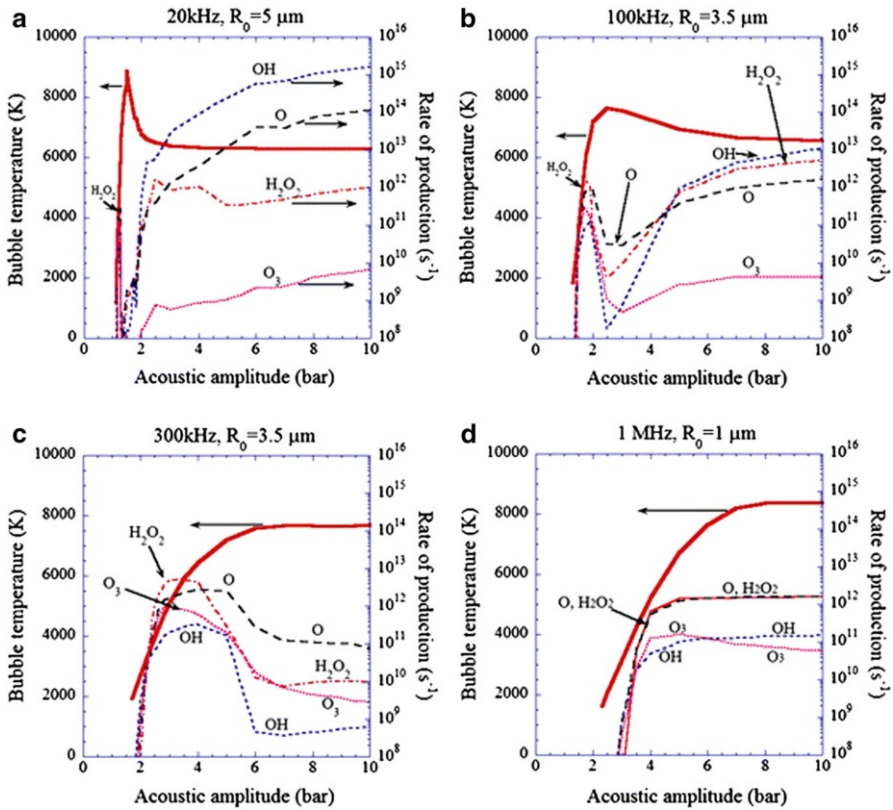


Fig. 14 Numerical simulations of the rate of production of each oxidant inside an isolated air bubble per second estimated by the first bubble collapse as a function of acoustic amplitude with the temperature inside a bubble at the end of the bubble collapse (*thick line*): **a** 20 kHz and $R_0 = 5 \mu\text{m}$. **b** 100 kHz and $R_0 = 3.5 \mu\text{m}$. **c** 300 kHz and $R_0 = 3.5 \mu\text{m}$. **d** 1 MHz and $R_0 = 1 \mu\text{m}$ [reprinted with permission from AIP Publishing LLC [48]; copyright (2007)]

amplitudes. This is due to bubble expansion to a relatively larger volume caused by the longer acoustic period, resulting in an increase in the amount of water vapour inside a bubble [104]. For a vaporous bubble, which is defined as a bubble with a molar fraction of vapour higher than 0.5 at the end of the bubble collapse, the main oxidant created is OH radicals [48].

The amount of H_2O_2 produced at 100 kHz is higher compared to that produced at 20 kHz because a high temperature is maintained at 20 kHz for a longer time as compared to higher frequencies, which can dissociate H_2O_2 into OH radicals. It has been shown that T_{max} is proportional to R_{max} for frequencies greater than 16 kHz [105]. It has been observed for a gaseous bubble that when the molar fraction of vapour is less than 0.5, the collapse temperature ranges from 4000 to 6500 K and the main oxidant is H_2O_2 . However, when the bubble temperature is greater than 6500 K in gaseous bubbles, the main oxidant is O atoms. The consumption of oxidants took place inside an air bubble by an oxidizing nitrogen when the bubble

temperature is higher than 7000 K, and the main chemical products are HNO_2 , NO and HNO_3 [48, 106].

While Yasui's calculations on frequency effect are based on a single bubble system, the overall chemical activity in a multibubble system should be looked at with a different approach. While single bubble dynamics calculations provide an avenue to theoretically calculate bubble temperatures, chemical yield, sonoluminescence intensity, etc., such calculations may not provide insight into multibubble systems. Single bubble calculations tend to provide overestimates of bubble temperatures and chemical yields when multibubble systems are considered. This is due to various factors that include bubble clustering, bubble coalescence, asymmetric collapse of bubbles, inhomogeneous nature of acoustic field, etc.

It is well known that with an increase in frequency, the number of antinodes and hence the number of cavitation bubbles generated increase. Figure 15 shows the schematic and photographic images of the standing waves observed at 37 and 440 kHz, which clearly illustrates the increase in the number of standing waves as well as the bubble population. It has been noted that the radical yield increases with an increase in frequency, reaches a maximum value and decreases with further increase in the frequency. The highest sonochemical yield is obtained between 200 and 800 kHz as demonstrated in various studies [61, 86, 107–109].

Figure 16 presents the OH radical yield as a function of sonication time obtained by sonicating water with different frequencies (20, 358 and 1062 kHz) at a power of 0.90 W/cm^2 [110]. The amount of OH radicals produced was highest at 358 kHz, whereas a decrease was observed when the frequency was increased to 1062 kHz.

This behaviour is due to a relatively lower bubble temperature generated at higher frequency and a lower amount of water vapour that could evaporate into a bubble during the expansion phase [110], as shown in Fig. 17 by theoretical calculations.

Using the resonance radius of the bubbles at each frequency, researchers could calculate the amount of water molecules in a monolayer on the surface of bubbles [110]. As for the evaporation process, a finite time is required. From the time required for evaporation and expansion cycle and the number of molecules at the

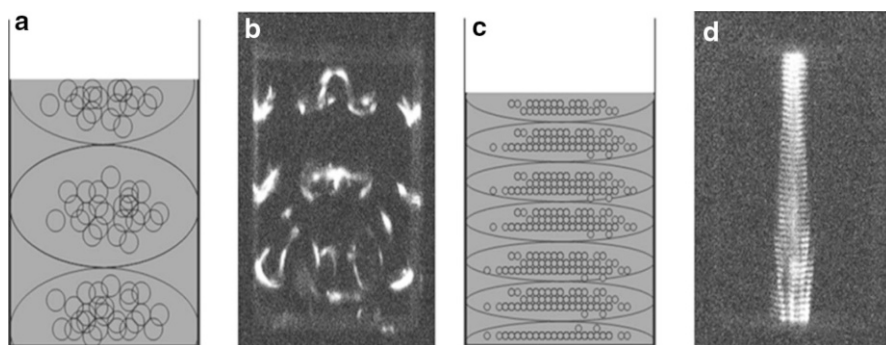


Fig. 15 a, c Schematic representation of the standing wave leading to increase in the number of bubbles with increasing frequency; b, d Images of sonoluminescence profile at 37 and 440 kHz, respectively [reprinted with permission from Springer [19]; copyright (2016)]

Fig. 16 Yield of OH radicals as a function of sonication time for different ultrasonic frequencies (*filled square* 358 kHz, *filled inverted triangle* 1062 kHz, *filled circle* 20 kHz) at 0.90 W cm^{-2} [reprinted with permission from Elsevier [110]; copyright (2008)]

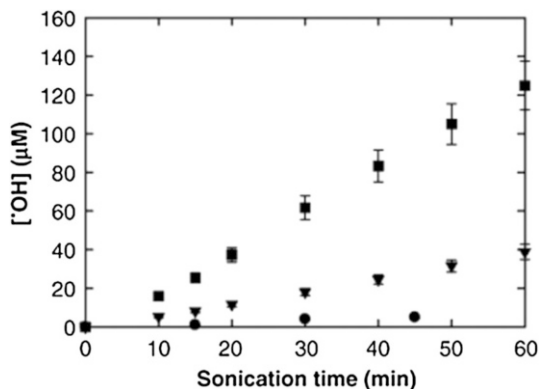
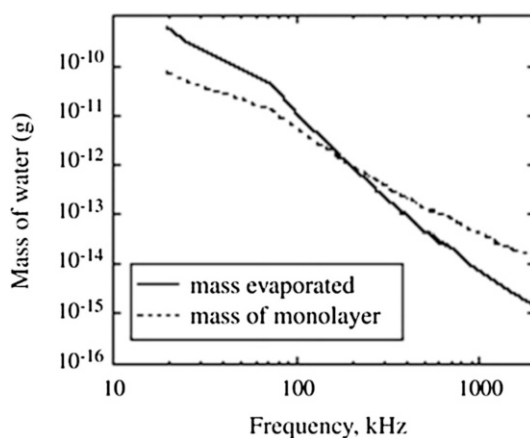


Fig. 17 Mass of water evaporated from a bubble surface during a single expansion phase at various frequencies [reprinted with permission from Springer [19]; copyright (2016)]



interface, it can be seen that the mass that evaporates exceeds the amount present in a monolayer on the bubble surface at lower frequencies. At higher frequencies, the amount that could evaporate is less than a monolayer, which is due to the very short expansion time available during bubble oscillations. Though a surge in bubble population occurs at higher frequency, the size of bubble reduces, thereby leading to a decrease in the bubble temperature and hence the radical yield. Thus, a combination of lower bubble temperature and lower amount of water vapour present inside a collapsing bubble is responsible for the decrease in sonochemical efficiency at very high frequencies.

7 Summary

This article has provided an overview of the basics and fundamentals of sonochemistry including the dynamics of bubble motion, growth and collapse as well as different physical and chemical effects generated after the bubble collapse. The primary and secondary radicals and physical effects such as microjetting,

microstreaming, shear forces and the shock waves generated during acoustic cavitation have been used in material synthesis, sonochemical degradation of pollutants, mass transfer enhancement, electrochemistry, food technology, phase separation, alteration of enzyme activity and removal of deposits and biofilms [111–116], which will be discussed in various articles of this journal.

References

1. Ashokkumar M, Mason TJ (2007) Sonochemistry. In: Kirk-Othmer encyclopedia of chemical technology. Wiley, New York. doi:[10.1002/0471238961.1915141519211912.a01.pub2](https://doi.org/10.1002/0471238961.1915141519211912.a01.pub2)
2. Duckhouse H, Mason T, Phull S, Lorimer J (2004) The effect of sonication on microbial disinfection using hypochlorite. *Ultrason Sonochem* 11:173–176
3. Ferrara K, Pollard R, Borden M (2007) Ultrasound microbubble contrast agents: fundamentals and application to gene and drug delivery. *Biomed Eng* 9:415–447
4. Thornycroft JI, Barnaby SW (1895) Torpedo-boat destroyers. In: Minutes of the proceedings of the Institution of Civil Engineers, Thomas Telford-ICE Virtual Library, pp 51–69
5. Rayleigh L (1917) VIII. On the pressure developed in a liquid during the collapse of a spherical cavity. *Lond Edinb Dubl Phil Mag* 34:94–98
6. Brohult S (1937) Splitting of the haemocyanin molecule by ultrasonic waves. *Nature* 140:805
7. Frenzel H, Schultes HF (1935) Luminescenz im Ultraschallbeschickten Wasser. *Z Phys Chem* 27:421
8. Weiss J (1944) Radiochemistry of aqueous solutions. *Nature* 153:48–50
9. Parke A, Taylor D (1956) The chemical action of ultrasonic waves. *J Chem Phys (Resumed)* 1956:4442–4450. doi:[10.1039/JR9560004442](https://doi.org/10.1039/JR9560004442)
10. Schulz R, Henglein A (1953) Notizen: Über den Nachweis von freien Radikalen, die unter dem Einfluß von Ultraschallwellen gebildet werden, mit Hilfe von Radikal-Kettenpolymerisation und Diphenyl-pikryl-hydrazyl. *Zeitschrift für Naturforschung B* 8:160–161
11. Noltingk BE, Neppiras EA (1950) Cavitation produced by ultrasonics. *Proc Phys Soc Sect B* 63:674
12. Makino K, Mossoba MM, Riesz P (1983) Chemical effects of ultrasound on aqueous solutions. Formation of hydroxyl radicals and hydrogen atoms. *J Phys Chem* 87:1369–1377
13. Henglein A (1987) Sonochemistry: historical developments and modern aspects. *Ultrasonics* 25:6–16
14. Leighton T (2012) *The acoustic bubble*. Academic, San Diego
15. Lorimer JP, Mason TJ (1987) Sonochemistry. Part 1—the physical aspects. *Chem Soc Rev* 16:239–274
16. Mason T, Paniwnyk L, Lorimer J (1996) The uses of ultrasound in food technology. *Ultrason Sonochem* 3:S253–S256
17. Mason TJ, Lorimer JP (1989) An introduction to sonochemistry. *Endeavour* 13:123–128
18. Leong T, Wu S, Kentish S, Ashokkumar M (2010) Growth of bubbles by rectified diffusion in aqueous surfactant solutions. *J Phys Chem C* 114:20141–20145
19. Ashokkumar M (2016) Ultrasonic synthesis of functional materials. In: *SpringerBriefs in green chemistry for sustainability*. Springer, Cham, pp 17–40
20. Crum LA (1982) Nucleation and stabilization of microbubbles in liquids. *Appl Sci Res* 38:101–115
21. Ashokkumar M (2010) Theoretical and experimental sonochemistry involving inorganic systems. Springer, Dordrecht
22. Yount DE (1979) Skins of varying permeability: a stabilization mechanism for gas cavitation nuclei. *J Acoust Soc Am* 65:1429–1439
23. Lim M, Ashokkumar M, Son Y (2014) The effects of liquid height/volume, initial concentration of reactant and acoustic power on sonochemical oxidation. *Ultrason Sonochem* 21:1988–1993
24. Crum L (1984) Acoustic cavitation series: part five rectified diffusion. *Ultrasonics* 22:215–223
25. Yasui K, Tuziuti T, Kanematsu W, Kato K (2016) Dynamic equilibrium model for a bulk nanobubble and a microbubble partly covered with hydrophobic material. *Langmuir*. doi:[10.1021/acs.langmuir.5b04703](https://doi.org/10.1021/acs.langmuir.5b04703)

26. Yasui K (2002) Influence of ultrasonic frequency on multibubble sonoluminescence. *J Acoust Soc Am* 112:1405–1413
27. Bremond N, Arora M, Dammer SM, Lohse D (2006) Interaction of cavitation bubbles on a wall. *Phys Fluids* 18:121505
28. Yount D, Gillary E, Hoffman D (1984) A microscopic investigation of bubble formation nuclei. *J Acoust Soc Am* 76:1511–1521
29. Calvisi ML, Lindau O, Blake JR, Szeri AJ (2007) Shape stability and violent collapse of microbubbles in acoustic traveling waves. *Phys Fluids* 19:047101
30. Wang W, Chen W, Lu M, Wei R (2003) Bubble oscillations driven by aspherical ultrasound in liquid. *J Acoust Soc Am* 114:1898–1904
31. Plesset M (1949) The dynamics of cavitation bubbles. *J Appl Mech* 16:277–282
32. Poritsky P (1952) The collapse or growth of a spherical bubble or cavity in a viscous fluid. In: *Proceedings of the 1st US National Congress in Applied Mathematics*, p 813
33. Tomita Y, Shima A (1986) Mechanisms of impulsive pressure generation and damage pit formation by bubble collapse. *J Fluid Mech* 169:535–564
34. Yasui K (1998) Effect of non-equilibrium evaporation and condensation on bubble dynamics near the sonoluminescence threshold. *Ultrasonics* 36:575–580
35. Grieser F, Ashokkumar M (2006) Sonochemical synthesis of inorganic and organic colloids. In: Caruso F (ed) *Colloids and colloid assemblies: synthesis, modification, organization and utilization of colloid particles*. Wiley-VCH, Weinheim, pp 120–149
36. Hsieh DY, Plesset MS (1961) Theory of rectified diffusion of mass into gas bubbles. *J Acoust Soc Am* 33:206–215
37. Eller A, Flynn H (1965) Rectified diffusion during nonlinear pulsations of cavitation bubbles. *J Acoust Soc Am* 37:493–503
38. Fyrrillas MM, Szeri AJ (1996) Surfactant dynamics and rectified diffusion of microbubbles. *J Fluid Mech* 311:361–378
39. Lee J, Kentish S, Ashokkumar M (2005) Effect of surfactants on the rate of growth of an air bubble by rectified diffusion. *J Phys Chem B* 109:14595–14598
40. Vinodgopal K, He Y, Ashokkumar M, Grieser F (2006) Sonochemically prepared platinum-ruthenium bimetallic nanoparticles. *J Phys Chem B* 110:3849–3852
41. Anandan S, Grieser F, Ashokkumar M (2008) Sonochemical synthesis of Au⁻Ag core⁻ shell bimetallic nanoparticles. *J Phys Chem C* 112:15102–15105
42. Kumar PSS, Manivel A, Anandan S, Zhou M, Grieser F, Ashokkumar M (2010) Sonochemical synthesis and characterization of gold-ruthenium bimetallic nanoparticles. *Colloids Surf A Physicochem Eng Asp* 356:140–144
43. Lee J, Ashokkumar M, Kentish S, Grieser F (2005) Determination of the size distribution of sonoluminescence bubbles in a pulsed acoustic field. *J Am Chem Soc* 127:16810–16811
44. Brothie A, Grieser F, Ashokkumar M (2009) Effect of power and frequency on bubble-size distributions in acoustic cavitation. *Phys Rev Lett* 102:084302
45. Burdin F, Tsochatzidis N, Guiraud P, Wilhelm A, Delmas H (1999) Characterisation of the acoustic cavitation cloud by two laser techniques. *Ultrason Sonochem* 6:43–51
46. Chen W-S, Matula TJ, Crum LA (2002) The disappearance of ultrasound contrast bubbles: observations of bubble dissolution and cavitation nucleation. *Ultrasound Med Biol* 28:793–803
47. Tsochatzidis N, Guiraud P, Wilhelm A, Delmas H (2001) Determination of velocity, size and concentration of ultrasonic cavitation bubbles by the phase-Doppler technique. *Chem Eng Sci* 56:1831–1840
48. Yasui K, Tuziuti T, Kozuka T, Towata A, Iida Y (2007) Relationship between the bubble temperature and main oxidant created inside an air bubble under ultrasound. *J Chem Phys* 127:154502
49. Merouani S, Hamdaoui O, Rezgui Y, Guemini M (2014) Theoretical estimation of the temperature and pressure within collapsing acoustical bubbles. *Ultrason Sonochem* 21:53–59
50. Mišík V, Miyoshi N, Riesz P (1995) EPR spin-trapping study of the sonolysis of H₂O/D₂O mixtures: probing the temperatures of cavitation regions. *J Phys Chem* 99:3605–3611
51. Suslick KS, Hammerton DA, Cline RE (1986) Sonochemical hot spot. *J Am Chem Soc* 108:5641–5642
52. Hart EJ, Fischer C-H, Henglein A (1990) Sonolysis of hydrocarbons in aqueous solution. *Int J Radiat Appl Instrum C Radiat Phys Chem* 36:511–516
53. Tauber A, Mark G, Schuchmann H-P, Sonntag C (1999) Sonolysis of tert-butyl alcohol in aqueous solution. *J Chem Soc Perkin Trans 2*:1129–1136

54. Rae J, Ashokkumar M, Eulaerts O, von Sonntag C, Reisse J, Grieser F (2005) Estimation of ultrasound induced cavitation bubble temperatures in aqueous solutions. *Ultrason Sonochem* 12:325–329
55. Ciawi E, Rae J, Ashokkumar M, Grieser F (2006) Determination of temperatures within acoustically generated bubbles in aqueous solutions at different ultrasound frequencies. *J Phys Chem B* 110:13656–13660
56. Crum L (1994) Sonoluminescence, sonochemistry, and sonophysics. *J Acoust Soc Am* 95:559–562
57. Mason TJ, Peters D (2002) *Practical sonochemistry: power ultrasound uses and applications*. Woodhead, Cambridge
58. Ashokkumar M, Lee J, Kentish S, Grieser F (2007) Bubbles in an acoustic field: an overview. *Ultrason Sonochem* 14:470–475
59. Marinesco M, Trillat JJ (1933) Action des ultrasons sur les plaques photographiques. *CR Acad Sci Paris* 196:858
60. Griffing V, Sette D (1955) Luminescence produced as a result of intense ultrasonic waves. *J Phys Chem* 23:503–509
61. Suslick KS, Crum LA (1998) *Sonochemistry and sonoluminescence*. Wiley-Interscience, New York
62. Yasui K (1999) Mechanism of single-bubble sonoluminescence. *Phys Rev E* 60:1754
63. An Y (2006) Mechanism of single-bubble sonoluminescence. *Phys Rev E* 74:026304
64. Jarman P (1958) Sonoluminescence. *Sci Prog* 46:632–639
65. Crum L, Walton A, Mortimer A, Dyson M, Crawford D, Gaitan D (1987) Free radical production in amniotic fluid and blood plasma by medical ultrasound. *J Ultras Med* 6:643–647
66. Finch R (1963) Sonoluminescence. *Ultrasonics* 1:87–98
67. Weissler A (1953) Sonochemistry: the production of chemical changes with sound waves. *J Acoust Soc Am* 25:651–657
68. Chendke P, Fogler H (1983) Sonoluminescence and sonochemical reactions of aqueous carbon tetrachloride solutions. *J Phys Chem* 87:1362–1369
69. Chambers LA (1937) The emission of visible light from cavitated liquids. *J Chem Phys* 5:290–292
70. Wu C, Roberts PH (1993) Shock-wave propagation in a sonoluminescing gas bubble. *Phys Rev Lett* 70:3424
71. Moss WC, Clarke DB, White JW, Young DA (1994) Hydrodynamic simulations of bubble collapse and picosecond sonoluminescence. *Phys Fluids* 6:2979–2985
72. Kondić L, Gersten JI, Yuan C (1995) Theoretical studies of sonoluminescence radiation: radiative transfer and parametric dependence. *Phys Rev E* 52:4976
73. Kwak H-Y, Na JH (1996) Hydrodynamic solutions for a sonoluminescing gas bubble. *Phys Rev Lett* 77:4454
74. Yasui K (1997) Alternative model of single-bubble sonoluminescence. *Phys Rev E* 56:6750
75. Yasui K (1999) Single-bubble and multibubble sonoluminescence. *Phys Rev Lett* 83:4297
76. S-i Hatanaka, Mitome H, Yasui K, Hayashi S (2002) Single-bubble sonochemiluminescence in aqueous luminol solutions. *J Am Chem Soc* 124:10250–10251
77. Ashokkumar M (2011) The characterization of acoustic cavitation bubbles—an overview. *Ultrason Sonochem* 18:864–872
78. Ashokkumar M, Lee J, Iida Y, Yasui K, Kozuka T, Tuziuti T, Towata A (2010) Spatial distribution of acoustic cavitation bubbles at different ultrasound frequencies. *ChemPhysChem* 11:1680–1684
79. Sunartio D, Yasui K, Tuziuti T, Kozuka T, Iida Y, Ashokkumar M, Grieser F (2007) Correlation between Na^{*} emission and “chemically active” acoustic cavitation bubbles. *ChemPhysChem* 8:2331–2335
80. Mišík V, Riesz P (1996) EPR study of free radicals induced by ultrasound in organic liquids II. Probing the temperatures of cavitation regions. *Ultrason Sonochem* 3:25–37
81. Mišík V, Riesz P (1996) Recent applications of EPR and spin trapping to sonochemical studies of organic liquids and aqueous solutions. *Ultrason Sonochem* 3:S173–S186
82. Mason T, Lorimer J, Bates D, Zhao Y (1994) Dosimetry in sonochemistry: the use of aqueous terephthalate ion as a fluorescence monitor. *Ultrason Sonochem* 1:S91–S95
83. Ashokkumar M, Niblett T, Tantiongco L, Grieser F (2003) Sonochemical degradation of sodium dodecylbenzene sulfonate in aqueous solutions. *Aust J Chem* 56:1045–1049
84. Ashokkumar M, Grieser F (2005) A comparison between multibubble sonoluminescence intensity and the temperature within cavitation bubbles. *J Am Chem Soc* 127:5326–5327
85. S-i Hatanaka, Yasui K, Kozuka T, Tuziuti T, Mitome H (2002) Influence of bubble clustering on multibubble sonoluminescence. *Ultrasonics* 40:655–660

86. Kanthale P, Ashokkumar M, Grieser F (2008) Sonoluminescence, sonochemistry (H_2O_2 yield) and bubble dynamics: frequency and power effects. *Ultrason Sonochem* 15:143–150
87. Yasui K (2001) Temperature in multibubble sonoluminescence. *J Chem Phys* 115:2893–2896
88. Weninger K, Camara C, Putterman S (2000) Observation of bubble dynamics within luminescent cavitation clouds: sonoluminescence at the nano-scale. *Phys Rev E* 63:016310
89. Yasui K, Tuziuti T, Sivakumar M, Iida Y (2005) Theoretical study of single-bubble sonochemistry. *J Chem Phys* 122:224706
90. Didenko YT, Suslick KS (2002) The energy efficiency of formation of photons, radicals and ions during single-bubble cavitation. *Nature* 418(6896):394–397
91. Matula TJ, Crum LA (1998) Evidence for gas exchange in single-bubble sonoluminescence. *Phys Rev Lett* 80:865
92. Kruus P (2000) Sonochemical formation of nitrate and nitrite in water. *Ultrason Sono* 7:109–113
93. Koda S, Tanaka K, Sakamoto H, Matsuoka T, Nomura H (2004) Sonochemical efficiency during single-bubble cavitation in water. *J Phys Chem A* 108:11609–11612
94. Yasui K, Tuziuti T, Iida Y, Mitome H (2003) Theoretical study of the ambient-pressure dependence of sonochemical reactions. *J Chem Phys* 119:346–356
95. Vazquez G, Camara C, Putterman S, Weninger K (2001) Sonoluminescence: nature's smallest blackbody. *Opt Lett* 26:575–577
96. Tuziuti T, Yasui K, Sivakumar M, Iida Y, Miyoshi N (2005) Correlation between acoustic cavitation noise and yield enhancement of sonochemical reaction by particle addition. *J Phys Chem A* 109:4869–4872
97. Matula TJ, Roy RA, Mourad PD, McNamara WB III, Suslick KS (1995) Comparison of multi-bubble and single-bubble sonoluminescence spectra. *Phys Rev Lett* 75:2602
98. Mettin R, Akhatov I, Parlitz U, Ohl C, Lauterborn W (1997) Bjerknes forces between small cavitation bubbles in a strong acoustic field. *Phys Rev E* 56:2924
99. Lucien E, Greer A (2001) Electrophilic oxidant produced in the photodeoxygenation of 1,2-benzodiphenylene sulfoxide. *J Org Chem* 66:4576–4579
100. Brown WG, Hart EJ (1972) The oxygen atom: a primary species in irradiated water. *Radiat Res* 51:249–253
101. Sauer MC Jr, Brown WG, Hart EJ (1984) Oxygen (3P) atom formation by the photolysis of hydrogen peroxide in alkaline aqueous solutions. *J Phys Chem* 88:1398–1400
102. Hart EJ, Henglein A (1985) Free radical and free atom reactions in the sonolysis of aqueous iodide and formate solutions. *J Phys Chem* 89:4342–4347
103. Thomas KB, Greer A (2003) Gauging the significance of atomic oxygen [O(3P)] in sulfoxide photochemistry. A method for hydrocarbon oxidation. *J Org Chem* 68:1886–1891
104. Yasui K (2001) Effect of liquid temperature on sonoluminescence. *Phys Rev E* 64:016310
105. Toegel R, Gompf B, Pecha R, Lohse D (2000) Does water vapor prevent upscaling sonoluminescence? *Phys Rev Lett* 85:3165
106. Yasui K, Tuziuti T, Iida Y (2004) Optimum bubble temperature for the sonochemical production of oxidants. *Ultrasonics* 42:579–584
107. Beckett MA, Hua I (2001) Impact of ultrasonic frequency on aqueous sonoluminescence and sonochemistry. *J Phys Chem A* 105:3796–3802
108. Capocelli M, Joyce E, Lancia A, Mason TJ, Musmarra D, Prisciandaro M (2012) Sonochemical degradation of estradiols: incidence of ultrasonic frequency. *Chem Eng J* 210:9–17
109. Petrier C, Jeunet A, Luche JL, Reverdy G (1992) Unexpected frequency effects on the rate of oxidative processes induced by ultrasound. *J Am Chem Soc* 114:3148–3150
110. Ashokkumar M, Sunartio D, Kentish S, Mawson R, Simons L, Vilku K, Versteeg CK (2008) Modification of food ingredients by ultrasound to improve functionality: a preliminary study on a model system. *Innov Food Sci Emerg* 9:155–160
111. Shanmugam A, Chandrapala J, Ashokkumar M (2012) The effect of ultrasound on the physical and functional properties of skim milk. *Innov Food Sci Emer* 16:251–258
112. Ashokkumar M, Lee J, Zisu B, Bhaskarcharya R, Palmer M, Kentish S (2009) Hot topic: sonication increases the heat stability of whey proteins. *J Dairy Sci* 92:5353–5356
113. Chandrapala J, Zisu B, Palmer M, Kentish S, Ashokkumar M (2011) Effects of ultrasound on the thermal and structural characteristics of proteins in reconstituted whey protein concentrate. *Ultrason Sonochem* 18:951–957
114. Price GJ (1996) Ultrasonically enhanced polymer synthesis. *Ultrason Sonochem* 3:S229–S238

115. Bhangu SK, Ashokkumar M, Lee J (2016) Ultrasound assisted crystallization of paracetamol: crystal size distribution and polymorph control. *Crys Growth Des* 16:1934–1941
116. Mason TJ (2003) Sonochemistry and sonoprocessing: the link, the trends and (probably) the future. *Ultrason Sonochem* 10:175–179

Advances in Green Organic Sonochemistry

Micheline Draye¹  · Nathalie Kardos¹

Received: 5 June 2016 / Accepted: 19 September 2016 / Published online: 4 October 2016
© Springer International Publishing Switzerland 2016

Abstract Over the past 15 years, sustainable chemistry has emerged as a new paradigm in the development of chemistry. In the field of organic synthesis, green chemistry rhymes with relevant choice of starting materials, atom economy, methodologies that minimize the number of chemical steps, appropriate use of benign solvents and reagents, efficient strategies for product isolation and purification and energy minimization. In that context, unconventional methods, and especially ultrasound, can be a fine addition towards achieving these green requirements. Undoubtedly, sonochemistry is considered as being one of the most promising green chemical methods (Cravotto et al. *Catal Commun* 63: 2–9, 2015). This review is devoted to the most striking results obtained in green organic sonochemistry between 2006 and 2016. Furthermore, among catalytic transformations, oxidation reactions are the most polluting reactions in the chemical industry; thus, we have focused a part of our review on the very promising catalytic activity of ultrasound for oxidative purposes.

Keywords Ultrasound · Sonochemistry · Green chemistry · Sustainable chemistry · Oxidation · Catalysis · Enzymatic catalysis

This article is part of the Topical Collection “Sonochemistry: From basic principles to innovative applications”; edited by Juan Carlos Colmenares Q., Gregory Chatel.

✉ Micheline Draye
micheline.draye@univ-savoie.fr

¹ Laboratoire de Chimie Moléculaire et Environnement, Université Savoie Mont Blanc, Campus Scientifique Savoie Technolac, 79376 Le Bourget du Lac Cedex, France

1 Introduction: General Interest in Ultrasound

At the turn of the twenty-first century, the chemical industry was one of the largest manufacturing industries in the world [2]. At the same time, it is one of the most polluting. It is from an awareness, at a global level, of the impact of human activities on the environment that the field of sustainability neologism was born. A key objective in current chemistry is thus to accommodate conventional procedures by making them both economically and environmentally acceptable. This is made possible through the design of solvent-free methodologies or by using fewer toxic solvents, via the development of efficient and benign catalytic system, and/or via the reduction of energy consumption using more energy-efficient activation techniques. In this context, ultrasound is known to enhance the reactivity and kinetics of some processes through a physical phenomenon called acoustic cavitation, which is the formation, growth and collapse of micrometer-sized bubbles when a pressure wave of sufficient intensity propagates through an elastic liquid [3]. By imploding, these bubbles create locally extreme temperatures and pressures that lead to high-energy radical reactions but also generate some interesting physical effects [4]. In addition, ultrasound is associated with energy savings [5], avoids the use of catalysts [6] or solvents [7], and leads to cleaner products with few or no by-products [5].

2 Use of Ultrasound in Green Solvents

The use of organic solvents in chemical laboratories, and more generally in the chemical industry, is considered an essential issue regarding the health and safety of workers and protection of the environment. Solvents represent at least half of the material used in a chemical process to produce a drug substance, defining them as having the largest impact on environmental performance, and affecting cost, safety and human health [8]. Indeed, the chemical industry uses large volumes of solvents, especially in the production of pharmaceuticals, biopharmaceuticals and agrochemicals [9]. Thus, governments, industries and research institutions are currently seeking for sustainable solutions aimed at promoting the use of “greener” solvents [10], solvent-free reactions [11] or alternative solutions [12–14] that would make processes safer for human health and the environment.

A way to reduce the environmental impact of the large-scale use of organic solvents is to use solvents with negligible vapor pressure such as ionic liquids (ILs), to use benign solvents and especially water, or to not use solvents at all [15]. The use of ILs as media for organic synthesis in combination with ultrasound will not be addressed in this review; it is one of the topics of the review by Chatel and coworkers in this issue.

2.1 Water

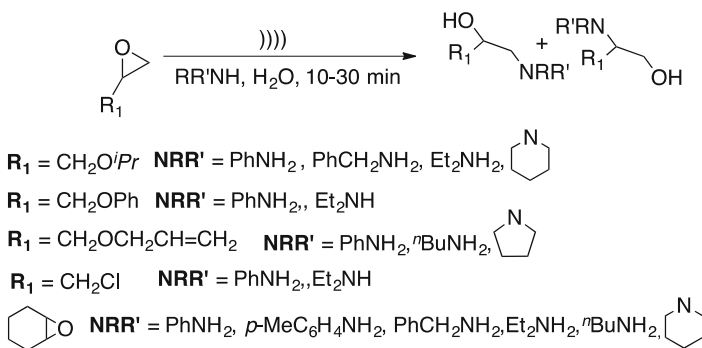
As stated by Sheldon in 1996 ‘if a solvent (diluent) is needed it should preferably be water’ [16]. The first “historical” report in the area of sonochemistry in water

appeared in 1927, with the seminal publication by Richards and Loomis [17] describing the acceleration of chemical reaction using ultrasonic irradiation. Since then, a substantial number of works has been published concerning sonochemical effects when organic reactions are performed in water.

Water is an economically and environmentally attractive solvent because it is cheap, abundant, readily available, non-toxic and non-flammable. Many organic compounds present a low solubility in water; however, the unique structure and physicochemical properties of water can greatly influence the course of reaction, and water has been shown to enhance the reactivity and selectivity of some organic reactions [18]. In addition, water is considered as the ideal solvent in sonochemistry because it favors cavitation, which is optimum between 318 K and 343 K [19].

A large number of publications have dealt with ultrasound-assisted synthesis in water. Nevertheless, we chose to focus on examples where ultrasound allows dispensing with the use of catalysts and additives.

In that context, Abaee and coworkers [20] described the ultrasound-promoted synthesis of β -aminoalcohols through aminolysis of epoxides in aqueous medium free from additives or pH adjustment. These compounds are usually synthesized by direct treatment of epoxides with large amount of amines at high temperature, precluding the use of sensitive groups on the substrate, and aqueous procedures commonly require additives or pH adjustment to proceed. Ultrasound-promoted reactions were performed using an ultrasonic-homogenizer at frequency of 24 kHz and a maximum output power of 400 W, without any additives (Scheme 1). The only compound formed was β -aminoalcohol, indicating that nucleophilic attack occurs regioselectively at the less hindered side of the epoxide. Of note, no change in pH value was observed after sonication. Interestingly, control experiments allowed possible simultaneous thermal activation to be excluded. In addition, the presence of water was shown to be crucial because it probably activates the epoxide through hydrogen bonding. The experimental conditions were extended to the reaction of various epoxides with different aliphatic and aromatic amines yielding to corresponding β -aminoalcohols in 10–30 min at 80–97 %. The more sterically hindered cyclohexene oxide led to the sole *trans* products in the same times and with the same yields. The unsymmetrically substituted epoxide styrene oxide gave

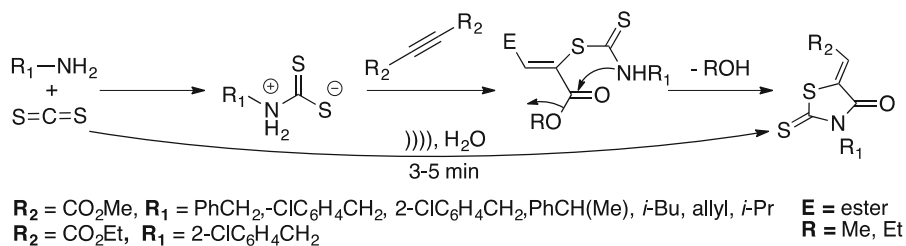


Scheme 1 Ultrasound-promoted synthesis of β -aminoalcohols in aqueous media (adapted from [20])

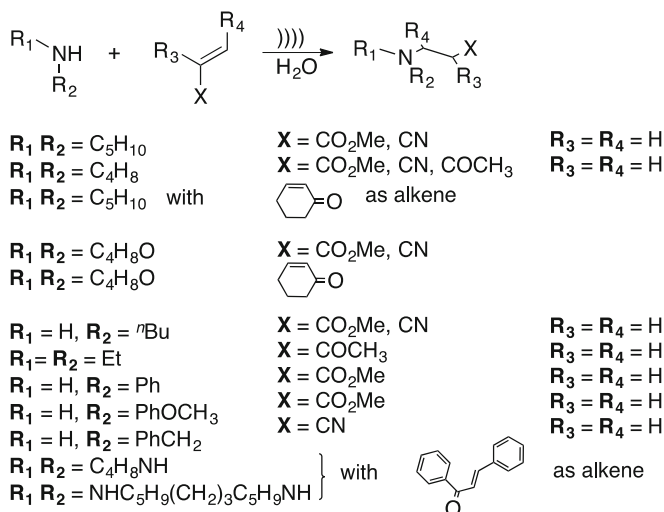
rise to the formation of two regioisomers resulting from the attack at the less hindered side of the epoxide with aliphatic amines, and at the α carbon of the epoxide with aromatic amines.

When aniline is used in competition with piperidine, the exclusive formation of piperidine-substituted products indicated a very high chemoselectivity. In the same way, Rhodanines can be synthesized in good yields and short time in catalyst-free conditions, using unusual experimental conditions. As an example, Rostmania and coworkers [21] proposed a swift and efficient catalyst-free one-pot procedure for the synthesis of Rhodanine derivatives using ultrasonic irradiation in water as the reaction medium (Scheme 2). Dimethyl acetylene-dicarboxylate, carbone disulfide and benzylamine were chosen as the model system and were reacted under irradiation of an ultrasonic probe at a frequency of 20 kHz and a maximum output power of 600 W. Surprisingly, under those conditions, with water as solvent, 94 % of Rhodanines were obtained in 3 min of reaction, whereas 1 h was required in silent conditions. Less than 10 % of product was obtained in silent conditions, regardless of the solvent used. The method has been applied to various substrates with success, leading to 86–94 % of Rhodanine derivatives in 5–3 min, probably through the mechanism postulated by the authors (Scheme 2).

Banik and coworkers [22] also described a catalyst-free procedure for the ultrasound-assisted synthesis of nitrogen heterocycles and derivatives in water (Scheme 3). Interestingly, high yields were obtained in water, in organic solvents, and also in solvent-free conditions; however, the reaction proceeded much faster in water. In addition, six- and three-fold rate accelerations were observed when reactions were conducted under ultrasound and solvent-free conditions rather than in water at room temperature. Several amines and unsaturated ketones, nitriles and esters were tested under the optimal conditions, leading to spectacular results: all ultrasonically assisted reactions in water were very fast without need of a catalyst, leading to excellent yields of 86–98 % with high regio- and chemo-selectivities and without side product formation. The increase in the reaction rate in the presence of water could be explained through hydrogen bond formation with the carbonyl group, increasing the electrophilic character of the α -carbon of the unsaturated compounds, which increases the nucleophilic attack by the amine. Moreover, hydrogen bond formation between the hydrogen of the amine and the oxygen of the water increases the nucleophilic power of the nitrogen atom of the amine. In



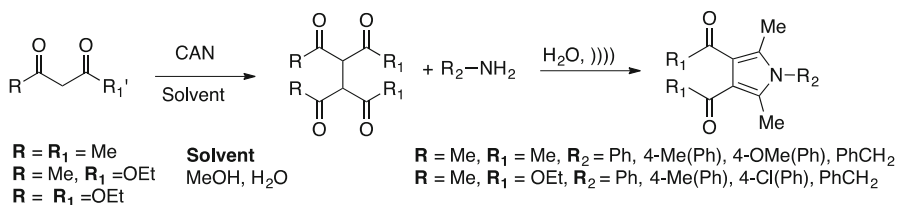
Scheme 2 Catalyst-free synthesis of Rhodanines in water under ultrasonic irradiation (adapted from [21])



Scheme 3 Catalyst-free ultrasound assisted synthesis in water of nitrogen heterocycles and derivatives through the aza-Michael reaction

addition, under ultrasonic irradiation, water acts as a pseudo-organic solvent at the high temperature of the implosion of the cavitation bubbles. After completion of the reaction, the mixture is cooled; this decrease in temperature leads to a decrease in the solubility of the organic products, facilitating their isolation.

Similarly, Almeida [23] described a two-step protocol for the catalyst-free synthesis of penta-substituted pyrroles in water (Scheme 4). In this protocol, the first step was the dimerization of the 1,3-dicarbonyl derivatives using ceric ammonium nitrate (CAN) as oxidant, to produce tetracarbonyl derivatives. The reaction was carried out in methanol under silent conditions, and in water under silent and ultrasonic conditions in a cleaning bath. Interestingly, 62–87 % of product was obtained after 2–5 min of ultrasonic irradiation in water, whereas 1 h was necessary to yield 45–56 % under silent conditions in water, and 61–80 % in methanol. The resulting compounds are then reacted with amines in water and without catalyst under ultrasonic irradiation to give the corresponding penta-substituted pyrroles in 37–70 % yield. Reactions performed with amines that bear electron-donating groups proceed faster, because of the increase in nucleophilicity of the amine. It is



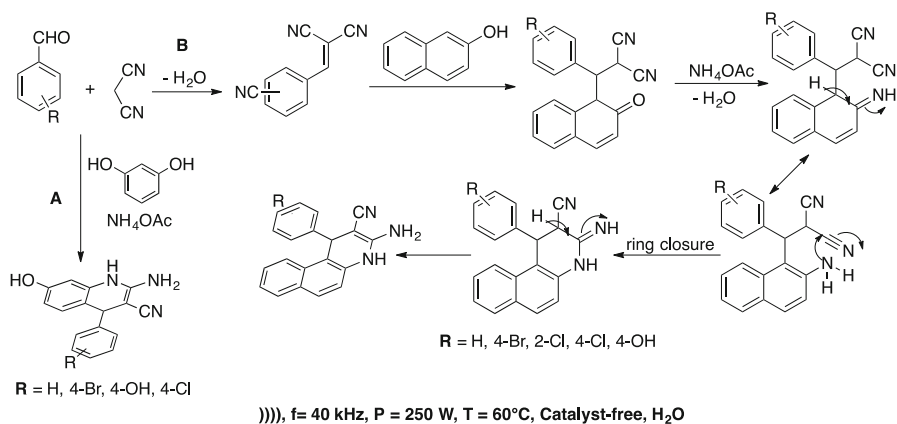
Scheme 4 Catalyst-free two step synthesis in water of penta-substituted pyrroles under ultrasonic irradiation (adapted from [23])

noteworthy that this efficient, mild and eco-friendly procedure had never been published in the literature before this paper.

In 2014, Jonnalagadda and coworkers [24] described an ultrasonic-mediated catalyst-free multicomponent protocol for the synthesis of substituted quinolones in aqueous medium. The synthesis of these compounds usually requires harsh reaction conditions and tedious work-up procedures. In this latter paper, the authors turned their attention to multicomponent (MCR) reactions that already present interesting features, such as high bond forming, convergence, operational simplicity and reduction in waste generation. In order to improve the sustainability of the reaction, they studied the possibility of designing catalyst-free ultrasonic MRC using water as the sole solvent. They first explored the reaction of benzaldehyde with 2-naphthol/resorcinol and ammonium acetate as a model (Scheme 5A). In silent conditions, and at room temperature, the reaction failed and the materials remained unreacted. When the mixture in ethanol was heated up to 60 °C, the reaction was completed in 5 h, affording 55 % yield in dihydroquinoline. When the same mixture in ethanol was irradiated using an ultrasound cleaner at a frequency of 40 kHz and a nominal power of 250 W, the reaction was completed in 3 h, affording a good 75 % yield. With the aim of further improving the green character of the reaction, the reaction was ultrasonically activated, in aqueous medium at 60 °C; 96 % of the desired product were obtained in a short time, without any by-product.

In order to broaden the scope of the reaction, various aromatic aldehydes were subjected to these optimized experimental conditions. Excellent yields of 90–97 % were obtained in 1.0–1.5 h. A mechanism occurring via a tandem system was then proposed to explain the formation of the dihydroquinoline (Scheme 5B).

Recently, Ramazani, Rouhani and Joo [25] reported for the first time a novel and swift, catalyst-free one-pot synthesis of highly substituted propanamide derivatives in water from a three-component reaction. As a model reaction, an equimolar concentration of cyclohexyl isocyanide, 4-methylcinnamic acid and 2-oxopropyl benzoate in water were irradiated with an ultrasonic probe (frequency = 20 kHz,



Scheme 5 Four components reaction for the synthesis of dihydroquinolines and its probable mechanism (adapted from [24])

nominal power = 250 W). Various parameters, such as the time of reaction, the ultrasonic power and the solvent, were then studied. A maximum yield of 92 % was obtained when the three components were irradiated for 40 min in water at a frequency of 20 kHz and a power of 100 W. To identify the role of ultrasound, the reaction was extended to several substituted carboxylic acids, isocyanides and 2-oxopropyl benzoate under ultrasonic or silent conditions. In all cases, the reactions carried out under ultrasonic irradiation led to higher yields in shorter time. The authors explained the acceleration of the reaction by the action of the physical effects of ultrasound, which increase mass transfer. However, they believe that the acceleration of the reaction could be ascribed to the chemical effects of ultrasound, which allow faster production of the conjugate base of the carboxylic acid. Whatever the carboxylic acid and isocyanide derivatives, excellent yields (87–95 %) are obtained in a short time of 40 min, without formation of undesirable by-products. Finally, the authors gave a mechanistic explanation of the reaction, which starts with the nucleophilic addition of isocyanide to 2-oxopropyl benzoate, assisted by the protonation of benzoate by carboxylic acid, which leads to a nitrilium intermediate. The intermediate is then attacked by the conjugate base of the carboxylic acid to form an adduct that undergoes a Mumm rearrangement, to give sterically congested propanamide derivatives.

Finally, the authors developed an easy, efficient and environmentally friendly catalyst-free one-pot and three-component procedure for the synthesis of propanamide derivatives in water under ultrasonic irradiation.

2.2 Ultrasound-Assisted Reactions in Glycerol

The use of green solvents from renewable resources has been the subject of huge interest in recent years. Among such solvents, glycerol, which is a main co-product of biodiesel and oleochemical production, can be considered a twenty-first century commodity [26]. In addition, glycerol allows excellent cavitation, that makes its use as a solvent for some reactions performed under ultrasonic irradiation very interesting [26].

In this context, Cravotto and coworkers proposed for the first time in 2011, ultrasound-assisted synthetic protocols using glycerol as solvent [27]. They first carried out the catalytic transfer hydrogenation of benzaldehyde into benzylic alcohol in glycerol as solvent and hydrogen donor, catalyzed by Ru (*p*-cumene) Cl₂ dimer. They experimented with this dual usage of glycerol under microwave, ultrasonic (ultrasonic horn, *P* = 30 W), and combined microwave/ultrasonic irradiation. The crucial role of ultrasound was evidenced in the transfer hydrogenation of benzaldehyde, for which the mixture was pre-sonicated (cup-horn, *f* = 10 kHz, *P* = 100 W) and then heated up with a bath of oil. Indeed, under those conditions the duration of the reaction was decreased by factor of two compared to the same reaction without pre-sonication; however, the yields were identical. Neither microwave irradiation nor combined ultrasound/microwave irradiations could compete with ultrasonic irradiation, which led to 100 % yield after 3 h.

The authors then studied a series of metal-catalyzed C–C couplings in glycerol, and compared the contribution of the different methods of activation. The coupling between 4-iodoanisole and phenylboronic acid in glycerol, using ligand-free palladium salts and palladium on charcoal, was used as a model reaction. Ultrasonic/oil bath, microwave and simultaneous ultrasound/microwave irradiation greatly improved the rate of the reaction. The optimal yields obtained under ultrasonic/oil bath and ultrasonic/microwave irradiation were ascribed to both heat input, and improvement of mass transfer.

The authors then used palladium-loaded cross-linked chitosan in place of ligand-free palladium salts and glycerol as solvent. Under those experimental conditions, ultrasonic, microwave/high pressure and ultrasonic/microwave irradiations markedly increased the reaction yield.

Finally, the authors experimented the Barbier reaction by using benzaldehyde as substrate; they compared the usual solvent system THF/NH₄Cl under stirring to the glycerol/NH₄Cl system under ultrasonic irradiation. Ultrasound improved the yield, and the kinetics of the reaction were increased by a factor 1.5. Nevertheless, contribution of the cleaning bath on the reaction rate was negligible, whereas the ultrasonic horn yielded 80 % of alcohol in 15 min and 100 % in 1 h, without formation of by-product.

In conclusion, glycerol is a very attractive bio-sourced and non-volatile solvent for many organic reactions. In addition, its smart combination with ultrasonic irradiation solves its problems of solubility and high viscosity by an enhancement of heat and of mass transfer in the organic reactions.

2.3 Solventless Synthesis

In the paper previously cited and devoted to the selective catalytic synthesis of fine chemicals, Sheldon said that the best solvent is no solvent [16]. Given the multiple roles of solvents in chemical processes, this is far from a dogma. For instance, solvents dissolve reactants, bring them together to facilitate the reaction, and affect chemical reactivity. Nonetheless, a couple of articles have reported “solvent-free” synthesis under ultrasonic activation.

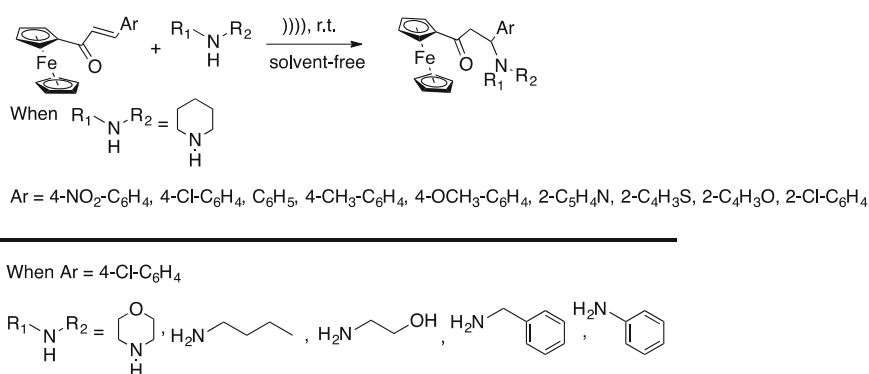
2.3.1 Synthesis of β -Aminocarbonyls

In this context, β -amino carbonyls are versatile intermediates that are used for the synthesis of a large number of organic compounds, such as amino alcohols, peptides and lactams, and as precursors to optically active amino acids [28]. The Mannich reaction provides one of the most basic and useful methods for their synthesis, while presenting serious disadvantages in its classical version. Indeed, due to the drastic reaction conditions and the long reaction times used, unwanted side reactions often take place [29]. Alternatively, the acid- or base-induced Michael additions of α , β -unsaturated carbonyls with amines have been used successfully. However, drawbacks, including use of expensive reagents or organic solvents, or an excess of catalyst and high temperature, still exist [30].

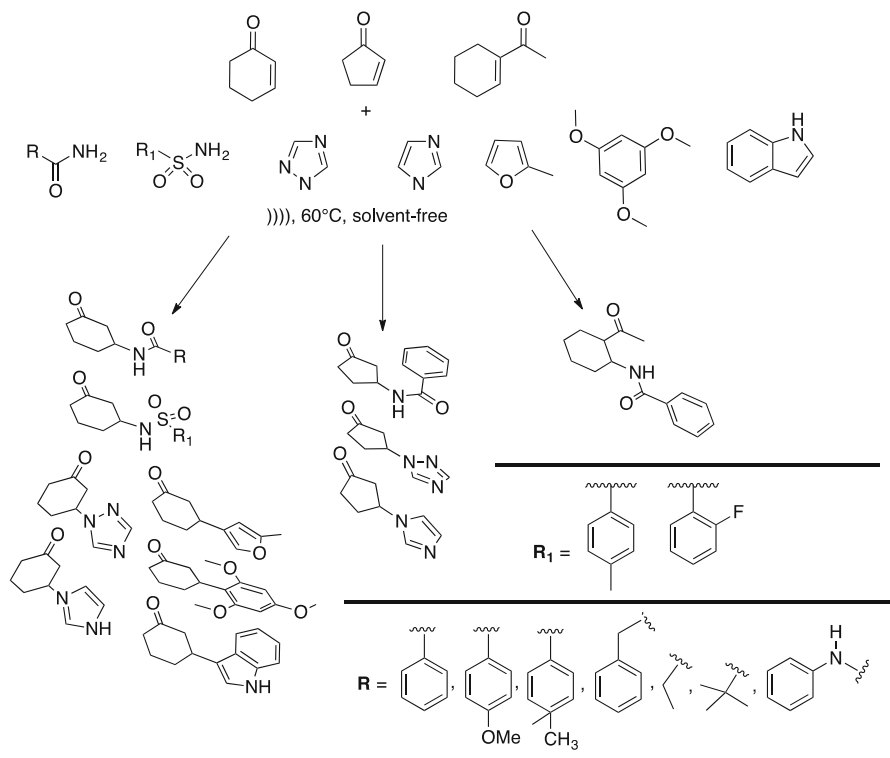
In 2005, Ji and coworkers [31] proposed an ultrasound-assisted Michael addition of amines to ferrocenylenones under solvent- and catalyst free conditions and at room temperature (Scheme 6). By using an ultrasonic cleaner at a frequency of 40 kHz and a power of 250 W, the addition products were obtained almost quantitatively in 0.5–2 h, except when the Michael acceptor was sterically hindered. Secondary amines were shown to add better than primary amines; and when primary amines such as *n*-butylamine, ethanolamine, or benzylamine were reacted with ferrocenylenones, highly chemoselectivity was observed and only mono-addition products were obtained. In addition, the reaction was extended successfully to 3-ferrocenyl chalcones, chalcones, ethylacrylates and acrylonitriles. In contrast to the existing method, this simple methodology was very efficient, high yielding and environmentally friendly.

Some years later, Zhao and coworkers [32] developed a new, solvent-free, method for the Michael addition of nitrogen- and carbon-containing nucleophiles to cyclic enones under ultrasonic irradiation. As model reaction, they used a mixture of cyclohexenone and benzamide that was irradiated at a frequency of 20 kHz and a power of 675 W (pulse-on time, 1.2 s, pulse-off time; 1.5 s) and thermostated at 60 °C. These ultrasound-assisted solvent-free conditions led to an increase in the rate of the reaction by a factor of 4 compared to when acetonitrile was used as solvent, whereas the yield increased from 73 % to 96 % with a slight increase of cyclohexenone (1.2–2 eq.); it was almost quantitative (99 %) when the amount of para-toluenesulfonic acid catalyst was decreased from 10 % to 1 %. But, under those optimal conditions, a decrease in temperature from 60 °C to 25 °C resulted in a decrease in yield from 99 % to 48 %, probably due to the increased viscosity of the medium. The authors then studied the generalization of the method to various Michael acceptors with three N-centered nucleophiles including benzamide, 1-phenylurea, and *p*-toluenesulfonamide (Scheme 7).

Michael addition of nitrogen-containing heterocycles such as 1,2,4-triazole and imidazole to cyclohex-2-enone and cyclopent-2-enone led to almost quantitative yields, whereas the reaction of benzamide or 4-benzensulfonamide with cyclopent-



Scheme 6 Ultrasound-assisted Michael addition of amines to ferrocenylenones under solvent- and catalyst-free conditions and at room temperature (adapted from [31])



Scheme 7 Michael-type addition of various Michael acceptors with three weak N-centered and carbon containing nucleophiles under optimized conditions (adapted from [32])

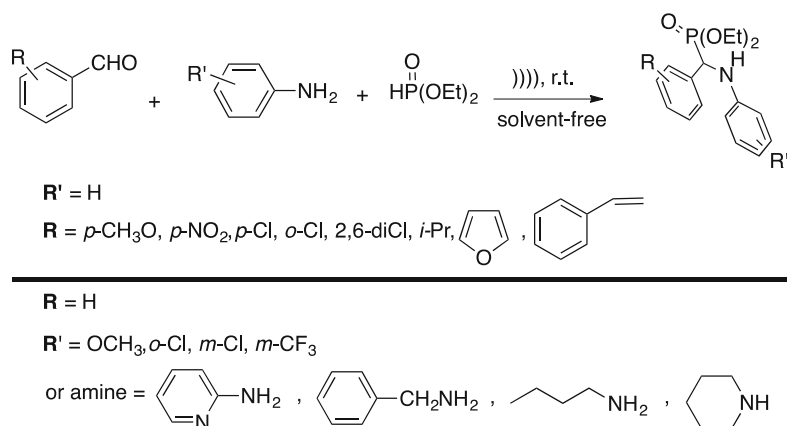
2-enone yielded 78 % addition products. When cyclohex-2-enone was reacted with aliphatic amides or aromatic amides bearing electron-withdrawing substituents on the aromatic ring, the yield in addition product was decreased to 60–55 %. Furthermore, it was necessary, in some cases, to increase the amount of catalyst or to double the duration of irradiation. When an acyclic enone such as 1-acetyl-1-cyclohexene was reacted with benzamide, a complex mixture was obtained whatever the amount of catalyst used. These optimized experimental conditions were used for Friedel-Crafts alkylation of electron-rich (hetero)arenes such as indoles, furans and 1,3,5-triethoxybenzenes to enones. The resulting yields were good to excellent, in 30 min of ultrasonic irradiation by adjusting the catalyst amount at 1 mol% or 10 mol%. In this work, the authors developed a solvent-free efficient, convenient and environmentally friendly protocol for the Michael type addition of nitrogen- and carbon-containing nucleophiles to cyclic enones under ultrasonic irradiation.

2.3.2 Synthesis of α -Aminophosphonates

α -Amino phosphonates are phosphorous analogs of α -amino acids, and transition state mimics of peptide hydrolysis. They have a wide range of biological and pharmacological activities, such as being peptide mimics, haptens of catalytic antibodies, enzyme inhibitors, anti-cancer agents, anti-viral agents, anti-thrombotic agents, anti-inflammatory agents, antibiotics, etc. [33], and are thus very interesting scaffolds that have generated much interest in organic synthesis.

Since the first one-pot synthesis of α -amino phosphonates described in the literature [34], many variations have been developed. Unfortunately, they all displayed some drawbacks, such as environmental impact due to the use of volatile organic solvents, and long reaction times.

In 2007, Xia and coworkers [35] described a one-pot procedure for a three-component coupling of aldehydes, amines and diethylphosphite under ultrasound-assisted solvent-free and catalyst-free conditions (Scheme 8). In order to investigate the ultrasonic effect, the authors first used *p*-methoxyaniline and benzaldehyde as model molecules together with diethylphosphite. The experiments were performed in an ultrasound cleaning bath with a frequency of 40 kHz and an output power of 250 W. Under ultrasound irradiation, 97 % of α -amino phosphonate was obtained in only 1.5 h whereas only 18 % was observed in silent conditions when the reaction was run overnight. They then investigated the reactivity of aldehydes and amines, pointing out both electronic and steric effects from aldehydes and no remarkable electron and position effects from the amines on the three-component couplings. Whatever the aldehyde, the yields were excellent, but aldehydes with an electron-donating group could be accomplished in a much shorter time than those with an electron-withdrawing group under ultrasonic irradiation. The impact of the steric effect was more obvious, and, for sterically hindered aldehydes, reaction times were greatly increased while yields of products were decreased, and were lower than in silent conditions with the aliphatic isobutyraldehyde. Because of their lower

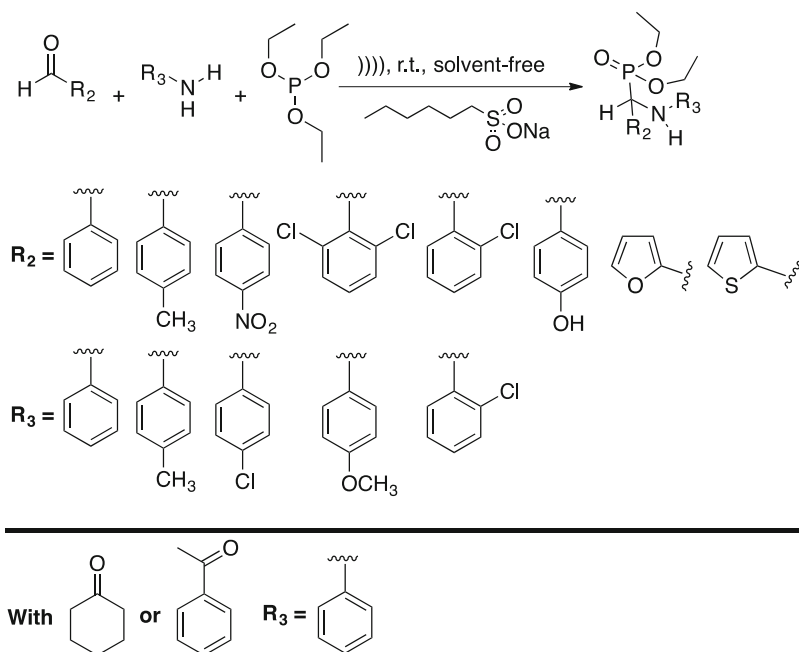


Scheme 8 Ultrasound-assisted one-pot coupling of aldehydes and amines with diethylphosphite under solvent-free conditions and catalyst-free conditions (adapted from [35])

reactivity, coupling reactions involving ketones had to be carried out at 70 °C under solvent-free and ultrasound conditions, leading to good yields in short times, except for acetophenone, for which only 25 % of product was obtained. Finally, using ultrasonic irradiation, the authors described an environmentally friendly solventless and catalyst-free convenient method for this three-component Mannich-type coupling.

Following this work, Shungare and coworkers [36] proposed a solvent-free procedure for the synthesis of α -aminophosphonates catalyzed by 1-hexanesulphonic acid sodium salt under ultrasonic irradiation (Scheme 9).

Various parameters such as catalyst amount, solvent need and effect of sonication were optimized with benzaldehyde, aniline and triethyl phosphite as model reagents. The use of 10 % mol of catalyst was sufficient to push the reaction forward. By using an ultrasonic bath at a frequency of 35 kHz, and a nominal power of 200 W, they observed an excellent 94 % yield under solvent-free conditions in 15 min of irradiation. However, in silent conditions, 60 min of reaction were needed to obtain a lower yield of 65 %. The presence of solvent decreased the yield to 68 % in the best case with dichloromethane and to 20 % in the worst case with water. The generality of the method was then examined by reacting different substrates with triethyl phosphite and 1-hexanesulphonic acid sodium, in solvent-free conditions and under ultrasonic irradiation. Satisfying yields were obtained except with ketones, which gave very low yields of products even after prolonged time of ultrasonic irradiation. In addition, under ultrasonic irradiation, whatever the



Scheme 9 Ultrasound-assisted synthesis of aminophosphonate catalyzed by 1-hexanesulphonic acid sodium salt under solvent-free conditions (adapted from [36])

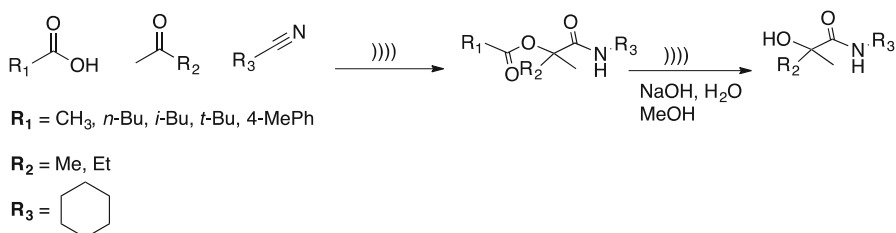
substrate studied, the yield of product obtained was superior, or at least identical, to that obtained under silent conditions. No remarkable difference in the reaction time and yields of products were observed with aldehydes substituted by electron-donating or -withdrawing functional groups.

2.3.3 Synthesis of α -Acyloxy Amides and α -Hydroxyl Amides

Depsides, depsipeptides and α -acyloxyamides are derivatives that show promising biological activities including anti-bacterial, anti-viral, antifungal and anti-inflammatory properties [37]; they also have great potential for Boron Neutron Capture Therapy (BNCT) applications [38].

A few years ago, Zhao and coworkers [39] published an ultrasound-promoted, easy, efficient and environmentally friendly protocol for the synthesis of α -acyloxyamides via sterically congested Passerini reactions under solvent-free conditions. The experiments were performed using an ultrasonic probe at a frequency of 25 kHz and 1200 W (pulse-on time = 2 s, pulse-off time = 2 s) for 1 h (Scheme 10), and the results were compared to those obtained at a pressure of 300 MPa.

In general, the use of ultrasound was shown to accelerate the reaction, and the reaction time decreased from 16.5 h at 300 MPa to 1 h under ultrasound, leading, in most cases, to higher yields. In addition, variation in the sizes of the substituents R_1 , R_2 and R_3 yielded 41–68 % of products under 1 h of ultrasonic irradiation compared to 28–89 % when the reactions were carried out at 16.5 h at 300 MPa pressure. Furthermore, when the reaction was performed in a low-polarity organic solvent, in water, or in aqueous LiCl, use of ultrasound was inefficient, and the product did not form. Under solvent-free conditions, 50 min of sonication of the mixture acetic acid, 2,2,2-trifluoro-1-phenylethanone and 1-isocyanato-4-methoxy-2-nitrobenzene led to a 49 % yield of product. An increase in the temperature of the mixture to 40 °C led to a maximum yield of 58 % in 40 min of sonication, whereas 24 h are necessary without solvent under conventional activation to get 52 % of products. In addition, the kinetics of the ultrasound-assisted procedure were 36-fold higher in solvent-free conditions than in the presence of solvent. The authors then decided to extend the optimized conditions to the reaction of several trifluorophenylethanones with isocyanides and acetic acid, and, for some of them, compared the efficiency of an ultrasonic horn to that of the ultrasonic bath ($f = 40$ kHz, $P = 100$ W).



Scheme 10 Synthesis of α -acyloxyamide under ultrasonic irradiation (adapted from [39])

Good to excellent conversions were observed whatever the electronic nature of the substituents of the trifluorophenylethanone, and of the isocyanide. Moreover, the bath cleaner was as efficient as the ultrasonic horn but the reaction was 4.5 to 8-fold faster when using the ultrasonic horn. With the objective of evaluating the bioactivities of the resulting α -hydroxyl amides, the authors experimented with a one-pot α -acyloxyamide synthesis-hydrolysis. After completion of the α -hydroxyl amide synthesis, the medium was hydrolyzed by aqueous sodium hydroxide in methanol under ultrasonic irradiation for 15 min, giving α -hydroxylamides in good yields.

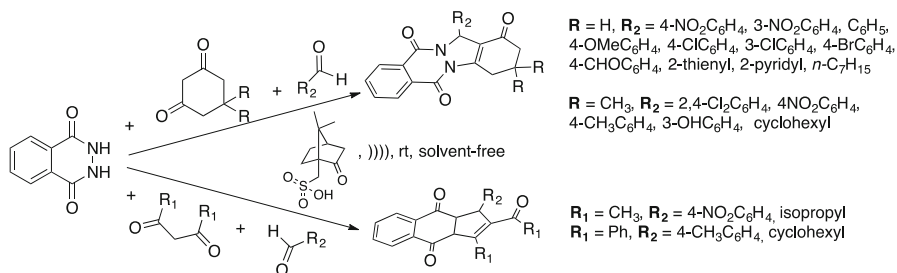
In conclusion, the authors described a new, efficient and environmentally friendly, solvent-free procedure for the synthesis of α -acyloxyamides via sterically congested Passerini reactions under ultrasonic irradiation; α -hydroxylamides were readily obtained by in situ basic hydrolysis under ultrasonic irradiation.

2.3.4 Synthesis of Heterocycles Scaffolds and Precursors

Reactions leading to interesting scaffolds and their precursors are especially useful for a large panel of 'drug like' molecules. 2*H*-Indazolo[2,1-*b*]phthalazine-1,6,11-triones, 1*H*-pyrazolo[2,1-*b*]phthalazine-5,10-diones and benzopyrano[4,3-*d*]pyrimidines are important N-heterocycles possessing several biological properties, such as anticonvulsant [40], cardiotoxic [41] and anti-thrombotic [42] activities. Due to their importance, various methods are available for their synthesis. Unfortunately, several of these present some drawbacks, such as harsh reaction conditions, use of toxic solvents, expensive catalysts, and low yield [43].

In 2011, Singh and coworkers [44] reported a swift and efficient solvent-free synthesis of 2*H*-indazolo[2,1-*b*]phthalazine-1,6,11-triones, 1*H*-pyrazolo[2,1-*b*]phthalazine-5,10-diones under ultrasonic irradiation, mediated by *S*-camphorsulfonic acid at room temperature (Scheme 11).

The reaction was first performed with phthalhydrazide, dimedone and 4-nitrobenzaldehyde in the absence of catalyst under solvent-free silent conditions at 80 °C, and under ultrasound irradiation, (ultrasonic bath, $P = 200$ W) at room temperature. In both conditions, the absence of desired product, even after 12 h of reaction, confirmed the indispensable nature of a catalyst. The above model reaction was then carried out under ultrasonic and silent conditions in the presence of various



Scheme 11 Solvent-free synthesis of 2*H*-indazolo[2,1-*b*]phthalazine-1,6,11-triones, 1*H*-pyrazolo[2,1-*b*]phthalazine-5,10-diones under ultrasonic irradiation (adapted from [44])

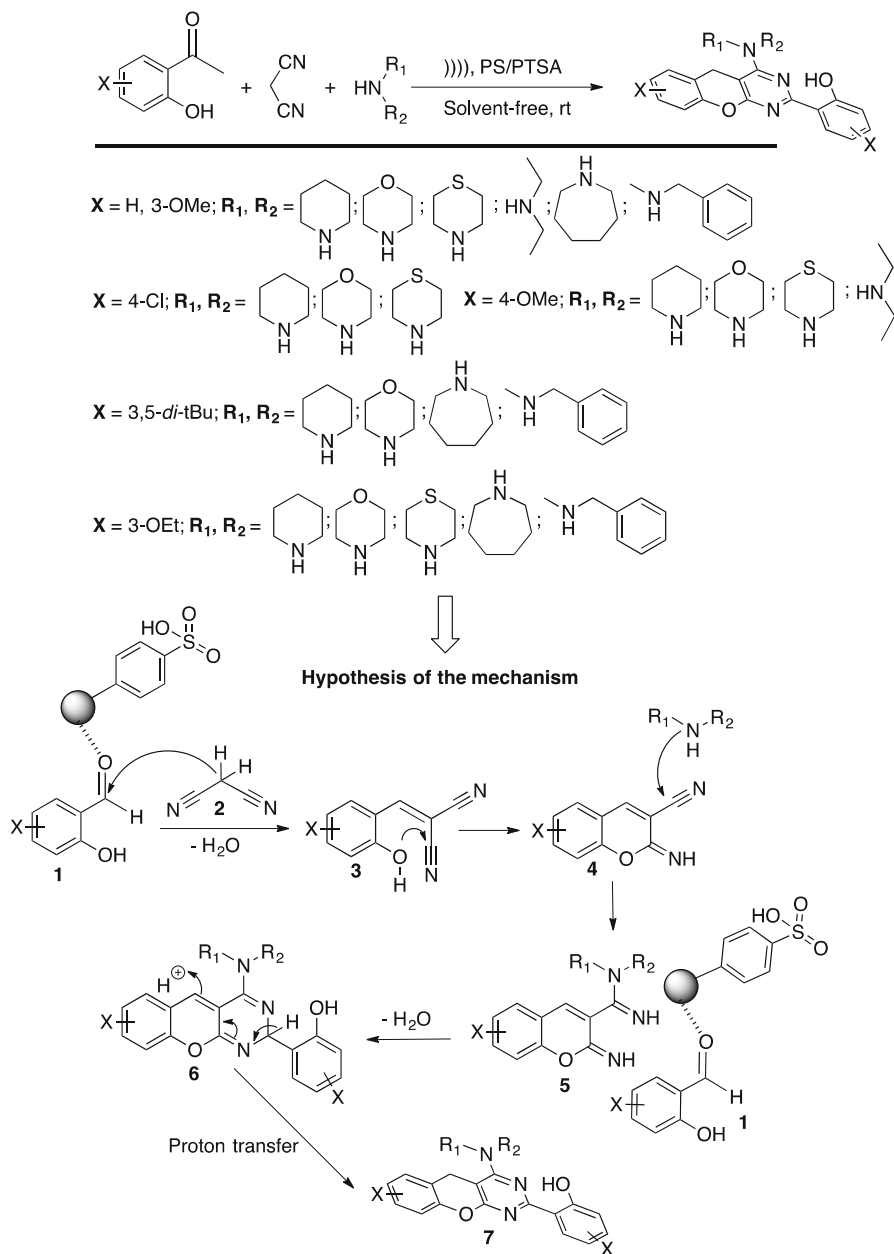
catalysts: *L*-proline, P_2O_5 , $InCl_3$, NH_3HSO_3 , $BF_3 \cdot OEt_2$ and *S*-camphorsulfonic acid (*S*-CSA). *S*-CSA was the most efficient and selectively provided the maximum 92 % of desired product in a minimum time of 20 min under solvent-free and ultrasonic irradiation conditions. Indeed, the other catalysts led to the desired product in lower yields, and to the Knoevenagel condensation product. The generality and the synthetic scope of this coupling protocol was then demonstrated by synthesizing a series of 2*H*-indazolo[2,1-*b*]phthalazine-1,6,11-triones, 1*H*-pyrazolo[2,1-*b*]phthalazine-5,10-diones under the optimized conditions. Main aromatic, heteroaromatic or aliphatic aldehydes, and cyclic or acyclic 1,3-diketones reacted successfully under the optimized conditions, although aliphatic aldehydes led to lower yields. Surprisingly, cyclic 1,3-diketones such as indane-1,3-dione, 1,3-dimethylbarbituric acid, and 4-hydroxycoumarin treated with phthalhydrazide and aldehyde under optimized conditions led selectively to the Knoevenagel condensation product.

Finally, in this work, the authors proposed a simple, eco-friendly and efficient approach to build structurally diverse 2*H*-indazolo[2,1-*b*]phthalazine-1,6,11-triones, 1*H*-pyrazolo[2,1-*b*]phthalazine-5,10-diones through domino Knoevenagel condensation / Michael addition / intramolecular cyclohydration sequence. This protocol could be used directly for biological assays.

In 2015, Jeong and coworkers [45] became interested in the synthesis of benzopyranopyrimidines in solvent-free conditions and under ultrasonic irradiation, catalyzed by a solid supported catalyst at room temperature (Scheme 12). The described strategy began with the development of the optimal conditions using salicylaldehyde, malonitrile, and piperidine as models in solvent-less conditions under silent and ultrasonic irradiation. A screening of various catalysts showed the efficiency of polymer-supported Lewis acid catalysts, and especially of the polystyrene *p*-toluenesulfonic acid (PS/PTSA) complex, the activity of which was excellent under ultrasonic irradiation. Indeed, an optimal amount of 30 mg of catalyst led to 94 % of product in 15 min of ultrasonic irradiation, whereas 50 min was necessary to obtain 81 % of product in silent conditions. The effect of solvent was then studied on the model reaction with 30 mg of catalyst, both under silent and ultrasonic conditions; it was established that 15 min of ultrasonic irradiation at room temperature in solvent-free conditions using 30 mg of PS/PTSA were the best conditions for this reaction. In addition, PS/PTSA catalyst was shown to be recyclable without significant loss of efficiency, and 87 % of product was obtained at its fourth use. The condensation of malonitrile with different salicylic aldehydes and various secondary amines under these optimized conditions led to a variety of benzopyranopyrimidines.

Salicylaldehydes bearing either electron-withdrawing or electron-donating groups reacted successfully with malonitrile and secondary amines under solvent-free and ultrasonic conditions in the presence of 30 mg of PS/PTSA at room temperature to give the corresponding benzopyrano[2,3-*d*]pyrimidines in 73–94 % yield. Unfortunately, no information is given in the paper on the ultrasonic conditions in terms of frequency, power, and material used.

The authors proposed a stepwise mechanism (Scheme 12), proceeding first via Knoevenagel condensation of the salicylaldehyde **1** with the malonitrile **2** leading to



Scheme 12 Synthesis of benzopyrano[3,4-d] pyrimidines in solvent-free conditions under ultrasonic irradiation using polystyrene *p*-toluenesulfonic acid (PS/PTSA) as catalyst and hypothesis of the mechanism (adapted from [45])

an intermediate **3** on the acidic active surface of the catalyst. Then, a Pinner reaction affords compound **4**, the cyano function of which is readily attacked by the secondary amine to produce intermediate **5**. Intermediate **5** reacts finally with

another molecule of salicylaldehyde **1** leading to compound **6**, which affords benzopyrano[2,3-d]pyrimidine **7** by proton transfer through the surface of the solid catalyst.

In conclusion, the authors describe an efficient and eco-friendly solvent-free procedure for the synthesis of benzopyrano[2,3-d]pyrimidines in the presence of a solid catalyst under ultrasonic irradiation at room temperature.

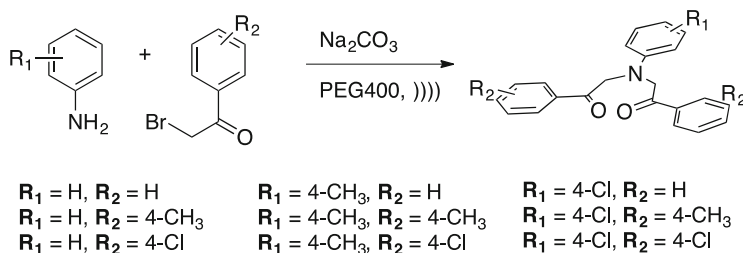
N,N-Bis(phenacyl)alanines are very important precursors of various N-containing heterocyclic compounds [46]. Unfortunately, the classical methods for their synthesis require organic volatile solvents, long reaction times, and lead to low yields [47]. Hence, He and coworkers [48] reported a solvent-free synthesis of *N,N*-bis(phenacyl)aniline under ultrasonic irradiation, using polyethylene glycol 400 (PEG400) as a phase transfer catalyst (PTC) (Scheme 13).

The reaction was first optimized using aniline, α -bromoacetophenone and sodium carbonate in the presence of PEG400 at room temperature. The mixture was irradiated using an ultrasonic probe at a frequency of 24 kHz, by increasing the power from 200 W to 400 W. In the presence of 2 mol% PEG400, an increase of the power from 200 W to 350 W led to an increase in yield from 38 % to 54 %, and a decrease in reaction time from 150 min to 50 min. Moreover, at a power of 350 W, an increase in the amount of PEG400 to 5 mol% led to a decrease in the reaction time to 30 min, and an increase in the yield to 81 %.

The optimized conditions were then extended to the condensation of substituted anilines, with substituted α -bromoacetophenone, but no obvious electronic effects of the substituents were evidenced. Yields of 73–83 % in the resulting *N,N*-bis(phenacyl)alanines were observed in 30–50 min of ultrasonic irradiation.

Finally, the authors developed an efficient and environmentally-friendly solvent-free procedure for the synthesis of bis(phenacylanilines) under ultrasonic irradiation in the presence of PEG400 as PTC.

Summing up the above, ultrasound-assisted solvent-less synthesis has been studied extensively for MCR reactions in the literature, but also for many other reactions, such as in the protection of chemical functions [49]. The use of this non-conventional activation method, in combination with solvent-less conditions, allows significant improvements in terms of yield, reaction time, by-product formation,



Scheme 13 Solvent-free synthesis of *N,N*-bis(phenacyl)alanines under ultrasonic irradiation (adapted from [48])

chemoselectivity, ease of experimentation, and sustainability of the reactions, that can often be performed in catalyst-free conditions.

3 Sustainable Catalytic Oxidations under Ultrasound

From among the numerous published works on sonochemistry, we choose here to highlight organic transformations with a synthetic purpose. Thus, degradation of organic pollutants, sludge or waste, desulfurization of fuel oil will not be reported. We will restrict our investigation to the few papers dedicated to oxidative transformations involving green oxidants (H_2O_2 or O_2) associated, or not, with green metals (Mn or W) as catalysts.

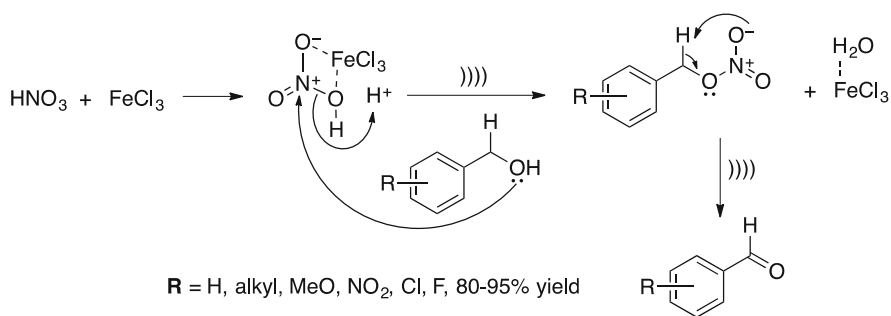
3.1 Synthesis of Carbonyl and Carboxylic Compounds

Aldehydes and ketones are of great interest in organic synthesis either as precursors, fine chemicals or solvents. Their syntheses have required toxic and expensive conditions, often unacceptable for polyfunctionalized compounds, that are no longer considered adequate for sustainable chemistry. It is necessary to develop environmentally benign and straightforward methods leading to such products. In order to minimize further oxidation of aldehydes to carboxylic acids, a two-phase system is often proposed.

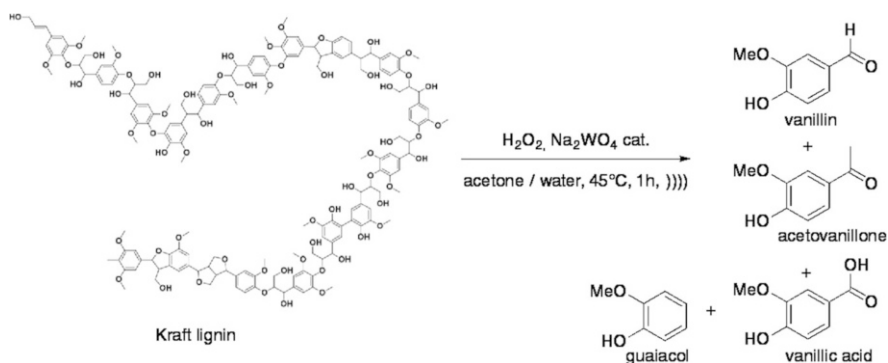
Although ultrasound promotes micromixing, increased reaction rate and mass transfer compare to silent conditions (magnetic or mechanical stirring), PTC is still needed. Pandit and coworkers [50] applied such a strategy to benzaldehyde synthesis, and showed that active oxidizing species are generated in the aqueous phase containing hydrogen peroxide and dodecatungstophosphoric acid ($\text{H}_3\text{PW}_{12}\text{O}_{40}$). Aliquat-336, used as PTC, is able to transfer the oxidant to the organic layer, thus allowing the reaction with benzyl alcohol, providing benzaldehyde with high selectivity in 125 min at 39 °C maximum. They studied the influence of all the parameters (concentrations of alcohol and H_2O_2 , amount of PTC and of catalyst, effect of ultrasound), and obtained best yield and selectivity in the sonochemically assisted process requiring a 22 kHz bath, and essential presence of PTC although dichloromethane appeared to be unavoidable.

Substituted benzyl alcohols were converted quantitatively within 10–25 min at room temperature, in acetone, using a mixture of the Lewis acid FeCl_3 and HNO_3 as oxidants according to the suggested mechanism (Scheme 14) [51]. A 35 kHz ultrasonic bath was revealed to be crucial in avoiding the overoxidized or nitrated by-products obtained under silent conditions.

These works led Draye and coworkers [52] to envisage the oxidative depolymerization of Kraft lignin (a paper industry waste) into four vanillin-based monomers: vanillin, acetovanillone, vanillic acid and guaiacol (Scheme 15), in silent but also acoustic conditions. This great renewable source of organic compounds, and especially of aromatics, is so stable that only 0.51 % yield was obtained with hydrogen peroxide and catalytic amount of Na_2WO_4 , $2\text{H}_2\text{O}$ under magnetic stirring. This result is one of the best ever reached with H_2O_2 . But,



Scheme 14 Suggested mechanism for oxidation of benzyl alcohols with FeCl₃ and HNO₃ under sonication (adapted from [51])



Scheme 15 Depolymerization of Kraft lignin in the presence of a H₂O₂ / Na₂WO₄ system (adapted from [52])

surprisingly, acoustic cavitation promoted the high coupling of phenoxy radicals generated by superoxide radical HO₂[•] at the end of polymer units, thus causing a decrease in the number of monomers. Thus ultrasound is used in the pretreatment and extraction of lignin rather than in an oxidative synthetic process [53].

This green transformation was also applied to cyclanols, which have five- to eight-membered rings, leading to corresponding ketones with excellent selectivity (> 99 %) in the presence of aqueous H₂O₂ [54]. The screening of the catalyst led to the choice of tungstic acid H₂WO₄; however, despite this, the solventless reaction is not efficient without PTC. Different ILs were added as co-catalysts, with hydrophobic ILs predicted to give modest yields and displaying poor mass transfer ability. In order to validate this hypothesis, Aliquat-336 was tested. Cyclohexanone was then obtained almost quantitatively in 15 min with an ultrasonic probe at 20 kHz. A radical mechanism might occur under sonication.

This was again proven in the oxidation of D-glucose into D-gluconic acid. The Sono-Fenton reaction occurred at low frequency in the presence of the H₂O₂/FeSO₄ system [55]. This very efficient and regioselective reaction afforded the acid with

99 % conversion and 97 % yield, in a very short time at room temperature, releasing no harmful waste.

Oxidative transformation of valeraldehyde into valeric acid with bubbling oxygen and di-tert-butylperoxide as catalyst was carried out with a 30 kHz probe [56]. The catalyst initiates the formation of a radical that traps oxygen to provide valeric peracid as an intermediate. It then reacts with valeraldehyde to give valeric acid at room temperature. This radical-chain oxidation is due solely to acoustic cavitation.

This phenomenon is powerful and versatile, and is efficient in both degradation and synthetic reactions.

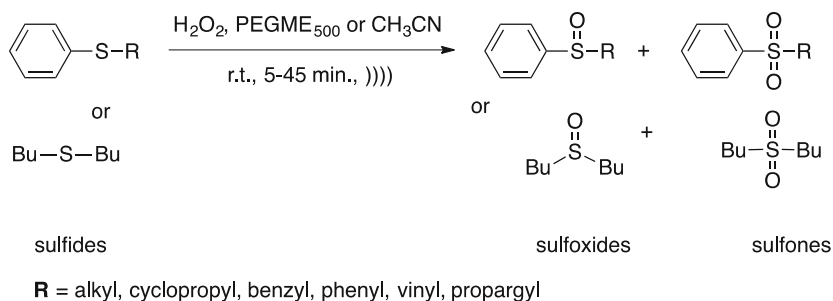
3.2 Synthesis of Sulfoxides and Sulfones

Sulfoxides are important compounds that exhibit various interesting properties and are thus used in many different domains of the chemical industry. They can be produced by direct oxidation of sulfides with a very good selectivity, and with environmentally benign methods.

Pandit and coworkers [57] investigated this reaction on thioanisole in water, with hydrogen peroxide under sonication at 22 kHz. All reaction parameters have been studied rigorously. For example, addition of H_2O_2 portionwise is more efficient than adding the total amount at the beginning. In fact, under ultrasound, this oxidant decreases because of homolytic cleavage occurring during bubble collapse. Thus, an excess of H_2O_2 is often used. In this work, conversion of thioanisole into sulfoxide was excellent and almost quantitative, and selectivity increased by the use of catalytic amounts of β -cyclodextrin. By-products such as sulfone were then lower.

To achieve this goal requires 2 h at 32 °C, although water has replaced methanol, making this new process more eco-friendly.

When Jain and coworkers [58] achieved this oxidation on various sulfides (phenyle, vinyle, propargyle and alkyle ones) in two different solvents at room temperature, they obtained 80–95 % of sulfoxides in polyethylene glycol PEGME500 and 85–98 % of sulfones in acetonitrile, respectively, within 5–45 min (Scheme 16). Unsaturated carbon–carbon bonds remained unchanged.



Scheme 16 Oxidation of sulfides with H_2O_2 in organic solvents under ultrasound (adapted from [58])

The advantage of using PEGME500 relies on its recyclability in several subsequent runs without significant loss of conversion and selectivity.

3.3 Epoxidation of Alkenes

Epoxides represent a class of molecules produced either chemically or biochemically that serve mainly as precursors for drugs and natural compounds. They are often issued from alkenes, requiring hazardous and expensive reactants and solvents. Selectivity might be low when polysubstituted substrates are used. It became necessary to work out new sustainable and efficient processes for synthesizing such intermediates, even in an enantioselective pathway [59, 60].

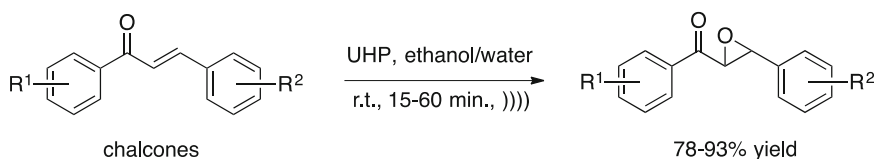
Jin and coworkers [61] developed a versatile and eco-friendly ultrasonically assisted method for the epoxidation of chalcones in the presence of urea-hydrogen peroxide (UHP) in ethanol/water. This oxidant is easy to handle, and safer than H_2O_2 . Sonochemical activation at 40 kHz leads to 78–93 % yield, in much shorter times than magnetic stirring, whether unsaturated ketones are activated or deactivated (Scheme 17).

Rayati and Sheybanifard studied the epoxidation of several alkenes using a biomimetic strategy involving Fe-porphyrin catalyst grafted on carbon nanotubes, H_2O_2 in large excess in ethanol [62]. The reaction improved when ultrasound was used to activate the mixture, in terms of time, conversion (maximum 80 %) and selectivity (epoxide towards aldehyde). The catalyst is even reusable four times without loss of efficiency.

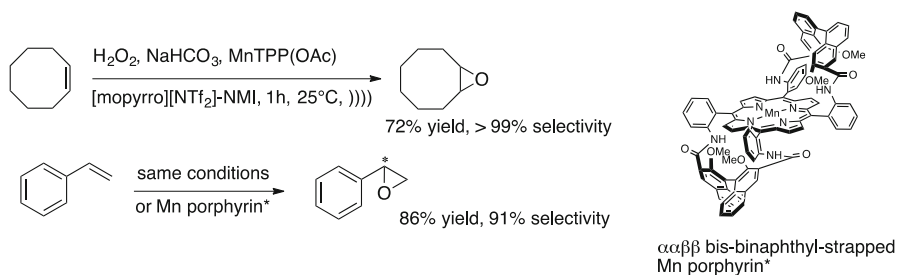
Exchanging iron for manganese led the authors to add acetic anhydride or acetic acid to generate peracid in the reaction medium [63]. Alkenes then reacted even faster, with better selectivity and conversion, especially for cyclooctene.

Draye and coworkers [64] combined both $\text{H}_2\text{O}_2/\text{NaHCO}_3/\text{imidazole}/\text{Mn}(\text{TPP})\text{OAc}$ oxidation system and [mopyrro][NTf₂] IL under ultrasonic irradiation to give an exceptionally favorable environment for Mn(TPP)OAc-catalyzed olefin oxidations such as cyclooctene or styrene (Scheme 18).

Under these conditions, the porphyrin is protected by immobilization in the IL phase, and the peroxymonocarbonate (generated in situ) has too short a lifetime under ultrasound. The classical mechanism of oxidation via porphyrin can occur, through the oxo-manganyl intermediate, which is the oxidizing species formed in situ. These two conditions allow the mechanism of the epoxidation reaction to be controlled. Thus, considering chiral epoxidation via design of the catalyst was



Scheme 17 Epoxidation of chalcones with urea-hydrogen peroxide (UHP) in a cleaning ultrasonic bath (adapted from [61])



Scheme 18 Ultrasonic-assisted epoxidation of olefins catalyzed by MnTPP(OAc) in [mopyrro][NTf₂] IL, and by chiral Mn porphyrin (adapted from [64, 66])

obvious and successful [65–67]. (S)-styrene oxide was obtained in 16 % yield after 5 min with a 40 % ee.

Moreover, the effect of ultrasound in ILs was investigated and, for the first time, some typical parameters of sonochemistry were determined in this solvent to better understand the powerful combination of ILs / ultrasound in green organic synthesis.

This sophisticated oxidative system is imitating biocatalyst processes. Researchers have not hesitated in crossing the line to investigate enzymes and microorganisms to improve organic transformations according to the principles of green chemistry.

4 Enzymatic Transformations

The mechanical effects of low-frequency ultrasound (20–100 kHz) enhance organic transformations by better micromixing due to microstreaming, better mass transfer, and better diffusion, especially in heterogenous media [59, 60]. It is obvious that it can also improve biotechnological processes, as ultrasound is known to alter cell membranes, increasing diffusion of materials, or to disrupt cells, thus releasing enzymes and proteins in the reactor, influencing kinetics [68, 69]. But submitting those macromolecules to very powerful irradiation can cause irreversible damage by means of oxidation with hydroxyl radical, breakage as a consequence of shear forces, or local heat spots. Thus, it is essential to design the right reactor for the right purpose: use of an ultrasonic bath, a cuphorn, or a directly immersed probe [60, 69].

Sonochemistry has already been widely applied to biocatalysis, such as in sludge or waste remediation [70], decontamination [71], microbial fermentations [72], anaerobic digestion [73], pretreatment of enzymes [74], or biodiesel production [75]. We chose here to report ultrasonically enzyme-assisted synthetic transformations for pharmaceutical, agrochemical, food, fragrances and flavors, or cosmetics applications. Indeed, research studies in these domains have not attracted as much attention as the organic syntheses discussed above, even though they are relevant to the principles of green chemistry.

4.1 Transesterification and Esterification

4.1.1 Transesterification

The most illustrative reaction in this context is transesterification carried out in the presence of lipase. In general, and in aqueous media, this enzyme hydrolyzes triacylglycerol esters. When the reaction is carried out in a non-aqueous organic medium, lipase catalyzes esterification or transesterification. Under ultrasound, and up to 70 °C, one of the most efficient is lipase B from *Candida antarctica*. It is immobilized mainly on a macroporous poly acrylic resin, and in this form is known as Novozym[®]435.

Despite the high cost of such enzymes, this synthetic strategy proved to be the best in carbohydrate chemistry, displaying excellent regioselectivity and yields, avoiding extra protection and deprotection steps [76]. Indeed, the natural polysaccharide Konjac glucomannan (KGM) has been acylated on C6-OH positions with vinyl esters (from C2 to C18) in tert-butanol with higher yields, higher degree of substitution (DS) and higher initial reaction rate under sonication at 20 kHz in a cleaning bath than with conventional methods. The acylated sugar appeared to be a good emulsifier and a promising medicine.

Cinnamyl acetate—a natural fragrance and flavor extracted from the bark of cinnamon—can be obtained successfully from transesterification between cinnamyl alcohol and vinyl acetate in the presence of Novozym[®]435 at 25 kHz in 20 min, solvent-free. Lipase is reusable seven times without any loss of activity [77].

In order to produce biodegradable polymers, the homopolymer poly(ethylene glutarate) was obtained for the first time by the same solventless strategy [78]. The reaction between ethylene glycol diacetate and diethyl glutarate was relatively fast (7 h at 45 kHz v. 24 h under silent conditions) with almost quantitative conversion of the monomer and a higher degree of polymerization. In this case, lipase B was immobilized on a glycidyl methacrylate polymer and is known as Fermase CALB[™] 10,000.

Lipase-catalyzed copolymer synthesis can be optimized in terms of rate, yields and molecular weight by using ultrasonic activation. Annuar and coworkers [79] succeeded in improving biodegradable copolymer production of poly-4-hydroxybutyrate-co-6-hydroxyhexanoate from γ -butyrolactone and ϵ -caprolactone in chloroform. Screening of lipase was realized, and Novozym[®]435 afforded the best results with the highest stability under ultrasound.

Transesterification with glycerol was first studied on methyl benzoate, with catalytic amounts of Novozym[®]435 at 37 kHz in 2-propanol, modestly yielding 1-glycerol benzoate [80], before applying it to glycerolysis of olive oil [81]. In the latter case, mono-(MAG) and diacylglycerols (DAG), very good for prevention of obesity, were obtained consistently with kinetic modeling, and without requiring any separation of solvent.

Flavonoids display interesting pharmacological properties, but their low liposolubility prevents them from crossing the blood–brain barrier. Thus, mono acylated flavonoids have been synthesized to enhance this activity, thus requiring the development of green processes. Divinyl dicarboxylates (C8–C17) were chosen as

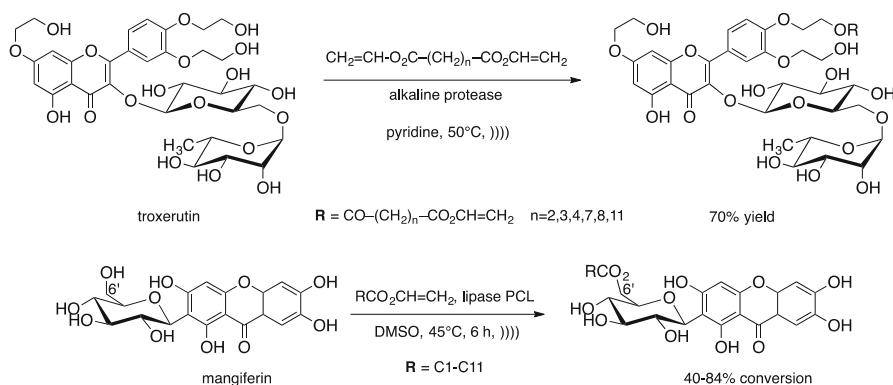
acyl donors along with troxerutin (also known as vitamin P4). Transesterification was catalyzed by an alkaline protease from *Bacillus subtilis* in pyridine, leading to high regioselectivity regardless of the activation system. Ultrasound frequency and power was investigated, and 80 kHz provided an excellent yield, almost the double (70 %) that of silent conditions (Scheme 19) [82].

Mangiferin, a xanthonoid extracted from mangoes and other plants, possesses similar pharmacological potential. For the same reason, mono acylated derivatives would exhibit greater activities. PCL enzyme, in DMSO at 45 °C, led to 84 % of 6'-OH acylation with vinyl acetate, under ultrasound (Scheme 19) [83].

Resveratrol, a naturally derived stilbene from grapes, berries and peanuts, exhibits pharmacological properties such as anti-oxidant, cardioprotective, anti-inflammatory and antitumor activities. However, 4'-acetoxyresveratrol seems to have enhanced metabolic stability, and can be achieved by same strategy, without the need to protect or deprotect phenolic groups from the aromatic aglycone moiety and hydroxyl groups from the sugar part. Novozym[®] 435 catalyzed efficiently acylation on the 4' position of the aromatic skeleton. Under ultrasonication, reaction time is decreased drastically and conversion reached more than 95 % [84].

4.1.2 Esterification

If transesterification is a green process, direct esterification catalyzed by enzymes is more eco-friendly in terms of atom-economy. Ultrasound is an effective activation system, increasing rates being due mainly to mass transfer. Thus, flavors like isoamylbutyrate can be produced almost quantitatively in solvent-free conditions from isoamyl alcohol and butyric acid, in the presence of catalytic amounts of Novozym[®] 435 [85]. Rathod and coworkers [86] optimized such a reaction in order to produce wax esters, used as cosmetic emollients. They synthesized cetyl oleate in the presence of Fermase CALB[™] 10,000 at 40 kHz, increasing yield by 7.5 fold compared to silent conditions. The kinetic model was still consistent with the experiment.



Scheme 19 Ultrasound-assisted enzyme-catalyzed transesterification of troxerutin and mangiferin with vinyl esters (adapted from [82, 83])

De Oliveira and coworkers [87] also envisaged trying direct ultrasonically assisted enzymatic esterification to afford ascorbyl esters like palmitate (in modest yields) and oleate (in very good yields, but with a large excess of oleic acid) [88]. They used tert-butanol to dissolve ascorbic acid and fatty acids.

Esters obtained from short chain alcohols display fruity flavors and are of great interest in the fragrance and food industries. Biocatalyzed esterification could lead to “natural flavors”. Fernandez-Lafuente and coworkers [89] developed their own strategy using phospholipase Lecitase-Ultra immobilized on styrene-divinylbenzene beads (MCI-Lecitase), and a variety of short primary and secondary alcohols and fatty acids from C4 to C18. Best results were obtained with C8 and C14 acids. Ultrasound allowed a higher initial rate and the use of a higher substrate concentration.

Enantioselective esterification was carried out by Zhi and coworkers [90] using the immobilized thermophilic esterase APE1547 for the resolution of ibuprofen. Enzyme is added to a stoichiometric mixture of 1-octanol and racemic ibuprofen in *n*-heptane at 45 °C, in an ultrasonic cleaning bath (40 kHz). Ten cycles were performed without any loss in APE1547 activity or enantioselectivity.

4.2 Transesterification and Esterification in Ionic Liquids

4.2.1 Transesterification in Ionic Liquids

Polyhydroxyalcanoates, PHAs, are easily biodegradable biopolymers. Anuar and coworkers [91] reported ring opening, transesterification and polymerization of ϵ -caprolactone in IL [emim][BF₄]. Such a solvent, with high viscosity, can limit mass diffusion, but this can be overcome with the help of ultrasound. Indeed, the molecular weight of the polymer was enhanced, increasing its crystallinity and reducing its polydispersity compared to poly-6-hydroxyhexanoate obtained in silent conditions.

4.2.2 Esterification in Ionic Liquids

ILs are versatile tools for solubilizing, extracting or immobilizing natural molecules. Ha and coworkers [92] decided to use ILs either in trans or direct esterification of glucose (as a model) to produce fatty acid sugar ester with surfactant properties. Indeed, glucose is hydrophilic while fatty acids are lipophilic. Two envisaged strategies appeared to be efficient starting from vinyl laurate (90 % conversion) or lauric acid (80 % conversion), catalyzed by Novozym[®]435 under ultrasonication. A supersaturated solution of glucose prepared in ILs, [bmim][OTf] gave the best results. In these conditions, formed monoester precipitated, thus limiting diester synthesis and facilitating the work-up.

ILs were also screened to prepare alkyl caffeate, which exhibits biological properties [93]. In this case, direct lipase-catalyzed esterification of caffeic acid in methanol and [bmim][NTf₂] (an hydrophobic IL) led to methyl caffeate in almost quantitative yield, under ultrasound. Novozym[®]435 was the more suitable and reusable lipase under such conditions (16 cycles), with significant decrease in yield observed after 11 cycles.

4.3 Other Organic Transformations

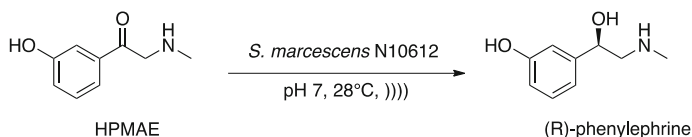
After dealing with oxidation, we now focus on enzyme-catalyzed enantiospecific bioreduction to afford (R)-phenylephrine, a drug substitute of ephedrine (Scheme 20) [94]. 1-(3-Hydroxyphenyl)-2-(methylamino)-ethanone (HPMAE) was converted at 95 % by adding whole cells of *Serratia marcescens* N10612 as biocatalyst; sonication enhanced cell permeability.

Lastly, we report a nice one-pot ultrasonically assisted synthesis of pure indolizines catalyzed by lipase [95]. *Candida antarctica* A and B were used as biocatalyst, but the former proved to give higher conversion (>70 %). Ultrasound improved the reaction rate dramatically, leading to indolizine in only 2 h instead of 2 days under silent conditions (Scheme 21). This cycloaddition involved the *in situ* generated ylide, which reacts even in aqueous media, making this strategy even greener.

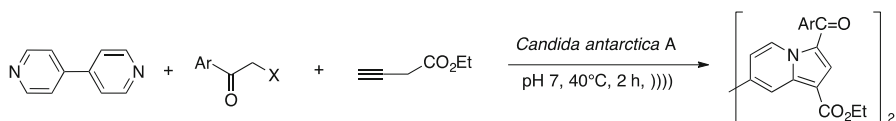
We have highlighted green organic transformations, mainly allowing biomass valorization. Biotechnological processes activated with an ultrasound/enzyme combination proved very efficient and encouraging. Reaction rates are increased dramatically thanks to enhancement of mass transfer and diffusion. It is also notable that enzymes, as macromolecules, remaining mostly unchanged by ultrasonic chemical and physical effects, allowing recycling. Thus, future industrial eco-friendly applications could emerge.

5 Perspectives

This chapter clearly demonstrates the huge potential of sonochemistry within Green Chemistry. The phenomena induced by cavitation are well established but not completely understood by the scientific community. Indeed, the use of ultrasound is still not rigorous enough, and a lot of technical information, such as acoustic power, frequency, etc., is missing from the experimental section of a large number of papers published in the literature, precluding rigorous interpretation of all the phenomena discussed above. In addition, this lack of information does not allow other researchers to accurately reproduce published experiments. Sonochemists still have a difficult task to accomplish before ultrasound can be used to its full potential, and wisely as a green tool or for green purposes. Progress in sustainable sonochemistry is based on the combined skills of various scientists, from chemists to physicists. And although some industrial processes already involve the use of ultrasound [96, 97], chemical engineers still have some hard work to do in the scale-



Scheme 20 Enantiospecific ultrasound-assisted enzyme-catalyzed reduction of 1-(3-hydroxyphenyl)-2-(methylamino)-ethanone (HPMAE) (adapted from [94])



Scheme 21 Ultrasound-assisted synthesis of indolizine by biocatalyzed one-pot cycloaddition (adapted from [95])

up of green sonochemical methodologies and processes in order to make them cost effective and transposable to the industrial scale.

References

- Cravotto G, Boretto E, Oliverio M, Propocio A, Penoni A (2015) *Catal Commun* 63:2–9
- Morris P J T, Murmann J P (2002) In: Mokyr j (ed) *The Oxford encyclopedia of economic history*. Oxford University Press, Oxford
- Chatel G, Leclerc L, Naffrechoux E, Bas C, Kardos N, Goux-Henry C, Andrioletti B, Draye M (2012) *J Chem Eng Data* 57:3385–3390
- Draye M, Estager J, Naffrechoux E, Lévêque JM (2011) In: Bazureau JP, Draye M (eds) *Ultrasound and microwaves: recent advances in organic chemistry*. Transworld Research Network, Kerala
- Cintas P (2016) *Ultrason Sonochem* 28:257–258
- Varma RS, Naicker K, Kumar D (1999) *J Mol Catal A Chem* 149:153–160
- Gawande MB, Bonifácio VDB, Luque R, Branco P, Varma RS (2014) *ChemSusChem* 7:24–44
- Prat D, Hayler J, Wells A (2014) *Green Chem* 16:4546–4551
- Jimenez-Gonzalez C, Ponder C, Broxterman QB, Manley JB (2011) *Org Process Res Dev* 15:912–917
- Shanab K, Neudorfer K, Schirmer E, Spreitzer H (2013) *Curr Org Chem* 17:1179–1187
- Varma RS (1999) *Green Chem* 1:43–55
- Nasir Baig RB, Varma RS (2012) *Chem Commun* 41:1559–1584
- Nasir Baig RB, Varma RS (2013) *Green Chem* 15:398–417
- Polshettiwar V, Varma RS (2008) *Chem Soc Rev* 37:1546–1557
- Sheldon RA (2005) *Green Chem* 7:267–278
- Sheldon RA (1996) *J Mol Catal A: Chem* 107:75–83
- Richards WT, Loomis AL (1927) *J Am Chem Soc* 49:3086–3100
- Simon M-O, Li C-J (2012) *Chem Soc Rev* 41:1415–1427
- Severa J, Bár J (1991) *Handbook of radioactive contamination and decontamination*. Elsevier, Amsterdam, p 126
- Abae AS, Hamidi V, Mojtahedi MM (2008) *Ultrasonics Sonochem* 15:823–827
- Rostmania S, Lamei K (2011) *Synthesis* 19:3080–3082
- Bandyopadhyay D, Mukherjee S, Turrubiarres LC, Banik BK (2012) *Ultrasonics Sonochem* 19:969–973
- Almeida AAR (2013) *Green Chem Lett Rev* 6:129–133
- Pagadala R, Maddila S, Jonnalagadda SB (2014) *Green Chem Lett Rev* 7:131–136
- Ramazani A, Rouhani M, Joo SW (2016) *Ultrasonics Sonochem* 28:393–399
- Cintas P, Tagliapietra S, Calcio Gaudino E, Palmisano G, Cravotto G (2014) *Green Chem* 16:1056–1065
- Cravotto G, Orio L, Calcio Gaudino E, Martina K, Tavor D, Wolfson A (2011) *ChemSusChem* 4:1130–1134
- Nagri DM, Ambhore DM, Gawande MB (2010) *Int J Chem* 2:98–101
- He L, Qin S, Chang T, Sun Y, Zhao J (2014) *Int J Mol Sci* 15:8656–8666
- Rulev AY (2011) *Russ Chem Rev* 80:197–2018
- Yang J-M, Ji S-J, Gu D-G, Shen Z-L, Wang S-Y (2005) *J Organomet Chem* 690:2989–2995
- Du X-J, Wang Z-P, Hou Y-L, Zhang C, Li Z-M, Zhao W-G (2014) *Tetrahedron Lett* 55:1002–1005

33. Zahra R, Hossein N, Ramin G (2015) RSC Adv 5:99148–99152
34. Qian C, Huang T (1998) J Org Chem 63:4125–4128
35. Xia M, Lu Y-D (2007) Ultrason Sonochem 14:235–240
36. Niralwad KS, Shingate BB, Shingare MS (2010) Ultrason Sonochem 17:760–763
37. Gulevich AV, Shpilevaya IV, Nenajdenko VG (2009) Eur J Org Chem 3801–3808
38. Jonnalagadda SC, Cruz JS, Connell RJ, Scott PM (2009) Tetrahedron Lett 50:4314–4317
39. Cui C, Zhu C, Du X-J, Wang Z-P, Li Z-M, Zhao W-G (2012) Green Chem 14:3157–3163
40. Zhang L, Guan LP, Sun XY, Wei CX, Chai KY, Quan ZS (2009) Chem Bio Drug Design 73:313–319
41. Nomoto Y, Obase H, Takai H, Teranishi M, Nakamura J, Kubo K (1990) Chem Pharm Bull 38:2179–2183
42. Bruno O, Brullo C, Schenone S, Ranise A, Bondavalli F, Barocelli E, Tognolini M, Magnanini F, Ballabeni V (2002) Farmaco 57:753–758
43. Zonouzi A, Hosseinzadeh F, Karimi N, Mirzazadeh R, Ng SW (2012) Comb Sci 15:240–246
44. Shukla G, Verma RK, Verma GK, Singh MS (2011) Tetrahedron Lett 52:7195–7198
45. Thirupathiah B, Reddy MV, Jeong YT (2015) Tetrahedron 71:2168–2176
46. Ravindran G, Muthusubramanian S, Selvaraj S, Perumal S (2007) J Heterocycl Chem 44:133
47. Almstrom GK (1916) Liebigs Ann Chem 411:350–382
48. He J, Shi L, Liu S, Jia P, Wang J, Hu R (2014) Monatsch Chem 145:213–216
49. Mojtahedi MM, Abaee MS, Hamidi V, Zolfagharu A (2007) Ultrason Sonochem 14:596–598
50. Mahamuni NN, Gogate PR, Pandit AB (2006) Ind Eng Chem Res 45:98–108
51. Naik R, Nizam A, Siddekha A, Pasha MA (2011) Ultrason Sonochem 18:1124–1127
52. Napoly F, Kardos N, Jean-Gérard L, Goux-Henry C, Andrioletti B, Draye M (2015) Ind Eng Chem Res 54:6046–6051
53. Chatel G, De Oliveira Vigier K, Jérôme F (2014) Chem Sus Chem 7:2774–2787
54. Chatel G, Monnier C, Kardos N, Voiron C, Andrioletti B, Draye M (2014) Appl Catal A 478:157–164
55. Rinsant D, Chatel G, Jérôme F (2014) Chem Cat Chem 6:3355–3359
56. Neuenschwander U, Neuenschwander J, Hermans I (2012) Ultrason Sonochem 19:1011–1014
57. Mahamuni NN, Gogate PR, Pandit AB (2006) Ind Eng Chem Res 45:8829–8836
58. Khatri PK, Jain SL, Sain B (2011) Ind Eng Chem Res 50:701–704
59. Martin-Aranda RM, Calvino-Casilda V (2010) Recent Pat Chem Eng 3:82–98
60. Chatel G, MacFarlane DR (2014) Chem Soc Rev 43:8132–8149
61. Jin H, Zhao H, Zhao F, Li S, Liu W, Zhou G, Tao K, Hou T (2009) Ultrason Sonochem 16:304–307
62. Rayati S, Sheybanifard Z (2015) J Porphyrins Phthalocyanines 19:622–630
63. Rayati S, Bholoulbandi Z (2014) C R Chimie 17:62–64
64. Chatel G, Goux-Henry C, Kardos N, Suptil J, Andrioletti B, Draye M (2012) Ultrason Sonochem 19:390–394
65. Rose E, Andrioletti B, Zrig S, Quelquejeu-Ethève M (2005) Chem Soc Rev 34:573–583
66. Chatel G, Goux-Henry C, Mirabaud A, Rossi T, Kardos N, Andrioletti B, Draye M (2012) J Catal 291:127–132
67. Collman JP, Wang Z, Straumanis A, Quelquejeu M (1999) J Am Chem Soc 121:460–461
68. Rokhina EV, Lens P, Virkutyte J (2009) Trends Biotechnol 27:298–306
69. Kwiatkowska B, Bennett J, Akunna J, Walker GM, Bremner DH (2011) Biotechnol Adv 29:768–780
70. Adulkar TV, Rathod VK (2014) Ultrason Sonochem 21:1083–1089
71. Sutar RS, Rathod VK (2015) Ultrason Sonochem 24:80–86
72. Herran NS, Casas Lopez JL, Sanchez Perez JA, Chisti Y (2008) J Chem Technol Biotechnol 83:593–600
73. Guo Y, Kim SH, Sung SH, Lee P (2010) Int J Hydrogen Energy 35:3450–3455
74. Wang Z, Lin X, Li P, Zhang J, Wang S, Ma H (2012) Bioresour Technol 117:222–227
75. Ramadoss G, Muthukumar K (2016) Ultrason Sonochem 28:207–217
76. Chen Z-G, Zong M-H, Gu Z-X, Han Y-B (2008) Bioprocess Biosyst Eng 31:351–356
77. Tomke PD, Rathod VK (2015) Ultrason Sonochem 27:241–246
78. Zhao X, Bansode SR, Ribeiro A, Abreu AS, Oliveira C, Parpot P, Gogate PR, Rathod VK, Cavaco-Paulo A (2016) Ultrason Sonochem 31:506–511
79. Gumel AM, Annuar MSM, Chisti Y (2013) Ultrason Sonochem 20:937–947
80. Ceni G, Costa da Silva P, Lerin LA, Oliveira JV, Toniazzo G, Treichel H, Oestreich EG, de Oliveira D (2011) Enzyme and Microbial Technology 48:169–174

81. Fiametti KG, Ustra MK, de Oliveira D, Corazza ML, Furigo A Jr, Oliveira JV (2012) *Ultrason Sonochem* 19:440–451
82. Xiao Y, Yang L, Mao P, Zhao Z, Lin X (2011) *Ultrason Sonochem* 18:303–309
83. Wang Z, Wang R, Tian J, Zhao B, Wei X-F, Su Y-L, Li C-Y, Cao S-G, Ji T-F, Wang L (2010) *J Asian Nat Prod Res* 12:56–63
84. Kuo C-H, Hsiao F-W, Chen J-H, Hsieh C-W, Liu Y-C, Shieh C-J (2013) *Ultrason Sonochem* 20:546–552
85. Bansode SR, Rathod VK (2014) *Process Biochem* 49:1297–1303
86. Khan NR, Jadhav SV, Rathod VK (2015) *Ultrason Sonochem* 27:522–529
87. Lerin LA, Feiten MC, Richetti A, Toniazzo G, Treichel H, Mazutti MA, Oliveira JV, Oestreicher EG, de Oliveira D (2011) *Ultrason Sonochem* 18:988–996
88. Balen M, Silveira C, Kratz JM, Simões CMO, Valério A, Ninow JL, Nandi LG, Di Luccio M, de Oliveira D (2015) *Biocatalysis and Agricultural Biotechnology* 4:514–520
89. Alves JS, Garcia-Galan C, Danelli D, Paludo N, Barbosa O, Rodrigues RC, Fernandez-Lafuente R (2015) *Catal Today* 255:27–32
90. Baiyi A, Hailin F, Zhuofu W, Lu Z, Lei W, Zhi W, Guang C (2016) *Molecules* 21:565–572
91. Gumel AM, Annuar MSM, Chisti Y, Heidelberg T (2012) *Ultrason Sonochem* 19:659–667
92. Lee SH, Nguyen HM, Koo Y-M, Ha SH (2008) *Process Biochem* 43:1009–1012
93. Wang J, Wang S, Li Z, Gu S, Wu X, Wu F (2015) *J Mol Catal B Enzym* 111:21–28
94. Zang C-Z, Kan S-C, Yeh C-W, Lin C-C, Shieh C-J, Liu Y-C (2015) *Ultrason Sonochem* 26:415–421
95. Dinica RM, Furdui B, Ghinea IO, Bahrim G, Bonte S, Demeunynck M (2013) *Mar Drugs* 11:431–439
96. McCausland LJ, Cains PW (2004) *Biotechnol Genet Eng Rev* 21:3–10
97. Rueroft G, Hipkiss D, Ly T, Maxted N, Cains PW (2005) *Org Process Res Dev* 9:923–932

Nanostructured Materials Synthesis Using Ultrasound

Jordan J. Hinman¹ · Kenneth S. Suslick¹

Received: 11 November 2016 / Accepted: 21 December 2016
© Springer International Publishing Switzerland 2017

Abstract Recent applications of ultrasound to the production of nanostructured materials are reviewed. Sonochemistry permits the production of novel materials or provides a route to known materials without the need for high bulk temperatures, pressures, or long reaction times. Both chemical and physical phenomena associated with high-intensity ultrasound are responsible for the production or modification of nanomaterials. Most notable are the consequences of acoustic cavitation: the formation, growth, and implosive collapse of bubbles, and can be categorized as primary sonochemistry (gas-phase chemistry occurring inside collapsing bubbles), secondary sonochemistry (solution-phase chemistry occurring outside the bubbles), and physical modifications (caused by high-speed jets, shockwaves, or inter-particle collisions in slurries).

Keywords Sonochemistry · Nanomaterials · Microspheres · Nanoparticles · Ultrasonic

1 Introduction

The production of nanostructured materials through the effects of high-intensity ultrasonic irradiation of materials has been a subject of interest for more than two decades [1–5]. The ultrasonic irradiation of a liquid can cause effects over a large range of size scales, from the mixing and heating of the bulk liquid to the concentration of energy in microscopic hot spots intense enough to produce high-energy chemical

This article is part of the Topical Collection “Sonochemistry: From basic principles to innovative applications”; edited by Juan Carlos Colmenares Q., Gregory Chatel.

✉ Kenneth S. Suslick
ksuslick@illinois.edu

¹ Department of Chemistry, University of Illinois at Urbana-Champaign, 600 S. Mathews Av., Urbana, IL 61801, USA

Published online: 11 January 2017

Reprinted from the journal

59

 Springer

reactions. Both the physical and chemical effects of ultrasound have been utilized in the production of nanostructured materials. The complex and wide range of processes caused by ultrasound—both chemical and physical—provides a diverse palette for the formation of nanomaterials with a variety of compositions and structures.

The chemical effects of ultrasonic irradiation in a liquid are not the result of direct coupling of the sound waves to molecular species, as they occupy very different time and length scales. Rather, sonochemistry arises as a consequence of the implosive collapse of bubbles produced by acoustic cavitations [6]. The process of nucleation, growth, and collapse of bubbles during acoustic cavitation is shown graphically in Fig. 1. When a liquid is subject to sufficiently strong acoustic waves, dissolved gases or other impurities nucleate cavities (bubbles) within the liquid during rarefaction. Through successive cycles, the cavities grow through rectified diffusion—the decrease in cavity volume during compression is less than the growth during rarefaction due to the reduced surface area of the bubble during compression. When the bubble reaches a certain size (microns for 20-kHz ultrasonic irradiation) it becomes resonant with the ultrasonic radiation and can rapidly increase in size. Soon the bubble becomes unstable and violently collapses, producing a hot spot within the liquid medium [7].

Spectroscopic studies of the light emitted during cavitation (i.e., sonoluminescence) by Suslick et al. have shown that these implosions generate conditions of 5000 K and 1000 bar in clouds of cavitating bubbles and even more extreme conditions in isolated single bubble cavitation [6, 8–11]. It is within these regions of extreme conditions that chemical reactions occur. Suslick et al. also studied the rate of ligand substitution for metal carbonyl sonolysis as a function of metal carbonyl vapor pressure and found the sonochemical reactions must be taking place in two regions—gas phase and liquid phase [7, 12]. The liquid phase is mostly composed of droplets injected into collapsing bubbles [12], and perhaps a thin shell surrounding the collapsing bubble. Temperatures of the two sonochemical regions in low vapor pressure alkanes were determined to be 5200 and 1900 K for the gas

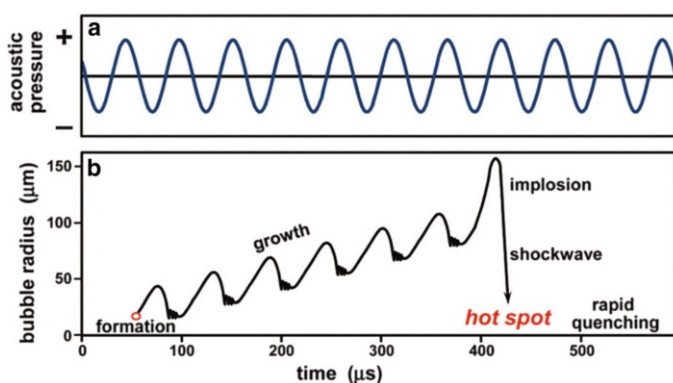


Fig. 1 Graphical representation of the growth and collapse of acoustic cavitation bubbles. As a liquid is irradiated with ultrasound, it is subjected to periodic compression and rarefaction (a). Bubbles formed in the liquid undergo expansion and compression and the size of the bubble oscillates until resonance occurs and implosive collapse follows (b). Reproduced with permission from Ref. [1]. Copyright 2012 Royal Society of Chemistry

phase and liquid phase, respectively. The extremely short lifetimes of cavitation events results in heating and cooling rates of more than 10^{10} K s^{-1} [6, 12]. As shown in Fig. 2, the conditions of sonochemistry are quite extreme in comparison to other chemical processes.

This review will focus on recent examples of the use of ultrasound for the synthesis of nanostructured materials and will be organized according to the mechanisms by which ultrasound can be used for the production of nanomaterials. Section 2 focuses on nanomaterials produced using the chemical effects of ultrasound, and this section is further divided by the use of primary sonochemistry or secondary sonochemistry. In Sect. 3, various methods for using the physical processes of ultrasound to create nanostructured materials are explored. This section is subdivided into (1) ultrasonic spray techniques to generate microdroplet reactors for the generation of nanostructured materials; (2) sonofragmentation and sonocrystallization; and (3) sonochemically produced protein microspheres, which are created by a combination of chemical and physical effects.

2 Chemical Effects of Ultrasound

As a result of the extreme conditions during cavitation bubble collapse, both physical and chemical processes are initiated. The implosive collapse of bubbles generates a shock wave that propagates out into the liquid medium. Bubble collapse near a solid surface disrupts the spherical symmetry of the bubble and causes the formation of microjets that can impact the surface in addition to the shock wave. These physical processes make ultrasonic irradiation an effective means to mix

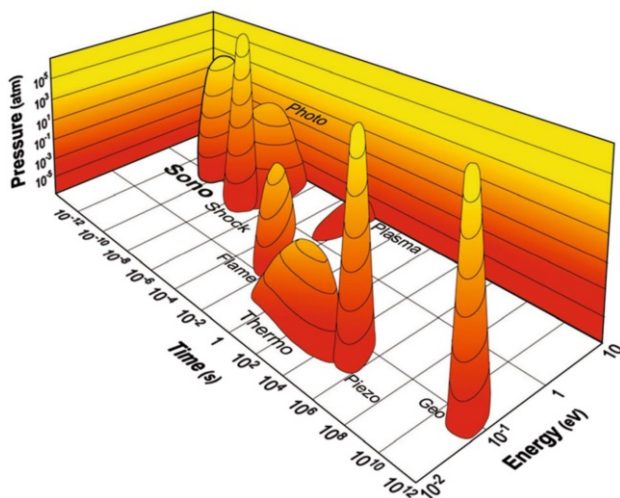


Fig. 2 Graph showing the “islands of chemistry”, a graphical comparison of the timescale, energy, and pressure of various chemical processes. As shown in the graph, sonochemistry is a comparatively fast, high-energy, and high-pressure process. These conditions allow for the sonochemical production of various materials. Reproduced with permission from Ref. [1]. Copyright 2012 Royal Society of Chemistry

liquids, erode solid surfaces, and facilitate interparticle collisions. Of course, another consequence of ultrasonic irradiation is the eventual bulk heating of the solution; with typical ultrasonic horns, ultrasonic intensities are $\sim 50 \text{ W cm}^{-1}$, such bulk heating can be significant in small liquid volumes.

Figure 3 provides a general scheme of the applications of sonochemical and ultrasonic processes to materials chemistry.

The chemical effects of ultrasound mostly derive from the hot spots created by collapsing bubbles. The effective compressional heating generates local temperatures high enough to cause the dissociation of all chemical bonds (up to and including N_2) [13]. Volatiles and gases present inside the collapsing bubble can undergo reaction and we refer to these as primary sonochemical reactions. Secondary sonochemical reactions occur involving these initially formed species after they have migrated into the surrounding liquid. Many radical species that will be formed within an ultrasonic hot spot can undergo a variety of secondary reactions with solutes in the surrounding liquid [14].

In the case where water is the sonicated liquid, sonolysis of water will generate highly reactive hydrogen atoms and hydroxyl radicals, and upon diffusion out of the hot spot, these species can initiate secondary sonochemical reactions (e.g., reductions, oxidation, hydroxylation of organics, etc.). The sonolysis of water is a well-studied process [15] and involves a number of rapid primary and secondary reactions that can also involve dissolved gases (e.g., O_2), as shown below.

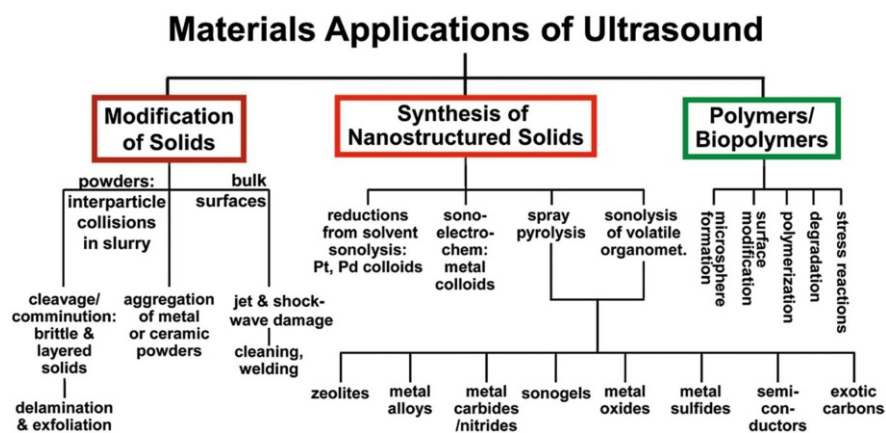
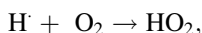
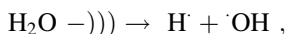
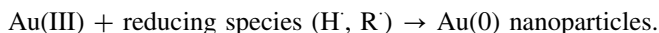
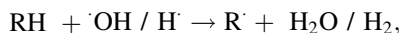


Fig. 3 This chart shows how the various physical and chemical aspects of ultrasound can be used in the production of nanostructured materials. Reproduced with permission from Ref. [1]. Copyright 2012 Royal Society of Chemistry

Thus, during the ultrasonic irradiation of aqueous solutions, both strong oxidants and reductants are formed, and the nature of the overall sonochemical reactions will depend on the conditions. The sonication of nonaqueous liquids also produces radical species [14, 16–18], which can undergo recombination, disproportionation and elimination reactions (e.g., similar to high temperature pyrolysis of hydrocarbons following Rice Radical Chain mechanisms), as well as redox reactions. For example, in the presence of an organic additive, species like Au(III) can be reduced [19], as discussed in more detail later:



2.1 Primary Sonochemistry for Nanoparticle Synthesis

The production of metal nanoparticles from volatile precursors has developed from the first report of amorphous iron nanoparticle synthesis [20]. When a volatile organometallic compound, such as $\text{Fe}(\text{CO})_5$, is dissolved in a low vapor pressure alkane solvent or ionic liquid [21, 22] and subjected to intense ultrasound, conditions favor dissociation of multiple metal–ligand bonds, and metal nanoparticles can thus be produced. Due to the short lifetime of a cavitation event, the particle is so rapidly cooled that crystallization is prevented, resulting in amorphous particles. The product appears as an agglomeration of 20-nm nanoparticles (Fig. 4). If oleic acid or a similar surfactant is added to the reaction mixture, colloidal iron nanoparticles 8 nm in diameter are obtained, as shown in the TEM image in Fig. 4 [23]. Using precursor compounds like $\text{Fe}(\text{CO})_5$ and $\text{Co}(\text{CO})_3\text{NO}$, amorphous iron, cobalt and mixed nanoparticles have been made [24].

The synthesis of amorphous metal nanoparticles can be modified by the addition of other reactants to yield a variety of nanomaterials. Addition of sulfur to a solution of $\text{Mo}(\text{CO})_6$ and subsequent sonication produces clustered and agglomerated nanoparticles of MoS_2 [25]. This product has a higher edge surface area than conventionally prepared MoS_2 , and the catalytic activity is only at the edges where Mo atoms are exposed, not on the flat sulfur faces. MoS_2 is the predominant industrial hydrodesulfurization catalyst, and the sonochemically prepared MoS_2 demonstrates comparatively high catalytic activity for hydrodesulfurization of thiophene as an example. The sonication of $\text{Mo}(\text{CO})_6$ [26] and $\text{W}(\text{CO})_6$ [27] in an aliphatic solvent produces molybdenum carbide and tungsten carbide, respectively. Sonication of $\text{Mo}(\text{CO})_6$ in the presence of air produces MoO_3 nanoparticles. When these precursors are sonicated in the presence of SiO_2 nanoparticles or other inorganic oxide particles, the catalytic material can be directly deposited onto a support during synthesis.

SiO_2 and carbon nanoparticles can also serve as removable templates to metal oxides or sulfides. After the sonochemical production of amorphous iron in the presence of carbon nanoparticles, exposure to air causes the particles to quickly oxidize, forming hollow iron oxide nanocrystals [28]. The crystallization is attributed to the energy generated during the combustion of the carbon nanoparticle template upon air exposure. Figure 5 shows the hollow nature of the resulting hematite nanoparticles. In a control experiment lacking the carbon template,

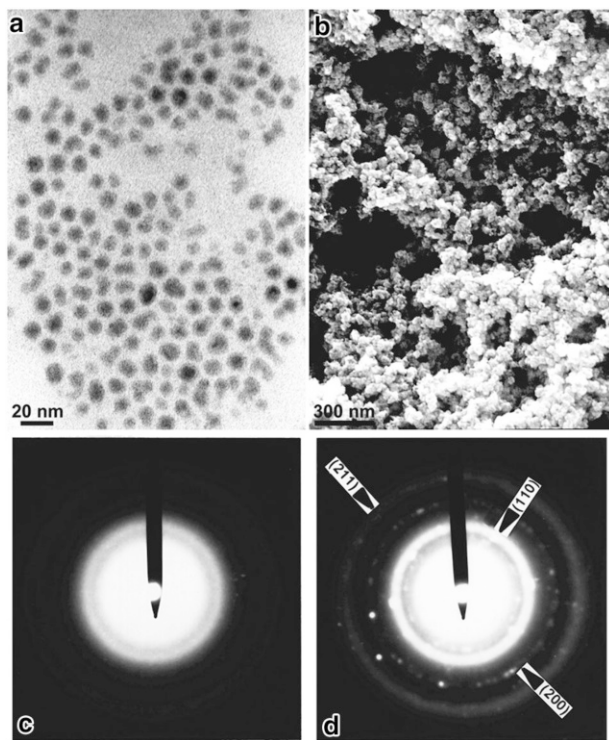


Fig. 4 **a** TEM showing sonochemically produced amorphous iron nanoparticles. **b** SEM of agglomerated amorphous iron nanoparticles. **c** The electron diffraction pattern of the as-produced iron colloid demonstrates its amorphous nature. **d** Heating from the electron beam induces crystallization in situ, as can be seen in the change of the electron diffraction pattern. Reproduced with permission from Ref. [23]. Copyright 1996 American Chemical Society

amorphous iron oxide particles were formed from amorphous iron. Similarly, the sonication of $\text{Mo}(\text{CO})_6$ with silica nanoparticles and sulfur or in the presence of air will produce hollow MoS_2 or MoO_3 particles, respectively [29]. An experiment showed the hydrodesulfurization catalytic activity of the sonochemically produced hollow MoS_2 nanospheres outperformed even the non-hollow sonochemically prepared MoS_2 . Washing the particles with HF removes the silica, leaving hollow nanoparticles. Annealing the MoO_3 particles forms hollow nanocrystals.

2.2 Secondary Sonochemistry for Nanoparticle Synthesis

Secondary sonochemistry, using a species produced within a cavitating bubble to effect chemical reactions in the liquid phase is widely employed, in part due to its ability to react with nonvolatile species. Even before the mechanisms of sonochemistry were fully understood, Baigent and Müller showed that ultrasound could be used as an alternative to traditional processes for the production of colloidal gold sols [30]. For a detailed discussion of the sonochemical production of metallic nanomaterials, refer to the recent review by Shchukin et al. [4]. Grieser and

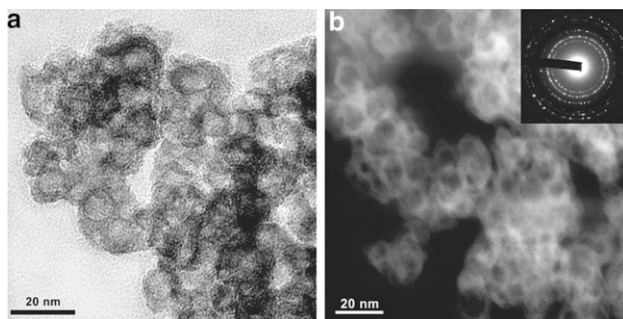


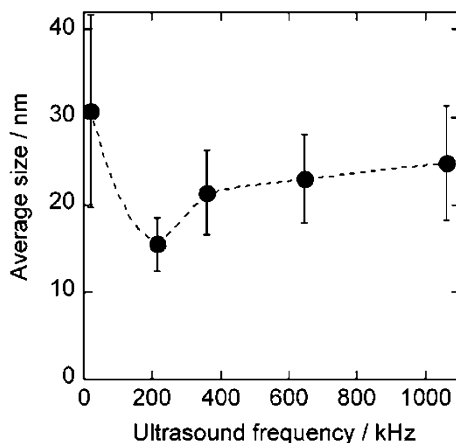
Fig. 5 TEM images of hollow hematite nanoparticles prepared sonochemically from iron pentacarbonyl and carbon nanoparticles in hexadecane. **a** Bright field TEM and **b** dark field TEM images show the nanoparticles and their hollow cores. The *inset* shows the selected-area electron diffraction pattern, demonstrating the crystalline nature of the nanoparticles. Reproduced with permission from Ref. [28]. Copyright 2007 American Chemical Society

coworkers described that when aqueous solutions of HAuCl_4 are sonicated in the presence of alcohols or a similar surfactant or organic additive, Au(III) is reduced to Au(0) , and gold nanospheres are formed. In a study of the effects of ultrasound frequency on the formation of gold nanoparticles ranging from 20 to 1062 kHz, the fastest rate of Au(III) reduction occurred using 213-kHz radiation [19] in the specific apparatus that they used (which was also the optimized mid-range of the instrument). The size of the gold nanoparticles was also smallest at 213 kHz, as shown in Fig. 6, although the effect on size is rather small compared to the errors in size measurement and may not be statistically significant.

Just as conventional nanoparticle syntheses are able to produce nonspherical nanoparticles, so too can sonochemical syntheses. In the presence of cetyltrimethylammonium bromide and AgNO_3 , gold nanorods can be formed [31]. Sonochemical nanoparticle synthesis techniques have been used to make gold nanobelts [32], gold nanodecahedra [33], and silver nanoplates [34]. Nie et al. have used the physical effects of acoustic cavitation to create gold nanoparticles with cone-like shapes [35]. In their proposed mechanism, 2-ethoxyaniline, a reductant, is dissolved in hexane. If mixed to with an aqueous gold solution, an emulsion forms. The gold is reduced at the hexane–water interface, forming hemispherical particles. If the phases are emulsified at much lower acoustic power with an ultrasonic bath, however, cone-like particles are made. The authors propose this may due to be a consequence of cavitation bubble collapse, although the exact mechanism is not at all clear; the cone shape may derive instead from larger, irregularly shaped micelles formed from the low acoustic intensities of a cleaning bath.

Ultrasound has been used to produce other noble metal nanoparticles as well. Mizukoshi et al. produced gold–palladium core-shell nanoparticles [36]; Au–Ag [37] and Au–Pt [38] have subsequently been produced as well. The sonochemical production of these core-shell bimetallic nanoparticles is likely in part due to the different reduction potentials for the different metal ions. In the Au–Pd system, the gold is reduced first and the nanoparticles serve as a nucleation site for Pd reduction [36]. Pt–Ru core shell particles were made by sequential sonication of a Pt solution

Fig. 6 A graph of gold nanoparticle size as a function of ultrasonic frequency. The particles size is minimized at 213 kHz, which corresponds to the maximum rate of Au(III) reduction observed at the same frequency. Reproduced with permission from Ref. [19]. Copyright 2005 American Chemical Society



followed by a Ru(III) solution in PVP or SDS [13]. Uniform bimetallic nanoparticles have also been produced sonochemically, including PtCu₃ [39], PdAg [40], and Pd/first-row transition metal particles [41].

Using poly(methacrylic acid) as a capping agent and hydroxyl radical scavenger, Suslick and coworkers were able to use high-intensity ultrasound to make extremely small (<2 nm) silver nanoclusters [42]. These nanoclusters exhibited a strong fluorescence at 610 nm, unlike larger silver nanoparticles, which do not exhibit fluorescence. Sonochemically produced Ag nanoclusters have been used for the detection of dopamine [43] and sulfide anions [44]. Gold nanoclusters [45] and copper nanoclusters [46] have been produced as well.

Sonochemistry has been employed to synthesize a variety of materials other than noble metals with a variety of structures. Among these materials, various metal oxide and hydroxide nanoparticles have been produced sonochemically, including MgO [47], Sr(OH)₂ [48], Dy₂O₃ [49], and Fe₃O₄ [50]. Metal oxides may be formed through sonochemical oxidation via radicals or through sonohydrolysis. Nanostructured zinc oxide is a material of interest as a wide band gap semiconductor, for use as a photocatalyst, and for its antimicrobial properties. Recently, a colloidal suspension of ZnO was produced when zinc acetate was ultrasonically irradiated in a basic solution with a colloidal stabilizer, poly(vinyl alcohol) [51]. The colloidal particles were 10 nm in diameter as determined by dynamic light scattering measurements.

To make a nanostructured ZnO layer as a matrix in an electrochemical sensor, ZnO nanorods and nanoflakes were grown on a Si substrate by sonicating a zinc salt with hexamethylenetetramine, which served as shape directing agent [52]. Similarly, ZnO nanoparticles have been sonochemically produced and simultaneously deposited on a textile surface in an effort to make an antimicrobial surface in a one-step process [53]. Silver [54] and CuO [55] nanoparticles have also been sonochemically formed on textiles and paper surfaces in a similar manner. The specific mechanism by which these nanoparticles inhibit microbial growth is not well understood, although it is well known that these metal ions are toxic to

bacteria. The ease of coating a variety of materials with inorganic nanoparticles using ultrasound may be useful for other applications besides antibacterial activity, such as modifying surface hydrophobicity.

Besides coating bulk textiles materials, sonochemistry can also be used to coat nanostructured surfaces with nanoparticles. Hierarchically structured ZnO microspheres were coated with sonochemically produced CdS nanoparticles as a photosensitizer to make a hierarchical photocatalyst that was more active through the absorbance of visible light than ZnO is alone [56]. While the ZnO was produced through a hydrothermal synthesis, CdS nanoparticles were produced by the sonication of an aqueous solution of cadmium chloride and thiourea with suspended ZnO microspheres. The thiourea was sonochemically reduced to produce sulfide anions, which precipitated with aqueous cadmium to form 50–100-nm spherical CdS nanoparticles (Fig. 7). The interface between the ZnO and the CdS nanoparticles is clean without a buffer zone between the two materials, as the TEM image of Fig. 7c demonstrates. It was suggested that the physical effects of the ultrasound may have a role in cleaning the ZnO surface and providing places for the CdS to nucleate. In photodegradation tests with rhodamine B, the hierarchical ZnO/CdS showed improved activity under solar irradiation than either material alone, which the authors attributed to more efficient charge separation in the composite material.

As with the metal nanoparticles, non-spherical nanoparticles can be made. Examples include ZnO nanorods and triangles [57], as well as SnO₂ nanobelts [58]. One example of this is the formation of Ag/AgCl nanocube plasmonic photocatalysts [59]. By sonicating a solution of silver nitrate, sodium chloride, and poly(vinyl pyrrolidone) in ethylene glycol, uniform nanocubes of AgCl (edge length 115 ± 20 nm) were produced with inclusions of silver nanoparticles, as shown in the SEM images in Fig. 8. The cubic shape was the result of particle growth in the presence of PVP. While the physical effects of the ultrasound helped increase the speed of Oswald ripening in the particles, some of the silver ions in solution were reduced to form silver nanoparticles by the radicals sonochemically generated. Some of these silver nanoparticles became embedded in the AgCl matrices of the nanocubes, giving them a mauve color rather than the usual white of AgCl alone. The Ag/AgCl nanocubes performed photocatalytic degradation of organic dyes better than other reported Ag/AgCl materials.

The ability of sonochemistry to prepare small particles quickly has motivated some research into the sonochemical preparation of porous materials as an alternative to more conventional, and often lengthy, solvothermal synthesis. In a comparative study, Jung and coworkers prepared MOF-177 (Zn₄O(BTB)₂, BTB=4,4',4''-benzene-1,3,5-triyl-tribenzoate) by solvothermal, microwave, and sonochemical methods using 1-methyl-2-pyrrolidone (NMP) as the solvent [60]. Both the microwave and sonochemical syntheses required only an hour to complete, in contrast to the 48 h required by the solvothermal method. Also, the particles produced by microwave and sonochemical methods were smaller than those produced using the conventional synthesis. The BET surface area of the microwave particles was less than that of the sonochemical and conventional particles, which

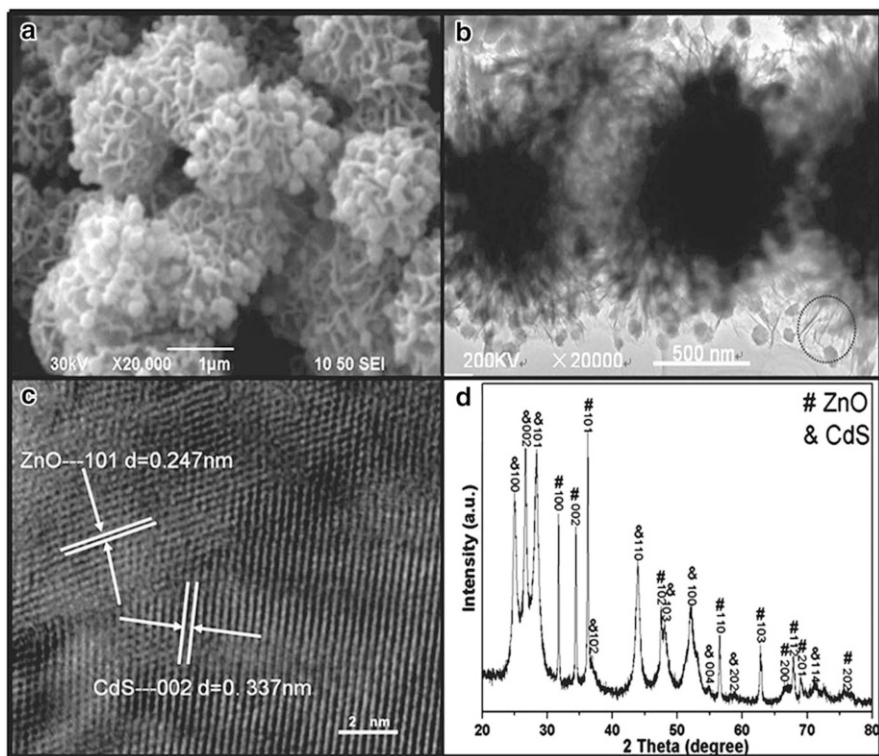


Fig. 7 ZnO/CdS hierarchical heterostructures. **a** SEM image showing CdS nanoparticles incorporated into the porous ZnO structure. **b** TEM of the ZnO/CdS hierarchical heterostructures. **c** High resolution TEM showing the heterojunction between a ZnO nanosheet and a CdS nanoparticle. The interface does not show any buffer layers. **d** Powder XRD pattern of the ZnO/CdS structures includes peaks from both phases. Reproduced with permission from Ref. [56]. Copyright 2012 Royal Society of Chemistry

had similar properties. In a test of CO₂ adsorption, the sonochemical particles exhibited the highest uptake of the three methods.

In another report, a sonochemical method for the preparation of Mg-MOF-74 (Mg₂(dhtp)(H₂O)₂·8H₂O, dhtp=2,5-dihydroxyterephthalate) was adapted from the conventional solvothermal method [61]. The sonochemical method did not work unless triethylamine was added to the solution to encourage deprotonation of the dhtp. Again, the sonochemical method was able to produce MOF particles with similar BET surface area and performance to the conventional preparation method in a reduced amount of time. The particle morphology differed between the methods. The conventional method produced agglomerated needle 14 μm particles, while the sonochemical method produced spherical 0.6 μm particles. Addition of triethylamine for the solvothermal method produced particles of intermediate structure and size, showing that this likely has some effect on the particle formation in addition to the ultrasound. The research of Ahn and coworkers has additionally produced sonochemical methods for the preparation of MOF-5 [62], ZIF-8 [63], and

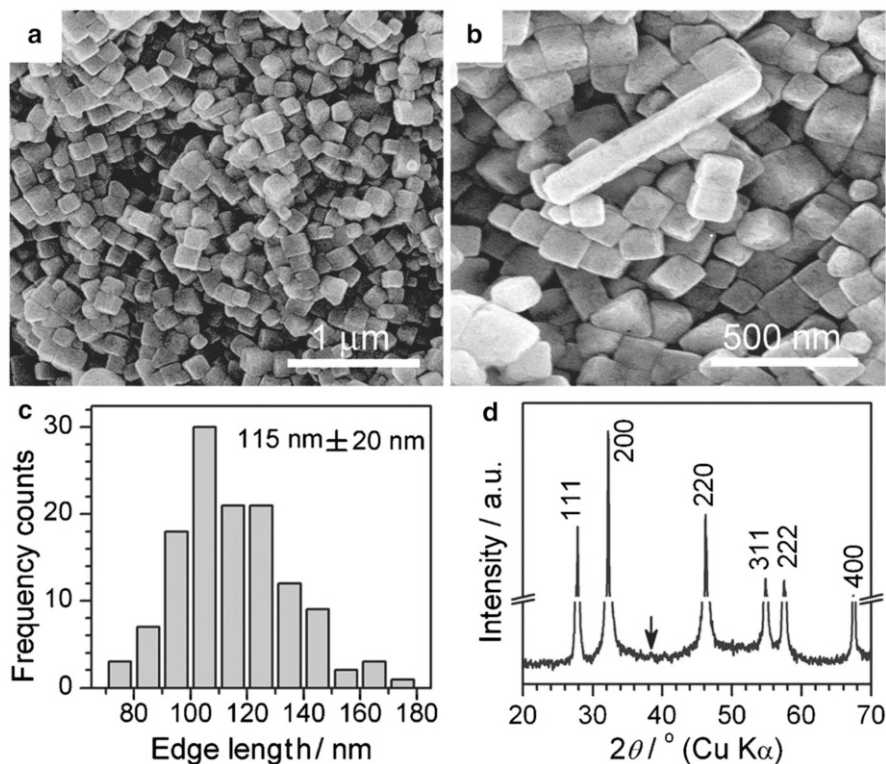


Fig. 8 **a, b** SEM images showing the cubic structure of the Ag/AgCl particles. **c** A histogram of the distribution of particle edge lengths. **d** The X-ray diffraction pattern of the Ag/AgCl particles is shown. The peaks match a cubic phase of AgCl, with the corresponding planes labeled. The *arrow* points to a weak peak that matches the Ag(111) plane. Reproduced with permission from Ref. [59]. Copyright 2012 Wiley-VCH Verlag GmbH & Co. KGaA

IRMOF-3 [64]. Other porous materials prepared by ultrasonic methods include manganese dioxide octahedral molecular sieves (OMS) [65].

Sonochemical synthesis of high surface area carbon materials have been of interest as well, as reviewed recently in detail by Skrabalak [66]. Much like the examples mentioned above, efforts have been made to deposit sonochemically produced nanoparticles onto a graphene substrate. Guo et al. prepared 5-nm TiO₂ nanoparticles deposited on graphene sheets by the ultrasonic irradiation of a suspension of graphene oxide with TiCl₄ in ethanol, followed by reduction of the graphene oxide [67]. The composite showed improved activity over TiO₂ alone in the photocatalytic degradation of methylene blue. The authors attribute this improvement in part to the ability of the graphene to reduce the recombination of electron-hole pairs. Sonochemistry has been used to couple graphene oxide and graphene to other nanoparticles as well, including Au [68] and Fe₃O₄ [69]. Graphene nanosheets themselves have reportedly been produced from the reduction of graphene oxide via the assistance of ultrasonic irradiation [70]. It was proposed that in addition to dispersing and activating the graphene oxide surface, the radical

species produced during cavitation collapse might also play a role in speeding up the reduction of graphene oxide by hydrazine.

Rather than prepare graphene through the reduction of graphene oxide, Xu and Suslick used sonochemistry to exfoliate graphene from graphite and simultaneously functionalize it with polystyrene to improve its dispersion [71]. Styrene was chosen as a suitable solvent for graphite exfoliation since it has a surface tension of 35 dyn cm^{-1} , which is a good match the surface energy of graphite. Also, under sonochemical conditions, styrene will produce radicals that can chemically attach to the surface of exfoliated graphene sheets and functionalize them, thus improving their dispersibility. This method produced a colloid of single- and few-layered graphene, as shown in the TEM of Fig. 9. The polystyrene-functionalized graphene was soluble in dimethylformamide, tetrahydrofuran, toluene, and chloroform, and the solutions were stable for months without precipitation. Other polymerizable solvents, like 4-vinylpyridine, were also able to produce functionalized graphene.

Sonochemistry has been useful in the synthesis of other carbon nanomaterials as well. Jeong et al. ultrasonically irradiated a suspension of silica powder in *p*-xylene with a small amount of ferrocene to produce single-walled carbon nanotubes (SWCNTs) [72]. The ferrocene decomposed as described above into amorphous iron particles that were able to catalyze the formation of the SWCNTs, and the *p*-xylene was the carbon source. Recently, Ha and Jeong reported the sonochemical formation of multiwalled carbon nanotubes (MWCNTs) as well [73]. The synthesis of MWCNTs was similar to that of SWCNTs but required a higher concentration of ferrocene in the reactant mixture as well as the addition of a small amount of water. With some adjustment, the authors propose this method may be modified to produce fullerenes and carbon onions.

Sonochemistry can also play a role in traditional carbon nanotube syntheses. Sonication is a popular method to disperse individual SWCNTs in solutions. Amide solvents, such as *N*-methyl pyrrolidone (NMP), tend to disperse SWCNTs well. Yau et al. investigated small impurities present when SWCNTs are dispersed in NMP [74]. They found that these impurities could be produced in NMP alone after similar ultrasonic treatment and are likely the result of sonochemical degradation of NMP.

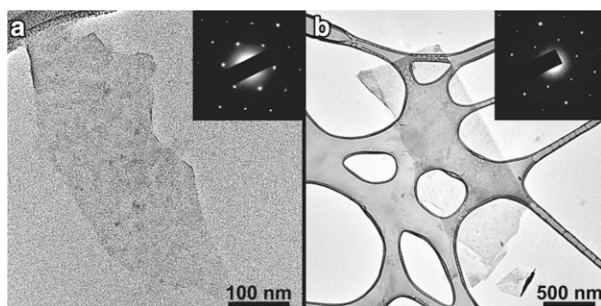


Fig. 9 TEM images showing **a** single-layer and **b** trilayer polystyrene-functionalized graphene prepared sonochemically. The *insets* in each image show the selected area electron diffraction patterns of the graphene samples, confirming the specimen structure. Reproduced with permission from Ref. [71]. Copyright 2011 American Chemical Society

Thermogravimetric analysis of the SWCNTs dispersed in NMP using ultrasound exhibited significant decomposition at 350–500 °C, whereas as-received SWCNT bundles and SWCNTs soaked in NMP without sonication lost only 10% of their mass over the 200–850 °C temperature range. These results suggest that the NMP degradation products adhere to or react with the sonicated SWCNTs, which may be important for their dispersion but detrimental to their thermal stability.

The production of luminescent carbon nanodots (CDs) via ultrasound by Xu et al. is both a further example of another possible carbon material made through sonochemistry as well as an instance where the delineation of primary and secondary sonochemistry becomes ambiguous [75]. The CDs were made from the sonication of an aqueous solution of citric acid as the carbon source and ethylenediamine as an N-doping source, both in rather high concentration (0.5–1 M). Sonication of the solution for 8 h produced 3–7-nm particles, as measured by TEM. X-ray diffraction suggested the particles were amorphous. The CDs had an absorbance band at 354 nm and luminescence at 450 nm when excited with 360-nm light. By optimizing the citric acid/ethylenediamine ratio and concentration, particles with a quantum yield up to 77% were made. This is high in comparison to other reported CD synthesis methods.

Xu et al. observed that the duration of sonication did not have a large impact on the CD quantum yield. If the CDs were formed from secondary reactions in solution, longer sonication should increase particle size and influence luminescence properties. Thus, they proposed that the CDs are formed within the collapsing bubbles. As shown in the diagram in Fig. 10, since citric acid and ethylenediamine are not volatile, they are entering collapsing bubbles via the injection of nanodroplets caused by unstable bubble collapse, as described earlier. In the intense conditions of the collapsing bubble, the droplet solvent evaporates, and the reactants are pyrolyzed to form the CDs. To further test this proposed mechanism, the citric acid was replaced with $M_w = 1800$ Da polyacrylic acid, and CDs were still formed. CDs have also been prepared in other studies using glucose and poly(ethylene glycol) as the carbon source [76].

3 Physical Effects of Ultrasound for Nanoparticle Production

The physical effects of high-intensity ultrasound (microjet formation, turbulence, rapid mixing, shock wave formation, and interparticle collisions in slurries) are also often important in the formation of nanostructured materials. As discussed earlier, cavitation collapse of bubbles generates shock waves that propagate out into the liquid medium. Bubble collapse near a solid surface is non-spherical and causes the formation of microjets that can impact surfaces and eject material out into solution. Turbulent flow and microstreaming make ultrasonic irradiation an effective means to mix liquids, erode solid surfaces, and facilitate interparticle collisions in suspensions of solid particles in liquids [1, 3, 5, 77–79].

This is exemplified by the production of ZnO hierarchically structured microspheres by Wang et al. [80]. They precipitated ZnO from an aqueous solution of $Zn(NO_3)_2$ and NaOH. The ZnO precipitated as interconnected nanosheets,

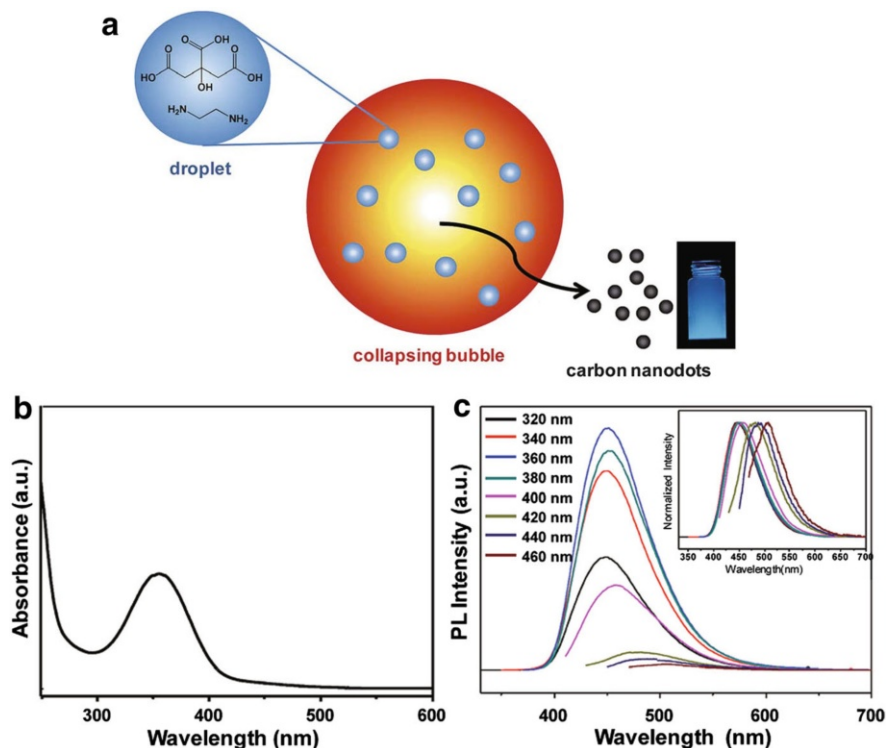


Fig. 10 **a** Schematic diagram of proposed sonochemical synthesis of carbon nanodots from aqueous citric acid. It was proposed that droplets containing citric acid are injected into collapsing cavitation bubbles, where the solvent is quickly evaporated and the citric acid pyrolyzed in the extreme sonochemical conditions, thus forming carbon dots. **b** UV/Vis absorption spectrum and **c** emission spectra of sonochemical carbon dots from various excitation wavelengths. Adapted with permission from Ref. [75]. Copyright 2014 Royal Society of Chemistry

forming flower-like structures. In the absence of ultrasonic irradiation, however, the structures took a longer time to form, were less uniform in size, and exhibited morphology differing from the nanosheets in places. These structures are shown for comparison in Fig. 11. The researchers attribute the structure of the ultrasonically irradiated samples to improved nucleation and diffusion as a result of ultrasound. They hypothesize that the hot spots generated via ultrasound increase the nucleation of the ZnO nanosheets and the shockwaves and microjets improve diffusion and dispersal of nanocrystals. A further experiment of interest would be to precipitate the ZnO while using a high-speed mixer to assess whether improved nucleation through hot spot generation is necessary for the formation of the hierarchical structures or if improved mass transfer suffices.

Similarly, the changes of the size and distribution of ZIF-8 (ZIF = zeolitic imidazolate framework, a Zn^{2+} -imidazolate metal-organic framework) nanoparticles under sonication utilizes the physical effects of ultrasound to alter the structure of nanoparticles [81]. ZIF-8 is prepared through precipitation when methanol

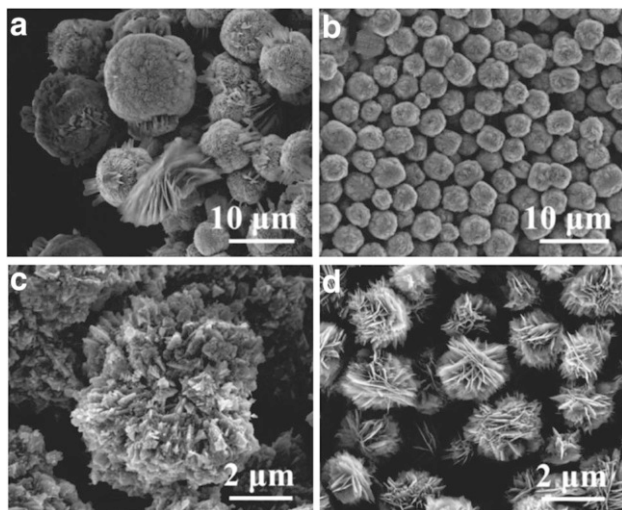


Fig. 11 SEM images demonstrating the effect of ultrasound on the precipitation of ZnO materials. In **a**, **c** ultrasound was not used, resulting in ZnO precipitates that vary widely in size and structure. In contrast, **b**, **d** show ZnO precipitates that were produced with sonication. The particles show a more uniform size distribution and exhibit nanosheet structures at higher magnification (as in **d**). The authors attribute these differences in morphology to the enhanced mixing caused by ultrasound, minimizing local inhomogeneous diffusion and nucleation. Reproduced with permission from Ref. [80]. Copyright 2013 American Chemical Society

solutions of zinc nitrate and 2-methylimidazole are mixed together, making particles about 200 nm in diameter. When these particles are subjected to sonication some particles increase in size while others diminish, resulting in a bimodal distribution. This bimodal distribution is evidence of Ostwald ripening. It is thought that cavitation events near the surface of the nanoparticles help facilitate the dissolution of the smaller particles, and the diffusion of materials in solution is also enhanced by the ultrasound.

3.1 Ultrasonic Spray Pyrolysis for Nanomaterials

Another method that utilizes the physical effects of ultrasound to make nanostructured materials is ultrasonic nebulization (also known as “atomization”, which of course it is not!). Ultrasonic irradiation of liquids with sufficient intensity can cause the ejection of liquid droplets from the crests of capillary waves on the liquid surface. The droplets ejected are of a generally uniform size, and the average size can be predicted from the Lang equation [82]:

$$D = 0.34 \left(\frac{8\pi\gamma}{\rho f^2} \right)^{1/3},$$

where D is the diameter of the droplet, γ is the surface tension of the liquid, ρ is the liquid density, and f is the frequency of the ultrasonic irradiation. For water nebulized with a 1.65-MHz transducer, the average droplet size is about 3 μm in

diameter. Each droplet is a small, individual chemical reactor that can be flowed through heat, light, or other stimuli to induce chemical reactions. One of the advantages of ultrasonic nebulization is that dense mists can be formed independent of gas flow rate. In addition, it is an easily scaled technique for both laboratory and pilot plant production. By varying reactants, solvent, auxiliary additives, reactor temperature, etc, a variety of different materials with nanostructured morphology can be produced.

Ultrasonic spray pyrolysis (USP) sends an ultrasonically nebulized precursor solution into a carrier gas stream through a heated region, where thermal decomposition can be used to create nano- and micromaterials [2, 3]. A diagram of a typical apparatus used for USP reactions is given in Fig. 12. A more detailed review of the principles and variations of USP has recently appeared [83]. Besides the obvious similarity of both sonochemistry and USP utilizing ultrasound, the two techniques also both restrict reaction zones into sub-micrometer regions—sonochemistry occurs in hot gaseous regions within the cavitation bubble a liquid medium, while USP uses hot liquid droplets isolated in a gas flow. A wide variety of nanostructured materials can be made with ultrasonic spray techniques, such as metals, metal oxides, carbon, semiconductor materials, and polymers.

The simplest forms of particles that USP will form are compact, solid microspheres and hollow shells. Whether solid or hollow particles are made can in part be described by the Peclet number, or the ratio of the solvent evaporation rate to the rate of solute diffusion through the droplet. If solvent evaporation is fast or the material quickly precipitates and forms, hollow shells can be produced. These shells may break apart, forming either a dense agglomeration of particles or small fragments, depending upon the material.

In a recent example of the formation of solid particles by an ultrasonic spray method, Suslick et al. prepared silicone microspheres [84]. The production of polydimethylsiloxane (PDMS) microsphere through emulsion polymerization (the typical method of making polymer microspheres) results in polydisperse particles with large sizes (100 μm) due to the very low surface energy of silicones; other methods that can make small microspheres could only produce particles one at a

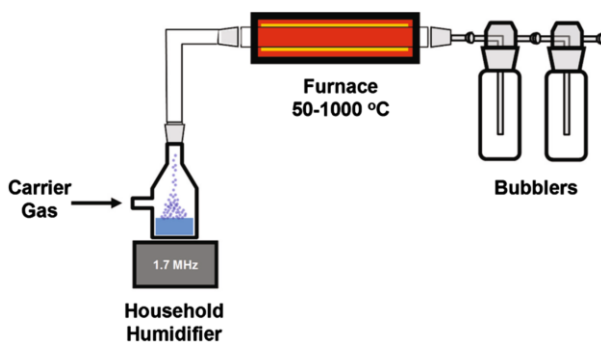


Fig. 12 Simplified diagram of the apparatus used for ultrasonic spray pyrolysis. The household humidifier has a 1.7-MHz ultrasonic transducer to induce nebulization of the reactant solution

time. By generating individual particles through an ultrasonically generated mist, however, microspheres of a uniform size can be readily prepared in quantity. Generally, PDMS oligomers were diluted in hexane or toluene solutions. The mist of this solution was conveyed through a 300 °C tube furnace on an Ar stream, where the solvent evaporated and the PDMS oligomers crosslinked to form solid microspheres <math><2\ \mu\text{m}</math> in diameter with a narrow size distribution. The size of the PDMS microspheres could be controlled by varying the concentration of the precursor solution, as shown in Fig. 13.

In order to explore the potential utility of the PDMS microspheres, several modifications were made to the basic preparation to produce a variety of microspheres. Incorporating Nile red into the precursor solution resulted in fluorescent PDMS microspheres. Even after thorough washing, the dye was still retained within the microspheres and made the microspheres fluorescent. To test whether the microspheres could be used for drug delivery, Rhodamine 6G was used

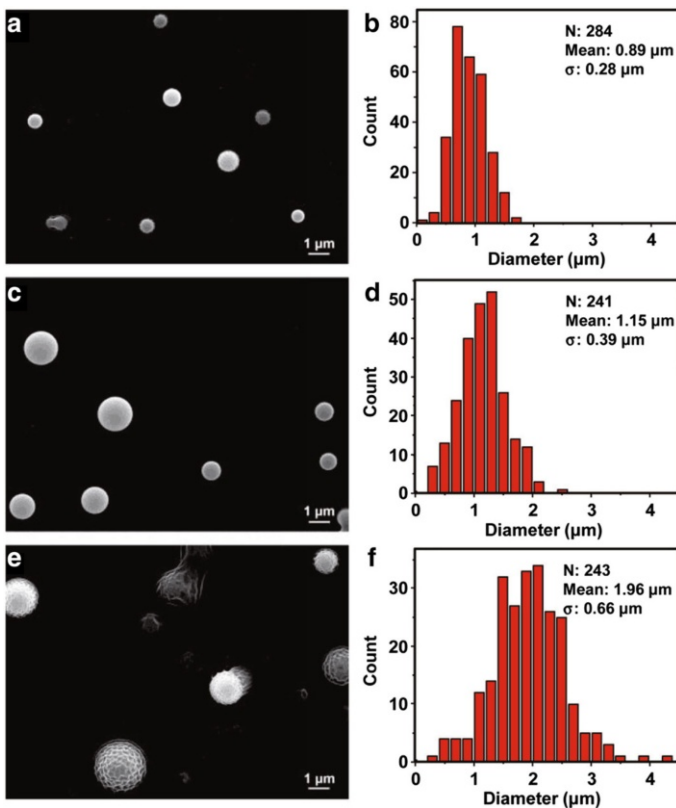


Fig. 13 The size of PDMS (polydimethylsiloxane) microspheres can be controlled by varying the concentration of PDMS in the precursor solution. These SEM images show PDMS microspheres prepared using **a** 4 mg mL⁻¹, **c** 20 mg mL⁻¹, **e** 100 mg mL⁻¹ PDMS in hexanes. **b**, **d**, **f** Size distributions of microspheres shown in **a**, **c**, **e**, respectively. Reproduced with permission from Ref. [84]. Copyright 2015 Wiley-VCH Verlag GmbH & Co. KGaA

to assess the loading and release properties of the PDMS microspheres with small hydrophobic molecules. The microspheres exhibited only 25% release after 200 h in phosphate buffered saline, likely due to the inhibition of particle wetting owing to the hydrophobicity of the PDMS. Incorporation of polar side chains or copolymers improved release properties. Magnetic cores could be incorporated into the PDMS microspheres by adding Fe_3O_4 nanoparticles to the precursor solution, which may make PDMS microspheres a possible platform for MRI contrast agents. Cytotoxicity studies showed that PDMS microspheres are not toxic to cells, even at a concentration of 10^5 microspheres/cell.

Suslick and coworkers have used USP to produce hollow microspheres of ZnS:Ni^{2+} [85] and aluminum metal [86]. The hollow ZnS:Ni^{2+} were formed from the removal of a colloidal silica core with HF etching. The segregation of ZnS toward the surface of the microsphere is attributed to low solubility of ZnS and its precursors in the aqueous precursor solution, causing it to precipitate out of solution soon after heating. The thin shell aluminum metal particles were formed by a slightly different mechanism, owing to the reaction of gaseous TiCl_4 as a reductant with trimethylamine aluminum hydride at the surface of the nebulized droplets. Conditions can be adjusted to form shells that are nonporous and trap some of the precursor solvent and TiCl_4 .

Materials made with USP are often porous. Porosity can be produced from the decomposition of the precursors, or it can be introduced through the use of templates. Some porous microspheres produced using aerosol procedures include γ -alumina [87], titania [88], and TiN [89]. The synthesis of MoS_2 by USP exemplifies the use of colloidal silica templates making porous nanostructured microparticles [90]. Microspherical particles were made from an aqueous precursor solution of colloidal silica and $(\text{NH}_4)_2\text{MoS}_4$. Silica in the microsphere product was etched away with HF, leaving a highly porous MoS_2 microspheres. Highly porous metal oxide particles can also be prepared using USP with template nanoparticles. The use of a colloidal silica template has been used to make porous titania microspheres [91]. When Suslick and coworkers added other transition metals [Co(II), Cr(II), Mn(II), Fe(II), and Ni(II) salts] to the Ti/Si precursor and partially etched the silica, the resulting microspheres had a ball-in-ball structure of a silica sphere within a porous titania shell, shown in Fig. 14.

Besides colloidal silica, other template materials can be used as well to increase the porosity of USP-produced particles. Colloidal polymeric particles, such as polystyrene, have been used in the production of porous silica microspheres. Polystyrene templates can be removed in the heated reaction zone through pyrolysis, thus requiring no additional removal steps after the product is collected. Suslick and Suh used styrene in a sequential heating setup to template worm-like pores into silica microspheres [92]. The styrene polymerized in the first heated zone, then a second hotter zone was used to decompose and remove the template.

Porous carbon microspheres have also been prepared through the use of colloidal silica templates. Lu and coworkers have used a sucrose precursor solution with different types and amounts of silica to produce carbon microspheres with a range of structures [37, 93, 94]. Recently, Choi and coworkers adapted a procedure to produce porous carbon microspheres to include the addition of silicon nanoparticles

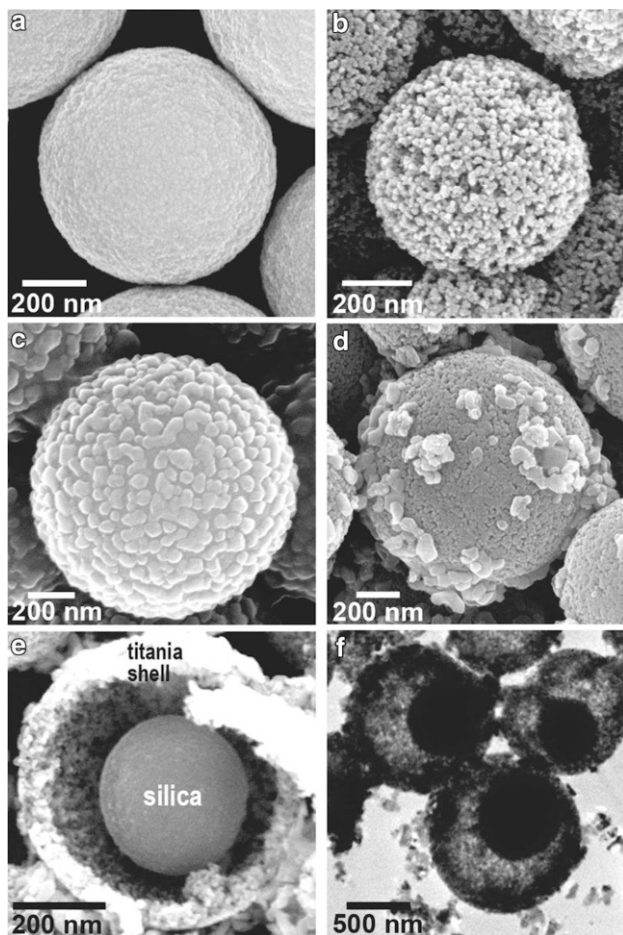


Fig. 14 Electron microscope images of ball-in-ball hollow titania microspheres produced by USP. **a** SEM images of titania and silica microspheres as prepared by USP and **b** after HF etching. **c** SEM of silica and titania microspheres prepared with cobalt shows cobalt oxide particles on the surface of the microsphere, and **d** the microspheres after etching. The ball-in-ball morphology of the etched titania/cobalt oxide microspheres is demonstrated by **e** SEM and **f** TEM. Reproduced with permission from Ref. [91]. Copyright 2006 Wiley-VCH Verlag GmbH & Co. KGaA

[95]. Ultrasonic nebulization of an aqueous sucrose solution containing silicon and silica nanoparticles followed by subsequent pyrolysis and HF etching produced porous carbon microspheres with embedded Si nanoparticles. This composite material was tested as an anode in a lithium ion battery since Si is known to have a large theoretical capacity. The microspheres exhibited high capacity, and retained 91% capacity over 150 cycles. The incorporation of Si nanoparticles in the porous carbon network allowed room for the Si to expand during electrochemical cycling. The coupling of porous carbon for the development of battery electrode materials using USP has also produced microspheres incorporating MoO_3 for lithium ion

batteries [96], sulfur for lithium–sulfur batteries [97], and $\text{Na}_2\text{FePO}_4\text{F}$ for sodium ion batteries [98],

Another templating method is to use precursor materials that form in situ templates upon reaction. For example, porous carbon microspheres have not only been produced through the use of colloidal templates, but also by in situ templates generated by the decomposition of the precursor materials. Porous carbon microspheres have been produced via USP using alkali carboxylates [99] and sucrose [100] as precursor materials. Salts generated by the decomposition of these precursors can act as templates for porosity which are dissolved away upon collection in a suitable solvent. Gaseous products generated by the precursor decomposition may also act as porogens. The nature of the precursor affects the nanostructure of the carbon microspheres. Figure 15 demonstrates the effect of using different alkali metal chloroacetates to produce very different structures in the resulting carbon microspheres.

Despite the production of a variety of porous metal oxides by USP, porous iron oxide had not yet been successfully prepared until recently. Suslick and Overcash were able to produce highly porous iron oxide microspheres using ferritin core analogs (Spiro–Saltman balls) as the precursor material [101]. When the precursor was prepared by mixing $\text{Fe}(\text{NO}_3)_3$ and Na_2CO_3 , porous microspheres with a BET surface area of $301 \text{ m}^2 \text{ g}^{-1}$ were produced. In contrast, replacing $\text{Fe}(\text{NO}_3)_3$ with FeCl_3 produces hollow porous spheres with a BET surface area of only $97 \text{ m}^2 \text{ g}^{-1}$. This difference is attributed to the lack of nitrate decomposition, which acts as a

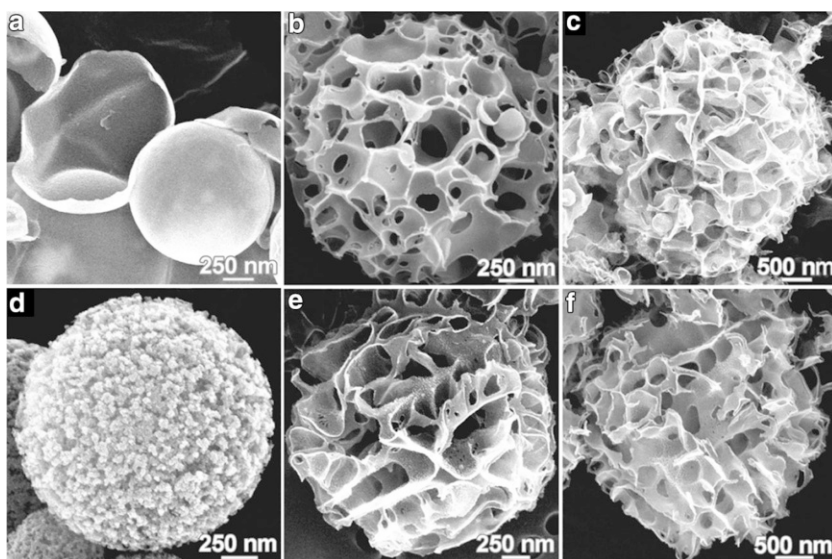


Fig. 15 SEM images of porous carbon microspheres produced by USP. The different morphologies of the microspheres result from the use of different precursor materials: **a** lithium chloroacetate (LiCA), **b** NaCA, **c** KCA, **d** lithium dichloroacetate (LiDCA), **e** NaDCA, and **f** KDCA. Reproduced with permission from Ref. [99]. Copyright 2006 American Chemical Society

porogen during pyrolysis by releasing gases (NO_x) in situ. Mixing the iron salts produced microspheres with intermediate properties.

Suslick and coworkers have also developed porous MnO_2 microspheres for use as a supercapacitor material [102]. Synthesis requires only a precursor solution of KMnO_4 and HCl in water. Depending on the reaction temperature, porous or crystalline microspheres could be formed. The different microspheres produced by varying the temperature are shown in the TEM images in Fig. 16. Optimized reaction conditions yielded microspheres which demonstrated a specific capacitance of 320 F g^{-1} . While the microspheres performed best at low charging and discharging rates, coating with poly(3,4-ethylenedioxythiophene) (PEDOT) improved the microsphere performance at higher charge/discharge rates. PEDOT microspheres themselves were also prepared by ultrasonic spray polymerization of a solution of EDOT and an oxidant [103]. The choice of oxidant affected the morphology of the microspheres, yielding either solid, hollow, and porous microspheres. The microspheres had a specific capacitance of 160 F g^{-1} , which is comparatively high relative to other reports of PEDOT materials.

While generally microspherical morphology predominates the products of USP, Skrabalak and coworkers were able to produce crystalline nanoplates using USP. Through the combination of USP with a molten salt synthesis, NaInS_2 nanoplates were prepared [104]. To prepare these nanoplates, InCl_3 and excess Na_2S are combined in water and react to form In_2S_3 nanoparticles and dissolved NaCl . Upon nebulization, the droplets are carried by a N_2 stream into a 625°C furnace. The water evaporates, leaving behind a molten salt flux. Within this flux, NaInS_2 crystals

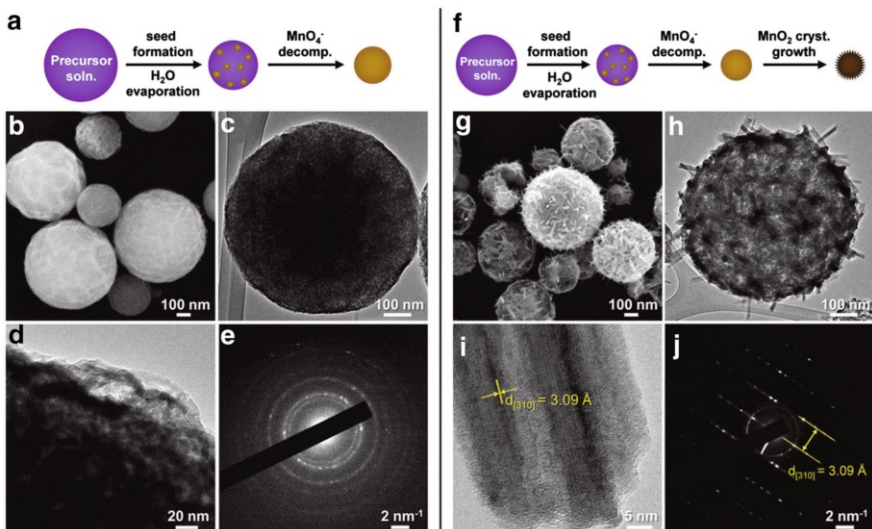


Fig. 16 Morphology of MnO_2 microspheres produced via USP varies according to reaction temperature, as demonstrated by comparison of materials produced at **a–e** 150°C and **f–j** 500°C . As shown in the **c, d, h, i** TEM images, increasing the reaction temperature causes the formation of larger crystals. Also shown are **b, g** SEM images, and **e, j** electron diffraction patterns. Reproduced with permission from Ref. [102]. Copyright 2015 Wiley-VCH Verlag GmbH & Co. KGaA

nucleate and grow to form hexagonal plates. After collection, the salt flux was removed from the nanoparticles with simple washing, yielding individual single-crystalline nanoplates. Figure 17 shows the NaInS_2 plates in comparison to the same material produced through a non-USP method. Without using USP, a similar reaction produced particles without any particular structure or size. The NaInS_2 nanoplates were used to construct a photoanode. USP-produced NaInS_2 photoanodes outperformed the non-USP samples. The coupling of USP and molten salt syntheses has been used to produce NaSbO_3 nanoplates [105], Fe_2O_3 nanoplates, rhombohedra, and octahedra [106], and CoFe_2O_4 nanoplates and octahedra [107]. With this technique, scalable flow chemistry can be used to produce unagglomerated, shaped colloidal particles.

The method used by Skrabalak bears similarity to the salt-assisted aerosol decomposition technique developed by Okuyama et al. [108]. This technique involves the production of nanoparticles via USP by preparing single salt or eutectic mixtures of alkali chlorides and nitrates along with the nanoparticle precursor salts so that nanoparticles could nucleate within the molten salt droplet during droplet heating. They reported the synthesis of $\text{Y}_2\text{O}_3\text{-ZrO}_2$, Ni, Ag-Pd, CdS, ZnS, LiCoO_2 ,

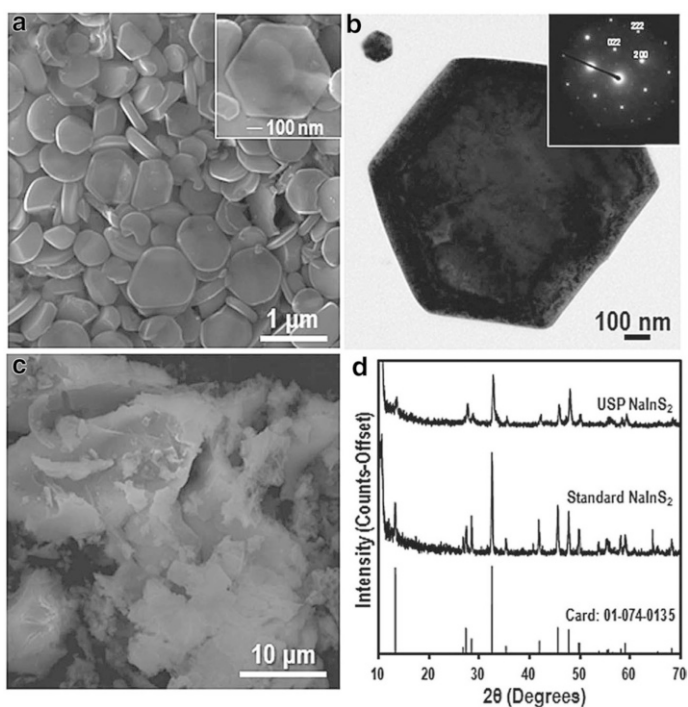


Fig. 17 Comparison of NaInS_2 produced by conventional means and molten salt-assisted USP. **a** SEM and **b** TEM images of the nanoplates produced via USP show the hexagonal shape of the nanoplates, and the inset electron diffraction pattern in **B** demonstrates the single-crystalline nature of the nanoplates. **c** An SEM image of NaInS_2 prepared through a non-USP method for comparison. **d** X-ray diffraction patterns of the USP and non-USP materials, as well as a reference for comparison. Reproduced with permission from Ref. [104]. Copyright 2012 Wiley-VCH Verlag GmbH & Co. KGaA

La_{0.8}Sr_{0.2}Co_{0.5}O_{3-x} [108], and CeO₂ [109] nanoparticles using this method, with these nanoparticles exhibiting higher crystallinity than particles produced without the additional salt.

Another similar technique for the production of nanoparticles by USP is chemical aerosol flow synthesis (CAFS), a method developed by Suslick and Didenko [110]. Rather than using salts and aqueous solutions, CAFS is performed with organic solvents. Precursor solutions are prepared with a solvent mixture composed of a high boiling solvent that will serve to establish liquid droplets in the heated zone where nanoparticles can form and a low boiling solvent that can dilute the precursor so that it can be nebulized. This method was used to produce semiconducting nanoparticles (i.e., quantum dots) of CdS, CdSe, and CdTe. As a specific example, for the production of ternary CdTeSe quantum dots [111], the Cd and chalcogenide precursors were prepared in octadecene with oleic acid and diluted with toluene. The toluene evaporates as the droplet is heated, and oleic acid-stabilized nanoparticles form in the hot droplets. Particle size could be changed by adjusting the temperature of the tube furnace, giving particles with emissions through the visible region. A blue shift in fluorescence was also observed for the ternary quantum dots due to photo-oxidation, as shown in Fig. 18. The CAFS synthesis of ternary quantum dots allowed emissions to be tuned into the far red and infrared regions as well.

3.2 Sonocrystallization and Sonofragmentation

The application of ultrasound to the preparation of crystalline materials has been an area of interest since the 1950s [112]. Sonocrystallization, using ultrasonic irradiation to aid in the crystallization of materials, is able to produce small crystals of uniform size distribution. The exact means by which ultrasonic irradiation aids in the crystallization of materials is not entirely clear; however, ultrasonic irradiation has been observed to reduce the induction time of crystal nucleation. Also, the width of the metastable zone, the region on a solubility graph between the temperature where equilibrium saturation is reached and the temperature where nucleation is observed, is reduced as well by the use of ultrasound [112]. Bubble collapse may produce areas of increased concentration that may increase the rate of nucleation. Also, the cavitation bubble surface itself may serve as a site for heterogeneous nucleation of crystals. Secondary nucleation can result from the erosion of crystal surfaces during cavitation.

Sonocrystallization has is a promising technique for the pharmaceutical industry. The size and uniform dispersity of pharmaceutical agents can be very important for its intended function, affecting the rate of solubility, how well the material can be delivered, and even its toxicity during use; in other circumstance, control of particle size is critical for efficacious delivery: for example, aerosol delivery of PAs has an optimal particle size, and for parenteral (e.g., intravenous) administration, crystals must be <5 μm to avoid embolisms. Sonocrystallization has been used to prepare crystals of acetylsalicylic acid [113], ibuprofen [114], cloxacillin benzathine [115], and paracetamol [116] in recent studies. For both the ibuprofen and paracetamol studies, sonocrystallization not only produced nano- and microcrystals, but these

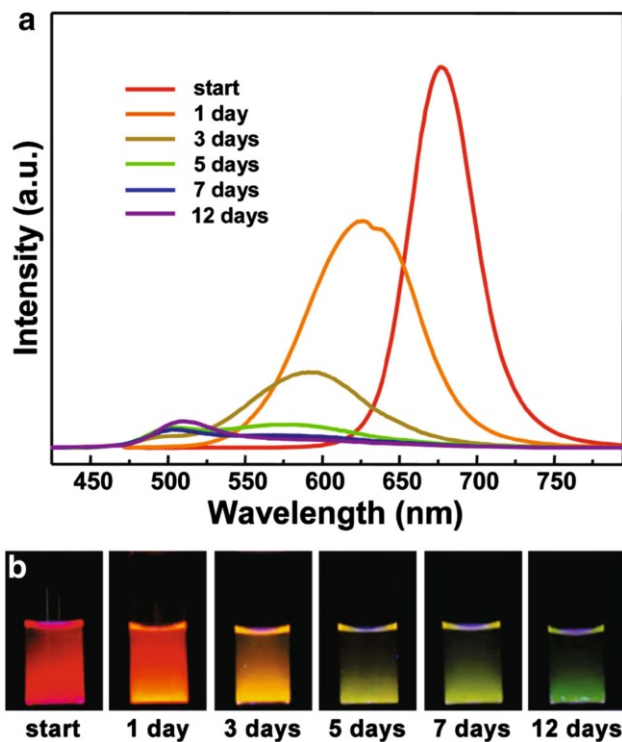


Fig. 18 USP-prepared CdTeSe quantum dots exhibited a blue-shift in fluorescence due to photo-oxidation. The **a** photoluminescence spectra and **b** photographs show the change in fluorescence with time as the CdTeSe quantum dots are exposed to light and air. Reproduced with permission from Ref. [111]. Copyright 2008 American Chemical Society

crystals exhibited better compactibility when forming tablets than conventionally made crystals. The properties responsible for improved compactibility are not entirely clear for either material, although in the case of the ibuprofen the researchers point to slight differences of the powder x-ray diffraction pattern from the reference crystalline material as an indication of possible differences of crystal habit.

Suslick et al. recently developed a spray sonocrystallization method for the preparation of 2-carboxyphenyl salicylate (CPS) [117]. An ethanol solution of CPS was mixed with water, an antisolvent, while passing through a specially prepared ultrasonic horn with a hollowed bore, shown schematically in Fig. 19. This produced well-dispersed crystals with an average size of 91 ± 5 nm. Crystals were also prepared in the presence of polyvinylpyrrolidone and sodium dodecyl sulfate to improve redispersibility after centrifugation. When ultrasound was replaced by mixing or when crystals were prepared without solvent flow, large crystals or aggregates were produced. Ultrasonic power, antisolvent flow rate, solvent flow rate, and the solvents used did not greatly influence the size of the particles produced by spray sonocrystallization. Only the initial concentration of CPS in the

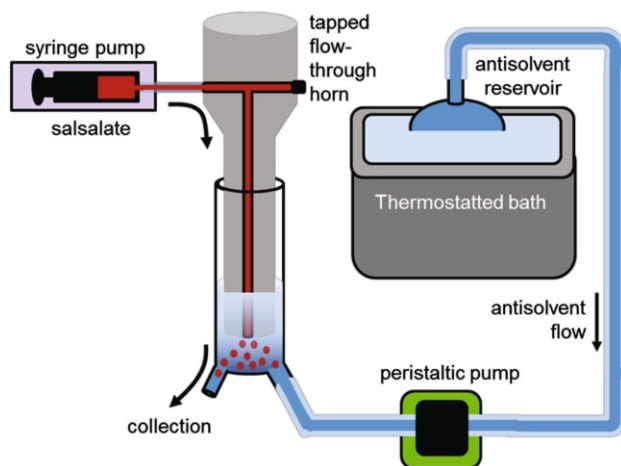


Fig. 19 Schematic diagram showing the apparatus used for spray sonocrystallization. A solution of the material to be crystallized is pumped through a tapped ultrasonic horn into a mixing cell full of a flowing antisolvent. Reproduced with permission from Ref. [117]. Copyright 2015 American Chemical Society

solvent seemed to affect the size of the crystals produced. From this, spray sonocrystallization seems like a robust flow method to produce nanoscale pharmaceutical crystals with a narrow size distribution.

The effects of ultrasound on crystalline materials are not only limited to the nucleation of crystals but also to the fragmentation of crystals in an ultrasonic field. The physical effects of ultrasound on a metal powder suspension were first investigated by Doktycz and Suslick [78] and quantitatively explained by Prozorov and Suslick [79]. Sonication of a slurry of zinc powder in decane produced fused agglomerations of particles. Figure 20 shows an example of two ultrasonically fused Zn particles. Fe, Sn, Cr, and Mo powders also produced fused particles when sonicated, but W powder did not. It was determined that this fusion was the result of interparticle collisions driven by cavitation shock waves.

In contrast to metal particles (which are malleable), the sonication of molecular and ionic crystals (which are friable) as slurries results in fragmentation of the crystals. Suslick et al. conducted a series of experiments to determine the mechanism of sonofragmentation [118]. To test the influence of interparticle collisions, different concentrations of aspirin crystals were suspended in decane and sonicated. Surprisingly, as Fig. 21 shows, it was found that the average particle size after sonication for 10 s did not vary with initial particle concentration, as would have been expected if interparticle collisions were the predominant factor of sonofragmentation. Other experiments were conducted to decouple the horn from the crystal suspension and the suspension from the vessel walls. In both cases, only minimal differences were observed in particle size in comparison to the normally sonicated crystals, ruling out particle–horn and particle–wall interactions as predominating sonofragmentation. These results suggest that shock wave–particle interactions is the major contributor to sonofragmentation.

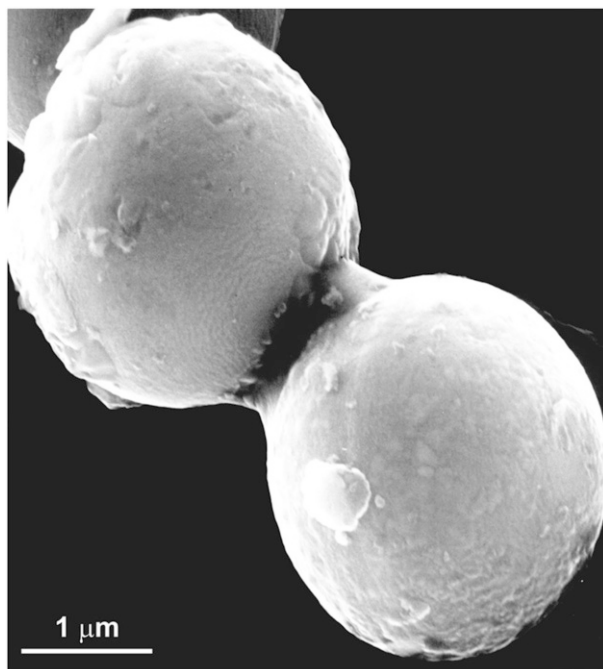


Fig. 20 SEM image showing two fused Zn metal particles. A Zn powder slurry in decane was irradiated with ultrasound, and the resulting shock waves caused interparticle collisions with enough force to fuse the metal particles together. Reproduced with permission from Ref. [78]. Copyright 1990 AAAS

A phenomenon related to sonocrystallization and sonofragmentation is the ability to produce enantiomerically pure crystals from a chiral mixture. Chen and coworkers first reported the growth of NaClO_3 crystals consisting predominantly of one enantiomer or the other if a supersaturated solution is ultrasonically irradiated to crystal nucleation and growth [119]. Ultrasonic chiral symmetry breaking in the crystallized portion is thought to be a modified example of Viedma ripening [120], where instead of mechanically grinding the crystals, ultrasound is used to reduce crystal size, i.e., sonofragmentation. In an experimental comparison of deracemization of NaClO_3 by ultrasound and by glass bead grinding, Stefanidis et al. subjected racemic suspension of crystals to one of the two methods [121]. The crystals exposed to ultrasound showed a faster initial rate of deracemization, but leveled out before reaching enantiomeric purity. The leveling was attributed to the particles all reaching uniform minimum size. The addition of enantiomerically pure crystals to an ultrasonically irradiated slurry resumed the deracemization, and enantiomeric purity could be reached in this manner.

Coquerel et al. were able to demonstrate the deracemization of chiral organic crystals [122]. They synthesized a precursor of paclobutrazol, a plant growth inhibitor and fungicide. The prepared crystals were suspended in a methanol–water mixture with NaOH as a racemizing agent for the compound. Experiments were both conducted by mixing the crystal suspensions with glass beads and

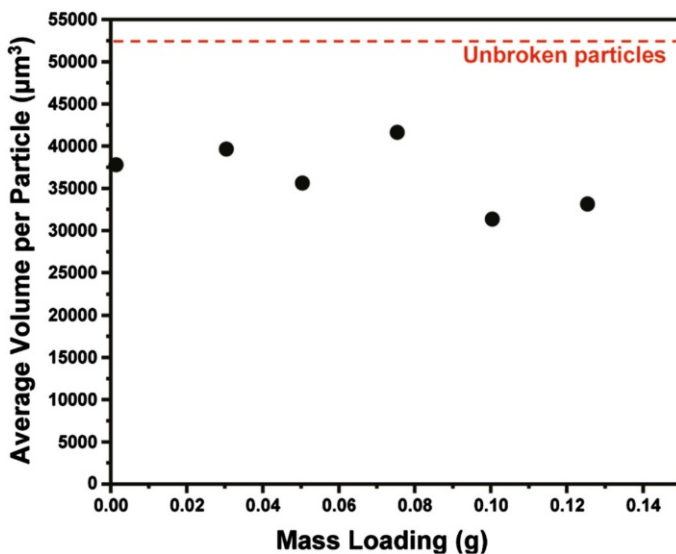


Fig. 21 Graph showing the volume of aspirin crystals as a function of total crystal mass loading as a suspension in dodecane after 10 s of sonication at 5.5 W. The negligible effect of mass loading on the final volume of the crystals is evidence against interparticle collisions as a major contributing mechanism to the sonofragmentation of molecular crystals. Reproduced with permission from Ref. [118]. Copyright 2011 American Chemical Society

ultrasonically irradiating the crystal suspensions. For these crystals, ultrasound was able to completely deracemize samples, and using ultrasound was faster than glass bead abrasion. The rate of deracemization was also found to increase with increasing power of ultrasound applied to the suspensions.

The bulk convection of liquids resulting from cavitation is potentially useful for the self-assembly of colloidal crystals. The formation of colloidal crystals requires a particle to have sufficient energy to move around until it can find a stable configuration relative to the other particles. For small particles, Brownian motion from the thermal energy of the system can drive the self-assembly of colloidal crystals, but larger particles tend to settle due to gravitational effects before a thermodynamically stable configuration can be arranged. Thus, other more complicated methods are usually required to direct the self-assembly of non-Brownian (i.e., larger) particles. The agitation provided by low power ultrasonic irradiation, may serve as an alternative means for larger particles to self-assemble by sedimentation. For example, the use of ultrasonic agitation to facilitate the formation of colloidal crystals was successfully demonstrated by Lash et al. [123]. Ultrasound provides two main advantages in this application. The force exerted by the acoustic waves can counter gravitational effects on particles, allowing the particles to move both macroscopically and microscopically. Second, the convection caused by cavitation also facilitates particle motion and collisions, which enhances the rate at which colloidal crystals form. When the ultrasonic amplitude is optimally set, the particles cluster together in a mechanism similar to inelastic collapse, where collision and

viscous dissipation promote the formation of crystalline structures. Both Brownian and non-Brownian crystals can be formed on the order of minutes.

3.3 Sonochemically Produced Protein Microspheres

The sonochemical production of oil- and gas-filled protein microspheres is an example of both the physical and chemical effects of ultrasound being used to create a nanostructured material [124]. When a mixture of oil and water are irradiated by high-intensity ultrasound, the turbulence generated can produce an emulsion. When an aqueous protein solution is sonicated with an immiscible liquid, protein microspheres are formed. As the oil is emulsified into droplets within the water, proteins attach to the oil–water interface. Meanwhile, cavitation is producing radicals through the sonolysis of water. In the presence of oxygen, superoxide radicals are formed, and these radicals crosslink the proteins through the formation of disulfide bonds. Thus, non-aqueous materials can be encapsulated in a thin, robust protein shell. If an ultrasonic probe is applied to the surface of a protein solution, a thin protein shell can similarly encapsulate gas bubbles [125]. The proteins composing the shell of the microsphere are not denatured by the process of shell formation.

Air- and oil-filled protein microspheres have been greatly studied for possible applications in drug delivery and medical imaging. Gas-filled protein microspheres can be used as a contrast agent for medical sonography [125]. Albunex[®] and Optison[®] are commercially available sonographic contrast agents composed of a protein microsphere encapsulating air or octafluoropropane, respectively [126, 127].

Protein microspheres have been used to encapsulate hydrophobic drugs to be used as passive delivery agents [128–130]. Most notably, VivoRx Pharmaceuticals commercialized Abraxane[™], albumin microspheres with a paclitaxel core, which is the predominant current delivery system for Taxol chemotherapy for breast cancer [131]; VivoRx became Abraxis Bioscience, which was acquired recently by Celgene for \$2.9 billion.

The surface of protein microspheres can be modified post synthesis using layer-by-layer techniques [132]. This technique was used to noncovalently attach peptides made to target integrin proteins overexpressed in some tumor types. The incorporation of gold, carbon, and melanin nanoparticles into the core or shell of the protein microspheres produced contrast agents for optical coherence tomography [133]. The inclusion of dyes or iron oxide nanoparticles in the oil phase produced protein microspheres with fluorescence imaging contrast and MRI contrast, respectively [134].

The sonochemical synthesis of albumin protein microspheres has inspired the use of ultrasound to make microcapsules of different proteins, other biopolymers, and even synthetic polymers. Using ultrasound to produce microspheres does not necessarily need to form covalent crosslinks in order to form somewhat stable microspheres. Biopolymer-stabilized emulsion droplets can be held together by noncovalent interactions (e.g., hydrogen bonding, hydrophobic interactions, and electrostatic interactions) in a manner similar to particle-stabilized pickering emulsions [135]. Avivi and Gedanken were able to produce streptavidin

microspheres despite the fact that streptavidin does not contain cysteine residues. The microspheres did not form under neutral pH but rather in a slightly acidic (pH 6.0) solution, which the authors attributed to hydrophobic interactions stabilizing the microspheres.

Suslick et al. were able to similarly use sodium polyglutamate (SPG) to form microspheres at neutral pH [136]. The presence of added radical scavengers did not affect the formation of the SPG microspheres, and MALDI-MS analysis showed no difference between sonicated and unsonicated SPG, thus showing that covalent bonding did not seem to be responsible in microsphere formation. Rather, hydrogen bonding is an important factor in the stabilization of SPG microspheres. To test whether hydrogen bonding or ion pairing influence microsphere stability, the ionic strength of the SPG solution was adjusted by the addition of NaNO_3 . Even moderate increases in ionic strength (e.g., adding small 0.1 M NaNO_3), which disrupts hydrogen bonding, significantly diminished microsphere stability and formation. Despite the effect of moderate ionic strength on microsphere formation, if microspheres were washed to remove excess counter ions, they were stable when placed in physiological condition buffer solutions, indicating their potential use in medical applications. The robustness of the microspheres was demonstrated by encapsulating and subsequently removing toluene, as shown in Fig. 22. The SPG shell wrinkled like a raisin, but still maintained its integrity.

While polypeptides with and without disulfide crosslinking have been shown to make stable microspheres using ultrasound, there have also been examples of using different biopolymers to sonochemically form core-shell microspheres. Tzanov and coworkers have made covalently cross-linked nanocapsules using thiolated chitosan [137]. Like the protein microspheres, the thiolated chitosan nanocapsules are stabilized by the formation of disulfide bonds. It was shown that a higher degree of disulfide bond formation could be achieved through increasing the pH of the reactant solution and increasing the degree of chitosan thiolation, resulting in nanocapsules that showed a greater stability against lysozyme degradation. The

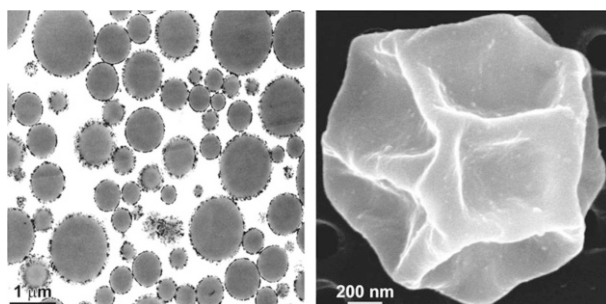


Fig. 22 TEM image (*left*) showing a cross-sectional view of vegetable oil-filled sodium polyglutamate microspheres. SEM image (*right*) of a single sodium polyglutamate microsphere that was prepared using a mixture of toluene and vegetable oil. As the toluene is evacuated, the microsphere contracts, but the shell maintains integrity, demonstrating its robust nature despite the lack of covalent crosslinking. Reproduced with permission from Ref. [136]. Copyright 2006 American Chemical Society

nanocapsules ranged in size from 250 to 570 nm in diameter, depending on the reaction conditions.

Research interest in sonochemically produced protein microcapsules has recently spread to include the remediation of heavy metal-contaminated water [138]. Waters and coworkers tested protein microspheres made from bovine serum albumin and chicken egg white protein, both proteins high in cysteine residues, as a means to remove copper ions from an aqueous solution. This idea was inspired from solvent extraction methods that use air bubble to increase the surface area between the aqueous solution and the extracting solvent. The cysteine residues, which allow for protein crosslinking in the sonochemical production of protein microspheres, should also have the ability to sorb metal ions. Air-filled protein microbubbles were prepared according to the Suslick method, and they were placed in an aqueous solution of copper(II) sulfate. A series of experiments varying temperature, copper concentration, microsphere concentration, and pH were conducted to determine the utility and optimum conditions of protein microbubble metal ion removal. Infrared and X-ray photoelectron spectroscopy of the microbubbles seemed to indicate that thiol, amine, amide, and carboxylate functional groups present on the surface of the microbubbles, and that all were involved in the sorption of copper ions. Under the best conditions tested, 10 g l^{-1} microspheres were able to remove 80% of copper ions from a solution of 1 g l^{-1} copper. Higher loading of microspheres actually resulted in poorer copper removal, possibly due to the formation of microsphere aggregates.

4 Conclusions

High-intensity ultrasound can be a powerful tool for the production of nanostructured materials, in large part stemming from the intense local conditions generated by acoustic cavitation. Such cavitation hot spots can be used to perform chemical reactions that can produce and modify materials. Ultrasound and cavitation also physically affect an irradiated fluid, causing increased mixing and shearing, heating, shock waves, microjets, and droplet nebulization. These processes can affect reaction rates, crystallization, and particle size. This complex variety of chemical and physical effects of ultrasound can be used in a multitude of ways by a discerning chemist, resulting in the wide range of nanostructured materials produced by sonochemical and ultrasound-assisted methods.

References

1. Xu H, Zeiger BW, Suslick KS (2013) Sonochemical synthesis of nanomaterials. *Chem Soc Rev* 42(7):2555–2567
2. Bang JH, Suslick KS (2010) Applications of ultrasound to the synthesis of nanostructured materials. *Adv Mater* 22(10):1039–1059
3. Bang JH, Didenko YT, Helmich RJ, Suslick KS (2012) Nanostructured materials through ultrasonic spray pyrolysis. *Aldrich Mater Matters* 7(2):15–18

4. Shchukin DG, Radziuk D, Möhwald H (2010) Ultrasonic fabrication of metallic nanomaterials and nanoalloys. *Annu Rev Mater Res* 40(1):345–362
5. Suslick KS, Price GJ (1999) Applications of ultrasound to materials chemistry. *Annu Rev Mater Sci* 29:295–326. doi:[10.1146/annurev.matsci.29.1.295](https://doi.org/10.1146/annurev.matsci.29.1.295)
6. Suslick KS, Flannigan DJ (2008) Inside a collapsing bubble: sonoluminescence and the conditions during cavitation. *Annu Rev Phys Chem* 59:659–683. doi:[10.1146/annurev.physchem.59.032607.093739](https://doi.org/10.1146/annurev.physchem.59.032607.093739)
7. Didenko YT, McNamara WB, Suslick KS (1999) Hot spot conditions during cavitation in water. *J Am Chem Soc* 121(24):5817–5818. doi:[10.1021/ja9844635](https://doi.org/10.1021/ja9844635)
8. Flint EB, Suslick KS (1991) The temperature of cavitation. *Science* 253(5026):1397–1399. doi:[10.1126/science.253.5026.1397](https://doi.org/10.1126/science.253.5026.1397)
9. Flannigan DJ, Suslick KS (2005) Plasma formation and temperature measurement during single-bubble cavitation. *Nature* 434(7029):52–55. doi:[10.1038/nature03361](https://doi.org/10.1038/nature03361)
10. Didenko YT, Suslick KS (2002) The energy efficiency of formation of photons, radicals and ions during single-bubble cavitation. *Nature* 418(6896):394–397. doi:[10.1038/nature00895](https://doi.org/10.1038/nature00895)
11. Didenko YT, McNamara WB, Suslick KS (2000) Molecular emission from single-bubble sonoluminescence. *Nature* 407(6806):877–879
12. Xu H, Eddingsaas NC, Suslick KS (2009) Spatial separation of cavitating bubble populations: the nanodroplet injection model. *J Am Chem Soc* 131(17):6060–6061
13. Ouerhani T, Pflieger R, Ben Massaoud W, Nikitenko SI (2015) Spectroscopy of sonoluminescence and sonochemistry in water saturated with N₂-Ar mixtures. *J Phys Chem B* 119(52):15885–15891. doi:[10.1021/acs.jpcc.5n10221](https://doi.org/10.1021/acs.jpcc.5n10221)
14. Riesz P, Berdahl D, Christman CL (1985) Free radical generation by ultrasound in aqueous and nonaqueous solutions. *Environ Health Perspect* 64:233–252
15. Makino K, Mossoba MM, Riesz P (1982) Chemical effects of ultrasound on aqueous solutions. Evidence for hydroxyl and hydrogen free radicals (.cntdot.OH and.cntdot.H) by spin trapping. *J Am Chem Soc* 104(12):3537–3539
16. Flint EB, Suslick KS (1989) Sonoluminescence from nonaqueous liquids—emission from small molecules. *J Am Chem Soc* 111(18):6987–6992. doi:[10.1021/ja00200a014](https://doi.org/10.1021/ja00200a014)
17. Suslick KS, Gawienowski JJ, Schubert PF, Wang HH (1983) Alkane sonochemistry. *J Phys Chem* 87(13):2299–2301. doi:[10.1021/j100236a013](https://doi.org/10.1021/j100236a013)
18. Suslick KS, Gawienowski JJ, Schubert PF, Wang HH (1984) Sonochemistry in non-aqueous liquids. *Ultrasonics* 22(1):33–36. doi:[10.1016/0041-624x\(84\)90059-3](https://doi.org/10.1016/0041-624x(84)90059-3)
19. Okitsu K, Ashokkumar M, Grieser F (2005) Sonochemical synthesis of gold nanoparticles: effects of ultrasound frequency. *J Phys Chem B* 109(44):20673–20675
20. Suslick KS, Choe SB, Cichowlas AA, Grinstaff MW (1991) Sonochemical synthesis of amorphous iron. *Nature* 353(6343):414–416
21. Flannigan DJ, Hopkins SD, Suslick KS (2005) Sonochemistry and sonoluminescence in ionic liquids, molten salts, and concentrated electrolyte solutions. *J Organomet Chem* 690(15):3513–3517. doi:[10.1016/j.jorganchem.2005.04.024](https://doi.org/10.1016/j.jorganchem.2005.04.024)
22. Oxley JD, Prozorov T, Suslick KS (2003) Sonochemistry and sonoluminescence of room-temperature ionic liquids. *J Am Chem Soc* 125(37):11138–11139. doi:[10.1021/ja029830y](https://doi.org/10.1021/ja029830y)
23. Suslick KS, Fang M, Hyeon T (1996) Sonochemical synthesis of iron colloids. *J Am Chem Soc* 118(47):11960–11961
24. Grinstaff MW, Cichowlas AA, Choe SB, Suslick KS (1992) Effect of cavitation conditions on amorphous metal synthesis. *Ultrasonics* 30(3):168–172
25. Mdleleni MM, Hyeon T, Suslick KS (1998) Sonochemical synthesis of nanostructured molybdenum sulfide. *J Am Chem Soc* 120(24):6189–6190
26. Hyeon T, Fang M, Suslick KS (1996) Nanostructured molybdenum carbide: sonochemical synthesis and catalytic properties. *J Am Chem Soc* 118(23):5492–5493
27. Cau C, Nikitenko SI (2012) Mechanism of W(CO)₆ sonolysis in diphenylmethane. *Ultrason Sonochem* 19(3):498–502
28. Bang JH, Suslick KS (2007) Sonochemical synthesis of nanosized hollow hematite. *J Am Chem Soc* 129(8):2242–2243
29. Dhas NA, Suslick KS (2005) Sonochemical preparation of hollow nanospheres and hollow nanocrystals. *J Am Chem Soc* 127(8):2368–2369
30. Baigent CL, Müller G (1980) A colloidal gold prepared with ultrasonics. *Experientia* 36(4):472–473

31. Okitsu K, Sharyo K, Nishimura R (2009) One-pot synthesis of gold nanorods by ultrasonic irradiation: the effect of pH on the shape of the gold nanorods and nanoparticles. *Langmuir* 25(14):7786–7790
32. Zhang J, Du J, Han B, Liu Z, Jiang T, Zhang Z (2006) Sonochemical formation of single-crystalline gold nanobelts. *Angew Chem Int Edit* 45(7):1116–1119
33. Sánchez-Iglesias A, Pastoriza-Santos I, Pérez-Juste J, Rodríguez-González B, García de Abajo FJ, Liz-Marzán LM (2006) Synthesis and optical properties of gold nanodecahedra with size control. *Adv Mater* 18(19):2529–2534
34. Jiang L-P, Xu S, Zhu J-M, Zhang J-R, Zhu J-J, Chen H-Y (2004) Ultrasonic-assisted synthesis of monodisperse single-crystalline silver nanoplates and gold nanorings. *Inorg Chem* 43(19):5877–5883
35. Zhang P, He J, Ma X, Gong J, Nie Z (2013) Ultrasound assisted interfacial synthesis of gold nanocones. *Chem Commun* 49(10):987–989
36. Mizukoshi Y, Fujimoto T, Nagata Y, Oshima R, Maeda Y (2000) Characterization and catalytic activity of core-shell structured gold/palladium bimetallic nanoparticles synthesized by the sonochemical method. *J Phys Chem B* 104(25):6028–6032
37. Anandan S, Grieser F, Ashokkumar M (2008) Sonochemical synthesis of Au-Ag core-shell bimetallic nanoparticles. *J Phys Chem C* 112(39):15102–15105
38. Ateez-Esfahani H, Wang L, Nemoto Y, Yamauchi Y (2010) Synthesis of bimetallic Au@Pt nanoparticles with Au core and nanostructured Pt shell toward highly active electrocatalysts. *Chem Mat* 22(23):6310–6318
39. Gümeç C, Cearnaigh DU, Casadonte DJ, Korzeniewski C (2013) Synthesis of PtCu₃ bimetallic nanoparticles as oxygen reduction catalysts via a sonochemical method. *J Mater Chem A* 1(6):2322–2329
40. Godínez-García A, Pérez-Robles JF, Martínez-Tejada HV, Solorza-Feria O (2012) Characterization and electrocatalytic properties of sonochemical synthesized PdAg nanoparticles. *Mater Chem Phys* 134(2–3):1013–1019
41. Matin MA, Jang J-H, Kwon Y-U (2014) PdM nanoparticles (M=Ni, Co, Fe, Mn) with high activity and stability in formic acid oxidation synthesized by sonochemical reactions. *J Power Sources* 262(C):356–363
42. Xu H, Suslick KS (2010) Sonochemical synthesis of highly fluorescent Ag nanoclusters. *ACS Nano* 4(6):3209–3214
43. Liu T, Zhang L, Song H, Wang Z, Lv Y (2013) Sonochemical synthesis of Ag nanoclusters: electrogenerated chemiluminescence determination of dopamine. *Luminescence* 28(4):530–535
44. Zhou T, Rong M, Cai Z, Yang CJ, Chen X (2012) Sonochemical synthesis of highly fluorescent glutathione-stabilized Ag nanoclusters and S₂⁻ sensing. *Nanoscale* 4(14):4103–4104
45. Li J, Ke CJ, Lin C, Cai ZH, Chen CY, Chang WH (2013) Facile method for gold nanocluster synthesis and fluorescence control using toluene and ultrasound. *J Med Biol*
46. Wang C, Cheng H, Huang Y, Xu Z, Lin H, Zhang C (2015) Facile sonochemical synthesis of pH-responsive copper nanoclusters for selective and sensitive detection of Pb²⁺ in living cells. *Analyst* 140(16):5634–5639
47. Alavi MA, Morsali A (2010) Syntheses and characterization of Mg(OH)₂ and MgO nanostructures by ultrasonic method. *Ultrason Sonochem* 17(2):441–446
48. Alavi MA, Morsali A (2010) Syntheses and characterization of Sr(OH)₂ and SrCO₃ nanostructures by ultrasonic method. *Ultrason Sonochem* 17(1):132–138
49. Salavati-Niasari M, Javidi J, Davar F (2010) Sonochemical synthesis of Dy₂(CO₃)₃ nanoparticles, Dy(OH)₃ nanotubes and their conversion to Dy₂O₃ nanoparticles. *Ultrason Sonochem* 17(5):870–877
50. Ghanbari D, Salavati-Niasari M, Ghasemi-Kooch M (2014) A sonochemical method for synthesis of Fe₃O₄ nanoparticles and thermal stable PVA-based magnetic nanocomposite. *J Ind Eng Chem* 20(6):3970–3974
51. Nagvenkar AP, Deokar A, Perelshtein I, Gedanken A (2016) A one-step sonochemical synthesis of stable ZnO-PVA nanocolloid as a potential biocidal agent. *J Mater Chem B* 4(12):2124–2132
52. Vabbina PK, Kaushik A, Pokhrel N, Bhansali S, Pala N (2015) Electrochemical cortisol immunosensors based on sonochemically synthesized zinc oxide 1D nanorods and 2D nanoflakes. *Biosens Bioelectron* 63(C):124–130
53. Singh G, Joyce EM, Beddow J (2012) Evaluation of antibacterial activity of ZnO nanoparticles coated sonochemically onto textile fabrics. *J*

54. Gottesman R, Shukla S, Perkas N, Solovoyov LA, Nitzan Y, Gedanken A (2011) Sonochemical coating of paper by microbicidal silver nanoparticles. *Langmuir* 27(2):720–726
55. Abramova A, Gedanken A, Popov V, Ooi E-H, Mason TJ, Joyce EM, Beddow J, Perelshtein I, Bayazitov V (2013) A sonochemical technology for coating of textiles with antibacterial nanoparticles and equipment for its implementation. *Mater Lett* 96(C):121–124
56. Xu F, Yuan Y, Han H, Wu D, Gao Z, Jiang K (2012) Synthesis of ZnO/CdS hierarchical heterostructure with enhanced photocatalytic efficiency under nature sunlight. *Cryst Eng Comm* 14(10):3615–3618
57. Zhang X, Zhao H, Tao X, Zhao Y, Zhang Z (2005) Sonochemical method for the preparation of ZnO nanorods and trigonal-shaped ultrafine particles. *Mater Lett* 59(14–15):1745–1747
58. Gao T, Wang T (2004) Sonochemical synthesis of SnO₂ nanobelt/CdS nanoparticle core/shell heterostructures. *Chem Commun* 22:2558–2559
59. Chen D, Yoo SH, Huang Q, Ali G, Cho SO (2012) Sonochemical synthesis of Ag/AgCl nanocubes and their efficient visible-light-driven photocatalytic performance. *Chem Eur J* 18(17):5192–5200
60. Jung D-W, Yang D-A, Kim J, Kim J, Ahn W-S (2010) Facile synthesis of MOF-177 by a sonochemical method using 1-methyl-2-pyrrolidinone as a solvent. *Dalton Trans* 39(11):2883–2885
61. Yang D-A, Cho H-Y, Kim J, Yang S-T, Ahn W-S (2012) CO₂ capture and conversion using Mg-MOF-74 prepared by a sonochemical method. *Energy Environ Sci* 5(4):6465–6473
62. Son W-J, Kim J, Kim J, Ahn W-S (2008) Sonochemical synthesis of MOF-5. *Chem Commun* 47:6336–6338
63. Lee Y-R, Jang M-S, Cho H-Y, Kwon H-J, Kim S, Ahn W-S (2015) ZIF-8: a comparison of synthesis methods. *Chem Eng J* 271(C):276–280
64. Lee Y-R, Cho S-M, Ahn W-S, Lee C-H, Lee K-H, Cho W-S (2015) Facile synthesis of an IRMOF-3 membrane on porous Al₂O₃ substrate via a sonochemical route. *Microporous Mesoporous Mater* 213(C):161–168
65. Dharmarathna S, King'ondeu CK, Pedrick W, Pahalagedara L, Suib SL (2012) Direct sonochemical synthesis of manganese octahedral molecular sieve (OMS-2) nanomaterials using cosolvent systems, their characterization, and catalytic applications. *Chem Mat* 24(4):705–712
66. Skrabalak SE (2009) Ultrasound-assisted synthesis of carbon materials. *Phys Chem Chem Phys* 11(25):4930–4942
67. Guo J, Zhu S, Chen Z, Li Y, Yu Z, Liu Q, Li J, Feng C, Zhang D (2011) Sonochemical synthesis of TiO₂ nanoparticles on graphene for use as photocatalyst. *Ultrason Sonochem* 18(5):1082–1090
68. Cui Y, Zhou D, Sui Z, Han B (2014) Sonochemical synthesis of graphene oxide-wrapped gold nanoparticles hybrid materials: visible light photocatalytic activity. *Chin J Chem* 33(1):119–124
69. Zhu S, Guo J, Dong J, Cui Z, Lu T, Zhu C, Zhang D, Ma J (2013) Sonochemical fabrication of Fe₃O₄ nanoparticles on reduced graphene oxide for biosensors. *Ultrason Sonochem* 20(3):872–880
70. Krishnamoorthy K, Kim G-S, Kim SJ (2013) Graphene nanosheets: ultrasound assisted synthesis and characterization. *Ultrason Sonochem* 20(2):644–649
71. Xu H, Suslick KS (2011) Sonochemical preparation of functionalized graphenes. *J Am Chem Soc* 133(24):9148–9151
72. Jeong S-H, Ko J-H, Park J-B, Park W (2004) A sonochemical route to single-walled carbon nanotubes under ambient conditions. *J Am Chem Soc* 126(49):15982–15983
73. Ha H, Jeong S-H (2016) Facile route to multi-walled carbon nanotubes under ambient conditions. *Korean J Chem Eng* 33(2):401–404
74. Yau HC, Bayazit MK, Steinke JHG, Shaffer MSP (2015) Sonochemical degradation of *N*-methylpyrrolidone and its influence on single walled carbon nanotube dispersion. *Chem Commun* 51(93):16621–16624
75. Wei K, Li J, Ge Z, You Y, Xu H (2014) Sonochemical synthesis of highly photoluminescent carbon nanodots. *RSC Adv* 4:52230–52234
76. Kumar VB, Ze Porat, Gedanken A (2016) Facile one-step sonochemical synthesis of ultrafine and stable fluorescent C-dots. *Ultrason Sonochem* 28:367–375. doi:10.1016/j.ultsonch.2015.08.005
77. Suslick KS (1990) Sonochemistry. *Science* 247(4949):1439–1445. doi:10.1126/science.247.4949.1439
78. Doktycz SJ, Suslick KS (1990) Interparticle collisions driven by ultrasound. *Science* 247(4946):1067–1069
79. Prozorov T, Prozorov R, Suslick KS (2004) High velocity interparticle collisions driven by ultrasound. *J Am Chem Soc* 126(43):13890–13891. doi:10.1021/ja049493o

80. Shi Y, Zhu C, Wang L, Zhao C, Li W, Fung KK, Ma T, Hagfeldt A, Wang N (2013) Ultrarapid sonochemical synthesis of ZnO hierarchical structures: from fundamental research to high efficiencies up to 6.42% for quasi-solid dye-sensitized solar cells. *Chem Mat* 25(6):1000–1012
81. Thompson JA, Chapman KW, Koros WJ, Jones CW, Nair S (2012) Sonication-induced Ostwald ripening of ZIF-8 nanoparticles and formation of ZIF-8/polymer composite membranes. *Microporous Mesoporous Mater* 158(C):292–299
82. Lang RJ (1962) Ultrasonic atomization of liquids. *J Acoust Soc Am* 34(1):6
83. Mwakikunga BW (2014) Progress in ultrasonic spray pyrolysis for condensed matter sciences developed from ultrasonic nebulization theories since Michael Faraday. *Crit Rev Solid State Mat Sci* 39(1):46–80. doi:[10.1080/10408436.2012.687359](https://doi.org/10.1080/10408436.2012.687359)
84. Rankin JM, Neelakantan NK, Lundberg KE, Grzincic EM, Murphy CJ, Suslick KS (2015) Magnetic, fluorescent, and copolymeric silicone microspheres. *Adv Sci* 2 (6)
85. Bang JH, Hehnich RJ, Suslick KS (2008) Nanostructured ZnS:Ni²⁺ photocatalysts prepared by ultrasonic spray pyrolysis. *Adv Mater* 20(13):2599. doi:[10.1002/adma.200703188](https://doi.org/10.1002/adma.200703188)
86. Helmich RJ, Suslick KS (2010) Chemical aerosol flow synthesis of hollow metallic aluminum particles. *Chem Mat* 22(17):4835–4837. doi:[10.1021/cm101342r](https://doi.org/10.1021/cm101342r)
87. Boissière C, Nicole L, Gervais C, Babonneau F, Antonietti M, Amenitsch H, Sanchez C, Grosso D (2006) Nanocrystalline mesoporous γ -alumina powders “UPMCI Material” gathers thermal and chemical stability with high surface area. *Chem Mat* 18(22):5238–5243
88. Li L, Tsung CK, Yang Z, Stucky GD, Sun LD, Wang JF, Yan CH (2008) Rare-earth-doped nanocrystalline titania microspheres emitting luminescence via energy transfer. *Adv Mater* 20(5):903–908
89. Bang JH, Suslick KS (2009) Dual templating synthesis of mesoporous titanium nitride microspheres. *Adv Mater* 21(31):3186–3190
90. Skrabalak SE, Suslick KS (2005) Porous MoS₂ synthesized by ultrasonic spray pyrolysis. *J Am Chem Soc* 127(28):9990–9991. doi:[10.1021/ja051654g](https://doi.org/10.1021/ja051654g)
91. Suh WH, Jang AR, Suh YH, Suslick KS (2006) Porous, hollow, and ball-in-ball metal oxide microspheres: preparation, endocytosis, and cytotoxicity. *Adv Mater* 18(14):1832–1837
92. Suh WH, Suslick KS (2005) Magnetic and porous nanospheres from ultrasonic spray pyrolysis. *J Am Chem Soc* 127(34):12007–12010. doi:[10.1021/ja050693p](https://doi.org/10.1021/ja050693p)
93. Hampsey JE, Hu Q, Rice L, Pang J, Wu Z, Lu Y (2005) A general approach towards hierarchical porous carbon particles. *Chem Commun* 28:3606–3608
94. Hu Q, Lu Y, Meisner GP (2008) Preparation of nanoporous carbon particles and their cryogenic hydrogen storage capacities. *J Phys Chem C* 112(5):1516–1523
95. Jung DS, Hwang TH, Park SB, Choi JW (2013) Spray drying method for large-scale and high-performance silicon negative electrodes in Li-ion batteries. *Nano Lett* 13(5):2092–2097
96. Ko YN, Park SB, Jung KY, Kang YC (2013) One-pot facile synthesis of Ant-cave-structured metal oxide-carbon Microballs by continuous process for use as anode materials in Li-Ion batteries. *Nano Lett* 13(11):5462–5466. doi:[10.1021/nl4030352](https://doi.org/10.1021/nl4030352)
97. Jung DS, Hwang TH, Lee JH, Koo HY, Shakoora RA, Kahraman R, Jo YN, Park M-S, Choi JW (2014) Hierarchical porous carbon by ultrasonic spray pyrolysis yields stable cycling in lithium-sulfur battery. *Nano Lett* 14(8):4418–4425
98. Langrock A, Xu Y, Liu Y, Ehrman S, Manivannan A, Wang C (2013) Carbon coated hollow Na₂FePO₄F spheres for Na-ion battery cathodes. *J Power Sourc* 223(C):62–67
99. Skrabalak SE, Suslick KS (2006) Porous carbon powders prepared by ultrasonic spray pyrolysis. *J Am Chem Soc* 128(39):12642–12643
100. Fortunato ME, Rostam-Abadi M, Suslick KS (2010) Nanostructured carbons prepared by ultrasonic spray pyrolysis. *Chem Mat* 22(5):1610–1612. doi:[10.1021/cm100075j](https://doi.org/10.1021/cm100075j)
101. Overcash JW, Suslick KS (2015) High surface area iron oxide microspheres via ultrasonic spray pyrolysis of ferritin core analogues. *Chem Mat* 27(10):3564–3567
102. Zhang Y, Huff LA, Gewirth AA, Suslick KS (2015) Synthesis of manganese oxide microspheres by ultrasonic spray pyrolysis and their application as supercapacitors. *Part Part Syst Charact* 32(9):899–906
103. Zhang Y, Suslick KS (2015) Synthesis of poly(3,4-ethylenedioxythiophene) microspheres by ultrasonic spray polymerization (USPo). *Chem Mat* 27(22):7559–7563
104. Mann AKP, Wicker S, Skrabalak SE (2012) Aerosol-assisted molten salt synthesis of NaInS₂ nanoplates for use as a new photoanode material. *Adv Mater* 24(46):6186–6191. doi:[10.1002/adma.201202299](https://doi.org/10.1002/adma.201202299)

105. Chen DP, Bowers W, Skrabalak SE (2015) Aerosol-assisted combustion synthesis of single-crystalline NaSbO₃ nanoplates: a topotactic template for ilmenite AgSbO₃. *Chem Mat* 27(1):174–180
106. Mann AKP, Fu J, DeSantis CJ, Skrabalak SE (2013) Spatial and temporal confinement of salt fluxes for the shape-controlled synthesis of Fe₂O₃ nanocrystals. *Chem Mat* 25(9):1549–1555. doi:[10.1021/cm3038087](https://doi.org/10.1021/cm3038087)
107. Fu J, DeSantis CJ, Weiner RG, Skrabalak SE (2015) Aerosol-assisted synthesis of shape-controlled CoFe₂O₄: topotactic versus direct melt crystallization. *Chem Mat* 27(5):1863–1868
108. Xia B, Lenggoro IW, Okuyama K (2001) Novel route to nanoparticle synthesis by salt-assisted aerosol decomposition. *Adv Mater* 13(20):1579–1582
109. Xia B, Lenggoro IW, Okuyama K (2001) Synthesis of CeO₂ nanoparticles by salt-assisted ultrasonic aerosol decomposition. *J Mater Chem* 11(12):2925–2927
110. Didenko YT, Suslick KS (2005) Chemical aerosol flow synthesis of semiconductor nanoparticles. *J Am Chem Soc* 127(35):12196–12197
111. Bang JH, Suh WH, Suslick KS (2008) Quantum dots from chemical aerosol flow synthesis: preparation, characterization, and cellular imaging. *Chem Mat* 20(12):4033–4038. doi:[10.1021/cm800453t](https://doi.org/10.1021/cm800453t)
112. Sander JRG, Zeiger BW, Suslick KS (2014) Sonocrystallization and sonofragmentation. *Ultrason Sonochem* 21(6):1908–1915
113. Eder RJP, Schrank S, Besenhard MO, Roblegg E, Gruber-Woelfler H, Khinast JG (2012) Continuous sonocrystallization of acetylsalicylic acid (ASA): control of crystal size. *Cryst Growth Des* 12(10):4733–4738
114. Manish M, Harshal J, Anant P (2005) Melt sonocrystallization of ibuprofen: effect on crystal properties. *Eur J Pharm Sci* 25(1):41–48
115. Li J, Bao Y, Wang J (2013) Effects of sonocrystallization on the crystal size distribution of cloxacillin benzathine crystals. *Chem Eng Technol* 36(8):1341–1346
116. Bučar D-K, Elliott JA, Eddleston MD, Cockcroft JK, Jones W (2014) Sonocrystallization yields monoclinic paracetamol with significantly improved compaction behavior. *Angew Chem Int Ed* 54(1):249–253
117. Kim HN, Sander JRG, Zeiger BW, Suslick KS (2015) Spray sonocrystallization. *Cryst Growth Des* 15(4):1564–1567
118. Zeiger BW, Suslick KS (2011) Sonofragmentation of molecular crystals. *J Am Chem Soc* 133(37):14530–14533
119. Song Y, Chen W, Chen X (2008) Ultrasonic field induced chiral symmetry breaking of NaClO₃ crystallization. *Cryst Growth Des* 8(5):1448–1450
120. Viedma C (2005) Chiral symmetry breaking during crystallization: complete chiral purity induced by nonlinear autocatalysis and recycling. *Phys Rev Lett* 94(6):065504
121. Xiouras C, Van Aeken J, Panis J, Ter Horst JH, Van Gerven T, Stefanidis GD (2015) Attrition-enhanced deracemization of NaClO₃: comparison between ultrasonic and abrasive grinding. *Cryst Growth Des* 15(11):5476–5484
122. Rougeot C, Guillen F, Plaquevent J-C, Coquerel G (2015) Ultrasound-enhanced deracemization: toward the existence of agonist effects in the interpretation of spontaneous symmetry breaking. *Cryst Growth Des* 15(5):2151–2155
123. Lash MH, Fedorchak MV, Little SR, McCarthy JJ (2015) Fabrication and characterization of non-Brownian particle-based crystals. *Langmuir* 31(3):898–905
124. Suslick KS, Grinstaff MW (1990) Protein microencapsulation of nonaqueous liquids. *J Am Chem Soc* 112(21):7807–7809
125. Grinstaff MW, Suslick KS (1991) Air-filled proteinaceous microbubbles—synthesis of an echo-contrast agent. *Proc Natl Acad Sci USA* 88(17):7708–7710. doi:[10.1073/pnas.88.17.7708](https://doi.org/10.1073/pnas.88.17.7708)
126. Quay SC (2004) Ultrasound contrast agents including protein stabilized microspheres of perfluoropropane, perfluorobutane, or perfluoropentane. US 6,723,303
127. Kiessling F, Huppert J, Palmowski M (2009) Functional and molecular ultrasound imaging: concepts and contrast agents. *Curr Med Chem* 16(5):627–642
128. Grinstaff MW, Soon-Shiong P, Wong M, Sandford PA, Suslick KS, Desai NP (1997) Methods for the preparation of pharmaceutically active agents for in vivo delivery. US 5665382
129. Soon-Shiong P, Desai NP, Grinstaff MW, Sandford PA, Suslick KS (1996) Methods for in vivo delivery of substantially water insoluble pharmacologically active agents and compositions useful therefor. US 5560933

130. Grinstaff MW, Soon-Shiong P, Wong M, Sandford PA, Suslick KS, Desai NP (1996) Composition useful for in vivo delivery of biologics and methods employing same. US 5498421
131. Hawkins MJ, Soon-Shiong P, Desai N (2008) Protein nanoparticles as drug carriers in clinical medicine. *Adv Drug Deliv Rev* 60(8):876–885. doi:[10.1016/j.addr.2007.08.044](https://doi.org/10.1016/j.addr.2007.08.044)
132. Toublan FJ-J, Boppart S, Suslick KS (2006) Tumor targeting by surface-modified protein microspheres. *J Am Chem Soc* 128(11):3472–3473
133. Lee TM, Oldenburg AL, Sitafalwalla S, Marks DL, Luo W, Toublan FJ-J, Suslick KS, Boppart SA (2003) Engineered microsphere contrast agents for optical coherence tomography. *Opt Lett* 28(17):1546–1548
134. John R, Nguyen FT, Kolbeck KJ, Chaney EJ, Marjanovic M, Suslick KS, Boppart SA (2011) Targeted multifunctional multimodal protein-shell microspheres as cancer imaging contrast agents. *Mol Imaging Biol* 14(1):17–24
135. Avivi S, Gedanken A (2002) S–S bonds are not required for the sonochemical formation of proteinaceous microspheres: the case of streptavidin. *Biochem J* 366(Pt 3):705–707
136. Dibbern EM, Toublan FJJ, Suslick KS (2006) Formation and characterization of polyglutamate core-shell microspheres. *J Am Chem Soc* 128(20):6540–6541. doi:[10.1021/ja058198g](https://doi.org/10.1021/ja058198g)
137. Francesko A, Fernandes MM, Perelshtein I, Benisvy-Aharonovich E, Gedanken A, Tzanov T (2014) One-step sonochemical preparation of redox-responsive nanocapsules for glutathione mediated RNA release. *J Mater Chem B* 2:6020–6029
138. Nazari AM, Cox PW, Waters KE (2014) Copper ion removal from dilute solutions using ultrasonically synthesised BSA- and EWP-coated air bubbles. *Sep Purif Technol* 132(C):218–225

Synthesis of Photoactive Materials by Sonication: Application in Photocatalysis and Solar Cells

Juan C. Colmenares¹ · Ewelina Kuna¹ ·
Paweł Lisowski¹

Received: 3 June 2016 / Accepted: 30 July 2016 / Published online: 10 August 2016
© The Author(s) 2016. This article is published with open access at Springerlink.com

Abstract In recent years, a good number of methods have become available for the preparation of an important group of photoactive materials for applications in photocatalysis and solar cells. Nevertheless, the benefits derived from preparing those materials through unconventional approaches are very attractive from the green chemistry point of view. This critical review work is focused on sonication as one of these promising new synthetic procedures that allow control over size, morphology, nanostructure and tuning of catalytic properties. Ultrasound-based procedures offer a facile, versatile synthetic tool for the preparation of light-activated materials often inaccessible through conventional methods.

Keywords Photoactive materials by sonication · Photocatalysis · Ultrasounds · Solar cells · Perovskites · Quantum dots

Abbreviations

UV	Ultraviolet
BFO	Bismuth ferrite
SPD	Sonophotodeposition
RT	Room temperature
RB5	Reactive black 5
SnS	Stannous sulfide
VOCs	Volatile organic compounds

This article is part of the Topical Collection “Sonochemistry: From basic principles to innovative applications”; edited by Juan Carlos Colmenares Q., Gregory Chatel.

✉ Juan C. Colmenares
jcarloscolmenares@ichf.edu.pl

¹ Institute of Physical Chemistry of the Polish Academy of Sciences (PAS), Kasprzaka 44/52, 01-224 Warsaw, Poland

USP	Ultrasonic spray pyrolysis
ESR	Electron spin resonance spectroscopy
QDSCs	Quantum dot sensitized solar cells
PSCs	Perovskite solar cells
PCE	Power conversion efficiency
DSSCs	Dye sensitized solar cells
CdTe	Cadmium telluride
NPs	Nanoparticles
QDs	Quantum dots
ROS	Reactive oxygen species
HSs	Hierarchical structures
UST	Ultrasound treatment technique
SVADC	Substrate vibration-assisted drop casting method
ITO	Indium tin oxide
spiro-OMeTAD	$N_2,N_2,N'_2,N'_2,N_7,N_7,N'_7,N'_7$ -octakis(4-methoxyphenyl)-9,9'-spirobi[9H-fluorene]-2,2',7,7'-tetramine

1 Sonochemical Preparation of Photoactive Catalytic Materials

The phenomenology of fabrication of highly efficient photocatalysts through an ultrasound route represents a very interesting and important area in science and technology, and it holds great potential for photocatalysts preparation in the near future [1–3]. In comparison with traditional sources of energy, ultrasound ensures unusual reaction conditions in liquid phase reactions due to the cavitation phenomenon (extremely high temperatures and pressures are formed in very short times in liquids) [3, 4]. Furthermore, application of ultrasound irradiation to a photocatalytic system might enhance both the bulk and localized mass transport and consequently expedite the molecular contact and the photocatalytic activity [1, 2, 4–6]. A considerable number of novel photocatalysts with novel nano-/microstructures (e.g., $ZnWO_4$ [7], $CdMoO_4$ [8], V_2O_5 [9], $CuMoO_4$ [10], TiO_2/Bi_2O_3 [11]) have been prepared by means of ultrasound-assisted methodology. In this subsection, we would like to focus the readers' attention on ultrasound-promoted procedures for the preparation of photocatalysts, and the potential application of these materials in the photocatalytic degradation and selective oxidation of organic compounds.

1.1 Sonochemical Synthesis of TiO_2 Photocatalyst

The current status of outstanding progress made by titanium dioxide (TiO_2), as the most widely used oxide semiconductor, has attracted considerable interest owing to its various applications in solar-driven hydrogen production, photocatalytic decomposition of pollutants, solar cells and so forth [12–14]. It is well known that overall efficiency for the solar-driven photocatalysis is very limited, because of its wide bandgap in the UV region, which accounts for less than 5 % of the total

solar irradiation [15]. Currently, hydrogenated TiO₂ nanoparticles (e.g., blue [16], brown [17] and black [18]) have opened a new avenue to the long-wavelength optical absorption and greatly enhanced photoactivity of the catalysts. Hydrogenated TiO₂ is intensively investigated due to its improvement in solar absorption, but there are major issues related to its structural, optical and electronic properties, and therefore an easily compatible method of preparation is much needed [19]. Recently, disorder-engineered TiO₂ nanocrystals treated in a hydrogen atmosphere under 20 bar of H₂ atmospheres and 200 °C for approximately 5 days showed a colour change to black with a reduction in the bandgap energy up to ~1.54 eV [20]. It should be pointed out that band gap narrowing may be traced back to the surface disorder without the formation of Ti³⁺ centres. In other words, formation of surface disorders, oxygen vacancies, Ti³⁺ ions, Ti–OH and Ti–H groups, and band edge shifting are responsible for the optical properties and photocatalytic activity of black or hydrogenated TiO₂. Interestingly, Ti³⁺ is not responsible for optical absorption of black TiO₂, while there is evidence of mid-gap states above the valence band edge due to hydrogenated disorders [21–23]. It should be also noted that hydrogen doping induced a high density of delocalized Ti3d electrons leading to improved charge transport properties [24]. Furthermore, the hydrogenated black TiO₂ exhibited highly efficient activity for the photocatalytic splitting of water [25]. Moreover, hydrogenation procedures need a high annealing temperature (over 400 °C) or high-pressure (e.g., 20 bar) and H₂ is flammable and explosive [16, 17, 23–26]. The first attempt to prepare amorphous hydroxylated TiO₂ with various degrees of blackness was based on the ultrasonic irradiation of high power intensity with enhanced photocatalytic activity of acid fuchsin degradation [27] (Table 1, Entry 1). A key feature of this system is that power density of employed ultrasonic irradiation was as high as 15 W mL⁻¹, and a low ultrasonic power density could not make such changes in colour. Furthermore, ultrasound was employed to modify the original TiO₂, which prepared amorphous hydroxylated TiO₂ with black appearance, large surface area (328.55 m² g⁻¹) and enhanced photocatalytic methylene blue decomposition. It was found out that ultrasonic irradiation could accelerate the hydrolysis of TiO₂ and reduce its particles size and form amorphous hydroxylated TiO₂ by long time ultrasonication, giving rise a material with higher absorbance intensity through the whole visible light and near-infrared regions.

Worth mentioning is the work by Mao et al. [28] on the preparation of mesoporous titanium dioxide (TiO₂) inside the periodic macropores of diatom frustules by sonochemical condensation of titania precursor, and then thermal treated at elevated temperatures, resulting in hierarchical macro/mesoporous materials. Furthermore, hierarchical structure provides a large number of accessible active sites for efficient transportation of guest species to framework binding sites. It was found that a high photocatalytic degradation of methylene blue as compared with P25 can be achieved with the composite having a certain loading amount of TiO₂ (30 wt%), attributing to its hierarchical macro/mesoporous structures. It should be also noted that mesoporous titanium TiO₂ with wormhole channel together with interconnected 3D structures inside diatom pores prepared by sonochemical synthesis with organic surfactant as structure directing agent has

Table 1 Selected research studies of ultrasound assisted processes in the synthesis of photocatalysts and photoactive catalytic materials

Entry	Photocatalyst	Ultrasound source	Reaction conditions	Remarks	Refs.
1	Black TiO ₂	15 W mL ⁻¹	0.5, 1, 2, 4 and 8 h at 80 °C, 100 mL	Totally disorder structure of amorphous TiO ₂ both before and after ultrasonic treatment was observed	[27]
2	CaTiO ₃ , BaTiO ₃ , SrTiO ₃	45 kHz, 60 W	Ambient conditions for 10 h, glass tube sealed with a screw cap	CaTiO ₃ and BaTiO ₃ nanoparticles with almost regular spherical shape and uniform particle size (~20 nm) were observed. SrTiO ₃ particles were found to agglomerate more strongly leading to cubic-like aggregates with edge lengths varying (100–300 nm)	[31]
3	ZnO/ Ag ₃ VO ₄	12 mm diameter Ti horn, 75 W, 20 kHz	1, 1.5, 2, 3, and 4 h at RT, 150 mL	The nanocomposites prepared by 2 h ultrasonic irradiation have the best activity	[40]
4	ZnO/AgI/ Fe ₃ O ₄	12 mm diameter Ti horn, 75 W, 20 kHz	0.5, 1, 2, and 4 h at RT, 150 mL	Photocatalyst prepared by ultrasonic irradiation for 1 hour has superior activity compared to other samples, and has remarkable stability and excellent magnetic filtration from the treated solutions	[41]
5	ZnO/AgI/ Ag ₂ CrO ₄	12 mm diameter Ti horn, 75 W, 20 kHz	0.25, 0.5, 1, 2, and 3 h at RT, 150 mL	Material prepared by ultrasonic irradiation for 1 h has the superior activity	[42]
6	g-C ₃ N ₄	12 mm, 33 Hz, 150 W	5 h at ambient temperature, 150 mL	g-C ₃ N ₄ sheet possesses porous structure with high surface area and large pore volume	[43]

potentially important structural features for photocatalytic reactivity, because channel branching within the framework may facilitate access to reactive sites on the framework wall, which is most critical for its use as photocatalyst.

In terms of improvement of TiO₂ photocatalytic properties under solar light by means of a suitable modification, enhanced photocatalytic activity of TiO₂ nanocomposites for the degradation of dyes and Gram negative bacteria (*Escherichia coli*) was obtained by doped TiO₂ with Al₂O₃, Bi₂O₃, CuO and ZrO₂ [29] and synthesized via sonochemical method. It is interesting to notice that

$\text{Bi}_2\text{O}_3\text{-TiO}_2$ nanocomposite is more efficient toward the degradation of the dyes under solar light and TiO_2 is the least efficient photocatalyst; the efficiency is in the order: $\text{Bi}_2\text{O}_3\text{-TiO}_2 > \text{Al}_2\text{O}_3\text{-TiO}_2 > \text{CuO-TiO}_2 > \text{ZrO}_2\text{-TiO}_2 > \text{TiO}_2$. It should be also noted that the antibacterial activity of all the five synthesized nanocomposites was tested against Gram negative bacteria (*E. coli*) by varying the concentrations (250, 500, 750 and 1000 μg). Among them, $\text{Al}_2\text{O}_3\text{-TiO}_2$ shows some significant zone of inhibition around the film under dark condition. Recently, certain novel promising photocatalysts prepared by ultrasound-assisted method have been described in several research papers and review articles [1–3].

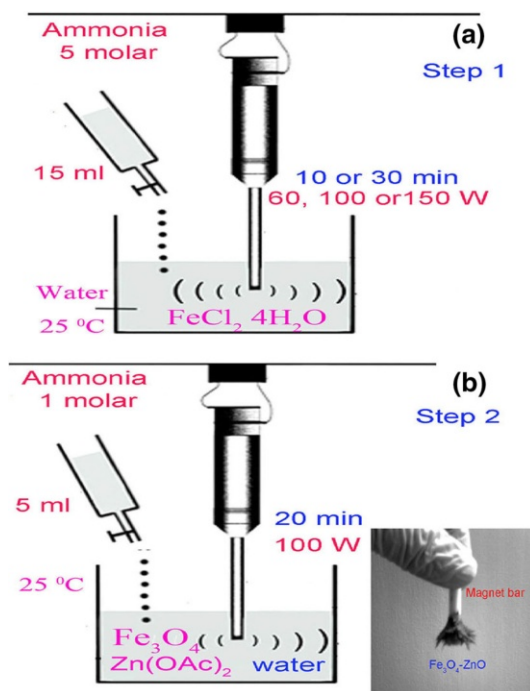
1.2 Sonochemical Synthesis of Selected Photocatalysts

Sonochemical method has been used extensively to generate novel materials with unusual (photo)-catalytic properties, due to its unique reaction effects. For example, addition of titanium iso-propoxide induces the generation of new linear polymeric chains type nickel-titanium-ethylene glycol (Ni-Ti-EG), as revealed by the color change (from green to light blue). This light blue polymer coagulates to form a uniform rod-like precursor by van der Waals interactions [30]. Another elegant strategy to prepare ternary CaTiO_3 , SrTiO_3 and BaTiO_3 materials by a one-step room-temperature ultrasound synthesis in ionic liquid for photocatalytic applications (photocatalytic hydrogen evolution and methylene blue degradation) was recently described [31] (Table 1, Entry 2). It is also important to note that the use of ionic liquids in sonochemistry is advantageous due to their low measurable vapor pressure, low viscosity, low thermal conductivity, and high chemical stability, which are all significant parameters to generate efficient cavitation.

Photoactive materials such as SrZrO_3 have been recently explored because they exhibit suitable properties for photocatalytic hydrogen evolution from water splitting [32]. The results confirm that SrZrO_3 was stable with time of hydrogen evolution and a very high rate ($35 \mu\text{mol g}^{-1} \text{h}^{-1}$) was exhibited by SrZrO_3 prepared by ultrasound-assisted synthesis. Recently, multiferroics such as BiFeO_3 (BFO) are worthy of notice due to their unique and strong coupling of electric, magnetic, and structural order parameters in terms of practical applications, since both ferroelectric and antiferromagnetic ordering temperatures are well above room temperature (Curie temperature 830°C and Neel temperature 370°C) [33]. Moreover, other researchers have applied BFO materials prepared by sono-synthesis with high photocatalytic activity under solar light in degradation of various compounds such as Rhodamine B [34], methylene blue [35], Reactive Black 5 (RB5) [36] and phenolic compounds [37]. As anticipated above, BiFeO_3 nanoparticles with measured band gap of 2.0 eV synthesized with ultrasound exhibited higher crystallization, smaller crystallite size and higher photocatalytic activity than the material synthesized with conventional methods.

In order to improve the photocatalytic activity of a semiconductor and exploit its advantageous properties, $\text{Fe}_3\text{O}_4/\text{ZnO}$ magnetic nanocomposites were synthesized via a surfactant-free sonochemical method in an aqueous solution (Fig. 1) and applied in the photo-catalytic degradation of various organic and azo dyes aqueous solution under UV light irradiation [38]. Surprisingly, these results showed that OH

Fig. 1 **a** Fe_3O_4 nanoparticles, **b** $\text{Fe}_3\text{O}_4\text{-ZnO}$ nanocomposite prepared by surfactant-free sonochemical method. Reproduced from Ref. [38] with kind permission from Springer Science and Business Media



radicals generated by ultrasonic treatment were responsible for inducing the oxidation of Fe^{2+} into Fe^{3+} . As soon as the required hydroxyl groups were available in the solution, the already-produced Fe^{3+} became saturated, and increasing the ultrasonic time did not help the dispersion of the formed nuclei. Additionally, prolongation of the reaction up to 30 min caused oxidation of most of the Fe^{2+} – Fe^{3+} and as a result, brown FeOOH nanoparticles which are more likely to agglomerate were also obtained. Moreover, it was shown that ultrasonic power (100 W) had a significant but rather unpredictable influence on the mean magnetite particle size (agglomeration size decreased to 100–500 nm). Nanocomposites with 10 % of ZnO exhibited a super-paramagnetic behavior.

Previous research [39] showed that orthorhombic stannous sulfide (SnS) nanoparticles synthesized via a sonochemical route by 20 kHz sonication had smaller crystalline size (4 ± 1 nm) in comparison to the nanoparticles that were synthesized by 50 kHz sonication (6 ± 1 nm). An optical investigation confirmed that the SnS particles had strong emission bands located at the UV and visible regions, suggesting that they have the potential to be used as optical devices.

It is known that n–n heterojunctions between two n-type semiconductors can effectively promote separation of photogenerated electron–hole pairs, due to formation of internal electric field. Hence, preparation of $\text{ZnO}/\text{Ag}_3\text{VO}_4$ nanocomposites prepared by an ultrasonic-assisted one-pot method led to the enhanced photocatalytic activity for organic pollutants degradation under visible-light irradiation [40] (Table 1, Entry 3). Interestingly, photocatalytic activity of $\text{ZnO}/$

Ag_3VO_4 nanocomposite under visible-light irradiation is about 21, 56, and 2.8-fold higher than that of the ZnO sample in degradation of rhodamine B, methylene blue, and methyl orange, respectively. Furthermore, it was revealed that the photocatalytic activity was attributed to greater generation of electron–hole pairs due to photosensitizing role of Ag_3VO_4 under visible-light irradiation and the efficient separation of the photogenerated electron–hole pairs due to formation of n–n heterojunction between the counterparts. Previous studies [41] (Table 1, Entry 4) showed that photocatalytic activity of the $\text{ZnO}/\text{AgI}/\text{Fe}_3\text{O}_4$ nanocomposite in degradation of rhodamine B, methylene blue, and methyl orange is about 32-fold higher than that of the $\text{ZnO}/\text{Fe}_3\text{O}_4$ sample prepared by ultrasonic irradiation method. The highly enhanced activity of novel ternary $\text{ZnO}/\text{AgI}/\text{Fe}_3\text{O}_4$ magnetic photocatalyst was mainly attributed to visible-light harvesting efficiency and decreasing recombination of the charge carriers as well. It should be noted that ultrasonic irradiation time and calcination temperature largely affect the photocatalytic activity. In another investigation [42] (Table 1, Entry 5), it was found that ternary $\text{ZnO}/\text{AgI}/\text{Ag}_2\text{CrO}_4$ photocatalyst with 20 % of Ag_2CrO_4 is active in rhodamine B degradation, with nearly 167-, 6.5-, and 45-fold higher conversion than that of ZnO, ZnO/AgI , and $\text{ZnO}/\text{Ag}_2\text{CrO}_4$, respectively, materials also prepared by ultrasonic irradiation method. Furthermore, visible-light activity of $\text{ZnO}/\text{AgI}/\text{Ag}_2\text{CrO}_4$ is about 6.5-, 16-, and 33-fold higher than that of the ZnO/AgI , whereas 45-, 22-, and 136-fold higher than that of the $\text{ZnO}/\text{Ag}_2\text{CrO}_4$ in degradation of rhodamine B, methylene blue, and methyl orange, respectively. It should be pointed out that photocatalyst prepared by ultrasonic irradiation for 60 min has the superior activity.

Recently, metal-free graphitic carbon nitride ($\text{g-C}_3\text{N}_4$) was synthesized via facile template-free sonochemical route and enhanced photodegradation of rhodamine B [43] (Table 1, Entry 6). The authors found that mesoporous $\text{g-C}_3\text{N}_4$ ($112.4 \text{ m}^2 \text{ g}^{-1}$) has almost 5.5 times higher photoactivity than that of bulk $\text{g-C}_3\text{N}_4$ ($8.4 \text{ m}^2 \text{ g}^{-1}$) under visible-light irradiation, which is attributed to the much higher specific surface area, efficient adsorption ability and the unique interfacial mesoporous structure that can favor the absorption of light and separation of photoinduced electron–hole pairs more effectively. Additionally, reactive oxidative species detection studies indicated that the photodegradation of rhodamine B over mesoporous $\text{g-C}_3\text{N}_4$ under visible-light is mainly via superoxide radicals.

Zhou et al. [44] prepared $\text{Zn}_3\text{V}_2\text{O}_7(\text{OH})_2(\text{H}_2\text{O})_2$ and $\text{g-C}_3\text{N}_4/\text{Zn}_3\text{V}_2\text{O}_7(\text{OH})_2(\text{H}_2\text{O})_2$ using sonochemical method with high photocatalytic activities in degradation of methylene blue. Interestingly, the absorption edge of $\text{g-C}_3\text{N}_4/\text{Zn}_3\text{V}_2\text{O}_7(\text{OH})_2(\text{H}_2\text{O})_2$ had red shift reaching 450 nm, and a significantly enhanced photocatalytic performance in degrading methylene blue, which increased to about 5.6 times that of pure $\text{Zn}_3\text{V}_2\text{O}_7(\text{OH})_2(\text{H}_2\text{O})_2$. During the ultrasound process, the heterojunction structure of $\text{g-C}_3\text{N}_4/\text{Zn}_3\text{V}_2\text{O}_7(\text{OH})_2(\text{H}_2\text{O})_2$ was formed and this special structure increased the separation efficiency of photogenerated electron–hole pairs, resulting in the enhancement of photocatalytic performances. Table 1 shows some detailed information about ultrasound assisted synthesis methods of photocatalysts made by selected research groups.

Another approach offering prospects for preparation of nanostructured $\text{TiO}_2/\text{STARBON}^\text{®}$ -polysaccharide-derived mesoporous materials by means of

ultrasound-assisted wet impregnation method was investigated [45]. Interestingly, carboxylic acid groups can be formed on the surface after initial thermal treatment at 400 °C under an oxygen-deficient atmosphere. Each carboxyl acid group acts as an individual nucleation site for TiO₂ formation, which is possible under hydrolysis and condensation reactions promoted by sonication. Finally, the hybrid material (TiO₂/STARBON[®]) is consolidated after thermal treatment at 400 °C. These conditions preserve pure, highly crystalline anatase phase (ca. 30 nm), leading to a reduction in the electron–hole recombination rate at the Starbon surface. TiO₂ nanoparticles are strongly anchored and have good contact with the STARBON-800 structure (i.e., no leaching after 240 min of photocatalytic degradation of phenol), believed to enhance the photoelectron conversion (i.e., as compared with Norit and Graphene oxide supports) of TiO₂ by reducing the recombination of photo-generated electron–hole pairs.

A similar study using a simple and effective ultrasound-assisted wet impregnation method was developed for the preparation of magnetically separable TiO₂/maghemite-silica photo-active nanocomposites tested in the liquid phase selective oxidation of benzyl alcohol [46]. Interestingly, photocatalytic selectivity in organic media (90 % in acetonitrile) towards benzaldehyde was achieved at a benzyl alcohol conversion of ca. 50 %. Solvents played a significant role in the photo-oxidation process with materials showing very good conversion and selectivity in acetonitrile but not in aqueous conditions. Additionally, spatially ordered heterojunction between TiO₂ and γ -Fe₂O₃ and a potential co-catalytic incorporation of Fe³⁺ into the TiO₂ structure might significantly increase the sensitization and decrease the band gap energy of TiO₂, effectively improving the photocatalytic activity and selectivity of these photocatalysts.

In an attempt to better understand the sonophotodeposition method (SPD), the iron-containing TiO₂/zeolite-Y photocatalyst for the selective oxidation of benzyl alcohol was investigated [47]. Generally, photocatalyst prepared by the sonophotodeposition method showed better results, in terms of alcohol conversion and yield of benzaldehyde, in comparison with the photocatalyst prepared by an ultrasound-assisted wet impregnation method. Furthermore, sonication probe and sun-imitating Xenon lamp were tested, and for the first time, a non-noble metal was deposited on the TiO₂ surface by using visible light, but with the help of ultrasound. It is worth noting that sonophotodeposition method is an innovative, simultaneous combination of ultrasonication and ultraviolet irradiation, and is highly energy efficient. Reactions can be carried out at room temperature and atmospheric pressure, very short reaction times and without using strong chemical reduction agents. Additionally, a considerable number of novel mono and bimetallic photocatalysts (e.g., Pd/TiO₂ [48], Pd-Au/TiO₂ [49], Pd-Cu/TiO₂ [50]) have been prepared by sonophotodeposition methodology for selective oxidation of volatile organic compounds (VOCs).

1.3 Ultrasonic Spray Pyrolysis for the Preparation of Photocatalysts

Ultrasonic spray pyrolysis (USP) method is a low-cost, continuous operation, and environmentally benign process with short processing time, which has been used to

synthesize functional materials [51]. A distinctive feature of the method is that it can produce porous microspheres of various compositions without template and with good phase purity, and the morphology can be easily controlled during the process to ensure homogeneous composition distribution in the spheres [52, 53]. In this approach of ultrasonic spray pyrolysis, Suslick et al. [54] synthesized BiVO_4 powders with particles ranging from thin, hollow and porous shells to ball-in-ball-type structures. Interestingly, materials prepared by USP are more active for oxygen evolving photocatalysts under visible-light irradiation ($\lambda > 400 \text{ nm}$) in AgNO_3 solution than commercial BiVO_4 and WO_3 powders, likely due to differences in the particle morphology. It was found that the increase of photocatalytic activity is likely due to the short distances electron-hole pairs must move to reach the surface in order to perform the desired redox reactions. Recently, USP was adapted to fabricate hierarchical porous ZnWO_4 microspheres and evaluated by the degradation of gaseous NO_x under simulated solar light irradiation [55]. It was found that synthesis temperature (650–750 °C) was a key factor influencing the microstructures of resulting ZnWO_4 samples, eventually affecting their photocatalytic activity, and which could be explained by improved optical absorption capability, high specific surface area, and fast separation/diffusion rate of the photogenerated charge carriers. Additionally, electron spin resonance spectroscopy (ESR) method indicated that O_2^- and $\cdot\text{OH}$ radicals function as the major reactive species for NO_x decomposition. Compared to solid spheres, hollow PbWO_4 spheres, which combine the merits of hollow and porous structures, could present improved mass transfer and high surface areas [56]. Moreover, hollow structured PbWO_4 spheres exhibited superior photocatalytic activity to solid spheres (NO removal rate is 35 ppb min^{-1}), due to the differences in microstructure and morphology.

Worth mentioning is the work by Tavares et al. [57] on the enhancement of the photocatalytic efficiency for the photodegradation of methylene blue applying the white emission of CaIn_2O_4 nanocrystals (band gap energy 3.83 eV) prepared by ultrasonic spray pyrolysis at 950 °C (Fig. 2). It should be noted that, USP provides a feasible approach for preparing shape- and size-controlled CaIn_2O_4 nanocrystals using short production times that hold great potential for photocatalytic applications and as photoluminescent materials capable of emitting white light. Moreover, the surface/bulk defects can influence the separation of photogenerated electron-hole pairs on the CaIn_2O_4 under irradiation, and the purity of the products is high and the composition of the powders is easily controlled.

On the other hand, pure and Al-doped ZnO nanostructured thin films were grown at 400 °C on glass substrates by ultrasonic spray pyrolysis after 30, 60 and 120 min, using a 0.5 M zinc acetate precursor solution (Fig. 3a) and 0.5 M zinc nitrate precursor solution (Fig. 3b). The authors [58] found that both pure and Al-doped ZnO nanostructured thin films show good photocatalytic activity regarding the degradation of stearic acid under UV-A light illumination (365 nm), a behavior which is mainly attributed to their good crystallinity and the large effective surface area.

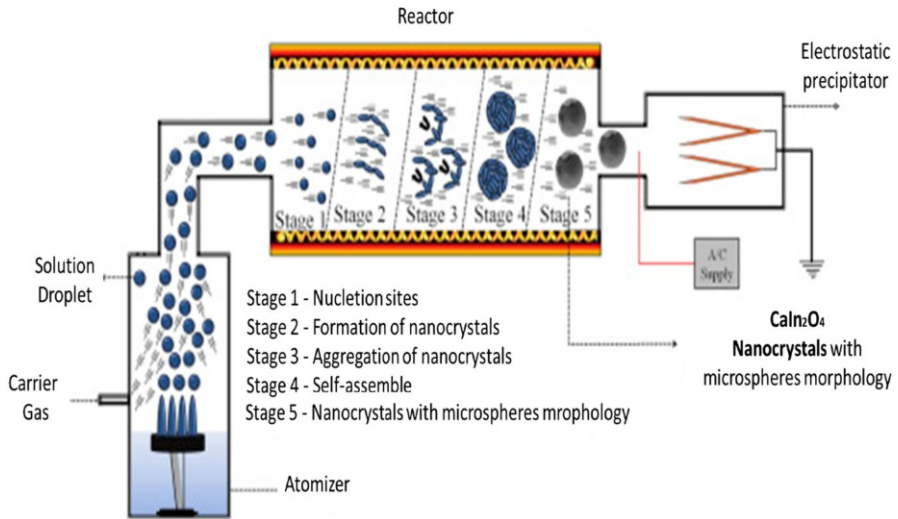


Fig. 2 Schematic representation of CaIn_2O_4 nanocrystals prepared by ultrasonic spray pyrolysis. Reproduced and modified from Ref. [57] with kind permission from Springer Science and Business Media

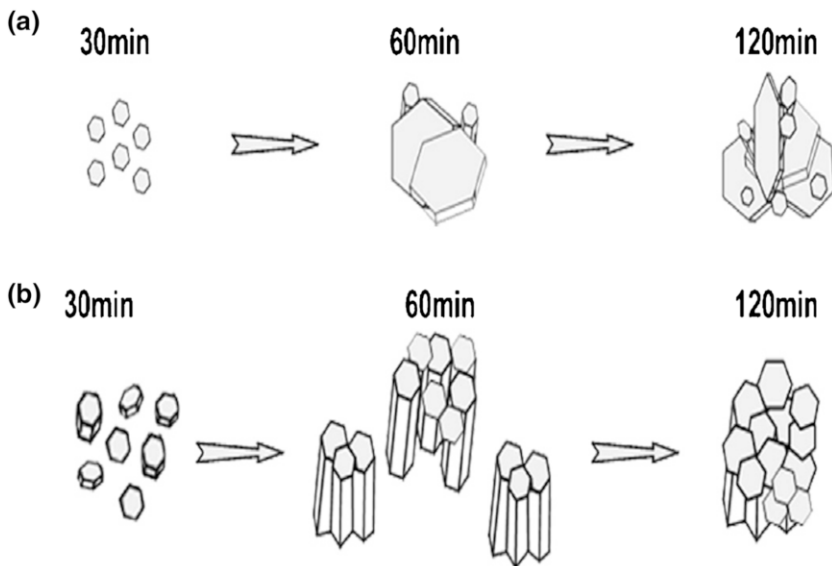


Fig. 3 ZnO growth mechanism using ultrasonic spray pyrolysis after 30, 60 and 120 min of spraying time, using **a** 0.5 M Zn acetate, **b** 0.5 M Zn nitrate precursor solution. Reproduced from Ref. [58] with kind permission from Springer Science and Business Media

2 Perovskite Solar Cells and Quantum Dots Photovoltaics

The interest in sonochemistry as a versatile tool for materials synthesis has been increasing, especially in the case of preparation of nanostructured materials for energy conversion like quantum dots, solar photovoltaic cells and dye-sensitized solar cells [59, 60]. The application of ultrasound allows to obtain a uniform shape and highly pure nanoparticles with a narrow size distribution, which has influence on the unique characteristics of photovoltaic devices. Additionally, ultrasound-assisted methodologies can decrease the time of synthesis, consequently reducing operating costs and develop effective manufacturing processes [60, 61]. Hence, it is a promising inexpensive alternative for the production of the next generation of solar cells such as quantum dot sensitized solar cells (QDSCs) or perovskite solar cells (PSCs) [62]. Perovskites are a class of compounds that possess well-defined crystal structure with formula ABX_3 , where, the A and B sites are engaged by cations and the X site is occupied by the anion. Depending on the type of the ions, they can form various perovskite crystal geometries with different features. The cations in the lattice are able to enhance and modify the band structure, which is particularly important from the point of view of photophysical properties [63, 64]. Thus, perovskites as an active layer in photovoltaic systems can deliver high open-circuit voltages and lead to the harvesting of light from a broad spectrum [64]. Perovskite solar cells are able to absorb the shorter wavelengths of visible light corresponding to photons with higher energy. Consequently, they can reach the maximum voltage of cells adequate to the maximum electrical power that comes from incident photons. Therefore, PSCs that stem from dye-sensitized solar cells (DSSCs) are considered as a forerunners of emerging photovoltaic technology [64, 65].

Perovskites first used for solar applications were documented in a seminal article by Miyasaka and co-workers in 2009 [66], and then by Park and co-workers 2 years later [67]. In all cases, the perovskite solar cells emerge as long-running, durable photovoltaic devices with high efficiency, and have been increasing from 10 to 20 % in the last few years [68, 69]. Due to fact that PCSs possess an enhanced light-harvesting system, improved charge separation process as well revised charge transfer and charge collection [68, 69], the power conversion efficiency (PCE) of perovskites solar cells is remarkable higher compared to the previous generation solar cells devices [i.e., wafer-based silicon devices or thin film SCs made from cadmium telluride (CdTe)]. The properties mentioned above can be attributed to the special structure of these materials, which mainly reflect on their application of photovoltaic technology as well as of other domains [70].

The next interesting possibility leading to more efficiently working solar cells is the development of quantum dot sensitized solar cells. It is worth noting that the energy conversion of solar cells directly depends on their structure, i.e., conductive substrates, semiconducting layers and in particular, sensitizing molecules (dye or quantum dots). The structure of DSSCs is similar to that of QDSCs; however, the power conversion efficiency (PCE) is remarkably lower in the case of QDSCs. Nevertheless, due to the relatively low cost related to using inexpensive

semiconductors and a simple fabrication, possible approaches for improving PCE are still under debate [61, 62, 71].

In this subsection, we would like to focus the readers' attention on the use of sonochemical methodology as a convenient tool for the preparation of solar cells with higher power conversion efficiency; indicating the influence of ultrasounds on the formation of quantum dots and perovskite solar cells, and pointing out the current state of the art.

2.1 Sonochemical Synthesis of Perovskites and Quantum Dots

The wide range of sonochemical methods used for the synthesis of perovskite-type oxides ABO_3 have been well reviewed by Colmenares group [72]. Among the most effective sonication-based processes, we can distinguish mainly co-precipitation methods, sol-gel methods, and hydrothermal methods as well aerosol synthetic techniques [e.g., the ultrasonic spray pyrolysis (USP)]. In comparison with conventional methodologies, which are mentioned above, the USP allows for control over size and shape of particles in a simple and more reproducible way. The selection of optimal parameters (such as ultrasound frequency, characteristic of the precursor solution and temperature) allows a nanomaterial with desirable properties to be obtained. However, it is not the only effective approach for the preparation of thin-films and ultrafine nanostructures in terms of manufacturing photovoltaic devices. An interesting concept that involves combination of ultrasonic spray technique and thermal evaporation process was reported by Xia et al. [73]. The modified deposition method assisted by ultrasonic spray coating used for the formation of $CH_3NH_3PbI_3$ thin film layers enables control of morphology. The obtained perovskite film possesses larger crystal size (>500 nm), which result in higher carriers mobility and lower charge recombination. Thereby, uniform coverage prevents an undesirable short circuit between the top and back surface contacts of a solar cell, resulting in an increase in the power conversion of photovoltaic devices [73].

$CH_3NH_3PbI_3$ nanoparticles (NPs) can also be synthesized by another sonochemical technique (Table 2; Entry 1) [74]. The method applied in this work involves ultrasonic irradiation for the preparation of ultrafine nanocrystal sensitizers for solar applications. The sonochemistry reaction is carried out in a non-aqueous solution, leading to the generation of nanoparticles with polygonal shapes in the narrow size-range. The sonochemical synthesis of methylammonium lead halide takes place only in isopropanol medium, and the presence of water reduces the reaction rate [74, 75]. Additionally, it has been shown that the morphology of the particles strictly depends on the irradiation time [74]. The nanoparticles obtained during 10 min of reaction exhibited irregular shapes, whereas the particles achieved after 20–30 min showed an opposite trend and formed hexagonal or triangles configuration [74]. Nevertheless, the shape of perovskites can be changed when the synthesis step is preceded by ultrasonic pretreatment of the precursor solution. Kesari and Athawale [75] demonstrated that ultrasound-assisted method arranged to $CH_3NH_3PbI_3$ synthesis allows to obtain a rod shape and a tetragonal crystal structure. Results indicate that the preparation route has an important impact on a

Table 2 Selected examples of sonochemical methods applied for the synthesis of active solar cells layers

Entry	Ultrasound source	Key parameters	Remarks	Refs.
Perovskites				
1	The ultrasonic transducer (frequency 20 kHz) was operated at an amplitude of 60 %	Time of irradiation increased from 10 to 30 min	The $\text{CH}_3\text{NH}_3\text{PbI}_3$ nanoparticles of polygonal shapes in the size range of 10–40 nm were obtained until 20 min reaction, whereas the shorter time of irradiation resulted in non-uniform shapes	[74]
2	A multiwave ultrasonic generator equipped with titanium oscillator (12.5 mm) operating at 20 kHz	Power of ultrasound was adjusted in the range from 50 to 70 W	The particle size of CuInS_2 was about 100 nm when the power of ultrasound was equal to 50 W—increasing the power led to formation of uniform particles with size of 60 nm	[81]
3	A sonication system operated at 59 kHz and a power output of 99 W	Concentration of precursor and sonication time (various variants)	The desired kesterite phase of CuZnSnS_2 was obtain using longer time of irradiation and higher precursor concentration	[82]
Quantum dots				
4	A ultrasound probe (frequency 20 kHz, 130 W/cm ²) operated at 50 % amplitude	The effect of ultrasound on the reduction process	The reduction process of tellurium does not exceed 15 min and allows to obtain CdTe QDs with the band gap value (2.3 eV)	[85]
5	Ultrasound horn with 1.9 cm diameter (20 kHz, output acoustic power 45.5 W)	The sonication time (0–45 min) and temperature (40–60 °C)	The CdS nanoparticles have uniform spherical morphology with size around 2 nm (60 °C after 45 min of irradiation).	[86]

sample's morphology and hence on its optical properties. It has been found that the band gap of the $\text{CH}_3\text{NH}_3\text{PbI}_3$ hybrid materials synthesized by ultrasonic method (from standard 1.5 to 2.25 eV) shifted into the blue region, which can be a sign that the materials possess features of quantum dots [74]. A similar behaviour of NaTaO_3 perovskite was observed by Vázquez-Cuchillo et al. [76], when the crystalline materials were more light sensitive in the UV-range compared to the same materials obtained by other technique (i.e., solid-state method). On the other hand, the defects forming on the surface due to cavitation effects can also turn to light electron capture centres and decrease the band-gap energy, which is rather more favorable from the photocatalytic point of view [77].

The application of ultrasound in perovskites' synthesis allows to obtain the required products using low temperature synthesis methods. The great number of cavitation active sites generated under ultrasonic irradiation led to materials that possess a small particle size and a uniform bulk [77, 78]. However, the formation and growth of nanosheets and face-like particles depend on ultrasound as well as on calcination conditions. The calcination temperature affects the crystallinity,

microstructure, optical and dielectric features of the samples. Consequently, the particles that were synthesized under the same ultrasonic conditions and calcined at different temperatures exhibited diverse properties as proved by various researcher groups [79, 80]. Interesting is the fact that contrary to previous studies, Wirunchit et al. [80] presented a facile sonochemical synthesis of perovskite oxides without any sintering and calcination step (Fig. 4). In this case, the formation of nanoparticles with a spherical morphology and a narrow particle size distribution occurs through the sonocrystallization process, whereas the effect of ultrasonic irradiation generates and promotes the nucleation as well as inhibits or delays the crystal growth process [80]. Furthermore, the crystal size and morphology of nanostructures also depend on the power energy of ultrasound (Table 2; Entry 2). Results presented by Amiri et al. indicate that increasing the power of ultrasound causes the production of uniform CuInS_2 nanoparticles with small size (~ 60 nm), whereas using the lower ultrasonic energy led to the creation of bigger aggregated particles with a lump-like structure [81].

The one-step sonochemical method proposed by Liu et al. [82] can be applied for the production of $\text{Cu}_2\text{ZnSnS}_4$ perovskites (Table 2; Entry 3). By this way, the propitious shape of nanoparticles can be obtained by facile and rapid synthesis through the selection of an optimal precursor's concentration as well the above-mentioned sonication time [82]. However, in the event of the production of high quality inks for solar-cells fabrication, a more suitable methodology seems to be the ultrasound-assisted microwave solvothermal method. Unlike the others, the nucleation–dissolution–recrystallization mechanism allows to obtain Cu_2ZnSn_4

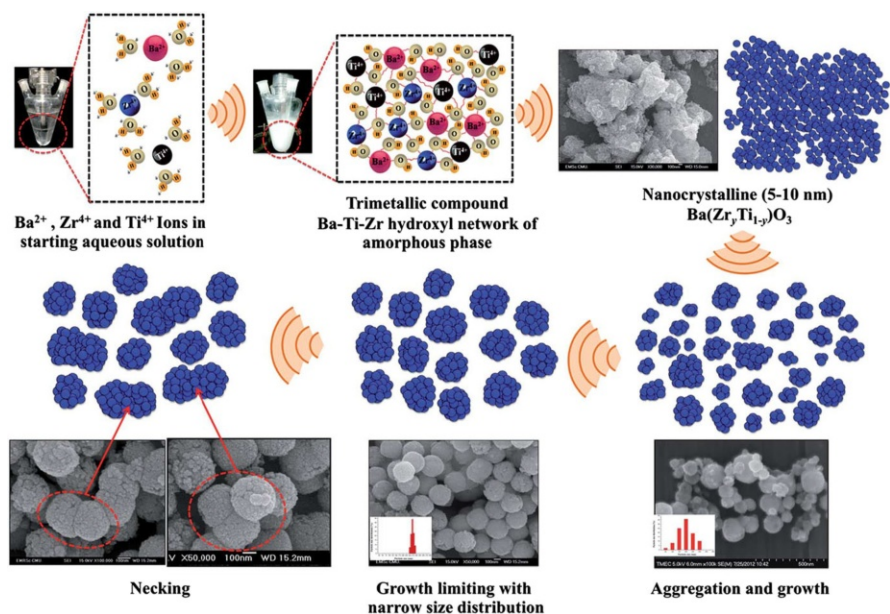


Fig. 4 Schematic diagrams illustrating formation of the crystal growth mechanism. Reproduced from [80] with permission of The Royal Society of Chemistry

nanosized particles with hexagonal prisms structure, due to fact that the synergistic effect of ultrasound and microwave plays a key role in the growth process of wurtzite phase [83, 84].

Ultrasound-assisted processes are also used to prepare quantum dot particles (QDs) for solar cells application. The simple and fast sonochemical methodology provides monodispersed CdTe QDs with a strong quantum confinement regime (Table 2; Entry 4). The application of ultrasound allows one to control the morphology and reduce the surface defects of quantum dots. As a result, this allowed the production of nanoparticles with only one fluorescence band, which is beneficial in terms of photovoltaic devices [85]. Furthermore, it is clearly shown that the application of ultrasound, in particular the sonication time, has an influence on the particle size distribution and the growth kinetics (Table 2; Entry 5) [86]. Results indicate that the increase of particle size at longer time is attributed to the diffusion-limited coarsening process, which is accelerated by cavitation. Thus, the effect of ultrasound irradiation causes that the synthesis of QDs nanoparticles occurs in shorter time using low temperature methodology such as the micro-emulsion method [86]. Additionally, sonochemically synthesized QDs possess better optical properties and are able to produce a large amount of reactive oxygen species (ROS), which may influence a further course of the photochemical processes [87].

2.2 Sonochemical Solar Cells Fabrication

Sonochemical methodology can be used as the first step toward the synthesis of photoactive layers or as the second step for the preparation of solar cells devices. The wide range of ultrasound parameters (i.e., ultrasonic power, frequency and time) have a positive influence on the size, morphology, structure or the surface area, and in consequence on optical as well as electrical properties of photovoltaic devices [81]. It was proven that the ultrasound irradiation accelerates the nucleation process, and promotes ionic and mass diffusion, which permit the synthesis of structures with desirable features in terms of the photovoltaic application [88]. For this reason, ultrasounds play a crucial role in the preparation of solar cells structures and cells' components.

The photoactive layers can consist of perovskite nanoparticles, quantum dots or hierarchical hollow spheres which can improve the efficiency of dye-sensitized solar cells (DSSCs), or quantum dots solar cells [89]. The DSSCs type of solar cells exhibited significant better parameters (i.e., a short circuit current density, open circuit voltage and fill factor) in comparison to standard nanoparticle photoelectrode, consequently increasing the power conversion efficiency and photocatalytic performance [90]. The hierarchical structures (HSs) (mainly ZnO, TiO₂, SnO₂) synthesized through the sonochemistry methodology demonstrate required properties caused by their nano/micro combined architectures. They enable fast electron transport due to an ideal network created by nanosheets connection. Additionally, HSs possess a large surface area, which improves the accessibility for incident photons [88, 91]. Furthermore, dye-sensitized solar cells based on hierarchical structures are able to enhance the light harvesting capability and improve the

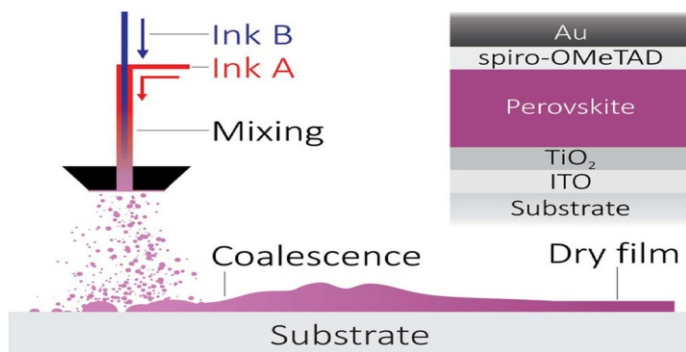


Fig. 5 Schematic of pumped ultrasonic spray coating for perovskite precursor deposition. Reproduced from [94] with permission of The Royal Society of Chemistry

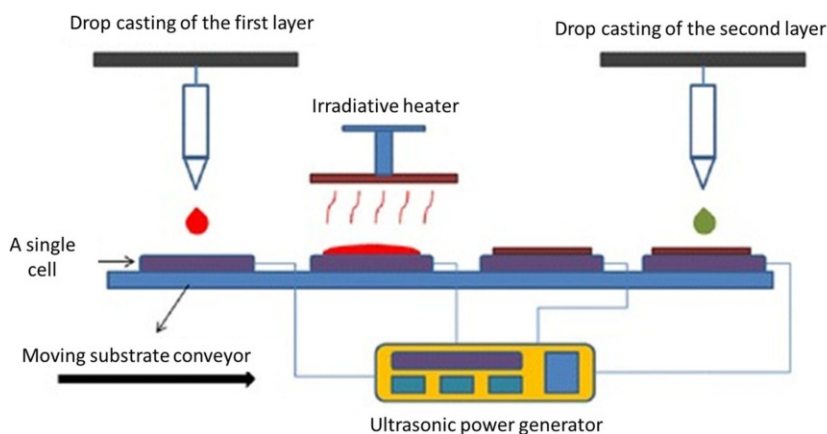


Fig. 6 Scheme of the automated manufacturing of SVADC process for solar cells fabrication. Reproduced and modified from Ref. [96] with kind permission from Springer Science and Business Media

efficiency of SCs [91]. Using ultrasound treatment technique (UST), the change of the solar power efficiency can be improved up to 50 % [92].

Among many sonochemical methods used for the fabrication of solar cells, we can spot the ultrasonic spray coating method (USP). The USP allows one to deposit uniform perovskite thin films on glass substrates (Fig. 5) [93, 94]. The formation of dense films having a surface coverage above 85 % guarantees maximum device efficiency. For this reason, the USP coating leads to an increase of the power conversion efficiencies of perovskite-based photovoltaics devices [94]. Concurrently, ultrasonic spray coating with various rates provides the quick optimization of thickness, precursor ratios and resulting pinhole-free layer crystallinity [95]. Furthermore, USP provides high-performance flexible perovskite solar cells by using a combination of ultrasonic spray-coating and low thermal budget photonic curing [94].

As the next promising tool for the fabrication of micro-thin as well as nano-thin films, the substrate vibration-assisted drop casting method (SVADC) has emerged. Due to fact that the SVADC is scalable casting methodology, it can be used to prepare an array of thin-film solar cells, perovskite, and quantum-dot solar cells or other thin-film devices through an automated fabrication process (Fig. 6). The same manufacturing process allows several layers of a thin-film solar cell to be deposited. It is worth to note that the solution properties, surface wettability, impingement conditions as well as substrate vibration have influence on the maximum effective and uniform surface of solar cells. Due to the fact that this method allows one to obtain a simple structure (possessing efficiency over 3 %) without requiring an optimization process and the application of expensive materials or treatments, the SVADC might replace the old generation techniques of ultrasound-assisted methods used for the fabrication of silicon wafers [96].

Acknowledgments Prof. Dr. Juan C. Colmenares would like to thank the National Science Centre (Poland) for support within the project Sonata Bis Nr. 2015/18/E/ST5/00306. Pawel Lisowski would like also to thank the National Science Centre (NCN) in Poland for the research project 2015/17/N/ST5/03330.

Open Access This article is distributed under the terms of the Creative Commons Attribution 4.0 International License (<http://creativecommons.org/licenses/by/4.0/>), which permits unrestricted use, distribution, and reproduction in any medium, provided you give appropriate credit to the original author(s) and the source, provide a link to the Creative Commons license, and indicate if changes were made.

References

1. Colmenares JC (2014) Sonication-induced pathways in the synthesis of light-active catalysts for photocatalytic oxidation of organic contaminants. *ChemSusChem* 7:1512–1527
2. Sathishkumar P, Mangalaraja RV, Anandan S (2016) Review on the recent improvements in sonochemical and combined sonochemical oxidation processes—a powerful tool for destruction of environmental contaminants. *Renew Sust Energ Rev* 55:426–454
3. Yu C-L, Yu JC, He H-B, Zhou W-Q (2016) Progress in sonochemical fabrication of nanostructured photocatalysts. *Rare Met* 35:211–222
4. Sander JRG, Zeiger BW, Suslick KS (2014) Sonocrystallization and sonofragmentation. *Ultrason Sonochem* 21:1908–1915
5. Skorb EV, Möhwald H (2016) Ultrasonic approach for surface nanostructuring. *Ultrason Sonochem* 29:589–603
6. Colmenares JC (2013) Ultrasound and photochemical procedures for nanocatalysts preparation: application in photocatalytic biomass valorization. *J Nanosci Nanotechnol* 13:4787–4798
7. Rahnamaeiyan S, Nasiri M, Alborzi A, Tabatabaei SM (2016) Sonochemical synthesis and characterization of zinc tungstate nanoparticles and investigation of its photocatalyst application. *J Mater Sci Mater Electron* 27:1113–1117
8. Khademolhoseini S, Zakeri M, Rahnamaeiyan S, Nasiri M, Talebi R (2015) A simple sonochemical approach for synthesis of cadmium molybdate nanoparticles and investigation of its photocatalyst application. *J Mater Sci Mater Electron* 26:7303–7308
9. Patil HR, Murthy ZVP (2016) Preparation of vanadium pentoxide nanoparticles by ionic liquid-assisted sonochemical method: effect of ionic liquid stericity on particle characteristics. *Chem Eng Process* 102:130–140

10. Sadeghi M (2016) Investigation of the structural, optical and magnetic properties of CuMoO_4 nanoparticles synthesized through a sonochemical method. *J Mater Sci Mater Electron* 27:5796–5801
11. An L, Wang G, Cheng Y, Zhao L, Gao F, Tian Y (2015) Ultrasonic-assisted synthesis of visible-light-driven $\text{TiO}_2/\text{Bi}_2\text{O}_3$ nanocomposite photocatalysts: characterization, properties and azo dye removal application. *Res Chem Intermed* 41:7449–7461
12. Fujishima A, Honda K (1972) Electrochemical photolysis of water at a semiconductor electrode. *Nature* 238:37–38
13. Graetzel M, Janssen RAJ, Mitzi DB, Sargent EH (2012) Materials interface engineering for solution-processed photovoltaics. *Nature* 488:304–312
14. Chen X, Shen S, Guo L, Mao SS (2010) Semiconductor-based photocatalytic hydrogen generation. *Chem Rev* 110:6503–6570
15. Chen X, Mao SS (2007) Titanium dioxide nanomaterials: synthesis, properties, modifications, and applications. *Chem Rev* 107:2891–2959
16. Zhu G, Shan Y, Lin T, Zhao W, Xu J, Tian Z, Zhang H, Zheng C, Huang F (2016) Hydrogenated blue titania with high solar absorption and greatly improved photocatalysis. *Nanoscale* 8:4705–4712
17. Wang M, Nie B, Yee K-K, Bian H, Lee C, Lee HK, Zheng B, Lu J, Luo L, Li YY (2016) Low-temperature fabrication of brown TiO_2 with enhanced photocatalytic activities under visible light. *Chem Commun* 52:2988–2991
18. Chen X, Liu L, Yu PY, Mao SS (2011) Increasing solar absorption for photocatalysis with black hydrogenated titanium dioxide nanocrystals. *Science* 133:746–750
19. Mehta M, Kodan N, Kumar S, Kaushal A, Mayrhofer L, Walter M, Moseler M, Dey A, Krishnamurthy S, Basu S, Singh AP (2016) Hydrogen treated anatase TiO_2 : a new experimental approach and further insights from theory. *J Mater Chem A* 4:2670–2681
20. Chen X, Liu L, Liu Z, Marcus MA, Wang W-C, Oyler NA, Grass ME, Mao B, Glans P-A, Yu PY, Guo J, Mao SS (2013) Properties of disorder-engineered black titanium dioxide nanoparticles through hydrogenation. *Sci Rep* 3:1510–1516
21. Sinhamahapatra A, Jeon J-P, Yu J-S (2015) A new approaches to prepare highly active and stable black titania for visible light-assisted hydrogen production. *Energy Environ Sci* 8:3539–3544
22. Lin T, Yang C, Wang Z, Yin H, Lu X, Huang F, Lin J, Xie X, Jiang M (2014) Effective nonmetal incorporation in black titania with enhanced solar energy utilization. *Energy Environ Sci* 7:967–972
23. Chen X, Liu L, Huang F (2015) Black titanium dioxide (TiO_2) nanomaterials. *Chem Soc Rev* 44:1861–1885
24. Wang Z, Yang C, Lin T, Yin H, Chen P, Wan D, Xu F, Huang F, Lin J, Xie X, Jiang M (2013) H-doped black titania with very high solar absorption and excellent photocatalysis enhanced by localized surface plasmon resonance. *Adv Funct Mater* 23:5444–5450
25. Hu YH (2012) A highly efficient photocatalyst-hydrogenated black TiO_2 for the photocatalytic splitting of water. *Angew Chem Int Ed* 51:12410–12412
26. Zhou W, Li W, Wang J-Q, Qu Y, Yang Y, Xie Y, Zhang K, Wang L, Fu H, Zhao D (2014) Ordered mesoporous black TiO_2 as highly efficient hydrogen evolution photocatalyst. *J Am Chem Soc* 136:9280–9283
27. Fan C, Chen C, Wang J, Fu X, Ren Z, Qian G, Wang Z (2015) Black hydroxylated titanium dioxide prepared via ultrasonication with enhanced photocatalytic activity. *Sci Rep* 5:11712–11721
28. Mao L, Liu J, Zhu S, Zhang D, Chen Z, Chen C (2014) Sonochemical fabrication of mesoporous TiO_2 inside diatom frustules for photocatalyst. *Ultrason Sonochem* 21:527–534
29. Magesan P, Ganesan P, Umopathy UJ (2016) Ultrasonic-assisted synthesis of doped TiO_2 nanocomposites: characterization and evaluation of photocatalytic and antimicrobial activity. *Optik* 127:5171–5180
30. Anandan S, Lana-Villarreal T, Wu JJ (2015) Sonochemical synthesis of mesoporous NiTiO_3 ilmenite nanorods for the catalytic degradation of tergitol in water. *Ind Eng Chem Res* 54:2983–2990
31. Alammar T, Hamm I, Wark M, Mudring AV (2015) Low-temperature route to metal titanate perovskite nanoparticles for photocatalytic applications. *Appl Catal B* 178:20–28
32. Huerta-Flores AM, Torres-Martínez LM, Sánchez-Martínez D, Zarazúa-Morín ME (2015) SrZrO_3 powders: alternative synthesis, characterization and application as photocatalysts for hydrogen evolution from water splitting. *Fuel* 158:66–71
33. Wang J, Neaton JB, Zheng H, Nagarajan V, Ogale SB, Liu B, Viehland D, Vaithyanathan V, Schlom DG, Waghmare UV, Spaldin NA, Rabe KM, Wuttig M, Ramesh R (2003) Epitaxial BiFeO_3 multiferroic thin film heterostructures. *Science* 299:1719–1722

34. Soltani T, Entezari MH (2013) Sono-synthesis of bismuth ferrite nanoparticles with high photocatalytic activity in degradation of Rhodamine B under solar light irradiation. *Chem Eng J* 223:145–154
35. Soltani T, Entezari MH (2013) Photolysis and photocatalysis of methylene blue by ferrite bismuth nanoparticles under sunlight irradiation. *J Mol Catal A: Chem* 377:197–203
36. Soltani T, Entezari MH (2013) Solar photocatalytic degradation of RB5 by ferrite bismuth nanoparticles synthesized via ultrasound. *Ultrason Sonochem* 20:1245–1253
37. Soltani T, Entezari MH (2014) Solar-Fenton catalytic degradation of phenolic compounds by impure bismuth ferrite nanoparticles synthesized via ultrasound. *Chem Eng J* 251:207–216
38. Saffari J, Mir N, Ghanbari D, Khandan-Barani K, Hassanabadi A, Hosseini-Tabatabaei MR (2015) Sonochemical synthesis of $\text{Fe}_3\text{O}_4/\text{ZnO}$ magnetic nanocomposites and their application in photocatalytic degradation of various organic dyes. *J Mater Sci Mater Electron* 26:9591–9599
39. Jamali-Sheini F, Yousefi R, Bakr NA, Cheraghizade M, Sookhakistan M, Huang NM (2015) Highly efficient photo-degradation of methyl blue and band gap shift of SnS nanoparticles under different sonication frequencies. *Mater Sci Semicond Process* 32:172–178
40. Kiantazh F, Habibi-Yangjeh A (2015) Ultrasonic-assisted one-pot preparation of $\text{ZnO}/\text{Ag}_3\text{VO}_4$ nanocomposites for efficiently degradation of organic pollutants under visible-light irradiation. *Solid State Sci* 49:68–77
41. Shekofteh-Gohari M, Habibi-Yangjeh A (2016) Ultrasonic-assisted preparation of novel ternary $\text{ZnO}/\text{AgI}/\text{Fe}_3\text{O}_4$ nanocomposites as magnetically separable visible-light-driven photocatalysts with excellent activity. *J Colloid Interface Sci* 461:144–153
42. Shaker-Agjeekandy S, Habibi-Yangjeh A (2016) Ultrasonic-assisted preparation of novel ternary $\text{ZnO}/\text{AgI}/\text{Ag}_2\text{CrO}_4$ nanocomposites as visible-light-driven photocatalysts with excellent activity. *Mater Sci Semicond Process* 44:48–56
43. Kumar S, Surendar T, Kumar B, Baruah A, Shanker V (2014) Synthesis of highly efficient and recyclable visible light responsive mesoporous $g\text{-C}_3\text{N}_4$ photocatalyst via facile template-free sonochemical route. *RSC Adv* 4:8132–8137
44. Zhan S, Zhou F, Huang N, Yin Y, Wang M, Yang Y, Liu Y (2015) Sonochemical synthesis of $\text{Zn}_3\text{V}_2\text{O}_7(\text{OH})_2(\text{H}_2\text{O})_2$ and $g\text{-C}_3\text{N}_4/\text{Zn}_3\text{V}_2\text{O}_7(\text{OH})_2(\text{H}_2\text{O})_2$ with high photocatalytic activities. *J Mol Catal A Chem* 401:41–47
45. Colmenares JC, Lisowski P, Łomot D (2013) A novel biomass-based support (Starbon) for TiO_2 hybrid photocatalysts: a versatile green tool for water purification. *RSC Adv* 3:20186–20192
46. Colmenares JC, Ouyang W, Ojeda M, Kuna E, Chernyayeva O, Lisovtyskiy D, De S, Luque R, Balu AM (2015) Mild ultrasound-assisted synthesis of TiO_2 supported on magnetic nanocomposites for selective photo-oxidation of benzyl alcohol. *Appl Catal B* 183:107–112
47. Magdziarz A, Colmenares JC, Chernyayeva O, Kurzydłowski K, Grzonka J (2015) Iron-containing titania photocatalyst prepared by the sonophotodeposition method for the oxidation of benzyl alcohol. *ChemCatChem* 8:536–539
48. Colmenares JC, Magdziarz A, Łomot D, Chernyayeva O, Lisovtyskiy D (2014) A new photocatalytic tool in VOCs abatement: effective synergetic combination of sonication and light for the synthesis of monometallic palladium-containing TiO_2 . *Appl Catal B* 147:624–632
49. Colmenares JC, Lisowski P, Łomot D, Chernyayeva O, Lisovtyskiy D (2015) Sonophotodeposition of bimetallic photocatalysts $\text{Pd-Au}/\text{TiO}_2$: application to selective oxidation of methanol to methyl formate. *ChemSusChem* 8:1676–1685
50. Lisowski P, Colmenares JC, Łomot D, Chernyayeva O, Lisovtyskiy D (2016) Preparation by sonophotodeposition method of bimetallic photocatalysts $\text{Pd-Cu}/\text{TiO}_2$ for sustainable gaseous selective oxidation of methanol to methyl formate. *J Mol Catal A Chem* 411:247–256
51. Wegner K, Vinati S, Piseri P, Antonini A, Zelioli A, Barborini E, Ducati C, Milani P (2012) High-rate production of functional nanostructured films and devices by coupling flame spray pyrolysis with supersonic expansion. *Nanotechnology* 23:185603–185615
52. Mwakikunga BW (2014) Progress in ultrasonic spray pyrolysis for condensed matter sciences developed from ultrasonic nebulization theories since michael faraday. *Crit Rev Solid State Mater Sci* 39:46–80
53. Overcash JW, Suslick KS (2015) High surface area iron oxide microspheres via ultrasonic spray pyrolysis of ferritin core analogues. *Chem Mater* 27:3564–3567
54. Dunkle SS, Helmich RJ, Suslick KS (2009) BiVO_4 as a visible-light photocatalyst prepared by ultrasonic spray pyrolysis. *J Phys Chem C* 113:11980–11983

55. Huang Y, Gao Y, Zhang Q, J-j Cao, R-j Huang, Ho W, Lee SC (2016) Hierarchical porous ZnWO_4 microspheres synthesized by ultrasonic spray pyrolysis: characterization, mechanistic and photocatalytic NO_x removal studies. *Appl Catal A* 515:170–178
56. Dong F, Huang Y, Zou S, Liu J, Lee SC (2011) Ultrasonic spray pyrolysis fabrication of solid and hollow PbWO_4 spheres with structure-directed photocatalytic activity. *J Phys Chem C* 115:241–247
57. Tavares MTS, Melo MM, Araújo VD, Tranquilin RL, Almeida CRR, Paskocimas CA, Bomio MRD, Longo E, Motta FV (2016) Enhancement of the photocatalytic activity and white emission of CaIn_2O_4 nanocrystals. *J Alloy Compd* 658:316–323
58. Kenanakis G, Katsarakis N (2014) Ultrasonic spray pyrolysis growth of ZnO and ZnO : Al nanostructured films: application to photocatalysis. *Mater Res Bull* 60:752–759
59. Bang JH, Suslick KS (2010) Applications of ultrasound to the synthesis of nanostructured Materials. *Adv Mater* 22:1039–1059
60. Babu SG, Neppolian B, Ashokkumar M (2015) Ultrasound assisted synthesis of nanoparticles for energy and environmental applications. In: Ashokkumar M (ed) *Handbook of ultrasonics and sonochemistry*, 1st edn. Springer, Singapore, pp 1–34
61. Kim H (2012) Ultrasonic synthesis of materials for energy conversion devices. Dissertation, University of California University of Illinois
62. Rühle S, Shalom M, Zaban A (2010) Quantum-dot-sensitized solar cells. *ChemPhysChem* 11:2290–2304
63. Ahmed MI, Habib A, Javid SS (2015) Perovskite solar cells: potentials, challenges, and opportunities. *Int J Photoenergy*. doi:10.1155/2015/592308
64. Kanhere P, Chen Z (2014) A review on visible light active perovskite-based photocatalysts. *Molecules* 19:19995–20022
65. Park NG (2015) Perovskite solar cells: an emerging photovoltaic technology. *Mater Today* 18(2):65–72
66. Kojima A, Teshima K, Shirai Y, Miyasaka T (2009) Organometal halide perovskites as visible-light sensitizers for photovoltaic cells. *J Am Chem Soc* 131:6050–6051
67. Im JH, Lee CR, Lee JW, Park SW, Park NG (2011) 6.5% efficient perovskite quantum-dot-sensitized solar cell. *Nanoscale* 3:4088–4093
68. Jung HS, Park NG (2014) Perovskite solar cells: from materials to devices. *Small* 11(1):10–25
69. Jasim KE (2015) Quantum dots solar cells. In: Kosyachenko LA (ed) *Solar cells—new approaches and reviews*, 1st edn. InTech, pp 304–329. doi:10.5772/59159
70. Zhao X, Park NG (2015) Stability issues on perovskite solar cells. *Photonics* 2:1139–1151
71. Jun HK, Careem MA, Arof A (2013) Quantum dot-sensitized solar cells—perspective and recent developments: a review of Cd chalcogenide quantum dots as sensitizers. *Renew Sustain Energy Rev* 22:148–167
72. Colmenares JC, Magdziarz A, Lisowski P (2015) Application of microwave and ultrasound irradiation in the synthesis of perovskite-type oxides ABO_3 . In: Granger P, Parvulescu VI, Parvulescu VI, Prellier W (eds) *Perovskites and related mixed oxides concepts and applications*, 1st edn. Wiley, Weinheim, pp 91–113
73. Xia Z, Chai G, Wang Y, Zhou H (2015) Uniform perovskite photovoltaic thin films via ultrasonic spray assisted deposition method. In: *Photovoltaic Specialist Conference (PVSC)*, New Orleans, IEEE, pp 1–4
74. Kumar VB, Gouda L, Porat Z, Gedanken A (2016) Sonochemical synthesis of $\text{CH}_3\text{NH}_3\text{PbI}_3$ perovskite ultrafine nanocrystal sensitizers for solar energy applications. *Ultrason Sonochem* 32:54
75. Kesari Y, Athawale A (2015) Ultrasound assisted bulk synthesis of $\text{CH}_3\text{NH}_3\text{PbI}_3$ perovskite at room temperature. *Mater Lett* 159:97
76. Vázquez-Cuchillo O, Manzo-Robledo A, Zanella R, Elizondo-Villareal N, Cruz-López A (2013) Characterization of NaTaO_3 synthesized by ultrasonic method. *Ultrason Sonochem* 20:498–501
77. Lishan SJ, Tong D, Qingbiao L, Yong T (2007) Study of photocatalytic performance of SrFeO_{3x} by ultrasonic radiation. *Catal* 8:963–966
78. Luevano-Hipolito E, Martinez-de la Cruz A, Lopez Cuellar E (2014) Synthesis, characterization, and photocatalytic properties of g- Bi_2MoO_6 prepared by co-precipitation assisted with ultrasound irradiation. *J Taiwan Inst Chem Eng* 45:2749–2754
79. Wattanawikkam CH, Pecharapa W (2015) Optical, dielectric and photocatalytic properties of perovskite ZnTiO_3 nanoparticle synthesized by sonochemical process. In: *Joint IEEE International Symposium on the Applications of Ferroelectric, International Symposium on Integrated Functionalities, and Piezoelectric Force Microscopy Workshop*, Singapore, IEEE, pp 280–284

80. Wirunchit S, Charoonsuk T, Vittayakorn N (2015) Facile sonochemical synthesis of near spherical barium zirconate titanate ($\text{BaZr}_{1-y}\text{TiyO}_3$; BZT); perovskite stability and formation mechanism. *RSC Adv* 5:38061–38096
81. Amiri O, Salavati-Niasari M, Sabet M, Ghanbari D (2014) Sonochemical method for preparation of copper indium sulfide nanoparticles and their application for solar cell. *Comb Chem High Throughput Screen* 17:183–189
82. Liu Y, Xu J, Ni Z, Fang G, Tao W (2015) One-step sonochemical synthesis route towards kesterite $\text{Cu}_2\text{ZnSnS}_4$ nanoparticles. *J Alloy Compd* 630:23–28
83. Wang W, Shen H, Yao H, Li J (2014) Preparation and properties of $\text{Cu}_2\text{FeSnS}_4$ nanocrystals by ultrasound-assisted microwave irradiation. *Mater Lett* 25:183–186
84. Long F, Chi S, He J, Wang J, Wu X, Mo S, Zou Z (2015) Synthesis of hexagonal wurtzite $\text{Cu}_2\text{ZnSnS}_4$ prisms by an ultrasound- assisted microwave solvothermal method. *J Solid State Chem* 229:228–234
85. Menezes FD, Galembeck A, Alves S (2011) Junior new methodology for obtaining CdTe quantum dots by using ultrasound. *Ultrason Sonochem* 18:1008–1011
86. Ghows N, Entezari MH (2013) Quantum sots of CdS synthesized by micro-emulsion under ultrasound: size distribution and growth kinetics. *Phys Chem Res* 1:166–174
87. Kumar VB, Perelshtein I, Lipovsky A, Porat Z, Gedanken A (2015) The sonochemical synthesis of Ga@C-dots particles. *RSC Adv* 5:25533–25540
88. Shi Y, Zhu C, Wang L, Zhao C, Li W, Fung KK, Ma T, Hagfeldt A, Wang N (2013) Ultrarapid sonochemical synthesis of ZnO hierarchical structures: from fundamental research to high efficiencies up to 6.42% for quasi-solid dye-sensitized solar cells. *Chem Mater* 25:1000–1012
89. Mousavi-Kamazani M, Salavati-Niasari M, Goudarzi M, Gharehbaai A (2015) A facile novel sonochemical-assistance synthesis of NiSe_2 quantum dots to improve the efficiency of dye-sensitized solar cells. *J Inorg Organomet Polym*. doi:10.1007/s10904-015-0300-8
90. He CX, Lei BX, Wang YF, Su CY, Fang YP, Kuang DB (2010) Sonochemical preparation of hierarchical ZnO hollow spheres for efficient dye-sensitized solar cells. *Chem Eur J* 16:8757–8761
91. Wang YF, Li XF, Li DJ, Sun YW, Zhang XX (2015) Controllable synthesis of hierarchical SnO_2 microspheres for dye sensitized solar cells. *J Power Source* 280:476–482
92. Dirnstorfer I, Burkhardt W, Meyer BK, Ostapenko S, Karg F (2000) Effect of ultrasound treatment on CuInSe_2 solar cells. *Solid State Commun* 16:87–91
93. Barrows AT, Pearson AJ, Kwak CK, Dunbar AD, Buckley AR, Lidzey DG (2014) Efficient planar heterojunction mixed-halide perovskite solar cells deposited via spray-deposition. *Energy Environ Sci* 7:2944–2950
94. Tait JG, Manghooli S, Qiu W, Rakocevic L, Kootstra L, Jaysankar M, Masse de la Huerta CA, Paetzold UW, Gehlhaar R, Cheyens D, Heremans P, Poortmans J (2016) Rapid composition screening for perovskite photovoltaics via concurrently pumped ultrasonic spray coating. *J Mater Chem A* 4:3792–3828
95. Das S, Yang B, Gu G, Joshi PC, Ivanov IN, Rouleau CM, Aytug T, Geohegan DB, Xiao K (2015) High-performance flexible perovskite solar cells by using a combination of ultrasonic spray-coating and low thermal budget photonic curing. *ACS Photonics* 2:680
96. Eslamian M, Zabihi F (2015) Ultrasonic substrate vibration-assisted drop casting (SVADC) for the fabrication of photovoltaic solar cell arrays and thin-film devices. *Nanoscale Res Lett* 10:462

The Role of Ultrasound on Advanced Oxidation Processes

Sundaram Ganesh Babu^{1,2} · Muthupandian Ashokkumar³ ·
Bernardshaw Neppolian¹

Received: 28 July 2016 / Accepted: 14 September 2016 / Published online: 5 October 2016
© Springer International Publishing Switzerland 2016

Abstract This chapter describes the use of ultrasound in remediation of wastewater contaminated with organic pollutants in the absence and presence of other advanced oxidation processes (AOPs) such as sonolysis, sono-ozone process, sonophotocatalysis, sonoFenton systems and sonophoto-Fenton methods in detail. All these methods are explained with the suitable literature illustrations. In most of the cases, hybrid AOPs (combination of ultrasound with one or more AOPs) resulted in superior efficacy to that of individual AOP. The advantageous effects such as additive and synergistic effects obtained by operating the hybrid AOPs are highlighted with appropriate examples. It is worth to mention here that the utilization of ultrasound is not only restricted in preparation of modern active catalysts but also extensively used for the wastewater treatment. Interestingly, ultrasound coupled AOPs are operationally simple, efficient, and environmentally benign, and can be readily applied for large scale industrial processes which make them economically viable.

Keywords Ultrasound · Advanced oxidation processes · Sonophoto process · SonoFenton process · Additive effect · Synergetic effect

This article is part of the Topical Collection “Sonochemistry: From basic principles to innovative applications”; edited by Juan Carlos Colmenares Q., Gregory Chatel.

✉ Bernardshaw Neppolian
neppolian.b@res.srmuniv.ac.in

¹ SRM Research Institute, SRM University, Kattankulathur, Chennai 603203, Tamilnadu, India

² Department of Chemical Engineering, Centre for Catalysis Research and c*change (DST-NRF Centre of Excellence in Catalysis), University of Cape Town, Cape Town 7701, South Africa

³ School of Chemistry, University of Melbourne, Parkville, VIC 3010, Australia

1 Introduction

The greatest challenge in the 21st century is to make a clean environment. Biological degradation processes are one of the most efficient and cost effective techniques to remove organic pollutants from wastewater. However, these systems have some limitations when persistent organic pollutants are present in the aquatic medium. Hence, new processes are required to degrade potentially hazardous toxic compounds from wastewater or effluents from industries. Advanced oxidative processes (AOPs) are efficient in the degradation organic pollutants in aqueous environment [1]. These AOPs generally produce stronger and non-selective hydroxyl radicals ($\cdot\text{OH}$) which, apart from fluorine, is the most powerful oxidant known [2, 3]. $\cdot\text{OH}$ radicals react with toxic organic pollutants and degrade them into smaller non-toxic molecules or in many cases fully mineralized to CO_2 and H_2O [4].

The frequency range of ultrasound is in the region between 18 kHz and >10 MHz. Sonication of water produces cavitation bubbles, which on collapse generate local heating. During acoustic cavitation, highly reactive hydrogen atoms ($\text{H}\cdot$) and $\cdot\text{OH}$ radicals [5] are generated. Organic and inorganic molecules present in the solution undergo oxidation or reduction depending on their reactivity. Ultrasonic effects on general/specific degradation processes are published as review articles [6–10]. In the past decades, the use of ultrasound in the degradation (oxidation) of variety of organic pollutants attracted many researchers because of its simple operational conditions [11–13].

It is generally accepted that sonochemical reactions occur in three zones: core of cavitation bubble, bubble–liquid interface, and bulk solution. The chemical industries discharge contaminated wastewater into aquatic environment. These waste effluents require proper treatment before safe discharge into the environment. Most effluents are toxic in nature, due to the presence of aromatic compounds like benzene, toluene, xylene, etc. There are many reports available in the literature for generating $\cdot\text{OH}$ radicals using AOPs. In this chapter only the ultrasound based AOPs for the wastewater treatment is discussed in detail.

2 Advance Oxidation Processes (AOPs)

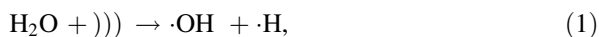
Glaze and co-workers established the concept of “advanced oxidation processes” in 1987. AOPs are defined as the oxidation processes assisted by strong oxidants such as hydroxyl radicals which could be used in waste water treatment. Hydroxyl radical ($\cdot\text{OH}$) is a powerful, non-selective chemical oxidant that cleave carbon–carbon, carbon–nitrogen, carbon–sulphur and also the other chemical bonds. These kinds of free radical assisted systems are categorized under this broad definition of AOP. In general, such free radicals could be generated using various methods such as ozonation (O_3), hydrogen peroxide (H_2O_2), potassium persulfate (KPS), catalysts (transition metal ions, noble metals or photocatalysts), light illumination (either ultraviolet light or visible light), ultrasound (US) or electron beam. Typical AOPs are listed in Table 1.

Table 1 List of typical AOP systems [1–13]

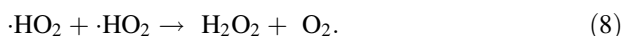
Non-photochemical	Photochemical
O ₃ at elevated pH (>8.5)	H ₂ O ₂ /UV
O ₃ /H ₂ O ₂	O ₃ /UV
O ₃ /US	O ₃ /H ₂ O ₂ /UV
O ₃ /AC (activated carbon)	H ₂ O ₂ /Fe ²⁺ /UV (photo-Fenton)
O ₃ /catalyst	UV/TiO ₂
Fe ²⁺ /H ₂ O ₂ (Fenton system)	H ₂ O ₂ /TiO ₂ /UV
Electro-Fenton	O ₂ /TiO ₂ /UV
Pulsed plasma	UV/US
Ultrasound (US)	Vacuum UV
H ₂ O ₂ /US	
Microwave	
Wet air oxidation	
Supercritical water oxidation	

Generally, photo-AOP techniques involve the use of ultraviolet light in the presence of H₂O₂, ozone, Fenton's reagent or a semiconductor surface [14, 15]. Some less common methods such as γ -radiolysis is also used as AOPs [16–18].

Ultrasound is one of the important AOPs, which could be operated either individually or coupled with other AOPs such as O₃/US, H₂O₂/US, UV/US and so on. As mentioned earlier, sonication of water leads to the formation of radicals [19, 20]. The chains of reactions that occur during sonication of pure water are shown in Reactions (1–4).



Additional radicals are also produced in the gas phase when the solution is saturated with oxygen [21]. Reactions (5–8).



Ultrasonication of organic pollutant in aqueous medium results in thermal and chemical degradation either in the gas phase or liquid phase or at the gas–liquid interface.

3 Effect of Ultrasound in AOPs

3.1 Sonolysis

In 2005, Marechal et al. published a review article to illustrate some fundamentals of the ultrasound and its broad application in textile wet processes [22]. They listed some of the important sonolysis processes for the degradation of textile dyes, mineralization of organic pollutants, degradation of volatile organic matters, heavy metal removals and oxidation of radioactive metals such as As(III). Ince and co-workers investigated the degradation of four different kinds of textile dyes in aqueous solutions by 520 kHz ultrasonic irradiation [23]. The cleavage of aromatic/olefinic carbon–carbon bonds in azo dyes was slower than that of color to be attributed to the priority of hydroxyl radical attack on the nitrogen–nitrogen bonds. This is mainly evident from the formation of numerous oxidation intermediates of organic character during the course of dye degradation. Significant reduction in toxicity of the dyes was accomplished along with color and aromatic carbon degradation.

Cephalexin is one of the most popular antibiotics which are produced in great quantities in pharmaceutical industries. A large amount of this drug is detected in aquatic environment. Guo and co-workers firstly studied the effect of ultrasound irradiation to improve the biodegradability of cephalexin in wastewater [24]. They evaluated the ultrasonic degradation of cephalexin in aqueous medium and investigated the biodegradability of the ultrasonically treated solution by the BOD₅/COD ([biological oxygen demand]₅/[chemical oxygen demand]) ratio. The results confirmed that the BOD₅/COD ratio value increased from zero to 0.36 after ultrasound treatment.

Figure 1 shows the chemical oxygen demand (COD) removal of ultrasonic irradiation of cephalexin in aqueous solution. 24 kHz ultrasonic frequency was used

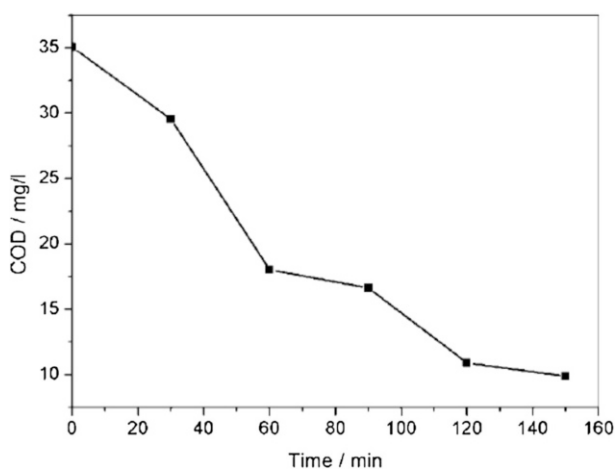


Fig. 1 Chemical oxygen demand during sonolysis of cephalexin in aqueous solution (Reprinted with permission from Ref. [24]. Copyright 2010 Water Research Commission)

for this sonolysis studies. A pH value of 7.5 was maintained under air atmosphere at 25 °C. It is evident from Fig. 1 that cephalexin was degraded by ultrasonic irradiation and the COD value decreased gradually with respect to the irradiation time. The COD value decreased to 70 % of the initial value after 150 min of ultrasound irradiation.

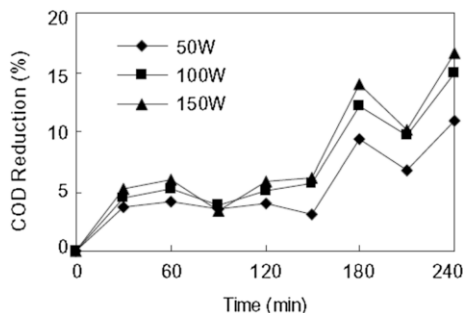
The effects of pH and ultrasonic power on the degradation process were studied. It was reported that the optimal ultrasound power for cephalexin degradation in the system was 200 W. This might be due to the increase in the number of cavitation bubbles at 200 W. This resulted in the increase of extend of degradation of cephalexin. Similarly, a higher rate of cephalexin degradation was observed in the pH range of 6.5–8.5. This is because the cephalexin mainly exists in zwitterionic form in solution at this pH range, which could have increased its concentration at the bubble surface. A higher interfacial concentration allows the compound to be effectively degraded by $\cdot\text{OH}$ radicals generated during acoustic cavitation. The degradation kinetics of cephalexin in aqueous solution under different experimental conditions was also investigated. They reported that the degradation followed pseudo-first order kinetics.

Leachates are generally augmented by rainwater or snowmelt and reaches the landfill [25]. The leachates more often possess a large volume of organic matter that is hazardous pollutants [26]. Biological degradation methods are efficient when applied to relatively younger leachates [27–32]. However, biodegradation is less efficient for the treatment of older leachates [33].

In recent years, ultrasonic technique is largely used for the mineralization of organic compounds from wastewater [34, 35]. Very few reports have been published on the sonochemical treatment of heavily polluted wastewater like landfill leachates contaminated with ammonia nitrogen. Wang et al. carried out ultrasound irradiation for the removal of organic matters and also ammonia nitrogen from landfill leachate wastewater [36]. The effects of ultrasonic power input, pH, aeration and initial concentration were studied in detail They observed that sonolysis of organic compounds took place via reaction with $\cdot\text{OH}$ radicals. A small contribution to the degradation was noted with thermal decomposition within the bubbles. The rise of COD was explained by the complexity of sonolysis of organic pollutant in landfill leachate. The ammonia nitrogen present in the landfill leachate was also effectively removed by sonolysis. Nearly, 96 % of the ammonia nitrogen was removed under ultrasonication after 180 min. The authors' analyzed the intermediates and found that the concentrations of $\text{NO}_2\text{-N}$ and $\text{NO}_3\text{-N}$ were increased which might be due to the formation of NO and NO_2 in cavitation bubbles from the N_2 and O_2 dissolved in water, which ultimately dissolve in water to generate nitrous and nitric acids. Further, they studied the reaction pathway of ammonia nitrogen removal by sonolysis proceeds via pyrolysis due to the high temperature developed within the cavitation bubbles. The authors concluded that the ammonia molecules in leachate enter into the cavitation bubbles and transform into N_2 and H_2 via pyrolysis under instant high temperature and high pressure in the cavitation bubbles.

The effect of ultrasonic power input on COD reduction in landfill leachate is illustrated in Fig. 2. It is clearly evident from Fig. 2 that ultrasonic power affected the COD removal in landfill leachate. The efficiency of COD removal increased

Fig. 2 Effect of power input on COD reduction efficiency (initial concentration 4770 mg L⁻¹; initial pH 8.1; without aeration) (Reprinted with permission from Ref. [36]. Copyright 2008 Elsevier)



with an increase in ultrasonic power. This is due to an increase in the number of cavitation bubbles with an increase in ultrasonic power, which results in enhanced $\cdot\text{OH}$ formation [37–41].

Similar to the above pollutants, namely, cephalixin and ammonia nitrogen in landfill leachate, arsenic is also a toxic metalloid. Arsenic is naturally found in ores and soil in many parts of the earth, and is released into the groundwater through natural processes [42, 43]. People live in Southeast Asian countries (e.g., Bangladesh, Nepal, West Bengal in India and Vietnam) and western U.S. are adversely affected by arsenic contamination in ground water [44–48]. Many important organs of the human body are very much sensitive towards the long term exposure to arsenic poisoning [49]. Hence, it is important to develop a suitable method for the oxidation of acutely toxic As(III) to the less toxic As(V). Neppolian et al. studied the effect of different operational parameters sono-oxidation of As(III) to As(V), such as power density and pulse mode [50].

Figure 3 shows the sono-oxidation of As(III) solutions (75 mL) over the different concentration range of 0.0013–0.0268 mM. It can be observed from Fig. 3 that complete oxidation of As(III) to As(V) was achieved within 15–50 min of ultrasonic irradiation.

In comparison to the continuous mode of operation, pulsed sonication showed significant effect on the oxidation of As(III) to As(V). As the amplitude of ultrasound was increased, the rate of oxidation also increased. The H_2O_2 production was considerably reduced as compared to that observed during the sonication of water alone [without As(III)]. This suggested that $\cdot\text{OH}$ radicals were involved in As(III) oxidation process. The sono-oxidation process was independent of the initial pH of the solution in the range of 3–10. The involvement of dissolved oxygen in As(III) oxidation was proven by performing experiments in nitrogen saturated solutions, where oxidation process was not observed. Hence, the authors concluded that the sonolysis treatment process is an effective technique for the oxidation of As(III) to As(V) without the use of external chemicals or catalysts.

Besides, the authors studied the effect of initial pH on the sonochemical oxidation of As(III). In general, the initial pH value of the solution greatly influenced the oxidation reaction rate. Nonetheless, in the present system it is observed that the rate of the reaction was not significantly changed by adjusting the initial pH of the As(III) solution. However, very interestingly, the final pH value

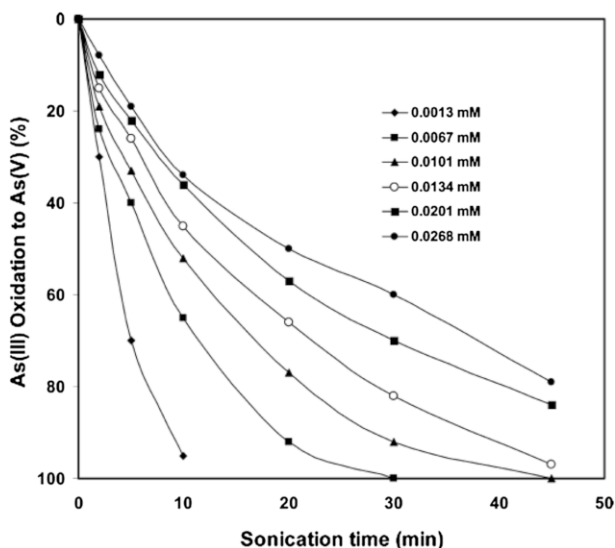


Fig. 3 Effect of the different initial concentrations of As(III) on the oxidation of As(III) to As(V). Experimental conditions: pH = 7, tip diameter = 19 mm, power = 36 W (Reprinted with permission from Ref. [50]. Copyright 2009 American Chemical Society)

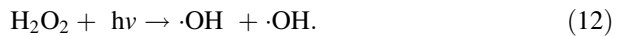
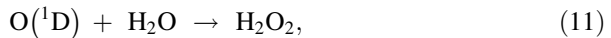
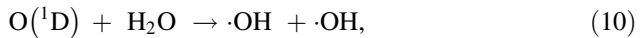
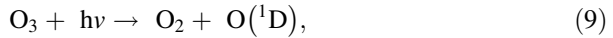
dropped almost to 3–4 in all the experiments performed. This is one of a better example for the sonochemical reaction was which not remarkably stimulated by initial pH value.

The same research group also studied the effect of addition of peroxydisulfate ion (PDS) towards the sonochemical oxidation of As(III) [51]. Along with $\cdot\text{OH}$ radicals, sulfate anion radicals produced during acoustic cavitation also involved in the oxidation of As(III) to As(V) in an aqueous environment. A tenfold enhancement was observed by the addition of PDS. The dissolved oxygen content also played a vital role in this oxidation process which was proved by nitrogen sparging experiment. Continuous aeration of oxygen (10 mg L^{-1}) increased the oxidation to 80 % over 5 min sonication. The addition of humic acid (HA) retarded the oxidation rate of As(III), but the effect could be offset by using larger amounts of PDS. Influence of ultrasound input power and frequency on the oxidation rate was examined. The authors found that rate of oxidation of As(III) was lower at the ultrasound frequency of 211 kHz as compared to that of at 20 kHz.

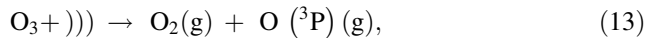
3.2 Ultrasound/Ozone Mineralization

Ozone (O_3) based AOP can be coupled with other AOPs such as photocatalysis, photolysis, Fenton reaction based processes and sonolysis. The key difference between the ozonation and AOP processes is that the ozone process relies mainly on the direct oxidation with aqueous ozone while AOPs rely primarily on oxidation with hydroxyl radicals. Ozone-sonolysis hybrid AOP is discussed in detail in this section.

Ozonation of water either in presence and absence of UV illumination is extensively reported in the literature [52–54]. Depending up on the solution pH, O_3 can react with organic pollutants either directly by electrophilic attack or indirectly by radical chain reactions. Combination of ozone with UV or US results in a net enhancement in the degradation of toxic organic pollutants due to direct and indirect production of $\cdot OH$ radicals. O_3 in aqueous medium generates H_2O_2 which in turn produces $\cdot OH$ that actively participate in the degradation process (Reactions 9–12) [55]



In the hybrid process, O_3 undergoes thermal decomposition within collapsing bubbles providing additional $\cdot OH$ radicals, as given in Eqs. (13, 14) [56].



In a typical case study, the hybrid O_3/US AOP was used for the degradation of a textile dye C.I. Acid Orange 7 [57]. To facilitate the degradation process further, UV light illumination was also used. The degradation reaction was monitored by UV–visible absorbance of the solution, total organic carbon analysis and five-day biochemical oxygen demand (BOD_5) of the solution. The authors varied the concentration of O_3 from 10 to 60 g m^{-3} . The rate of color decay with respect to the concentration of O_3 is depicted in Fig. 4.

Besides, the authors performed a comparative study with various coupled AOPs namely O_3/US , O_3/UV and $O_3/UV/US$ for the degradation of C.I. Acid Orange 7

Fig. 4 The relation between time rate of color decay and the ozonation with ultrasound (subscripts of k refer to the ozone outputs of the generator as g m^{-3}) (Reprinted with permission from Ref. [57]. Copyright 2004 Elsevier)

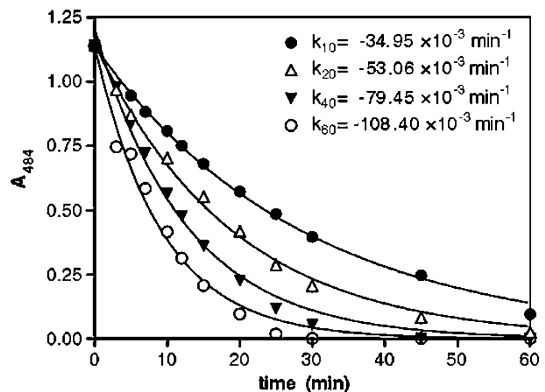
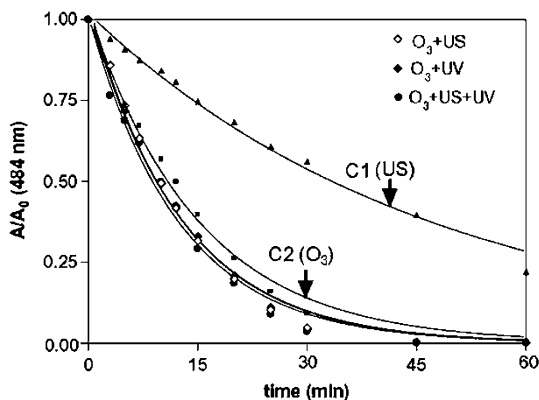


Fig. 5 Comparative profiles of color decay rates in O₃/UV, O₃/US and O₃/UV/US schemes (C1 and C2 show performances of the two controls, i.e. individually applied US and ozone schemes, respectively) (Reprinted with permission from Ref. [57]. Copyright 2004 Elsevier)



dye and the results are depicted in Fig. 5. Based on the degradation rate constants, the authors made a conclusion that no significant improvement in decolourization was provided by the simultaneous operation of the three AOPs (O₃/US/UV).

Similarly, the degradation of sulfamethoxazole was investigated using ultrasound (US), ozone (O₃) and O₃/US oxidation process [58]. Guo et al. showed that ultrasound significantly enhanced sulfamethoxazole ozonation by assisting ozone in producing more ·OH radicals in O₃/US oxidation process. The rate of degradation was increased by 6–26 % by combining ultrasound and ozonation processes under different pH conditions. The formation of different intermediates during the three AOPs namely US alone, O₃ alone and O₃/US hybrid oxidation process was identified and the results clearly revealed that the major intermediates in O₃ alone and O₃/US hybrid oxidation process are similar. However, the introduction of ultrasound in O₃/US hybrid oxidation process significantly improved the cleavage of C–S bond. Under the optimal reaction condition the degradation of sulfamethoxazole was much easier. Noticeable enhancement in sulfamethoxazole removal rate was observed by the O₃/US oxidation process as compared to the other two examined processes (US alone and O₃ alone).

The role of individual (US alone and O₃ alone) and coupled AOP (O₃/US) processes were examined towards the sulfamethoxazole removal. The authors discussed the ultrasonic energy using the calorimetric method, in detail [59]. As can be seen from Fig. 6, only 3 % of the sulfamethoxazole was removed in the presence of US alone process. O₃ alone system showed comparatively better efficiency. The O₃/US hybrid oxidation process exhibited superior performance than the individual AOP system. Hence, the authors concluded that it was paramount important to combine ultrasound with other technologies to improve the removal rate.

Fan et al. examined the influence of ultrasound on O₃ based AOP for the degradation of methamidophos and dichlorvos which are organophosphorous pesticides that commonly used for pest control in agriculture to obtain better yields [60]. The authors varied various experimental parameters including O₃ flow rate, water temperature, treatment time and initial concentration of organophosphorous pesticides to evaluate their effects on the degradation rate under O₃/US condition. A maximum degradation rate of 82 % was observed with the O₃/US oxidation process

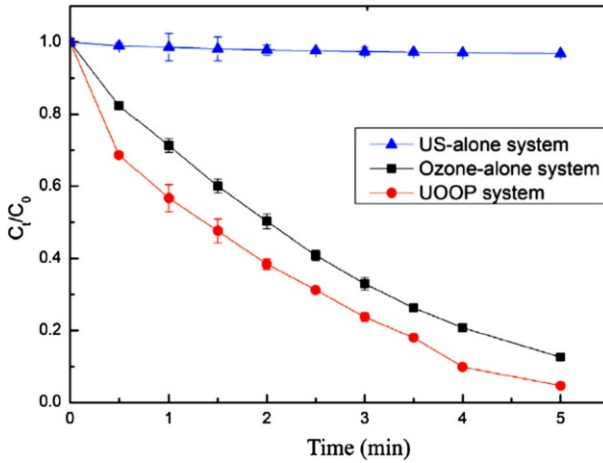


Fig. 6 The sulfamethoxazole degradation curve under US-alone, ozone-alone and O_3 /US oxidation process (UOOP) systems (Reprinted with permission from Ref. [58]. Copyright 2015 Elsevier)

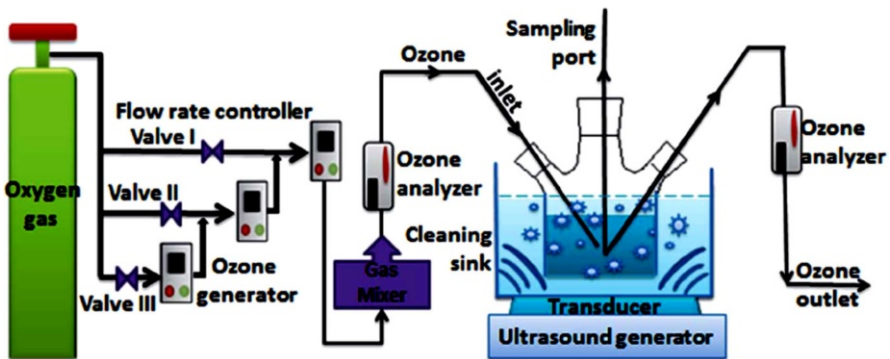


Fig. 7 Schematic representation of the O_3 /US combination cleaning apparatus (JY-92-II ultrasonic generator, frequency rate 25 kHz, ultrasound power 0–1000 W; DHX-SS-1G ozone generator) (Reprinted with permission from Ref. [60]. Copyright 2015 Royal Society of Chemistry)

under optimal experimental conditions. Figure 7 illustrates the schematic of the experimental set up for the O_3 /US oxidation process used for the degradation of methamidophos and dichlorvos organophosphorous pesticides.

Temperature of the system played a vital role in O_3 /US oxidation process. The degradation of methamidophos and dichlorvos (the model organophosphorous pesticides) showed a significant difference with respect to the temperature of the system. The authors varied the initial water temperature from 8 to 32 °C and studied the O_3 /US oxidation process for the degradation of organophosphorous pesticides. Higher temperature increases the rate of chemical reaction between oxidant and substrate which promotes the reaction faster. However, too high temperature possibly decreases the partial pressure of dissolved O_3 in the reaction medium which in turn decrease the O_3 concentration. This resulted in less production of $\cdot OH$

radicals. Based on the observation the authors concluded that the most favourable temperature for the degradation of organophosphorous pesticides under O_3/US oxidation process is $8^\circ C$.

Very often, the combination of more than two AOPs resulted in a very good performance. To support this, three AOP components viz, US, UV and O_3 were utilized for the lab-scale degradation of aryl-azo-naphthol dye and C.I. Acid Orange 8 [61]. Simultaneous and single operations of US and O_3 operations in presence of different wavelength light illumination for 30 min were studied and the results are presented in Fig. 8. A remarkable decay profile was observed by the combined process. This is due to generation of excess $\cdot OH$ radicals and other oxidative species such as singlet oxygen, peroxy and/or superoxide.

In contrary, single AOP processes were found to show better efficiency as compared to the combined AOPs in other studies. For instance, ultrasound assisted O_3 based degradation of pararosaniline (C.I. Basic Red 9) was studied under different AOP conditions [62]. It was observed that ozonation of pararosaniline solution was more efficient than ultrasonic irradiation alone or in combination with O_3 . The intermediate compounds formed by degradation process of the pararosaniline was analysed by GC-MS and some of the oxygenated by-products such as long-chain carboxylic acids and alcohols were identified [63]. Authors prepared a comparison table to understand the efficacy of the system based on the identified intermediate compounds (Table 2).

3.3 Sonophoto Degradation

Combinations of different AOPs for environmental detoxification have recently been exploited, especially for waste water treatment [65–73]. Among the different hybrid AOPs, the so-called sonophotocatalysis, i.e., the simultaneous use of ultrasound (US) and photocatalysis, is one of the widely studied systems under different experimental conditions [74–76]. The simultaneous use of the two

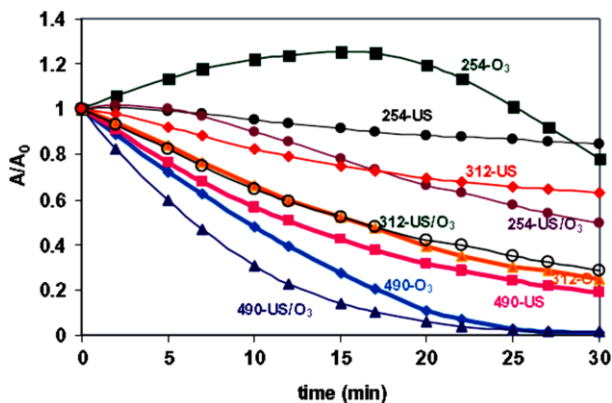


Fig. 8 Profiles of visible and UV absorption decay during 30 min contact of AO8 with US, O_3 and O_3/US combined schemes (Reprinted with permission from Ref. [61], Copyright 2006 Elsevier)

Table 2 Comparison of the by-products generated from ozonized aqueous solutions of the two different dyes (Reprinted with permission from Ref. [62]. Copyright 2006 Elsevier)

Dye	Pararosaniline ^a		Reactive Red 120 ^b	
	[62]	% ^c	[64]	% ^c
[Dye] ₀	1.2×10^{-5} M	(19 mg L ⁻¹)	1.4×10^{-4} M	(200 mg L ⁻¹)
Aldehyde/ketone				
Formaldehyde (μM)	0.94	57	n.i.	
Acetaldehyde (μM)	0.26	16	n.i.	
Acetone (μM)	0.45	27	n.i.	
Others (μM)	n.d.		n.i.	
Total (μM)	1.7	100		
[Carbon] ₀ (%)	0.9			
Carboxylic acids				
Formic (μM)	9.11	75	20	14
Acetic (μM)	1.00	8	0.0	0
Glycolic (μM)	0.28	2	n.i.	
Pyruvic (μM)	0.54	4	n.i.	
Oxalic (μM)	1.25	10	125	86
Total (μM)	12.2	100	145	100
[Carbon] ₀ (%)	8.2		2.4	
Nitrate (μM)	97		200	
[N] ₀ (%)	73		10	

n.d. Not detected, *n.i.* not informed or not measured

^a Dye ozonized (7 mg O₃ L⁻¹) during 15 min

^b Data from unpurified dye ozonized (8.9 mg O₃ L⁻¹) during 150 min

^c Percentage contribution of individual compound to each specie's classes

techniques was reported to be more effective than their sequential combination in many instances [77–79]. Synergistic effects between the two techniques were more often observed when employing small particle size semiconductors or when operating at relatively low US frequency for the degradation of organic species [80].

Mrowetz et al. investigated the degradation of 2-chlorophenol and two azo dyes in aqueous solutions under sonolysis, photocatalysis in the presence of TiO₂ and simultaneous sonolysis and photocatalysis, i.e., sonophotocatalysis [81]. Ultrasound significantly influenced the rate of photocatalytic degradation by promoting deaggregation of the photocatalyst. Ultrasound greatly induced desorption of organic matters and intermediates from the photocatalyst surface. The degradation result for the acid orange 8 under different hybrid AOPs is given in Fig. 9. It is evident that sonophotocatalysis showed significantly better efficiency.

A similar trend was observed with sonophotocatalytic degradation systems developed for the mineralization of different organic pollutants namely salicylic acid, methyl tert-butyl ether and 2,4,6-trichlorophenol [82–85]. In all these systems, the degradation efficiency increased by the introduction of ultrasonic irradiation.

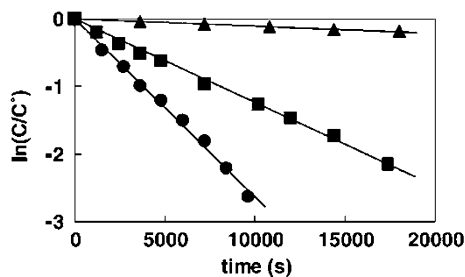


Fig. 9 First order kinetic plots of AO8 degradation under (*filled upright triangle*) ultrasound in the presence of TiO_2 particles (US/ TiO_2), (*filled square*) photocatalysis (UV/ TiO_2) and (*filled circle*) sonophotocatalysis (US/UV/ TiO_2). Initial dye concentration: 4×10^{-5} M; TiO_2 amount: 0.1 g L^{-1} (Reprinted with permission from Ref. [81]. Copyright 2003 Elsevier)

In some cases, the efficacy of the sonophotocatalysis system was increased greatly by the doping of the catalysts with noble metals. For example, the photocatalytic and sonophotocatalytic efficiencies of Au– TiO_2 photocatalysts prepared by three different procedures were evaluated towards the degradation of a representative organic pollutant, nonylphenol ethoxylate surfactant in aqueous environment [86]. No synergistic effect was observed with the as-synthesized Au– TiO_2 photocatalysts towards the sonophotocatalytic degradation of Teric GN9 which might be due to the interference of the degradation products generated during the simultaneous irradiation by light and ultrasound.

The concentration of Teric GN9 was monitored by high performance liquid chromatography (HPLC). Sonolytic, photocatalytic and sonophotocatalytic degradation of Teric GN9 is shown in Fig. 10. The $\cdot\text{OH}$ radicals were found to be the responsible species for the degradation of Teric GN9 surfactant under all the three

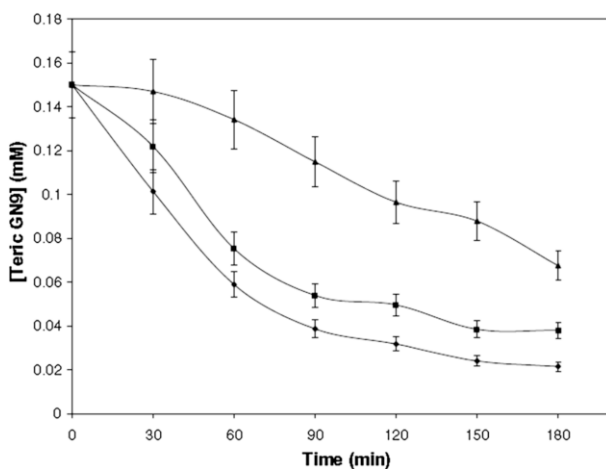


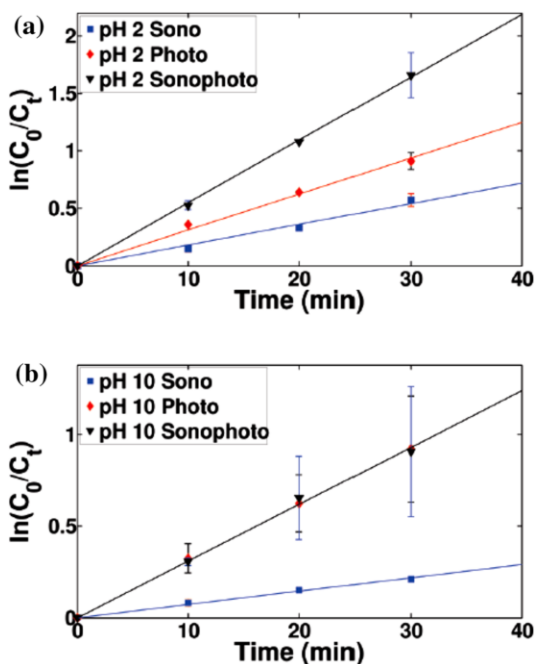
Fig. 10 The degradation plot for Teric GN9 surfactant (1.5×10^{-4} M) using conventional Au– TiO_2 nanoparticles by photocatalysis (*filled diamond*), sonophotocatalysis (*filled square*) and sonolysis (*filled upright triangle*) methods (Reprinted with permission from Ref. [86]. Copyright 2009 Elsevier)

AOPs i.e. sonolysis, photocatalysis and sonophotocatalysis [87]. Based on the previous studies and the experimental data, the authors confirmed that the initial step of this degradation is the attack of $\cdot\text{OH}$ radical on the surfactant [88, 89].

A hybrid AOP by means of coupling the sonolysis and photocatalysis was developed for the degradation of *p*-chlorobenzoic acid in ambient air saturated aqueous solutions [90]. Under the sonophotocatalytic degradation experimental conditions, 20 % synergistic enhancement was evidenced compared with the sum of the individual processes. Individual and hybrid AOPs were performed for the degradation of *p*-chlorobenzoic acid under different pH conditions and the results are depicted in Fig. 11. All the systems followed a pseudo-first-order reaction kinetics for degradation process [91–95].

Ultrasound mediated UV light induced ZnO sonophotocatalytic system was demonstrated for the enhanced degradation of Chrome Intra Orange G in aqueous solution [96]. A high intensity ultrasonic treatment was applied for the degradation of chitosan polymer in the presence of TiO_2 under UV light illumination and found an additive effect by the combination of sono- and photocatalytic systems [97]. A similar TiO_2 based sonophoto degradation system was used for the degradation of malachite green in water by Berberidou et al. [98]. The accelerated sonophotocatalytic degradation of Reactive Red 120 dye under visible light using dye sensitized TiO_2 activated by ultrasound was carried out to illustrate the effect of ultrasound in photocatalysis in dye sensitized system [99]. The results emphasized that the oxidative species such as singlet oxygen ($^1\text{O}_2$) and superoxide (O_2^-) radicals are the responsible species for the effective degradation of Reactive Red 120 dye in the

Fig. 11 Pseudo-first-order kinetics curves observed during the sonophotocatalytic degradation of an aqueous solution containing $100\ \mu\text{M}$ *p*-chlorobenzoic acid at **a** pH 2 and **b** pH 10. (condition: TiO_2 loading was $1\ \text{mg mL}^{-1}$. The applied ultrasonic power was $55\ \text{mW mL}^{-1}$ and frequency was 213 kHz. The detector wavelength used in HPLC was 238 nm) (Reprinted with permission from Ref. [90]. Copyright 2011 American Chemical Society)



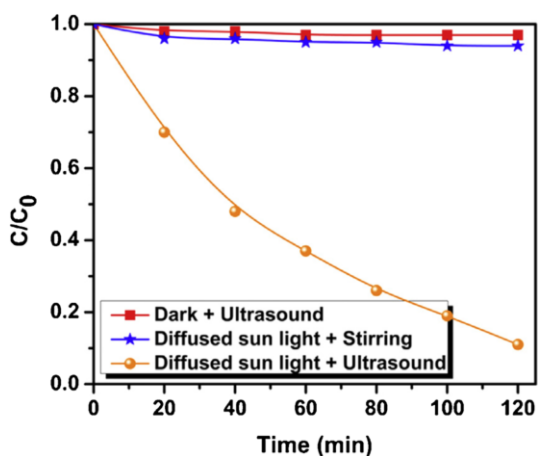
presence of oxygen. Sonophotocatalytic degradation of an azo dye namely Reactive Black 5 was also investigated under ambient reaction condition [100]. The hybrid AOPs (combined sono- and photo- catalytic system) showed superior degradation performance than that of the individual AOPs (sono- alone and photo- alone).

The sonophotocatalytic AOP system was not only efficient for the textile dyes but also for the colourless organic hazardous pollutants. Oxidative degradation of 4-chlorophenol by sonolytic, photocatalytic and sonophotocatalytic processes was studied in aqueous solutions using $\text{Bi}_2\text{O}_3/\text{TiZrO}_4$ as a visible light driven photocatalyst and with 20 kHz ultrasound [101]. A cumulative effect was observed by the coupled method for the oxidative degradation of 4-chlorophenol which is an added advantage of the system.

Very recently, Babu et al. demonstrated that diffused sunlight is an effective light source for the efficient degradation and mineralization of methyl orange dye by sonophotocatalytic degradation [102]. They used reduced graphene oxide (rGO) supported CuO-TiO_2 photocatalyst for the sonophotocatalytic degradation process. It is worth to mention here that they achieved a tenfold synergy for the first time by combining sono- and photocatalytic degradation under diffused sunlight. The addition of rGO augmented the activity of bare CuO-TiO_2 more than two fold. This sonophotocatalytic system shows similar activity for the degradation of methylene blue and 4-chlorophenol which clearly indicating the versatility of the sonophotocatalytic system.

For comparison, they performed the sono-, photocatalytic and sonophotocatalytic degradation studies and the results are shown in Fig. 12. Only 3 and 6 % degradation was observed with the sono- alone and individual photocatalytic reaction under diffused sunlight. However the combination of these two systems, i.e., sonophotocatalytic reaction increased the degradation percentage to 89. The synergistic effect was found to be tenfold. The synergistic effect is mainly due to the production of $\cdot\text{OH}$ radicals by both ultrasound and $\text{CuO-TiO}_2/\text{rGO}$ photocatalyst. In previous reports, a maximum of 1–1.5 fold synergistic by the ultrasound assisted photocatalytic process [103].

Fig. 12 Synergistic effect of ultrasound on photocatalytic degradation of methyl orange dye under diffused sunlight (Reprinted with permission from Ref. [102]. Copyright 2015 Elsevier)



Neppolian et al. studied the oxidative degradation of 4-chlorophenol (4-CP) by sonolytic, photocatalytic and sonophotocatalytic processes in aqueous solutions using $\text{Bi}_2\text{O}_3/\text{TiZrO}_4$ as a visible light driven photocatalyst and with 20 kHz ultrasound [104]. The authors claim that $\text{Bi}_2\text{O}_3/\text{TiZrO}_4$ photocatalyst is a potential catalyst for the degradation of 4-CP by both photocatalytic and sonophotocatalysis processes. They studied the formation of intermediates by the sonolysis of 4-CP using HPLC. Interestingly, there were no intermediates identified during the sonophotocatalytic degradation of 4-CP solution using $\text{Bi}_2\text{O}_3/\text{TiZrO}_4$ photocatalyst under visible light illumination. Rapid mineralization of 4-CP during the sonophotocatalytic process was confirmed by total organic carbon (TOC) studies and found to be superior to that of sonolysis alone. Furthermore, the initial pH of 4-CP was not affected the sonophotocatalytic degradation. However, the situation for sonolysis alone was greatly influenced by the initial pH values where the degradation rate decreased as the pH was raised from acidic to basic conditions. Based on the results, the authors reported a cumulative/additive effect for the hybrid sono- and photo- catalytic degradation of 4-CP using $\text{Bi}_2\text{O}_3/\text{TiZrO}_4$ photocatalyst under visible light illumination.

The additive effect of the sonophotocatalysis is clearly evidenced from the Fig. 13. This is because the degradation efficiency of sonophotocatalysis was the sum of the efficiencies of sonolysis and photocatalysis of the same system. Furthermore, among the three methods used, sonophotocatalysis (coupled sonolysis and photocatalysis AOPs) showed excellent activity than that of the individual AOP.

Moreover, the authors studied the effect of initial pH on the sonocatalytic degradation of 4-CP. It is observed that sonolytic degradation of 4-CP was higher at lower pH value, especially showed utmost degradation at the initial pH 3. Controversially, the photocatalysis displayed lower efficiency at pH 3. However, no

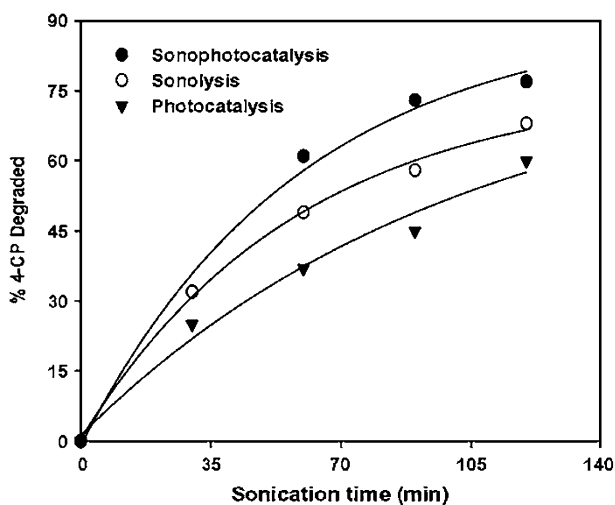


Fig. 13 4-CP degradation (%) with respect to reaction time by using three different processes (Experimental conditions: $[\text{4-CP}] = 1.25 \times 10^{-4}$ M, $\text{pH} = \sim 5$, 20 kHz horn diameter = 19 mm, power = 51 W) (Reprinted with permission from Ref. [104]. Copyright 2001 Elsevier)

notable influence of the pH was observed during the sonophotocatalytic degradation. This clearly evidenced the advantage of the coupled sono- and photo- catalytic system for the effective degradation of 4-CP at any pH below 10.

Similarly, Kritikos et al. also observed a cumulative effect while coupling the sono- and photocatalytic system for the degradation of reactive black 5 (RB 5), a representative diazo dye found in textile effluents, by means of ultraviolet irradiation (9 W UVA) over TiO₂ suspensions and ultrasound irradiation (80 kHz, 135 W) [105]. They investigated several commercial TiO₂ catalysts and an anatase Hombicat UV 100 TiO₂ photocatalyst exhibited considerable activity in terms of solution decoloration, COD and ecotoxicity reduction. With their operational conditions, complete degradation was achieved within 60 min of reaction. Additionally, the external addition of H₂O₂ up to 0.01 M hindered degradation by scavenging the photogenerated holes (h⁺) and ·OH radicals. Nevertheless, only 10 % of the decolorization was observed with sonolysis of RB 5 by continuous sparging of oxygen (O₂). The simultaneous application of ultraviolet and ultrasound irradiation resulted in increased decoloration compared to that achieved by individual photocatalysis and sonolysis. The overall sonophotocatalytic effect clearly revealed that the process was slightly higher than additive effect of the two processes.

The beneficial effect of coupling photocatalysis with sonolysis was attributed to the increased production of hydroxyl radicals in the reaction mixture arising from the sonolytic cleavage of water, enhanced mass transfer of organics between the liquid phase and the catalyst surface, catalyst excitation by ultrasound induced luminescence, increased catalytic activity due to ultrasound de-aggregating catalyst particles (which increased the surface area) [106–108]. It is really difficult to distinguish the contributions from the above effects. However the overall total effect resulted in the slight enhancement in additive effect and the results are given in Fig. 14.

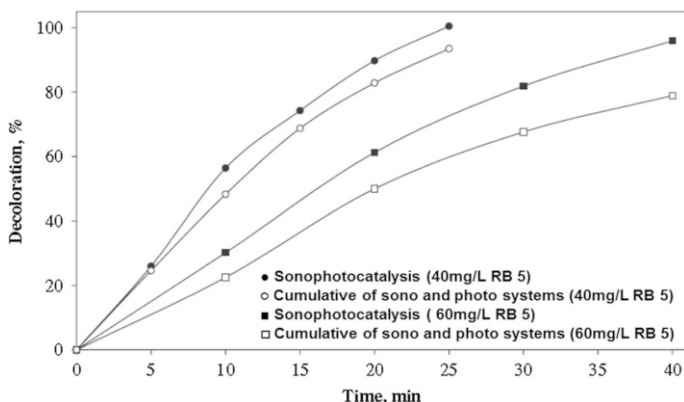
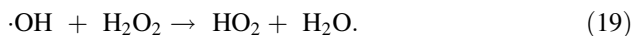
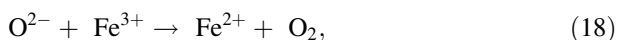
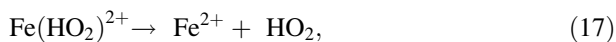
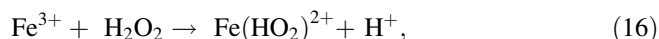
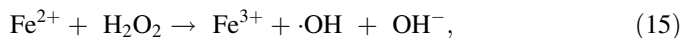


Fig. 14 Decoloration–time profiles during combined sonochemical and photocatalytic (sonophotocatalytic) degradation at 0.25 g L⁻¹ catalyst loading and (filled circle) 40 mg L⁻¹ RB 5; (filled square) 60 mg L⁻¹ RB 5. Open symbols show the cumulative effect of the respective individual sonochemical and photocatalytic runs (Reprinted with permission from Ref. [105]. Copyright 2007 Elsevier)

On the other hand, Lirong et al. experienced a very high synergism in a sonophotocatalytic system for the degradation of organophosphate pesticide [109]. A magnetic sonophotocatalyst namely $\text{Fe}_3\text{O}_4@\text{SiO}_2@\text{TiO}_2$ was synthesized and well characterized by physicochemical techniques. The as-synthesized catalyst was tested against the degradation of the commercial organophosphate viz dichlorvos (DDVP). The degradation efficiency of the sonophotocatalytic systems were identified by measuring the chemical oxygen demand and also by the enhancement in biodegradability. The highest synergistic effect was observed in the combined sonolysis and photocatalysis which was proved to be significant than that of the solo photocatalysis. Based on the results, the author reported a very high synergism for the sonophotocatalysis which can be applied as a pre-treatment step for the biological degradation of pesticide wastewater. Very importantly, the reported $\text{Fe}_3\text{O}_4@\text{SiO}_2@\text{TiO}_2$ photocatalyst showed very good performance and also stable under reaction condition.

3.4 SonoFenton Process

In recent years, AOPs which involved in situ generation of highly potent chemical oxidants such as $\cdot\text{OH}$ radicals find much attention [110]. Among the AOPs, Fenton and sonochemical reactions are widely used for the destruction of recalcitrant organic contaminants in wastewater. The classic Fenton reagent is a combination of Fe^{2+} and H_2O_2 ($\text{Fe}^{2+}/\text{H}_2\text{O}_2$). The combination of Fe^{3+} and H_2O_2 is known as Fenton-like reagent ($\text{Fe}^{3+}/\text{H}_2\text{O}_2$). As Fe^{3+} can be produced from Fenton reagent during reactions, Fenton chemistry and Fenton-like chemistry often occur simultaneously [111, 112]. The following reactions show the mechanism of $\cdot\text{OH}$ formed when either Fe^{2+} or Fe^{3+} is present (Eqs. 15–19) [113, 114].



The main drawback of these systems for the application on a large scale is the high cost of H_2O_2 which limits the practical applicability of these systems. However, combination of sonolysis with these Fenton and Fenton-like reagents are the suitable solution to overcome this drawback.

Hence many researchers studied the ultrasound assisted Fenton and Fenton like systems for the degradation studies [115–124]. For instance, Iordache et al. explored the potential application of ultrasound in Fenton based oxidation process for the wastewater treatment [125]. They studied the individual Fenton and the hybrid sono-Fenton decomposition systems for the degradation of different pesticides such

as 2,4-dichlorophenoxyacetic acid, 4-(2,4-dichlorophenoxy)butyric acid, 4-chloro-o-toloxoacetic acid, 3,5-dibromo-4-hydroxybenzotrile and 3-(4-chlorophenyl)-1,1-dimethylurea. In all the cases, the ultrasound irradiation improved the wet oxidation process.

Similarly, Fe_3O_4 magnetic nanoparticles were synthesized as heterogeneous catalysts for the effective degradation of bisphenol A in presence of ultrasonic irradiation [126]. The ability of Fe_3O_4 magnetic nanoparticles in $\text{US}/\text{Fe}_3\text{O}_4/\text{H}_2\text{O}_2$ system under different operational condition was investigated in detail. They also found that the $\cdot\text{OH}$ radicals were promptly generated due to the catalysis of the Fe_3O_4 MNPs and are responsible for the degradation. Very importantly, the ultrasound augmented this Fenton degradation system.

For comparison, degradation of bisphenol A was studied under different individual and hybrid combinations such as $\text{US}/\text{Fe}_3\text{O}_4/\text{H}_2\text{O}_2$, $\text{US}/\text{Fe}_3\text{O}_4$, $\text{US}/\text{H}_2\text{O}_2$, US , $\text{Fe}_3\text{O}_4/\text{H}_2\text{O}_2$, Fe_3O_4 and H_2O_2 with different initial pH values. The result is given in Fig. 15. In control experiments (individual AOPs, Fe_3O_4 alone or US alone), no significant degradation was observed. Nevertheless, a higher degradation efficiency was obtained in $\text{US}/\text{H}_2\text{O}_2$ system compared to H_2O_2 alone system. This might be due to the fact that the complex chemical and physical processes caused by collapse of cavitation bubble increases the formation of reactive radicals, but due to

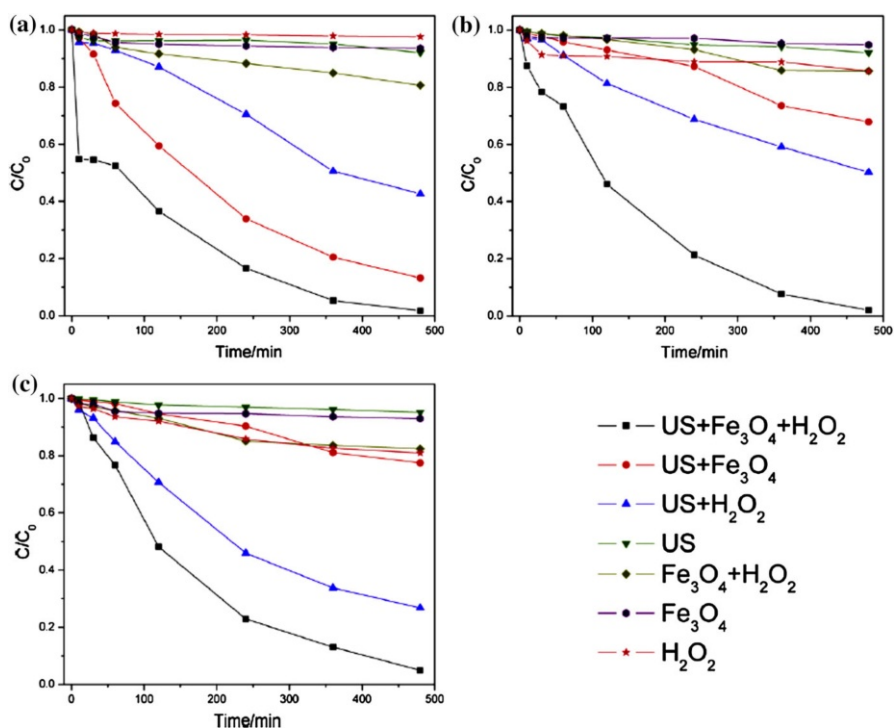


Fig. 15 Bisphenol A degradation in different system at different pH condition of **a** pH = 3, **b** pH = 7, **c** pH = 9 (concentrations of Fe_3O_4 and H_2O_2 were 585 mg L^{-1} and 160 mmol L^{-1} , respectively) (Reprinted with permission from Ref. [126]. Copyright 2012 Elsevier)

the low volatility of H_2O_2 in water limited ultrasonic degradation rate [127, 128]. However, a strong synergistic effect was observed with US/ Fe_3O_4 system which was attributed to the continuous formation of H_2O_2 in the solution under ultrasonic irradiation [129, 130]. A maximum degradation was evidenced with US/ $\text{Fe}_3\text{O}_4/\text{H}_2\text{O}_2$ system.

A novel sono-Fenton system was developed based on $\text{Fe}@\text{Fe}_2\text{O}_3$ core-shell nanowires for the degradation of pentachlorophenol [131]. The effect of individual and combined AOPs for the degradation is illustrated in Fig. 16. The authors noted that pentachlorophenol cannot be degraded by either ultrasonic irradiation or $\text{Fe}@\text{Fe}_2\text{O}_3$ core-shell nanowires alone. However, the combined sono-Fenton system based on the $\text{Fe}@\text{Fe}_2\text{O}_3$ core-shell nanowires showed phenomenal degradation efficiency against pentachlorophenol. More than 40 % of the pentachlorophenol was decomposed after 60 min by this sono-Fenton system.

Similar sono-Fenton systems were developed for the degradation of diethyl phthalate, dichlorophenol and Rhodamine B by different researchers [132–134]. In all the systems, a maximum degradation was experienced with the hybrid sono-Fenton process.

Ultrasonicator power plays a vital role in many of the ultrasound assisted AOPs. For instance, Khim et al., examined the degradation rate as a function of power density [132]. The results clearly revealed that the first order degradation rate constant increased linearly with increasing power density in both sonocatalytic system and sonoFenton process. The increased cavitation activity at the higher power level increased the sono-oxidation process. The cavitation activity greatly influenced by the number of bubbles generated, in addition to the temperature and pressure inside the bubble. Besides, the degree of enhancement mainly depends on the cavitation, pyrolysis and/or radical reaction.

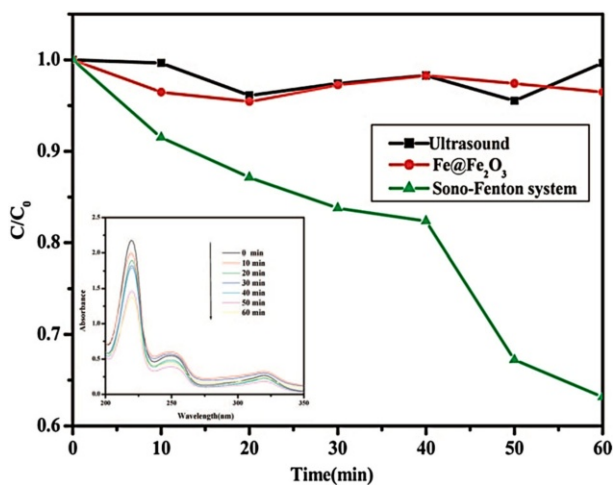


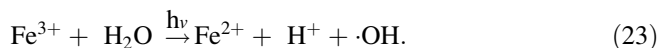
Fig. 16 The degradation curves of PCP in the solution during the sono-Fenton process based on $\text{Fe}@\text{Fe}_2\text{O}_3$ core-shell nanowires. The inset is the UV-vis spectral changes of PCP with reaction time at neutral pH (Reprinted with permission from Ref. [131]. Copyright 2008 American Chemical Society)

3.5 Sonophoto-Fenton Systems

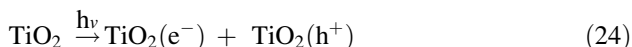
Sonophoto-Fenton process represents a combination of sonolysis with homogeneous or heterogeneous Fenton and heterogeneous photocatalysts. The major advantage of this coupled AOP is that to achieve faster degradation efficiency. The formed Fe^{2+} species during the sonolysis mimics the Fenton's reagent as the sonolysis of water produces hydrogen peroxide (H_2O_2). The corresponding reactions are given in Eqs. (20–22) [135–137].



Besides, the regeneration of Fe^{2+} can be achieved by the light (<450 nm) induced reaction as it is sonophoto-Fenton process (Eq. 23).



This photo and Fenton AOPs coupled with ultrasound (US), i.e., sonophoto-Fenton reaction continuously produces the reactive $\cdot\text{OH}$ radicals. This in turn assisted the complete degradation of toxic pollutants of both hydrophilic and hydrophobic nature. The $\cdot\text{OH}$ radicals formed through both band gap excitation of TiO_2 photocatalyst under light illumination, as depicted in Eqs. (24–26), as well as sonolytic splitting of water molecules [138]. The significant benefit of this combination process is that US continuously cleans the surface of the photocatalyst and is useful in preserve its reactivity over longer irradiation times.



where e^- is photogenerated electron in the conduction band, h^+ is the valence band hole and OH_{ads}^- is the hydroxide ion adsorbed on the TiO_2 surface.

The sonolytic, photocatalytic and sonophotocatalytic degradation of Monocrotophos (MCP), an organophosphate insecticide, in the presence of homogeneous (Fe^{3+}) and heterogeneous photocatalysts (TiO_2) were studied in detail by Madhavan et al. [139]. Poor degradation results were observed with photocatalysis by TiO_2 than the sonolysis which might be due to the interference of phosphate ions formed as an intermediate product. Nevertheless, a 15 fold increase was observed by the addition of Fe^{3+} ions into the photocatalysis system. The authors found the synergy indices of 0.62 and 0.87 by the sonophotocatalytic degradation of MCP in the presence of TiO_2 and Fe^{3+} , respectively. Complete mineralization of MCP was identified by the TOC and HPLC analyses. The sonication of MCP led to the

formation of dimethyl phosphate, dimethylphosphonate, 3-hydroxy 2-buteneamide and N-methyl 3-oxobutanamide as the intermediate products which were evidenced by the LC–MS analysis.

Babuponnusami and Muthukumar focused on the oxidative degradation of phenol in aqueous medium using Fenton, sono-Fenton, and sono-photo-Fenton [140]. The authors noticed that during the sonophoto-Fenton process the Fe^{2+} concentration was reduced by 30–50 % and the H_2O_2 concentration was decreased by 12.5 %. Furthermore, the phenol degradation was found to be 71.0, 55.8 and 50.5 % for sonophoto-Fenton, sono-Fenton and Fenton methods, respectively. The results clearly revealed that the sonophoto-Fenton technique was superior to that of the Fenton and sono-Fenton processes for the oxidation of phenol under operational condition. Figure 17 shows the effect of reaction time on phenol degradation under three processes (Fenton, sono-Fenton and sonophoto-Fenton) studied. Very interestingly, the sonophoto-Fenton process was found to be efficient compared to the other two processes. This might be due to the additional formation of H_2O_2 and Fe^{2+} by combined effect of UV and US [141]. The phenol degradation percentage observed for sonophoto-Fenton, sono-Fenton and Fenton methods were 71, 56 and 51 %, respectively.

Sonophoto-Fenton process was studied for the degradation of ethylenediaminetetraacetic acid (EDTA), a commercial chelating agent that used for decontamination purposes in nuclear industry, by Chitra et al. [142]. The authors investigated the kinetics of degradation of EDTA by employing either photo-Fenton process using UV light or sono-Fenton process using ultrasound (130 kHz) or simultaneous sonophoto-Fenton process. The results confirmed that EDTA is effectively degraded by the synergistic effect of both photo-Fenton and sono-Fenton process. All the processes were found to follow a first order reaction kinetics. The loss of chelating ability of EDTA during this oxidative degradation was proved by change in the pH value. Amide formation during the oxidation process was also observed.

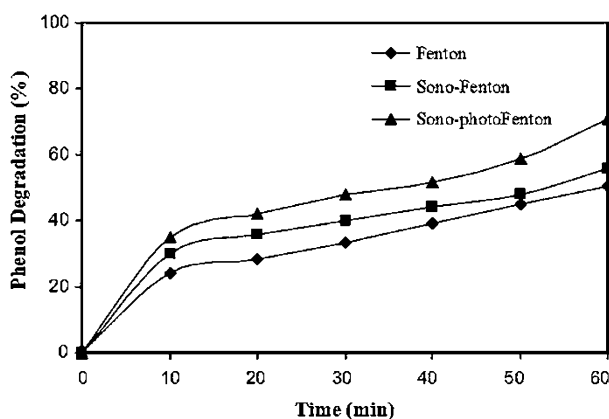


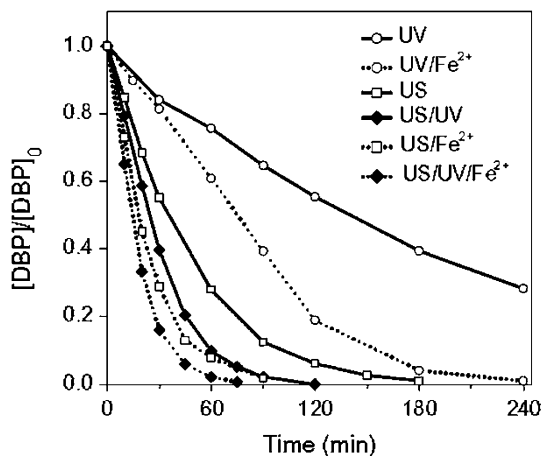
Fig. 17 Effect of reaction time on phenol degradation for Fenton, sono-Fenton, and sono-photo-Fenton processes (conditions: initial phenol concentration = 200 mg L^{-1} , $\text{Fe}^{2+} = 45 \text{ mg L}^{-1}$, $\text{pH} = 3$, $\text{H}_2\text{O}_2 = 1000 \text{ mg L}^{-1}$) (Reprinted with permission from Ref. [140]. Copyright 2011 Wiley online library)

Bisphenol A was also degraded by the combined AOPs, sonolysis, Fe^{2+} and TiO_2 photo-assisted route [143]. Researchers experienced a pronounced synergistic effect that led to the complete and rapid degradation of bisphenol A. In the present system, ultrasound was found to play a principal role in supplying H_2O_2 to enhance the degradation process. However, the photo-Fenton and TiO_2 photocatalysis are mainly responsible protocols for the mineralization of the intermediates to generate CO_2 and H_2O .

Homogeneous sonophoto-Fenton process ($\text{US}/\text{UV}/\text{Fe}^{2+}$) was investigated against the degradation of di-*n*-butyl phthalate (DBP) [144]. To illustrate the exclusive performance of the sonophoto-Fenton process, different hybrid AOPs such as US/Fe^{2+} , US/UV , and UV/Fe^{2+} processes were examined and the results were compared. A maximum performance was evidenced by the sonophoto-Fenton, $\text{US}/\text{UV}/\text{Fe}^{2+}$, process. The DBP degradation was found to be inversely related to pH and greatest at an optimal Fe^{2+} concentration for the $\text{US}/\text{UV}/\text{Fe}^{2+}$ process. Because at lower pH values the formation of $[\text{Fe}(\text{OH})]^{2+}$ was facilitated and increased the concentration of Fe^{3+} and thereby promoting the $\cdot\text{OH}$ generation. As a result, the DBP degradation was favorable at lower pH levels.

Figure 18 illustrates the DBP degradation by the photo- (UV), photo-Fenton (UV/Fe^{2+}), sono- (US), sonophoto- (US/UV), sonoFenton (US/Fe^{2+}) or sonophoto-Fenton ($\text{US}/\text{UV}/\text{Fe}^{2+}$) processes. Except in photo-Fenton (UV/Fe^{2+}), the degradation of DBP generally followed pseudo first-order kinetics in all other processes. The results showed that a complete and best degradation performance was obtained with the hybrid process of sonophoto-Fenton ($\text{US}/\text{UV}/\text{Fe}^{2+}$) within 75 min. The relative degradation performance was found to be in the order: $\text{US}/\text{UV}/\text{Fe}^{2+} > \text{US}/\text{Fe}^{2+} > \text{US}/\text{UV} > \text{US} > \text{UV}/\text{Fe}^{2+} > \text{UV}$. A maximum synergism of 1.43 was observed with the US/UV process [145]. The active involvement of Fe^{2+} in the US/Fe^{2+} , UV/Fe^{2+} and $\text{US}/\text{UV}/\text{Fe}^{2+}$ processes greatly increased DBP degradation compared to the corresponding processes without Fe^{2+} (i.e. US, UV, and US/UV). This clearly indicates the beneficial role of Fe^{2+} ions in these hybrid AOPs processes. Besides, the rate constants of these hybrid AOPs processes were

Fig. 18 DBP degradation performance under different processes (conditions: $[\text{DBP}]_0 = 0.01 \text{ mM}$; $[\text{Fe}^{2+}]_0 = 0.1 \text{ mM}$; $[\text{pH}]_0 = 6.5 \pm 0.05$) (Reprinted with permission from Ref. [144]. Copyright 2014 Elsevier)



$k_{\text{sonophoto-Fenton}} > k_{\text{sono-Fenton}} + k_{\text{photo}} > k_{\text{photo-Fenton}} + k_{\text{sono}}$. This clearly inferred that there may be complex synergistic mechanisms present in the US/UV/Fe²⁺ process.

Combination of ultrasound with other AOPs not always resulted in additive effect. In some cases more than additive effect, i.e. synergistic effect also experienced. For example, Dural et al. studied the ultrasound based degradation of antiepileptic drug carbamazepine (CBZ) and experienced a synergism [146]. They examined the degradation reactions under different coupled AOPs condition namely UV–H₂O₂, US–UV–H₂O₂ and US–UV–H₂O₂–Fe systems. An utmost synergism of 27.7 % was quantified while coupling sonolysis and UV irradiation. Besides, the carbamazepine degradation followed first order rate kinetics. Degradation of carbamazepine pursued radical mechanism which was strongly evident by the scavenger experiments. Based on the TOC results, the authors claim that during the first 10–15 min, carbamazepine is completely degraded. Furthermore the complete mineralization was observed afterwards by degrading formed the intermediates. During this process the dissolved oxygen remained low. The ·OH radicals are the responsible species for the degradation of relatively stable intermediates. The important contribution of ·OH radicals was confirmed by performing the degradation reaction under the US–UV–H₂O₂–Fe system condition. A maximum of 93 % was observed after 35 min with this system. A detailed study of the flow pattern inside the reactor augmented that mineralization rate increased with ultrasound radiation that cannot be attributed to a positive effect in mixing.

In order to find the synergism of this degradation reaction, CBZ degradation was performed under different conditions such as UV, US and UV/US and the results are depicted in Fig. 19. The rate constant values by photolysis (UV), sonolysis (US) and sonophoto (UV/US) process were found to be 0.028, 0.001 and 0.0401 min⁻¹, respectively for CBZ degradation. Based on this value the synergistic value was found by following the Eq. (27) [147].

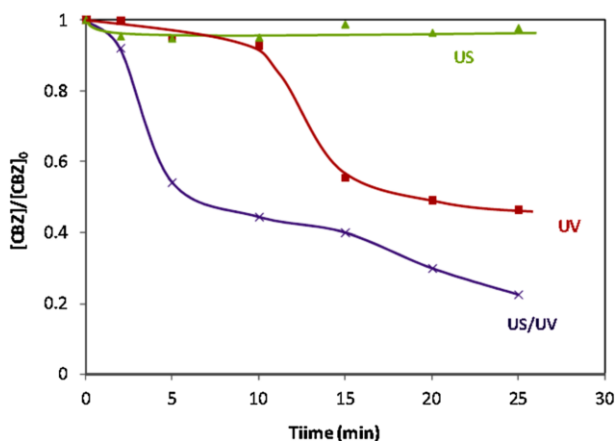


Fig. 19 Degradation of CBZ under different processes (UV, US and UV/US) (conditions: [CBZ]₀ = 78.2 ppm; pH = 2.7) (Reprinted with permission from Ref. [146]. Copyright 2016 Elsevier)

$$\text{Synergy (\%)} = \frac{k_{\text{US+UV}} - (k_{\text{UV}} + k_{\text{US}})}{k_{\text{US+UV}}} \times 100 \%. \quad (27)$$

In the same way, to achieve high synergism, Chakma et al., prepared zirconium ferrite (ZrFe_2O_5) and tested as a catalyst in advanced oxidation processes (AOPs) using decolorization/degradation of azo and non-azo dyes as model processes [148]. They compared the activity of the present catalyst, ZrFe_2O_5 , with the conventional TiO_2 catalyst which prepared by sonochemical sol-gel process. From the UV-visible diffused reflectance spectral results the authors confirmed that ZrFe_2O_5 photocatalyst has lower band gap energy than TiO_2 . Sonochemically synthesized ZrFe_2O_5 photocatalyst also exhibit high adsorption capacity for the textile dyes which assists their effective degradation through Fenton and photocatalytic process. To illustrate the phenomenal synergistic activity of ZrFe_2O_5 photocatalyst, the degradation studies were performed under individual AOPs such as sonolysis, photocatalysis, Fenton and also by the combination of these AOPs. The combined AOPs for ZrFe_2O_5 photocatalyst showed superior performance as compared to the photocatalytic performance of pristine TiO_2 . Nonetheless, the Fenton activity of ZrFe_2O_5 overcomes the photocatalytic activity in dye degradation. The sono-photo-Fenton hybrid AOPs was registered as an efficient system in which both photo- and Fenton- activities of ZrFe_2O_5 are utilized.

Several mechanisms may occur simultaneously that contribute to the overall degradation for any particular degradation procedure. The synergies between the mechanisms were resulted the enhancement in degradation in any hybrid AOPs. The synergies obtained by the ZrFe_2O_5 photocatalyst-catalyzed degradation of acid red B (ARB) and methylene blue (MB) is illustrated in Fig. 20. The synergy effect in hybrid advanced oxidation processes (HAOPs) was calculated with Eq. (28).

$$\text{Synergy factor (S}_F\text{)} = \frac{[\text{hybrid AOP}] - \{[\text{hybrid AOP}] + [\text{adsorption}]\}}{\{[\text{individual AOP}] + [\text{adsorption}]\}}. \quad (28)$$

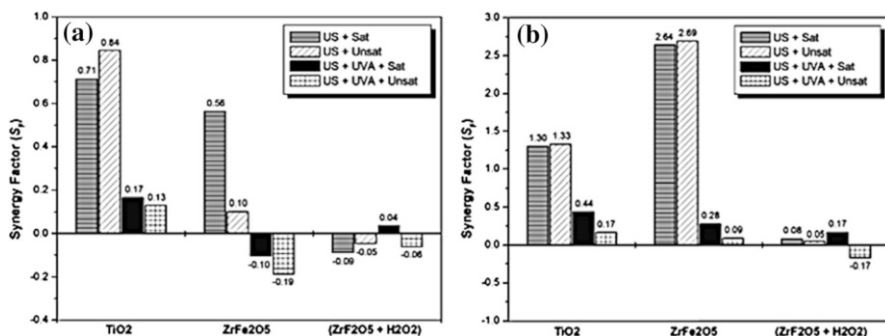


Fig. 20 Synergism of hybrid AOPs: **a** synergistic effect for decolorization of ARB (azo dye), and **b** synergistic effect for decolorization of MB (non-azo dye). Note: while calculation of the synergies, the extent of adsorption of the dye onto the photocatalyst (after total reaction time of the advanced oxidation treatment) was accounted (Reprinted with permission from Ref. [148]. Copyright 2015 Royal Society of Chemistry)

4 Conclusions and Future Directions

The application of ultrasonic technology has received world-wide attention in environmental remediation. The beneficial effects of ultrasound include a reduction in reaction time in waste water treatment processes. It is well known fact that ultrasound alone is generally not feasible in environmental remediation because not all the cavitation energy can be transferred into chemical and physical effects. Hence, the efficiency of the sonolysis can be enhanced by adding external oxidants such as H_2O_2 and potassium persulfate. On the other hand, the combinations of two or more AOPs along with ultrasound showed pronounced enhancement in performance without the addition of expensive external oxidizing agents. Very interestingly, hybrid AOPs showed synergistic effect as compared to individual AOP systems, in most cases. In summary, there is no doubt that ultrasound is a powerful tool in the area of AOPs.

References

1. Glaze WH (1994) An overview of advanced oxidation processes: current status and kinetic models. *Chem Oxid* 2:44–57
2. Karthik P, Vinoth R, Babu SG, Wen M, Kamegawa T, Yamashita H, Neppolian B (2015) Synthesis of highly visible light active TiO_2 -2-Naphthol surface complex and its application in photocatalytic chromium (VI) reduction. *RSC Adv* 5:39752–39759
3. Babu SG, Vijayan AS, Neppolian B (2015) SnS_2/rGO : an efficient photocatalyst for the complete degradation of organic contaminants. *Mater Focus* 4:272–276
4. Kumar PS, Selvakumar M, Babu SG, Jaganathan S, Karuthapandian S (2015) Novel CuO/Chitosan nanocomposite thin film: facile hand picking recoverable, efficient and reusable heterogeneous photocatalyst. *RSC Adv* 5:57493–57501
5. Kumar PS, Selvakumar M, Babu SG, Karuthapandian S, Chattopadhyay S (2015) CdO nanospheres: facile synthesis and bandgap modification for the superior photocatalytic activity. *Mater Lett* 151:45–48
6. Suslick KS (1988) *Ultrasound: its chemical, physical and biological effects*. VCH, New York
7. Mason TJ, Lorimer JP (1988) *Sonochemistry: theory, applications and uses of ultrasound in chemistry*. Ellis Horwood, Chichester
8. Suslick KS (1989) The chemical effects of ultrasound. *Sci Am* 260:80–86
9. Mason TJ, Tiem A (2001) *Advances in sonochemistry*. JAI, Oxford
10. Lifka J, Ondrushka B, Hofmann J (2003) The use of ultrasound for the degradation of pollutants in water: aquasonolysis—a review. *Eng Life Sci* 3:253–262
11. Ince NH, Tezcanli G, Belen RK, Apikyan IG (2001) Ultrasound as a catalyzer of aqueous reaction systems: the state of the art and environmental applications. *App Cat B Environ* 29:167–176
12. Chowdhury P, Viraraghavan T (2009) Sonochemical degradation of chlorinated organic compounds, phenolic compounds and organic dyes—a review. *Sci Tot Env* 407:2474–2492
13. Gopiraman M, Babu SG, Khatri Z, Kim BS, Wei K, Karvembu R, Kim IS (2015) Photodegradation of dyes by a novel $\text{TiO}_2/\text{u-RuO}_2/\text{GNS}$ nanocatalyst derived from Ru/GNS after its use as catalyst in aerial oxidation of primary alcohols (GNS = graphene nanosheets). *React Kinet Mech Catal* 115:759–772
14. Glaze WH, Kang JW, Chapin DH (1987) The chemistry of water treatment processes involving ozone, hydrogen peroxide, and ultraviolet radiation. *Ozone Sci Eng* 9:335–352
15. Ince NH, Tezcanli G (1999) Treatability of textile dyebath effluents by advanced oxidation: preparation for reuse, water. *Sci Technol* 40:183–190

16. Babu SG, Vinoth R, Narayana PS, Bahnemann D, Neppolian B (2015) Reduced graphene oxide wrapped Cu₂O supported on C₃N₄: an efficient visible light responsive semiconductor photocatalyst. *APL Mater* 3:104415–104418
17. Naffrechoux E, Chanoux S, Petrier C, Suptil J (2000) Sonochemical and photochemical oxidation of organic matter. *Ultrason Sonochem* 7:255–259
18. Suslick KS (1990) Sonochemistry. *Science* 247:1439–1445
19. Yanagida H, Masubuchi Y, Minagawa K, Ogata T, Takimoto J, Koyama K (1999) A reaction kinetics model of water sonolysis in the presence of a spin-trap. *Ultrason Sonochem* 5:133–139
20. Boffito DC, Crocella V, Pirola C, Neppolian B, Cerrato G, Ashokkumar M, Bianchi CL (2013) Ultrasonic enhancement of the acidity, surface area and free fatty acids esterification catalytic activity of sulphated ZrO₂–TiO₂ systems. *J Catal* 297:17–26
21. Joseph JM, Destailhats H, Hung HM, Hoffmann MR (2000) The sonochemical degradation of azobenzene and related azo dyes: rate enhancements via Fenton's reactions. *J Phys Chem A* 104:301–307
22. Vajnhandl S, Le Marechal AM (2005) Ultrasound in textile dyeing and the decolouration/mineralization of textile dyes. *Dyes Pigment* 65:89–101
23. Tezcanli-Guyer G, Ince NH (2003) Degradation and toxicity reduction of textile dyestuff by ultrasound. *Ultrason Sonochem* 10:235–240
24. Guo W, Wang H, Shi Y, Zhang G (2010) Sonochemical degradation of the antibiotic cephalixin in aqueous solution. *Water SA* 36:651–654
25. Koerner R, Soong T (2000) Leachate in landfills: the stability issues. *Geotext Geomembr* 18:293–309
26. Kang K, Shin H, Park H (2002) Characterization of humic substances present in landfill leachates with different landfill ages and its implications. *Water Res* 36:4023–4032
27. Mott H, Hartz K, Yonge D (1987) Landfill leachates. *J Environ Eng* 113:476–485
28. Tatsi A, Zouboulis A (2002) A field investigation of the quantity and quality of leachate from a municipal solid waste landfill in a Mediterranean climate (Thessaloniki, Greece). *Adv Environ Res* 6:207–219
29. Ehrig H (1984) Treatment of sanitary landfill leachate: biological treatment. *Waste Manage Res* 2:131–152
30. Trebouet D, Schlumpf J, Jaouen P, Quemeneur F (2001) Stabilized landfill leachate treatment by combined physicochemical-nanofiltration processes. *Water Res* 35:2935–2942
31. Marttinen S, Kettunen R, Sormunen K, Soimasuo R, Rintala J (2002) Screening of physical-chemical methods for removal of organic material, nitrogen and toxicity from low strength landfill leachates. *Chemosphere* 46:851–858
32. Amokrane A, Comel C, Veron J (1997) Landfill leachates pre-treatment by coagulation flocculation. *Water Res* 31:2775–2782
33. Li X, Zhao Q, Hao X (1999) Ammonium removal from landfill leachate by chemical precipitation. *Waste Manage* 19:409–415
34. Yusuf G (2001) Sonochemistry: environmental science and engineering applications. *Ind Eng Chem Res* 40:4681–4715
35. Parag R (2008) Treatment of wastewater streams containing phenolic compounds using hybrid techniques based on cavitation: a review of the current status and the way forward. *Ultrason Sonochem* 15:1–15
36. Wang S, Wu X, Wang Y, Li Q, Tao M (2008) Removal of organic matter and ammonia nitrogen from landfill leachate by ultrasound. *Ultrason Sonochem* 15:933–937
37. Entezari M, Kruus P (1996) Effect of frequency on sonochemical reactions II. Temperature and intensity effects. *Ultrason Sonochem* 3:19–24
38. Goel M, Hongqiang H, Mujumdar A, Ray M (2004) Sonochemical decomposition of volatile and non-volatile organic compounds—a comparative study. *Water Res* 38:4247–4261
39. Jiang Y, Petrier C, Waite T (2002) Kinetics and mechanisms of ultrasonic degradation of volatile chlorinated aromatics in aqueous solutions. *Ultrason Sonochem* 9:317–323
40. Klavarioti M, Mantzavinos D, Kassinos D (2009) Removal of residual pharmaceuticals from aqueous systems by advanced oxidation processes. *Environ Int* 35:402–417
41. Arslan-Alaton I, Akmehtmet BI (2002) Biodegradability assessment of ozonated raw and biotreated pharmaceutical wastewater. *Arch Environ Con Toxicol* 43:425–431
42. Oremland RS, Stolz JF (2003) The ecology of arsenic. *Science* 300:939–944

43. Iqbal J, Kim HJ, Yang JS, Baek K, Yang JW (2007) Removal of arsenic from groundwater by micellar-enhanced ultrafiltration (MEUF). *Chemosphere* 66:970–976
44. Karim MM (2000) Arsenic in groundwater and health problems in Bangladesh. *Water Res* 34:304–310
45. Meharg AA, Rahman MM (2003) Arsenic contamination of Bangladesh paddy field soils: implication for rice contribution to arsenic consumption. *Environ Sci Technol* 37:229–234
46. Deschamps E, Ciminelli VST, Holl W (2005) Removal of As (III) and As (V) from water using a natural Fe and Mn enriched sample. *Water Res* 39:5212–5220
47. Ryu J, Choi W (2004) Effects of TiO₂ surface modifications on photocatalytic oxidation of arsenite: the role of superoxides. *Environ Sci Technol* 38:2928–2933
48. Dutta PK, Pehkonen SO, Sharma VK, Ray AK (2005) Photocatalytic oxidation of arsenic (III): evidence of hydroxyl radicals. *Environ Sci Technol* 39:1827–1834
49. Elless MP, Poynton CY, Willms CA, Doyle MP, Lopez AC, Sokkary DA, Ferguson BW, Blaylock MJ (2005) Pilot-scale demonstration of phytofiltration for treatment of arsenic in the New Mexico drinking water. *Water Res* 39:3863–3872
50. Neppolian B, Oronila A, Grieser F, Ashokkumar M (2009) Simple and efficient sonochemical method for the oxidation of arsenic(III) to arsenic(V). *Environ Sci Technol* 43:6793–6798
51. Neppolian B, Doronila A, Ashokkumar M (2010) Sonochemical oxidation of arsenic(III) to arsenic(V) using potassium peroxydisulfate as an oxidizing agent. *Water Res* 44:3687–3695
52. Beckett MA, Hua I (2000) Elucidation of the 1,4-dioxine decomposition pathway at discrete ultrasonic frequencies. *Environ Sci Technol* 34:3944–3953
53. Gould JP, Groff KA (1987) The kinetics of ozonolysis of synthetic dyes. *Ozone Sci Eng* 9:153–157
54. Snider EH, Porter JJ (1974) Ozone treatment of dye waste. *J Water Pollut Contr Fed* 46:886–894
55. Peyton GR, Glaze WH (1985) The mechanism of photolytic ozonation. *Photochemistry of Environmental Aquatic Systems ACS Symposium Series* 327:76–88
56. Destailhats H, Colussi AJ, Joseph JM, Hoffmann MR (2000) Synergistic effects of sonolysis combined with ozonolysis for the oxidation of azobenzene and methyl orange. *J Phys Chem* 104:8930–8935
57. Tezcanli-Guyer G, Ince NH (2004) Individual and combined effects of ultrasound, ozone and UV irradiation: a case study with textile dyes. *Ultrasonics* 42:603–609
58. Wan-Qian G, Ren-Li Y, Xian-Jiao Z, Juan-Shan D, Hai-Ou C, Shan-Shan Y, Nan-Qi R (2015) Sulfamethoxazole degradation by ultrasound/ozone oxidation process in water: kinetics, mechanisms, and pathways. *Ultrason Sonochem* 22:182–187
59. Koda S, Kimura T, Kondo T, Mitome H (2003) A standard method to calibrate sonochemical efficiency of an individual reaction system. *Ultrason Sonochem* 10:149–156
60. Xiao-Dan F, Wen-Li Z, Hai-Yan X, Tai-Qiu Q, Jian-Guo J (2015) Effects of ultrasound combined with ozone on the degradation of organophosphorus pesticide residues on lettuce. *RSC Adv* 5:45622–45630
61. Gultekin I, Ince NH (2006) Degradation of aryl-azo-naphthol dyes by ultrasound, ozone and their combination: effect of α -substituents. *Ultrason Sonochem* 13:208–214
62. Martins AO, Canalli VM, Azevedo CMN, Pires M (2006) Degradation of pararosaniline (C.I. Basic Red 9monohydrochloride) dye by ozonation and sonolysis. *Dyes Pigm* 68:227–234
63. Zhao W, Shi H, Wang D (2004) Ozonation of cationic Red X-GRL in aqueous solution: degradation and mechanism. *Chemosphere* 57:1189–1199
64. Zhang F, Yediler A, Liang X, Kettrup A (2004) Effects of dye additives on the ozonation process and oxidation by-products: a comparative study using hydrolyzed C.I. Reactive Red 120. *Dyes Pigm* 60:1–7
65. Ince NH, Tezcanlı G (2001) Reactive dyestuff degradation by combined sonolysis and ozonation. *Dyes Pigm* 49:145–153
66. Andreozzi R, Caprio V, Insola A, Marotta R (1999) Advance oxidation processes (AOP) for water purification and recovery. *Catal Today* 53:51–59
67. Toma S, Gaplovsky A, Luche J-L (2001) The effect of ultrasound on photochemical reaction. *Ultrason Sonochem* 8:201–207
68. Ruppert G, Bauer R, Heisler G (1994) UV–O₃, UV–H₂O₂, UV–TiO₂ and photo-Fenton reaction-comparison of advanced oxidation processes for wastewater treatment. *Chemosphere* 28:1447–1454
69. Benitez FJ, Beltran-Heredia J, Acero JL, Rubio FJ (2000) Contribution of free radicals to chlorophenols decomposition by several advanced oxidation processes. *Chemosphere* 41:1271–1277

70. Xie Y, Chen F, He J, Zhao J, Wang H (2000) Photoassisted degradation of dyes in the presence of Fe^{3+} and H_2O_2 under visible irradiation. *J Photochem Photobiol A Chem* 136:235–240
71. Esplugas S, Gimenez J, Contreras S, Pascual E, Rodriguez M (2002) Comparison of different advanced oxidation processes for phenol degradation. *Water Res* 36:1034–1042
72. Weavers LK, Ling FH, Hoffmann MR (1998) Aromatic compounds degradation in water using a combination of sonolysis and ozonolysis. *Environ Sci Technol* 32:2727–2733
73. Kopf P, Gilbert E, Eberle SH (2000) TiO_2 photocatalytic oxidation of monochloroacetic acid and pyridine: influence of ozone. *J Photochem Photobiol A Chem* 136:163–168
74. Colmenares JC (2014) Sonication-induced pathways in the synthesis of light-active catalysts for photocatalytic oxidation of organic contaminants. *ChemSusChem* 7:1512–1527
75. Theron P, Pichat P, Guillard C, Petrier C, Chopin T (1999) Degradation of phenyltrifluoromethylketone in water by separate or simultaneous use of TiO_2 photocatalysis and 30 or 515 kHz. *Phys Chem Chem Phys* 1:4663–4668
76. Stock NL, Peller J, Vinodgopal K, Kamat PV (2000) Combinative sonolysis and photocatalysis for textile dye degradation. *Environ Sci Technol* 34:1747–1750
77. Vaishnav P, Kumar A, Ameta R, Punjabi PB, Ameta SC (2014) Photo oxidative degradation of azure-B by sono-photo-Fenton and photo-Fenton reagents. *Arab J Chem* 7:981–985
78. Theron P, Pichat P, Petrier C, Guillard C (2001) Water treatment by TiO_2 photocatalysis and/or ultrasound: degradations of phenyltrifluoromethylketone, a trifluoroacetic-acid-forming pollutant, and octan-1-ol, a very hydrophobic pollutant. *Water Sci Technol* 44:263–270
79. Ragaini V, Selli E, Bianchi CL, Pirola C (2001) Sono-photocatalytic degradation of 2-chlorophenol in water: kinetic and energetic comparison. *Ultrason Sonochem* 8:251–258
80. Petrier C, Lamy M-F, Francony A, Benahcene A, David B, Renaudin V, Gondrexon N (1994) Sonochemical degradation of phenol in dilute aqueous solutions: comparison of the reaction rates at 20 and 487 kHz. *J Phys Chem* 98:10514–10520
81. Mrowetz M, Pirola C, Selli E (2003) Degradation of organic water pollutants through sonophotocatalysis in the presence of TiO_2 . *Ultrason Sonochem* 10:247–254
82. Davydov L, Reddy EP, France P, Smiriotis PG (2001) Sonophotocatalytic destruction of organic contaminants in aqueous systems on TiO_2 powders. *App Catal B Environ* 32:95–105
83. Harada H (2001) Sonophotocatalytic decomposition of water using TiO_2 photocatalyst. *Ultrason Sonochem* 8:55–58
84. Selli E, Bianchi CL, Pirola C, Bertelli M (2005) Degradation of methyl tert-butyl ether in water: effects of the combined use of sonolysis and photocatalysis. *Ultrason Sonochem* 12:395–400
85. Shirgaonkar IZ, Pandit AB (1998) Sonophotocatalytic destruction of aqueous solution of 2,4,6-trichlorophenol. *Ultrason Sonochem* 5:53–61
86. Anandan S, Ashokkumar M (2009) Sonochemical synthesis of Au- TiO_2 nanoparticles for the sonophotocatalytic degradation of organic pollutants in aqueous environment. *Ultrason Sonochem* 16:316–320
87. Vinodgopal K, Ashokkumar M, Grieser F (2001) Sonochemical degradation of a polydisperse nonylphenol ethoxylate in aqueous solution. *J Phys Chem B* 105:3338–3342
88. Babu SG, Vinoth R, Kumar DP, Shankar MV, Chou HL, Vinodgopal K, Neppolian B (2015) Influence of electron storing, transferring and shuttling assets of reduced graphene oxide at the interfacial copper doped TiO_2 *p-n* hetero-junction for the increased hydrogen production. *Nanoscale* 7:7849–7857
89. Brand N, Mailhot G, Bolte M (1998) Degradation photoinduced by Fe(III): method of alkylphenol ethoxylates remove in water. *Environ Sci Technol* 32:2715–2720
90. Yuanhua HE, Grieser F, Ashokkumar M (2011) Kinetics and mechanism for the sonophotocatalytic degradation of *p*-chlorobenzoic Acid. *J Phys Chem A* 115:6582–6588
91. Adewuyi YG (2005) Sonochemistry in environment remediation. 2. Heterogeneous sonophotocatalytic oxidation processes for the treatment of pollutants in water. *Environ Sci Technol* 39:8557–8570
92. Peller J, Wiest O, Kamat PV (2003) Synergy of combining sonolysis and photocatalysis in the degradation and mineralization of chlorinated aromatics compounds. *Environ Sci Technol* 37:1926–1932
93. Singla R, Ashokkumar M, Grieser F (2004) The mechanism of the sonochemical degradation of the benzoic acid in aqueous solution. *Res Chem Intermed* 30:723–733
94. Fujishima A, Hashimoto K, Watanabe T (1999) *Photocatalysis: fundamentals and applications*, 1st edn. BKC Inc., Tokyo

95. Okitsu K, Iwasaki K, Yobiko Y, Bandow H, Nishimura R, Maeda Y (2005) Sonochemical degradation of azo dyes in aqueous solution: a new heterogeneous kinetics model taking into account the local concentration of OH radicals and azo dyes. *Ultrason Sonochem* 12:255–262
96. Talebiana N, Nilforoushanb MR, Mogaddas FJ (2013) Comparative study on the sonophotocatalytic degradation of hazardous waste. *Ceram Int* 39:4913–4921
97. Taghizadeh MT, Abdollahi R (2011) Sonolytic, sonocatalytic and sonophotocatalytic degradation of chitosan in the presence of TiO₂ nanoparticles. *Ultrason Sonochem* 18:149–157
98. Berberidou C, Poullos I, Xekoukoulotakis NP, Mantzavinos D (2007) Sonolytic, photocatalytic and sonophotocatalytic degradation of malachite green in aqueous solutions. *Appl Cat B Environ* 74:63–72
99. Kavitha SK, Palanisamy PN (2011) Photocatalytic and sonophotocatalytic degradation of reactive red 120 using dye sensitized TiO₂ under visible light. *Inter J Civil Environ Eng* 5:1–6
100. Son Y, Cho E, Lim M, Khim J (2010) Effects of salt and pH on sonophotocatalytic degradation of azo dye reactive black 5. *Japanese J Appl Phy* 49:7
101. Neppolian B, Ciceri L, Bianchi CL (2011) Franz Grieser a, Muthupandian Ashokkumar. Sonophotocatalytic degradation of 4-chlorophenol using Bi₂O₃/TiZrO₄ as a visible light responsive photocatalyst. *Ultrason Sonochem* 18:135–139
102. Babu SG, Vinoh R, Neppolian B, Dionysiou DD, Ashokkumar M (2015) Diffused sunlight driven highly synergistic pathway for complete mineralization of organic contaminants using reduced graphene oxide supported photocatalyst. *J Hazard Mater* 291:83–92
103. Zhang J, Xiong Z, Zhao XS (2011) Graphene–metal–oxide composites for the degradation of dyes under visible light irradiation. *J Mater Chem* 21:3634–3640
104. Neppolian B, Ciceri L, Bianchi CL, Grieser F, Ashokkumar M (2001) Sonophotocatalytic degradation of 4-chlorophenol using Bi₂O₃/TiZrO₄ as a visible light responsive photocatalyst. *Ultrason Sonochem* 18:135–139
105. Kritikos DE, Xekoukoulotakis NP, Psillakis E, Mantzavinos D (2007) Photocatalytic degradation of reactive black 5 in aqueous solutions: effect of operating conditions and coupling with ultrasound irradiation. *Water Res* 41:2236–2246
106. Shimizu N, Ogino C, Dadjour MF, Murata T (2007) Sonocatalytic degradation of methylene blue with TiO₂ pellets in water. *Ultrason Sonochem* 14:184–190
107. Gogate PR, Pandit AB (2004) A review of imperative technologies for wastewater treatment II: hybrid methods. *Adv Environ Res* 8:553–597
108. Uchida T, Hamano A, Kawashima N, Takeuchi S (2007) Disaggregation and surface modification of nano-size diamond by ultrasound exposure: relationships among acoustic intensity, disaggregation, and surface modification. *Electron Comm Jpn Pt III* 90:10–18
109. Lirong M, Jianjun S, Ming Z, Jie H (2014) Synthesis of magnetic sonophotocatalyst and its enhanced biodegradability of organophosphate pesticide. *Bull Korean Chem Soc* 35:3521–3526
110. Ai ZH, Yang P, Lu XH (2005) Degradation of 4-chlorophenol by microwave irradiation enhanced advanced oxidation processes. *Chemosphere* 60:824–827
111. Voelker B, Sulzberger B (1996) Effects of fulvic acid on Fe(II) oxidation by hydrogen peroxide. *Environ Sci Technol* 30:1106–1114
112. Zepp RG, Faust BC, Hoigne J (1992) Hydroxyl radical formation in aqueous reactions (pH 3–8) of iron (II) with hydrogen peroxide: the photo-Fenton reaction. *Environ Sci Technol* 26:313–319
113. De Laat J, Gallard H (1999) Catalytic decomposition of hydrogen peroxide by Fe(III) in homogeneous solution: mechanism and kinetic modelling. *Environ Sci Technol* 33:2726–2732
114. Kwan WP, Voelker BM (2002) Decomposition of hydrogen peroxide and organic compounds in the presence of dissolved iron and ferrihydrite. *Environ Sci Technol* 36:1467–1476
115. Chou S, Huang C (1999) Application of a supported iron oxyhydroxide catalyst in oxidation of benzoic acid by hydrogen peroxide. *Chemosphere* 38:2719–2731
116. Fernandez J, Bandara J, Lopez A, Kiwi J (1999) Photoassisted Fenton degradation of non-biodegradable azo dye (Orange II) in Fe-free solution mediated by cation transfer membranes. *Langmuir* 15:185–192
117. Parra S, Henao L, Mielczarski E, Mielczarski J, Albers P, Suvorova E, Guindet J, Kiwi J (2004) Synthesis, testing, and characterization of a novel Nafion membrane with superior performance in photoassisted immobilized Fenton catalysis. *Langmuir* 20:5621–5629
118. Bozzi A, Yuranova T, Mielczarski J, Kiwi J (2002) Abatement of oxalates catalysed by Fe-silica structured surface via cyclic carboxylate intermediates in photo-Fenton reaction. *Chem Commun* 19:2202–2203

119. Cheng MM, Ma WH, Li J, Huang YP, Zhao JC (2004) Visible-light-assisted degradation of dye pollutants over Fe(III)-loaded resin in the presence of H_2O_2 at neutral pH values. *Environ Sci Technol* 38:1569–1575
120. Dhananjeyan M, Mielczarski E, Thampi K, Bensimon M, Kiwi J (2001) Photodynamics and surface characterization of TiO_2 and Fe_2O_3 photocatalysts immobilized on modified polyethylene films. *J Phys Chem B* 105:12046–12055
121. Fernandez J, Dhananjeyan M, Kiwi J, Senuma Y, Hilborn J (2000) Evidence for Fenton photoassisted processes mediated by encapsulated Fe ions at Biocompatible pH values. *J Phys Chem B* 104:5298–5301
122. Parra S, Guasaquillo I, Enea O, Mielczarski E, Mielczarki J, Albers P, Kiwi-Minsker L, Kiwi J (2003) Abatement of an azo dye on structured C-Nanfion/Fe-ion surfaces by photo-Fenton reactions leading to carboxylate intermediates with a remarkable biodegradability increase of the treated solution. *J Phys Chem B* 107:7026–7035
123. Parra S, Nadtotechenko V, Albers P, Kiwi J (2004) Discoloration of azo-dyes at biocompatible pH-values through an Fe-histidine complex immobilized on Nafion via Fenton-like processes. *J Phys Chem B* 108:4439–4448
124. Beckett MA, Hua I (2003) Enhanced sonochemical decomposition of 1,4-dioxane by ferrous iron. *Water Res* 37:2372–2376
125. Iordache I, Wilson S, Lundanes E, Iordache M, Pave VL, Aelenei N (2010) The Fenton and sono-Fenton processes applied for pesticide degradation. *Environ Eng Manag J* 9:519–525
126. Huang R, Fang Z, Yan X, Cheng W (2012) Heterogeneous sono-Fenton catalytic degradation of bisphenol A by Fe_3O_4 magnetic nanoparticles under neutral condition. *Chem Eng J* 197:242–249
127. Zhang H, Zhang JH, Zhang CY, Liu F, Zhang DB (2009) Degradation of CI acid orange 7 by the advanced Fenton process in combination with ultrasonic irradiation. *Ultrason Sonochem* 16:325–330
128. Drijvers D, van Langenhove H, Beckers M (1999) Decomposition of phenol and trichloroethylene by the ultrasound/ H_2O_2 /CuO process. *Water Res* 33:1187–1194
129. Nie M, Wang Q, Qiu G (2008) Enhancement of ultrasonically initiated emulsion polymerization rate using aliphatic alcohols as hydroxyl radical scavengers. *Ultrason Sonochem* 15:222–226
130. Guo X, Chen S, Hu Y, Li G, Liao N, Ye X, Liu D, Xue C (2014) Preparation of water-soluble melanin from squid ink using ultrasound-assisted degradation and its anti-oxidant activity. *J Food Sci Technol* 51:3680–3690
131. Luo T, Ai Z, Zhang L (2008) Fe@ Fe_2O_3 core-shell nanowires as iron reagent. 4. Sono-Fenton degradation of pentachlorophenol and the mechanism analysis. *J Phys Chem C* 112:8675–8681
132. Hwang A, Na S, Ha J, Kim J (2011) Degradation of diethyl phthalate by sono-Fenton process and its dependence on the power density. *Japan J Appl Phys* 50:7–9
133. Ranjit PJD, Palanivelu K, Lee CS (2008) Degradation of 2,4-dichlorophenol in aqueous solution by sono-Fenton method. *Korean J Chem Eng* 25:112–117
134. Ai Z, Lu L, Li J, Zhang L, Qiu J, Wu M (2007) Fe@ Fe_2O_3 core-shell nanowires as iron reagent efficient degradation of rhodamine b by a novel sono-Fenton process. *J Phys Chem C* 111:4087–4093
135. Makino K, Mossoba MM, Riesz P (1983) Chemical effects of ultrasound on aqueous solutions. Formation of hydroxyl radicals and hydrogen atoms. *J Phys Chem* 87:1369–1377
136. Weissler A (1959) Formation of hydrogen peroxide by ultrasonic waves: free radicals. *J Am Chem Soc* 81:1077–1081
137. Tay KS, Rahman NA, Abas MRB (2011) Fenton degradation of dialkylphthalates: products and mechanism. *Environ Chem Lett* 9:539–546
138. Carp O, Huisman CL, Reller A (2004) Photoinduced reactivity of titanium dioxide. *Prog Solid State Chem* 32:33–177
139. Madhavana J, Kumara PSS, Anandanb S, Griesera F, Ashokkumar M (2010) Sonophotocatalytic degradation of monocrotophos using TiO_2 and Fe^{3+} . *J Hazard Mater* 177:944–949
140. Babuponnusami A, Muthukumar K (2011) Degradation of phenol in aqueous solution by fenton, sono-Fenton and sono-photo-Fenton methods. *CLEAN Soil Air Water* 39:142–147
141. Wu C, Liu X, Wei D, Fan J, Wang L (2001) Photosonochemical degradation of phenol in water. *Water Res* 35:3927–3933
142. Chitra S, Paramasivan P, Sinha PK (2013) Sono-photo Fenton treatment of liquid waste containing ethylenediaminetetraacetic acid (EDTA). *Int J Nonferrous Metall* 2:89–94

143. Ricardo A, Palma T, Nieto JI, Combet E, Pétrier C, Pulgarin C (2010) An innovative ultrasound, Fe₂D and TiO₂ photoassisted process for bisphenol a mineralization. *Water Res* 44:2245–2252
144. Xu LJ, Chu W, Graham N (2014) Degradation of di-*n*-butyl phthalate by a homogeneous sono-photo-Fenton process with in situ generated hydrogen peroxide. *Chem Eng J* 240:541–547
145. Xu LJ, Chu W, Graham N (2013) Sonophotolytic degradation of dimethyl phthalate without catalyst: analysis of the synergistic effect and modeling. *Water Res* 47:1996–2004
146. Duran A, Monteagudo JM, Exposito AJ, Monsalve V (2016) Modeling the sonophoto-degradation/mineralization of carbamazepine in aqueous solution. *Chem Eng J* 284:503–512
147. Joseph CG, Li Puma G, Bono A, Taufiq-Yap YH, Krishnaiah D (2011) Operating parameters and synergistic effects of combining ultrasound and ultraviolet irradiation in the degradation of 2,4,6-trichlorophenol. *Desalination* 276:303–309
148. Chakma S, Moholkar VS (2015) Sonochemical synthesis of mesoporous ZrFe₂O₅ and its application for degradation of recalcitrant pollutants. *RSC Adv* 5:53529–53542

Effects of ultrasonic disintegration of excess sewage sludge

Ewa Zielewicz¹

Received: 30 May 2016 / Accepted: 23 August 2016 / Published online: 12 September 2016
© Springer International Publishing Switzerland 2016

Abstract Breaking down sludge floc (sonodispersion effect) and destruction of the cell membranes of microorganisms forming floc is a direct effect of ultrasonic disintegration of sludge excess. This results in release of organic material by liquid sludge (the sonolysis effect). Desired technological effects of the disintegration are: to shorten the hydrolytic phase of fermentation, to increase the production of biogas (source of renewable energy) and an increased mineralization (stability) of fermented sludge. The presented study demonstrates research covering thickened excess sludge of various physicochemical properties, collected from nine municipal sewage treatment plants. The sludge was subjected to ultrasonic disintegration using three differently constructed disintegrators and different proportions of sonification area. Direct effects of disintegration were monitored and recorded using selected indicators describing changes in the properties of sludge and increase of substance dispersed and dissolved in the supernatant liquid to be filtered. Studies have demonstrated that those (direct) effects of ultrasonic disintegration depend on the physicochemical properties of the sludge (foremost the concentration of dry solids) that determine their variable susceptibility to the disintegration methods. The direct effects also depend on optimal process conditions (which consist of the construction of the ultrasonic disintegrator), the geometric proportions of the sonication area and the operating parameters of disintegration (which could be appropriately matched to the characteristics of sludge). The most preferable results were obtained for ultrasonic disintegration of sludge with a dry matter concentration $C_0 < 4.2$ %. The

This article is part of the Topical Collection “Sonochemistry: From basic principles to innovative applications”; edited by Juan Carlos Colmenares Q., Gregory Chatel.

✉ Ewa Zielewicz
ewa.zielewicz@polsl.pl

¹ Institute of Water and Wastewater Engineering, Silesian University of Technology, Konarskiego18A, 44-100 Gliwice, Poland

highest effect of sonolysis—an almost 30-fold increase in the COD dissolved in the supernatant—was obtained for the sludge of lowest dry matter ($C_0 = 2.0\%$), which was sonicated in a reactor with a short transducer of the largest radiating surface area, as well as the lowest ratio between this area and area of reactor. The best effects of disagglomeration of flocks have corresponded with the high value of power density $U_{UD} = 880\text{--}900\text{ WL}^{-1}$.

Keywords Ultrasounds · Excess sludge · Lysis · Disagglomeration · Cell disruption · Disintegration · Fermentation · Volumetric energy · Specific energy

1 Introduction

Sludge produced in biological wastewater treatment is considered waste and should be processed. One of the main processes used in large wastewater treatment plants (WWTPs) involves stabilization by methane digestion. In this biochemical process, part of the organic matter of sludge is converted to mineralized substances, water and biogas. Mesophilic digestion is a complicated process that requires expensive and complex installation, and thus considerable investment. Nonetheless, it is perceived as a suitable method of sludge processing due to heat and energy gains. Easily fermenting preliminary sludge and difficult to the biodegradation process of excess sludge of aerobic microorganisms are compounds of digested sludge. Deterioration of biodegradability of excess sludge is associated with two important technological challenges.

Firstly, after several years of operation in wastewater treatment plants using biological removal process of biogenic substances, difficulties with hydrolysis under aerobic conditions were observed.

Secondly, a significant part of the excess sludge entering the digesters in present-day WWTPs is mechanically thickened to a concentration of 3–6 % TS, which reduces the size of the digesters and amount of heat required to heat up sludge, although it has negative impact on transport, stirring of the sludge and heat exchange. Large, compact sludge flocks that form from the polyelectrolyte help with thickening process and hinder the biodegradation of organic matter during biochemical stabilization; especially during first hydrolytic phase of digestion, which limits the entire process and extends processing time [1]. That results with extent of time and decrease of efficiency of mesophilic digestion (also affecting extent of mineralization and biogas production). Intensification of excess sludge digestion has been on the agenda of researchers and engineers.

One of the methods of improving the susceptibility of excess sludge for biodegradation includes disintegration, considered as the introduction of a determined quantity of energy into excess sludge, enough to produce what are called direct disintegration effects by the author (Zielewicz 2010) [2]. First, the particle agglomerates of the sludge are brought up, which isolates activated sludge microorganisms from the flocks and flocules, and thus makes it susceptible to degradation. Next, cell matter, proteins, and enzymes among others, are released to the liquid phase as a result of microbial cell disruption, i.e., liquefaction of the solid phase—hydrolysis [2–6]. Contemporary disintegration methods can be divided into:

- Mechanical—(ball mills, hydrodynamic reducers, lysis centrifuges, high-speed stirrers, ultrasounds),
- Non-mechanical methods, which include:
 - Physical (heat treatment, freezing, osmotic shock, decompression, plasma)
 - Biological (enzymatic lysis, autolysis)
 - Chemical (action of acids or bases, detergents, ozone, oxygen)

Hybrid methods are also employed. They are a combination of two (or more) techniques mentioned above (i.e., thermal and pressure, thermal and chemical, mechanical and chemical). Zielewicz at all [7] showed that hybrid disintegration that combines the mechanical destruction of sludge particles with ultrasonic cell lysis is most efficient due to better direct disintegration effects with lower energy consumption; hence, ultrasonic energy is not wasted during floc size reduction—this effect can be achieved using simpler and less energy-consuming methods, such as homogenisation. Research of chemical and ultrasonic disintegration in which lysis is supported by NaOH or ozone was also carried out [8, 9]. A review of mechanical disintegration technologies (including ultrasounds) along with schematics of the most common equipment and its applications in German wastewater treatment plants from 1993 to 1996 were presented in publication by scientists from Brunswick and Munich [10–12]. In Poland, 15 out of 17 installations of excess sludge disintegration are mechanical, with eight of them using ultrasonic disintegrators. Figure 1 shows schematics of disintegrating installation of excess sludge before entering digesters (based upon Müller's scheme [3]). Each type of disintegration of thickened excess sludge brings specific technological benefits and should be presented to designers, investors and operators of wastewater treatment plants. Mechanical disintegration, notably ultrasonic disintegration, is still most common [13–16].

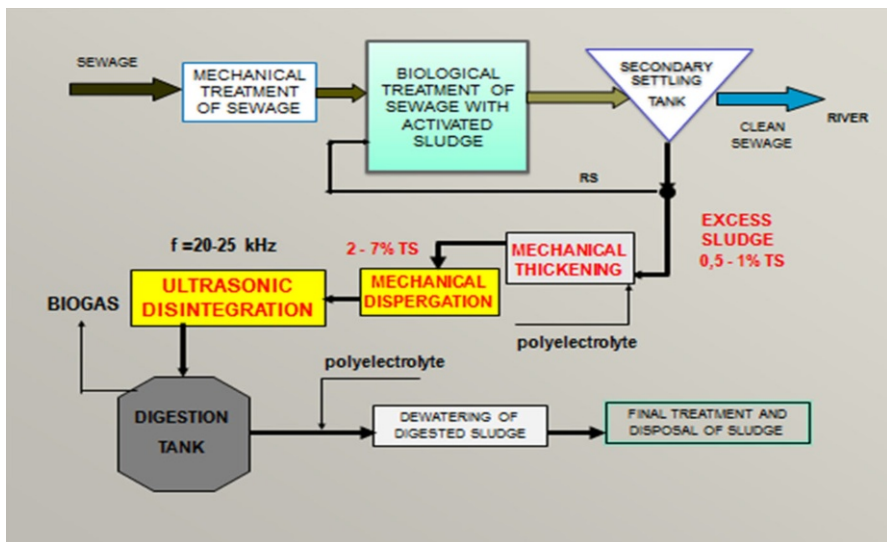


Fig. 1 The placement of ultrasonic disintegration at WWTP

An important advantage of the ultrasonic technique (despite its high energy consumption necessary to obtain the required effects of disintegration) is not only almost 100 % lysis of cells of microorganisms [17], but also that it brings about a number of sonochemical phenomena that help with decomposition of non-biodegradable sewage sludge compounds. Ultrasonic treatment of sludge attracts lot of attention due to the wide area of applications in multiple disciplines, i.e., chemistry, biology, medicine [18–21] and environmental science and research carried out for many years.

The author's own research (Kowalska, Bień, Zielewicz) [22–24] conducted on various types of sludge (from municipal and industrial WWTPs) in the 1970s and 1980s proved that ultrasound preconditioning of raw or digested sludge, prior to its conditioning with polyelectrolytes, can improve sedimentation, thickening and dewatering. Those researches focused on the effect of frequencies used and exposition time found that the best effect is obtained in the field of 20 kHz and exposition time of 1.5–2.0 min [22, 23]. It is known that an ultrasonic field with strictly defined parameters changes the physical and chemical properties of sludge, i.e., the structure of components, surface of solid particles and stability of its hydration layer, and, in consequence, its sedimentation properties [24]. A sequence of sonochemical and biochemical changes initiated in ultrasonic field forms the basis for the introduction of ultrasonic disintegration techniques to intensify the stabilization of sludge. Since the 1990s, the author's research has focused on supporting the biochemical degradation of organic compounds in excess sewage sludge by ultrasonic disintegration.

2 Fundamentals of Ultrasonic Disintegration and its Evaluation

Despite various technological applications, processes of ultrasonic disintegration of sludge are still an area of intense research [25–27]. However, the effects of sludge disintegration in an ultrasonic field are not yet fully recognized due to complex, multiphase, polydisperse and biochemical composition of sludge, which has characteristics that differ between wastewater treatment plants and within the same installation.

Both main effects of disintegration of sludge in ultrasonic field—dispergation and lysis—are mainly attributed to ultrasonic cavitation, which is recognized as the primary cause of changes in ultrasonic treatment of sludge. This phenomenon is proportional to the value of the parameters of the ultrasonic field, such as frequency, power, energy versus time of sonication, location of transducer with batch and others which determine the acoustic field [28–34].

2.1 Ultrasonic Disintegration Conditions

The practical applications of ultrasounds for disintegration, homogenization, washing, welding and the like, focus on the determination of the actual size of an ultrasonic field. Usually, the quantity of electrical energy E_{UD} that enters a medium and characterizes the system of transducer–medium is given. It is very important,

for both researchers of the process and operators of wastewater treatment plants, to know the amount of energy needed to measure a required effect of disintegration. The energy consumed during disintegration (usually understood as electrical energy or heat) is described in relation to the volume of disintegrated sludge as volumetric energy E_V . Quantitatively, E_V corresponds to the density of ultrasonic energy with respect to the power of the generator P_G (kW), or the power consumed by a head during disintegration— P_{UD} (kW) in ultrasonic disintegrators.

$$E_V = E_{UD}V^{-1} = P_{UD}t_{UD}V^{-1}(\text{kWhm}^{-3}, \text{kJm}^{-3}, \text{kJL}^{-1}) \quad (1)$$

Specific energy E_S is another popular energy indicator in relation to the dry weight of disintegrated sludge TS (kg) [35, 36].

$$E_S = E_{UD}TS^{-1} = P_{UD}t_{UD}TS^{-1}(\text{kWh kgTS}^{-1}) \quad (2)$$

Mues [35], like other designers of disintegrators and operators of wastewater treatment plants, thinks that this indicator should not exceed the value of $E_S = 0.5 \text{ kWh kg TS}^{-1}$. The amount of consumed energy may also relate to a disintegration effect produced, e.g., increase in ΔSCOD_{UD} of the matter dissolved in sludge liquid after disintegration as the indicator of lysis energy— E_L ($\text{kWh kg } \Delta\text{SCOD}_{UD}^{-1}$) [2, 37]. Similarly, other indicators of energy consumption can be related to the amount of biogas benefit, loss of organic matter and the like, e.g., indicators of biodegradation energy suggested by Benabdallah et al. [38].

The benefits obtained during the digestion of sonicated sludge depend first of all on:

- Physical and chemical properties of excess sludge before sonication, such as: size and structure of the particles, concentration of dry substances, COD of sludge, SCOD of sludge liquid, concentration of volatile fatty acids (VFA) and others [2, 20, 39],
- Characteristics of ultrasounds, such as: frequency f (kHz) and intensity I (Wcm^{-2}) which for the most of investigated sludge were about 20 kHz and above 1 Wcm^{-2} , respectively,
- Construction of sonochemical reactor, such as kind of transducer his field A_E and the field of the reactor chamber perpendicular to the irradiation direction A_C , location of transducer/transducers inside reactor [33, 34, 40],
- Volumetric energy E_V (kWh m^{-3}) as well as specific energy E_S (kJ kg TS^{-1}); both are related to the time of sonication and E_S is connected with the concentration of total solids (TS). Researches in field of ultrasonic disintegration conducted by Kopp et al. (1997), Lehne and Muller (2002), Bougrier et al. (2005), Zhang et al. (2008) [36, 41–43] emphasize that qualitatively significant disintegration effects can be expected after a use specific energy of $E_S \geq 1000 \text{ kJ kg TS}^{-1}$ (i.e., $0,28 \text{ kWh kg TS}^{-1}$) and most disintegration research is carried out over a range of $E_S = 1000\text{--}100,000 \text{ kJ kg TS}^{-1}$.

Sewage sludge disintegration involves use of ultrasounds of low frequency and high power capable of inducing ultrasonic cavitation in the sludge liquid that might

result in a number of physical, chemical and biochemical processes mentioned above [41].

The author's own researches (Zielewicz-Madej 2003, Zielewicz 2007, Zielewicz 2010) [2, 6, 37] show that the basic design parameters of disintegrator should ensure:

- Frequency in a range of $f = 20\text{--}25$ kHz,
- Sonication time t_{UD} (corresponding to the hydraulic retention time in the disintegration chamber) providing appropriate energy density E_V for specific sludge ranging from 5 to 25 kWh m⁻³ in commercial installations.
- Thickness of a sonicated sludge layer should not exceed 5 cm in static conditions, without exchanging the sludge layer in the sonicated area, and 10 cm in dynamic conditions. It was found that the best disintegration results were obtained for a layer of 3 cm [2, 37].

2.2 Indicators of the Direct Effects of Ultrasonic Disintegration

Cavitation induced by acoustic wave passing through sludge causes a number of mechanical and sonochemical effects, called (by the author) direct effects of disintegration. They include destruction of structure of excess sewage sludge—flocks are fragmented and broken down (dispergation) and there is disruption of microorganism cells, releasing the cell matter to the sludge liquid (lysis). The maximum release of organic matter from the dead microorganism cells is achieved when the size of the particles resulting from disintegration is not larger than 100 μm [44, 45]. Dispersion and lysis alter a number of other physicochemical properties of sludge (not only the susceptibility to biochemical decomposition), e.g., sedimentation abilities and rheological properties, which may help assess disintegration effectiveness. The first well-known important effect of ultrasonic disintegration is defined as the dispersive effect. Zielewicz [2, 37] suggests that the fragmentation of flocks and sludge particles (sonodispergation) can be described by changes in susceptibility to dewatering of sludge which can be described based on the capillary suction time—CST (s) test [46, 47]. The changes of filterability has been expressed as the indicator defined by Zielewicz [2], indirectly being the sonodispergation indicator:

$$kd_{CST} = CST_{UD}CST_{ND}^{-1} \quad (3)$$

where:

kd_{CST} —indicator of dispergation, (—)

CST_{ND} —capillary suction time of unsonicated sludge, (s)

CST_{UD} —capillary suction time of sonicated sludge, (s)

The effect of mechanical dispergation of sludge is best shown by the changes in size of particles. A number of authors describe a method of quantifying the size of sludge particles with a laser particle size analyser [48–50]. Authors highlight the importance of determining the size of particles directly after disintegration and after 1 h, because of substances released by microorganism cells may affect the sludge

particles in a way similar to polyelectrolytes, causing re-flocculation, especially if the disintegration is accompanied by stirring. The phenomenon of re-flocculation was observed by Biggs and Lant [47], who found that the greater the cell lysis, the greater the susceptibility to re-flocculation. Effect of dispersion can be described by comparing the amount of very fine particles, e.g., changes in the percentage contribution of $d < 100 \mu\text{m}$ particles in a microscopic image, and also by researching SCOD_{cf} of supernatants after centrifugation and filtration through a filter with a specified pore size. Zielewicz [2, 37] suggests the indicator described by the equation:

$$kd_{\text{CODcf}} = \text{COD}_{\text{cfUD}} \text{COD}_{\text{cfND}}^{-1} \quad (4)$$

where:

kd_{CODcf} —sonodyspergation indicator, (–)

COD_{cfUD} —COD of supernatant of sonicated sludge, (s)

COD_{cfND} —COD of the supernatant of unsonicated sludge, (s)

“cf” denotes that the fluid was separated by centrifugation and filtration through a 3- μm quality filter (as opposed to the methodology for the determination of SCOD of dissolved matter).

Destruction of microorganism cell membranes and the release of cell matter into sludge liquid, i.e., cell sonolysis, are the most expected effects of ultrasonic disintegration of sludge and are the main effects of this process. Because of this, ultrasonic pretreatments were proposed as a strategy to accelerate the first, hydrolytic phase of digestion. Cell sonolysis effect can be observed as an increase in soluble chemical oxygen demand (SCOD). The most common indicator of this direct effect used thus far was defined by Müller [3] as disintegration degree. It is based on SCOD determination in sludge liquid after centrifugation of sludge at 20,000 rpm and filtration through a 0.4- μm cellulose acetate membrane [3, 13].

$$\text{DD}_{\text{COD}} = (\text{SCOD}_1 - \text{SCOD}_2) (\text{SCOD}_3 - \text{SCOD}_2)^{-1} 100 \quad (5)$$

where:

D_{COD} —disintegration degree (lysis/sonolysis indicator as well), (%)

SCOD_1 —COD of soluble substances in disintegrated sludge liquid, ($\text{mg O}_2 \text{L}^{-1}$)

SCOD_2 —COD of soluble substances in untreated sludge liquid, ($\text{mg O}_2 \text{L}^{-1}$)

SCOD_3 —COD of soluble substances in chemically disintegrated sludge liquid, ($\text{mg O}_2 \text{L}^{-1}$) in various preparations (a, b, c)

- using 1-mol NaOH solution, 1:1 ratio, at 90 °C, for 10 min or
- using 0.5-mol NaOH solution, 1:1 ratio, at 20 °C, for 22 h or
- using 0.5-mol NaOH solution, 1:1 ratio, at 20 °C, for 24 h.

Zielewicz [2] suggests using a simpler indicator (patterned after indicator of solubilisation by Baier and Schmidheiny (1997) [51], which compares soluble COD of disintegrated sludge liquid (SCOD_{UD}) to the SCOD of untreated sludge liquid (SCOD_{ND}):

$$kd_{(\text{COD})} = \text{SCOD}_{\text{UD}} \text{SCOD}_{\text{ND}}^{-1} \quad (6)$$

where:

$kd_{(\text{COD})}$ —indicator of sonolysis (–)

SCOD_{ND} and SCOD_{UD} values describe changes in the concentration of soluble substances in sludge liquid on account of sonolysis, ($\text{mg O}_2 \text{ L}^{-1}$).

The author's own research revealed that cell lysis (sonolysis) was the predominant direct effect of ultrasonic disintegration and was not always accompanied by the mechanical break-up of sludge particles. Instead, another effect strongly associated with sonolysis occurred, i.e., an increase in the concentration of volatile fatty acids (VFAs) directly after ultrasonic treatment. The absolute increase in VFAs was frequently accompanied by an increase in acidification, defined as a ratio between VFAs and SCOD of the matter dissolved in sludge liquid ($\eta_A = \text{VFAs}/\text{SCOD}$). This indicates that the higher concentration of organic matter before ultrasonic treatment, expressed as SCOD, was converted into simple organic matter as a result of ultrasonic treatment, which is the product of phase II or phase III of digestion. This effect, named sonoacidification by Zielewicz [2, 37], was separate from the effect of the cell sonolysis, and the conditions for its best results were determined.

$$kd_{\text{VFAs}} = \text{VFA}_{\text{UD}} \text{VFA}_{\text{ND}}^{-1} \quad (7)$$

where:

kd_{VFAs} —indicator of sonoacidification determined by the author, (–)

VFA_{UD} and VFA_{ND} —describe a change in the concentration of VFAs in sludge liquid on account of sonoacidification ($\text{mg CH}_3\text{COOH L}^{-1}$).

There are a number of other values whose changes after disintegration can be used to assess the direct effect of disintegration (as indicators), e.g., concentrations of biogenic matter, nitrogen and phosphorus in supernatants. Liquids, returned to the technological cycle in a wastewater treatment plant, may affect the quality of sewage and effects of its treatment. Instead of commonly used SCOD liquefaction of sludge, investigations into the liquefaction of only organic matter present in the sludge (V_S) were conducted and are described by the following equation (Eq. 15) [44] are suggested:

$$X_{\text{VS}} = 100(V_S - V_{\text{S0}}) V_{\text{S0}}^{-1} \quad (8)$$

where:

X_{VS} —indicator expressing the degree of organic matter solubilisation, (%)

V_S —concentration of organic matter dissolved in disintegrated sludge, (mg L^{-1})

V_{S0} —concentration of organic matter dissolved in non-disintegrated sludge, (mg L^{-1})

The effect of protein increases in the sludge liquid as a degree of protein liquefaction during disintegration— DD_P can be expressed by the equation [52]:

$$\text{DD}_P = (\text{P}_{\text{sup}} - \text{P}_{\text{sup}_0}) \text{P}_{\text{total}}^{-1} \quad (9)$$

where:

DD_P —degree of disintegration based on protein measurements, (–)

P_{total} —proteins in an uncentrifuged sample, (mg L^{-1})

P_{sup_0} —proteins in the leachate of a non-disintegrated sample, (mg L^{-1})

P_{sup} —proteins in the leachate of a disintegrated sample, (mg L^{-1})

The degree of microorganism disintegration can also be assessed on the basis of the velocity of oxygen uptake [49]:

$$A_s = (1 - OV / OV_0)100 \quad (10)$$

where:

A_s —degree of aerobic bacteria destruction, (%)

OV —rate velocity of oxygen intake for the sludge after disintegration, ($\text{mg L}^{-1} \text{min}^{-1}$)

OV_0 —velocity of oxygen intake for the sludge prior to disintegration, ($\text{mg L}^{-1} \text{min}^{-1}$)

The indicators used to describe the direct effects of ultrasonic disintegration herein are presented in Sect. 3.

3 Methods

The main focus of this study was to determine the susceptibility of sludge collected from various wastewater treatment plants to ultrasonic disintegration, using disintegrators of different construction.

3.1 Materials

The research was conducted on waste-activated sludge (excess sludge) collected at nine Polish municipal wastewater treatment plants of $RLM > 50,000$. The sewage treatment lines in those plants contained activated sludge tanks that exploited the technologies of integrated removal of BOD_5 , N and P. The samples of waste activated sludge collected after mechanical thickening enhanced by flocculation were stored at 4°C during analysis. Apart from the concentration of total solids (TS), organic matter (VS) and total COD_0 of sludge (determined according to standard methods [53]), the examination of the samples prior to disintegration also covered all other parameters whose changes are monitored during disintegration processes, such as the concentration of dissolved (SCOD, VFAs, P, N) or dispersed matter (COD_{cf}) in supernatants and filterability measured by the capillary suction time test (CST), according to the methods used by Baskerville and Galle methodology, based on the measurements of transition of frontal boundary layer of the filtrate as a result of the effect of suction forces in the used paper (Whatman 17) [47]. The physical and chemical characteristics of excess sludge and its supernatants prior to disintegration are given in Table 1 (in order of increasing total solids).

Table 1 Physicochemical characteristics of excess sludge and its supernatants before ultrasonic disintegration

Sludge	Characteristics of sludge							Characteristics of supernatants					
	TS mgL ⁻¹	Co %	VS mgL ⁻¹	VS/TS %	pH	CST _{ND} s	ChZTo mgO ₂ L ⁻¹	SCOD _{ND} mgO ₂ L ⁻¹	SCOD _{cf,ND} mgO ₂ L ⁻¹	VFA _{ND} mgL ⁻¹ CH ₃ COOH	N _{ND} mg L ⁻¹	TOC _{ND} mgO ₂ L ⁻¹	
SLG1	20.4	2.0	14.2	69.8	7.2	5.3	54200	40	501	18.6	69.7	12	
SLG2	37.2	3.7	27.9	75.0	7.0	20.1	98710	54	323	27.7	17.7	18	
SLG3	40.0	4.0	31.3	78.2	6.6	74.1	70120	107	138	24.6	92.5	47	
SLG4	40.6	4.1	31.2	76.8	6.6	9.5	60160	42	465	11.5	8.4	10	
SLG5	41.1	4.1	30.4	73.9	6.8	7.8	36520	62	86	19.8	24.2	192	
SLG6	41.8	4.2	29.0	69.4	6.9	20.7	101900	53	81	11.6	8.34	110	
SLG7	56.6	5.7	43.1	76.2	6.8	23.6	59060	51	66	15.4	14.4	60	
SLG8	62.1	6.2	45.8	73.8	6.6	74.9	88830	166	219	24.6	74.0	101	
SLG9	66.6	6.7	41.4	62.2	6.8	65.3	91400	111	147	19.1	27.9	89	

3.2 Characteristics of Ultrasonic Disintegrators Used in the Research

The ultrasonic disintegration of excess sludge was carried out, using three sonochemical reactors (DEZ1, DEZ2 and DEZ3) of different design and technical operating parameters. Their characteristics are given in Table 2 and Fig. 2. The WK-2010 ultrasonic reactor with novel piezoelectric transducer (mosaic head) was called DEZ3. It works on the operating parameters as frequency of 20–30 kHz and power of 100–1500 W. The generator and conical transducer of big radiating surface area were developed in the Scientific and Teaching Centre of the Silesian University of Technology and manufactured by Semiinstruments for the grant N N523 756440 awarded by the Polish Ministry of Science and Higher Education [54]. The DEZ3 generator was equipped with a “TFT touch panel,” which enabled tasks and results to be set, checked and displayed, and a “LED panel,” which displayed the current mode of operation. The device was also fitted with an RS-232 connector and software, allowing for the device to be operated with a PC. The software offered adjustments of the device’s parameters and operation with respect to the type of sonicated medium. The workstation equipment allowed setting up the frequency of irradiation f_{UD} , corresponding power P_{UD} , as well as monitoring and registration data of process. Prior to and after disintegration, the sludge was tested to compare the changes in its properties (parameters listed in Table 1). The parameters were used to calculate direct disintegration effects, such as: kd_{CST} , $kd_{COD_{def}}$, kd_{SCOD} , kd_{VFA} and DD_{COD} , following the definitions and equations given in Sect. 2.2.

The stand for the disintegration heads allows change of location in the sonication chamber, depending on specified process parameters. In this research, the location of the emitter at the bottom of the tank and the thickness of sludge layers were constant: $h_E = 3$ cm and $h_O = 6$ cm, respectively (Fig. 2). This location was determined in previous researches [2, 6, 16]. Disintegration effectiveness was compared to results in horn type reactor DEZ2 (WK-2000), as well as in Washer (DEZ1) with a flat emitter at the bottom, produced by InterSonic (Poland).

Sonication was carried out in static conditions, using times of irradiation t_{UD} , relative to volumetric energy $Ev = 100$ kWh m^{-3} . This value of volumetric energy is five times higher than the one usually applied on industrial scale, but was used in the author’s research as the boundary value determining the susceptibility of sludge to ultrasound disintegration. The tests were carried out on excess sludge samples, mechanically thickened with polyelectrolytes to various concentrations of dry solids, which meant different consumption of specific energy E_S [kWh $kg\ TS^{-1}$] (presented in Table 3) due to the different concentrations of dry solids.

4 Results and Discussion

The main purpose of this study was to show that the direct effects caused by the ultrasonic cavitation depend on two main agents: physicochemical parameters of the medium subjected to ultrasonic treatment as well as the construction of sonochemical reactor (disintegrator) and the parameters of sonication.

Table 2 Construction and technological parameters of the process of ultrasonic disintegration

Symbol description	Power (P_G) W	Power (P_{UD}) W	Freq. (f) kHz	Time (t_{UD}) s	d_E mm	d_{CH} mm	$A_{CH}A_E^{-1}$ -	V_{CH} L	$V_{CH}A_E^{-1}$ -	Intensity with respect to emitter area $I_{UD(E)}$ $W\ cm^{-2}$	Intensity with respect to chamber area $I_{UD(CH)}$ $W\ cm^{-2}$	Power density U_{UD} $W\ L^{-1}$
DEZ1 Washer with one flat emitter on the bottom	90	98	25	1800	50	150×138	6.2	0.72	36.7	5.0	0.5	136
DEZ2 WK-2000 sandwich head with horn	400	270	23	270	20	80	16.9	0.30	95.5	86.0	5.4	900
DEZ3 WK-2010 mosaic head with short emitter	950	660	21	270	120	220	3.5	0.75	6.6	5.8	1.7	880

Construction of disintegrator		
Acronym Name description	Schema	Foto
<p>DEZ1 Washer with flat emitter on the bottom</p>		
<p>DEZ2 WK-2000 sandwich head with thin sonotrode (horn)</p>		
<p>DEZ3 WK-2010 mosaic head with short flat emitter</p>		

Fig. 2 Schematics and photographs disintegrators

Table 3 Juxtaposition of specific energy E_S and TS

Sludge (acronym)		SLG1	SLG2	SLG3	SLG4	SLG5	SLG6	SLG7	SLG8	SLG9
TS	g L^{-1}	20.4	37.2	40.0	40.6	41.1	41.8	56.5	62.1	66.6
Specific Energy E_S	$\frac{\text{kWh}}{\text{kgTS}^{-1}}$	5.0	2.7	2.5	2.5	2.5	2.4	1.8	1.6	1.5

Under technical conditions in a WWTPs, using a commercial disintegrator of a specific construction and ultrasonic operating parameters, special attention should be drawn to that physicochemical properties of excess sludge, which determine their susceptibility to ultrasonic disintegration. In this study, usage of very high energy $E_V = 100 \text{ kWh/m}^3$ output (the level not acceptable in technical applications) was very helpful to demonstrate that some sewage sludge, e.g., SLG1, is susceptible to this kind of disintegration, but some, e.g., SLG4, is not. The susceptibility of sludge was determined on a basis of three groups of direct effects of ultrasonic disintegration, i.e., sonodispersion, sonolysis and sonoacidification, and some well known indicators describing these effects as disintegration degree DD_{COD} , which were defined in Sect. 2.2.

A comparison of direct effects after the disintegration of nine investigated sludges in the DEZ3 (its best efficiency will be demonstrated in further discussion) is presented in Table 4, and Figs. 3 and 4. The susceptibility of the nine different types of sludge to ultrasonic disintegration appeared to be extremely diversified. SLG1 showed the highest susceptibility in every aspect, as mentioned earlier. Determining which sludge showed the lowest susceptibility was not that obvious after examining all the indicators. Indicators of sonodispersion kd_{CST} and $kd_{\text{COD}_{\text{ef}}}$ pointed out that SLG9 was less susceptible to dispersion in an ultrasonic field (Fig. 3). On the other hand, a comparison of indicators of sonolysis kd_{SCOD} and DD_{UD} indicates the weakest lysis in sediments SGL4 and SGL8. A similar susceptibility to lysis, but slightly lower than for SLG1, was demonstrated by SLG2, SLG5 and SLG6 (Fig. 4); however, the indicators mentioned above did not correlate with increase in TOC_{UD} and N_{UD} . This research revealed release of volatile fatty acids (VFAs) during sonolysis and confirmed previous findings by the author [2]. Like sonolysis, the highest sonoacidification was typical of SLG1, while the lowest of SLG8 and SLG4 (Fig. 4). This study shows typical parameters of sludge that influenced the differences in susceptibility, but were neither the concentration of organic matter in dry solids (VS/TS), SCOD_{ND} nor other parameters of supernatants of non-disintegrated sludge. However, considerably better effects were observed for the lower values of TS, COD_0 and COD_{NaOH} , when considerably less satisfying outcome was observed for high values of these parameters. This indicates that the direct effects of ultrasonic disintegration were inferior at very high concentrations of dry mass (SLG8 and SLG9), as was already observed in the author's previous studies [2, 37, 55–58]. More commending ramifications of ultrasonic disintegration at low TS concentrations resulted from the corresponding high values of E_S , but also the physical properties of the medium—lower TS indicates lower wave damping

Table 4 The comparison of the effects of ultrasonic disintegration of various sludge in DEZ3 disintegrator

Sludge TS (%)	Susceptibility to chemical lysis for DD _{UD} determination				Spec. ener. E _S				Sonodispersion				Sonolysis						
	SCOD _{N₂O₄H}		kd _{N₂O₄H}		CST _{UD}	kd _{CST}	COD _{UD}	kd _{COD}	CST _{UD}	kd _{CST}	COD _{UD}	kd _{COD}	SCOD _{UD}	kd _{SCOD}	DD _{UD}	N _{UD}	kd _{Neg}	TOC _{UD}	kd _{TOC}
	mgO ₂ L ⁻¹	%	mgO ₂ L ⁻¹	%															
SLG1	6412	11.83	5.0	526	99.9	2380	56.3	1147	28.6	11.4	197	2.8	664	55.8					
C ₀ = 2.0																			
SLG2	6380	6.46	2.7	30	1.5	2181	17.9	1090	20.1	7.15	140	7.9	35	2.0					
C ₀ = 3.7																			
SLG3	9514	13.57	2.5	70	1.0	458	3.3	298	3.1	2.5	60.0	0.7	550	1.2					
C ₀ = 4.0																			
SLG4	9418	15.65	2.5	12	1.2	551	7.6	47.5	1.1	0.6	9.5	1.13	34	3.2					
C ₀ = 4.1																			
SLG5	7700	21.08	2.5	344	43.9	1898	22.9	1046	13.6	17.4	128	5.3	437	2.3					
C ₀ = 4.1																			
SLG6	15,820	15.52	2.4	22	1.1	1212	16.5	1190	22.5	18.0	316	37.9	100	0.9					
C ₀ = 4.2																			
SLG7	6373	10.79	1.8	36.8	1.6	1007	13.5	577	9.1	27.9	51.7	3.6	36	1.4					
C ₀ = 5.7																			
SLG8	14,660	16.50	1.6	174	2.3	717	3.5	432	2.6	1.7	39.4	0.5	261	2.6					
C ₀ = 6.2																			
SLG9	9850	10.78	1.5	41	0.6	448	3.2	438	3.9	5.2	44.3	1.6	199	2.2					
C ₀ = 6.7																			

Table 4 continued

Sludge TS (%)	Sonoacidification				
	VFA _{SUD} mgL ⁻¹ CH ₃ COOH	kdVFA _S	K _{AC(UD)} = VFA _{UD} /SCOD _{UD} %	pH _{UD}	-ΔpH
SLG1	136.0	7.3	7.2	6.77	0.43
C ₀ = 2.0					
SLG2	42.0	1.5	7.0	6.83	0.17
C ₀ = 3.7					
SLG3	53.9	2.2	6.6	6.52	0.08
C ₀ = 4.0					
SLG4	16.5	1.4	6.6	6.59	0.01
C ₀ = 4.1					
SLG5	66.5	3.4	6.8	6.48	0.32
C ₀ = 4.1					
SLG6	249.0	2.2	6.9	6.74	0.16
C ₀ = 4.2					
SLG7	50.4	3.3	6.8	6.67	0.13
C ₀ = 5.7					
SLG8	25.8	1.0	6.6	6.69	0
C ₀ = 6.2					
SLG9	33.5	1.8	6.8	6.84	0
C ₀ = 6.7					

The best results, acceptable results are in bold

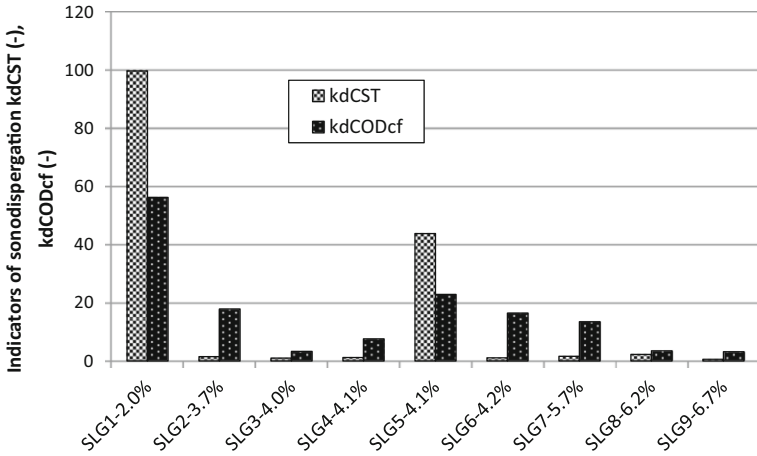


Fig. 3 Susceptibility of various sludge to sonodispersion

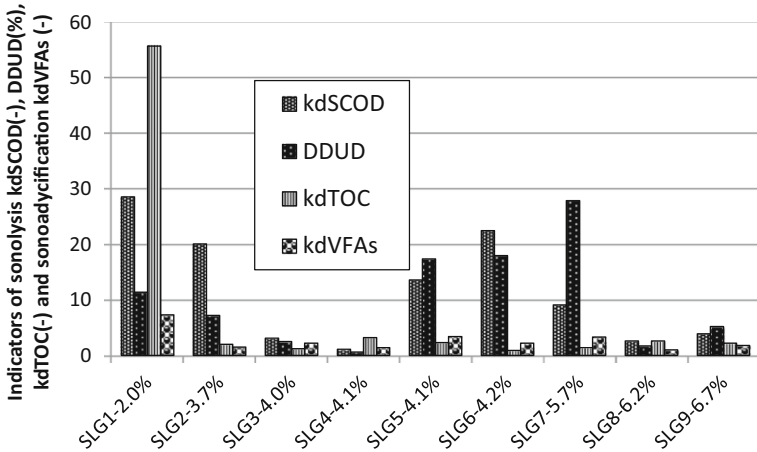


Fig. 4 Susceptibility of various sludge to sonolysis and sonoacidification

and higher hydration favours cavitation. Nevertheless, as shown by the previous author’s own research [37], very low concentrations of TS < 1 % indicate a smaller amount of released matter in the form of SCOD, and hence a decrease in lysis effects. These studies confirm earlier observations that the most beneficial lysis occurs for hydration at about 98–96 % [2, 37].

A second object of observation was the impact of sonochemical reactor design on the effectiveness of disintegration of the sludge. Therefore, four sludge with various physicochemical properties were chosen to show the impact of three-reactor design on all direct effects of disintegration. The study compared the effects obtained for SLG1 of the lowest concentration $C_0 = 2\%$ (at the same time the most susceptible to an ultrasonic field), and, in turn, the sludge with the average and highest

concentrations of dry solids which corresponded to the decreasing values of specific energy E_S (Table 5).

Analysing the results of disintegration, with the same energy consumption of $E_V = 100$ kWh/m³, proved that higher efficiency of sonodispersion was obtained in the DEZ3 (WK-2010) and the less satisfying effects were obtained in DEZ1 (washer), which can be seen in Fig. 5. It means that disagglomeration of flocs (sonodispersion) was more effective when power density was high, regardless of the type of disintegrator, e.g., for common horn reactor DEZ2 ($U_{UD} = 900$ WL⁻¹) and new type reactor DEZ3 ($U_{UD} = 880$ WL⁻¹). These are also suitably high values of intensity (with respect to chamber area) $I_{UD(CH)} \approx 5.4$ Wcm⁻² for DEZ2 and $I_{UD(CH)} = 1.7$ Wcm⁻² for DEZ3.

Sonolysis and sonoacidification appeared to be the best in DEZ3 and the worst in DEZ2, i.e., in horn reactor (Fig. 5). It was found that these effects of disintegration strongly depended on the design of a disintegrator mainly with respect to the emitters area A_E and the area of the reactor's chamber A_{CH} , as well as the volume of the chamber (Table 2). These parameters determined the intensity $I_{UD(E)}$, $I_{UD(CH)}$ (Wcm⁻²) and power density U_{UD} (WL⁻¹). As shown in Table 5, the best effects of sonolysis were obtained in a reactor with transducer of the biggest radiating surface area as well as the lowest ratio between this area and the area of reactor. The degree of lysis is dependent on the cavitation activity, which in the multiphase medium as sludge can be found out by measuring the change in SCOD and other substances such as VFAs, N, and P dissolved in supernatants. It has been shown in researches conducted by other authors and described by Sutkar and Gogate [33] that the cavitation activity is maximum very near to the transducer, so this could be explained best effect of sonolysis and sonoacidification for the largest emitters' surface area (Figs. 6, 7).

The best effects of sonochemical phenomena were obtained in DEZ3 and the worst in DEZ2, which may also indicate that the effects presented above are dependent upon the temperature increase during sonication and the achieved final temperature (Table 5). Cavitation, when it occurs in a reactor, generates conditions of very high temperatures and pressures (500–15000 K of temperature and 100–50000 atmospheres of pressure) locally [33], which by dissipation increases the temperature in the sonicated medium. During sonication with a Washer (DEZ1), of a relatively low power, the temperature of the sludge increased slowly with increase of irradiation time t_{UD} . The long sonication – 1800 s, was necessary for achieving the same, as in other reactors, constant density of energy E_V . Comparable and even slightly higher increase in temperature was obtained during a short sonication, using a high-power head (DEZ3). This means that for sonochemical reactor DEZ3, more cavitation activity was obtained. The two disintegrators had a common feature, i.e., low values of the chamber field/emitter field ratio: $A_{CH}/A_E = 6.2$ for DEZ1 and $A_{CH}/A_E = 3.5$ for DEZ3 (while the ratio A_{CH}/A_E for DEZ2 equaled 16.9), and it played an important role in achieving higher temperatures [57] and therefore more efficient lysis of microorganism cells.

Table 5 Comparison of the direct effects of ultrasonic disintegration in various disintegrators: DEZ1, DEZ2 and DEZ3

Symbol of reactor Acro	Acronym of sludge (%)	Spe. Ener E_s kWh kg ⁻¹	T_{UDmin} (ΔT_{UD}) °C	Sonodispersion			kd _{corp} cf —
				CST _{UD} s	kd _{CST} —	SCOD _{UD} cf mgO ₂ L ⁻¹	
DEZ1	SLG1	5.0	38.2 (19.8)	142	26.9	1071	25.3
	C ₀ = 2.0						
	SLG5	2.5	19.0 (8.6)	19	2.4	849	10.2
	C ₀ = 4.1						
	SLG7	1.8	31.0 (16.0)	15	0.6	120	1.6
	C ₀ = 5.7						
	SLG8	1.6	22.2 (7.2)	188	2.5	464	2.2
	C ₀ = 6.2						
DEZ2	SLG1	5.0	27.7 (9.3)	386	73.2	1106	26.2
	C ₀ = 2.0						
	SLG5	2.5	21.4 (9.8)	486	61.9	1113	13.4
	C ₀ = 4.1						
	SLG7	1.8	28.0 (13.0)	18	0.8	360	4.8
	C ₀ = 5.7						
	SLG8	1.6	19.0 (4.0)	171	2.3	378	1.8
	C ₀ = 6.2						
DEZ3	SLG1	5.0	43.0 (24.6)	526	99.9	2380	56.3
	C ₀ = 2.0						
	SLG5	2.5	27.5 (5.9)	344	43.9	1898	22.9
	C ₀ = 4.1						
	SLG7	1.8	35.0 (20.0)	37	1.6	1007	13.5
	C ₀ = 5.7						
	SLG8	1.6	26.6 (11.6)	174	2.3	717	3.5
	C ₀ = 6.2						

Table 5 continued

Symbol of reactor	Acro	Sonolysis					Sonoacidification						
		Acronym of sludge (%)	SCOD _{UD} mgO ₂ L ⁻¹	kd _{COB}	DD _{UD} %	N _{UD} mg L ⁻¹	kd _{SOG} %	TOC _{UD} mgO ₂ L ⁻¹	kd _{ROC} %	VFA _{SUD} mgL ⁻¹ CH ₃ COOH	kd _{VFAS}	pH _{UD}	ΔpH
DEZ1	SLG1		559	13.9	8.1	54.4	0.8	157	13.2	53.0	2.9	6.69	0.53
	C ₀ = 2.0												
	SLG5		561	9.1	18.7	61.8	2.6	341	1.8	62.0	3.1	6.67	0.12
	C ₀ = 4.1												
	SLG7		212	4.1	0.96	21.2	1.5	31.2	1.2	32.1	2.1	6.68	0.14
	C ₀ = 5.7												
	SLG8		287	1.7	0.83	60.0	0.8	156	1.5	42.6	1.7	6.65	0.0
	C ₀ = 6.2												
DEZ2	SLG1		444	11.1	6.3	69.9	1.0	138	11.6	51.4	2.2	6.69	0.53
	C ₀ = 2.0												
	SLG5		686	11.1	8.2	55.9	2.3	329	1.7	64.3	3.2	6.48	0.31
	C ₀ = 4.1												
	SLG7		272	5.3	3.5	34.5	2.4	40.3	1.5	21.4	1.4	6.66	0.16
	C ₀ = 5.7												
	SLG8		266	1.6	0.7	54.3	0.7	127	1.3	43.5	1.8	6.69	0.0
	C ₀ = 6.2												
DEZ3	SLG1		1147	28.6	11.4	197	2.8	664	55.8	136.0	7.3	6.77	0.43
	C ₀ = 2.0												
	SLG5		1046	13.6	17.4	128	5.3	437	2.3	66.5	3.4	6.48	0.32
	C ₀ = 4.1												
	SLG7		577	9.1	27.9	51.7	3.6	35.6	1.4	50.4	3.3	6.67	0.13
C ₀ = 5.7													

Table 5 continued

Symbol of reactor	Acro	Sonolysis					Sonoacidification					
		SCOD _{UD} mgO ₂ L ⁻¹	kd _{COB}	DD _{UD} %	N _{UD} mg L ⁻¹	kd _{S^{NOG}} %	TOC _{UD} mgO ₂ L ⁻¹	kd _{TOC} %	VFA _{SUD} mgL ⁻¹ CH ₃ COOH	kd _{VFA_S}	pH _{UD}	ΔpH
	SLG8	432	2.6	1.7	39.4	0.5	261	2.6	25.8	1.0	6.69	0.0

*C*₀ = 6.2

The best results, acceptable results are in bold

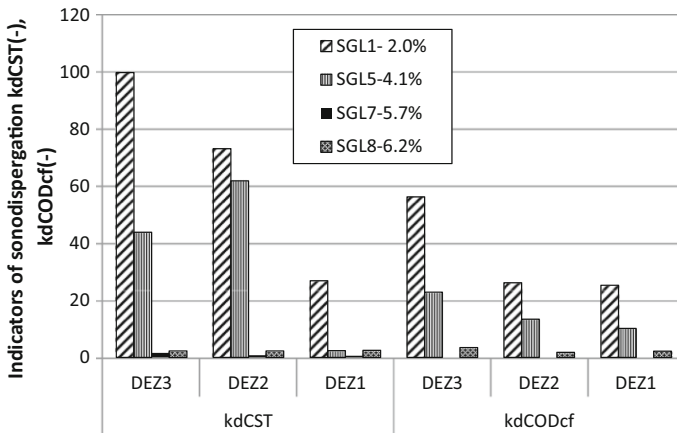


Fig. 5 The impact of the type of disintegrator on the effect of sonodispersion

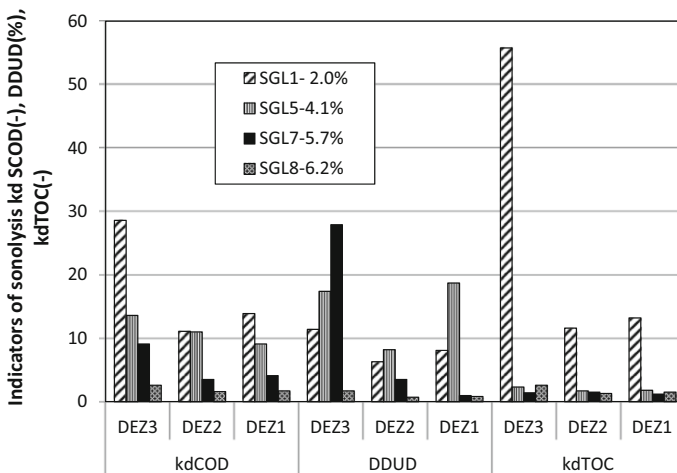


Fig. 6 The impact of the type of disintegrator on the effect of sonolysis

5 Conclusions

The susceptibility of excess sludge collected at various wastewater treatment plants to ultrasonic disintegration may vary, and therefore the decision to employ that particular method in a given plant must be preceded by tests and sampling carried out by scientific research institute offering appropriate equipment.

Ultrasonic disintegration is a “clean” process that does not require any other energy sources apart from electrical energy, but it is very sensitive to the changes in the physicochemical characteristics of sludge, because its effect depends on the occurrence of cavitation in a liquid medium. Then, it should not be considered if operator of wastewater treatment plant considers thickening excess sludge

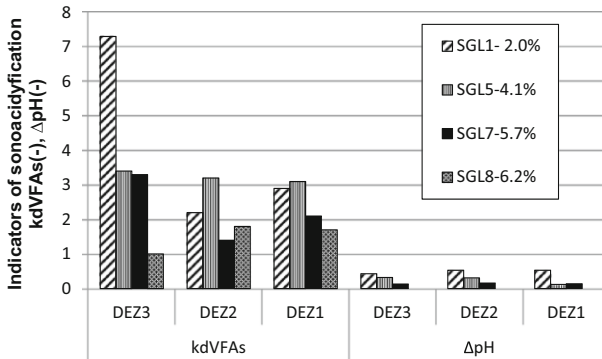


Fig. 7 The impact of the type of disintegrator on the effect of sonoacidification

substantially by employing flocculation with cation-active polyelectrolytes, which results in generating large, compact flocks causing damping of ultrasonic wave. In such media, ultrasonic energy is “wasted” on disagglomeration of flocks that should be treated mechanically [7]. Ultrasonic energy should be utilized to achieve the most desirable effects, i.e., sonolysis and sonoacidification, which initiate biochemical hydrolysis—the first limiting stage of digestion. Apart from sludge susceptibility to ultrasonic disintegration, it is important to match operating parameters to the characteristics of sludge. The best direct effects of sewage sludge disintegration were usually achieved at low frequencies of 20–25 kHz; however, there is a suitable resonance frequency for each generator–transducer–sludge combination, which improves disintegration efficiency. The best matching combination was used in the DEZ3 disintegrator. Adjustment of the sonochemical reactors’ operating parameters to properties of medium (thanks to the equipment used) improved the effects of sludge disintegration, compared to the effects for the other disintegrators, which is clearly seen for SLG1 sludge, the most susceptible to disintegration, notably to sonolysis.

The interest in disintegration expressed by operators of WWTPs may bring this process as a standard element of the technological line of sludge treatment and will improve efficiency. This will depend on investors’ approach to disintegration and their understanding of the importance of conscious selection of installations and operating parameters (not only ultrasonic ones) in terms of the physicochemical properties of sludge.

Acknowledgments Scientific work presented in the paper was funded by Grant NN523 756440 resource sponsored by the State Committee for Scientific Research (KBN) Poland in the years 2011–2014.

References

1. Eastman J, Ferguson J (1981) Solubilization of particulate organic carbon during the acid phase of anaerobic digestion. *J WPCF* 5(3):352–366
2. Zielewicz E (2010) Indicators on ultrasonic disintegration of sewage sludge. *Pol J Environ Stud* 2:268–272

3. Müller J (1996) Mechanischer Klärschlamm-aufschluss. Dissertation TU Braunschweig. Shaker-Verlag, Aachen
4. Hogan F, Mormede S, Clark P, Crane (2004) Enhanced anaerobic digestion using ultrasound. In: Proceedings of the 10th World Congress on Anaerobic Digestion. National Research Council Canada, Montreal, pp 136–141
5. Onyeche TI, Schläfer C, Bormann H, Schröder C, Sievers M (2002) Ultrasonic cell disruption of stabilized sludge with subsequent anaerobic digestion. *Ultrasonics* 40:31–35
6. Zielewicz-Madej E (2003) The influence of parameters of ultrasonic disintegration on the intensification of anaerobic biodegradation of organic compounds from sewage sludge. *Environ Prot Eng* 6(3–4):455–468
7. Zielewicz E, Sorys P, Janik M, Fukas-Płonka Ł (2008) The hybrid disintegration as a method of improving the effects of sludge stabilization. *Environ Prot Eng* 11(3):397–409 (in Polish)
8. Bougrier C, Albasi C, Delgenes JP, Carrere H (2006) Effect of ultrasonic, thermal and ozone pre-treatments on waste activated sludge solubilisation and anaerobic biodegradability. *Chem Eng Process* 45:711–718
9. Yuan HY, Chen YG, Zhang HX, Zhou Q, Gu GW (2006) Improved bioproduction of short-chain fatty acids (SCFAs) from excess sludge under alkaline conditions. *Environ Sci Technol* 40(6):2025–2029
10. Müller J, Lehne G, Schwedes J, Battenberg S, Näveke R, Kopp J, Dichtl N (1998) Disintegration of sewage sludge and influence on anaerobic digestion. *Water Sci Technol* 38(8–9):425–433
11. Müller J et al (2000) Verfahren und Anwendungsgebiete der mechanischen Klärschlamm-disintegration. *Korrespondenz Abwasser* 47(4):570–576
12. Müller J, Thiem A, Eder B, Günther F, Hruschka H, Kopp J, Kunz P, Otte-Witte R, Schmelz K, Seiler K (2001) Verfahrensvergleich und Ergebnisse der mechanischen Klärschlamm-disintegration. *Korrespondenz Abwasser* 48(3):393–400
13. Tiehm A, Nickel K, Zellhorn M, Neis U (2001) Ultrasonic waste activated sludge disintegration for improving anaerobic stabilization. *Water Res* 35:2003–2009
14. Nickel K, Neis U (2007) Ultrasonic disintegration of biosolids for improved biodegradation. *Ultrason Sonochem* 14:450–455
15. Eder B, Günther F (2002) Practical experience of sewage sludge disintegration by ultrasound. *TU Hamburg-Harbg Rep Sanit Eng* 35:173–188
16. Zielewicz E, Sorys P (2007) Comparison of ultrasonic disintegration in laboratory and technical scale disintegrators. *Eur Phys J Spec Top* 154(1):289–294 (Springer, Berlin/Heidelberg)
17. Zhang PY, Zhang GM, Wang W (2007) Ultrasonic treatment of biological sludge: floc disintegration. Cell lysis and inactivation. *Bioresour Technol* 98(1):207–210
18. Mason T (2003) Sonochemistry and sonoprocessing: the link, the trends and (probably) the future. *Ultrason Sonochem* 10:175–179
19. Mason T, Tiehm A (2001) Ultrasound in environmental protection. *Advances in sonochemistry*, vol 6. Elsevier, Amsterdam
20. Gogate PR, Kabadi AM (2009) A review of applications of cavitation in biochemical engineering/biotechnology. *Biochem Eng J* 44:60–72
21. Blume T, Neis U (2004) Improved wastewater disinfection by ultrasonic pre-treatment. *Ultrason Sonochem* 11:333–336
22. Kowalska E, Bieñ J, Zielewicz E (1978) The influence of ultrasound on the thickening of the sludge from municipal and industrial wastes. *Acustica* 40(2):99–103
23. Kowalska E, Bieñ J, Zielewicz E (1980) The effects of the thickening of various sewage deposits subjected to the influence of ultrasonic field. Pergamon Press, Oxford, pp 205–210
24. Kowalska E, Bieñ J, Zielewicz-Madej E (1988) Ultrasound in the suspension separation methods. *Dry Technol Int J Spec Issue Comb Field Separation Tech Dewatering, Batteele Columb Div* 6(3):447–471
25. Pilli Sridhar, Bhunia Puspendu, Song Yan, LeBlanc RJ, Tyagi RD, Surampalli RY (2011) Ultrasonic pretreatment of sludge: a review. *Ultrason Sonochem* 18:1–18
26. Tuan Le Ngoc, Ratsimba B, Julcour-Lebigue C, Delmas H (2012) Effect of external pressure on the efficacy of ultrasonic pretreatment of sludge. *Int Proc Chem Biol Environ Eng* 42:86–94
27. Tuan Le Ngoc, Chau Pham Ngoc (2013) Evaluation approaches of sludge ultrasonic pretreatment efficiency: a review. *Sci Technol Dev* 16(1):68–83
28. Miller M, Miller D, Brayman A (1996) A review in bioeffects of inertial ultrasonic cavitation from a mechanistic perspective. *Ultrasound Med Biol* 22(9):1131–1154

29. Zielewicz-Madej E, Sorys P (2006) Occurrence of ultrasonic cavitation in sewage sludge. *Eur Phys J. Journal de Physique IV, Proc EDP Sci* 137:227–230
30. Yan Y, Feng L, Zhang C, Zhu H, Zhou Q (2010) Effect of ultrasonic specific energy on waste activated sludge solubilization and enzyme activity. *Afr J Biotechnol* 9(12):1776–1782
31. Chu C, Lee D, Chang B, You C, Tay J (2002) “Weak” ultrasonic pre-treatment on anaerobic digestion of flocculated activated biosolids. *Water Res* 36:2681–2688
32. Śliwiński A (2001) Ultrasound and their applications WNT Warszawa 15-108/347-372 (in Polish)
33. Sutkar VS, Gogate PR (2009) Design aspects of sonochemical reactors: techniques for understanding cavitation activity distribution and effect of operating parameters. *Chem Eng J* 155(1–2):26–36
34. Gogate PR, Sutkar VS, Pandit AB (2011) Sonochemical reactors: important design and scale up considerations with a special emphasis on heterogeneous system. *Chem Eng J* 166(3):1066–1082
35. Mues A (1998) Verfahrenstechnik und Kosten des Ultraschalleinsatzes auf Kläranlagen. Klärschlammdeintegration, TU Braunschweig H 61:271–280
36. Zhang G, Zhang P, Yang J, Liu H (2008) Energy-efficient sludge sonication: power and sludge characteristics. *Bioresour Technol* 99:9029–9031
37. Zielewicz E (2007) Ultrasonic disintegration of excess sludge for receiving of VFA. Monography Silesian University of Technology, Gliwice (in Polish)
38. Beanabdalach EL-Hadji T, Dosta J, Marquez-Serrano R, Mata-Alvarez J (2007) Effect of ultrasound pretreatment in mesophilic and thermophilic anaerobic digestion with emphasis on naphthalene and pyrene removal. *Water Res* 41:87–94
39. Gronroos A, Kyllonen H, Korpijarvi K, Pirkonen P, Paavola T, Jokela J, Rintala J (2005) Ultrasound assisted method to increase soluble chemical oxygen demand (SCOD) of sewage sludge for digestion. *Ultrason Sonochem* 12:115–120
40. Zielewicz-Madej E (2003) The influence of parameters of ultrasonic disintegration on the intensification of anaerobic biodegradation of organic compounds from sewage sludge. *Environ Prot Eng* 6(3–4):455–468
41. Lehne G, Muller J (2002) The influence of the energy consumption on the sewage sludge disintegration, *Ultrasound in Environmental Engineering. Rep Sanit Eng* 35:205–215
42. Kopp J, Dichtl W, Müller J, Schwedes J (1997) Anaerobic digestion and dewatering characteristics of mechanical disintegrated excess sludge. *Int Konf Sludge Manag Wastewater Sludge-Waste Res* 2:231–242
43. Bougrier C, Carrere H, Delgenes JP (2005) Solubilisation on waste-activated sludge by ultrasonic treatment. *Chem Eng J* 106:163
44. Neis U (2002) Intensification of biological processes by ultrasound. *TU Hambg-Harbg Rep Sanit Eng* 35:79–90
45. Onyeche TI, Schäfer C, Bormann H, Schröder C, Sievers M (2002) Ultrasonic cell disruption of stabilized sludge with subsequent anaerobic digestion. *Ultrasonics* 40:31–33
46. Wolski P, Zawieja I (2012) Effect of ultrasound field on dewatering of sewage sludge *Archives of Environmental Protection* (38) 2:25–31
47. Wolski P, Zawieja I (2015) Susceptibility of conditioned excess sewage sludge to biodegradation and dewatering. *Environ Prot Eng*. doi:10.5277/EPE15030145
48. Neis U, Thiem A (1997) Particle size analysis in primary and secondary waste water effluents. *Water Sci Technol* 36(4):151–158
49. Sorys P, Zielewicz E (2007) Impact of selected physicochemical properties of excess sludge on the effects of ultrasonic disintegration. *Pol J Environ Stud 2A Part III* (16):568–572
50. Biggs CA, Lant P (2000) Activated sludge flocculation: on-line determination of floc size and the effect of shear. *Water Res* 34(9):2542–2550
51. Baier U, Schmidheiny P (1997) Enhanced anaerobic degradation of mechanically disintegrated sludge. *Water Sci Technol* 36(11):137–143
52. Schmitz U, Berger C, Orth H (2000) Protein analysis as simple method for the quantitative assessment of sewage sludge disintegration. *Water Res* 34(14):3682–3685
53. APHA, AWWA, WEF (1995) Standards methods for the examination of water and wastewater, 19th edition, APHA, Washington DC
54. Zielewicz E, Kasprzyk W (2012) The construction of a new sewage sludge ultrasonic disintegrator. 40 Winter School on wave and quantum acoustics. In: Workshop on molecular acoustics, relaxation and calorimetric methods. <http://ogpta.polsl.pl/wswqa/abstracts/41/wwomaracm>
55. Zielewicz E (2014) Effects of ultrasonic disintegration of excess sewage sludge with the heads of various construction. In: 43rd Winter School on wave and quantum acoustics, 10th Winter workshop

- on molecular acoustics, relaxation and calorimetric methods. <http://ogpta.polsl.pl/wswqa/abstracts/43/wwomaracm>
56. Zielewicz E, Tytła M (2015) Effects of ultrasonic disintegration of excess sludge obtained in disintegrators of different constructions. *Environ Technol* 4:1–8 (**Taylor and Francis Group**)
 57. Tytła M, Zielewicz E (2016) The effect of ultrasonic disintegration process conditions on the physicochemical characteristics of excess sludge. *Arch Environ Prot* 42(1):19–26
 58. Zielewicz E (2016) Effects of ultrasonic disintegration of excess sewage sludge. *Appl Acoust* 103:182–189

Combined Microwaves/Ultrasound, a Hybrid Technology

Katia Martina¹ · Silvia Tagliapietra¹ ·
Alessandro Barge¹ · Giancarlo Cravotto¹

Received: 16 August 2016 / Accepted: 2 November 2016 / Published online: 10 November 2016
© Springer International Publishing Switzerland 2016

Abstract The combination of microwave heating and ultrasound irradiation has been successfully exploited in applied chemistry. Besides saving energy, these green techniques promote faster and more selective transformations. The aim of this review is to provide a practical overview of the complimentary and synergistic effects generated by the combination of microwaves and either ultrasound or hydrodynamic cavitation. This will begin with a brief history, as we outline pioneering achievements, and will also update the reader on recent developments. Such hyphenated techniques are able to offer reliable and efficient protocols for basic chemistry, organic and inorganic synthesis as well as processing. The development of dedicated hybrid reactors has helped scientists to find solutions to new synthetic challenges in the preparation of nanomaterials and new green catalysts. This research topic falls within the confines of process intensification as it facilitates the design of substantially cleaner, safer and more energy efficient technologies and chemical processes.

Keywords Microwaves · Ultrasound · Enabling technologies · Hybrid reactors · Synergistic effects

This article is part of the Topical Collection “Sonochemistry: From basic principles to innovative applications”; edited by Juan Carlos Colmenares Q., Gregory Chatel.

✉ Giancarlo Cravotto
giancarlo.cravotto@unito.it

¹ Dipartimento di Scienza e Tecnologia del Farmaco and NIS-Centre for Nanostructured Interfaces and Surfaces, University of Turin, Via P. Giuria 9, 10125 Turin, Italy

1 Introduction

The use of ultrasound (US) in chemical reactions in solution provides specific activation based on the physical phenomenon of acoustic cavitation. US irradiation causes compression of the liquid followed by rarefaction and a sudden pressure drop that form small oscillating bubbles of gaseous substances. The bubbles expand until they reach an unstable size; they can collide and/or violently collapse. Moreover, the interaction of acoustic waves with a chemical system is not merely a way for improving dissolution and dispersion as it involves complex physico-chemical phenomena, which are currently a matter of advanced research. What makes sonochemistry unique is the remarkable phenomenon of cavitation, which is strongly dependent on the solvent vapour pressure, currently the subject of intense research that has already yielded thought-provoking results (Fig. 1).

Microwave (MW) irradiation has been successfully applied in organic chemistry. Spectacular accelerations, higher yields under milder reaction conditions and higher product purities have all been reported. Indeed, a number of authors have described successful reactions that do not occur by conventional heating and even modifications of selectivity (chemo-, regio- and stereoselective). The effect of MW irradiation on organic synthesis is a combination of thermal effects arising from the heating rate, superheating or “hot spots” and the selective adsorption of radiation by polar substances. Such phenomena are not usually accessible by classical heating and the existence of a non-thermal effect of highly polarising radiation is still a controversial topic. Due to the electromagnetic nature of MW non-polar solvent are not fully eligible for this kind of application (Fig. 2).

In 1995, Japanese researchers first described the surprising synergistic effects that occurred in sono- and chemo-luminescence experiments carried out under simultaneous MWs/US (MW/US) irradiation [1]. This now-typical hyphenated technique gives remarkable improvements in mass transfer, in particular in heterogeneous catalysis or biphasic aqueous systems [2, 3]. Sonochemistry can boast of a longer history than the other techniques; however, MW applications have seen impressive growth over the last 2 decades. While popular wisdom simply associates MW with superior heating and US with efficient agitation, these techniques are capable of

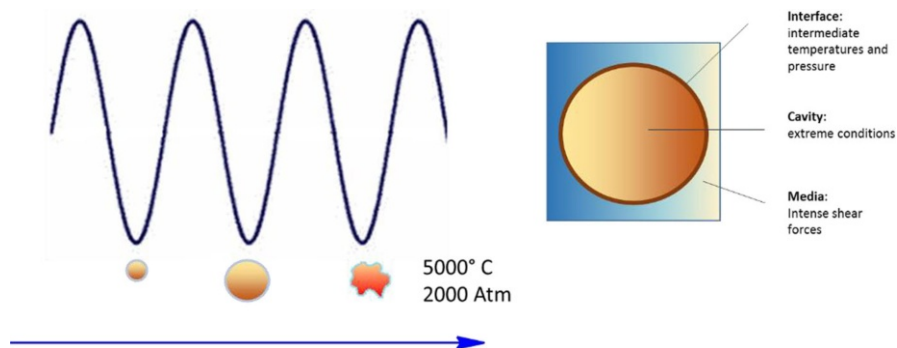


Fig. 1 Representation of acoustic cavitation

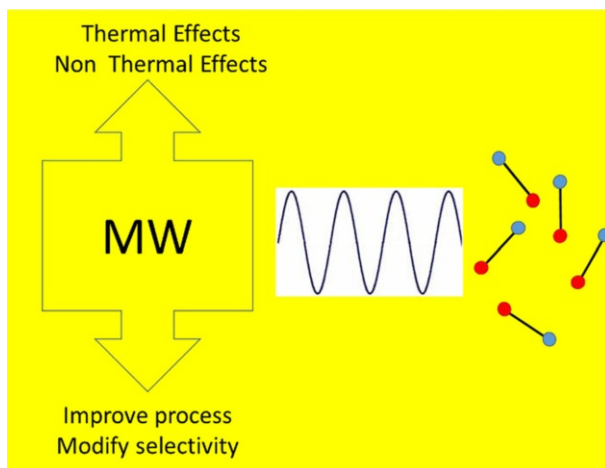


Fig. 2 Effect of MW on polar substances

doing so much more and this potential has provided additional impulse to their increased use in chemical processes [4]. Combined MW/US irradiation can be performed in simultaneous mode or otherwise sequentially by circulating the reacting mixture through the two compartments [5].

2 Combined MW/US Reactors

US can be conveyed inside a modified MW oven by inserting a non-metallic horn through its wall and down into the reaction vessel. These US horns are typically made of ceramic material, quartz, Pyrex[®] or special PEEK[®] containing glass fibres [6]. Simultaneous MW/US irradiation (SMUI) usually requires constant cooling, which can be provided by a circulating refrigerating fluid that is transparent to MW and thus avoids increasing the temperature to the boiling point, which would result in negligible cavitation. The first prototype, made at the University of Turin (2004), was built around a probe that held a cylindrical quartz horn inserted into a modified domestic oven inside which the PTFE vessel was cooled by a fluid circulating around an external jacket (Fig. 3). Chemat et al. avoided subjecting the horn to the electromagnetic field by using decalin (a low-viscosity apolar liquid) to convey the US waves to the reaction mixture, which was placed in a double-jacketed Pyrex vessel inside the oven [7].

As part of the authors' collaboration with Milestone Srl (Bergamo, IT), a more professional system was created, seen in Fig. 4, which can monitor and record all of the main parameters.

Combined irradiation can otherwise be achieved using flow loop reactors for sequential MW/US treatment, meaning that commercially available metallic horns can be used. In these reactors, a pump circulates the reacting mixture through two separate reaction cells, one placed inside the MW oven and the other (fitted with a

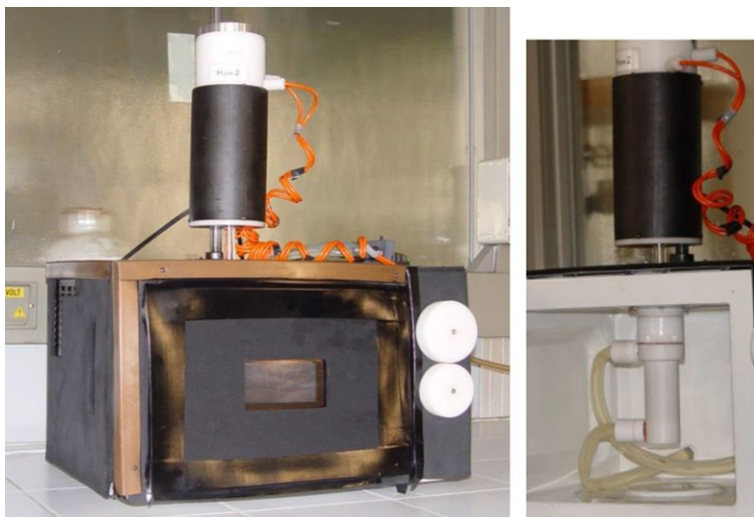


Fig. 3 First prototype of SMUI with a cooling system (authors' laboratory)



Fig. 4 SMUI with a cooling system (authors' laboratory)

US probe) outside it (Fig. 5). The Suzuki homo- and cross-couplings of aryl halides and arylboronic acids carried out in this reactor afforded products in higher yields than reactions performed under MW or US alone. Commercially available Pd/C or Pd(OAc)₂ were used as the catalysts and neither phosphine ligands nor phase-transfer catalysts were required. Even electron-deficient aryl chlorides gave acceptable yields [8].

Fig. 5 Loop reactor providing MW and US irradiation (authors' laboratory)

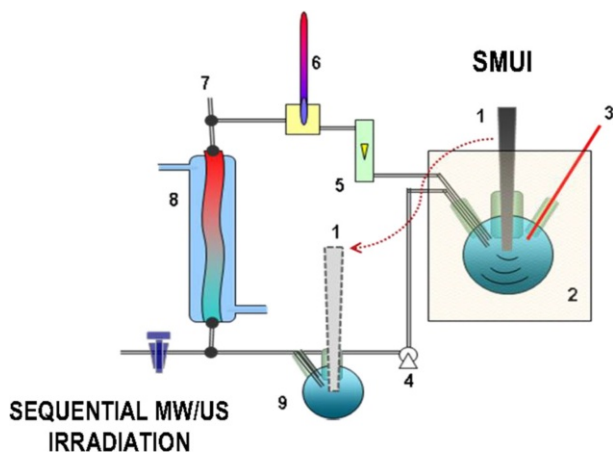


Fig. 6 Loop MW/US reactor for simultaneous and sequential irradiation. 1 US non-metallic horn, 2 MW oven, 3 optical fibre thermometer, 4 pump, 5 flow meter, 6 thermometer, 7 inlet and sampler, 8 heat exchanger and 9 external flask

A 5-l hybrid MW/US loop reactor prototype has also been used to decontaminate water [9]. The degradation of 2,4-dibromophenol (0.1 g/l) by Fenton's reagent was achieved by pumping the aqueous solution through a MW oven and an ultrasonic reactor that consisted of two generators working at 20 and 300 kHz.

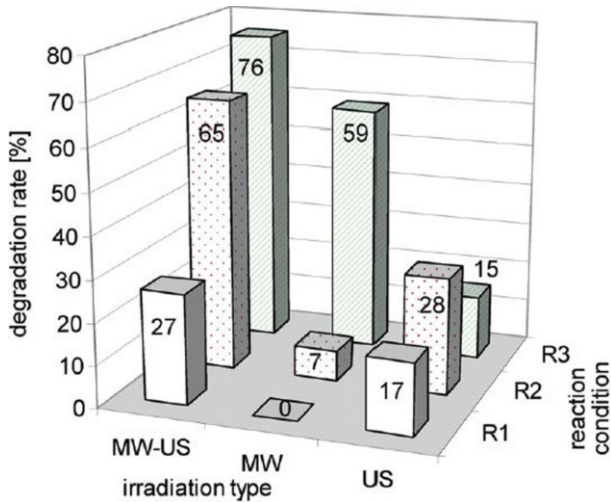


Fig. 7 Synergistic effects of SMUI phenol degradation. Reaction conditions: Phenol (1250 ml of 1 mM). MW: 360 W irradiated. US: 850 kHz, 40 W at 27 °C, flow rate 140 ml min⁻¹. R1: without H₂O₂, T_{MW} 93 °C, 4 h. R2: 20 mmol H₂O₂, T_{MW} 60 °C, 4 h. R3: 20 mmol H₂O₂, T_{MW} 93 °C, 2 h (reprinted with permission from Ref. 10; copyright American Chemical Society)

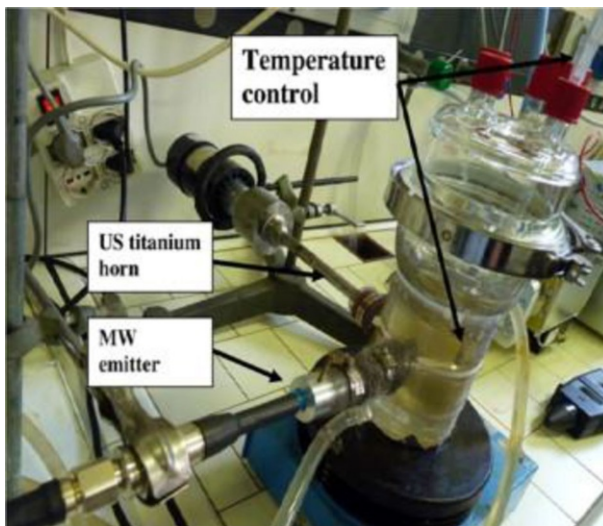


Fig. 8 SMUI with MW antenna and US horn (reprinted with permission from Ref. [11]; copyright Elsevier)

The degradation of phenol under combined MW/US irradiation, tested in both simultaneous and sequential loop systems, gave impressive synergistic effects, with and without the addition of H₂O₂ (Figs. 6, 7) [10].

Instead of placing the flask into a MW oven, Ragaini et al. used a coaxial dipole antenna as a MW wave guide to deliver MW. A titanium horn was placed

orthogonally to the antenna in the same vessel (Fig. 8) [11]. This kind of reactor enables the SMUI of chemical reactions using metallic horns, although its volume is limited.

3 Organic Reactions Under Combined MW/US Irradiation

Thirty years ago, Otteson and Michl described a pioneering gas-phase dehalogenation of organic dihalides using alkali metal vapours in excess argon under MW/US irradiation [12]. Several examples of this marriage appeared in the literature in the decades that were to come as innovative approaches to classical organic reactions and metal-assisted catalysis were described [13].

3.1 Transesterification Reaction

Of the several methods for enhancing oil transesterification that have been reported in the literature, simultaneous MW/US has given excellent results. Besides the high yield and shorter reaction time, superior biodiesel quality and lower energy consumption were observed thanks to optimal mass and heat transfer. The combination of MW and US irradiation is extremely effective in oil transesterifications because of the fast and selective MW heating, whereas US produces efficient mixing. Heat and mass transfer are strongly enhanced by combining the two different techniques in a single reactor that is well suited for the transesterification of waste vegetable oils. Martinez-Guerra et al. have developed a very fast protocol for waste vegetable oil to biodiesel production (in 82 min) under simultaneous irradiation [14]. Best conditions were: a 6:1 methanol/oil ratio, 0.75% sodium hydroxide, MW/US power 100 W (each source), giving a 98% yield, which was higher than MW (87%) or US (90%) alone. Besides efficiency and selectivity, safety, cost, robustness and environmental impact were all improved (Fig. 9).

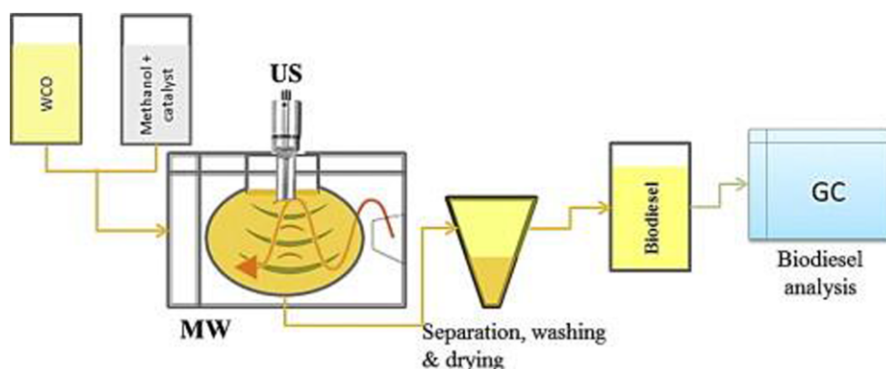


Fig. 9 Experimental set-up for transesterification reaction under US/MW (reproduced with permission from Ref. [14])



Fig. 10 Transesterification under SMUI (authors' laboratory)

The same authors published another work on MW/US-assisted transesterification under heterogeneous catalysis with BaO, with evident advantages for work-up and separation processes [15]. Very recently, they evaluated the effect of different alcohols on oil transesterification. Under simultaneously MW/US irradiation, the biodiesel yields for methanol and ethanol were comparable, whilst ethanol gave higher yields by individual MW or US irradiation [16].

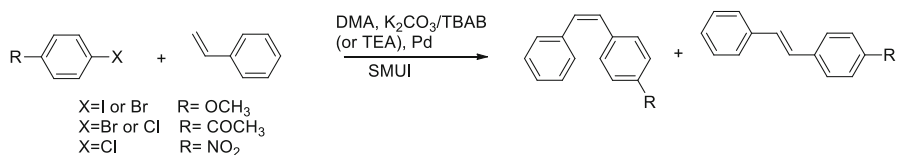
Response surface methodology (RSM) has been used by Cravotto et al. to optimise simultaneous MW/US-assisted palm oil transesterification; the methanol/oil ratio, catalyst concentration, reaction temperature and irradiation time were all improved [17] (Fig. 10). Full conversion (yield 98%) was achieved in about 2.2 min at 58 °C (1.09% catalyst concentration, 7:3.1 methanol/oil molar ratio), whereas the reaction time under classic conductive heating and stirring was about 40–50 min. This work demonstrated that simultaneous irradiation provokes an additive effect via an increase in contact area between oil and alcohol, leading to an increase in reaction rate. Simultaneous application can also address the issues that are found when carrying out consecutive irradiation. Total energy consumption was much lower than in the conventional method [0.36 MJ/l vs. 1.92 MJ/l (heating + stirring 400 W for 40 min)].

3.2 C-C Coupling

The Heck reaction, one of the most useful protocols in organic synthesis, has become a veritable classic over the last few decades. It has been carried out in all manner of reaction media (organic solvents, water, supercritical CO₂, ionic liquids) and, of course, under US and MW irradiation. In 2007, Palmisano et al. [18] reported Heck couplings that they had carried out without ligands in air and with very low catalyst loads under simultaneous US/MW irradiation. Ligand-free palladium (II) acetate (0.01–0.1 mol%) or palladium-on carbon (Pd/C 10%), in the 1.0–2.0 mol% range, gave most aryl iodides and bromides in high yields under conventional heating (120 °C) in 18 h. Combined US/MW, however, strongly promoted the reaction and generally decreased reaction times to 1 h. Even barely reactive electron-poor aryl chlorides, such as 4-chloroacetophenone and 1-chloro-4-nitrobenzene, reacted with styrene to afford high product yields (Scheme 1). In several cases, the addition of a co-catalyst, either 0.005 mol% rhodium *tris*(triphenylphosphine) chloride or 2.0–4.0 mol% copper (I) salt (iodide or bromide), proved highly advantageous. It is worth noting, however, that 4-bromo- and 4-chloroacetophenone gave up to 15% oxidation products, namely the corresponding 4-halobenzoic acid and 4-styrylbenzoic acid. This drawback was avoided by working under a nitrogen atmosphere.

Glycerol is a very suitable solvent for both MW and US promoted reactions. Although glycerol alone can be a valid alternative in environmentally friendly organic transformations, its use is still limited in most organic protocols because of the intrinsic reactivity of the –OH groups and the poor solubility of most organic compounds in it. The micellar catalysis approach may well be an alternative for improving the solubility of organic substrates, while enhancing their diffusion in this particular medium and inhibiting the reactivity of its polyol system. The fascinating possibility of applying SMUI hybrid technology to micellar catalysis in glycerol could lead to the much wider use of green protocols in synthesis and processing. This approach can simultaneously boast of the effective heating of glycerol under MW irradiation, efficient mixing under US and also avoiding side reactions. In 2014, Sacco et al. [19] described the application of SMUI to this approach using a monomodal apparatus equipped with a semiconductor generator and a coaxial cable. The monomode resonant MW cavity was also irradiated with US from the bottom using a suitable sonotrode (indirect sonication).

The authors reported on the efficient SMUI-assisted Ru-catalysed ring-closing metathesis of diethyl diallyl malonate in glycerol hydrophobic micellar conditions



Scheme 1 Schematic representation of a Heck reaction under SMUI (Ref. [18])

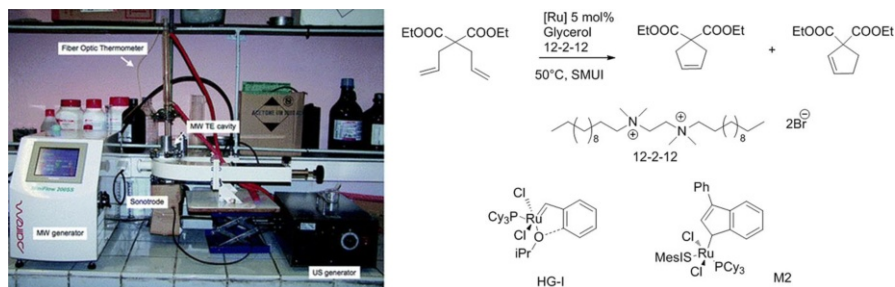
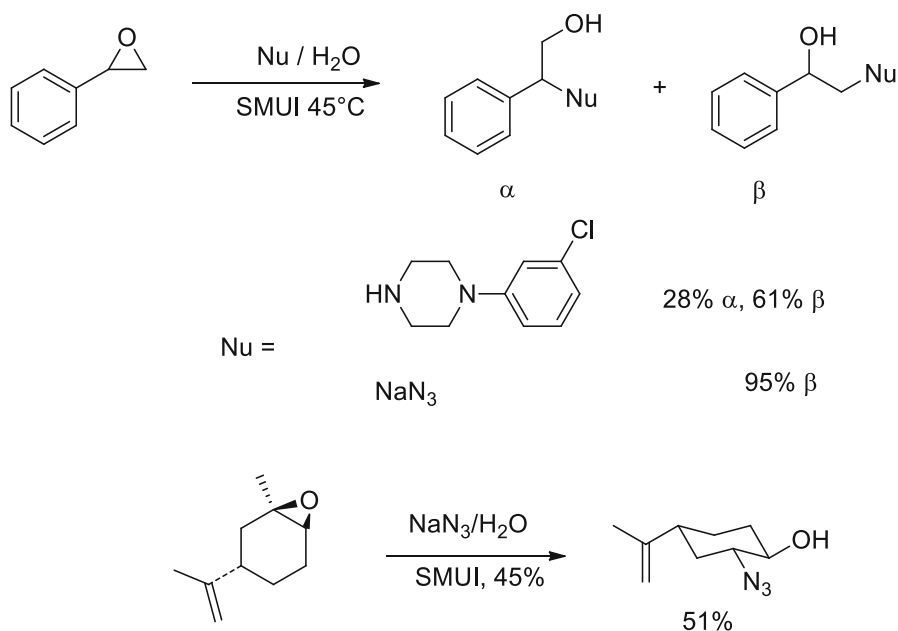


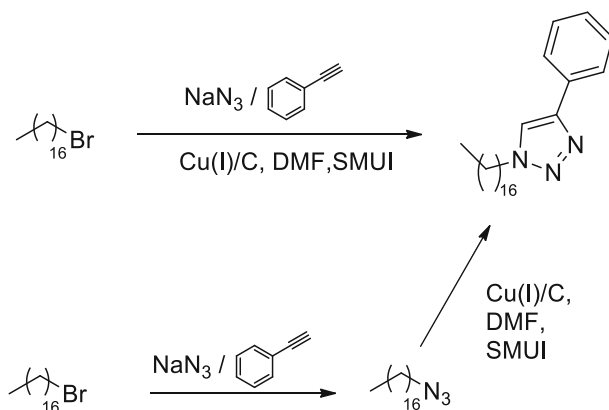
Fig. 11 A modified monomode SAIREM Miniflow cavity for SMUI and an example of ring-closing metathesis (reproduced from Ref. [19] with permission from the Centre National de la Recherche Scientifique (CNRS) and The Royal Society of Chemistry)

by means of a dicationic surfactant (Fig. 11). The SMUI reaction (US 200 W and MW 10 W) occurred in around 18 min, faster than with MW alone.

Epoxide cleavage by nucleophiles in aqueous media can generally incur competition from water itself, yielding the diol as the by-product. However, under high-intensity US or MW, the attack by the nucleophile was strongly promoted and water no longer reacted. In 2007, Palmisano et al. [20] reported the syntheses of a series of commercially available oxiranes, at different degrees of substitution, using sodium azide and 1-(3-chlorophenyl)piperazine in water at neutral pH without a metal catalyst. Four different reaction conditions were compared: (1) “on water” conventional conditions at 50 °C; (2) under MW irradiation at 50 °C; (3) under US



Scheme 2 Schematic representation of epoxide opening under SMUI (Ref. [20])

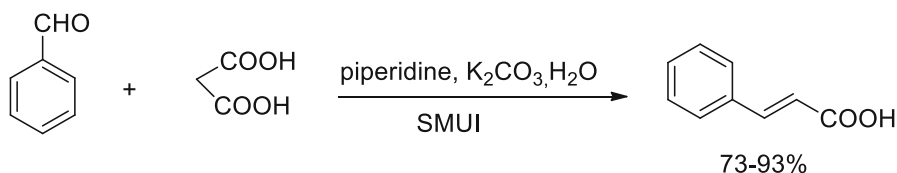


Scheme 3 SMUI promoted CuAAC reaction (Ref. [21])

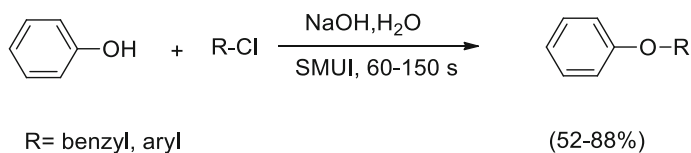
at 45 °C; (4) under SMUI at 45 °C. The last set of conditions strongly accelerated the cleavage and gave high regioselectivity for unsymmetrical epoxides. The *N*-nucleophile attack took place on the less hindered epoxide carbon, except for in 2-phenyloxirane. Reactions carried out in these conditions are completely *anti*-stereoselective, as shown by the exclusive formation of the *anti*-products in the cyclic epoxide reactions. An example can be found in (+)-(1*R*,2*S*,4*R*)-*cis*-limonene 1,2 epoxide, which exclusively afforded the 1*R*,2*R*,4*R* stereoisomer in moderate yield (51%) via reaction with sodium azide, as seen in Scheme 2.

The Huisgen 1,3-dipolar cycloaddition of azides and acetylenes leading to 1,2,3-triazoles and catalysed by Cu (I) salts is one of the most versatile “click” reactions. In 2007, the authors reported a series of optimised protocols and new applications of this reaction starting from several substrates [21]. Comparisons of heterogeneous vs. homogeneous catalysis [as based on charcoal-supported Cu (II) or Cu (I)] as well as conventional heating vs. MW irradiation vs. SMUI were made. Excellent results were obtained even with bulky molecules, such as azido β -cyclodextrins (β -CD), which afforded triazole cycloaddition with benzyl bromide and phenylacetylene. MW and SMUI dramatically accelerated the reaction in all cases (Scheme 3), the latter by means of a non-metallic US horn placed in the MW cavity. Very interesting results have also been achieved using metallic copper (turnings) instead of Cu (I) or Cu (II) salts [22]. The simultaneous use of US and MW promotes the reaction between CuO and Cu on the metal surface to give the catalytic species Cu_2O (US promoted reaction), while allowing the temperature required for 1,3-dipolar cycloaddition (MW enhanced reaction) to be reached at the same time. The combined MW/US approach gave better yields (in the same reaction time) than MW or US used alone. This new protocol was successfully applied to the derivatisation of 6-monoazido-6-monodeoxy- β -cyclodextrin and 6-monoazido-6-monodeoxy-2,3,6-*O*-permethyl- β -cyclodextrin with phenylacetylene.

Cinnamic acid and its derivatives are important reagents in organic synthesis as both intermediates and final products. They are routinely obtained from the reaction between aromatic aldehydes and malonic acid (Knoevenagel-Doebner reaction) in



Scheme 4 Knoevenagel-Doebner reaction promoted by SMUI (Ref. [23])



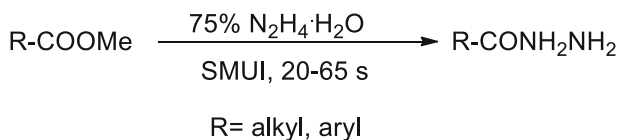
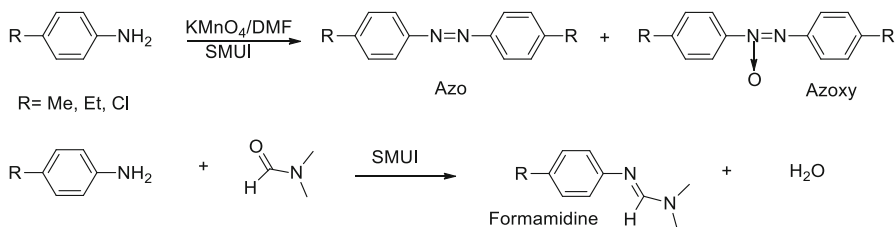
Scheme 5 SMUI promoted Williamson ether synthesis (Ref. [24])

organic solvents, catalysed by either primary or secondary amines. SMUI furnished significant rate enhancements and improved yields in the heterogeneous organic reactions. The SMUI technique has been applied by Peng and Song [23] for the preparation of 3-aryl acrylic acids in aqueous media with excellent yields (73–93%), as seen in Scheme 4. The presence of electron-withdrawing or -releasing groups on the substrates only had a slight influence on the yields. Results showed that the SMUI reaction proceeded much faster than under classic reflux, 65 s vs. 7 h. An additional advantage of using water as the solvent is the fact that many organic products can be separated via simple filtration or decantation from the resulting mixture.

3.3 C-Heteroatom Bond Formation

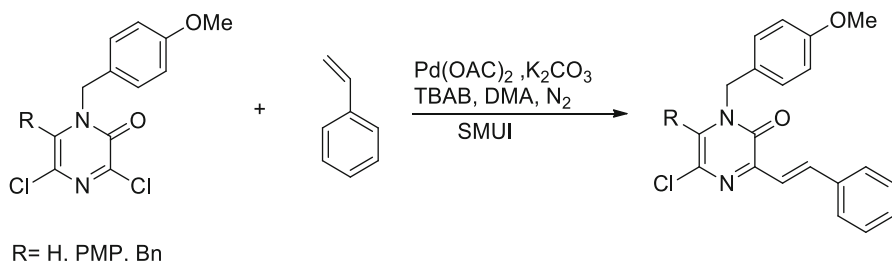
The Williamson synthesis of ethers usually makes use of an alkali-metal salt of the hydroxy compounds and halides working in either organic solvents or under phase transfer catalysis. The direct etherification of phenols with an alkylating agent and a base is, however, troublesome; the etherification of nitrophenols requires aprotic solvents if large excesses of alkylating agents and side reactions are to be avoided. Moreover, the selective monoetherification of bisphenols is not an easy task because it is inevitably accompanied by bietherified products. In this context, Peng and Song [24] reported an SMUI-assisted etherification that afforded a series of benzyl phenyl ethers and diphenyl ethers in good yields without the need for phase-transfer catalysis (Scheme 5). Control experiments, which were carried out under conductive heating and stirring, clearly displayed the great advantage of SMUI; benzyl phenyl ether was obtained in 16 h vs. 2 min and at 41 vs. 83% yield, respectively.

The solvent and surfactant free SMUI procedure was applied to the synthesis of hydrazides from esters and hydrazine monohydrate by the same authors [25]. Acyl anhydrides and acid chlorides both react rapidly with hydrazine to give hydrazides, but it was not possible to stop the monoacylation reaction. The most widely used method for the preparation of hydrazides is the hydrazinolysis of the corresponding esters with hydrazine monohydrate. This is, however, a reaction with some

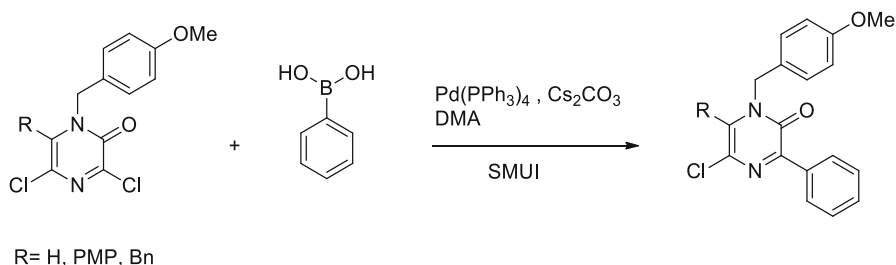
**Scheme 6** Schematic representation of the synthesis of hydrazide under SMUI (Ref. [25])**Scheme 7** Schematic representation of the synthesis of azo and/or azoxy compounds (Ref. [26])

drawbacks, such as the long reaction time and the diacylation products. Using the hydrazinolysis of methyl salicylate as a model system, the reaction was studied under a number of different reaction conditions (US, MW and SMUI), as seen in Scheme 6. Results clearly show that SMUI achieved the best results in terms of both reaction time and yield (84 vs. 73% in 40 s instead of 9 h under conventional heating with reflux).

Aromatic azo and azoxy compounds are important dyes and are widely used as analytical reagents, reducing agents, stabilisers and polymerisation inhibitors in biological and chemical research. Aromatic azo compounds are traditionally synthesised via the coupling of diazo compounds with amines or phenols, the oxidation of hydrazine and hydrazo compounds, the reduction of nitro compounds in alkaline solution or the molecular rearrangement of diazoamines. The formation of azobenzene via the oxidation of aniline in basic solution has been known since 1960 and the mechanism was explained using sonochemical experiments in water. US generated $\text{H}\cdot$ and $\text{OH}\cdot$ radicals that converted aniline to $\text{PhNH}\cdot$ and $\text{PhN}\cdot$ radicals that combined to yield PhNHNHPh and $\text{PhN}=\text{NPh}$. The oxidation of aniline using $\text{MnO}_2/\text{SiO}_2$ under MW irradiation (420 W) for just 4 min gave azobenzene in an 84% yield. In 2008, Ondruschka et al. [26] reported an efficient MW/US procedure for the preparation of azo and/or azoxy compounds from primary aromatic amines (Scheme 7). *p*-Methylaniline and *p*-ethylaniline conversions of more than 70% were obtained in 20 min under MW or SMUI, whereas 57 and 54% *p*-ethylaniline conversions were observed under US irradiation and plain heating in a water bath, respectively. SMUI significantly enhanced the conversion of *p*-chloroaniline as well. DMF is commonly used in MW irradiation chemistry as it is a good polar, aprotic solvent with a high boiling point. However, when present, it leads to the formation of formamidine and other by-products resulting in poor selectivity towards azo and azoxy products. No by-product was formed when the amount of water in the medium was increased from 15 to 35 ml. However, the yields of azo and azoxy compounds also decreased in this case. Other solvents such



Scheme 8 Heck reaction of 3,5-dichloro-2-(1*H*)-pyrazinones with styrene (Ref. [27])

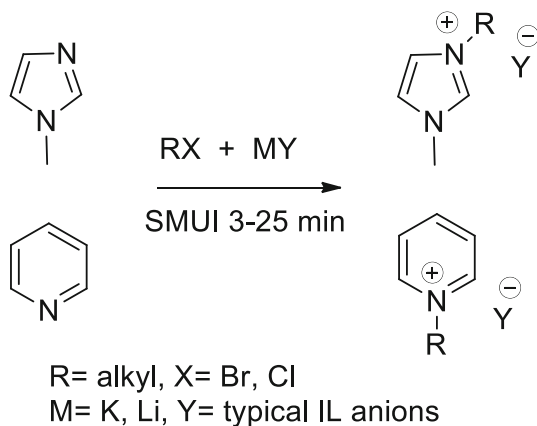


Scheme 9 Preparation of 3,5-dichloro-2-(1*H*)-pyrazinones (Ref. [27])

as dimethyl sulphoxide (DMSO), acetonitrile and ethanol have been studied with the aim of avoiding the formation of formamidine and other by-products.

3.4 Heterocyclic Compounds

Interest in the synthetic applications of SMUI in palladium-catalysed reactions with very low catalyst loads [27] led the authors to investigate the efficiency of this technique for the selective functionalisation of 3,5-dichloro-2-(1*H*)-pyrazinones in 2010. In spite to the poor reactivity in Pd-catalysed Suzuki and Heck reactions owing to the 5-chloro atom, SMUI strongly promoted the reaction leading to good yields by reducing the extent of degradation that can arise from prolonged heating. SMUI requires an efficient cooling system if strict temperature control is to be achieved and superheating, which would hamper cavitation, is to be prevented. This can be attained by circulating a MW-transparent refrigerated fluid such as Galden[®], a perfluoropolyether with a high boiling point and low viscosity. A Heck reaction of 3,5-dichloro-2-(1*H*)-pyrazinones with styrene was carried out using three different techniques: conventional heating, MW and SMUI (Scheme 8). Reactions were carried out in dimethylacetamide (DMA) under a nitrogen atmosphere in all cases. Yields were generally low because of partial degradation and the formation of by-products when the reaction was stirred under conductive heating, whereas yields were greatly improved under MW irradiation and were even better under MW/US irradiation. Complete conversion was observed after only 20 min with excellent reproducibility. The same 3,5-dichloro-2-(1*H*)-pyrazinones were subjected to Suzuki-Miyaura cross-couplings with phenylboronic acid in dimethylacetamide

Scheme 10 Preparation of ionic liquids (Ref. [28])

using very low catalyst loading (0.005 mmol of *tetrakis* (triphenylphosphine) palladium) and caesium carbonate as the base, as seen in Scheme 9. Yields increased from 7 to 14% under conventional heating to 63–86% under SMUI, which proved itself to be a fantastic tool for the chemical decoration of pyrazinones. Simultaneous MW/US irradiation greatly improved the kinetics and yields of these chemical modifications because of the optimal heat- and mass-transfer that they provide.

The first generation of ionic liquids (ILs) that saw widespread use was mainly composed of cations, such as dialkylimidazolium and alkyipyridinium derivatives, and anions, such as chloroaluminate and other metal halides that have been described as toxic and non-biodegradable. This generation of ILs was also oxygen-sensitive and can only be handled under inert-gas atmosphere. Research was thus directed towards the synthesis of air- and water-stable ILs, the second generation of ILs. The water- and oxygen-reactive anions were replaced by either halides (Cl⁻, Br⁻, I⁻) or anions, such as BF₄⁻, PF₆⁻ and C₆H₅CO₂⁻, which are stable in water and air. This second generation of ILs attracted a great deal of attention from the wider scientific community and has been providing interesting and novel applications in a number of areas. The “green” properties of ILs are linked to their negligible vapour pressure and flammability as well as their ease of recycling. However, their biodegradability is still open to debate and further toxicological studies are required if we are to ascertain their complete safety. They are usually prepared over two consecutive steps: (1) the quaternarisation of a nitrogen-bearing compound (Menshutkin reaction) and (2) the exchange of the halide with a different anion (metathesis). Non-conventional techniques, such as irradiation with MW and power US, have been successfully employed in the synthesis of ILs and have cut down reaction times and improved yields. In 2007, Cravotto et al. [28] described an efficient one-pot synthesis of second-generation ILs (Menshutkin reaction and anion metathesis) under SMUI; a series of ILs with 1-methylimidazole or pyridine cores were obtained in high yields in just a few minutes (80–97% isolated). The yields for the Menshutkin reaction are strongly temperature-dependent, meaning that strict temperature monitoring, using either optical-fibre thermometers or infrared (IR)

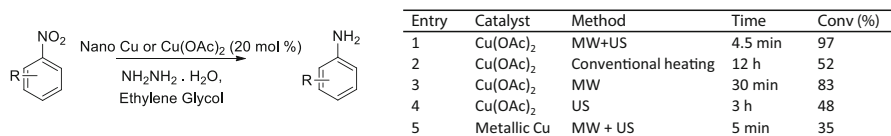
pyrometers, is required (Scheme 10). Preliminary experiments were also carried out on chloroalkanes. The one-pot synthesis of [C8 mim][PF₆] from 1-chlorooctane under SMUI for 10 min (140 °C) only gave a moderate yield (55%). Work on optimising the protocol for use with notoriously poorly reactive chloroalkanes is in progress. An efficient cooling system, which allows MW and US power levels to be increased sufficiently, was used. The reaction yield rose to 97% when carried out under external cooling at 140 °C (10 min).

3.5 MW/US Assisted Digestion

Ammonia and organic nitrogen can be analytically determined using the Kjeldahl method, which requires a previous sample digestion. A systematic study was carried out by Domini et al. [29] on a series of amino acids and on real samples where the classical Kjeldahl approach and MW/US combined method were compared. The total nitrogen values determined by the MW/US combined digestion method are closer to theoretical ones than those obtained using the classical approach. Furthermore, the mineralisation time was reduced from 30 min (classical approach) to 7 min (MW/US). The process was carried out in a glass round-bottom flask heated in a professional MW oven. A Pyrex horn was inserted into the flask to simultaneously irradiate the sample with US and MW.

4 Nanoparticles

Nanoparticles (NPs) are becoming key components of a wide range of applications. Research encompasses numerous disciplines, including nanotechnology, pharmaceuticals manufacture, chemistry, physics, optical components and polymer science. The size, morphology and dimensionality of NPs can strongly affect the properties of nanostructured materials. Nanostructured metallic and semiconducting materials of various structures and morphologies have recently received a great deal of attention because of their novel applications, peculiar properties and quantum size effects [30]. Nanostructured materials have thus been prepared via a variety of synthetic methods, including gas phase techniques, liquid phase methods (e.g., reduction of metal salts) and mixed phase approaches (e.g., synthesis of conventional heterogeneous catalysts on oxide supports). However, reducing agent strength as well as interactions with stabilising agents and solvents can affect the size and shape of metal nanoparticles in the production of metallic NPs. The use of MW irradiation in this context is not affected by safety concerns because of the high dilution of the metal in the *ab initio* preparation of nanoparticles. Of particular interest here is the use of MW radiation as the heat source as it can produce high-quality nanoparticles in a short time [31]. Moreover, US irradiation has been extensively examined in this field over many years [32, 33] and is now positioned as one of the most powerful tools in nanostructured material synthesis. It was only natural to consider the combination of MW and US irradiation, which has, in fact, recently been used to synthesise nanoparticles in a short time and was also able to tune particle properties and size [34].



Scheme 11 Reaction scheme and conversions of the copper-catalysed reduction of nitrobenzene under differing conditions (Ref. [35])

SMUI has been used to generate copper nanoparticles via Cu(OAc)₂ reduction by hydrazine hydrate in ethylene glycol [35]. The nanoparticles were fully characterised using X-ray diffraction (XRD) and transmission electron microscopy (TEM) to confirm that the spherical nanoparticles were made of pure metallic copper. Cu nanoparticles then catalysed nitrobenzene reduction with hydrazine hydrate. The reaction was repeated with Cu(OAc)₂ under SMUI to obtain the reduced aniline and Cu nanoparticles that were isolated by centrifugation. The optimised protocol was performed with 20% Cu(OAc)₂ and 3 eq of hydrazine hydrate and was heated at 105–110 °C in ethylene glycol. The same reaction, performed under conventional conditions lasted 12 h and had a yield of 52%, whereas the SMUI promoted reaction took 4.5 min and the yield was 97% (Scheme 11).

US and MW irradiations were also used sequentially to obtain a solid supported Pd catalyst for the semi-hydrogenation of alkyne to alkene [36]. Pd was reduced using US irradiation and supported under MW promotion to obtain Pd clusters of approximately 100 nm. This catalyst showed enhanced activity in the semi-hydrogenation reaction and high selectivity. This method is truly a novel and green route to the production of Pd nanoparticles, even in the absence of a surfactant.

The beneficial effects of MW and US irradiation in the preparation of CuO nanoparticles has also been demonstrated by Zhu et al. as they aimed to obtain nanofluids with enhanced thermal conductivity [37]. In this study, Cu(OH)₂ was converted to CuO in water under SMUI. The suspension was treated for 30 min in a US disrupter for the conversion from green to puce, while a subsequent 3 min of MW irradiation was enough to obtain the black nanofluid. The authors demonstrated that the transformation was not completed and the particles were aggregate when only US was used and that, analogously, some large aggregates were obtained when MW irradiation alone was used.

Nanostructures, such as wires, tubes and ribbons, have fast become the focus of intensive research in recent years because their small dimensions can be employed for both the efficient transport of electrons and optical excitation. Nowadays, light-emitting diodes, solar cells, single-electron transistors, lasers and biological labels are currently making full use of these ideal one-dimension nanostructures. Developing an efficient and sustainable approach to their preparation is, understandably, a subject of great interest and the MW/US combination is showing great promise in their environmentally benign production. Surfactants and ionic liquids are commonly used as templates to promote the formation of nanostructures. The combination of MW and US irradiation and the use of 1-butyl-3-methylimidazolium bromide [BIMB]Br has been successfully employed for the rapid synthesis of Pb(OH)Br nanowires [38]. Pb(OAc)₂·3 H₂O and [BIMB]Br were

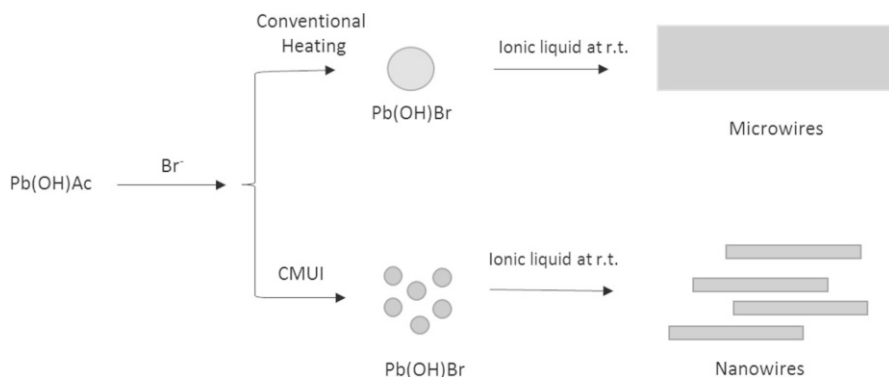


Fig. 12 Schematic representation of Pb(OH)Br nanowire formation (Ref. [38])

dissolved in deionised water and irradiated for 10 min by MW-US (50–50 W) irradiation. A comparison of nanowires obtained via conventional heating (70 °C, 24 h), those by MW irradiation and US irradiation alone and finally by the combined method highlighted the drastic differences in diameter and length of the nanowires produced by the differing methods. Under conventional conditions, Pb(OH)Br typically crystallised as a multiangular prism of 20–30 μm diameter and 2–3 mm of length. MW irradiation alone produces a uniform and smooth morphology, while US alone resulted in less uniform wires. Under combined US-MW irradiation furnished increased yields of straight and smooth wires (80–800 nm diameter and 50–100 μm length). A dramatic reduction in crystallisation time (24 h to 80 s) was also observed, which confirms that SMUI leads to the fast growth of crystal seed masses and causes a depletion in reaction nutrients over a short period of time, producing thinner and shorter wires (Fig. 12).

Of the different types of absorbing material used for thin-film solar cells, Cu₂ZnSnS₄ (CZTS) is one of the most promising as it contains earth-abundant, low-cost and nontoxic elements [39]. Many approaches to prepare CZTS thin films have been described in the literature in an attempt to reduce preparation costs. High cell efficiency is currently obtained via a non-vacuum-based approach in the absence of hydrazine, which is highly toxic, reactive and requires delicate handling and storage. The main methods for the preparation of CZTS nanoparticles include hot injection [36], solvothermal [40], mechanochemical [41] and MW irradiation [42]. MW irradiation has been combined with US in order to reduce nanoparticle aggregation; Wang et al. obtained CZTF nanoparticles by exposing a solution of zinc acetate dihydrate, tin (II) chloride dihydrate, copper (II) nitrate trihydrate and thioacetamide in polyethylene glycol 400 to simultaneous MW-US irradiation (MW power 800 and 400 W). The precursors were irradiated at different temperatures, from 130 to 180 °C, for 30 min and, after the nanoparticles had been characterised, it was observed that crystallinity, to form hexagonal-plate-like-nanoparticles, increased with increased temperature [43]. Long et al. described the preparation of wurtzite, rather than the kesterite phase, CZTF via the addition of a solution of thiourea in polyvinylpyrrolidone to a solution of copper (II) acetate monohydrate, zinc acetate dehydrate and tin

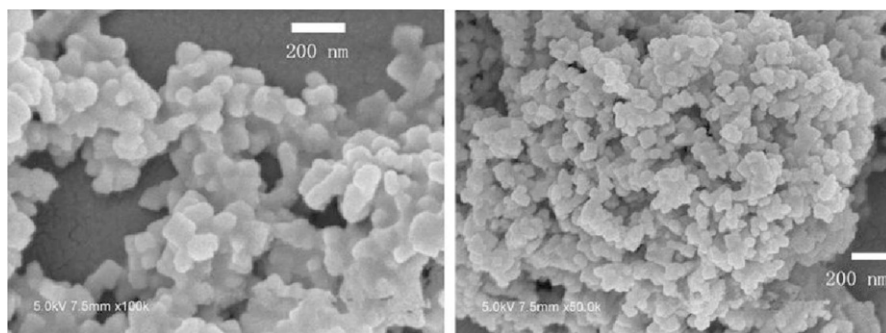


Fig. 13 SEM images of $\text{BiVO}_4: \text{Eu}^{3+}$ (reaction time: 60 min upper; 100 min bottom) (reproduced with permission from Ref. [44])

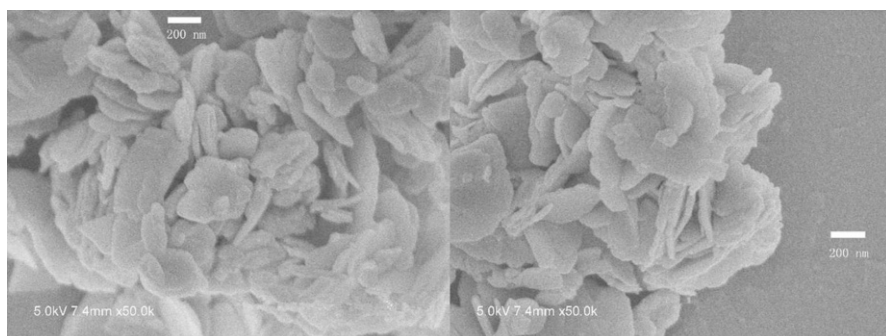


Fig. 14 SEM images of $\text{Gd}_2(\text{MoO}_4)_3: \text{Eu}^{3+}$ (reproduced with permission from Ref. [45])

(IV) chloride dihydrate in PVP at 150 °C under SMUI. The crystalline structure of CZTF was fully characterised by XRD, FESEM, EDS and TEM and the hexagonal prisms obtained were found to measure 0.5–2 μm wide and 5–12 μm long [44].

Eurpium or terbium activated phosphors, with characteristic lanthanide luminescence, were assembled under SMUI to obtain nanocrystals [45]. $\text{Bi}(\text{NO}_3)_3 \cdot 5\text{H}_2\text{O}$, $\text{Ln}(\text{NO}_3)_3 \cdot 6\text{H}_2\text{O}$ and NH_4VO_3 were irradiated by MW and US (MW power 400 W) in water at 80 °C for 1 h ($\text{Ln} = \text{La}, \text{Lu}, \text{Tb}, \text{Eu}$). The ultrasonic probe worked in pulsed mode (0.1 s and inter-pulse 0.2 s). SEM images showed quasi 1-D nanounits of $\text{BiVO}_4: \text{Eu}^{3+}$ of 60–80 nm average diameter (Figs. 13, 14). When SMUI was exploited to prepare $\text{GdBO}_3: \text{Eu}^{3+}$, a spontaneous nano-assembly was formed in flower-like morphology. Characteristic Eu^{3+} emissions were detected upon excitation. The $\text{La}_x\text{-Lu}_{1-x}\text{PO}_4: \text{Tb}^{3+}$ particle exhibited strong green emissions under UV excitation.

Yttrium aluminium garnet (YAG, $\text{Y}_3\text{Al}_5\text{O}_{12}$) is a chemically stable laser material. Highly dispersed ultrafine YAG powder is necessary to obtain transparent YAG ceramics of high density. Si et al. described the preparation of YAG under US irradiation as well as under US and MW sequential irradiation [46]. Al and Y metal particles, isopropanol, AlCl_3 and NH_4CO_3 were sonicated for 3–4 h. Several

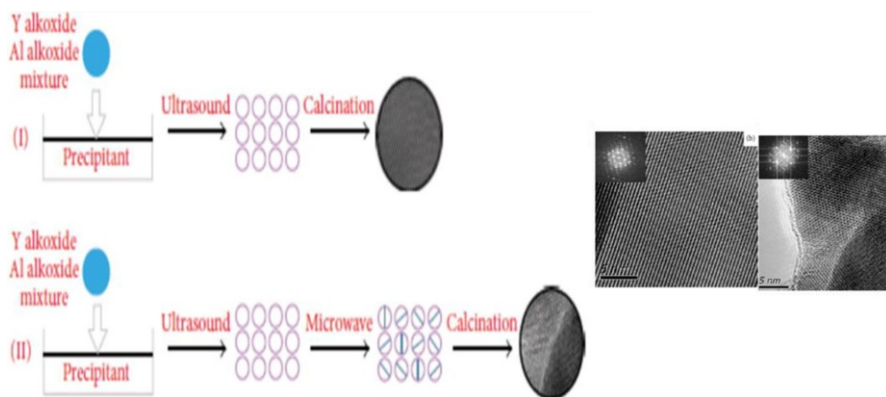


Fig. 15 Schematic diagram of the growth mechanism of YAG prepared by US-assisted synthesis (I) and US-MW-assisted synthesis (II). Reproduced with permission from Ref. [46]

samples were irradiated with MW before calcination for the sake of comparison. The TEM images of the different YAGs thus obtained demonstrated that US-MW irradiation produced a narrower distribution size and a more uniform shape than US-assisted precipitation. Interestingly, it was demonstrated, using HRTEM images and FFT patterns, that single crystalline and crystal grains were grown in the same direction under US-assisted synthesis, while the US/MW-assisted synthesis gave crystal grain growth in random orientations (Fig. 15). MW irradiation produced molecular movement and has an effect on the energy distribution of the crystal planes meaning that the YAG particle size was finer and uniform so as to avoid the addition of agents that suppress the agglomeration.

ZnO is a common photocatalyst that is active under ultraviolet light irradiation. In fact, nanoscaled ZnO is of very great interest indeed thanks to its unique optical and elective properties. ZnO microstructures exhibit enhanced performance over nanoparticles, nanorods and nanosheets. However, their preparation involves a complicated procedure and the addition of a surfactant or structure directing reagent. The synergic effect that MW and US provide allows for the preparation of well-defined flower-like nanostructures in surfactant-free conditions [47]. The optimised procedure entails sonication for 5 min, at a power of 1000 W, of a solution of zinc acetate in hydroxide aqueous solution, followed by treatment with MW heating combined with discontinuous US irradiation (1 s sonication and 2 s interruption) at a power of 500 W for 30 min (Fig. 16). The flower-like ZnO nanostructures showed superior methylene blue degradation catalytic activity to ZnO microrods.

Another attempt at obtaining ZnAlO nanoparticles was carried out with an eye to evaluating sterilisation activity [48]. A homogeneous and stable dispersion of the crystal structure was obtained upon the subsequent US and MW irradiation of $\text{Al}_2(\text{SO}_4)_3 \cdot 18\text{H}_2\text{O}$, $\text{Zn}(\text{NO}_3)_2 \cdot 6\text{H}_2\text{O}$ (molar ratio: $\text{Al}_2\text{O}_3:\text{ZnO} = 1:100$) in deionised water with a dispersant. The smallest nanoparticles, of 20 nm, showed the highest sterilisation activity against the proliferation of DH 5a bacteria.

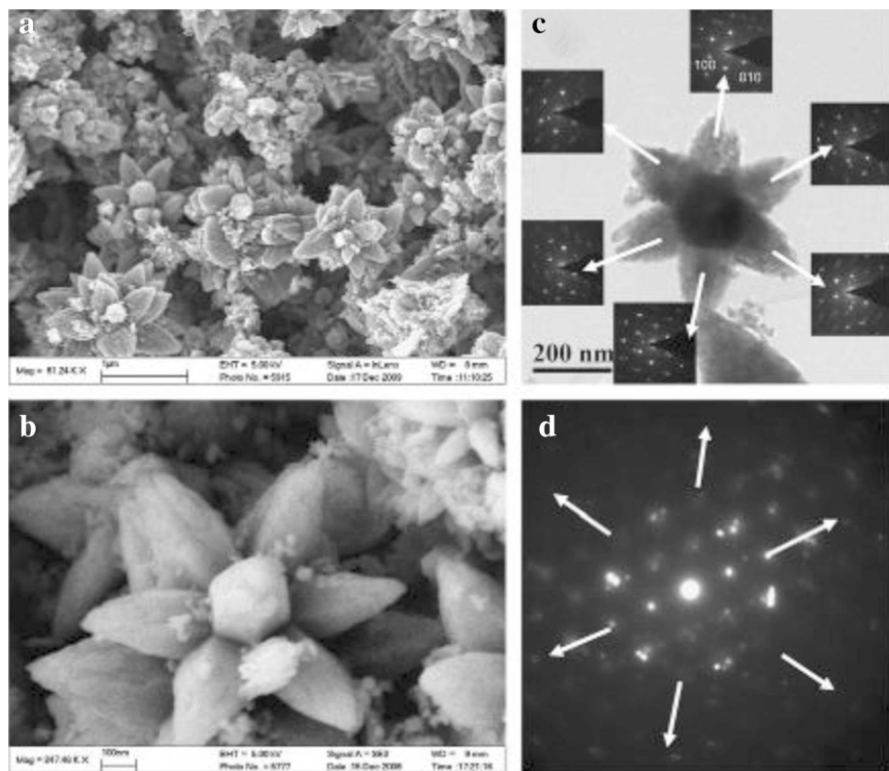


Fig. 16 SEM images (a, b), TEM image (c) and SAED patterns (d and insets of c) of the flower-like ZnO nanostructures (reproduced with permission from Ref. [47])

The micro- and nano-particles of bismuth vanadate (BiVO_4) have recently become the object of some interest as they show promise as visible light-driven photocatalysts. Various BiVO_4 nanostructures have been reported as promoting the degradation of numerous organic pollutants and microorganisms under visible light irradiation, and it has been documented that the shape and size of the nanostructures both have a significant effect on activity. The controlled fabrication of the *m*- BiVO_4 nanostructure generally requires harsh conditions: high temperature, long reaction time, and the addition of organic additives or a template. Combined MW/US irradiation is an attractive technique here as it enables the preparation of BiVO_4 nanoparticles with an average size of 150 nm at pH = 2. At higher pH values, the growth process leads to microspheres with a diameter of 3 μm (pH = 8) [49]. Different shapes were obtained with different solvents leading to a variety of nanostructures with differing optical properties and photocatalytic activity. The optimised procedure for BiVO_4 micro-/nanostructure preparation is performed in a MW/US combined reactor at 110 $^\circ\text{C}$ (HC-300A, Beijing Xianghu Technology Co., Ltd., MW power 500 W, US 800 W, 2 s sonication and 1 interruption).

Cadmium sulphide (CdS) is an important direct band gap material that is widely used for optoelectronic applications. The preparation of the pure crystal is an object

of interest in the fields of non-linear optical devices, lasers, thin-film transistors, light emitting diodes and also hydrothermal processes. Guo et al. used SMUI to control the syntheses of high-purity nanostructures [50]. CdCl_2 and either $\text{CS}(\text{NH}_2)_2$ or $\text{C}_2\text{H}_5\text{NS}$ and sulphur were dissolved in ethylene glycol and heated at 140°C for 45 min by MW irradiation and sonicated in pulsed mode with a titanium horn. The CdS obtained was deeply characterised and hexagonal wurtzite crystals combined to obtain a nanoflower. A mixture of hexagonal and triangular pyramid nanostructures was observed when MW irradiation was used alone. The photoluminescence spectra of the obtained CdS showed a large blue shift in the flower nanostructure as compared to the simple 2D CdS nanostructure. In 2010, the same authors applied the optimised procedure to the preparation of Ag-doped CdS nanoparticles in an attempt to enhance their efficacy as photocatalysts [51]. CdS was doped with 1, 3 and 5% Ag^+ , which led to spherical crystals of $\sim 5\text{--}15\text{ nm}$ being obtained. This work investigated the contribution of US and MW to the phase evolution and it was observed that MW alone cannot induce chemical reaction while simultaneous pulsed US allows Ag to dissolve into the CdS matrix. The photocatalytic degradation of rhodamine B occurs under visible light irradiation and only showed a slight improvement over the doped material when compared to CdS because the doping ratio was not optimal.

Goethite and akaganeite are ferric oxyhydroxides (α - and β - FeOOH) employed in the degradation of organic compounds with hydrogen peroxide under relatively weak UV irradiation. Xu et al. published a paper on the preparation of α - FeOOH via the SMUI of a $\text{FeCl}_3\cdot 6\text{H}_2\text{O}$ solution in urea and deionised water [52]. A high-intensity ultrasonic probe (from Xinzhi Co., China, JY92-2D) with a 10-mm-diameter titanium horn of 20 kHz in a pulsed mode was used in this process. It had a duty cycle of 1 s and was directly immersed 1 cm into the solution. For the sake of comparison, the akaganeite was also prepared under conventional conditions, under US and MW irradiation alone and using the combined method. The samples were all characterised by XRD and TEM. It was shown that morphologies depended greatly on the heating technique. As already observed for the preparation of $\text{Pb}(\text{OH})\text{Br}$ nanowires, the crystals are biggest under conventional conditions, while the smallest are obtained under SMUI. US used alone reduces crystal size and aggregation, while larger agglomeration was observed under MW irradiation alone. The β - FeOOH sample, prepared using SMUI (MW 400 W, US 200 W) at 70°C for 3 h, gave the highest catalytic activity under visible light irradiation and shows promise for use in practical photo-Fenton-like processes, which degrade organic pollutants (Table 1).

Transition metal oxides such as iron and titanium oxide show superior thermoelectric properties and high stability. Combining oxides with conducting

Table 1 Comparison of conventional heating, MW, US and SMUI in the synthesis of β - FeOOH

Preparation technique	Width (nm)	Length (nm)
Conventional condition	75	250
MW	25	80
US	50	175
MW-US combined	35	35

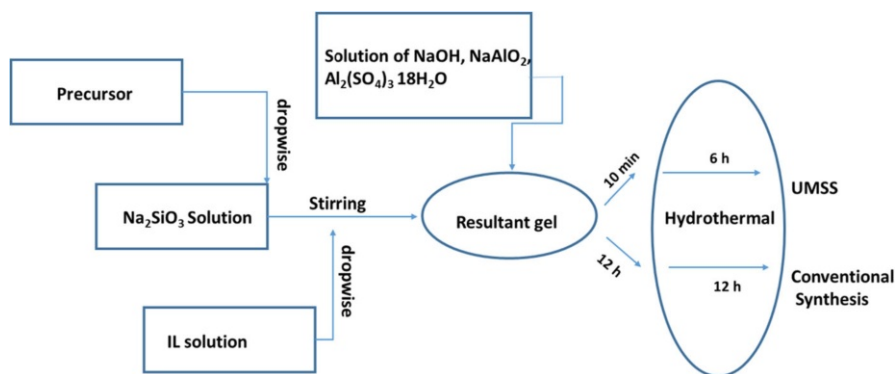


Fig. 17 Schematic representation of micro-mesoporous zeolite Y synthesis by SMUI and conventional synthesis

materials, such as graphene, or doping polymers with graphene and an oxide provides significant increases in electric conductivity, as demonstrated by Dey et al. [53–55]. MW/US irradiation was used sequentially to obtain excellent oxide nanoparticle (TiO_2 and Fe_2O_3) dispersion over graphene. Anatase TiO_2 nanoparticles were supported on graphene and the composite was studied as a burn rate enhancer and a combustion catalyst for the decomposition of ammonium perchlorate. The graphene- TiO_2 and Fe_2O_3 nanocomposites were then dispersed in 20% polyvinyl acetate and used successfully as thermoelectric polymers.

The MW/US combination has also been used for the preparation of zeolite with the aim of making it mesoporous and improving its catalytic activity [56]. The strategy for the preparation was based on the addition of an ionic liquid (1-methyl-3-[3'-(trimethoxysilyl) propyl] imidazolium chloride) for use as a mesoporous structure directing template (Fig. 17). SMUI facilitated the hydrothermal crystallisation of the Al silicate gel containing IL at 80 °C for 10 min (200 W) and did so in a shorter crystallisation time than the conventional process. A detailed characterisation of the zeolite showed that the structure obtained under SMUI had increased surface area and pore volume. The micro-mesoporous zeolite exhibited a well-dispersed, cauliflower-like morphology and a more uniform particle size. Catalytic activity was investigated on the alkylation reaction of styrene with *o*-xylene. The SMUI-obtained catalyst gave higher yields as well as improved stability and reusability.

Nano-hydroxyapatite has been obtained using the combined MW-US technique, which was used with an eye to improving its performance in adsorbing fluorine from contaminated water [57, 58]. The two published procedures solubilised $\text{Ca}(\text{NO}_3)_2 \cdot 4\text{H}_2\text{O}$ in water at pH values from 10.8 to 9.0. After the addition of KH_2PO_4 or $(\text{NH}_4)_2\text{HPO}_4$, the sample was treated with SMUI until a white agglomerate mass was produced. One of the procedures pre-treated the mixture with US (50 W, 30 Hz) for 1 h before SMUI. Ultrafine and highly crystalline particles of uniform size were obtained.

The sorption capacity of nano-HAp for the removal of fluoride ions from test solutions of fluorine in water was found to be higher than that of other synthetic nano-

HAp materials reported in the literature. Analogously, Liang et al. obtained mesoporous hydroxyapatite nanoparticles using SMUI [59]. In this publication, it was found that flake-like morphology without a mesoporous structure was recovered at low MW power and temperature (10–50 °C), while a clear mesoporous derivative was observed when the reaction was carried out from 50 to 90 °C. An increase in MW power, from 50 to 200 W, furnished a more mesoporous structure, whereas prolonging the MW irradiation from 10 to 30 min did not influence the morphology of the nanoparticles.

5 Plant Extraction

Both MW-assisted extraction (MAE) and US-assisted extraction (UAE) have been used independently in the extraction of vegetable matrices [60] and in efficient green extractions [61]. US alone improves extraction as cavitation disrupts cell walls, thereby releasing soluble components into the solution and increasing mass transfer. MW causes efficient in-core heating and promotes the migration of dissolved ions and polar species. Combined irradiation increases the solubility, and hence yields, of extracted compounds and requires less time than either source alone. Prolonged irradiation, however, may lead to the partial degradation of sensitive molecules. Simultaneous irradiation has thus been successfully employed in the extraction of essential oils from soybean germ and marine microalgae [62].

6 Conclusion

A number of papers have reported on environmentally friendly applications that use combined MW-US irradiation in a number of fields, including organic/inorganic synthesis, pollutant degradation, chemical digestion and even plant extraction. Besides nanoparticle preparation and heterogeneous phase reactions, a predictable reaction rate enhancement under SMUI is expected for radical reactions. MW and US generate hot spots, and these harsh localised conditions promote the formation of reactive radicals and electron-transfer paths. The present review summarises such developments and gives insight into future possibilities in particular in nanoparticle preparation and heterogeneous catalysis. Process implementation and scale-up to pilot plants have also been highlighted, although industrial applications will need a specialised engineering design. We believe that, as time passes, non-conventional hyphenated techniques and hybrid reactors will be recognised still further as a powerful ally to green synthetic chemistry and beyond.

Acknowledgements The University of Turin is warmly acknowledged for its financial support (Fondi Ricerca Locale 2015).

References

1. Maeda M, Amemiya H (1995) Chemical effects under simultaneous irradiation by microwaves and ultrasound. *New. J Chem* 19:1023–1028

- Cravotto G, Cintas P (2007) The combined use of microwaves and ultrasound: new tools in process chemistry and organic synthesis. *Chem Eur J* 13:1902–1909
- Cravotto G, Borretto E, Oliverio M, Procopio A, Penoni A (2015) Catalysis in water or biphasic aqueous systems under sonochemical conditions. *Catal Commun* 63:2–9
- Cintas P, Cravotto G, Canals A (2012) Combined ultrasound-microwave technologies, in *Handbook on Applications of Ultrasound: Sonochemistry for Sustainability*. CRC Press, Boca Raton, pp 659–673
- Cravotto G, Cintas P (2006) Power ultrasound in organic synthesis: moving cavitation chemistry from academia to innovative and large-scale applications. *Chem Soc Rev* 35:180–196
- Cravotto G, Garella D, Calcio Gaudino E, Lévêque JM (2008) Microwaves-ultrasound coupling: a tool for process intensification in organic synthesis. *Chem Today* 26:39–41
- Chemat F, Poux M, Di Martino JL, Berlan J (1996) An original microwave-ultrasound combined reactor suitable for organic synthesis: application to pyrolysis and esterification. *J Microwav Power Electromagn Energy* 31:19–22
- Cravotto G, Beggiato M, Penoni A, Palmisano G, Tollari S, Lévêque JM, Bonrath W (2005) High-intensity ultrasound and microwave, alone or combined, promote Pd/C-catalyzed aryl-aryl couplings. *Tetrahedron Lett* 46:2267–2271
- Cravotto G, Di Carlo S, Curini M, Tumiatti V, Roggero C (2007) A new flow reactor for the treatment of polluted water with microwave and ultrasound. *J Chem Technol Biotech* 82:205–208
- Wu Z, Ondruschka B, Cravotto G (2008) Degradation of phenol under combined irradiation with microwaves and ultrasound. *Environ Sci Technol* 42:8083–8087
- Ragaini V, Pirola C, Borrelli S, Longo I (2012) Simultaneous ultrasound and microwave new reactor: detailed description and energetic consideration. *Ultrason Sonochem* 19:872–876
- Otteson D, Michl J (1984) A procedure for gas-phase dehalogenation of organic dihalides with alkali metal vapors using microwave and/or ultrasound excitation and matrix isolation of products. *J Org Chem* 49:866–873
- Cravotto G, Rinaldi L, Carnaroglio D (2015) Efficient Catalysis by combining Microwaves with other enabling Technologies, Chapt. 8 in *Microwaves in Catalysis* Ed. Horikoshi S, Serpone N, Wiley-VCH Verlag GmbH & Co. KGaA Boschstr. 12, 69469 Weinheim, Germany
- Martinez-Guerra E, Gnanaswar Gude V (2014) Synergistic effect of simultaneous microwave and ultrasound irradiations on transesterification of waste vegetable oil. *Fuel* 137:100–108
- Martinez-Guerra E, Gnanaswar Gude V (2014) Transesterification of used vegetable oil catalyzed by barium oxide under simultaneous microwave and ultrasound irradiations. *Energy Convers Manage* 88:633–640
- Martinez-Guerra E, Gude VG (2016) Alcohol effect on microwave-ultrasound enhanced transesterification reaction. *Chem. Eng Process* 101:1–7
- Ardebili SMS, Hashjin TT, Ghobadian B, Najafi G, Mantegna S, Cravotto G (2015) Optimization of biodiesel synthesis under simultaneous ultrasound-microwave irradiation using response surface methodology (RSM). *Green Process Synth* 4:259–267
- Palmisano G, Bonrath W, Boffa L, Garella D, Barge A, Cravotto G (2007) Heck reactions with very low ligandless catalyst loads accelerated by microwaves or simultaneous microwaves/ultrasound irradiation. *Adv Synth Catal* 349:2338–2344
- Sacco M, Charnay C, De Angelis F, Radoiu M, Lamaty F, Martinez J, Colacino E (2015) Microwave-ultrasound simultaneous irradiation: a hybrid technology applied to ring closing Metathesis. *RSC Adv*. 5:16878–16885
- Palmisano G, Tagliapietra S, Binello A, Boffa L, Cravotto G (2007) Efficient regioselective opening of epoxides by nucleophiles in water under simultaneous ultrasound/microwave irradiation. *Synlett* 2007:2041–2044
- Cintas P, Martina K, Robaldo B, Garella D, Boffa L, Cravotto G (2007) Improved protocols for microwave-assisted Cu(I)-catalyzed Huisgen 1,3-dipolar cycloadditions. *Collect Czech Chem Commun* 72:1014–1024
- Cintas P, Barge A, Tagliapietra S, Boffa L, Cravotto G (2010) Alkyne-azide click reaction catalyzed by metallic copper under ultrasound. *Nat Protocol* 5:607–616
- Peng Y, Song G (2003) Combined microwave and ultrasound accelerated Knoevenagel-Doebner reaction in aqueous media: a green route to 3-aryl acrylic acids. *Green Chem* 5:704–706
- Peng Y, Song G (2002) Combined microwave and ultrasound assisted Williamson ether synthesis in the absence of phase-transfer catalysts. *Green Chem* 4:349–351

25. Peng Y, Song G (2001) Simultaneous microwave and ultrasound irradiation: a rapid synthesis of hydrazides. *Green Chem* 3:302–304
26. Wu Z, Ondruschka B, Cravotto G, Garella D, Asgari J (2008) Oxidation of primary aromatic amines under irradiation with ultrasound and/or microwaves. *Synth Commun* 38:2619–2624
27. Garella D, Tagliapietra S, Metha VP, Van der Eycken E, Cravotto G (2010) Straightforward functionalization of 3,5-Dichloro-2-pyrazinones under simultaneous microwave and ultrasound irradiation. *Synthesis* 2010:136–140
28. Cravotto G, Boffa L, Levêque JM, Estager J, Draye M, Bonrath W (2007) A speedy one-pot synthesis of second-generation ionic liquids under ultrasound and/or microwave irradiation. *Aust J Chem* 60:946–950
29. Domini C, Vidal L, Cravotto G, Canals A (2009) A simultaneous, direct microwave/ultrasound-assisted digestion procedure for the determination of total Kjeldahl nitrogen. *Ultrason Sonochem* 16:564–569
30. Cui Y, Lieber CM (2001) Functional nanoscale electronic devices assembled using silicon nanowire building blocks. *Science* 291:851–853
31. Boffa L, Tagliapietra S, Cravotto G (2013) Combined energy sources in the synthesis of nanomaterials in Microwaves 55–74. Chapt. 4 in *Nanoparticle Synthesis—Fundamentals and Applications*. Ed. Horikoshi S, Serpone N, Wiley-VCH Verlag GmbH & Co. KGaA Boschstr. 12, 69469 Weinheim
32. Bang JH, Suslick KS (2010) Application of ultrasound to the nanostructured materials. *Adv Mater* 22:1039–1059
33. Colmenares JC (2014) Sonication-induced pathways in the synthesis of light-active catalysts for photocatalytic oxidation of organic contaminants. *ChemSusChem* 7:1512–1527
34. Cravotto G, Boffa L (2014) Combined Ultrasound-Microwave irradiation for the preparation of nanomaterials, 203–226. Chapt. 7. In: Sivakumar M, Ashokkumar M (eds.) *Cavitation—a novel energy efficient technique for the generation of nanomaterials*. Pan Stanford Publishing Pte Ltd., eBook ISBN: 978-981-4411-55-4
35. Feng H, Li Y, Lin S, Van der Eycken E, Song G (2014) Nano Cu-catalyzed efficient and selective reduction of nitroarenes under combined microwave and ultrasound irradiation. *Sustain Chem Process* 2:14–19
36. Wu Z, Cherkasov N, Cravotto G, Borretto E, Ibhaddon AO, Medlock J, Bonrath W (2015) Ultrasound- and microwave-assisted preparation of lead-free palladium catalysts: effects on the kinetics of diphenylacetylene semi-hydrogenation. *ChemCatChem* 7:952–959
37. Zhu HT, Zhang CY, Tang YM, Wang JX (2007) Novel synthesis and thermal conductivity of CuO nanofluid. *J Phys Chem C* 111:1646–1650
38. Shen X-F (2009) Combining microwave and ultrasound irradiation for rapid synthesis of nanowires: a case study on Pb(OH)Br. *J Chem Technol Biotechnol* 84:1811–1817
39. Guo QJ, Ford GM, Yang WC, Walker BC, Stach EA, Hillhouse HW, Agrawal R (2010) Fabrication of 7.2% efficient CZTSSe solar cells using CZTS nanocrystals. *J Am Chem Soc* 132:17384–17386
40. Zhou YL, Zhou WH, Du YF, Li M, Wu SX (2011) Sphere-like kesterite Cu₂ZnSnS₄ nanoparticles synthesized by a facile solvothermal method. *Mater Lett* 65:1535–1537
41. Wang Y, Gong H (2011) Cu₂ZnSnS₄ synthesized through a green and economic process. *J Alloy Compd* 509:9627–9630
42. Madiraju VA, Taneja K, Kumar M, Seelaboyina R (2016) CZTS synthesis in aqueous media by microwave irradiation. *J Mater Sci: Mater Electron* 27:3152–3157
43. Wang W, Shen H, Yao H, Li J, Jiao J (2015) Influence of solution temperature on the properties of Cu₂ZnSnS₄ nanoparticles by ultrasound-assisted microwave irradiation. *J Mater Sci Mater El* 26:1449–1454
44. Long F, Chi S, He J, Wang J, Wu X, Mo S, Zou Z (2015) Synthesis of hexagonal wurtzite Cu₂ZnSnS₄ prisms by an ultrasound-assisted microwave solvothermal method. *J Solid State Chem* 229:228–234
45. Zheng Y, Tan J, Huang L, Tan D, Li Y, Lin X, Huo S, Lin J, Wang Q (2013) Sonochemistry-assisted microwave synthesis of nano-sized lanthanide activated phosphors with luminescence and different microstructures. *Mater Lett* 113:90–92
46. Si W, Ding C, Ding S (2014) Synthesis and characterization of YAG nanoparticles by ultrasound-assisted and ultrasound-microwave-assisted alkoxide hydrolysis precipitation methods. *J Nanomater* 2014:8, Art ID 408910. doi:10.1155/2014/408910
47. Li H, Liu E, Chan FYF, Lu Z, Chen R (2011) Fabrication of ordered flower-like ZnO nanostructures by a microwave and ultrasonic combined technique and their enhanced photocatalytic activity. *Mater Lett* 65:3440–3443

48. Luo C-X, Liu J-K, Lu Y, Du C-S (2012) Controllable preparation and sterilization activity of zinc aluminium oxide nanoparticles. *Mater Sci Eng C* 32:680–684
49. Zhang Y, Li G, Yang X, Yang H, Lu Z, Chen R (2013) Monoclinic BiVO₄ micro-/nanostructures: microwave and ultrasonic wave combined synthesis and their visible-light photocatalytic activities. *J Alloy Compd* 551:544–550
50. Tai G, Guo W (2008) Sonochemistry-assisted microwave synthesis and optical study of single-crystalline CdS nanoflowers. *Ultrason Sonochem* 15:350–356
51. Ma J, Tai G, Guo W (2010) Ultrasound-assisted microwave preparation of Ag-doped CdS nanoparticles. *Ultrason Sonochem* 17:534–540
52. Xu Z, Yu Y, Fang D, Xu J, Liang J, Zhou L (2015) Microwave–ultrasound assisted synthesis of β -FeOOH and its catalytic property in a photo-Fenton-like process. *Ultrason Sonochem* 27:287–295
53. Dey A, Panja S, Sikder AK, Chattopadhyay S (2015) One pot green synthesis of graphene–iron oxide nanocomposite (GINC): an efficient material for enhancement of thermoelectric performance. *RSC Adv* 5:10358–10364
54. Dey A, Hadavale S, Khan MAS, More P, Khanna PK, Sikder AK, Chattopadhyay S (2015) S Polymer based graphene/titanium dioxide nanocomposite (GTNC): an emerging and efficient thermoelectric material. *Dalton Trans* 44:19248–19255
55. Dey A, Nangare V, More PV, Shageeulla Khna MA, Khanna PV, Kanti Sikder A, Chattopadhyay S (2015) A graphene titanium dioxide nanocomposite (GTNC): one pot green synthesis and its application in a solid rocket propellant. *RSC Adv* 5:63777–63785
56. Fu X, Sheng X, Zhou Y, Fu Z, Zhao S, Zhang Z, Zhang Y (2016) Ultrasonic/microwave synergistic synthesis of well-dispersed hierarchical zeolite Y with improved alkylation catalytic activity. *Korean J Chem Eng* 33:1931–1937
57. Poinerna GEJ, Ghoshc MK, Nga Y-J, Issa TB (2011) Defluoridation behavior of nanostructured hydroxyapatite synthesized through ultrasonic and microwave combined technique. *J Hazard Mater* 185:29–37
58. Zou Z, Lin K, Chen L, Chang J (2012) Ultrafast synthesis and characterization of carbonated hydroxyl apatite nanopowders via sonochemistry-assisted microwave process. *Ultrason Sonochem* 19:1174–1179
59. Liang T, Qian J, Yuan Y, Liu C (2013) Synthesis of mesoporous hydroxyapatite nanoparticles using a template-free sonochemistry-assisted microwave method. *J Mater Sci* 48:5334–5341
60. Cravotto G, Cintas P (2007) Chapter 3: Extraction of flavourings from natural sources. In: Taylor A, Hort J (eds) *Modifying flavour in food*. Woodhead Publishing Ltd./CRC Press, Cambridge, pp 41–63. ISBN: 978-1-84569-074-8
61. Chemat F, Abert-Vian M, Cravotto G (2012) Review: green extraction of natural products: concept and principles. *Int J Mol Sci* 13:8615–8627
62. Cravotto G, Boffa L, Mantegna S, Perego P, Avogadro M, Cintas P (2008) Improved extraction of natural matrices under high-intensity ultrasound and microwave, alone or combined. *Ultrason Sonochem* 15:898–902

Ultrasound in Combination with Ionic Liquids: Studied Applications and Perspectives

Gregory Chatel^{1,2} 

Received: 3 June 2016 / Accepted: 12 July 2016 / Published online: 26 July 2016
© Springer International Publishing Switzerland 2016

Abstract Ionic liquids (ILs) as reaction media, and sonochemistry (US) as activation method, represent separately unconventional approaches to reaction chemistry that, in many cases, generate improvements in yield, rate and selectivity compared to traditional chemistry, or even induce a change in the mechanisms or expected products. Recently, these two technologies have been combined in a range of different applications, demonstrating very significant and occasionally surprising synergetic effects. In this book chapter, the advantages and limitations of the IL/US combination in different chemical applications are critically reviewed in order to understand how, and in which respects, it could become an essential tool of sustainable chemistry in the future. Fundamental aspects and practical considerations of the combination are discussed to better control and demonstrate the brought synergetic effects.

Keywords Sonochemistry · Ultrasound · Ionic liquids · Solvents · Cavitation · Green chemistry

This article is part of the Topical Collection “Sonochemistry: From basic principles to innovative applications”; edited by Juan Carlos Colmenares Q., Gregory Chatel.

✉ Gregory Chatel
gregory.chatel@univ-smb.fr

¹ Institut de Chimie des Milieux et Matériaux de Poitiers (IC2MP), Université de Poitiers, CNRS, 1 rue Marcel Doré, Bât. 1 ENSIP, 86073 Poitiers Cedex 9, France

² Present Address: Laboratoire de Chimie Moléculaire et Environnement (LCME), Université Savoie Mont Blanc, 73376 Le Bourget du Lac Cedex, France

1 Introduction

The combination of ultrasound with other innovative technologies starts to bring some synergetic effects (note that synergetic effects are defined as greater effects than the sum of parts considered separately). Some exciting routes are reported in this book by coupling ultrasound irradiation with microwave, electrochemistry or enzymes. This chapter is focusing on the combination of power ultrasound with ionic liquids as solvents.

In the recent years, the use of ionic liquids (often abbreviated “ILs”), salts with low or no melting point (typically less than 100 °C at atmospheric pressure), have attracted a lot of attention in different areas of chemistry, especially from the green chemistry community [1]. ILs have indeed been identified as a new class of solvents offering opportunities to transfer the traditional chemical processes to new, clean and eco-friendly technologies [2]. ILs present some unique properties often unavailable with traditional solvents including, in various cases, negligible vapour pressure, air and moisture stabilities, high polarity, chemical and electrochemical stabilities, etc. [3, 4].

Their applications as reaction media is an area of very active research, and new approaches involving ILs have been proposed for aspects of organic and pharmaceutical chemistry [5], preparation of materials [6], analytical chemistry [7], energy chemistry [8], electrochemistry [9], microextraction [10], biomass valorization [11], etc. Holbrey and Seddon made the estimation of nearly one million simple ILs that can be easily prepared in the laboratory, leading to 10^{18} possible ILs, and even more if multi-ionic systems are considered [12, 13]. This represents a great advantage in terms of tunability for these solvents, but also a limiting drawback in terms of the lack of theoretical and fundamental data about their properties to guide their use.

The most used ILs are generally composed of a bulky organic cation (ammonium, phosphonium and sulfonium) with an alkyl chain associated to an organic or inorganic anion (several cations and anions in the case of Double-Salt Ionic Liquids, DSILs [13]). The synthesis of ILs is generally performed through the first alkylation of an amine or phosphine (through a quaternization reaction, called Menshutkin reaction) or sulfide leading to an intermediate salt, followed by anion exchange with a Lewis acid, a metal salt, a Brønsted acid or via an ion exchange resin (Fig. 1) [2–4]. The purification of ILs during and after their synthesis is a

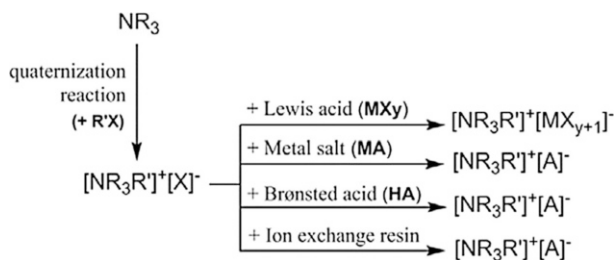


Fig. 1 Principle of the synthesis of ammonium based ILs

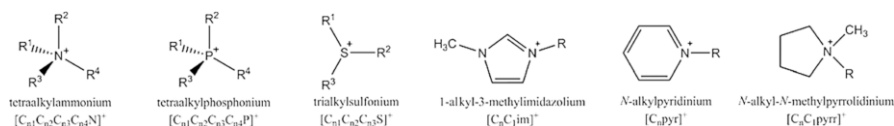


Fig. 2 Main used cations in ILs

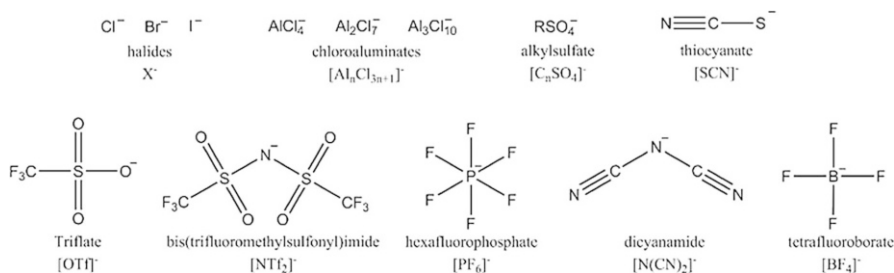


Fig. 3 Main used anions in ILs

challenging step since impurities can have important effects, even at trace levels, for example when biomass is involved in ILs-based processes [14].

The most commonly used cations are 1-alkyl-3-methylimidazolium, 1-alkylpyridinium, 1-alkyl-1-methylpyrrolidinium, tetraalkylammonium, tetraalkylphosphonium and trialkylsulfonium (Fig. 2) and the common anions are chlorides, chloroaluminates, hexafluorophosphate, tetrafluoroborate, triflate (or trifluoromethanesulfonate), thiocyanate, dicyanamide, bis(trifluoromethylsulfonyl)imide, etc. (Fig. 3). The alphanumeric nomenclature allows naming an IL as a function of the cation and its alkyl chain and the nature of the anion [4]. For example, the 1-butyl-3-methylimidazolium chloride is noted $[C_4C_1im]Cl$ and *N*-octylpyrrolidinium hexafluorophosphate is noted $[C_8pyrr][PF_6]$.

Ionic liquid media as well as sonochemistry are two technologies recently widely developed in different fields of chemistry. Often, their uses in a reaction or process produce improvements in terms of efficiency, selectivity, yield, reaction time, recycling, and/or, in some cases, other unexpected results. The idea of combining these two efficient technologies was innovative and produced clear synergies in some cases, but it is important to look closely at the literature to understand how this unique combination can be optimized as a highly effect approach to a number of chemical processes [15]. To better understand how the IL/US combination has developed recently, we studied publications reporting the combined use of these two technologies (Fig. 4). Thus, the main applications involving the ILs/ultrasound combination are about: (1) the use of ultrasound for the synthesis of ILs; (2) the synergetic effects found in organic chemistry; (3) for materials preparation (catalysts, nanoparticles, nanotubes, etc.); (4) for extraction and micro-extraction; (5) for biomass processing such as dissolution or pretreatment of lignocellulosic feedstocks and (6) others applications (electrochemistry, sonochemical degradation of ILs, fundamental studies, etc.).

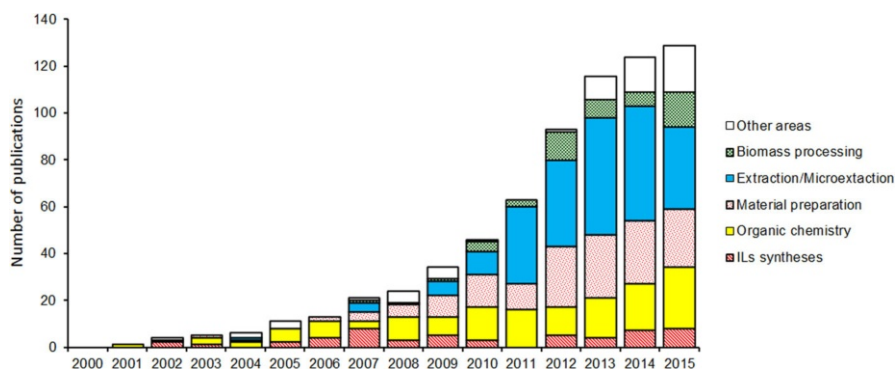


Fig. 4 Evolution of publications found for “ionic liquid and ultrasound” SciFinder® search, classified by applications and by year. (Data of June, 2016). Publications dealt with ultrasonic velocity in ILs were not included in this diagram (about 18 % of total publications)

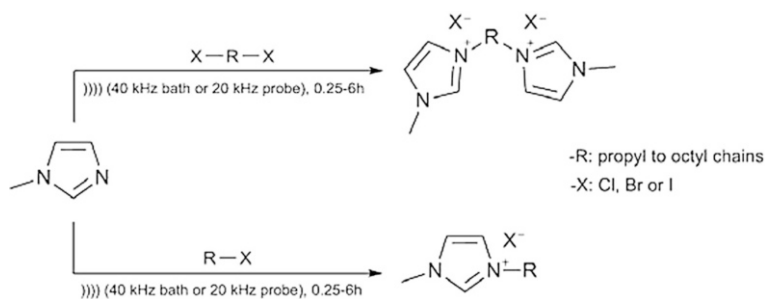


Fig. 5 Synthesis of 1-alkyl-3-methylimidazolium halides under low frequency ultrasonic irradiations [16]

2 Synthesis of Ionic Liquids Under Ultrasound

In the 2000s, Varma's and Lévêque's groups proposed separately the use of ultrasound to improve the synthesis of ILs [16, 17]. The first group developed a solvent-free sonochemical protocol for the preparation of some 1-alkyl-3-methylimidazolium halides ILs, comparing both the use of an ultrasonic bath (40 kHz, 320–881 W), a probe system (20 kHz, 750 W) and oil bath conditions (Fig. 5) [16]. From methylimidazole and chloro-, bromo- and iodoalkanes, yields up to 92 % were obtained in reduced times (from 0.25 to 6 h under US against 25–34 h under traditional conditions). Interestingly, butyl, hexyl and octyl dicationic salts were also efficiently prepared though this method from dihalides.

Lévêque et al. reported the US-assisted synthesis of several 1-butyl-3-methylimidazolium salts ($[\text{BF}_4]^-$, $[\text{PF}_6]^-$, $[\text{OTf}]^-$ and $[\text{BPh}_4]^-$) as shown in Fig. 6 [17]. The maximal isolated yield (80–90 %) was obtained after only 1 h under ultrasound 30 kHz at 20–24 °C (maintained by a cooling bath) while was 30 h were needed in the absence of US at room temperature. Indeed, the salt metathesis (anions exchange) was clearly enhanced under ultrasonic conditions.

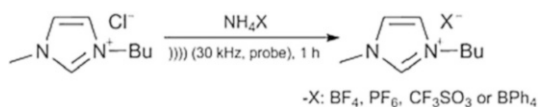


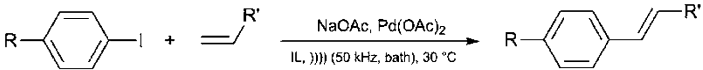
Fig. 6 Synthesis of 1-alkyl-3-methylimidazolium salts under 30 kHz ultrasonic irradiations [17]

The use of ultrasound during the syntheses of ILs were widely reported by Zhao [18] Cravotto [19, 22, 23], Li [20] Varma [21], Lévêque [22, 23], and more recently by Messali [24–28], Punjabi [29] and Moldoveanu [30], leading to important reductions of reaction time compared to traditional methods (called “silent conditions”). For example, Punjabi et al. showed the advantages of ultrasound (40 kHz, nominal power of 115 W) in the three steps of preparation of ILs: (1) *N*-alkylation of imidazole with *n*-butyl lithium in ethanol (3 h, US, room temperature); (2) quaternization of 1-butylimidazole with 1-bromobutane (2.5 h, US, 10 °C); (3) anion metathesis with silver/sodium/potassium salts (US, room temperature to 50 °C) [29]. Some reviews have also discussed the use of low-frequency ultrasound or/and microwaves as activation methods for ILs syntheses [31–33]. Interestingly, Deetlefs and Seddon assessed the green credentials of the syntheses of ILs promoted by US [34]. Indeed, the reduced preparation times induced by cavitation phenomenon, represent a significant green advantage compared to traditional methods, especially when the preparation is performed solvent-free. However, the authors noted that the coloration and slight decomposition sometimes observed when ILs are exposed to ultrasound is an issue [35, 36]. From an industrial point of view, this could be very limiting since the purification and decolorization of the salts that is required as a consequence leads to poor E-factors. In resume, the main challenge for the US-assisted synthesis of ILs is the scale-up, in regards to the possible slight degradation of the ILs under ultrasound and the optimization of ultrasound based processes.

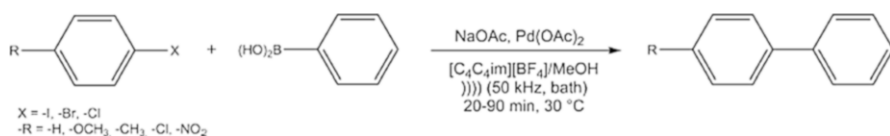
3 Applications in Different Fields of Chemistry

3.1 Organic Sonochemistry

The first example of ILs-based organic sonochemistry was reported by Srinivasan et al. [37] to promote C–C bond formation via a Heck reaction under ambient conditions in 1,3-di-*n*-butylimidazolium bromide ([C₄C₄im]Br) and 1,3-di-*n*-butylimidazolium tetrafluoroborate ([C₄C₄im][BF₄]) with an ultrasonic cleaning bath (50 kHz) [37]. The ultrasound assisted Heck reaction of the iodobenzenes with alkenes at 30 °C showed complete conversion in less than 3 h to afford the desired products in excellent isolated yields (73–87 %, Table 1). No reaction under similar ultrasonic conditions was observed when the ILs were replaced by molecular solvents such as dimethylformamide (DMF) and *N*-methyl-2-pyrrolidone (NMP) and no product, even at a trace level, was observed under ambient conditions in the absence of ultrasound. This example confirmed that both IL and US are required for

Table 1 Heck reaction of iodobenzenes with activated alkenes under 50 kHz in $[C_4C_4im]Br/[C_4C_4im][BF_4]$ ILs [37]


Entry	R	R'	Sonication time (h)	Isolated yield (%)
1	-H	-COOMe	2.0	81
2	-H	-COOEt	1.5	87
3	-H	-Ph	1.5	82
4	-OMe	-COOMe	3.0	82
5	-OMe	-COOEt	3.0	79
6	-OMe	-Ph	3.0	80
7	-Cl	-COOMe	1.5	79
8	-Cl	-COOEt	1.5	77
9	-Cl	-Ph	1.5	73

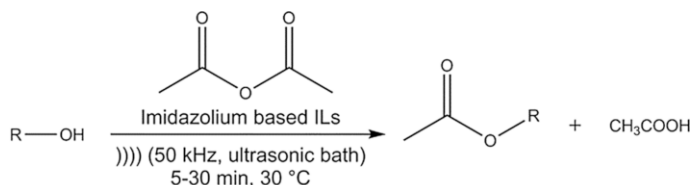
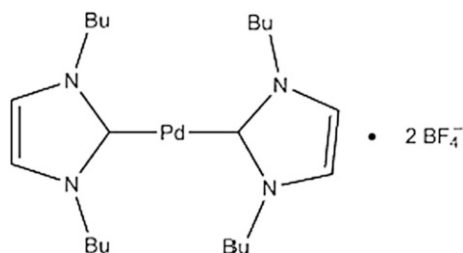
**Fig. 7** Suzuki coupling reaction in $[C_4C_4im][BF_4]$ under 50 kHz ultrasonic irradiations [39]

the reaction, showing an enhancement of reaction rates and a decrease of reaction times, compared to the classical and silent conditions.

The same research group reported several organic reactions in an ultrasonic cleaning bath (50 kHz) such as the nitration of phenols [38], the Suzuki cross-coupling [39], the synthesis of 3,4-dihydropyrimidin-2-(1*H*)-ones [40], the acetylation of alcohols [41], the synthesis of 1,8-dioxo-octahydro-xanthene derivatives [42] and the Sonogashira reaction [43]. For all these reactions, authors systematically compared their results to those under silent conditions during several hours in the IL medium and under sonication in molecular solvents such as acetonitrile, methanol, ethanol, THF, DMSO, hexadecane, PEG-400 and/or dichloromethane to show the synergetic effect brought by IL/US combination.

For example, the Suzuki coupling reaction in $[C_4C_4im][BF_4]$ under ultrasonic conditions showed significant conversions (42–52 % from chlorobenzenes, 82–92 % from bromo- and iodo-benzenes, see Fig. 7) [39]. The coupling reaction of iodobenzene with phenylboronic acid performed at 30 °C in the absence of ultrasound showed only 25 % conversion even after 10 h vs. 92 % after 20 min under US. The authors explained these results by the acceleration of the formation of a Pd-biscarbene complex from interaction of the Pd and the $[C_4C_4im]^+$ cation and the subsequent in situ generation of a zero-valent Pd-species as the active catalyst (Fig. 8).

Fig. 8 Pd-biscarbene complex proposed by Srinivasan et al. [39]



-R: aryl alkyl, alkyl, cinnamyl, carbohydrates, ...

Fig. 9 Sonochemical O-acetylation of alcohols in $[C_4C_4im]$ based ILs [41]

The choice of the IL can be crucial. For example, the sonochemical O-acetylation of alcohols (50 kHz, 120 W output power, ultrasonic bath) performed in imidazolium based ILs (Fig. 9) in the absence of any catalyst was tested in other types of ILs such as ethylammonium nitrate and 1-*n*-butylpyridium tetrafluoroborate [41]. In these conditions, the conversion decreased to less than 50 % even after several hours of sonication, while 80–95 % isolated yields was obtained in 5–30 min in the presence of imidazolium based ILs. The authors showed that hydrogen bond (Lewis/Brønsted acid) interaction of the C2-hydrogen of the imidazolium cation with the oxygen of the acetic anhydride was essential in the mechanism of the reaction. In addition, the reaction time decreased under ultrasonic conditions compared to silent ones (4–12 times shorter). The synergistic role of the IL was confirmed by the fact that there was no reaction after several hours in a series of molecular solvents under ultrasonic irradiation [41].

Interestingly, the IL/US combination was also efficient in the phase-transfer catalysis based synthesis of butyl salicylate or mandelic acid [44, 45]. For example, mandelic acid was prepared under ultrasound (40–80 kHz, input power of 120 W) in $[C_4C_1im][PF_6]$ from benzaldehyde with chloroform in the presence of tetrabutyl ammonium bromide as a phase transfer catalyst [44]. In the absence of ultrasound, the reaction must be performed for 8 h to produce only 42 % yield, while it reached 90 % after 2 h under 60 kHz ultrasound irradiation. Here, it is possible that an additional effect of the ultrasound is to increase the dispersion of the phase transfer catalyst, increasing its surface area.

In previous studies, we worked on the epoxidation of cyclohexene, cyclooctene, styrene and α -pinene with good yields in only 1 h in the presence of a manganese tetraphenylporphyrin and hydrogen peroxide, using the hydrophobic

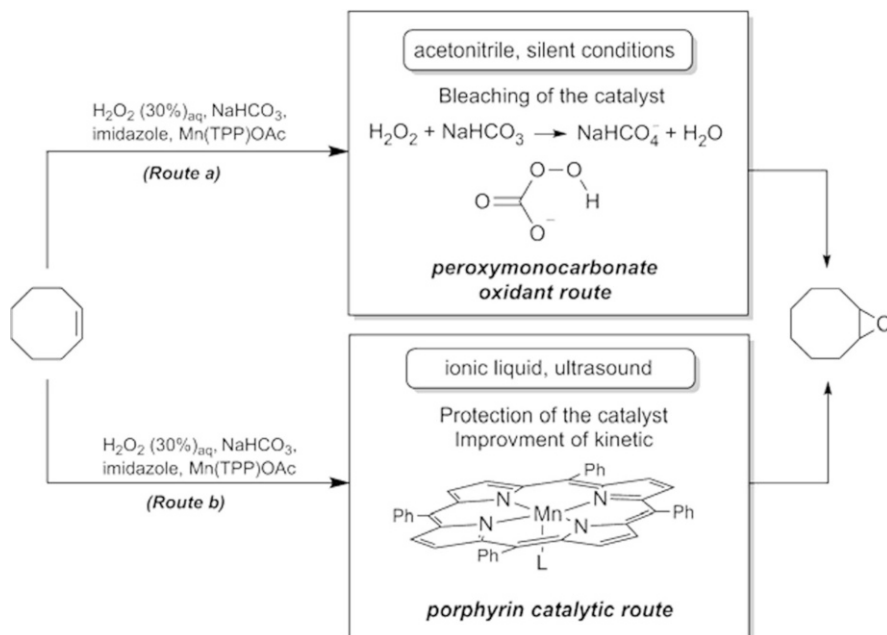


Fig. 10 Proposed routes for olefins epoxidation reaction **a** in acetonitrile/silent conditions and **b** in IL/US conditions [47]

methyloctylpyrrolidinium bis(trifluoromethylsulfonyl)imide ($[\text{C}_8\text{C}_1\text{pyrr}][\text{NTf}_2]$) under 20 kHz ultrasound irradiation [46]. The results suggested a switch of reaction mechanism according to the chosen experimental conditions (Fig. 10): (a) acetonitrile/silent stirring or (b) IL/US activation (Fig. 10). In the first case, the metalloporphyrin was quickly degraded and its recycling was not possible. In the optimized conditions (b), the IL prevented the degradation of the catalyst. Moreover, the reaction time was significantly reduced under US. In the latter conditions, the epoxidation reaction could occur via a classical high-valent oxomanganese porphyrin complex.

To unambiguously prove the proposed routes represented in Fig. 10, a chiral Mn porphyrin complex was used as catalyst for the enantioselective epoxidation of styrene: in the classical conditions (a), the racemic mixture of epoxides was obtained while in the conditions (b), the ultrasonic asymmetric catalysis in IL clearly showed that the mechanism involves the metalloporphyrin catalyst route [47]. Thus, the IL/US combination improved the yields and decreased reaction times, but also involved a new reactivity for this epoxidation reaction.

In summary, it is clear that, in a wide range of organic reactions, the IL/US combination is often described in catalytic reactions as improving the yield, the selectivity and the global efficiency of the process. However, the contribution of physical and/or chemical effects of these outcomes may be several-fold depending on the sonochemical conditions and equipment, as well as the nature of the studied reaction [48–54]. A valid and systematic comparison with classical conditions is

required to prove the true synergy of the IL/US combination. In addition, we recommend all researchers studying these fascinating effects to provide a clear set of control experiments to provide a basis for unambiguous conclusions.

3.2 Material Preparation

The combined use of ILs and US was investigated in the synthesis and the preparation of different materials such as methanofullerene derivatives, [55, 56] graphene sheet [57, 58], nanocrystals (ZnS, ZnO, Sb₂S₃, SnS, etc.) [59–65], nanoparticles (SnO₂, CuS, PbS, CdS, TiO₂, Ag, Fe₂O₃, etc.), [66–72] energetic materials [73, 74], mesoporous silica [75], specific photocatalysts, [76] etc.

For example, a stable graphene suspension was prepared in [C₄C₁im][NTf₂] from a dispersion of graphite under 20 kHz ultrasonic irradiation (60 min) with a high concentration up to 0.95 mg.mL⁻¹ [57]. The preparation of an IL-Pd-graphene nanocomposite was also reported through a sonoelectrochemical route, as an efficient electrochemical sensor for chlorophenols [58]. In this case, the ILs played the role of a linker and enhanced the catalytic activity [77]. Sonication presents known effects on the synthesis and modification of graphene, including the exfoliation of the graphite into discrete graphene sheets, suppressed aggregation in the reduction of graphite oxide compared to classical mechanical stirring [78]. Liu et al. also reported the exfoliation of graphite into graphene sheets in 1-butyl-3-methylimidazolium cholate, and their stable dispersions that were achieved under 20 kHz ultrasonic irradiation [79]. They also applied this technique to achieve a Pd-nanoparticle-graphene hybrid, which was used as a catalyst for CO oxidation [80].

Numerous papers have reported nanoparticle synthesis and stabilization in ILs [81–83], and their sonochemical activation was observed in catalytic processes via dispersion improvement and surface depassivation [84–87]. Associating both technologies led to synergetic effects in many cases. For example, Jin et al. developed a sonochemical method for the preparation of gold nanoparticles capped by a thiol-functionalized IL using hydrogen peroxide as a reducing agent [88]. In this case, ultrasound (40 kHz, 80 W) accelerated the formation of gold nanoparticles and helped their dispersion in the IL. The function of the thiol groups in the selected IL was used to prevent Au⁰ particles from aggregating and the 1-(2',3'-dimercaptoacetoxypyl)-3-methylimidazolium 3''-mercapto-1''-propanesulfonic acid IL controlled the subsequent growth of nanoparticles in the aqueous media, thanks to the thiol groups both in the cation and anion [89]. Behboudnia et al. applied their sonochemical preparation method in a 1-ethyl-3-methylimidazolium ethyl sulfate/water mixture for the synthesis of several nanoparticles such as SnO₂, CuS, PbS, CdS [66–69]. In all cases, the preparation was fast, efficient and led to very small and highly dispersed nanoparticles. Others examples have reported the same advantages in different ILs [70–72].

Recently, Li et al. prepared BiOCl/*m*-BiVO₄ heterojunctions under ultrasound (probably low frequency ultrasound) with different BiOCl content by changing the amount of [C₄C₁im]Cl during the preparation process [90]. Authors reported that the amount of IL has a significant effect on the structures of the obtained samples based on XRD patterns. The surface morphology of the prepared samples was

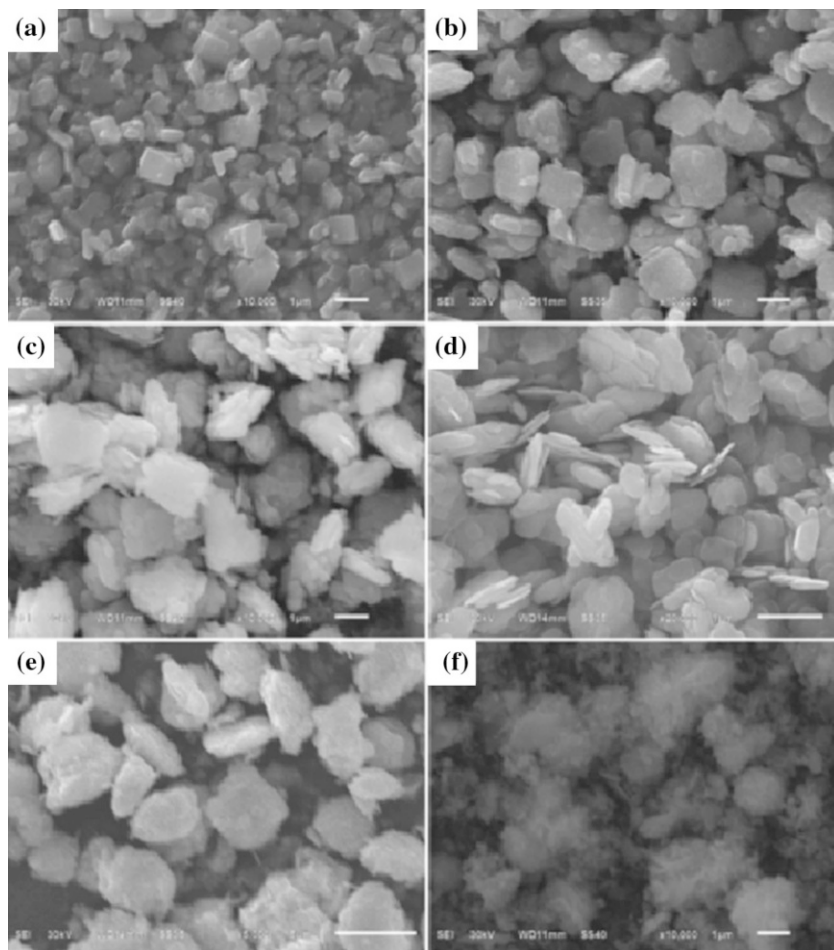


Fig. 11 SEM images of BiOCl/*m*-BiVO₄ heterojunction samples prepared under ultrasound from different amounts of IL: **a** 0 g (blank sample), **b** 1.0 g, **c** 2.0 g, **d** 3.0 g, **e** 4.0 g and **f** 5.0 g [90]

examined by scanning electron microscopy (SEM, Fig. 11). In fact, pure *m*-BiVO₄ consisted of a large number of irregular nanoplates with smooth surfaces. With the proposed method of preparation, square blocks with approximately the same diameters were observed (10–20 nm). TEM and EDS analyses showed that the as-prepared heterostructures are composed of BiOCl nanoparticles growing on the BiVO₄ nanoplates. These materials were efficiently used in photocatalytic reactions, showing a significant improvement activity. In this study, the advantage of using ultrasound was the short preparation time (<2 h), but no specific investigation on the role of US was performed.

In resume, low frequency ultrasonic irradiations have been extensively used for the synthesis of materials in ILs, in particular to improve the dispersion of the

particles. The main consequence of this combination is the reduction of preparation times, and often, a better quality of the synthesized materials.

3.3 Extraction and Microextraction

Nowadays, the extraction and microextraction area represents the main application of IL/US combination [15]. Extensive literature is available in the area and reports some advantages compared to the sometimes laborious, time- and volatile solvent-consuming heat-reflux extraction. In particular, ILs have been widely investigated for extraction processes for their solvation properties, high chemical stability and the tuning opportunities that they offer [91–93]. On another hand, ultrasonic extraction have been also efficiently developed to rapidly extract polysaccharides or active ingredient, as a function of the chosen ultrasonic parameters [94–96]. For some years, the IL/US combination for extraction has become an efficient approach, especially to reduce the reaction time and facilitate the procedures. For example, Cao et al. extracted piperine from white pepper via an ultrasonic pretreatment (ultrasonic bath, 40 kHz) in imidazolium based ILs [97]. The procedure only consisted of treating the sample powder in a water/IL mixture with low frequency ultrasound, and after filtration and dilution, the solution was analyzed by UPLC. No effects attributable to the ILs were observed on peak resolution, elution order and elution time. Liquid-phase micro-extraction for determination of aromatic amines in water samples also used the same kind of procedure showing the performance, simplicity, stability, low cost, ease of operation and low consumption of organic solvents offered by this method [98].

In resume, a synergistic IL/ultrasound combination has been extensively demonstrated in the efficient extraction and microextraction of organic compounds from liquid or solid products, coupled to different analysis techniques such as chemiluminescence detection [99], GC–MS [100, 101], HPLC [102–106], high-speed counter-current chromatography [107], flame atomic absorption spectrometry [108–110], liquid chromatography-quadrupole-linear ion trap-mass spectrometry [111], fluorescence detection [112], etc. The origins of this synergy is certainly related to mass transport effects at the micro- and nano-levels, the ultrasound compensating for the elevated viscosity of the ILs.

3.4 Electrochemical Processes

Ultrasonic electrochemical applications using ILs have also shown some advantages in the recent literature. Hardacre et al. compared the electroreduction of *N*-methylphthalimide to 3-hydroxy-2-methyl-isoindolin-1-one in ILs using phenol as a proton donor under silent and ultrasonic conditions [113]. The rate of electroreduction increased under 25 kHz ultrasound irradiation (3 mm diameter titanium probe, 95 W cm⁻²). It is noted that some darkening of the IL phase was observed during the reaction and the identification by ion chromatography of fluoride from the anion decomposition [113].

Fuchigami et al. worked on the electrochemical fluorination of ethyl α -phenylthioacetate in fluoride and imidazolium based ILs under 45 kHz ultrasound

irradiation via an immersible transducer positioned at the level of the anode during the electrolysis [114, 115]. The mass transfer was improved in these experimental conditions, leading to increased yield and selectivity of the corresponding α -monofluorinated and α,α -difluorinated products, as a function of the imposed current. In addition, sonication changed the stereoselectivity of the anodic fluorination of 4-thiozolidinone.

Electrochemistry and sonochemistry have also been combined, successively, for the synthesis of imidazole-2-thiones [116]. In this case, the electrochemical reduction of 1,3-dialkylimidazolium ILs gave first the corresponding *N*-heterocyclic carbenes that, after reaction with elemental sulfur under ultrasound (22.5 kHz, 100 W), led to 1,3-dialkylimidazole-2-thiones in very high yields in very short times.

In general, low frequency ultrasound activation appears to improve electrochemical processes mainly via stirring effects (increase of mass-transfer coefficients) [117], continuous cleaning of the electrode surface and enhancement of reaction rates [118]. For these reasons, some examples of ultrasonic-electrodeposition processes in ILs were reported by B. Zeng's [119–122] and J. Zheng's [123, 124] research groups.

3.5 Biomass processing

The IL/US combination has been also investigated in the biomass conversion field, since numerous advantages of the use of ILs and US have been widely showed separately [125]. Indeed, IL based strategies allow generally (1) a simple dissolution of cellulose, and possible regeneration for development of advanced materials (2) a direct dissolution of lignocellulosic biomass with separation of major components for direct use of the resulting biopolymers (3) a homogeneous dispersion for a facile depolymerization into low molecular weight chemicals, and (4) a facile pretreatment of wood for the access of enzymes or chemicals to react more easily [126]. Ultrasound irradiation can meet the challenge of processing recalcitrant and multicomponent lignocellulosic biomass, providing a severe physico-chemical environment that is difficult to obtain with other engineering methods. After treatment, no remarkably change in the chemical structure of biomass and in mechanism reactions is generally observed [127], but reaction kinetics are often accelerated, enhancing the efficiency and economic aspect of the biomass conversion processes [128, 129].

In 2007, Mikkola et al. functionalized microcrystalline cellulose, cotton linters and Kraft cellulose in the presence of 2-chloropropanoic acid or 2-chlorobutanoic acid using low frequency ultrasound [130]. The process involved 1-allyl-3-methylimidazolium chloride or 1-butyl-3-methylimidazolium chloride which are able to dissolve the biopolymer in a few minutes (<25 min) under ultrasound. In this case, ultrasound enhanced the dissolution procedure, without any negative effects on the cellulose units.

Rogers et al. also reported that an ultrasonic pretreatment (42 kHz ultrasonic bath, 135 W) improved the dissolution of cellulose in 1-ethyl-3-methylimidazolium acetate ([C₂C₁im][OAc]) [131, 132] and facilitated the separation of lignin and

hemicellulose components in choline acetate ([Cho][OAc]) [133]. The same IL was used by Takahashi et al. for IL/ultrasound-assisted pretreatment and in situ enzymatic saccharification of bagasse [134]. The cellulose and hemicellulose saccharification percentage was 80 and 72 %, respectively, when the in situ saccharification was performed for 48 h in the presence of 10 % [Cho][OAc]. These percentages reached 72 and 53 %, respectively, even in the case of 20 % [Cho][OAc]. In this case, ultrasound was irradiated for 60 min at 24 kHz (output power of 35 W) using an ultrasonic probe in a water bath maintained at 25 °C, only for the first step, improving the pretreatment of bagasse.

Liu et al. used an ultrasonic probe (frequency not indicated, probably less than 50 kHz, 20–75 W) to dissolve cellulose in 1-butyl-3-methylimidazolium chloride ([C₄C₁im]Cl) [135]. The authors showed that ultrasound with high power results in oxidative degradation of the cellulose. Ju et al. explained that ultrasonic treatment improved the solubility of cellulose because it facilitated the penetration and diffusion of 1-allyl-3-methylimidazolium into the structure of the samples [136].

In the biomass conversion area, the most studied application of the IL/US combination is in the pretreatment of cellulose or lignocellulosic biomass to enhance enzymatic reactions [137–144]. ILs could access the cellulose and disrupt the hydroxyl bonds more efficiency during sonication through mass transfer improvement. Yu et al. showed that, in the sonochemical driven enzymatic isomerization of glucose to fructose in imidazolium ILs, the association of the two technologies helped to off-set the disadvantages of the cavitation effect on the enzyme caused by ultrasound as well as the mass transfer limitations caused by the high viscosity of the IL [145].

Hernoux-Villière et al. converted starch-based industrial waste (potato peels) into reducing sugars in 1-allyl-3-methylimidazolium chloride and 1-(4-sulfobutyl)-3-imidazolium chloride [146]. Microwave and low frequency ultrasound activations were investigated to perform the depolymerization of the raw starch based material; only microwaves appeared to reduce the reaction time by reaching the required temperature in a short time period. The ultrasonic bath was not powerful enough to allow the mixing of a highly heterogeneous and viscous system that requires the use of an ultrasonic probe directly immersed in the solution for a direct irradiative mode.

Guo et al. used a Bronsted acidic IL as catalyst instead of as a solvent for the production of biodiesel from soybean [147]. Thus, in methanol and under ultrasonic conditions (24 kHz, 200 W), the methyl ester conversion reached 93.2 % after 60 min. It appears that the IL/US combination should be, after optimization of all the parameters, an efficient and eco-friendly tool for synthesis of biodiesel [148].

In resume, many advantages have been already showed for the pretreatment of biomass for fuels production and extraction processes, but the possibility to produce high-value chemicals is, in many cases, not identified or reported [125]. The IL/US combination should provide innovative results in the next future.

Table 2 Headgas composition during sonication of ILs [35]

Entry	IL	Headgas components
1	[C ₄ C ₁ im]Cl	Chlorobutane (25.6 %), chloromethane (51.1 %), imidazole decomposition products (23.3 %) ^a
2	[C ₄ C ₁ im][BF ₄]	Imidazole decomposition products ^a
3	[C ₄ C ₁ im][PF ₆]	Imidazole decomposition products ^a
4	[C ₁₀ C ₁ im][BPh ₄]	Benzene (71.6 %), toluene (7.8 %), cyclopentadiene (1.4 %), 1-hexene (0.5 %), 2,4-hexadiene (0.7 %), imidazole decomposition products (18 %) ^a

^a Imidazole decomposition products : 1,3-butadiene (0.4 %), 1,3-butadiyne (2.2 %), acetonitrile/isocyanomethane (21.9 %), 2-methylpropane (60.7 %), 2-propenenitrile (7.4 %) and pent-3-en-1-yne (7.4 %)

4 Effects of Ultrasound on Non-Volatile ILs

A classical observation during the sonication of ILs is their darkening from colorless to amber as a function of the irradiation time, indicating some decomposition of the IL. Generally, the IR, ¹³C NMR, ¹⁹F, fast atom bombardment mass (FAB-MS), UV–visible spectra and elemental analysis of irradiated ILs contained no significant difference before and after sonication. Suslick's group investigated the sonochemistry and sonoluminescence of some imidazolium based ILs ([C₄C₁im]Cl, [C₄C₁im][BF₄], [C₄C₁im][PF₆]) and decylmethylimidazolium tetraphenylborate ([C₁₀C₁im][BPh₄]) under 20 kHz irradiation (60 W.cm⁻²) for 3 h at 85 and 135 °C under an Ar flow [35]. After sonication, the ¹H NMR spectrum of the ILs showed some additional peaks in the imidazole region amounting to 0.44 % of total hydrogen. Interestingly, the headgas over each sonication was analyzed by GC–MS (Table 2). During sonication, the imidazolium based ILs produced gases containing traces of light hydrocarbons and nitriles, clearly due to the degradation of the imidazolium rings. Headgases from sonication of [C₄C₁im][BF₄] and [C₄C₁im][PF₆] contained no detectable fluoride-containing species and from [C₁₀C₁im][BPh₄] contained 72 % benzene and traces of other cyclic products.

Suslick et al. also compared the multibubble sonoluminescence (MBSL) spectra of [C₄C₁im]Cl, 1-methylimidazole and 1-methylimidazole with 1.5 % *n*-butyl chloride, showing molecular emission from excited states of C2 carbon and CH. They concluded from the products analyzed by ¹H NMR, that the headgases and the MBSL spectra are a result of the ultrasonic decomposition of both the ILs themselves and of their primary sonolysis products [35, 149]. The primary decomposition products for the imidazolium based ILs are *N*-alkylimidazoles and 1-alkylhalides.

Interestingly, the identification of the degradation products of hydrophobic bis(trifluoromethylsulfonyl)imide [NTf₂]⁻-based ILs irradiated under 20 kHz ultrasound allowed to determine the mechanisms of degradation via the formation of the primary and secondary sonolysis products [36]. Pyrolysis reactions were suggested at the site of collapse of the cavitation bubbles. No product of oxidation by HO[•] radicals was detected. For the irradiation of [C₈C₁pyrr][NTf₂], analyses reported degradation products of the octyl chain (44 %), benzene derivatives

obtained through reforming mechanisms (20 %), derivatives of acrylonitrile obtained from ammoxidation of propene under air (6 %) and sulfur-containing compounds resulting from the degradation of the $[\text{NTf}_2]^-$ anion (3 %). The temperatures and pressures required for pyrolysis reactions fit with the intense local heating (about 5000 K) established when cavitation bubbles collapse.

These results obtained on ILs [35, 36, 149] are consistent with the two-site model of sonochemical reactions involving the bubble's gas-phase interior and the immediately surrounding shell of liquid phase [150]. Ashokkumar et al. determined a temperature of about 3500 K generated in the imploding cavitation bubbles in 1-ethyl-3-methylimidazolium ethylsulfate ($[\text{C}_2\text{C}_1\text{im}][\text{EtSO}_4]$) and observed an enhancement in the sonoluminescence intensity with increase in bulk fluid temperature and the corresponding decrease of the IL viscosity [151].

To limit the degradation of hydrophobic ILs under ultrasonic irradiation, we proposed a water/IL biphasic system leading to a reduction by 20 times of the amount of degradation products [36]. In this case, the hot spots could be preferentially located in the aqueous phase rather in the IL, mainly due to their difference of viscosities and vapor pressures. We also determined the acoustic power of some $[\text{NTf}_2]^-$ -based ILs submitted to ultrasound [152]. Despite very different specific heat capacities (c_p) for water and for ILs, the measured acoustic powers were very similar for both media. Thus, the faster heating up of the ionic liquids compared with water can lead to interesting effects as a solvent for organic reactions. Further investigations are needed to probe whether the cavitation model can be applied more broadly to all non-volatile ILs.

Physico-chemical characterizations of ILs such as heat capacities, enthalpies, entropies of vaporization, H-bonding abilities, etc., are increasing [153, 154] and should be of importance to further better understand physical and chemical reactivity under ultrasound.

5 Sonochemical Degradation Treatment of Ionic Liquids

With their growing use as solvents and their high chemical stability, ILs could be detected in technological wastewaters, and they could break through classical treatment systems into natural waters, becoming persistent pollutants [155]. In addition, it is difficult to exactly determine the toxicity towards cells and environment with the current data, and the millions of possible cation/anion combinations lead to a complex evaluation of their impact on health and environment [156, 157]. Hence, degradative processes that could be applied as a waste treatment strategy are of importance to the field.

Li et al. developed an efficient process for oxidative degradation of 1,3-dialkylimidazolium ILs in hydrogen peroxide and acetic acid medium under high frequency ultrasound (330 kHz, 750 W) [158]. The authors achieved a degradation efficiency of 93 % after 12 h, and 99 % after 72 h. Degradation products were determined using GC-MS to propose a possible mechanism of degradation (Fig. 12).

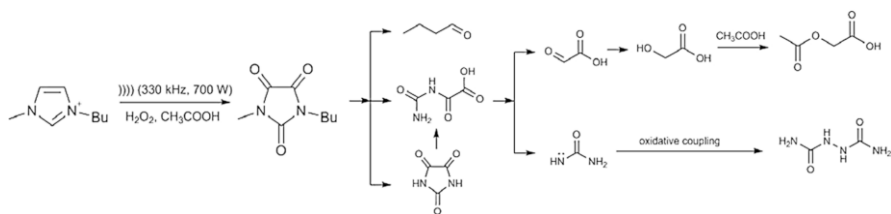


Fig. 12 Oxidation degradation mechanism of $[C_4C_1im]^+$ cation under high frequency ultrasound [158]

Wang et al. developed a zero-valent iron activated carbon micro-electrolysis system under low frequency US (ultrasonic bath, 45 kHz, 300 W) to degrade 1-butyl-3-methylimidazolium chloride residues in water [159]. More than 81 % of $[C_4C_1im]Cl$ was mineralized after a 110 min degradation reaction. The authors suggested that the imidazolium ring was oxidized to 1-butyl-3-methyl-2,4,5-trioxoimidazolidine, and then the ring was opened to form *N*-butylformamide and small molecular compounds. The authors demonstrated the efficiency of this method on different ILs showing that the degradation mechanism was dependent of the nature of the IL [160]. However, this technique has only been applied to treatment of low concentrations of IL in water (about 1 mmol L^{-1}) and investigation of higher concentrations would be an important step.

6 Conclusions and Outlook

In the two last decades, the use of ultrasound has been increasingly investigated in the presence of, or for the synthesis of ILs. The main areas where this synergistic combination are applied are organic chemistry, the synthesis of ILs, and more recently for materials preparation (catalysts, nanoparticles, nanotubes, propellants, etc.), for extraction and micro-extraction, electrochemistry, biomass processing, sonochemical degradation of ILs, etc. For instance, the use of low frequencies is predominant with IL media, probably for its ease of processing and its accessibility at lab. Most often, the beneficial consequences of the IL/US combination are the decrease of reaction/preparation times with improvements in yield, selectivity and/or quality of the products, compared to silent conditions. In some cases unexpected results can also be obtained under ultrasonic irradiations, thereby offering the potential for new synthesis pathways. Increasingly, low frequency ultrasound in an IL medium is also particularly valuable in the extraction area, offering significant benefits in terms of processing time and energy reduction, efficiency in mass and energy transfer, high reproducibility and simplification of manipulations.

The potential for further promising opportunities to emerge from the ILs/ultrasound combination is already based on numerous examples. We especially identify some important issues, trends and potentials for this combination:

6.1 Rigorous Experimental Data About Ultrasound and ILs

It is true for all uses of ultrasound, but even more so when ILs are chosen as propagation media: all the ultrasonic parameters should be reported in the literature to better understand the phenomenon occurring in ILs during the cavitation. The purity of ILs, the identification of impurities and the water content also represent significant issues and should be clearly specified in all experimental sections. The more systematic physico-chemical characterizations of ILs should lead to collect crucial data to better understand the behaviours of ILs under ultrasonic irradiations.

6.2 Investigation of Mechanisms

Ultrasound activation is not a simple tool of stirring and ILs have not the classical behaviours of organic solvents. It is a huge challenge to collect more detailed investigations of the mechanisms involved under ultrasonic irradiation in ILs in order to better understand the phenomena and better control the expected effects.

6.3 Right Balance in Terms of Energy

At low frequencies, it is necessary to provide enough energy to favor the physical effects. In many cases, the highly heterogeneous and viscous systems obtained in ILs require a direct irradiative mode via an ultrasonic probe directly immersed in the solution, since ultrasonic baths are not always sufficiently powerful. However, depending on the IL nature and purity, an acoustic power that is too high can cause partial degradation of the IL. Many papers reported the darkening of the irradiated IL as a function of the time; this represents a real issue for industrial applications.

6.4 Water Amount in ILs Under Ultrasound

The presence of water or organic impurities in irradiated ILs may impact significantly the acoustic cavitation phenomenon. This direction needs to be investigated in depth and could represent an opportunity to avoid the darkening and degradation of ILs under US.

6.5 Investigation of High Frequency Ultrasound

As described previously, high frequency ultrasound seems currently to be mostly of interest as a means for IL degradation via advanced oxidation processes. However, the use of high frequency ultrasound needs to be further explored in order to provide a basis for optimising reactivity in the presence of IL based media, for organic and catalytic reactions.

6.6 New Opportunities for IL/Ultrasound Combination

This combination opens the door to interesting opportunities in new research areas. The combination with other technologies represents a great potential in term of

innovation, for examples coupling with enzymatic catalysis for enhancing enzymatic activity in ILs [161, 162]. In these cases, it will be important to study silent, coupled and non-coupled conditions separately, for comparison and to highlight the synergetic effects. The combination with microwave can also bring new insight in the area [163–165].

Based on the numerous advantages discussed in this chapter, in terms of time reduction, yield improvement, energy economy and innovation, the US/IL combination clearly has a strong potential to contribute to innovation broadly in green and sustainable chemistry.

References

1. Rogers RD, Seddon KR (2003) *Science* 302:792–793
2. Rogers RD, Seddon KR (2003) *Ionic liquids as green solvents: progress and prospects*. American Chemical Society, Washington, D.C.
3. Wasserscheid P, Welton T (2008) *Ionic liquids in synthesis*. Wiley-VCH, Weinheim
4. Hallett JP, Welton T (2011) *Chem Rev* 111:3508–3576
5. Cojocaru OA, Bica K, Gurau G, Narita A, McCrary PD, Shamshina JL, Barber PS, Rogers RD (2013) *MedChemComm* 4:559–563
6. Zhang P, Wu T, Han B (2014) *Adv Mater* 26:6810–6827
7. Ho TD, Zhang C, Hantao LW, Anderson JL (2014) *Anal Chem* 86:262–285
8. MacFarlane DR, Tachikawa N, Forsyth M, Pringle JM, Howlett PC, Elliot GD, Davis JH Jr, Watanabe M, Simon P, Austen Angell C (2014) *Energy Environ Sci* 7:232–250
9. Torriero AAJ (2015) *Electrochemistry in Ionic Liquids*, Springer International Publishing, p 738
10. Stanisz E, Werner J, Zgoła-Grzeskowiak A (2014) *TrAC Trends Anal Chem* 61:64–66
11. Tadesse H, Luque R (2011) *Energy Environ Sci* 4:3913–3929
12. Holbrey JD, Seddon KR (1999) *Clean Products and Processes*. In: Matsunaga T (ed.), Vol. 1, Springer-Verlag, New York, p 223
13. Chatel G, Pereira JFB, Debbeti V, Wang H, Rogers RD (2014) *Green Chem* 16:2051–2083
14. Stark A, Behrend P, Braun O, Müller A, Ranke J, Ondruschka B, Jastorff B (2008) *Green Chem* 10:1152–1161
15. Chatel G, MacFarlane DR (2014) *Chem Soc Rev* 43:8132–8149
16. Nambodiri VV, Varma RS (2002) *Org Lett* 4:3161–3163
17. Lévêque J-M, Luche J-L, Pétrier C, Roux R, Bonrath W (2002) *Green Chem* 4:357–360
18. Zhao S, Zhao E, Shen P, Zhao M, Sun J (2008) *Ultrason Sonochem* 15:955–959
19. Cravotto G, Boffa L, Lévêque JM, Estager J, Draye M, Bonrath W (2007) *Aust J Chem* 60:946–950
20. Li W, Lin Q, Ma L (2010) *Ultrason Sonochem* 17:752–755
21. Varma RS (2006) *J Chem* 45B:2305–2312
22. Lévêque JM, Desset S, Suptil J, Fachinger C, Draye M, Bonrath W, Cravotto G (2006) *Ultrason Sonochem* 13:189–193
23. Cravotto G, Gaudino EC, Boffa L, Lévêque JM, Estager J, Bonrath W (2008) *Molecules* 13:149–156
24. Messali M, Almtiri MN, Abderrahman B, Salghi R, Aouad MR, Alshahateet SF, Ali AAS (2015) *S Afr J Chem* 68:219–225
25. Messali M (2014) *Arabian J Chem* 7:63–70
26. Messali M, Asiri MAM (2013) *J Mater Environ Sci* 4:770–785
27. Messali M, Aouad MR, Ali AAS, Rezki N, Ben Hadda T (2015) *Med Chem Res* 24:1387–1395
28. Messali M (2015) *Molecules* 20:14936–14949
29. Ameta G, Kumar Pathak A, Ameta C, Ameta R, Punjabi PB (2015) *J Mol Liq* 211:934–937
30. Zbancioc G, Mangalagiu II, Moldoveanu C (2015) *Ultrason Sonochem* 23:376–384
31. Varma RS (2003) *Expeditious synthesis of ionic liquids using ultrasound and microwave irradiation*. In: Rogers R D and Seddon K R (eds.) Vol. 856, *Ionic liquids as green solvents*, ACS Symposium Series, American Chemical Society: Washington, Chap. 7, p 82–92

32. Varma RS (2007) *Green Chem Lett Rev* 1:37–45
33. Lévêque JM, Estager J, Draye M, Cravotto G, Boffa L, Bonrath W (2007) *Monatsh Chem* 138:1103–1113
34. Deetlefs M, Seddon KR (2010) *Green Chem* 12:17–30
35. Oxley JD, Prozorov T, Suslick KS (2003) *J Am Chem Soc* 125:11138–11139
36. Chatel G, Pflieger R, Naffrechoux E, Nikitenko SI, Suptil J, Goux-Henry C, Kardos N, Andrioletti B, Draye M (2013) *ACS Sustainable Chem Eng* 1:137–143
37. Deshmukh RR, Rajagopal R, Srinivasan KV (2001) *Chem Commun* p 1544–1545
38. Rajagopal R, Srinivasan KV (2003) *Ultrason Sonochem* 10:41–43
39. Rajagopal R, Jarikote DV, Srinivasan KV (2002) *Chem Commun* p 616–617
40. Gholap AR, Venkatesan K, Daniel T, Lahoti RJ, Srinivasan KV (2004) *Green Chem* 6:147–150
41. Gholap AR, Venkatesan K, Daniel T, Lahoti RJ, Srinivasan KV (2003) *Green Chem* 5:693–696
42. Venkatesan K, Pujari SS, Lahoti RJ, Srinivasan KV (2008) *Ultrason Sonochem* 15:548–553
43. Gholap AR, Venkatesan K, Pasricha R, Daniel T, Lahoti RJ, Srinivasan KV (2005) *J Org Chem* 70:4869–4872
44. Yang HM, Hung YH, Tu CY (2014) *J Taiwan Inst Chem Eng* 45:1421–1427
45. Hua Q, Dabin L, Chunxu L (2011) *Ultrason Sonochem* 18:1035–1037
46. Chatel G, Goux-Henry C, Kardos N, Suptil J, Andrioletti B, Draye M (2012) *Ultrason Sonochem* 19:390–394
47. Chatel G, Goux-Henry C, Mirabaud A, Rossi T, Kardos N, Andrioletti B, Draye M (2012) *J Catal* 291:127–132
48. Mamaghani M, Pourranjbar M, Nia RH (2014) *J Sulfur Chem* 1:1–6
49. Wang J, Zong Y, Fu R, Niu Y, Yue G, Quan Z, Wang X, Pan Y (2014) *Ultrason Sonochem* 21:29–34
50. Li D, Zang H, Wu C, Yu N (2013) *Ultrason Sonochem* 20:1144–1148
51. Suresh, Sandhu JS (2013) *Org Med Chem Lett* 3:2–8
52. Qian H, Wang Y, Liu D (2013) *Ind Eng Chem Res* 52:13272–13275
53. Estager J, Lévêque JM, Turgis R, Draye M (2007) *Tetrahedron Lett* 5:755–759
54. Yinghuai Z, Bahnmüller S, Hosmane NS, Maguire JA (2003) *Chem Lett* 32:730–731
55. Yinghuai Z, Bahnmüller S, Chibun C, Carpenter K, Hosmane NS, Maguire JA (2003) *Tetrahedron Lett* 44:5473–5476
56. Yinghuai Z (2004) *J Phys Chem Solids* 65:349–353
57. Wang X, Fulvio PF, Baker GA, Veith GM, Unocic RR, Mahurin SM, Chib M, Dai S (2010) *Chem Commun* 46:4487–4489
58. Shi JJ, Zhu JJ (2011) *Electrochim Acta* 56:6008–6013
59. Wu Y, Hao X, Yang J, Tian F, Jiang M (2006) *Mat Lett* 60:2764–2766
60. Behboudnia M, Habibi-Yangjeh A, Jafari-Tarzanag Y, Khodayari A (2008) *J Cryst Growth* 310:4544–4548
61. Goharshadi EK, Ding Y, Jorabchi MN, Nancarrow P (2009) *Ultrason Sonochem* 16:120–123
62. Barzegar M, Habibi-Yangjeh A, Behboudnia M (2009) *J Phys Chem Solids* 70:1353–1358
63. Salinas-Estevan P, Sanchez EM (2010) *Mater Lett* 64:2627–2630
64. Salinas-Estevan P, Sanchez EM (2010) *Cryst Growth Des* 10:3917–3924
65. Garcia-Gomez NA, De la Parra-Arcieniega SM, Garza-Tovar LL, Torres-Gonzalez LC, Sanchez EM (2014) *J Alloys Compd* 588:638–643
66. Taghvaei V, Habibi-Yangjeh A, Behboudnia M (2009) *Powder Technol* 195:63–67
67. Behboudnia M, Habibi-Yangjeh A, Jafari-Tarzanag Y, Khodayari A (2009) *J Optoelectron Adv Mater* 11:134–139
68. Behboudnia M, Habibi-Yangjeh A, Jafari-Tarzanag Y, Khodayari A (2008) *Bull Korean Chem Soc* 29:53–56
69. Behboudnia M, Habibi-Yangjeh A, Jafari-Tarzanag Y, Khodayari A (2010) *J Phys Chem Solids* 71:1393–1397
70. Alamar T, Birkner A, Shekhah O, Mudring AV (2010) *Mater Chem Phys* 120:109–113
71. Sang Shin U, Hong HK, Kim HW, Gong MS (2011) *Bull Korean Chem Soc* 32:1583–1586
72. Zhang S, Zhang Y, Wang Y, Liu S, Deng Y (2012) *Phys Chem Chem Phys* 14:5132–5138
73. McCrary PD, Beasley PA, Cojocar OA, Schneider S, Hawkins TW, Perez JPL, McMahon BW, Pfeil M, Boatz JA, Anderson SL, Son SF, Rogers RD (2012) *Chem Commun* 48:4311–4313
74. Qian H, Ye ZW, Lv CX (2007) *Lett Org Chem* 4:482–485
75. Putz AM, Len A, Ianăși C, Savii C, Almásy L (2016) *Korean J Chem Eng* 33:749–754

76. Yang C, Li F, Li T (2015) *CrystEngComm* 17:7676–7683
77. Zhu CZ, Guo SJ, Zhai ZY, Dong SJ (2010) *Langmuir* 26:7614–7618
78. Nalajala VS, Moholkar VS (2011) *Ultrason Sonochem* 18:345–355
79. Xiao W, Sun Z, Chen S, Zhang H, Zhao Y, Huang C, Liu Z (2012) *RSC Adv* 2:8189–8193
80. Mao BH, Liu CH, Gao X, Chang R, Liu Z, Wang SD (2013) *Appl Surf Sci* 283:1076–1079
81. Luska KL, Moores A (2012) *Green Chem* 14:1736–1742
82. Luska KL, Moores A (2012) *ChemCatChem* 4:1534–1546
83. Luska KL, Moores A (2011) *Adv Synth Catal* 353:3167–3177
84. Wittmar A, Ruiz-Abad D, Ulbricht M (2012) *J Nanopart Res* 14:651–661
85. Shafi KVPM, Ulman A, Dyal A, Yan X, Yang NL, Estournès C, Fournès L, Wattiaux A, White H, Rafailovich M (2002) *Chem Mater* 14:1778–1787
86. Bazureau JP, Draye M (2011) *Ultrasound and Microwaves: Recent Advances in Organic Chemistry, Research Signpost*
87. Suslick KS, Hammerton DA, Cline DE (1986) *J Am Chem Soc* 108:5641–5645
88. Jin Y, Wang P, Yin D, Liu J, Qin L, Yu N, Xie G, Li B (2007) *Colloids Surf A* 302:366–370
89. Kim KS, Demberelnyamba D, Lee H (2004) *Langmuir* 20:556–560
90. Yang C, Li F, Li T (2015) *CrystEngComm* 17:7676–7683
91. Poole CF, Poole SK (2010) *J Chromatogr A* 1217:2268–2286
92. Huddleston JG, Willauer HD, Swatloski RP, Visser AE, Rogers RD (1998) *Chem Commun* p 1765–1766
93. Sun X, Luo H, Dai S (2012) *Chem Rev* 112:2100–2128
94. Tan ZJ, Wang CY, Yang ZZ, Yi YJ, Wang HY, Zhou WL, Li FF (2015) *Molecules* 20:17929–17943
95. Liao J, Qu B, Liu D, Zheng N (2015) *Ultrason Sonochem* 27:110–116
96. Li C, Fu X, Huang Q, Luo F, You L (2015) *Eur Food Res Technol* 240:49–60
97. Cao X, Ye X, Lu Y, Yu Y, Mo W (2009) *Anal Chim Acta* 640:47–51
98. Zhou Q, Zhang X, Xiao J (2009) *J Chromatogr A* 1216:4361–4365
99. Abolhasani J, Amjadi M, Hassanzadeh J, Ghorbani-Kalhor E (2014) *Anal Lett* 47:1528–1540
100. He SW, Shen CY, Wei XQ, Jin MC, Cai MQ (2013) *Adv Mater Res* 726–731:74–80
101. Shamsipur M, Yazdanfar N, Ghambarian M (2016) *Food Chem* 204:289–297
102. Han D, Row KH (2011) *J Sci Food Agric* 91:2888–2892
103. Wu K, Zhang Q, Liu Q, Tang F, Long Y, Yao S (2009) *J Sep Sci* 32:4220–4226
104. Dong S, Hu Q, Yang Z, Liu R, Huang G, Huang T (2013) *Microchem J* 110:221–226
105. Gong A, Zhu X (2015) *Talanta* 131:603–608
106. Qin H, Zhou G, Peng G, Li J, Chen J (2015) *Food Anal Methods* 8:1673–1681
107. Sun Y, Li W, Wang J (2008) *J Chromatogr B* 879:975–980
108. Molaakbari E, Mostafavi A, Afzali D (2011) *J Hazard Mater* 185:647–652
109. Stanisz E, Werner J, Matusiewicz H (2013) *Microchem J* 110:28–35
110. Tuzen M, Pekiner OZ (2015) *Food Chem* 188:619–624
111. Parrilla Vazquez MM, Parrilla Vazquez P, Martinez Galera M, Garcia MDG, Ucles A (2013) *J Chromatogr A* 1291:19–21
112. Asensio-Ramos M, Hernandez-Borges J, Borges-Miquel TM, Rodriguez-Delgado MA (2011) *J Chromatogr A* 1218:4808–4816
113. Villagran C, Banks CE, Pitner WR, Hardacre C, Compton RG (2005) *Ultrason Sonochem* 12:423–428
114. Fuchigami T, Sunaga T, Ishii H, Atobe M (2002) In: *Workentin M S, Maran F and Chiba K (eds.) Organic Electrochemistry, The electrochemical society: Pennington*
115. Fuchigami T, Tajima T (2005) *J Fluorine Chem* 126:181–187
116. Feroci M, Orsini M, Inesi A (2009) *Adv Synth Catal* 35:2067–2070
117. Costa C, Doche ML, Hihn JY, Bisel I, Moisy P, Lévêque JM (2010) *Ultrasonics* 50:323–328
118. Compton RG, Hardcastle JL, Del Campo J (2003) In: *Encyclopedia of electrochemistry (Ed. Bard Stratmann), Instrumentation and Electroanalytical Chemistry (Ed. P. Unwin), Vol. 3, Wiley-VCH, Weinheim*
119. Xiao F, Mo Z, Zhao F, Zeng B (2008) *Electrochem Commun* 1:1740–1743
120. Xiao F, Zhao F, Mei D, Mo Z, Zeng B (2009) *Biosens Bioelectron* 24:3481–3486
121. Xiao F, Zhao F, Zhang Y, Guo G, Zeng B (2009) *J Phys Chem C* 113:849–855
122. Zhao F, Xiao F, Zeng B (2010) *Electrochem Commun* 12:168–171
123. He Y, Zheng J, Dong S (2012) *Analyst* 2012(137):4841–4848

124. He Y, Zheng J (2013) *Anal Methods* 5:767–772
125. Chatel G, De Oliveira Vigier K, Jérôme F (2014) *ChemSusChem* 7:2774–2787
126. Sun N, Rodriguez H, Rahman M, Rogers RD (2011) *Chem Commun* 47:1405–1421
127. Garcia A, Gonzalez Alriols M, Llano-Ponte R, Labidi J (2011) *Bioresour Technol* 102:6326–6330
128. Gogate PR, Abhijeet MK, Kabadi M (2009) *Biochem Eng J* 44:60–72
129. Rokhina EV, Lens P, Virkutyte J (2009) *Trends Biotechnol* 5:298–306
130. Mikkola JP, Kirilin A, Tuuf JC, Pranovich A, Holmbom B, Kustov LM, Murzin DY, Salmi T (2007) *Green Chem* 9:1229–1237
131. Sun N, Rahman M, Qin Y, Maxim ML, Rodriguez H, Rogers RD (2009) *Green Chem* 11:646–655
132. Maxim ML, Sun N, Wang H, Sterner JR, Haque A, Rogers RD (2012) *Nanomater Energy* 1:225–236
133. Cheng F, Wang H, Chatel G, Gurau G, Rogers RD (2014) *Bioresour Technol* 164:394–401
134. Ninomiya K, Kohori A, Tatsumi M, Osawa K, Endo T, Kakuchi R, Ogino C, Shimizu N, Takahashi K (2015) *Bioresour Technol* 176:169–174
135. Lan W, Liu C, Yue FX, Sun RC, Kennedy JF (2011) *Carbohydr Polym* 86:672–677
136. Liu L, Ju M, Li W, Hou Q (2013) *Carbohydr Polym* 98:412–420
137. Yang F, Li L, Li Q, Tan W, Liu W, Xian M (2010) *Carbohydr Polym* 81:311–316
138. Ho Ha S, Hiep NM, Koo YM (2010) *Biotechnol Bioprocess Eng* 15:126–130
139. Liu Z, Lu L (2011) *Adv Mater Res* 236–238:169–172
140. Lozano P, Bernal B, Recio I, Belleville MP (2012) *Green Chem* 14:2631–2637
141. Wang Y, Pan Y, Zhang Z, Sun R, Fang X, Yu D (2012) *Process Biochem* 47:976–982
142. Ninomiya K, Kamide K, Takahashi K, Shimizu N (2012) *Bioresour Technol* 103:259–265
143. Wang F, Chen ZG, Zhu HJ (2013) *Biochem Eng J* 79:25–28
144. Ninomiya K, Ohta A, Omote S, Ogino C, Takahashi K, Shimizu N (2013) *Chem Eng J* 215–216:811–818
145. Wang Y, Pan Y, Zhang Z, Sun R, Fang X, Yu D (2012) *Process Biochem* 47:976–982
146. Hernoux-Villière A, Lévêque JM, Kärkkäinen J, Papaiconomou N, Lajunen M, Lassi U (2014) *Catal Today* 223:11–17
147. Guo W, Li H, Ji G, Zhang G (2012) *Bioresour Technol* 125:332–334
148. Bi YG, Wu SS (2013) *Adv Mat Res* 791–793:196–199
149. Flannigan DJ, Hopkins SD, Suslick KS (2005) *J Organomet Chem* 690:3513–3517
150. Suslick KS, Hammerton DA, Cline RE (1986) *J Am Chem Soc* 108:5641–5642
151. Kanthale PM, Brothie A, Grieser F, Ashokkumar M (2013) *Ultrason Sonochem* 20:47–51
152. Chatel G, Leclerc L, Naffrechoux E, Bas C, Kardos N, Goux-Henry C, Andrioletti B, Draye M (2012) *J Chem Eng Data* 57:3385–3390
153. Paulechka YU (2010) *J Phys Chem Ref Data* 39:033108
154. Rocha MAA, Coutinho JAP, Santos LMNBF (2014) *J Chem Phys* 141:134502
155. Stepnowski P, Zaleska A (2005) *J Photochem Photobiol A* 170:45–50
156. Jastorff B, Störmann R, Ranke J, Mölter M, Stock F, Oberheitmann B, Hoffman W, Hoffmann J, Nüchter M, Ondruschka B, Filser J (2003) *Green Chem* 5:136–142
157. Bubalo MC, Radosevic K, Redovnikovic IR, Halambek J, Sreck VG (2014) *Ecotoxicol Environ Saf* 99:1–12
158. Li X, Zhao J, Li Q, Wang L, Tsang SC (2007) *Dalton Trans* 1875–1880
159. Zhou H, Shen Y, Lv P, Wang J, Fan J (2013) *Sep Purif Technol* 104:208–213
160. Zhou H, Lv P, Shen Y, Wang J, Fan J (2013) *Water Res* 47:3514–3522
161. Lee SH, Nguyen HM, Koo YM, Koo SH, Ha SH (2008) *Process Biochem* 43:1009–1012
162. Wang J, Wang S, Li Z, Gua S, Wu X, Wu F (2015) *J Mol Catal B Enzym* 111:21–28
163. Li C, Lu Z, Zhao C, Yang L, Fu Y, Shi K, He X, Li Z, Zu Y (2015) *J Sep Sci* 38:291–300
164. Bubalo MC, Sabotin I, Radoš I, Valentinčič J, osiljkov T, Brnčić M (2013) *Green Process Synth* 2:579–590
165. Lévêque JM, Cravotto G (2006) *CHIMIA Int J Chem* 60:313–320

Synergy of Microfluidics and Ultrasound Process Intensification Challenges and Opportunities

David Fernandez Rivas¹  · Simon Kuhn²

Received: 26 May 2016 / Accepted: 30 August 2016 / Published online: 21 September 2016
© The Author(s) 2016. This article is published with open access at Springerlink.com

Abstract A compact snapshot of the current convergence of novel developments relevant to chemical engineering is given. Process intensification concepts are analysed through the lens of microfluidics and sonochemistry. Economical drivers and their influence on scientific activities are mentioned, including innovation opportunities towards deployment into society. We focus on the control of cavitation as a means to improve the energy efficiency of sonochemical reactors, as well as in the solids handling with ultrasound; both are considered the most difficult hurdles for its adoption in a practical and industrial sense. Particular examples for microfluidic clogging prevention, numbering-up and scaling-up strategies are given. To conclude, an outlook of possible new directions of this active and promising combination of technologies is hinted.

Keywords Microfluidics · Ultrasound · Sonochemistry · Process intensification · Chemical engineering · Solids handling

This article is part of the Topical Collection “Sonochemistry: From basic principles to innovative applications”; edited by Juan Carlos Colmenares Q., Gregory Chatel.

✉ David Fernandez Rivas
d.fernandezrivas@utwente.nl

Simon Kuhn
simon.kuhn@kuleuven.be

¹ Mesoscale Chemical Systems, MESA+ Institute for Nanotechnology, Carre 1.339, 7500 AE Enschede, The Netherlands

² Department of Chemical Engineering, KU Leuven, Celestijnenlaan 200F, 3001 Leuven, Belgium

1 Introduction and Definitions

1.1 The Basics of Ultrasound

We present in Fig. 1 a comprehensive diagram with terms and concepts that will be described and expanded in the text. After reading this work, it will be clearer to the reader how synergy, understood in the framework of process intensification (PI), has the largest relevance when analysing the combination of microfluidics and ultrasound applications.

Ultrasound effects on matter are widely known in academic and industry circles. There are several practical applications that have been extensively covered in the literature, ranging from mechanical and chemical processing, medicine, food industry, to cleaning. Use of ultrasound can be either continuous or pulsed and across a broad range of frequencies (20 kHz up to 1 MHz) and acoustic pressures depending on the application [1–6]. Frequencies higher than 1 MHz are known to be used, especially when talking about particle handling and acoustic streaming [7, 8]. Sonochemistry describes the chemical effects of ultrasound on molecular transformations. Different from other energy sources to drive reactions, the chemical effect of ultrasound in liquids is not linked to a direct interaction with the molecules [9]; instead, the energy contained in the sound is channeled into acoustic

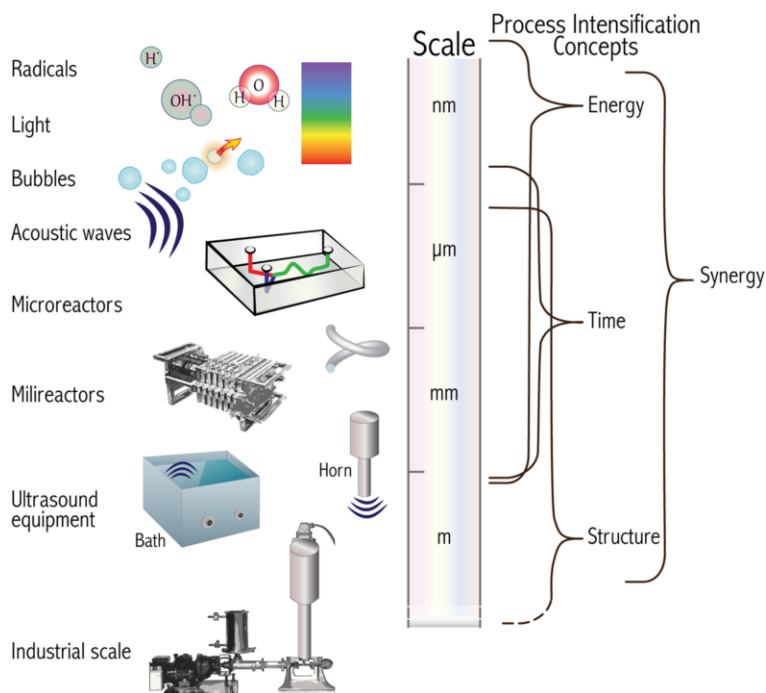


Fig. 1 Diagram with terms and concepts described in this chapter. The relative sizes of the items described on the left increase from top to bottom. On the right we connect the different sizes where the process intensification concepts have the greatest influence

cavitation, i.e. the formation, growth, and subsequent collapse of bubbles in a liquid [10]. These collapse events lead to temperature and pressure hot spots inside the bubble (high temperatures >5000 K and pressures >1000 atm), which in turn activate chemical transformations without altering much the liquid medium [9, 11]. Actually, although the high temperatures and pressures are inside the bubble, most of the relevant chemistry happens in the liquid phase. The importance of bubble collapse is such that it appears that chemical reactions as a result of cavitation might have played a role in producing complex organic molecules in prebiotic times [12]. We can fairly say that ultrasonication, or the exposure of matter to ultrasound, has reached a state of maturity.

Despite the wide use of cavitation, the borders between the physical and chemical phenomena remain blurred, which contributes to an extended use of sonochemistry in a *black-box* manner. The reason behind this is that cavitation effects such as of liquid jets, streaming, chemical radical molecules production, plasma formation with light emission, and shockwaves, are intertwined in complex dependencies that are hard to resolve in space and time [13]. Often, users of sonochemistry and outsiders tend to confuse the definition of a bubble (gas in a liquid, or gas in gas as in soap bubbles) and cannot correlate a given effect with a specific phenomenon. This situation has not prevented sonochemistry from being widely exploited in several useful applications, yet we think it could be done more efficiently.

1.2 The Basics of Microreactors

Using microstructured devices in chemical engineering provides several advantages over conventional, and mostly batch, reaction systems. Because of the decrease in characteristic length scale, an increased surface-to-volume ratio (m^2/m^3) is obtained, with benefits such as enhanced heat and mass transfer coefficients, as well as improved energy conversion efficiencies [14–19]. In addition, the typically small volumes allow a safer handling of hazardous materials and reduced risk when performing high-parameter reactions (pressure and temperature). Early studies showed the potential of using microreactors for chemical synthesis in small-scale flows [14, 15]. Research over the past decade focused on developing complex microchemical systems to enable multi-step processes, especially focusing on transformations involving multiphase flows. A prime example of such a multi-step microchemical synthesis is the continuous flow, multi-step Heck synthesis performed by integrating microreactors, liquid–liquid extraction, and microfluidic distillation [20]. These early studies highlight the potential and the usability of microchemical devices, especially for rapid experimentation and shortening product development cycles.

In order to define the size range of microchannels or capillaries it is not sufficient to consider only their characteristic dimension, e.g. in terms of their hydrodynamic diameter D_H . Also, the wall roughness of microfluidic devices ($D_H \sim \mathcal{O}(10^{-6} \text{ m})$) cannot be neglected at this scale, and it is associated with the tolerances of microfabrication techniques [21]. The roughness and hydrophobic properties of a

surface have a strong influence in the existence of small gas pockets that can eventually serve as nucleation of bubbles, as will be discussed further in this text. The existence of surface nanobubbles is related to the pinning of the three-phase contact line at chemical or geometric surface heterogeneities, and such bubbles can form when the liquid comes into contact with the surface, but also from gas supersaturation during the immersion process [22].

On the other hand, concentration, temperature, and other gradients are reduced significantly when compared to equivalent conventional devices. Singular behaviour of matter at the microscale is rather attributed to the application of models derived for large-scale geometries, describing pressure drop and transport processes (e.g. wall heat transfer) that deviate considerably when applied to microchannels.

An important observation of chemical processes in microchannels is that the two-phase flow regime is independent of the channel orientation, i.e. the phase distribution will be the same in horizontal and vertical channel alignment. These differences between macro- and microchannels arise from the relative importance of gravity and interfacial forces: interfacial effects dominate phenomena at the microscale. Consequently, the definition of microchannels does not just depend on their physical size, but also on the properties of the considered fluid system. One proposed criterion is to calculate the Laplace length scale λ [23], which uses the ratio of interfacial and gravitational forces to quantify a cut-off dimension below which the effect of gravity can be neglected

$$\lambda = \sqrt{\frac{\sigma}{g(\rho_L - \rho_G)}} \quad (1)$$

where σ denotes the interfacial tension, g is the acceleration due to gravity, and ρ_L and ρ_G are the densities of the liquid and gas (or second immiscible liquid) phase, respectively. If the hydrodynamic diameter of the flow channel is smaller than this Laplace length scale ($D_H < \lambda$) it can be considered a microchannel, and this dependence on the fluid properties results in a rather wide size range.

Table 1 shows selected (and commonly encountered classes) of two-phase flow systems and their corresponding values of the Laplace length scale. Gas-liquid systems are characterized by large density differences, but also large interfacial tension, which then results in Laplace constants of $\lambda \sim 3$ mm. In liquid-liquid systems the determining parameter is interfacial tension, as the density difference between two liquid phases is negligible. Table 1 quantifies one example each for

Table 1 Fluid properties and associated Laplace length scale for selected two-phase flow systems [24, 25]

Property	Water	Nitrogen	1-Butanol	Toluene	DMSO
Density ρ (kg m ⁻³)	998	1.25	810	867	1100
Interfacial tension σ (N m ⁻¹)		0.072	0.002	0.037	0.057
Laplace length scale λ (mm)		2.71	0.98	5.33	7.65

Values for the interfacial tension and Laplace length scale assume water as the primary phase

low (1-butanol), intermediate (toluene), and large (DMSO) interfacial tension, and the accompanying wide size range below which gravitational effects can be neglected.

It is known that acoustic cavitation relying on nuclei does not occur easily in microfluidics because the static pressure inside the microchannels is high, which tends to promote the fast dissolution of gas bubbles [26]. For a cavity or bubble to be formed in a liquid, the energy required theoretically is extremely high. For a small bubble forming in water with a radius $\sim 10^{-10}$ m, the minimum negative pressure (also referred to as Blake threshold pressure) required to overcome water molecule cohesion forces is ca. 1400 atm [27]. The pressure inside a gas bubble $p_g(t)$ is a result of the sum of the ambient pressure P_0 and the Laplace pressure (not considering the vapor pressure)

$$p_g(t) = P_0 + \frac{2\sigma}{R(t)} \quad (2)$$

where σ is the surface tension and $R(t)$ is the bubble radius. When the first term in the right hand side of Eq. 2 dominates, bubbles can be considered “large”, meaning that the gas pressure inside the bubble is dominated by the ambient pressure; as a reference, $R \gg 2\sigma/P_0$, corresponds to a radius $R \approx 1.4\mu\text{m}$, for air in water at ambient pressure. For small bubbles the Laplace pressure dominates. During the expansion phase (lower pressure) of a sound wave, bubbles can be formed (see Fig. 2).

In practice, values much smaller than the Blake threshold pressure (1–3 atm) are sufficient to create bubbles [28]. This is due to the presence of small particles or defects in the container holding the liquid, that can entrap gas nuclei, which serve as a weakening spot for molecular cohesion. Once a bubble is formed and reaches a resonance size depending on the ultrasonic frequency, it can suddenly grow to a larger size, become unstable, and violently collapse, hence the term transient cavitation. Alternatively the bubble may oscillate during several cycles at its resonance size, meanwhile generating large local streaming; this is known as

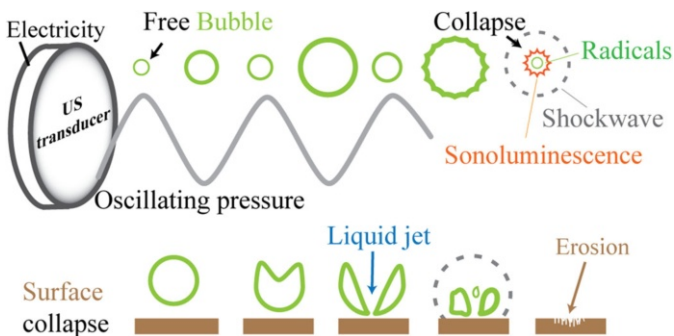


Fig. 2 Schematic representation of a free bubble and a bubble close to a wall, oscillating due to pressure variations imposed by an ultrasound transducer. At the moment of collapse, radicals, shockwaves and light emission (sonoluminescence) can be produced as detailed in the text. When near a surface or another bubble, jetting can also occur. Repeated collapse events against a surface can lead to erosion of surfaces

stable cavitation. Acoustically driven capillary waves can also induce cavitation in microfluidics. Capillary waves travel on the surface of a liquid while restoring forces are provided by the interfacial tension when the wavelengths are short enough for gravity to be neglected. There are comprehensive works covering several aspects of the types of bubbles, and cavitation, for which we refer to the literature [22, 26, 27, 29].

1.3 Synergistic Effects When Combining Ultrasound with Microreactors

The use of the term synergy is not always correct in specialised literature. Most definitions or examples fail to illustrate how two or more techniques are able to produce a combined effect greater than the sum of their separate effects, particularly in sonochemistry [30–32]. The concept of process intensification is highly linked to modern chemical engineering as it aims for a more sustainable and efficient way to manufacture chemical products [33]. This is achieved by the introduction of innovative principles in both process and equipment design, which will then lead to significant improvement in process efficiency and product quality, that in turn further reduces waste streams.

Figure 3 depicts the main goals of PI together with the associated length scales:

1. Maximize the effectiveness of intra- and intermolecular events,
2. Give each molecule the same processing experience,

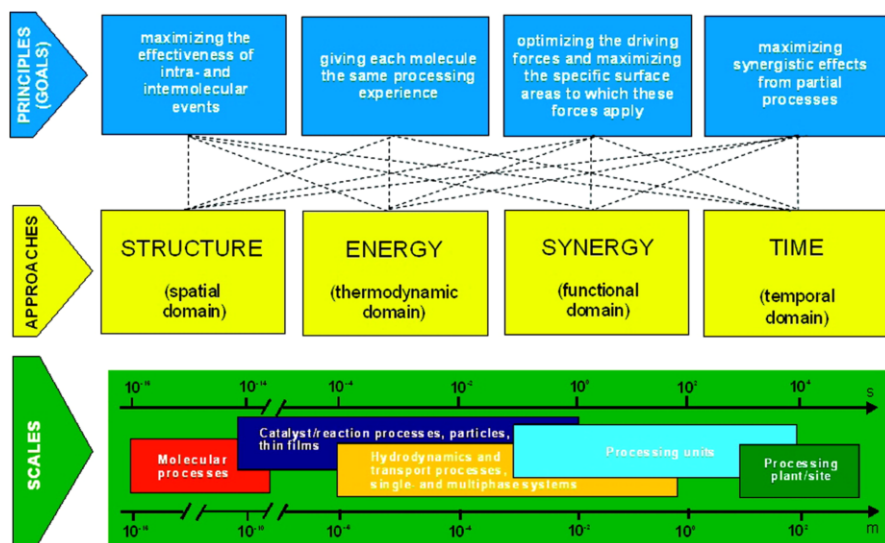


Fig. 3 Fundamental view on process intensification showing the connection between the involved scales, approaches and goals [33]. The approaches to successfully intensify a process can be categorized in four domains: spatial, thermodynamic, functional, and temporal. These approaches need to be applied on all the relevant time and length scales depicted in the green bar. These scales range from the molecular level to the size of a chemical plant. Reprinted with permission from [33]. Copyright 2009 American Chemical Society

3. Optimize the driving forces at every scale and maximize the specific surface area, and
4. Maximize the synergistic effects from partial processes.

Given its inherent properties, microfluidic systems can address all these goals, and in parallel chemical engineers have assimilated the fact that “larger” equipment is not always necessary to reach an economy of scale. In the past three decades several academicians and companies have adopted a “scaling-down” strategy of processes [34–36]. In addition to the benefits mentioned earlier in Sect. 1.2, microfluidic systems represent a well-defined reaction platform for a wide array of chemical manipulations and synthesis. Among other properties, the residence time of species and the reactor temperature can be precisely controlled [37, 38]. This also allows rapid experimentation in terms of high-throughput screening (e.g. reaction conditions, catalysts) [39–41] and automated optimization [42–44]. In addition, microfluidic systems open novel process windows [45], as they allow safe synthesis in harsh conditions [46] and increase the achievable reaction space by e.g. performing synthesis in supercritical solvents [47–49]. All these studies highlight the potential of using micro-reactors for chemical synthesis in small-scale flows, and consequently more complex microchemical systems to enable multi-step processes have been developed [20, 50].

Owing to the small length scales and associated small fluid penetration depths, microfluidic devices also allow the integration of various external energy sources, and thus open up novel routes for PI. Selected applications include photo- and electrochemistry [51, 52], and acoustic microfluidics [53]. While acoustic microfluidics is mostly related to the manipulation of particles via the acoustophoretic force [54], here we focus on the synergistic effects of microfluidics and ultrasound. Since quantifying the separate effects of using microfluidics with ultrasound and comparing the results with their combined effect is required to demonstrate a synergy, we perform a mind experiment. Take a microfluidic reactor that can operate for 1 h until it clogs. The application of ultrasound (even below the pressure amplitudes that yield cavitation) will have improved mixing, heat, and mass transfer, but no direct effect whatsoever in the reaction progress (radicals, light, etc). Most likely, the clogging of the microreactor will be reduced and the reactor will be able to operate for a longer time. This has a clear synergy result, in terms of mechanical effects, since the combination of both techniques will lead to the desired products and longer operation time.

Progress in the field of continuous manufacturing has also been well received by industry. In a collaborative paper co-authored by several major pharmaceutical and fine chemistry companies (GSK, DSM, Boehringer Ingelheim, Pfizer, AstraZeneca, Eli Lilly, Johnson & Johnson, Merck) the need for further research efforts in process intensification was already identified recently [55]. This also includes the demand for novel concepts for continuous reaction systems to enable fine chemicals manufacture.

Despite the many advantages of microchemical systems and their successful applications in chemical engineering research and pioneering companies, one major practical drawback greatly limiting their use in commercial environments and larger

scales, is their susceptibility to channel clogging for flows containing particulate matter. This is especially problematic when solid particles are formed as a by-product of a particular chemical reaction, as the amount of solid matter gradually increases along the axial extent of the microchannel. Integrating microfluidic reactors with ultrasonic actuators has been proven successful to mitigate clogging and to ensure long-term operation [56–58]. We expect that more attention to the potential of combining microfluidics and ultrasound will be given in the coming years, and more studies able to highlight the “real” synergy will see the light. Other examples will also be given in Sect. 3.

2 Economical Drivers and Scientific Impact

Fundamental transformations have taken place in the ways that society and the economy influence each other over the last decade. The current growth model has been exhausted as we observe a slowdown in the global economy. A possible alternative to the ways we produce and exploit the natural resources in a sustainable way can be supported by technological changes or innovations. Ecological aspects, such as the impact on the environment and other phenomena such as global warming and the realization that natural resources are not unlimited, has triggered a more conscious approach on how we can continue exploiting natural resources in a sustainable, safer, and responsible way. Ultrasound and microfluidics separately have contributed to significant advances in this respect [30, 59, 60]. Scientific innovation is being accelerated both in globalised markets and our more interconnected world, at a pace not reported before. Some experts credit the Fourth Industrial Revolution for which enabling technologies such as alternative fuels, 3-D printing, and nanotechnology, have already been linked to microfluidics and ultrasound [61–68]. On the other hand, with the current power of social media, some scientists team up with designers, marketing and other professionals across disciplines, in such a way that it is possible to address better the existing needs of society. This can result in a market-pull approach where new ideas and products are tailored to specific costumers, and in turn will accelerate deployment into society.

Currently, the ultrasonics and microfluidics communities are induced to innovate and revisit existing knowledge toolboxes in order to ensue a technology-push with the hope to commercialise new inventions. Since 1996, the number of research publications and patents having as keywords “microfluidics”, “chemistry”, and “ultrasound” indexed in Scopus is 1908 and 1262 respectively. The number of articles in 2015 was 357, and the number of patents was 128, with an estimated 10 % increase per year in both categories over the last 5 years. Microfluidics as a commercial activity is in its hype phase, where established companies and new spin-offs amount to an estimated 670 according to industrial observers [69]. An interesting trend is seen towards integration of platforms such as plug-and-play components and standardisation. Further, several universities are active in the creation of spin-offs that can eventually be bought by larger companies (e.g. pharmaceutical and electronic) depending on their potential to produce components, and the services they can provide.

We refer the reader to some references and interesting developments around microreactor technology given by Sigma-Aldrich's product manager [70], including the possibility to buy generic "all-in-one solution" microreactors, which are labeled as "the chemist's round bottomed flask of the twenty-first century". Several companies provide commercial micro- and milli-reactor solutions, e.g. Chemtrix, Corning, ESK, Micronit and Velocys. Among the companies involved in the commercialization of ultrasound integrated reactors we are aware of, Hielscher commercialises an Ultrasonic Mini flow cell and a GDmini2 Ultrasonic Inline Micro-reactor; Prosonix has catered to larger scale reactors in its Prosonitron project for Auginish Alumina (Glencore) [71].

Conversely, some larger transnational companies are shedding their research and development groups that sometimes become start-ups on its own. The spun-out researchers that assemble in new companies toughen the competition between academics and other institutes for subsidies or research funds. Shorter product-life cycles, together with continuously changing market trends and offer-demand balance are the new normal in most commercial activities [72]. This situation has had a tremendous impact worldwide on the chemical industry and research as a whole, twisting, or skewing governmental financing towards private investment in many countries. Since subsidies and funding scheme for research are drying out, the advent of social campaigns has become an alternative. Researchers are increasingly more active in social media and stream their research and products to meet non conventional demands, such as for cooking [73, 74]. Non-traditional ways to fund research such as for innovative ultrasonic equipment for cleaning applications have been funded through crowd-sourcing schemes [75].

Nevertheless, there are certain risks that need to be addressed and minimized. To begin with, the regulations and amount of information ruling the use of US equipment are scarce. Logically, until they are not clarified, it will be hard to expand the current industrial applications of ultrasound and sonochemistry towards the consumers market with revolutionary ultrasonic equipment [76].

3 Overcoming Challenges and Opening New Opportunities

3.1 Integrating Ultrasound with Microfluidics

Going "micro" with ultrasound is not straightforward, neither is interpreting the results of experiments or processes, yet its potential for different chemical uses has already been identified [77]. Microfluidics enable the manipulation of chemical reactions using very small amounts of fluid, and ultrasound offers a good "non-invasive" alternative for several processes. Additionally, the small quantities of reagents, solvents, and waste, a precise control of reaction conditions, as well as the integration of functionality for process intensification, have all been highlighted as greener, safer, and often faster protocols [30]. On the other hand, answering the perennial question on how to process or produce larger volumes of liquids with microfluidics, several numbering-up and scaling-up strategies, as well as manifold-ing have been explored with varied success [78–81].

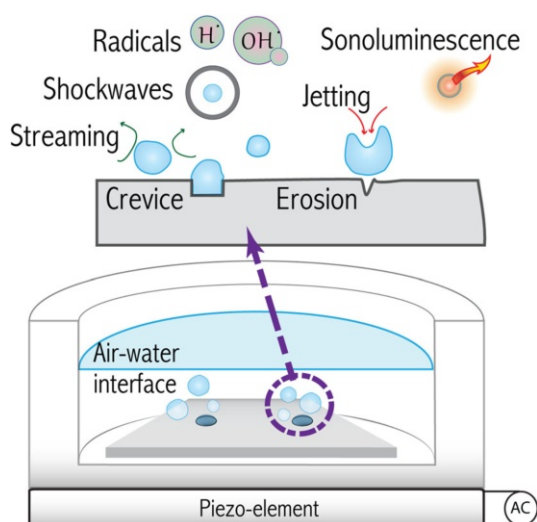
In designing the experimental setups that researchers have used to perform microfluidics and sonochemistry we can identify two main directions based on the final objective of the researchers and availability of resources of each group:

- Use of commercial existing equipment, where a capillary or microfluidic device is placed inside ultrasonic baths or in close contact with ultrasonic horns (see Fig. 1) [82–84].
- Tailor made ultrasonic setups, where a transducer or set of them are glued or clamped against the microfluidic device (see Fig. 4 Bottom) [85–90].

While using commercial devices will lead to fast implementation in the lab, bespoke setups allow an additional degree of customization and optimization in terms of energy efficiency, but also reaction yield. One key design parameter is the coupling between the ultrasound transducer and the microfluidic reactor [91], and such designed systems can then be applied to microfluidic liquid–liquid extraction [89], degradation of contaminants [92–94], and particle synthesis [95, 96].

The large number of techniques at hand and disparate existing knowledge on its effects, has detrimentally influenced the modest utilisation and adoption of ultrasonic cavitation and microfluidics in industry. Furthermore, the differences in experiments designed by chemists and physicists are as varied as the ways a lab researcher and a plant engineer interpret their results. Because of the complex interrelation of physicochemical phenomena resulting from the collapse of a bubble or a cluster of bubbles, replicating results and the choice of quantification techniques (calorimetry, chemical dosimetry, acoustics, optics, etc.) has been troublesome [97–103]. In the particular case of sonochemistry, it has reached the point of being labeled a “black art” [104]. Overall, there is an increasing interest in exploring the potential positive results brought up by combining these two techniques (ultrasound and microfluidics), as observed in specialized conferences

Fig. 4 *Top* Diagram illustrating the main phenomena associated to acoustic cavitation: radical production, shockwaves, sonoluminescence, jetting, and erosion. Bubbles are formed from crevices existing in the walls of the reactor or dissolved solid particles. *Bottom* A tailor-made ultrasonic setup in which a transducer (piezo-element) converts electricity into mechanical oscillations that are transferred to the liquid contained in the reactor. This configuration has been used for microfluidics studies



and other media. It is still in its early phases, and the reason why the progress is modest will be made more clear in the subsequent sections.

3.2 Entangled Effects of Cavitation

Acoustic cavitation can produce phenomena difficult to explain since it has interconnected variables with non-linear dependencies. The acoustic frequency, pressure amplitude, and other complex physicochemical parameters dictate the creation (or nucleation) and dynamic interaction of collapsing bubbles. The collapse of a bubble can be stable or transient, bubbles inside a cluster can be shielded by those outside; interaction forces between the acoustic field and bubbles (Bjerkness forces) are affected by the liquid properties (gas content, surface tension) and the geometry and materials of the reactors, to name a few [105, 106]. All of the above is further complicated “going down” in scale by confinement effects due to small scales, heat, and mass transfer phenomena. For example, when comparing 1D, 2D and 3D equivalent sonochemical reactors [107], an apparent increase in the reaction rate over the volume change was suggested to be due to the relaxation of space confinement when changing from 1D to 2D geometry. The reaction rate increased by 10 times while the volume increased by 57 times from 2D to 3D. A logical explanation was given by the fact that the total volume of a 3D reactor is not used as efficiently as the thinner layered channel, where nodes and antinode planes are not present. The power input dependencies also exhibit behaviours difficult to explain without a proper understanding of the underlying physicochemical mechanisms of cavitation (e.g. adiabatic compression of gas content dependence on the maximum and minimum radius, number, and spacial distribution of bubbles, shielding effects, etc.). In the same study, a decrease in the production rate of hydro-terephthalic acid (HTA) at higher input power density was found for 2D and 3D, but not in the 1D channel. In later studies, other puzzling correlations of power and an unexpected drop in radical production efficiency [85, 108] were explained by the change in the sphericity of bubble collapses. More details will be provided in the following Sect. 3.3.

From the chemical engineering and practical point of view, the most difficult hurdle for the wide acceptance of ultrasound and sonochemistry as a useful tool has been the measly energy efficiency values. The acoustic transducers transform electrical power into mechanical energy which is transmitted to the liquid. Part of the energy generates cavitation and another heats the whole system, hence not all of the energy produces the desired chemical and physical effects, making it difficult to establish a robust energy balance. For simplification purposes and using a relation reported in the literature [82, 109], we can define the sonochemical efficiency (or yield) as X_{US} = measured effect/input power; which in our particular case we define it as:

$$X_{US} = \frac{\Delta H(\Delta N_{rad}/\Delta t)}{P_{US}} \quad (3)$$

where ΔH is the energy required for the formation of $\text{OH}\cdot$ radicals, which is equal to the enthalpy of formation of the chemical reaction with a value of 5.1 eV per molecule [110]:



P_{US} is the electric power absorbed by the transducer which can be obtained from the measured voltage, current and their phase difference. This is clearly an underestimated value that can help in practical as well as in academic comparisons. Other “measured effects” can be used depending on the specific case, e.g. color dye degradation, mixing efficiency, calorimetric measurements. Depending on the specific study, on average the values reported for $OH \cdot$ radicals are in the order of $X_{US} \sim \mathcal{O}(10^{-6})$ [4, 85, 100, 111].

Ultrasonic cavitation is known to be difficult to reproduce since bubbles are normally created from impurities randomly distributed inside the reactor. Impurities such as defects on the walls (crevices) or dissolved solid particles are efficient traps for gas nuclei, and the acoustic nucleation threshold for bubbles trapped in cavities has theoretically and empirically been predicted [29, 112, 113]. The event of nucleation of a bubble from a crevice serves as a seed for subsequent cavitation. Depending on the acoustic conditions characteristic clouds of bubbles, also known as streamers, can persist for long periods [106, 114–117]. Effects such as inertia, surface tension, and viscous forces in a liquid influence the generation of microbubbles and have been studied with the help of non-dimensional numbers such as the ultrasound Weber number (We) and the ultrasound Womersley number (Wo).

$$We = \rho f^2 d_{in}^3 / \sigma \quad (5)$$

$$Wo = d_{in}(f/\nu)^{1/2} \quad (6)$$

where ρ is the density of the liquid, f is the ultrasound frequency, d_{in} is the diameter of the pinned bubble, σ stands for the interfacial tension and ν is the kinematic viscosity. The ratio of inertial and surface tension forces is given by the Weber number, We , and the Womersley number, Wo , represents the ratio of pulsatile to viscous forces. According to a particular study [114], a uniform diameter of bubbles is obtained when $8.16 < We < 300$ and $2 < Wo < 5$. For $Wo > 5$, the inertial effect dominates the viscous effect, resulting in bubbles of various sizes being released from the gas-liquid interface. When $Wo < 2$, the interface was not distorted sufficiently to release bubbles. When $We > 300$, the inertia dominates surface tension effects producing bubbles of various sizes. For small We , the interface oscillations are stable without strong distortion, and no bubbles are produced due to dominating surface tension effects.

In general, it has been possible to study to a good level of detail physicochemical exotic phenomena such as plasma formation inside the bubbles, the emission of light (sonoluminescence), radical production, shockwaves, streaming and jetting (see Fig. 4) [11, 98, 106, 111, 118–120]. The interaction of individual bubbles or clusters as they collapse among themselves and against nearby surfaces (see Fig. 2) has also been studied given its importance for applications such as erosion prevention, cleaning, surface modifications, biology, and several chemical processes [13, 121–126].

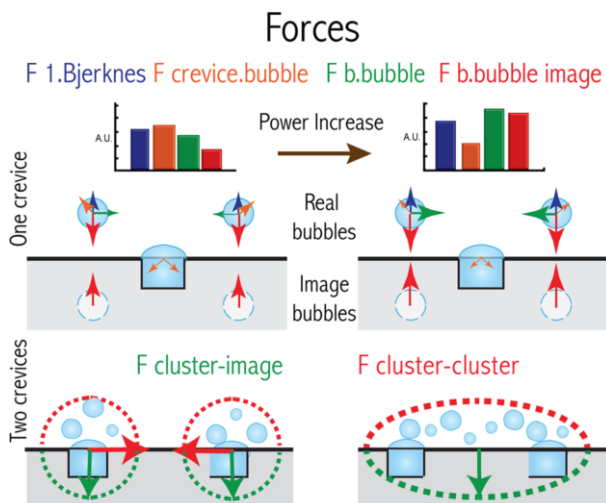


Fig. 5 Simplified representation of forces and colors associated to them represented in arbitrary units in a *bar plot* for two different power settings (higher to the *right*). The *top chart* depicts the case of a single crevice and how the bubbles around it interact with each other. The *bottom chart* shows similar information, but when two crevices are etched and how the clusters of bubbles interact (see Fig. 6 for more details)

In the particular cases that acoustic cavitation takes place close to a surface (see Fig. 5), interaction forces among the bubbles and the acoustic field alter the otherwise “ideal” spherical collapse. Oscillating bubbles, and bubble clusters oscillating close to a surface are attracted to their “image” on the virtual mirrored space. Jets and shockwaves emitted at different instants during acoustic cavitation are the main mechanisms responsible for the erosion of surfaces (see Fig. 4) [6, 13, 122, 127].

3.3 Controlling Cavitation with Microscopic Crevices

For a newcomer to the sonochemistry realm, it is important to understand that the rationale behind all the effects of cavitation begins with considering each bubble as a reactor in itself. Then, a working ultrasonic bath or horn will produce an undetermined number of bubbles of different sizes, and consequently each collapse will result in different temperatures and pressures inside of the bubble. It should be no surprise that as a result, the chemical or physical effects have a broad distribution of values, simply because all bubble-reactors behave different.

Despite the careful experimental precautions, the number of bubbles can be underestimated since some large bubbles overlap, and many smaller bubbles are not counted due to the optical resolution [108]. Nevertheless the qualitative and quantitative measurements of their number, coupled to the radical formation values can give relevant information to compare with other reports. Dividing the radical production per cycle by the average number of bubbles per cycle, gave bubble radical productions in the same order of magnitude measured by Didenko and

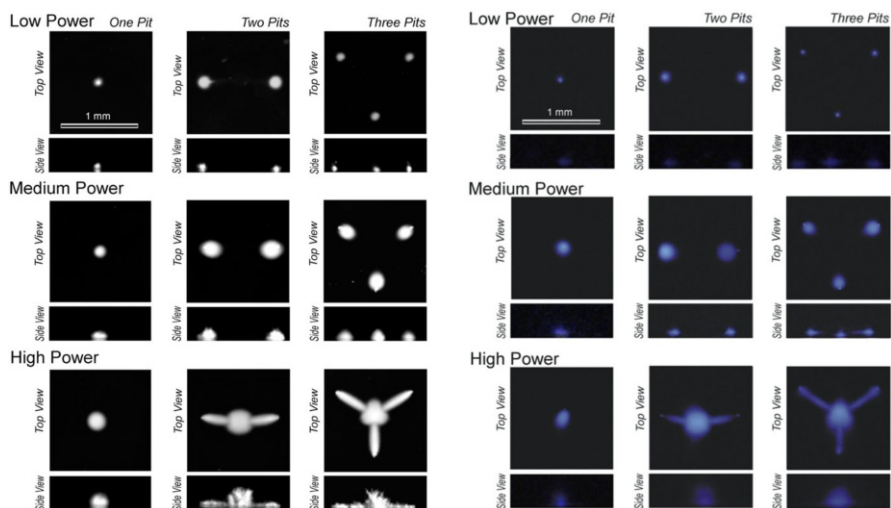


Fig. 6 *Left* Images showing *top* and *side* views of the bubble structures generated from micromachined silicon surfaces for different configurations (1, 2, and 3 crevices) and for increasing power level. Low (electrical) power corresponds to 74 mW, medium power to 182 mW, and high power to 629 mW. *Right* Corresponding Luminol luminescence in dark room conditions. The *scale bar* represents 1 mm of a microreactor with total volume of ca. 250 μl . Reproduced with permission from [85]. Copyright 2010 Wiley-VCH Verlag GmbH & Co. KGaA

Suslick [111] who reported data for a single bubble of maximum radius of 28.9 μm driven at 52 kHz producing $\text{OH}\cdot$ radical generation at a rate of 6.6×10^5 per cycle. These values for radical production can be taken as a reference of the order of magnitude that can be produced by a generic bubble in an ultrasonic reactor [128].

The quest to trap bubbles for the study of nucleation and collapse was initially driven by fundamental research questions. Different approaches have been used, from acoustic trapping to geometrical confinement of conical bubbles or micromachined crevices [86, 111, 114, 129, 130]. Focusing on aspects relevant for the chemical engineering community, we will elaborate on a series of recent results motivated by two practical questions:

1. How can the energy efficiency of sonochemical reactors be improved?
2. How can bubble generation be controlled reproducibly?

The challenge was, not surprisingly, conquered as a result of an interdisciplinary collaboration between microfabrication experts, physicists, and chemists. A microfluidic sonochemical reactor was designed, modeled and tested under laboratory conditions [85, 108, 131, 132], and more recently the same concept has been patented, scaled up, numbered up, and commercialised [133–135]. We consider this case a good example of the positive outcome of the synergy of microfluidics, ultrasound and process intensification concepts.

3.3.1 Batch Micro-Sono-Reactor

The structure of a batch ultrasonic reactor was modified by micromachining artificial crevices of ca. 30 μm diameter and 10 μm depth, unto the surface of silicon substrates. This passive modification was used as a trap for a determined number of bubbles (see Fig. 4). Upon sonication, the bubbles served as a seeding gas volume that ensured continuous formation of smaller bubbles (streamers) containing a mixture of gas and water vapor. This continued formation of bubbles can be sustained by virtue of a phenomenon termed “rectified diffusion” [27, 136]. This phenomenon occurs as a bubble expands, and gas-solvent molecules diffuse–evaporate into the bubble; conversely, when the compression part of the sound field arrives, gas-solvent molecules diffuse–condense out of the bubble. Because of an unbalance in the area in the expansion (larger) and compression phase (smaller), there is a net gain inside the bubble which can compensate any mass loss as the smaller bubbles are created from the crevice.

In the first report of a series of studies based on the same device [85], the streamers were demonstrated to produce hydroxyl radicals ($\text{OH}\cdot$) by imaging its reaction with luminol. The reaction rates were measured as a function of electrical power with terephthalic dosimetry (see Fig. 6).

As introduced in Sect. 3.2, though the efficiency when crevices were present was higher at the three powers tested (about one order of magnitude), at the highest power there was an unexpected drop. The efficiency values calculated with Eq. (4), are shown in Fig. 7. From a speculative analysis it was concluded that at high power, when the bubble pattern changes (see Fig. 6) a different radical generation

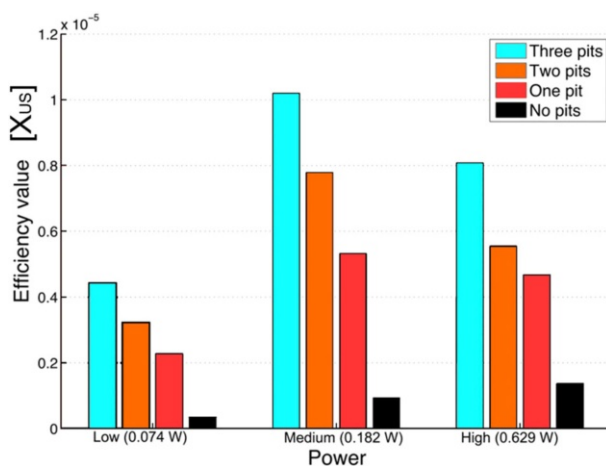


Fig. 7 Experimental efficiency values (X_{US}) for different number of crevices and different US powers calculated from Eq. (3) [108]. For each power the presence of crevices results in an increase in efficiency as the number of crevices is increased. As the power is increased from low to medium the trends increase for any number of crevices, except for high power, as it seems to decrease in all cases. Whether this result corresponds to true differences in the acoustic and sonochemical processes or to a decreased efficiency of conversion from electrical to mechanical power has not been clarified. Reprinted from [108]. Copyright 2013, with permission from Elsevier

distribution over the reactor volume could take place. Looking at each bubble as individual reactors, the energy efficiency of each collapse is strongly determined by the sphericity of the collapse, and the maximum size reached before collapsing. The smaller bubbles were thought to be stiffer due to a surface tension contribution and were not expected to grow considerably large during expansion. This leads to a consequently weaker compression and lower maximum temperatures reached after each collapse. Conversely, larger bubbles do not collapse spherically especially when close to a solid surface, hence limiting its maximum compression potential.

To clarify these assumptions, two complementary studies were devised. In the first one, the light emission from the collapse of bubbles (sonoluminescence) and as the result of the reaction of $\text{OH}\cdot$ with luminol (sonochemiluminescence) was measured with a photomultiplier [131]. Transient cavitation conditions were verified by measuring the SL intensity in propanol solutions. The different light intensities of SL and SCL helped to establish a difference in the bubble population able to emit light and those chemically active. This type of photosensitive study is important when it is impossible to capture the fast dynamics of bubble collapse with the available equipment. The second study was directed at taking short exposure images and fast-imaging movies for the determination of the number and sizes of bubbles [108]. The quantification of radicals was correlated with the number of bubbles and radius-time evolution in an acoustic cycle. The main conclusions from this study were that at higher powers, hence larger pressure fields in which bubbles expand and collapse, the shape of each bubble deviates from the ideal sphericity which corresponds to a maximum conversion of potential energy into sonochemical effects (shockwaves, liquid jets, sonoluminescence, and radical formation, see Fig. 8). Those bubbles that collapse towards each other, or in the proximity of an interface, deform and result in jet formation. As a result, not all the energy that could heat the bubble content is available for the rupture of chemical bonds, such as that of water molecule which is measured by the formation of $\text{OH}\cdot$ radicals.

From the reactor design perspective, the fact that bubbles remain close to the surface from which they were created can have negative consequences. With this microreactor that allows control over cavitation, the erosion caused by bubbles collapsing in the vicinity of different silicon substrates could be studied right from the initial incubation period and through more advanced stages [127]. The same effect of various sources of damage formation such as jetting, shock waves, direct bubble impact, and surface stress corrosion that can cause the damage observed for three crystallographic silicon surfaces studied, was later used for another useful application: the rapid removal from substrates of deposited organic and inorganic materials, such as biofilms [137]. The practical relevance of these results will be continued in the following subsection.

Contrary to what happens with most commercial ultrasonic equipment, tailor-made devices can in principle be operated at different frequencies. The studies of this micro-sono-reactor were conducted at one frequency (200 kHz) where it was more active. Based on what was discussed in Sect. 3.2, for the case of water and air on a 30 μm crevice we have $We = 15$ and $Wo = 13.4$, indicating that relatively small interface oscillations of the bubble in the crevice (small We) are unbalanced by inertia dominated effect resulting in bubbles of different sizes (large Wo).

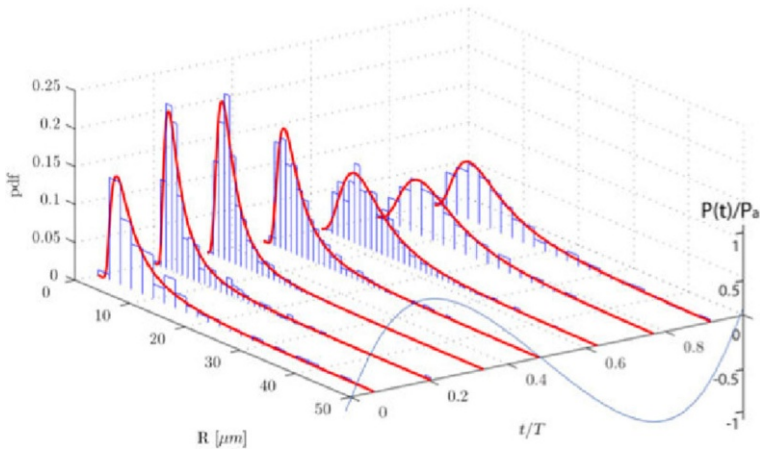
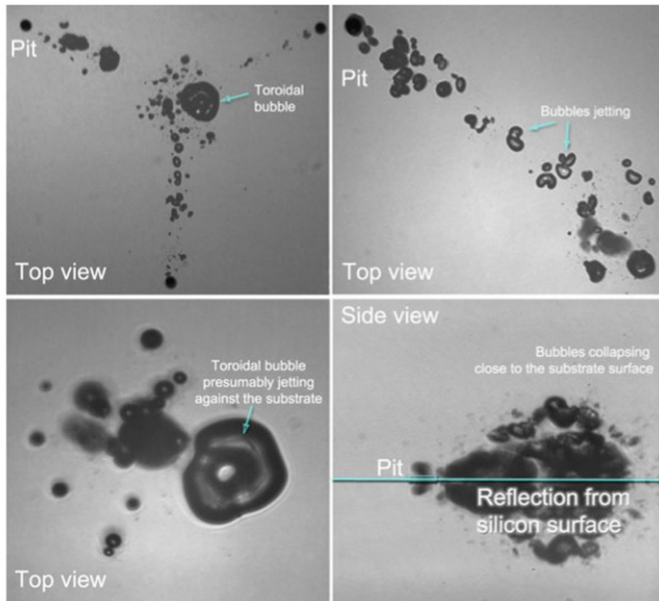


Fig. 8 *Top* Short time exposure image at high power settings (0.981 W) where the deformation of bubbles and jetting phenomena is visible. *Bottom* Bubble size distribution histograms at a power of 0.981 W for three pits. The axis to the *extreme right* represents the normalized pressure for the acoustic cycle. Reprinted from [108]. Copyright 2013, with permission from Elsevier

Snapshots of videos from experiments of this system indeed show significant bubble deformations of the bubbles ejected from the bubble stabilised on the crevice (see Fig. 8) [108, 117]. We have not found in the literature other studies reporting on such large values for both numbers, hence a parametric study in this direction would be highly valued for future applications. Similar studies addressing the effect of different frequencies in the same reactor will shine more light into the challenging “black” field of sonochemistry.

3.3.2 Scaled-Up Non-Conventional Batch Reactor

Scaling-up or numbering-up are the most frequent strategies used in microfluidics whenever there is an interest in practical applications beyond the lab-scale. Small volumes ca. 250 μl , such as the ones used in the studies mentioned in the previous sections are of limited relevance for practical or industrial uses. Making larger crevices or higher amplitudes to obtain larger bubbles before collapse does not correlate linearly with better results, as explained in Sect. 3.3.1. Additionally, despite the unique control over the location of bubble clouds, it is difficult to envisage any commercial appeal that the presence of a few crevices etched on the bottom of a batch reactor can produce. Even when the numbering-up of crevices might be possible by drilling crevices on the surfaces of ultrasonic baths or the tips of horns, it seems like an improbable option for all manufacturers of baths and horns.

In trying to find a universal solution that could be used in most ultrasonic equipment, the new concept of the Bubble Bag was devised [134]. The inner surface of a bag that serves as a container can be indented with crevices for gas entrapment (see Fig. 9). It has been described as a cavitation intensifying bag since it enables a production of bubbles that does not take place on a simple bag. The Bubble Bag can be interpreted as sophisticated beaker, initially made of plastic, but it can be manufactured in any other material since the principle for creating bubbles from crevices has already been demonstrated in silicon and glass. The first and most versatile advantage is that it does not depend on a particular frequency for cavitation to happen as demonstrated with several pieces of ultrasonic equipment; see in Fig. 9 the results of two ultrasonic baths with different frequencies with and without crevices. The second advantage schematically represented in Fig. 10 is that numbering-up of such a beaker is straightforward.

Designed originally for cleaning arbitrary objects [135], the current dimensions and potential use for radical generation allows us to classify it as a milli-reactor [138]. Using the same configuration, the bags can also be used for other applications such as emulsification, and presumably for any physicochemical processes where ultrasound is currently used [139, 140]. The most relevant scientific advantage is that reproducibility of results and energy efficiency are considerably better than when compared with a bag not having crevices. The standard deviation of radicals detected was reduced by 22 %, accompanied by an increase of 45.1 % in efficiency (see Fig. 9). The number of pits and bags can be in principle as large as the ultrasonic equipment allows for. New optimisation and characterisation studies will be required to find the best position or configuration of transducer-bag positioning. So far, the Bubble Bag has been operated in batch mode; we expect to provide more results as a flowing reactor in the near future in a multiple-stage assembly. We believe this concept will lead to new applications and improved versions to be reported in the specialised literature.

To conclude with this section, in Fig. 10 we illustrate the trends identified up to now and where we believe the future developments will head to: intensified continuous flow and industrial scale sonochemical reactors.

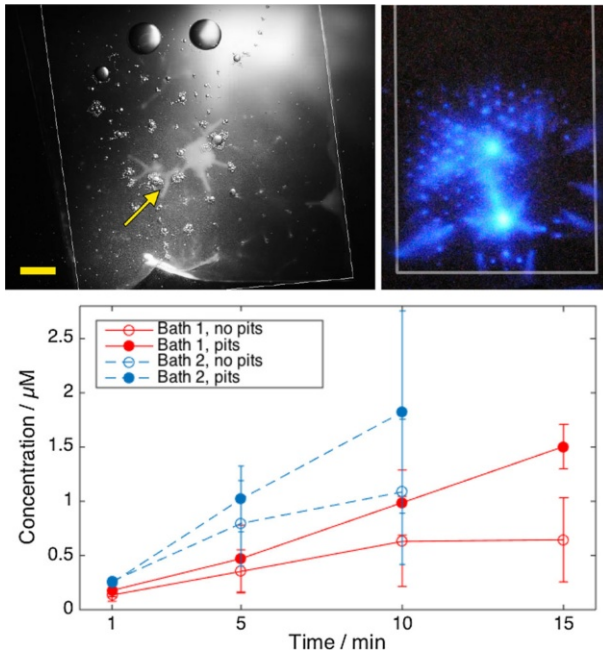


Fig. 9 *Left* Clouds of bubbles inside a cavitation intensifying bag; *right* sonochemiluminescence as a result of the radicals produced by the bubbles upon reaction with luminol. The *arrow* indicates the bubble clouds emerging from the crevices. The *scale bar* corresponds to 5 mm. *Bottom* Radical production in bags with and without pits, as a function of time and for a large (45 kHz, 364 kPa and 33.3 W/L) and a small (35 kHz, 427 kPa and 24.2 W/L) ultrasonic bath. Reproduced with permission from [134]. Copyright 2010 Wiley-VCH Verlag GmbH & Co. KGaA

3.4 Acoustic Streaming

A phenomena increasingly exploited in microstructured devices is acoustic streaming. In general terms, acoustic streaming is the generation of a convective motion (i.e. fluid flow) through the presence of an acoustic field [141]. Real fluids exhibit a viscous attenuation towards an acoustic wave traveling through them, which in the case of an oscillatory acoustic field results in a time-averaged displacement of individual fluid elements. This local displacement can develop into a steady fluid flow, termed acoustic streaming [142]. Depending on the location and length-scale of the fluid motion several sub-categories of acoustic streaming can be defined, such as boundary layer driven streaming (Schlichting and Rayleigh streaming), Eckart streaming in the bulk fluid, and cavitation microstreaming [141, 143]. In the following we will discuss each streaming phenomena and provide application examples in microfluidics.

Boundary layer driven streaming Because of the no-slip condition at a solid interface, the fluid flow in the boundary layer is characterized by a steep velocity gradient. In turn, this steep velocity gradient is also responsible for a larger viscous dissipation of acoustic energy compared to bulk flow [144]. Applying a standing acoustic wave parallel to the solid interface results in spatially fixed pressure nodes

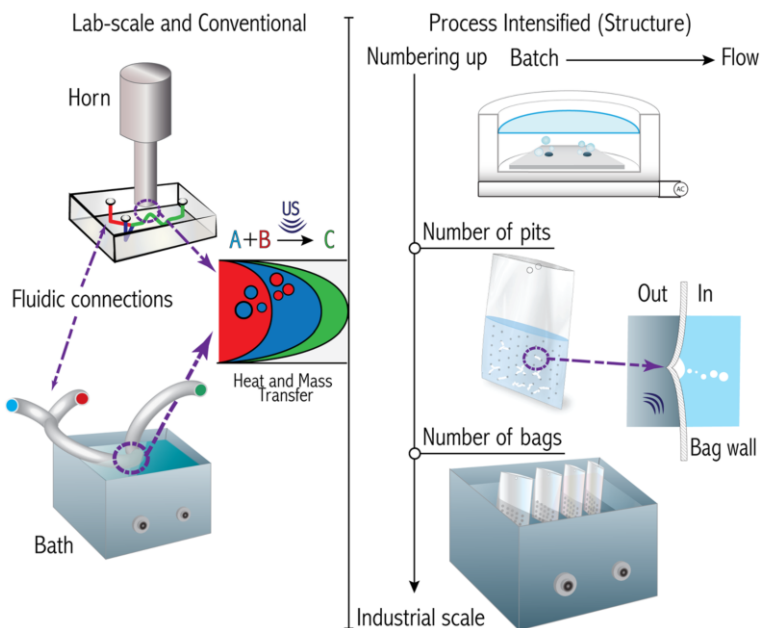


Fig. 10 *Left pane* conventional and lab-scale uses in which existing ultrasonic devices such as horns and baths are used to promote reactions. *Right pane* An example of scaling-up a micro-sonochemical reactor by increasing its volume and numbering-up the amount of crevices and the Bubble bag

and antinodes, which leads to a steady vortical fluid motion in the boundary layer (termed Schlichting streaming). These vortices in the inner boundary layer will excite counter-rotating vortices in the outer boundary layer, and this induced streaming motion is termed Rayleigh streaming [145].

Boundary layer driven streaming in microfluidics is often employed for particle trapping, e.g. to either control local particle concentration [146], particle aggregation [147], or to separate particles based on their size (in combination with the acoustic radiation force acting on the particles) [54, 143, 148]. However, it can also be used to overcome one of the disadvantages of microstructured devices, i.e. that the only means of mixing is by diffusion due to the predominant laminar flow. Rayleigh streaming has been shown to improve micromixing [149].

Eckart streaming When the dissipation of the acoustic energy takes place in the bulk of the fluid, Eckart streaming is observed. However, as microstructured devices are characterized by a large surface-to-volume ratio, their hydrodynamics is governed by boundary layers, and bulk flow is rarely encountered [141]. In general, Eckart streaming will only occur when high frequency ultrasound is applied, and when the characteristic dimension (defined as the propagation direction of the acoustic wave) is in the order of millimeters.

Consequently, the applications of Eckart streaming are limited in microfluidics. However, based on the experimental observation that the resulting convective motion is characterized by high velocity jets [150], it has been used to design a valveless ultrasonic pump [151].

Cavitation microstreaming Cavitation microstreaming is generated by the acoustically driven oscillations of microbubbles in a liquid. These oscillations are transferred via the boundary layer surrounding the bubble and generate vorticity and convective motion in the fluid [152]. In addition to the streaming motion, oscillating bubbles will also create stress fields in their surrounding, which largely depend on their mode of oscillation [153].

These stress fields coupled with the streaming effect enable the therapeutic use of microbubble-mediated ultrasound. An increased permeability of cell membranes has been observed, which allows e.g. targeted drug delivery. In addition, the combination of microbubbles and ultrasound have been shown to accelerate the breakdown of blood clots (thrombolysis) [154]. Furthermore, cavitation microstreaming is also applied to enhance mixing in microfluidic devices [155].

3.5 Clogging Prevention

In this section we will review the handling of solids in microfluidic systems. The solid material can either be comprised of an unwanted and insoluble by-product of a reaction, or the target compound (e.g. nanoparticle synthesis or crystallization of organic molecules). In general, managing solid particles in flow represents a major challenge for the upstream, continuous processing of fine chemicals in microreactors [56]. Many synthetic organic reactions either involve the use or the generation of insoluble compounds [57]. In the following we will discuss the ultrasound application strategies to control the particle formation within the microchannel.

The impact of channel clogging on continuous manufacturing is best illustrated with a study conducted at Lonza [156]: In a screen of 86 different reactions it was found that 59 % would benefit from a continuous process, however, this number reduced to 19 % due to the presence of solids. Consequently, to assist the transition from conventional batch to continuous manufacturing processes exploiting microreaction technology, reliable solids handling needs to be established.

Figure 11 depicts the main interactions governing particle behavior in microfluidic channels, namely particle-fluid, particle-particle, and particle-surface interactions [58].

The relative importance of these interactions differs on a case by case basis, which leads to several phenomena discussed below: Deposition of particles (Fig. 11a) is initiated by particle-fluid interactions transporting the solid to the microchannel wall where it finally sticks due to a dominating particle-surface interaction. Increasing the particle-fluid interaction by e.g. increasing the fluid velocity will lead to resuspension (Fig. 11b). The particles will agglomerate in the bulk of the fluid by particle-particle interactions (Fig. 11c); however, agglomerate break-up can again occur when the particle-fluid interactions overcome the inter-particle interactions. As we will discuss later, this is one of the main avenues where ultrasound comes into play, as the induced cavitation will give rise to hydrodynamic forces on the agglomerates and thus decrease their size. The clogging phenomena itself (Fig. 11d) is governed by all three interactions, and usually occurs via bridging of a constricted microchannel cross-section [56, 57].

The most used passive means to prevent microchannel clogging are:

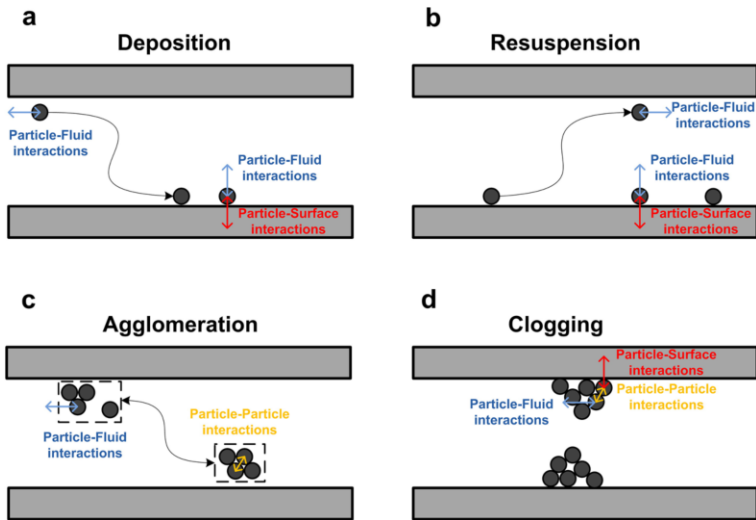


Fig. 11 Interactions governing the behavior of solid particles in microchannels [58]. Particle-fluid, particle-particle, and particle-surface interactions are always present, but their relative importance differs widely depending on the considered case (deposition, resuspension, agglomeration, and clogging). Reproduced with permission from [58]. Copyright 2014 Tekno Scienze Srl

- Application of two-phase flow, allowing the introduction of a secondary phase which dissolves the solids. However, this also introduces additional mass transport limitations.
- Increasing the wall shear stress by increasing the fluid velocity.
- Reactor surface modification, mostly based on fluoropolymers, to achieve non-sticking reactor walls.

The passive techniques are reviewed elsewhere [56–58], here we primarily focus on active clogging prevention using ultrasound.

The integration of acoustic actuators with microstructures is a new and emerging area, where the acoustic energy is mostly supplied using transducers or piezoelectric microdevices with different sizes and geometries [77, 157–161]. One application of ultrasound integration in microfluidics is the excitation of a standing acoustic wave in the fluidic channel [53]. Particles in an acoustic standing wave field will experience an acoustic radiation force [54], which can be exploited for the manipulation of their trajectories [162]. This concept can even be extended to controlling the trajectory of single bubbles [163].

At increased power, acoustic irradiation has been shown to be successful in reducing agglomerate particle size, which is essential to prevent clogging [158, 159, 164]. A well studied reaction system and also a challenge under flow conditions due to clogging is that of Pd-catalyzed CN cross-couplings [158]. Under typical reaction conditions inorganic by-products precipitate immediately in the non-polar solvents needed for this transformation. Furthermore, the recent

developments of highly active palladium catalysts which allow for extremely fast reactions, and thus also a fast generation of these inorganic salts.

One approach to prevent clogging is to immerse Teflon tubing in an ultrasonic bath for irradiation, as shown in Figs. 10 and 12a [159] and discussed in Sect. 3.1.

However, when using an ultrasonic bath, one has to be aware of the fact that not a single frequency is excited, but the resulting waveform can be quite complex [158]. Furthermore, the emitted ultrasonic waves first need to couple with the media in the bath before transferring to the microreactor. As such, integrating a piezoelectric actuator directly into the microfluidic assembly to directly transmit the acoustic waveform to the reactor is energetically more efficient, as mentioned in Sect. 3.1. An example of such a layered microreactor system is shown in Fig. 12b, which was also successfully applied to the aforementioned Pd-catalyzed CN cross-couplings and allowed for long term operation [160]. High-speed imaging revealed the formation of gas bubbles upon ultrasonic irradiation via the mechanism of stable cavitation, and the pressure forces associated with this formation lead to the breakup of the particle agglomerates [165–167]. This phenomena is clearly depicted in Fig. 13, which shows the fragmentation of a calcite crystal due to the collapse of a bubble.

Furthermore, using piezoelectric actuators allows for a precise control of the operating frequency, which is important to control the resulting size of the agglomerates. Figure 12c depicts the particle size distribution of inorganic precipitates subject to the applied ultrasound frequency, and for the particular setup the identified optimum frequency corresponded to 50 kHz.

3.6 Microfluidics As a Tool for Particle Synthesis

Microfluidic systems have also seen an increase in use for cases where the particulate matter is the desired product. Continuous manufacturing enables the formation of particles with narrow size distribution, which is an important property for their final application. In general, particles of similar properties will be formed when they experience similar conditions in the reactor, which is difficult to achieve in batch systems due to mixing limitations associated with their large size, but feasible on the micro-scale using continuous flow.

However, focusing on particle formation processes, these devices need not only overcome clogging of the microchannels, but also ensure kinetic control of nucleation, growth, and agglomeration. The same Teflon reactor design with integrated piezoelectric actuator as outlined above was applied to the crystallization of hydroxyapatite (HAp) in continuous flow [168, 169]. Compared to the batch process (stirred tank reactor), the HAp particles formed were more crystalline and less carbonate contaminated. The sonication strategy also lead to a reduction in particle aggregation and primary particle size; however, the resulting particle size distribution was poly-modal, which strongly suggested that the nucleation, growth and agglomeration processes were not precisely enough controlled in this system. A decoupling of nucleation and growth of particles in the reactor will increase this kinetic control, and one example to achieve this is the use of an ultrasonic horn next to the microchannel [95]. This will create a spatially localized zone within the reactor for the generation of

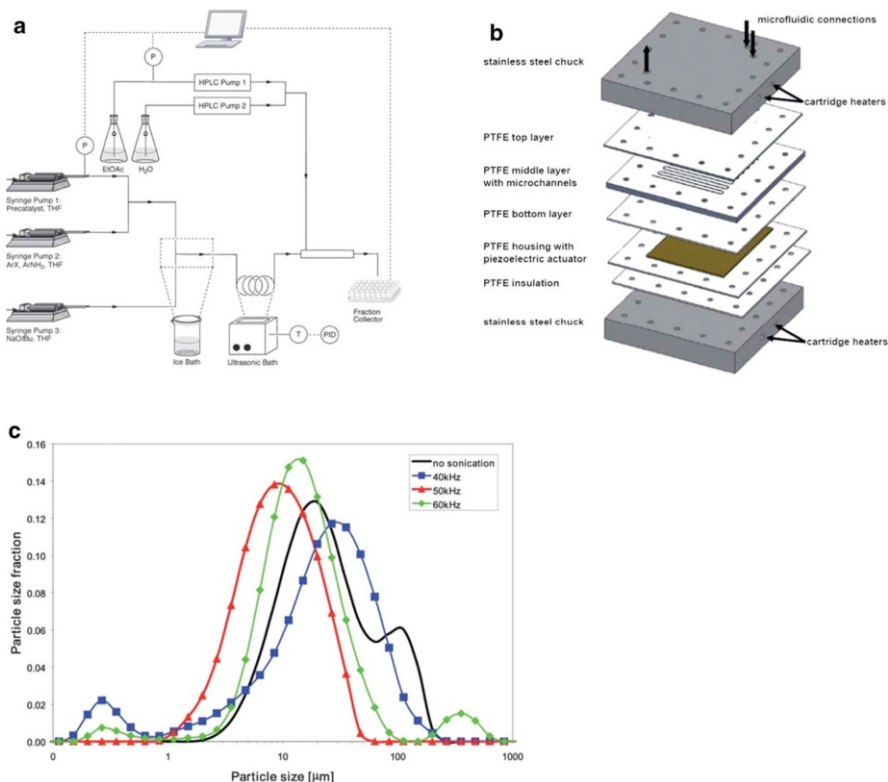


Fig. 12 Examples of the use of ultrasound in microfluidic systems to prevent clogging. The methods of ultrasound integration range from immersing the reactor in an ultrasonic bath (**a**) to a full reactor assembly with the ultrasound transducer positioned next to the microfluidic channels (**b**). **a** Using an ultrasonic bath to handle solids formed during palladium-catalyzed amination reactions [159]. Reproduced from [159] with permission of The Royal Society of Chemistry. **b** A Teflon microreactor with integrated piezoelectric actuator to handle solid forming reactions [160]. Reproduced from [160] with permission of The Royal Society of Chemistry. The latter design eliminates the need of a transfer medium for the acoustic wave, and allows precise control of the applied ultrasound frequency and power. **c** The final precipitate particle size depends on the applied ultrasound frequency, and consequently a precise control of the operating parameters is desired for the combination of ultrasound and microfluidics [160]. Reproduced from [160] with permission of The Royal Society of Chemistry

crystal nuclei. Using a similar setup, Rossi et al. [96] studied the effect of supersaturation and ultrasound power on nucleation in more detail, and it was concluded that the transient cavitation of bubbles is a significant mechanism for enhancing crystal nucleation.

4 Outlook and Future Applications

We aimed to cover most of the recent examples of the use of microfluidics and ultrasound in which given processes have been intensified. As mentioned in the text, we shared our conclusion that synergy, as described in process intensification terms,

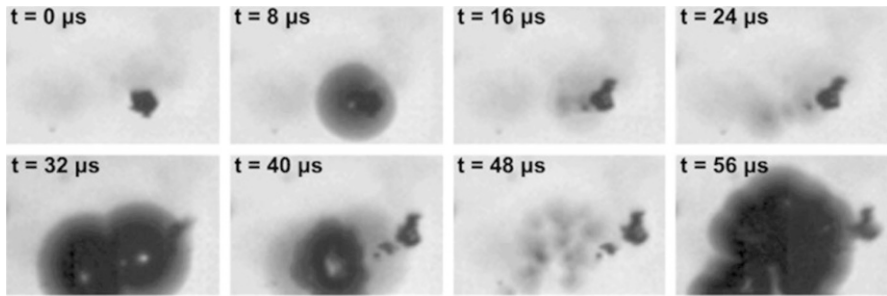


Fig. 13 Images of an oscillating cavitation bubble that nucleated on the surface of a calcite crystal. The single crystal fragmentizes as a result of the violent collapse of the bubble [165]. Reprinted from [165]. Copyright 2013, with permission from Elsevier

plays the largest role in the combination of microfluidics and ultrasound applications.

We have highlighted the emerging availability of commercial devices, but also stated that customisation leads to increased efficiency and product yield. As such, we see the future need for a plug-and-play approach, with readily available off-the-shelf components, which allow custom designed experimental setups. We speculate that market and society requirements will be the drivers for the developments we might see along this line, particularly in the food processing, nanomaterials synthesis, cosmetics, medicine, and other relevant applications.

On the scientific front we identified several developments which warrant further investigation to gain a more fundamental understanding. In terms of cavitation, we pose the following research questions:

- Is it possible to control further processes and applications such as the synthesis of nanomaterials, exfoliation of nanoparticles, or the improved properties of emulsions of relevance in food processing, coatings, etc.?
- How much more can a sonochemical reactor based on artificial crevices be scaled-up efficiently with a continuous flow operation? This is of relevance for applications where large volumes need to be processed as in water treatment or food processing.
- Can the surface of bubbles be further used as a “meeting point” for reactive species, so that bubbles can act as catalytic reaction spots with higher control than currently achieved?

In the field of particle synthesis and solid precipitation the following questions should be addressed:

- What is the influence of cavitation intensity on crystal nucleation rates? Using crevices for obtaining controlled transient cavitation could improve crystal nucleation mechanisms, and hence will be worth addressing in future studies.
- Is there a critical cavitation bubble size to enhance nucleation?

- What is the effect of ultrasound irradiation on crystal growth; e.g. can we exploit acoustic streaming to enhance convective mass transfer to achieve increased growth rates?

Our vision of where the field is going is open to debate and we invite colleagues to enrich it with future ideas.

Acknowledgments We thank our colleagues P. Cintas, H. Gardeniers, B. Verhaagen, for useful suggestions. S.K. acknowledges funding from the European Research Council under the ERC Starting Grant Agreement n. 677169–MicroParticleControl.

Open Access This article is distributed under the terms of the Creative Commons Attribution 4.0 International License (<http://creativecommons.org/licenses/by/4.0/>), which permits unrestricted use, distribution, and reproduction in any medium, provided you give appropriate credit to the original author(s) and the source, provide a link to the Creative Commons license, and indicate if changes were made.

References

1. Neppiras EA (1972) *Ultrasonics* 10(1):9
2. Suslick KS, Price GJ (1999) *Annu Rev Mater Sci* 29:295
3. Cravotto G, Cintas P (2006) *Chem Soc Rev* 35(2):180
4. Gogate PR (2008) *Chem Eng Process* 47(4):515
5. Chandrapala J, Oliver C, Kentish S, Ashokkumar M (2012) *Ultrason Sonochem* 19(5):975
6. Mason TJ (2016) *Ultrason Sonochem* 29:519
7. Petersson F, Åberg L, Swärd-Nilsson AM, Laurell T (2007) *Anal Chem* 79(14):5117
8. Bernassau A, Glynn-Jones P, Gesellchen F, Riehle M, Hill M, Cumming D (2014) *Ultrasonics* 54(1):268
9. Suslick K (1990) *Science* 247:1439
10. Neppiras EA (1980) *Phys Rep Rev Sect Phys Lett* 61(3):159
11. Lohse D (2005) *Nature* 434(7029):33
12. Dharmarathne L, Grieser F (2016) *J Phys Chem A* 120(2):191
13. Verhaagen B, Rivas DF (2016) *Ultrason Sonochem* 29:619
14. Jensen KF (2001) *Chem Eng Sci* 56(2):293
15. Ehrfeld W, Hessel V, Loewe H (2000) *Microreactors: new technology for modern chemistry*. Wiley, Germany
16. Hessel V, Angeli P, Gavriilidis A, Löwe H (2005) *Ind Eng Chem Res* 44(25):9750
17. Hessel V, Noël T (2012) *Ullmann's encyclopedia of industrial chemistry*, chap. 1. Introduction. Wiley, Germany
18. Hessel V, Noël T (2012) *Ullmann's encyclopedia of industrial chemistry*, chap 2. Processing. Wiley, Weinheim
19. Modestino M, Fernandez Rivas D, Hashemi S, Gardeniers HJGE, Psaltis D (2016) *Energy Environ Sci*. doi:10.1039/c6ee01884j
20. Hartman RL, Naber JR, Buchwald SL, Jensen KF (2010) *Angewandte Chemie* 49(5):899
21. Qin D, Xia Y, Rogers J, Jackman R, Zhao XM, Whitesides G (1998) *Microsystem technology in chemistry and life science*. In: *Microfabrication, microstructures and microsystems*, vol 194. Springer, Berlin, pp 1–20
22. Lohse D, Zhang X (2015) *Rev Mod Phys* 87(3):981
23. Serizawa A, Feng Z, Kawara Z (2002) *Exp Thermal Fluid Sci* 26(6–7):703
24. Berger R, Misek T, Schröter J (1985) *Standard test systems for liquid extraction*. Tech rep
25. Cheong WJ, Carr PW (1987) *J Liq Chromatogr* 10(4):561

26. Tandiono SW, Ohl DSW, Klaseboer E, Wong VVT, Camattari A, Ohl CD (2010) *Lab Chip* 10(14):1848
27. Ashokkumar M, Mason TJ (2000) *Sonochemistry*. Wiley, Hoboken
28. Neppiras E, Noltingk B (1951) *Proc Phys Soc Sect B* 64(12):1032
29. Atchley AA, Prosperetti A (1989) *J Acoust Soc Am* 86(3):1065
30. Cintas P (2016) *Ultrason Sonochem* 28:257
31. Compton RG (2016) *Electrochem Commun* 64:A1
32. Cintas ECGP, Cravotto G, Rivas DF (2016) 15th Meeting of the European Society of Sonochemistry
33. Van Gerven T, Stankiewicz A (2009) *Ind Eng Chem Res* 48(5):2465
34. Kockmann N (2006) Micro process engineering: fundamentals, devices, fabrication, and applications. In: *Process engineering methods and microsystem technology*. Wiley, New York, pp 1–45
35. Reay D, Ramshaw C, Harvey A (2008) *Process intensification*. Elsevier, Amsterdam, pp 103–186
36. Gardeniers J (2011) *Microchem Eng Pract* 449–474
37. Hartman RL, Jensen KF 9(17):2495
38. Hartman RL, McMullen JP, Jensen KF (2011) *Angewandte Chemie Int Ed*
39. Hatakeyama T, Chen DL, Ismagilov RF (2006) *J Am Chem Soc* 128(8):2518
40. Song H, Chen DL, Ismagilov RF (2006) *Angewandte Chemie Int Ed* 45(44):7336
41. Kreutz JE, Shukhaev A, Du W, Druskin S, Daugulis O, Ismagilov RF (2010) *J Am Chem Soc* 132(9):3128
42. McMullen JP, Stone MT, Buchwald SL, Jensen KF (2010) *Angewandte Chemie* 49(39):7076
43. McMullen JP, Jensen KF (2010) *Annu Rev Anal Chem* 3:19
44. McMullen JP, Jensen KF (2011) *Organic Process Res Dev* 15(2):398
45. Hessel V, Wang Q (2011) *Chimica oggi/Chem Today* 29(3)
46. Gutmann B, Cantillo D, Kappe CO (2015) *Angewandte Chemie International Edition*
47. Trachsel F, Hutter C, Rudolf von Rohr P (2008) *Chem Eng J* 135:S309
48. Trachsel F, Tidona B, Desportes S, Rudolf von Rohr P (2009) *J Supercrit Fluids* 48(2):146
49. Marre S, Roig Y, Aymonier C (2012) *J Supercrit Fluids* 66:251
50. Noël T, Kuhn S, Musacchio AJ, Jensen KF, Buchwald SL (2011) *Angewandte Chemie Int Ed* 50:5943
51. Cambié D, Bottecchia C, Straathof NJW, Hessel V, Noël T (2016) *Chem Rev*
52. Rackus DG, Shamsi MH, Wheeler AR (2015) *Chem Soc Rev* 44(15):5320
53. Friend J, Yeo LY (2011) *Rev Mod Phys* 83:647
54. Bruus H (2012) *Lab Chip* 12:1014
55. Jimenez-Gonzalez C, Poechlauer P, Broxterman Q, Yang B, Am Ende D, Baird J, Bertsch C, Hannah R, Dell’Orco P, Noorman H, Yee S, Reintjens R, Wells A, Massonneau V, Manley J (2011) *Organic Process Res Dev* 15(4):900
56. Flowers BS, Hartman RL (2012) *Challenges* 3(2):194
57. Hartman RL (2012) *Organic Process Res Dev* 16:870
58. Wu KJ, Kuhn S (2014) *Chem Today* 32:62
59. Anastas PT, Zimmerman JB (2003) *Environ Sci Technol*
60. Mason TJ (2007) *Ultrason Sonochem* 14(4):476
61. Kjeang E, Djilali N, Sinton D (2009) *J Power Sour* 186(2):353
62. Symes MD, Kitson PJ, Yan J, Richmond CJ, Cooper GJT, Bowman RW, Vilbrandt T, Cronin L (2012) *Nat Chem* 4(5):349
63. Comina G, Suska A, Filippini D (2014) *Lab Chip* 14(16):2978
64. Porta R, Benaglia M, Puglisi A (2015) *Org Process Res Dev*. [acs.oprd.5b00325](https://doi.org/10.1021/acs.oprd.5b00325)
65. Modestino MA, Haussener S (2015) *Annu Rev Chem Biomol Eng*
66. Fernandez Rivas D, Verhaagen B, Walsh S (2015) *Commer Micro Manuf Int* 8(6):30
67. Cintas P, Tagliapietra S, Caporaso M, Tabasso S, Cravotto G (2015) *Ultrason Sonochem* 25(C):8
68. Schwab K (2016) *World economic forum*
69. <http://www.enablingmnt.com> (2016)
70. Junkers M (2016) *Microreact Technol*. <http://www.sigmaaldrich.com/technical-documents/articles/chemfiles/microreactor-technology.html>
71. Burns J (2007) 21st PIN Meeting November
72. Corsi P, Dulieu M (2013) *The marketing of technology intensive products and services: driving innovations for non-marketers*. Wiley, New York
73. Leonelli C, Mason TJ (2010) *Chem Eng Process* 49(9):885

74. <https://www.hielscher.com/ultrasonic-cooking-basics-recipes.htm> (2016)
75. <https://www.indiegogo.com/projects/dolfi-next-gen-washing-device/> (2016)
76. Leighton TG (2016) *Proc R Soc Lond A Math Phys Eng Sci* 472:2185
77. Fernandez Rivas D, Cintas P, Gardeniens J (2012) *Chem Commun* 48(89):10935
78. Tonkovich A, Kuhlmann D, Rogers A, McDaniel J, Fitzgerald S, Arora R, Yuschak T (2005) *Chem Eng Res Des* 83(6A):634
79. Roberge DM, Zimmermann B, Rainone F, Gottsponer M, Eyholzer M, Kockmann N (2008) *Org Process Res Dev* 12(5):905
80. Elvira KS, Solvas XCI, Wootton RCR, Demello AJ (2013) *Nat Chem* 5(1):905
81. Su Y, Kuijpers K, Hessel V, Noël T (2016) *React Chem Eng*
82. Berlan J, Mason TJ (1992) *Ultrasonics* 30(4):203
83. Thangavadiel K, Owens G, Lesniewski PJ, Okitsu K (2013) *Ind Eng Chem Res* 52(51):18175
84. Chen H, Li J, Zhou W, Pelan EG, Stoyanov SD, Arnaudov LN, Stone HA (2014) *Langmuir* 30(15):4262
85. Fernandez Rivas D, Prosperetti A, Zijlstra AG, Lohse D, Gardeniens JGE (2010) *Angewandte Chemie International Edition* 49(50):9699
86. Tandiono SW, Ohl DSW, Klaseboer E, Wong VV, Dumke R, Ohl CD (2011) *Proc Natl Acad Sci USA* 108(15):5996
87. Navarro-Brull FJ, Poveda P, Ruiz-Femenia R, Bonete P, Ramis J, Gómez R (2014) *Green Process Synth* 3(5):311
88. Dong Z, Yao C, Zhang X, Xu J, Chen G, Zhao Y, Yuan Q (2015) *Lab Chip* 15(4):1145
89. John JJ, Kuhn S, Braeken L, van Gerven T (2016) *Chem Eng Process Process Intensif* 102:37
90. Matsuoka M, Takahashi F, Asakura Y, Jin J (2016) *Jpn J Appl Phys* 55(7S1):07KB01
91. Bora M, Shusteff M (2015) *Lab Chip* 15:3192
92. Thangavadiel K, Konagaya M, Okitsu K, Ashokkumar M (2014) *J Environ Chem Eng* 2(3):1841
93. Colmenares JC (2014) *ChemSusChem*
94. Sathishkumar P, Mangalaraja RV, Anandan S (2016) *Renew Sustain Energy Rev* 55:426
95. Jiang M, Papageorgiou CD, Waetzig J, Hardy A, Langston M, Braatz RD (2015) *Crystal Growth Des* 15(5):2486
96. Rossi D, Jamshidi R, Saffari N, Kuhn S, Gavriilidis A, Mazzei L (2016) *Cryst Growth Des* (2015)
97. Price GJ, Lenz EJ (1993) *Ultrasonics* 31(6):451
98. Matula TJ, Roy RA, Mourad PD, McNamara WB III, Suslick KS (1995) *Phys Rev Lett* 75(13):2602
99. Segebarth N, Eulaerts O, Reisse J, Crum LA, Matula TJ (2002) *J Phys Chem B* 106(35):9181
100. Sutkar VS, Gogate PR (2009) *Chem Eng J* 155(1–2):26
101. Zhou M, Yusof NSM, Ashokkumar M (2013) *RSC Adv* 3(24):9319
102. Al-Juboori RA, Yusaf T, Bowtell L, Aravinthan V (2015) *Ultrasonics* 57:18
103. Verhaagen B, Zanderink T, Fernandez D (2016) *Rivas Appl Acoust* 103:172
104. Mason TJ, Lorimer JP, Bates DM (1992) *Ultrasonics* 30(1):40
105. Leighton TG (1994) The acoustic bubble. In: *An introduction for surface scientists and nanoscientists*. Academic Press, London
106. Lauterborn W, Kurz T (2010) *Rep Prog Phys* 73(10):106501
107. Iida Y, Yasui K, Tuziuti T, Sivakumar M, Endo Y (2004) *Chem Commun* 2280–2281
108. Fernandez Rivas D, Stricker L, Zijlstra AG, Gardeniens JHGE, Lohse D, Prosperetti A (2013) *Ultrason Sonochem* 20(1):510
109. Mason TJ, Lorimer JP, Bates DM, Zhao Y (1994) *Ultrason Sonochem* 1(2):S91
110. Toegel R, Hilgenfeldt S, Lohse D (2002) *Phys Rev Lett* 88:034301
111. Didenko YT, Suslick KS (2002) *Nature* 418(6896):394
112. Borkent BM, Gekle S, Prosperetti A, Lohse D (2009) *Phys Fluids* 21(10)
113. Trevena DH (1984) *J Phys D Appl Phys* 17(11):2139
114. Makuta T, Takemura F, Hihara E, Matsumoto Y, Shoji E (2006) *J Fluid Mech* 548(1):113
115. Ashokkumar M, Lee J, Iida Y, Yasui K, Kozuka T, Tuziuti T, Towata A (2010) *ChemPhysChem* 11(8):1680
116. Birkin PR, Offin DG, Vian CJB, Leighton TG (2011) *J Acoust Soc Am* 130(5):3379
117. Zijlstra A, Fernandez D, Gardeniens RHGE, Versluis M, Lohse D (2015) *Ultrasonics* 56:512
118. Suslick KS, Flannigan DJ (2008) *Annu Rev Phys Chem* 59(1):659
119. Gielen B, Marchal S, Jordens J, Thomassen LCJ, Braeken L, Van Gerven T (2016) *Ultrason Sonochem* 31(C):463
120. Nikitenko SI, Pflieger R (2016) *Ultrason Sonochem* 1–8

121. Howkins SD (1966) *J Acoust Soc Am* 39(1):55
122. Leighton TG (1995) *Ultrason Sonochem* 2(2):S123
123. Gogate PR, Tatake PA, Kanthale PM (2002) *AIChE J*
124. Shchukin DG, Skorb E, Belova V, Möhwald H (2011) *Adv Mater* 23(17):1922
125. Lajoinie G, De Cock I, Coussios CC, Lentacker I, Le Gac S, Stride E, Versluis M (2016) *Biomicrofluidics* 10(1):011501
126. Skorb EV, Möhwald H (2016) *Ultrason Sonochem* 29(C):589
127. Fernandez Rivas D, Betjes J, Verhaagen B, Bouwhuis W, Bor TC, Lohse D, Gardeniers HJGE (2013) *J Appl Phys* 113:064902
128. Koda S, Tanaka K, Sakamoto H, Matsuoka T, Nomura H (2004) *J Phys Chem A* 108(52):11609
129. Leighton TG, Cox BT, Phelps AD (2000) *J Acoust Soc Am* 107(1):130
130. Bremond N, Arora M, Ohl CD, Lohse D (2006) *Phys Rev Lett* 96(22):224501
131. Fernandez Rivas D, Ashokkumar M, Leong T, Yasui K, Tuziuti T, Kentish S, Lohse D, Gardeniers HJGE (2012) *Ultrason Sonochem* 19(6):1252
132. Stricker L, Dollet B, Fernandez D, Lohse RD (2013) *J Acoust Soc Am* 134(3):1854
133. Verhaagen B, Fernandez Rivas D, Gardeniers HJGE, Versluis M (2015) Micropits for ultrasonic treatment. Patent Pending. PCT/EP2015/056806
134. Verhaagen B, Liu Y, Pérez AG, Castro-Hernandez E, Fernandez Rivas D (2016) *Chem Select* 1(2):136
135. <http://www.bubclean.nl/bubble-bags-2/> (2016)
136. Brennen CE (1995) Cavitation and bubble dynamics. In: Oxford engineering science series. Oxford University Press, Oxford
137. Fernandez Rivas D, Verhaagen B, Seddon J, Zijlstra AG, Jiang LM, Van der Sluis LWM, Prosperetti A, Versluis M, Lohse D, Gardeniers HJGE (2012) *Biomicrofluidics* 6:034114
138. Rivas DF, Verhaagen B, Perez AG, Castro-Hernandez E, van Zwieten R, Schroen K (2015) *J Phys Conf Ser* 656(1):012112
139. van Zwieten R, Verhaagen B, Schroen K, Rivas DF (2016) *Ultrason Sonochem* (**under review**)
140. <http://www.bubclean.nl/chemical-processes-in-the-bubble-bag/> (2016)
141. Wiklund M, Green R, Ohlin M (2012) *Lab Chip* 12:2438
142. Riley N (2001) *Annu Rev Fluid Mech* 33(1):43
143. Leong T, Johansson L, Juliano P, McArthur SL, Manasseh R (2013) *Ind Eng Chem Res* 52(47):16555
144. Nyborg WL (1958) *J Acoust Soc Am* 30(4):329
145. Sadhal SS (2012) *Lab Chip* 12:2292
146. Spengler JF, Coakley WT, Christensen KT (2003) *AIChE J* 49(11):2773
147. Spengler JF, Coakley WT (2003) *Langmuir* 19(9):3635
148. Devendran C, Gralinski I, Neild A (2014) *Microfluid Nanofluid* 17(5):879
149. Bengtsson M, Laurell T (2004) *Analyt Bioanalyt Chem* 378(7):1716
150. Cosgrove J, Buick J, Pye S, Greated C (2001) *Ultrasonics* 39(6):461
151. Rife J, Bell M, Horwitz J, Kabler M, Auyeung R, Kim W (2000) *Sens Actuat A Phys* 86(1–2):135
152. Paul RM, Ooi A (2007) *J Fluid Mech* 576:191
153. Collis J, Manasseh R, Liovic P, Tho P, Ooi A, Petkovic-Duran K, Zhu Y (2010) *Ultrasonics* 50(2):273 (**Selected Papers from ICU 2009**)
154. Dijkmans P, Juffermans L, Musters R, van Wamel A, ten Cate F, van Gilst W, Visser C, de Jong N, Kamp O (2004) *Eur Heart J Cardiovasc Imag* 5(4):245
155. Liu RH, Yang J, Pindera MZ, Athavale M, Grodzinski P (2002) *Lab Chip* 2:151
156. Roberge DM, Ducry L, Bieler N, Cretton P, Zimmermann B (2005) *Chem Eng Technol* 28(3):318
157. Nilsson J, Evander M, Hammarström B, Laurell T (2009) *Analytica Chimica Acta* 649(2):141
158. Hartman RL, Naber JR, Zaborenko N, Buchwald SL, Jensen KF (2010) *Organic Process Res Dev* 14(6):1347
159. Noël T, Naber JR, Hartman RL, McMullen JP, Jensen KF, Buchwald SL (2011) *Chem Sci* 2(2):287
160. Kuhn S, Noël T, Gu L, Heider PL, Jensen KF (2011) *Lab Chip* 11(15):2488
161. Hübner S, Kressler S, Kralisch D, Bludszuweit-Philipp C, Lukow K, Jänich I, Schilling A, Hieronymus H, Liebner C, Jähnisch K (2012) *ChemSusChem* 5(2):279
162. Lenshof A, Magnusson C, Laurell T (2012) *Lab Chip* 12(7):1210
163. Kok MP, Segers T, Versluis M (2015) *Lab Chip* 15(18):3716
164. Sedelmeier J, Ley SV, Baxendale IR, Baumann M (2010) *Organic Lett* 12:3618
165. Wagterveld RM, Boels L, Mayer MJ, Witkamp GJ (2011) *Ultrason Sonochem* 18(1):216

166. Zeiger BW, Suslick KS (2011) *J Am Chem Soc* 133(37):14530
167. Wagterveld RM, Miedema H, Witkamp GJ (2012) *Cryst Growth Des* 12(9):4403
168. Castro F, Kuhn S, Jensen KF, Ferreira A, Rocha F, Vicente A, Teixeira JA (2013) *Chem Eng J* 216:979
169. Castro F, Kuhn S, Jensen KF, Ferreira A, Rocha F, Vicente A, Teixeira JA (2013) *Chem Eng Sci* 100:352

Sonochemical Reactors

Parag R. Gogate¹ · Pankaj N. Patil²

Received: 4 June 2016 / Accepted: 5 August 2016 / Published online: 20 August 2016
© Springer International Publishing Switzerland 2016

Abstract Sonochemical reactors are based on the generation of cavitation events using ultrasound and offer immense potential for the intensification of physical and chemical processing applications. The present work presents a critical analysis of the underlying mechanisms for intensification, available reactor configurations and overview of the different applications exploited successfully, though mostly at laboratory scales. Guidelines have also been presented for optimum selection of the important operating parameters (frequency and intensity of irradiation, temperature and liquid physicochemical properties) as well as the geometric parameters (type of reactor configuration and the number/position of the transducers) so as to maximize the process intensification benefits. The key areas for future work so as to transform the successful technique at laboratory/pilot scale into commercial technology have also been discussed. Overall, it has been established that there is immense potential for sonochemical reactors for process intensification leading to greener processing and economic benefits. Combined efforts from a wide range of disciplines such as material science, physics, chemistry and chemical engineers are required to harness the benefits at commercial scale operation.

Keywords Sonochemical reactors · Design aspects · Operating parameters · Guidelines · Process intensification · Scale-up strategies

This article is part of the Topical Collection “Sonochemistry: From basic principles to innovative applications”; edited by Juan Carlos Colmenares Q., Gregory Chatel.

✉ Parag R. Gogate
pr.gogate@ictmbai.edu.in

¹ Chemical Engineering Department, Institute of Chemical Technology, Matunga, Mumbai 40019, India

² Chemical Engineering Department, Gharda Institute of Technology, Lavel, Tal. Khed 415708, India

1 Introduction

Cavitation reactors, are a novel and promising form of multiphase reactors, based on the principle of release of large magnitudes of energy due to the violent collapse of the cavities in the liquid medium. Cavitation reactors used for intensification of physical and chemical processing applications are generally classified into sonochemical reactors and hydrodynamic cavitation reactors. In the case of sonochemical reactors, the pressure variations induced by the passage of ultrasound results in the generation of cavities which undergo subsequent growth and finally collapse releasing large magnitudes of energy over a very small volume resulting in very high energy densities [1]. In the case of hydrodynamic cavitation, cavities are generated using the pressure variations induced by an interchange in the flow and local pressure based on inserting a cavitating device in the fluid flow. Another classification of cavitation, which is based on the nature of the radius-time profile for the different phases of cavitation, is the stable and transient cavitations. These two forms of cavitation, which differ significantly in the collapse conditions, can be obtained both in sonochemical and hydrodynamic cavitation reactors based on suitable adjustment of the operating parameters. In the case of stable cavitation, the bubbles oscillate around their equilibrium position over several refraction/compression cycles and the maximum growth is only about 2–10 times the original size of the cavity. As such, the collapse is also not too violent, and intermittent pressure/temperature pulses are generated corresponding to each cycle of partial collapse. In transient cavitation, the bubbles grow over one (sometimes two or three) acoustic cycle to a maximum size which can be a few hundred times the initial size and finally collapse violently over a quick time duration generating local hot spots and very high energy densities.

Cavitation generated by the passage of ultrasonic waves is also described as acoustic cavitation. Ultrasound induces alternate compression and rarefaction cycles in the liquid. In the compression cycle, the average distance between the molecules decreases and during the rarefaction cycle, the distance increases as the liquid molecules are typically pulled apart. If adequately large negative pressure is applied to the liquid so that the average distance between the molecules exceeds the critical molecular distance required to hold the liquid intact, cavities are formed [2]. These formed cavities grow in size through oscillations until a maximum size is obtained which would be dependent on the operating conditions in the reactor and subsequently undergo a rapid collapse phase over a very small interval of time (of the order of few microseconds). The collapse of cavities typically induces localized supercritical conditions such as high-pressure and high-temperature pulse ranging to about a few thousands, as well as intense turbulence coupled with high levels of fluid shear and liquid circulation. The magnitude of the pressure pulse or the intensity of shock waves (together described generally as the cavitation intensity) depend on various factors, namely the operating parameters such as ultrasound frequency and intensity, the initial radius of the nuclei which is typically decided by the liquid physicochemical properties and the compressibility of the cavitating medium [2]. In addition to the cavitation intensity, the active volume of

the cavitation is also very important particularly deciding the feasibility of using sonochemical reactors at a large scale. The active volume is mainly decided by the geometric parameters viz. the area of the transducer (unit used for transmission of ultrasonic waves into the liquid medium and for transfer of supplied electric energy into the vibrational energy) and the number of transducers. The aim of the design engineers should be to maximize both these parameters of cavitation intensity and the active volume.

The benefits obtained due to the use of sonochemical reactors in chemical and physical processing are many. The different applications which can be intensified due to the use of sonochemical reactors include chemical synthesis (with benefits of shorter reaction time, higher yields, better selectivity and use of ambient conditions), wastewater treatment (oxidation of complex pollutants, molecular rearrangement leading to enhanced biodegradability), enzymatic reactions (enhanced enzyme activity as well as intensification due to improved transfer processes), crystallization (better crystal characteristics and obtaining correct polymorphs sometimes without seeding), emulsification (better droplet size distribution), etc. [3–15]. It is also important to note that though there are so many successful applications demonstrated at laboratory- and pilot-scale capacity, successful operation at a commercial scale has not been well established, though some success has been reported for water treatment and crystallization. There are various factors providing hindrance to successful application of sonochemical reactors on an industrial scale. The main factor is that intense cavitation activity is concentrated very close to the transducer which could prove harmful to the functioning of the transducer (possible erosion of the surface) and also there would be a large fraction of dead zones in the large-scale reactor resulting in lower overall yields. Reduced energy efficiency at larger scales of operation is also another challenge for the conventional designs. The use of multi-frequency multiple transducer reactors (can be tailored to have a capacity over the range of 5–500 L) has tried to address some of these issues with good effectiveness for a variety of applications as compared to the conventional designs.

The present work provides useful discussion on the mechanisms for intensification in different applications, an overview of different sonochemical reactor configurations, the effect of operating parameters with guidelines for achieving the maximum benefits and some typical illustrations of success stories in recent years. The possible combinations of the sonochemical reactors with microwave, ultraviolet (UV) and hydrodynamic cavitation have also been discussed and, finally, the scope for future work required to achieve commercial applications has been elucidated. Overall, the work has focused on providing the state-of-the-art understanding into the current status with possible recommendations for the future work for establishing the scale-up strategies.

2 Effects/Mechanisms of Acoustic Cavitation Governing Intensification

In general, the acoustic cavitation phenomenon, which provides the controlling mechanism for intensification due to the use of sonochemical reactors, is dictated by the following steps:

- Liquid is exposed to the acoustic field of varying intensity (type of liquid mainly in terms of presence of heterogeneity in the form of dissolved gases or solid particles decides the critical intensity required for inception).
- Formation of cavities due to fluctuations in the pressure field which contains small quantities of dissolved gases and vapors from the surrounding medium (the fraction will be dependent on the type of liquid medium, especially the use of vaporous solvents).
- Growth of the cavity due to compression and rarefaction cycles of ultrasonic waves.
- Achieving a maximum cavity size depending on the operating conditions.
- Collapse of the cavity releasing a large magnitude of energy creating conditions with extreme pressures and temperatures (duration of collapse will determine the intensity and, also, the overall intensity will be dependent on the number of cavities generated in the reactor).

Before exploring the possible use of sonochemical reactors for process intensification, it is very important to understand the cavitation effects and the controlling mechanism governing the specific application under question [16, 17]. Cavitation typically results in generation of very high temperatures (in the range of 500–10,000 K) and pressures (500–5000 bars) often described as hot spots coupled with generation of highly reactive free radicals due to the dissociation of molecules exposed to hot spots. Generally, these effects are described as the chemical effects and are useful for intensification of chemical processing applications such as chemical synthesis and wastewater treatment, which are, most of the time, limited by intrinsic chemical kinetics [17]. On the other hand, cavitation also results in the generation of high-intensity turbulence coupled with liquid streaming and intense shear. These effects are described as physical effects and are useful for intensification of physical processing applications such as enzymatic reactions or other biotechnological applications, crystallization and emulsification, which are often limited by the transport processes. Sometimes, the physical effects also can contribute to intensification of chemical reactions (catalytic and heterogeneous reactions). The physical effects can lead to an increase in the surface area of the solid catalysts and also continuous cleaning of the catalyst surface which can improve the efficiency of catalytic reactions. Also, enhancement in the mass transfer rates due to turbulence generated as a result of acoustic streaming can yield intensification of heterogeneous reactions limited by the resistances between two or more phases. It is important to understand that the typical operating parameters (intensity and frequency of irradiation) can be optimized so as to obtain the dominating physical or chemical effects suitable for the specific application under question [16], though, in reality, both these effects will be existent and contribute to

the net intensification of the process. Typically, lower frequencies of irradiation (20–100 kHz) would result in dominating physical effects whereas higher frequencies (200–2000 kHz) would result in generation of dominant chemical effects. A combination of multiple frequencies can also be tailored so as to suit the specific applications.

Bubble dynamics analysis which usually predicts the radius time profiles for different phases of the cavitation can be used to predict the chemical and physical effects as a function of different operating parameters [18–21]. The simulations can be performed under different assumptions (single cavity approach or the cluster approach, incompressible or the compressible nature of liquid and type of the cavity generated, i.e. void or vaporous) and the behavior of the cavity can be predicted quantifying the maximum growth of the cavity as well as the temperature and pressure pulse generated at the collapse of the cavities. Integration of the chemical reaction kinetics for the typical dissociation or thermal pyrolysis reactions based on the expected components in the collapsing cavity can also give an idea about the quantum of free radicals that are likely to be generated in the reactor. Three reaction zones have been identified for the chemical reactions as inside the collapsing cavity (mainly dissociation reactions leading to formation of radicals, intensity is maximum here), interface between the cavity and liquid (lower intensity as compared to the center of the collapsing cavity, the radical concentration is still higher and radicals can attack the molecules present in the vicinity) and, finally, the liquid bulk itself where the migrated radicals will react with the chemicals present in the bulk (the rate of reaction would be lower as compared to the center or the interface, also the quantum of migrated radicals is limited). The bubble dynamic simulations can also be used to predict the pressure field distribution as well as the zones with maximum cavitation intensity in the reactor, and this approach can be effectively used for optimization of the designs for large-scale operations as well as in deciding the placement of reactors with a coupling fluid in the main sonochemical vessel.

The observed sonochemical effects are generally explained on the basis of hot-spot theory [22] and electrical theory [23]. According to the hot spot theory, a small gas bubble or cavity subjected to acoustic pressure amplitude of more than a few bars experiences violent pulsation, such that the bubble wall velocity for a collapsing bubble approaches the velocity of sound. At this point, the bubble shatters upon collapse and results in significant adiabatic heating resulting in conditions similar to hot spots (thousands of degrees of temperature and thousands of atmospheres of local pressure). These hot spots result in the dissociation of the water molecules or other chemical species entrapped in the cavitating bubble and result in the formation of the free radicals. Margulis [23] reported that some observations could not be completely explained by the “hot-spot” theory and proposed an alternative electrical theory, which considers the charge distribution due to dipoles in water and their distribution around a bubble. It was reported that, during the bubble formation and collapse, enormous electrical field gradients of about 10^{11} V/m are generated which are sufficiently high to cause bond breakage and induce chemical activity. It is important to note that the hot spot theory is the

most common accepted explanation for the intensification of chemical reactions involving cavitation [22, 24].

After understanding the important effects that can be induced using cavitation and its role in deciding the degree of intensification, it is important to provide some guidelines regarding the usage of sonochemical reactors. While thinking about the application of sonochemical reactors, the first important point to be considered is whether the given application is homogeneous or heterogeneous. Typically, for the heterogeneous systems (involving two or more phases), stronger intensification benefits can be obtained due to simultaneously acting mechanisms involving both the physical and chemical effects. Further, the application of sonochemical reactors can be either as an addition to the existing reactors or as a complete replacement. The decision would be dependent on the controlling mechanism of the expected intensification and the nature of problems in the conventional processing. For example, if the conventional processing is only limited by mixing issues or lower surface areas for the solid materials, intermittent application of sonochemical reactors as an add-on facility would be sufficient as this can provide the necessary activation as well as enhanced surface areas based on deagglomeration or particle breakage. Such an intermittent application would give the desired intensification benefits but, more importantly, at much lower energy inputs. The application time and the duration of each pulse treatment using ultrasound will have to be decided based on the detailed understanding of the controlling mechanisms. The scale-up issues for the pretreatment vessel might be minimal as ultrasound is to be used only as a supporting technique to the existing stirred reactor configuration. An easier design approach would be to use transducer attached to the walls of a stirred reactor. If the controlling mechanism for intensification is truly based on the chemical effects involving requirement of continuous formation of free radicals or hot spots improving the intrinsic chemical kinetics, application of sonochemical reactors would be required continuously and the design needs to consider all the aspects from chemical reaction engineering, multiphase reactor and the material science prospects.

Analysis of the scientific database available in the open literature or the data generated using laboratory-scale investigations for an entirely new application can help in identifying the scale-up strategy in terms of obtaining an efficient design and selection of the effective operational window for the important parameters such as frequency and power dissipation. The proper selection of these parameters as well as the design configuration of sonochemical reactor is a must to achieve the expected levels of process intensification for the desired application. The liquid physicochemical properties decide both the ease of inception and the collapse intensity and, hence, play a decisive role in the expected intensification. It is also important that this intensification is achieved at minimum possible levels of energy consumption. Overall, a detailed analysis of controlling mechanisms for the progress of the specific application and interactions between the operating and design parameters is very important to balance the degree of intensification and the associated costs for the operation.

3 Overview of Sonochemical Reactor Designs

Various sonochemical reactor designs, differing in terms of the basic configuration in terms of geometry, number of transducers and position of transducers, are available and reported in the literature. We now discuss some of the important reactor configurations, also commenting on the suitability for the large-scale operations. Ultrasonic horns and ultrasonic baths were the most commonly used reactor designs, especially in most of the literature illustrations. More recent developments have employed direct bonding of the transducer to the surface of the vessel and different arrangements such as a triangular or square pitch in the case of ultrasonic bath [25], parallel plate reactors with each plate irradiated with either the same or different frequencies [26], tubular reactors with two ends either irradiated with transducers or one end with a transducer and other with a reflector [27], and flow cell-type configurations with transducers on sides of the vessel [28] can be constructed. It is important to understand that while selecting a sonochemical reactor for the specific application, the aim of the design engineer should be to achieve uniform distribution of cavitation activity and maximize the cavitation yields (typically defined as the net effects per unit energy consumption).

3.1 Ultrasonic Horn

A basic configuration of sonochemical reactors is the ultrasonic horn which is mostly used for the laboratory-scale characterization studies. Typically, an ultrasonic horn operates at a fixed frequency and only variable power dissipation (controlled by varying the amplitude) is possible to control the cavitation intensity in the reactor. The ultrasonic horn has to be directly immersed into the liquid medium as shown in Fig. 1 (vertical horn as well as horizontal horn) and very high cavitation activity is obtained close to the transducer, especially in the case of vertical configuration. It is also observed that the cavitation activity decreases as one moves away from the transducer [3] and, hence, there is a possibility that considerable dead zones will be obtained if a large volume is used for the treatment. In the case of vertical configuration, the recommended capacity for obtaining desirable effects is over the range of 50–500 mL, whereas, for the horizontal configuration (also described as the longitudinally vibrating horn), capacity can be over the range of 1–10 L. It is also important to understand that the power density (power dissipation per unit volume) will be reduced at higher processing volumes, and lower intensity of cavitation activity would be obtained which may not be suited for chemical processing applications such as oxidation of complex molecules or the synthesis reactions. Another disadvantage of the ultrasonic horn is that due to the direct exposure of the horn to the liquid medium, there is a possibility of contamination of the processed liquid due to the erosion of the transducer surface which may not be allowed in the case of pharmaceutical or food-processing applications.

Most of the operations with ultrasonic horns have been in a batch mode but a continuous mode of operation is also possible based on the use of an ultrasonic horn

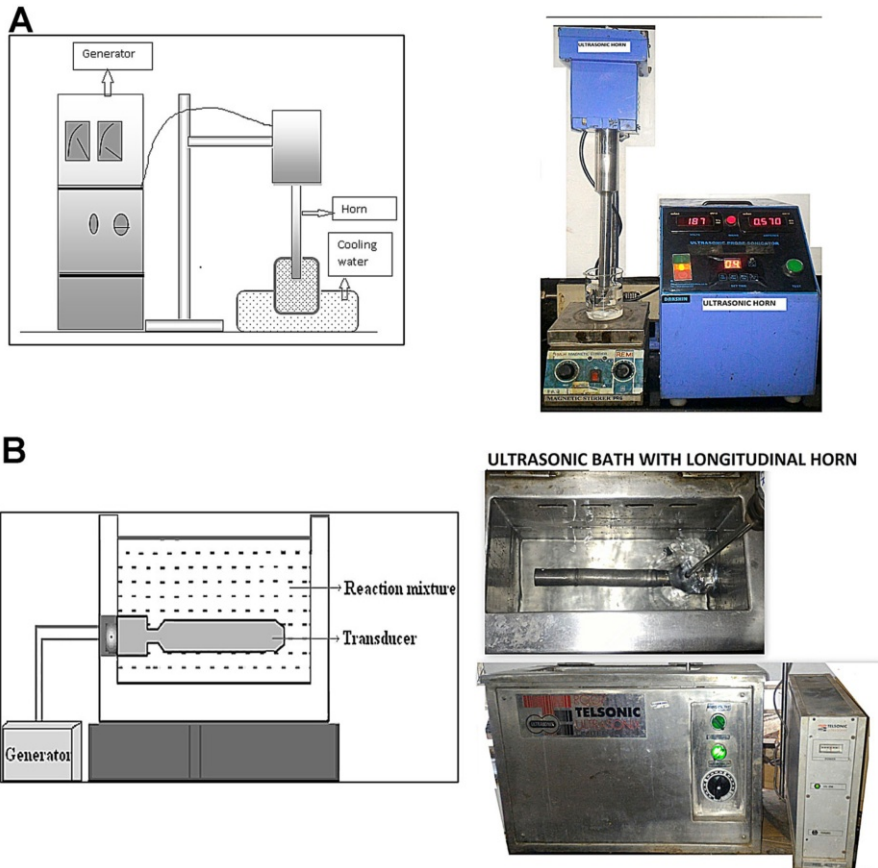


Fig. 1 Schematic representation and actual photograph of ultrasonic horn (a) vertical configuration (b) horizontal configuration

in a flow loop. Ultrasonic horns can be inserted at multiple locations using T joints and this can give flexibility of enhancing the active treatment zone based on the use of a number of ultrasonic horns. It is important to note that such a configuration also suffers from uncertainty about possible leakage, especially in the case of high-pressure systems.

3.2 Ultrasonic Bath

The ultrasonic bath is typically a cleaning tank type configuration and the schematic representation has been shown in Fig. 2. The capacity of the tank can be varied and, based on the capacity, a desired number of transducers can be introduced at the base of the reactor. This flexibility also allows maintaining the desired power density for the specific application. Also, as multiple transducers are being used, there is flexibility in terms of deciding the arrangement of transducers which can aid in obtaining uniform cavitation activity distribution in the reactor [29]. An ultrasonic

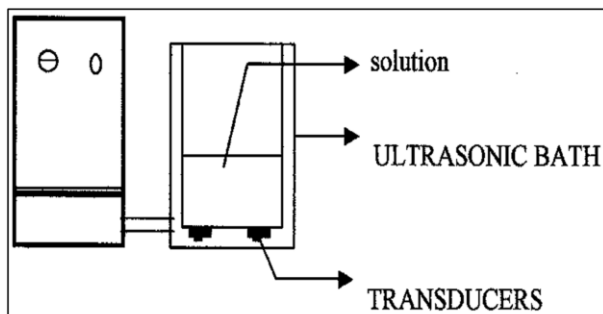


Fig. 2 Schematic representation and actual photograph of an ultrasonic bath

bath can be operated in a batch mode or in a continuous mode based on the overflow type of operation. Also, direct and indirect modes of irradiation can be used with an ultrasonic bath. In the case of direct mode of irradiation, the liquid is taken in the directly in the bath whereas in the case of indirect mode of irradiation liquid is taken in a reactor which is immersed in the ultrasonic bath using a coupling fluid. The required cavitation intensity for the specific application would decide the selection of mode of irradiation. If intense cavitation activity is required, say, for applications such as wastewater treatment, a direct mode of irradiation will be preferred. Consequently, if milder cavitation activity is essential and intense cavitation is detrimental, such as in the case of enzymatic reactions, an indirect mode of irradiation will be recommended. Usage of coupling fluid for the indirect mode also implies restriction on the operating conditions, especially temperature, as this cannot exceed the boiling point of the coupling fluid which, most of the time, would be water.

3.3 Multiple-Frequency Flow Cell

For large-scale applications of sonochemical reactors, it is a must to design a continuous configuration and a flow cell offers good potential in this respect. The flow cell is based on the attachment of transducers to the wall of the reactor, and different geometries, such as rectangular and hexagonal, can be used as depicted schematically in Fig. 3. The dimensions of the vessel can be decided based on the processing conditions and the length of the flow cell can be adjusted so as to extend treatment times. A modular unit can also be constructed which can be replicated as the scale-out philosophy. Adjustment of the pitch of the multiple transducers can help in achieving uniform distribution of the cavitation activity similar to an

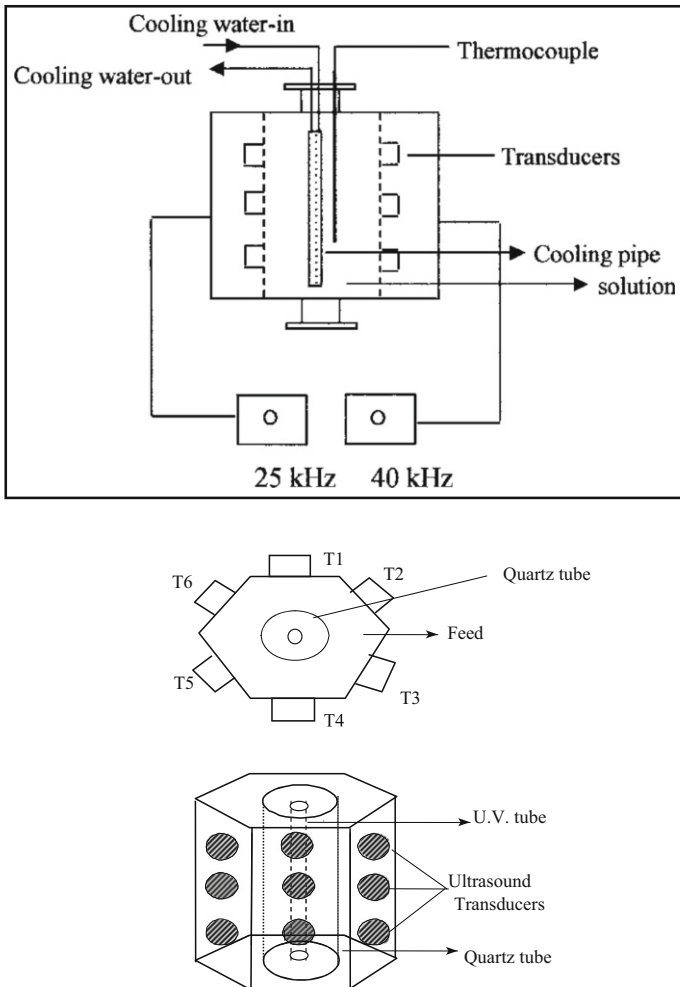


Fig. 3 Schematic representation of multiple-frequency flow cell (a) dual-frequency rectangular configuration (b) triple-frequency hexagonal configuration

ultrasonic bath. Also, due to the lower power dissipation per unit transducer, the decoupling losses can be reduced which means that a higher magnitude of energy will be available for the desired transformations. The design of the multiple-transducer units also allows concentrating the intensity at the central zone away from the transducers which reduces the problem of surface erosion and localized operation of cavitation. It is also important to understand that the use of multiple transducers in different sets allows using multiple frequencies of irradiation. The use of a multiple-frequency operation can help in achieving both the chemical and physical effects (for example, a combination of 20 and 500 kHz would give both physical and chemical effects) and also can result in intense cavitation as compared to the use of only one frequency at the same power dissipation. The design of flow cells can also be modified to insert an annular quartz tube at the center of the reactor (Fig. 3b) which can be equipped with an UV lamp. Such a modification can allow simultaneous energy dissipations based on the use of ultrasound and UV irradiations, which can give synergistic results for the applications with similar controlling mechanisms such as chemical synthesis or wastewater treatment governed by hydroxyl radical oxidation [30].

It is important to note that most of the research dealing with application of sonochemical reactors for process intensification has been at the laboratory scale and only recently some illustrations of large-scale designs can be seen in the open literature. Mhetre and Gogate [31] reported a rectangular box type configuration (length = 30 cm, width = 30 cm and height = 80 cm) which can be operated in both batch and continuous mode. The ultrasonic flow cell has an operating capacity of 72 L and all the transducers operate at a fixed driving frequency of 40 kHz. The schematic representation of the flow cell with the arrangement of the transducers has been given in Fig. 4. The ultrasonic flow cell has been reported to operate at four different input power dissipation levels as 600, 1200, 1800 and 2400 W based on the use of a different selector switch provided on the generator. Son et al. [32] also reported the use of a large-scale design with a rectangular type cross-section and having capacity of 250 L. The reported dimensions of the reactor are 1.2 m × 0.6 m × 0.4 m and a transducer module having nine transducers has been introduced on the wall. The transducers are capable of operating at different frequencies over the range of 35–170 kHz and have a fixed power rating as 400 W per transducer. Asakura et al. [33] also reported a similar design having a capacity of 120 L with use of multiple transducers having fixed frequencies of 500 kHz and maximum power rating of 620 W. The actual power dissipated into the liquid measured using the calorimetric studies revealed energy efficiency of 70 %. It was also reported that the liquid height in the reactor played an important role in deciding the cavitation activity as established using the Weissler reaction. The iodine yield was reported to be the maximum for the liquid height over the range of 400–435 mm. Also, the iodine yield increased with an increase in the power dissipation. The sonochemical efficiency obtained for this large scale reactor was also reported to be similar to a laboratory scale reactor which confirmed the proper scale-up procedures.

As part of providing a discussion on large-scale configurations, it is also important to provide an overview of the applications with continuous operation of

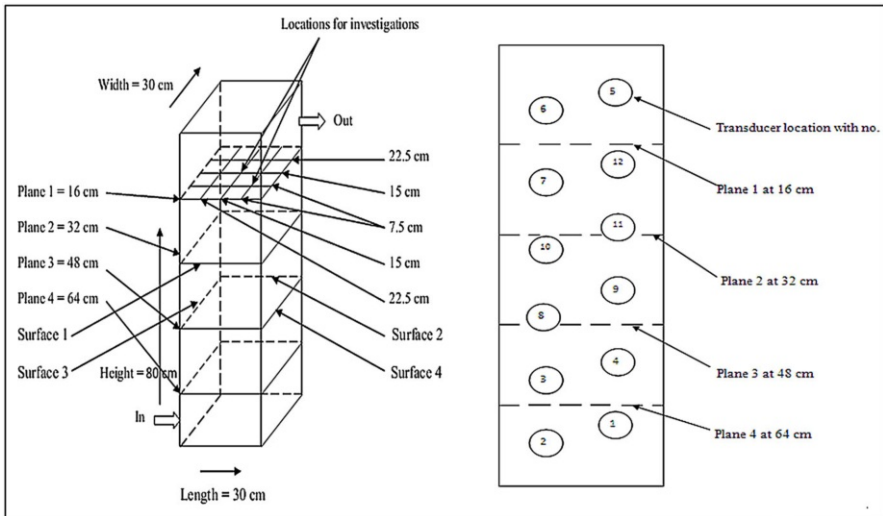


Fig. 4 Schematic view and actual photograph of pilot-scale ultrasonic flow cell with different locations of transducers [31]

sonochemical reactors as this is the main requirement for large-scale processing. Palanisamy et al. [34] investigated the synthesis of cadmium sulfide nanoplatelets having a thickness of less than 10 nm in a continuously operated ultrasonic horn reactor with use of inserts for reducing the residence time of the liquid mixture as well as to form a narrow film around the surface of the horn. It was reported that the

use of inserts allowed reduction in the available volume from 65 mL to only 8 mL. It was also reported that the continuous configuration allowed synthesis of the desired form of platelets with significant (around eight times) reduction in the overall processing time and giving good control over the final product characteristics. Shirsath et al. [35] reported the continuous synthesis of calcium carbonate using a stirred reactor in the presence of ultrasonic irradiations. The reactor assembly consisted of a sequential operation of a continuously stirred reactor followed by an ultrasonic horn which was immersed in a continuous-flow reactor. It was reported that the use of ultrasound resulted in production of smaller particles of calcium carbonate as compared to only stirring which was attributed to the enhanced nucleation and reduced agglomeration of the formed particles. Jolhe et al. [36] investigated the synthesis of peracetic acid in a combination of a sonochemical and a continuous-flow microreactor. For the combination approach, the microreactor was immersed in the ultrasonic bath in the presence of water as the coupling fluid provided with temperature control. Comparison of the results obtained for the continuous reactor with the conventional batch reactor revealed significant intensification with the reaction time being reduced from 100 min in the batch operation to only 10 min and, also, the final product yield was about 50 % higher. It was also reported that the role of ultrasound was to provide the formation of hydrogen peroxide in situ which helped in acceleration of the reaction. An additional benefit of ultrasound was enhanced activity for the solid catalyst, and it was also demonstrated that the deactivation of catalyst was reduced in the presence of ultrasound.

4 Effect of Operating Parameters

The cavitation intensity generated in the sonochemical reactors which also decides the degree of the obtained intensification for any chemical or physical processing applications is strongly dependent on the different operating parameters such as intensity of irradiation, frequency of irradiation and power dissipation in addition to the geometry of the reactor and arrangement of the transducers. The liquid phase physicochemical properties that decide the size of the nuclei generated as well as the ease of generation of cavities also affect the cavitation intensity but not much variation can be obtained in these parameters due to the fixed conditions of the processing. The current section deals with understanding the effect of different parameters and presents guidelines for the optimum selection of the same.

4.1 Intensity of Irradiation

The intensity of irradiation is defined as power dissipation per unit area of transducers used for irradiation. The intensity can be varied by either changing the power dissipation into the reactor which also affects the power density or by changing the area of transducers (this may not be always possible as an operational parameter once the given geometry for the reactor is fixed). Typically, bubble dynamics studies have confirmed that intense cavitation collapse can be obtained

using lower operating intensity [2] and, also, the number of cavities formed is directly dependent on the levels of power dissipation into the reactors. Considering these two counteracting effects, usually an optimum power dissipation level exists and it is also recommended to dissipate same power through higher areas of irradiation (of course this has to be considered at the design stage). Entezari and Kruus [37] have reported that the rate of iodine liberation at constant power input increased with an increase in the area of irradiating surface. Auzay and Naffrechoux [38] compared the use of different dosimetry techniques as nitrite, nitrate and the more commonly used iodine dosimetry to understand the effect of power density on the sonochemical efficiency. It was reported that the sonochemical efficiency increased with an acoustic power for all the dosimetry approaches though, more importantly, the extent of increase was different in each of the approaches. This observation allows understanding that the use of enhanced power dissipation will be dependent on the specific application and usually optimum power dissipation levels specific to the application needs to be selected.

4.2 Frequency of Irradiation

Frequency of irradiation usually dominates the type of cavitation effects as physical or chemical. Typically, an increase in the frequency of irradiation leads to more intense collapse resulting in stronger chemical effects in term of radical formation. At a constant intensity and for a fixed initial radius of the nuclei, the magnitude of pressure pulse generated at the end of collapse of a single cavity increases with an increase in the frequency of irradiation, as demonstrated using the bubble dynamics studies [2]. Furthermore, as the collapse is adiabatic, increased collapse pressures naturally increase the maximum temperatures reached in the cavity and, hence, in accordance with the hot-spot theory, the rate of chemical reaction increases. Seymore and Gupta [39] reported that oxidation of KI significantly enhanced with an increase in the frequency of the ultrasound.

It is important to note that the use of a multiple-frequency operation can give more intense collapse as compared to the single-frequency operation and, also, a combination of physical and chemical effects can be obtained. Servant et al. [40] reported that the volume fraction of cavitation bubbles was significantly higher in the case of dual-frequency operation as compared to the single-frequency sonochemical reactors. Tataka and Pandit [41] also reported similar results for multiple (both triple and dual) frequencies with higher intensity of cavitation collapse as compared to the single-frequency operation. It was also reported that the use of multiple frequencies with lower magnitude difference and in phase gives higher cavitation intensity.

4.3 Operating Temperature

The effect of temperature is usually complex due to the multiple effects induced by the changes in the temperature on the liquid phase physicochemical properties and the rates of chemical reactions. An important effect of temperature is on the vapor pressure which allows easy generation of cavities but at the same time, presence of

vapors in the collapsing cavity results in lower cavitation intensity due to the cushioned collapse. In the case of applications involving chemical reactions, presence of vapors in the collapsing cavity will lead to higher dissociation rates and, hence, enhanced product yields. Usually, it is recommended to select an optimum temperature beyond which either marginal effects or reduced yields will be obtained. Enhancing the temperature for a large-scale operation also means additional operating costs for heating and, hence, it becomes even more important to weigh the intensification benefits obtained due to the use of higher temperatures against the associated costs.

4.4 Operating Pressure

Usually the operating pressure is kept fixed as the atmospheric pressure in the operation of sonochemical reactors. An increase in the pressure generally results in a marginal increase in the sonochemical effect till an optimum pressure, though this needs to be quantified for the specific application and compared against the higher operating and capital costs required for maintaining the higher pressures. There have not been many reports dealing with understanding the effect of operating pressure using different experimental systems and, to the best of our knowledge, only one such report could be seen. Yotsumoto et al. [42] investigated the effect of pressure over the range of 0.03–0.3 MPa (gauge) on the sonochemical reaction using a flow reactor and reported that maximum sonochemical efficiency was obtained at an optimum pressure of 0.1 MPa and temperature of 333 K.

4.5 Sonication Time

Cavitation yields typically increase with the time of operation but, beyond a certain time, only marginal changes or even reduced yields can be observed. One of the contributing factors for this trend is the presence of dissolved gases in the initial period, which assists the formation of cavities, but the degassing action of ultrasound results in lower cavitation effects in the subsequent operation. Subjecting the process fluids to ultrasound over extended time periods can be detrimental such as in the case of enzymatic reactions or the food-processing applications or the crystallization of pharmaceutical products and, in such cases, it is very important to establish clearly the optimum treatment times.

4.6 Liquid Physicochemical Properties

The important physicochemical properties of the liquid affecting the cavitation intensity as well as the ease of generation of cavities are viscosity, vapor pressure and surface tension. Usually, most of the applications rely on the use of water or aqueous solutions as the process fluid and this meets the optimum criteria for maximum benefits. For the other cases involving solvents, some decision-making factors need to be considered. Typically, lower viscosity would be more beneficial and excessively high viscosity such as in the case of oils would completely arrest the generation of cavitation events. Similarly, liquids with lower surface tension will

also be recommended as the ease of formation of cavities will be enhanced due to considerable ease to overcome the natural cohesive forces. Higher surface tension effects mean that higher threshold pressure and, hence, energy will be required for the inception of cavitation.

Presence of dissolved gases or any other impurities including solids is beneficial for the cavitation till an optimum quantum. Dissolved gases or solid particles provide nucleation sites for cavitation thereby reducing the threshold energy requirement and, also, the number of cavitation events increases. Bubbling gases through the mixture, again at an optimum rate dependent on the geometry of the sonochemical reactor [43], would enable obtaining higher cavitation effects as this also helps in counteracting the negative effects of degassing. The type of gas used also plays a major role in deciding the cavitation intensity and, in general, gases with a high specific heat ratio give a higher cavitation effect. On the other hand, gases with higher solubility reduce the cavitation intensity due to cushioned collapse. Presence of solid particles gives similar counteracting mechanisms in terms of enhanced surface cavitation and reduced effects due to scattering of the incident sound waves leading to reduced energy dissipation. Thus, an optimum loading of the solid particles will also exist [44] and the other decisive factors would be the size of solid particles and the nature of the solids (whether it can act as a catalyst to enhance the rates of chemical reactions).

4.7 Geometry of the Sonochemical Reactor

The geometry of the reactor in terms of the configuration of the transducers (number and position), ratio of diameter of transducer to the reactor diameter, liquid height and shape of reactor decides the cavitation activity distribution and, hence, the observed degree of process intensification due to the use of sonochemical reactors. The following important guidelines can be given for maximizing the effects:

- Usually, a higher number of transducers provides the beneficial effects in terms of uniform cavitation activity distribution with the required intensities. Selecting parallel plate reactors is recommended as this allows interactions of the incident sound waves, giving resonating effects and continuous processing can also be obtained. Theoretical analysis in terms of the pressure field mapping based on the numerical simulations of the wave propagation equations is very useful for obtaining an optimum design configuration [45–47]. The use of multiple transducers also allows controlling the hydrodynamic conditions and the mixing characteristics in the reactor which will be very important for the physical processing applications and also chemical processing applications limited by mass transfer.
- An increase in the diameter of transducer immersed in the reactor till an optimum is beneficial resulting in an increase in the cavitation activity. The ratio of horn diameter to the reactor diameter mainly affects the intensity of liquid circulation, including the turbulence, and is more important for the physical processing application as the controlling mechanisms are based on the physical effects of cavitation.

- Similar to the diameter of the transducer, the depth of the transducer in the liquid also decides the intensity of the physical effects, mainly on the basis of the degree of reflection of the incident sound waves from the base of the reactor and from the reactor wall. It is also important to understand that an optimum depth of the transducer also exists.
- For continuous operation, the flow cell type configuration is more suited and the ability to arrange the transducers on the opposite faces gives flexibility in controlling the intensity of cavitation based on the formation of standing waves. In the literature, rectangular or hexagonal cross-sections have been demonstrated to give excellent results both in terms of the theoretical simulations and experimental measurements of the cavitation activity distribution.

5 Applications of Sonochemical Reactors

It is useful to overview the different applications, where sonochemical reactors can be used efficiently. There are large illustrations available in the literature where spectacular effects of cavitation have been successfully harnessed for a variety of applications worldwide, although mostly under laboratory-scale operations. Few of the important applications are now discussed briefly.

5.1 Biochemical Engineering/Biotechnology

The foremost application in the area of biotechnology is cell disruption for release of intracellular enzymes, as the conventional devices, mainly the mechanical disintegrators such as high-speed agitator bead mills and high-pressure homogenizers, result in energy efficiencies of only about 5–10 %. Application of ultrasound as a cell disruption approach allows intensified recovery with lower energy requirements as compared to the conventional approaches. Balasundaram and Pandit [48] reported the beneficial effects for the release of invertase enzyme by disruption of *S. cerevisiae* cells using sonication, whereas Kurokawa et al. [49] reported similar enhanced efficiency of ultrasonic disruption for the case of *Chaetocerosgracilis*, *Chaetoceroscalcitrans*, and *Nannochloropsis* sp.

Sonochemical reactors also offer immense potential for the microbial disinfection, either operated individually or in combination with chemical methods. The physical effects of cavitation in terms of turbulence associated with liquid circulation are dominant, though chemical and heat effects also play a supporting role. The use of ultrasonic reactors for microbial disinfection has been substantially investigated [50–52]. Phull et al. [50] investigated the application of ultrasound in combination with chlorine as a disinfection technique for *E. coli* and reported that sonication was seen to amplify the effect of chlorination and the combination was significantly better than sonication alone. Blume and Neis [52] also reported similar beneficial effects for sewage treatment plant (STP) effluents with different concentrations of suspended solids after exposure to sonication in combination with chlorine.

Sonochemical reactors can also be used as a pretreatment to biological oxidation with the objective of reducing the toxicity of the effluent or, in other words, increase the biodegradability. Sangave and Pandit [53] and Sangave et al. [54] reported the enhancement effects on the biodegradability of distillery wastewater due to the use of ultrasonic reactors. Though there is not much reduction in the actual chemical oxygen demand (COD) of the effluent during the pretreatment using ultrasound, there is a significant rearrangement in the molecular structures with formation of lower molecular weight compounds which are easily digested by the microorganisms.

In biological wastewater treatment, a major problem is the production of large quantities of sewage sludge which are highly susceptible to decay and, hence, proper disposal approaches are required. The sludge has to be stabilized by anaerobic digestion in order to enable environmentally safe utilization and disposal. Ultrasonic reactors have been reported to be effective in improving sludge hydrolysis [55] based on the reduction in the size or the deagglomeration of the microbial flocs, giving significant reduction in the digestion time. Ultrasonic waves at low frequency and low energy are also reported to enhance the bioreactor performance, giving higher microbial activity [56]. Zhang et al. [57] reported the use of an external sonication chamber in combination with the activated sludge system and demonstrated significant reduction in the generation of sludge during the treatment, which can control the overall treatment costs effectively.

5.2 Chemical Synthesis

The different beneficial effects induced by use of sonochemical reactors in the case of chemical synthesis are reaction time reduction, increase in the reaction yield, use of less forcing conditions as compared to the conventional routes, reduction in the induction period of the desired reaction, possible switching of the reaction pathways resulting in an increased selectivity and increasing the effectiveness of the catalyst used in the reaction [1, 5, 58]. For the case of homogeneous reactions, cavitation can intensify reactions proceeding through radicals, whereas ionic reactions are not likely to be affected. In the case of heterogeneous reactions, reactions proceeding through ionic intermediates can also be intensified using the physical effects of cavitation.

Ultrasound forms very fine emulsions in systems with immiscible liquids, which is very beneficial and can result in intensified processing even in the case of phase transfer-catalyzed reactions. When very fine emulsions are formed, the surface area available for reaction between the two phases is significantly increased, thus increasing the rate of the reaction. Similarly, in the case of heterogeneous systems involving solids, application of sonochemical reactors can give enhanced surface area and also avoid the deactivation or fouling of the solid particles which is especially important when solids are the catalyst for the reaction.

In the case of aqueous systems, the intensification effects of ultrasound in organic systems are not directly related to thermal effects but are instead a result of acceleration of the single-electron transfer (SET) process. The SET step is required as an initial step in several reactions, such as cycloadditions involving carbodienes

and heterodienes [59]. The application of ultrasound can also alter the stereoselectivity of a particular reaction, as observed in the case of the cyclization of the tetracyclic 19-iodotabersonine to the vindolinie epimers [60].

5.3 Crystallization

The use of ultrasound provides a non-invasive way of improving the crystal properties and process controllability, mainly in terms of controlling the size distribution and the habit and morphology of the crystals [61–63]. Ultrasound can also be used to replace seeding and provide enough formation of the nuclei in the difficult-to-nucleate systems. By varying the power and duration of ultrasonic irradiation, the crystal size distribution can be tailored to optimize downstream processing, which is very important in the case of pharmaceutical processing. Ultrasound also results in reduction in the induction period and the metastable zone width providing the desired crystallization conditions. It is important to note that low-frequency ultrasound (20–50 kHz) is most favorable with optimum levels of power dissipation and the irradiation time as application of higher operating frequency (>100 kHz) coupled with high power and extended time periods can lead to radical-induced degradations.

Crystallization is one such operation where commercial-scale application of sonochemical reactors has also been reported with many successful results, especially for pharmaceutical compounds. The scale-up is usually recommended based on the modular flow cell type configurations where the number of modules can be decided on the basis of required residence time and the capacity of the operations. For small-capacity specialty chemicals, an external loop containing the sonochemical reactor can also be constructed where the liquid mixture can be circulated through the sonication unit at predesigned time intervals and with desired residence times.

5.4 Wastewater Treatment

Sonochemical reactors can also be used effectively for the destruction/degradation of the pollutants in water because of the localized high concentrations of the oxidizing species such as hydroxyl radicals and hydrogen peroxide, higher magnitudes of localized temperatures and pressures and the formation of the transient supercritical water. The hydrophobic compounds react with $\text{OH}\cdot$ and $\text{H}\cdot$ at the hydrophobic gas/liquid interface, while the hydrophilic species react to a greater extent with the $\text{OH}\cdot$ radicals in the bulk aqueous phase. Optimization of organic compound degradation rates can be achieved by adjusting the energy density, the irradiation intensity and the nature and properties of the saturating gas in solution. The variety of chemicals that have been destructed using sonication using different equipments and on a wide range of operating scales are imidacloprid, *p*-nitrophenol, rhodamine B, 1,1,1 trichloroethane, methyl parathion, pentachlorophenate, potassium ferrocyanide, phenol, CFC 11 and CFC 113, *o*-dichlorobenzene and dichloromethane, potassium iodide, sodium cyanide, carbon tetrachloride etc. [64–66].

5.5 Extraction

Considering the growing importance of the natural products, extraction of active ingredients using a specific solvent with the desired affinity has become an important operation in many of the food and pharmaceutical sectors. The extraction process is extremely difficult as the fraction of the active ingredients in natural sources is very small and harsh conditions cannot be used for extraction due to the possible loss of the activity of the compounds. Considering the complex structure of the natural sources, the mass transfer resistances often dominate the recovery resulting in a requirement of significant treatment times and also possibly incomplete recoveries. The use of ultrasound, based on its dominant physical effects, can give significant process intensification benefits such as enhanced recovery, reduced time and lower energy consumption. The collapse of cavities near the solid surface creates micro-jets at significantly higher velocities which, coupled with the shear and turbulence, results in a reduction in the particle size and surface peeling providing higher access for the solvent to the active ingredient. Application of ultrasound for intensified recovery has been reported for a variety of compounds such as aroma compounds, flavonoids, natural dyes, pigments, essential oils, citrus compounds and medicinal products [67, 68].

5.6 Medicinal Uses

The use of ultrasound for medicinal purposes has also been on a significantly increasing trend. Though, this forms an entirely different field of analysis, some important possibilities are illustrated here. Ultrasound promotes the production of free radicals in a given solvent and this fact has been used in the improved production of hydroxyl radicals from two anticancer drugs, adriamycin and mitomycin C [69], which lead to better management of the introduced drug. Ultrasound was also used in a patented process in which pharmaceuticals were delivered to the body using the preformed porous polymeric microparticles [70]. Ultrasound-assisted atomization has also been applied for obtaining encapsulated drugs with proper morphological characteristics so as to result in the improved drug delivery systems. Use of ultrasound has been reported to yield uniform particle size distribution with enhanced encapsulation efficiencies confirming the utility of ultrasonic atomization in the pharmaceutical field [71].

6 Combinations with Microwave, UV and Hydrodynamic Cavitation

Ultrasound can be effectively combined with different techniques like microwave, UV and hydrodynamic cavitation resulting in intensified processing with better energy and cost efficiency. These combinations can yield synergistic results due to the complimentary effects and sometimes similarity in the controlling mechanisms. For example, a combination of microwave and ultrasound can be effective due to complimentary action resulting into elimination of heat and mass transfer barriers. Microwave is based on rapid dipolar moment of a polar molecule, which helps in

diminishing heat transfer barriers. The physical effects associated with ultrasound removes the mass transfer limitation in the system. The combination of microwave with ultrasound techniques can improve the process chemistry, and reduce the process time by 2–10 fold as compared to the individual operations. Development of this combination is also dependent on the material of construction for the ultrasonic horn. The presence of metal in microwave cavity produces an electric arc and, hence, it is difficult to use a simultaneous operation of microwave and ultrasound [15]. Most of the studies have been based on the use of sequential operation or using a Teflon-based ultrasonic horn, but this gives reduced efficiency for the sonochemical operation. Boukroufa et al. [72] studied the extraction of essential oil, polyphenols and pectin from orange peel using microwave and ultrasound technology without adding any solvent but only water which was recycled and used as solvent. It was reported that combination of microwave, ultrasound and the recycled water of citrus peels allows one to obtain high value compounds in shorter time and lower energy with reduced generation of wastewater. Gude [73] reported that individual, sequential, as well as simultaneous applications of microwave and ultrasound irradiations can be utilized for process intensification of various biofuel productions and selective recovery of high-value products from natural sources.

The efficacy of sonochemical reactors for intensification can be enhanced based on the use of UV irradiations either in sequential operation or simultaneous operation. The combination results in the enhanced generation of hydroxyl radicals, which can result in higher extents of oxidation [30]. Another advantage of the combination approach is that the problem of deactivation of the photocatalyst due to the product inhibition can be avoided due to the continuous cleaning action induced by the ultrasound. Degradation of phenol at a pilot scale of operation was investigated by Khokhawala and Gogate [74] using the combination of UV irradiations with ultrasonic (US) irradiations. It was reported that combined operation of US and UV leads to much better results in terms of enhanced degradation. Tenster et al. [75] also reported that combination of high-frequency ultrasound and UV resulted in rapid disinfection for the application of cleaning microbially contaminated surfaces. In the sequential mode, a contaminated surface was pretreated with sonication and then irradiated with UV light. It was reported that high-frequency ultrasound exposure time and UV doses for complete inactivation decreased by a factor of 2 and 6 to 7, respectively, compared to high-frequency ultrasound or UV alone. Tezcanli-Giiyer and Ince [76] investigated the individual and combined application of ultrasound and UV irradiation for the degradation of azo dye. It was reported that combination of UV with ultrasound induced a synergistic effect, which was attributed mainly to the formation of an enhanced quantum of OH radicals due to the photolysis of US-generated H_2O_2 .

A novel combination of hydrodynamic and acoustic cavitation (hydrodynamic–acoustic cavitation/HAC) has been reported by Franke et al. [77] with investigated application as the decomposition of chloroform. In the combination reactor, an US horn was introduced in the recirculation loop used for the hydrodynamic cavitation reactor just after the cavitating device. Using such an arrangement allows for the collapse of the cavities generated using hydrodynamic cavitation under the influence of ultrasound, which is considered to be more violent as compared to the

hydrodynamic cavitation-induced collapse. The distance between the sonochemical reactor and the cavitating device needs to be properly optimized so as to achieve proper interactions between the two modes of cavitation. It was reported that the hybrid method is the most efficient method in terms of energy transformation efficiency and the individual application of ultrasound was less efficient as compared to the combination approach. Franke et al. [78] also reported the use of a combined hydrodynamic–acoustic cavitation reactor for the transesterification of rapeseed oil with methanol for the production of the biodiesel. Studies related to the understanding of the effect of different parameters such as the molar ratio of methanol to oil, ultrasound amplitude, catalyst loading and temperature revealed that the catalyst loading and the US amplitude are the parameters with maximum influence on the biodiesel production. It was also reported that a biodiesel yield of 96.5 % was achieved in just 10 s of operation using the combined operation. Beneficial results have also been reported for other applications such as degradation of carbamazepine in environmentally relevant concentrations in wastewater [79].

Gogate et al. [80] described the development of a combined reactor based on the simultaneous use of acoustic cavitation, hydrodynamic cavitation, electrochemical oxidation/precipitation and ozonation. The reactor has been reported to have successful applications for water treatment and recycling of “frac” water (used water in the hydraulic manufacturing operations that need to be recycled back) at over 1200 installations across the USA and Canada. The hybrid oxidation reactor is described to give process intensification benefits and about 10–20 times higher processing rates as compared to use of ozone or the sonochemical reactors alone which has been attributed to the generation of additional oxidants in situ during the treatment and also elimination of mass transfer resistances leading to enhanced utilization of the introduced oxidants (ozone). Apart from disinfection of the microorganisms and reduction in COD introduced due to the presence of organic contaminants, passage through a hybrid reactor has also been reported to reduce scale formation and also result in increased flowability, which can lead to energy savings for the actual fracturing operations.

7 Efforts Needed in the Future

In spite of extensive potential for different applications with many proven results from laboratory-scale operations, only limited illustrations of successful application of sonochemical reactors at a commercial scale can be seen. The main reasons for poor translation are identified as lower rates of processing, uneven distribution of cavitation activity, material problems for high power application and lower energy transfer efficiencies leading to higher treatment costs. It is also important to understand that suitable design strategies linking the theoretically available information with the experimental results are lacking, which has restricted the optimum scale-up and operation of sonochemical reactors. Some of the guidelines for the required future work for transforming the successful laboratory-scale approach into commercial-scale technology include:

1. There is a current need to design reactors with uniform cavitation activity above the threshold required for inception of specific application. The design should be optimized based on the theoretical simulations of the pressure field distribution and understanding the effect of operating/geometric parameters on the activity distribution.
2. Experimental investigations at different scales of operation are needed to understand the dependency of the flow field, turbulence characteristics and the collapse intensity on the scale of operation with an objective of establishing well-defined scale strategies.
3. The significant problems related with the efficiency, power and scaling up of the transducers have been the root cause in delaying industrial development. Further research should be directed in terms of development of transducers operating with high power capacity and minimum erosion. The problem has more of a material science background, though inputs from chemical engineers and chemists will always be required.
4. The combination of sonochemical reactors with the hydrodynamic cavitation reactors as well as with microwave and UV need to be applied for a variety of applications so as to establish clearly the expected synergism. Development of hybrid designs capable of operating in continuous operation and as simultaneous combinations is very essential.
5. Development of user-friendly computer codes (similar to modern CFD codes) to predict the expected chemical effects as a function of the different operating parameters would be useful which can avoid trial-and-error-type experimentation.
6. The effect of process-intensifying parameters such as the presence of dissolved salts, suspended solids and gases should be studied in detail at different operating scales with the aim of intensification so as to minimize the operating costs and to increase the applicability of cavitation reactors.

8 Concluding Remarks

Analysis of different aspects of sonochemical reactors including the mechanism of generation, the key effects, the reactor configurations and the existing literature on different applications has revealed the following key considerations:

1. Passage of ultrasound into the liquid medium generates cavitating conditions and subsequent effects classified as physical and chemical which can drive the intensification of different applications.
2. Identification of the key controlling mechanisms for the specific application and subsequent optimization of the use of sonochemical reactors is very important to maximize the benefits in a cost-effective manner.
3. Almost all the operating parameters including intensity and frequency of irradiation as well as the operating temperature show an optimum dependent on

- the specific application, which needs to be established using laboratory/pilot-scale studies maintaining the geometric similarity.
4. Theoretical simulations can be effectively used to predict the cavitation activity and the pressure field distributions in the reactor which can also help in arriving at an optimum design for the large-scale operations. Multiple transducer reactors with flow cell type arrangement is the recommended configuration for successful commercial-scale installations with already proven results for some applications such as water treatment and crystallization.
 5. It has been conclusively established that application of sonochemical reactors can give intensified processing with the use of greener conditions and reduced energy requirements as compared to the conventional approach.
 6. The suggested guidelines for the possible work in the area of material development, understanding the controlling mechanism and developing scale-up strategies would be very helpful in efficient design and operation of large-scale sonochemical reactors.

References

1. Mason TJ (1992) Practical sonochemistry: users guide in chemistry and chemical engineering. Ellis Horwood series in organic chemistry. Ellis Horwood, Chichester
2. Gogate PR, Pandit AB (2004) Sonochemical reactors: scale up aspects. *Ultrason Sonochem* 11(3–4):105–117
3. Kanthale PM, Gogate PR, Pandit AB, Wilhelm AM (2003) Mapping of ultrasonic horn: link primary and secondary effects of ultrasound. *Ultrason Sonochem* 10:331–335
4. Lorimer JP, Mason TJ (1987) Sonochemistry. Part 1—the physical aspects. *Chem Soc Rev* 16:239–274
5. Lindley J, Mason TJ (1987) Sonochemistry: part 2—synthetic applications. *Chem Soc Rev* 16:275–311
6. Mason TJ (1990) A survey of commercially available sources of ultrasound suitable for sonochemistry, in sonochemistry—uses of ultrasound in chemistry. Royal Society of Chemistry, Cambridge
7. Mason TJ (1999) Sonochemistry. Oxford University Press, Oxford
8. Pandit AB, Moholkar VS (1996) Harness cavitation to improve processing. *Chem Eng Prog* 96:57–69
9. Vichare NP, Senthilkumar P, Moholkar VS, Gogate PR, Pandit AB (2000) Energy analysis in Acoustic cavitation. *Ind Eng Chem Res* 39:1480–1486
10. Ashokkumar M, Grieser F (1999) Ultrasound assisted chemical processes. *Rev Chem Eng* 15:41–83
11. Gogate PR, Pandit AB (2000) Engineering design methods for cavitation reactors I: sonochemical reactors. *AIChE J* 46(2):372–379
12. Gogate PR (2002) Cavitation: an auxiliary technique in wastewater treatment schemes. *Adv Environ Res* 6(3):335–358
13. Mason TJ, Lorimer JP (2002) Applied sonochemistry: uses of power ultrasound in chemistry and processing. Wiley, New York
14. Kumar Ajay, Gogate PR, Pandit AB, Delmas H, Wilhelm AM (2004) Gas liquid mass transfer studies in sonochemical reactors. *Ind Eng Chem Res* 43:1812–1819
15. Gole VL, Gogate PR (2012) A review on intensification of synthesis of biodiesel from sustainable feed stock using sonochemical reactors. *Chem Eng Process* 53:1–9
16. Yusof NM, Bandar B, Yousef A, Mecit A, Jagannathan M, Ashokkumar M (2016) Physical and chemical effects of acoustic cavitation in selected ultrasonic cleaning applications. *Ultrason Sonochem* 29:568–576

17. Gogate PR (2008) Cavitation reactors for process intensification of chemical processing applications: a critical review. *Chem Eng and process* 47:515–527
18. Moholkar VS, Pandit AB (1997) Bubble behavior in hydrodynamic cavitation: effect of turbulence. *AIChE J* 43(6):1641–1648
19. Naidu DV, Rajan R, Kumar R, Gandhi KS, Arakeri VH, Chandrasekaran S (1994) Modeling of a batch sono-chemical reactor. *Chem Eng Sci* 49(6):877–888
20. Vichare NP (1999) Studies in sonochemistry and cavitation phenomena. M Chem Eng Thesis Univ of Mumbai, Mumbai
21. Kidak R, Ince NH (2006) Ultrasonic destruction of phenol and substituted phenols: a review of current research. *Ultrason Sonochem* 13:195–199
22. Flynn HG (1964) Physics of acoustic cavitation in liquids in physical acoustics. In: Mason WP (ed) *Physical acoustics*, vol 1, Part B. Academic, New York
23. Margulis MA (1981) Investigations of electrical phenomena connected with cavitation I On electrical theories of chemical and physicochemical actions of ultrasonics. *Russ J Phy Chem* 55:154–158
24. Noltingk BE, Neppiras EA (1950) Cavitation produced by ultrasonics. *Proceed Phyl Soc (Lond)* B63:674–685
25. Dahlem O, Demaiffe V, Halloin V, Reisse J (1998) Direct sonication system suitable for medium scale sonochemical reactors. *AIChE J* 44:2724–2730
26. Thoma G, Swofford J, Popov V, Som M (1997) Sonochemical destruction of dichloromethane and *o*-dichlorobenzene in aqueous solution using a nearfield acoustic processor. *Adv Environ Res* 1:178–193
27. Gonze E, Gonthier Y, Boldo P, Bernis A (1998) Standing waves in a high frequency sonoreactor: visualisation and effects. *Chem Eng Sci* 53:523–532
28. Gogate PR, Mujumdar S, Pandit AB (2003) Large scale sonochemical reactors for process intensification: design and experimental validation. *J Chem Technol Biotechnol* 78:685–693
29. Gogate PR, Tatake PA, Kanthale PM, Pandit AB (2002) Mapping of sonochemical reactors: review. Analysis and experimental verification. *AIChE J* 48(7):1542–1560
30. Gogate PR, Pandit AB (2004) Sonophotocatalytic reactors for wastewater treatment: a critical review. *AIChE J* 50(5):1051–1079
31. Mhetre AS, Gogate PR (2014) New design and mapping studies of sonochemical reactor operating at capacity of 72 L. *Chem Eng J* 258:69–76
32. Son Y, Lim M, Khim J (2009) Investigation of acoustic cavitation energy in a large-scale sonoreactor. *Ultrason Sonochem* 16:552–556
33. Asakura Y, Yasuda K, Kato D, Kojima Y, Koda S (2008) Development of a large sonochemical reactor at a high frequency. *Chem Eng J* 139:339–343
34. Palanisamy B, Paul B, Chang C-H (2015) The synthesis of cadmium sulfide nanoplatelets using a novel continuous flow sonochemical reactor. *Ultrason Sonochem* 26:452–460
35. Shirsath SR, Sonawane SH, Saini DR, Pandit AB (2015) Continuous precipitation of calcium carbonate using sonochemical reactor. *Ultrason Sonochem* 24:132–139
36. Jolhe PD, Bhanvase BA, Patil VS, Sonawane SH (2015) Sonochemical synthesis of peracetic acid in a continuous flow micro-structured reactor. *Chem Eng J* 276:91–96
37. Entezari MH, Kruus P (1996) Effect of frequency on sonochemical reactions II: temperature and intensity effects. *Ultrason Sonochem* 3:19–24
38. Auzay SR, Naffrechoux JBE (2010) Comparison of characterization methods in high frequency sonochemical reactors of differing configurations. *Ultrason Sonochem* 17:547–554
39. Seymore JD, Gupta RB (1997) Oxidation of aqueous pollutants using ultrasound—salt induced enhancement. *Ind Eng Chem Res* 36:3453–3457
40. Servant G, Laborde JL, Hita A, Caltagirone JP, Gerard A (2003) On the interaction between ultrasound waves and bubble clouds in mono- and dual-frequency sonoreactors. *Ultrason Sonochem* 10:347–355
41. Tatake PA, Pandit AB (2002) Modelling and experimental investigation into cavity dynamics and cavitation yield: influence of dual frequency ultrasound sources. *Chem Eng Sci* 57:4987–4995
42. Yotsumoto T, Morita T, Noiri Y, Kojima Y, Asakura Y, Koda S (2014) Influence of pressure and temperature on sonochemical reaction in a flow-type reactor equipped with a PZT transducer. *Jpn J Appl Phys* 53 (7 SPEC ISSUE) art no 07KE09
43. Gogate PR, Shaha S, Csoka L (2015) Intensification of cavitation activity using gases in different types of sonochemical reactors. *Chem Eng J* 262:1033–1042

44. Gogate PR, Katekhaye SN (2012) A comparison of the degree of intensification due to the use of additives in ultrasonic horn and ultrasonic bath. *Chem Eng Proc* 61:23–29
45. Wei Z, Weavers LK (2016) Combining COMSOL modeling with acoustic pressure maps to design sono-reactors. *Ultrason Sonochem* 31:490–498
46. Tudela I, Sáez V, Esclapez MD, Díez-García MI, Bonete P, González-García J (2014) Simulation of the spatial distribution of the acoustic pressure in sonochemical reactors with numerical methods: a review. *Ultrason Sonochem* 21(3):909–919
47. Sutkar VS, Gogate PR, Csoka L (2010) Theoretical prediction of cavitation activity distribution in sonochemical reactors. *Chem Eng J* 158:290–295
48. Balasundaram B, Pandit AB (2001) Selective release of invertase by hydrodynamic cavitation. *Biochem Eng J* 8:251–256
49. Kurokawa M, King PM, Wu X, Joyce EM, Mason TJ, Yamamoto K (2016) Effect of sonication frequency on the disruption of algae. *Ultrason Sonochem* 31:157–162
50. Phull SS, Newman AP, Lorimer JP, Pollet B, Mason TJ (1997) The development and evaluation of ultrasound in the biocidal treatment of water. *Ultrason Sonochem* 4:157–164
51. Piyasena P, Mohareb E, McKellar RC (2003) Inactivation of microbes using ultrasound: a review. *Int J Food Microbiol* 87:207–216
52. Blume T, Neis U (2005) Improving chlorine disinfection of wastewater by ultrasound application. *Water Sci Technol* 52:139–144
53. Sangave PC, Pandit AB (2004) Ultrasound pre-treatment for enhanced biodegradability of the distillery wastewater. *Ultrason Sonochem* 11:197–203
54. Sangave PC, Gogate PR, Pandit AB (2007) Ultrasound and ozone assisted biological degradation of thermally pretreated and anaerobically pretreated distillery wastewater. *Chemosphere* 68:42–50
55. Nickel K, Neis U (2007) Ultrasonic disintegration of bio solids for improved biodegradation. *Ultrason Sonochem* 14:450–455
56. Chisti Y (2003) Sonobioreactors: using ultrasound for enhanced microbial productivity. *Trends Biotechnol* 21:89–93
57. Zhang G, Zhang P, Gao J, Chen Y (2008) Using acoustic cavitation to improve the bio-activity of activated sludge. *Bioresour Technol* 99:1497–1502
58. Cravatto G, Cintas P (2006) Power ultrasound in organic synthesis: moving cavitation chemistry from academia to innovative and large-scale applications. *Chem Soc Rev* 35:180–196
59. Nebois P, Bouaziz Z, Fillion H, Moeini L, Aurell Piquer MJ, Luche JL, Riera A, Moyano A, Pericas MA (1996) The Diels-Alder cycloaddition an intriguing problem in organic sonochemistry. *Ultrason Sonochem* 3:7–13
60. Luche JL, Einhorn C, Einhorn J, de Souza Barboza JC, Petrier C, Dupuy C, Delair P, Allavena C, Tuschl T (1990) Ultrasonic waves as promoters of radical processes in chemistry: the case of organometallic reactions. *Ultrasonics* 28(5):316–321
61. Luque de Castro MD, Priego-Capote F (2007) Ultrasound-assisted crystallization (sonocrystallization). *Ultrason Sonochem* 14:717–724
62. Amara N, Ratsimba B, Wilhelm AM, Delmas H (2001) Crystallization of potashalum: effect of power ultrasound. *Ultrason Sonochem* 8:265–270
63. Li H, Li H, Guo Z, Liu Y (2006) The application of power ultrasound to reaction crystallization. *Ultrason Sonochem* 13:359–363
64. Adewuyi YG (2001) Sonochemistry: environmental science and engineering applications. *Ind Eng Chem Res* 40:4681–4715
65. Adewuyi YG (2005) Sonochemistry in environmental remediation 2 heterogeneous sonophotocatalytic oxidation processes for the treatment of pollutants in water. *Environ Sci Technol* 39:8557–8570
66. Patil AL, Patil PN, Gogate PR (2014) Degradation of imidacloprid containing wastewaters using ultrasound based treatment strategies. *Ultrason Sonochem* 21:1778–1786
67. Shirsath SR, Sonawane SH, Gogate PR (2012) Intensification of extraction of natural products using ultrasonic irradiations—a review of current status. *Chem Eng Proc* 53:10–23
68. Vinatoru M (2001) An overview of the ultrasonically assisted extraction of bioactive principles from herbs. *Ultrason Sonochem* 8:303–313
69. Tata DB, Biglow J, Wu J, Tritton TR, Dunn F (1996) Ultrasound-enhanced hydroxyl radical production from two clinically employed anticancer drugs: adriamycin and mitomycin C. *Ultrason Sonochem* 3:39–45

70. Supersaxo A, Kou JH (1995) Controlled delivery of pharmaceuticals from preformed porous polymeric microparticles. US Patent 5:470–582
71. Dalmoro A, Barba AA, Lamberti G, d'Amore M (2012) Intensifying the microencapsulation process: ultrasonic atomization as an innovative approach. *Euro J Pharma Biopharma* 80:471–477
72. Boukroufa M, Boutekedjiret C, Petigny L, Rakotomanoman N, Chemat F (2015) Bio-refinery of orange peels waste: a new concept based on integrated green and solvent free extraction processes using ultrasound and microwave techniques to obtain essential oil polyphenols and pectin. *Ultrason Sonochem* 24:72–79
73. Gude VG (2015) Synergism of microwaves and ultrasound for advanced biorefineries. *Resour Eff Tech* 1:116–125
74. Khokhawala IM, Gogate PR (2010) Degradation of phenol using a combination of ultrasonic and UV irradiations at pilot scale operation. *Ultrason Sonochem* 17:833–838
75. Tenster I, Matafonov G, Batoev V (2015) Combination of high-frequency ultrasound and UV radiation of excilamp for surface disinfection. *Eng Life Sci* 15:830–834
76. Tezcanli-GiiUyer G, Ince NH (2004) Individual and combined effects of ultrasound ozone and UV irradiation: a case study with textile dyes. *Ultrasonics* 42:603–609
77. Franke M, Braeutigam P, Wu ZY, Ren Y, Ondruschka B (2011) Enhancement of chloroform degradation by the combination of hydrodynamic and acoustic cavitation. *Ultrason Sonochem* 18:888–894
78. Franke M, Ondruschka B, Braeutigam P (2014) Hydrodynamic-acoustic-cavitation for biodiesel synthesis. In: 3rd international conference on environment chemistry and biology singapore IPCBEE 78. doi:[10.7763/IPCBE.2014.V78.6](https://doi.org/10.7763/IPCBE.2014.V78.6)
79. Braeutigam P, Franke M, Schneider RJ, Lehmann A, Stolle A, Ondruschka B (2012) Degradation of carbamazepine in environmentally relevant concentrations in water by Hydrodynamic-Acoustic - Cavitation (HAC). *Water Res* 46:2469–2477
80. Gogate PR, McGuire D, Mededovic Thagard S, Cathey R, Blackmon J, Chapas G (2014) Hybrid advanced oxidation reactor technology: from concept to practical reality. *Ultrason Sonochem* 21:590–598